

DISSERTATION

THE DEVELOPMENT OF NOVEL N-HETEROCYCLIC CARBENES FOR ASYMMETRIC
C-C BOND FORMING REACTIONS

Submitted by

Daniel A. DiRocco

Department of Chemistry

In partial fulfillment of the requirements

For the Degree of Doctor of Philosophy

Colorado State University

Fort Collins, Colorado

Summer 2012

Doctoral Committee:

Advisor: Tomislav Rovis

Robert M. Williams

Richard G. Finke

Travis S. Bailey

Delphi Chatterjee

ABSTRACT

THE DEVELOPMENT OF NOVEL N-HETEROCYCLIC CARBENES FOR ASYMMETRIC C-C BOND FORMING REACTIONS

A variety of novel *N*-heterocyclic carbenes have been developed as organocatalysts for highly efficient and selective intermolecular C-C bond forming reactions. Problems associated with attaining high selectivity while retaining high efficiency in asymmetric intermolecular acyl anion pathways have been resolved through non-traditional manipulation of the catalyst architecture.

In the context of the asymmetric intermolecular Stetter reaction, a new series of fluorinated triazolium salt pre-catalysts have been developed that catalyze the highly enantioselective coupling of heteraryl aldehydes and nitroalkenes. Stereoelectronic effects in the ground state suggest that conformation of the catalyst plays a role in determining selectivity. DFT calculations provide evidence for an electrostatic interaction between the fluorine-induced dipole and the electrophiles as the source of increased selectivity.

The scope of the asymmetric intermolecular Stetter reaction of nitroalkenes has been further expanded to incorporate α,β -unsaturated aldehydes as partners. Mechanistic studies point to the initial proton-transfer event leading to generation of the acyl-anion equivalent as being turnover limiting. With this knowledge, an additive has been introduced that effectively increases the rate of proton transfer leading to substantially shorter reaction times and dramatically lower catalyst loadings.

Further catalyst development has led to the realization of another mode of catalyst control, using the C-F bond as an additional source of substrate differentiation. This complementary fluorinated

catalyst architecture substantially increases the reactivity of enolizable aldehydes in the asymmetric intermolecular Stetter reaction of nitrostyrenes, and for the first time allows for their inclusion in this transformation.

An asymmetric aza-benzoin reaction of aliphatic aldehydes and *N*-Boc imines has been developed after identifying an extremely selective amino-indanol derived catalyst scaffold and mild reaction conditions. The direct enantioselective acylation of amines has been realized using a dual catalysis manifold, incorporating a photoactive metal complex as a catalyst to activate amines toward acyl-anion addition and a chiral NHC catalyst. This methodology has led to the isolation and full characterization of a series of aza-Breslow intermediates by X-ray crystallography. Studies of these intermediates provide crucial information about the fundamental reactivity of the Breslow intermediate and show that it is not only a catalyst resting state in these transformation but its generation is also reversible in the presence of a weak acid.

ACKNOWLEDGMENTS

I would like to thank my advisor, Professor Tomislav Rovis, for not only creating an outstanding environment in which to become a scientist, but also one full of comradery, friendship, and tradition. Tom's insatiable passion for science is motivating and contagious and has provided the momentum that has carried me through this stage of my career.

I want to thank the entire Rovis group for being such a wonderful bunch of individuals to work with for the past years. To put it lightly, leaving you all will be the most difficult part of this process. I especially want to thank my classmates Kevin Oberg and Derek Dalton for selflessly offering their assistance in solving the numerous X-ray structures that were crucial to my success. Also, Professor Ken Houk, Liz Noey, and Joann Umm for all of their hard work during our collaborations.

I thank Mr. John Capwell, my high school chemistry teacher, for going out of his way to introduce me to organic chemistry and truly inspiring the rest of my life. Also, Professor Holly Bendorf and Professor Chriss McDonald for their dedication to undergraduate research as well as serving as my role models in college and to this day.

A very special thanks goes to my family who have always encouraged me to do great things, especially my parents, who made sure that I always had what I needed when it came to my education.

Most importantly, I thank my wife Christen, who left everything and everyone she knew behind to be with me, while I followed my dreams.

TABLE OF CONTENTS

Chapter 1. N-Heterocyclic Carbene Catalysis and the Development of Chiral Triazolylidene Carbenes for the Asymmetric Intermolecular Stetter Reaction	1
1.1 N-Heterocyclic Carbene Catalysis	1
1.1.1 Introduction	1
1.1.2 Development of the Asymmetric Benzoin Reaction	2
1.1.3 Development of the Asymmetric Stetter Reaction	5
1.1.4 A Mechanistic Study of the Intramolecular Stetter Reaction	9
1.1.5 The Asymmetric Intermolecular Stetter Reaction	10
1.2 Results	13
1.2.1 Catalyst Development and Application to the Asymmetric Intermolecular Stetter Reaction	13
1.2.2 Development of an Asymmetric Intermolecular Stetter Reaction of Hetaryl Aldehydes and Nitroalkenes	21
1.3 Investigation Into the Effect of Catalyst Fluorination	37
1.4 Conclusion	48
References	50
Chapter 2. Expanding the Scope of the Asymmetric Intermolecular Stetter Reaction of Nitroalkenes	54
2.1 Introduction	54
2.2 Results	56
2.2.1 The Role of the α -Heteroatom	56

2.2.2 Mechanistic Study of the Effect of Catechol	61
2.2.3 The Scope of the Asymmetric Intermolecular Stetter Reaction of Enals and Nitroalkenes	65
2.3 A [4+2] Cycloaddition of Enals and Nitroalkenes.....	72
2.4 Aliphatic Aldehydes in the Asymmetric Intermolecular Stetter Reaction.....	74
2.4.1 Introduction.....	74
2.4.2 Initial Studies and Catalyst Development.....	75
2.4.3 The Scope of the Asymmetric Intermolecular Stetter Reaction of Aliphatic Aldehydes and Nitrostyrenes.....	82
2.4.4 DFT Study of the Effect of Catalyst Fluorination	89
2.5 Conclusion	93
References.....	94
Chapter 3. Addition of Catalytically Generated Acyl Anion Equivalents to Imines and Iminium Ions.....	96
3.1 Additions of Acyl Anion Equivalents to Imines.....	96
3.1.1 Introduction.....	96
3.1.2 Catalytic Asymmetric Cross Aza-Benzoin Reactions of Aliphatic Aldehydes and <i>N</i> -Boc Imines	99
3.1.3 The Role of the Carboxylic Acid.....	107
3.2 Addition of Acyl Anion Equivalents to Iminium Salts.....	109
3.2.1 Introduction.....	109
3.2.2 Results.....	112

3.3 Conclusion	133
3.4 References.....	135
Chapter 4. Isolation and Characterization of Aza-Breslow Intermediates	137
4.1 Introduction.....	137
4.2 Results.....	140
4.3 Conclusion	151
4.4 References.....	152
Appendix 1	153
Appendix 2.....	224
Appendix 3.....	276
Appendix 4.....	322

Chapter 1

N-Heterocyclic Carbene Catalysis and the Development of Chiral Triazolylidene Carbenes for the Asymmetric Intermolecular Stetter Reaction

1.1 *N*-Heterocyclic Carbene Catalysis

1.1.1 Introduction

Since the 1960's, *N*-heterocyclic carbenes have grown increasingly popular in the fields of organic and organometallic chemistry due to their versatility as organocatalysts and ligands.¹ The pioneering work of Wanzlick established nucleophilic carbenes as reactive intermediates, although isolation proved difficult because of their inherent reactivity.² Breslow also proposed the existence of nucleophilic carbenes in 1958 during his investigation of the thiamine mode of action.³ It was not until 1988, nearly thirty years later that the first stable carbene species was isolated by Bertrand and subsequently Arduengo and characterized by X-ray crystallography (Figure 1.1).⁴ Since Arduengo's reports, imidazole, thiazole, and triazole derived stable carbenes have been reported the most common uses are as σ -donor ligands for metals and organocatalysts for a variety of transformations, notably the benzoin and Stetter reactions.⁵

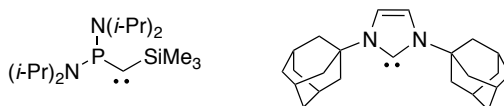
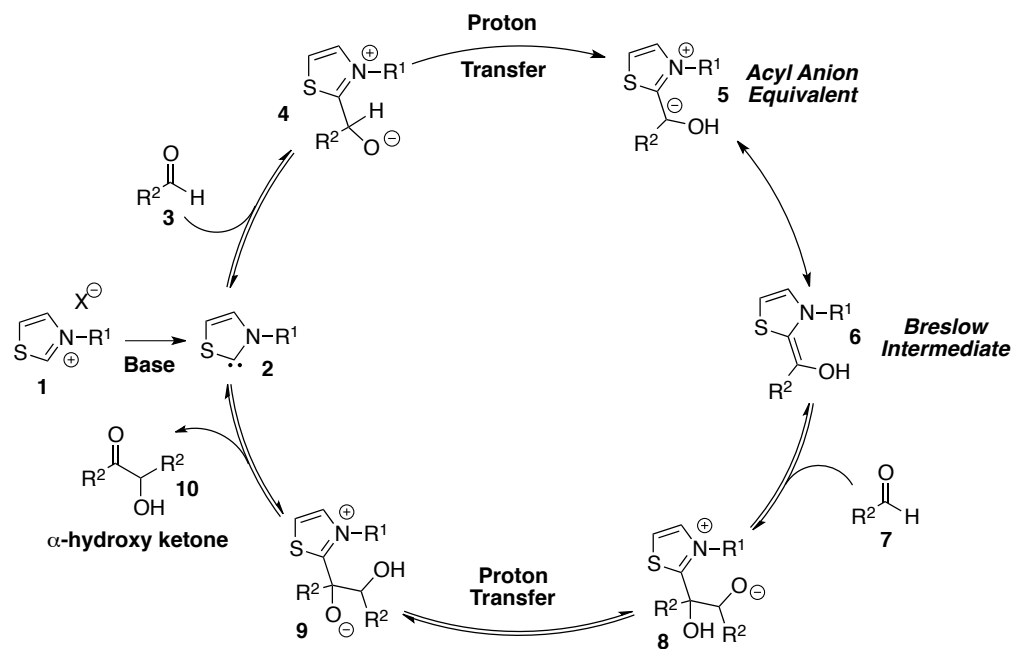


Figure 1.1

1.1.2 Development of the Asymmetric Benzoin Reaction

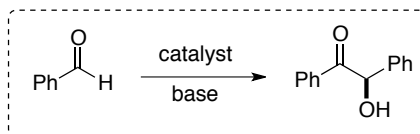
Wohler and Liebig first reported the benzoin reaction in 1832, which described the use of cyanide as a catalyst for the formation of benzoin from benzaldehyde.⁶ The reversal of reactivity from an electrophilic aldehyde into a nucleophilic acyl anion equivalent was one of the first examples of what is now known as *umpolung* reactivity. Some seventy years later, Lapworth described his studies on the action of potassium cyanide with benzaldehyde wherein the currently accepted proposed mechanism was first reported.⁷ In 1943, Ukai demonstrated that thiazolium salts could also catalyze the benzoin condensation,⁸ although it was not until 1958 that the currently accepted mechanism was elucidated by Breslow.⁹ The mechanism of the thiazolium catalyzed benzoin reaction is closely related to Lapworth's initial proposal; the nucleophilic carbene (**2**) is formed *in situ* by deprotonation of a thiazolium salt (**1**) with base. The carbene (**2**) can undergo nucleophilic addition to an aldehyde (**3**) generating tetrahedral intermediate **4**. Subsequent proton transfer generates the acyl anion equivalent (**5**), commonly referred to as the "Breslow intermediate" in resonance structure **6**. This nucleophilic species can then undergo addition to another molecule of aldehyde yielding tetrahedral intermediate **8**. After a final proton transfer, intermediate **9** collapses to liberate the carbene (**2**) and a α -hydroxy ketone (**10**) (Scheme 1.1).



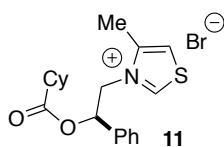
Scheme 1.1

With Ukai's discovery of the thiazolylidene carbene-catalyzed benzoin reaction came a newly found interest in the area. The use of thiazolium salts as precatalysts enabled the reaction to be rendered asymmetric through the development of chiral scaffolds. The first example of an asymmetric benzoin reaction was reported in 1966 by Sheehan using chiral thiazolium salt **11** to yield benzoin in 22% ee (Table 1.1).¹⁰ Over the next thirty years many groups attempted to improve the reactivity and enantioselectivity of this transformation with only modest success (Table 1.1).¹¹ Enders achieved the first significant advancement in the area when chiral triazolylidene carbenes were introduced, providing dramatic increases in yields and enantioselectivity over previous thiazolium derived catalysts (Table 1.1, **16**).¹² By developing a more rigid bicyclic framework, Leeper was able to increase enantioselectivity while maintaining modest reactivity (Table 1.1, **17-18**).¹³

Table 1.1

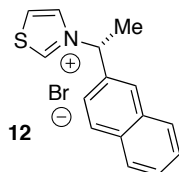


Sheehan 1966



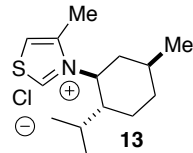
**9% yield
22% ee**

Sheehan 1974



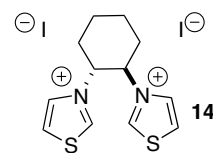
**6% yield
51% ee**

Tagaki 1980



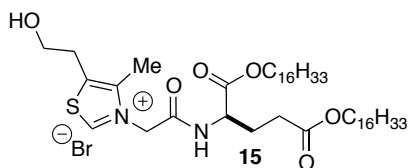
**20% yield
35% ee**

Lopez-Calahorra 1994



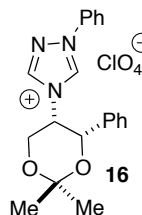
**11.5% yield
27% ee**

Tsuda 1995



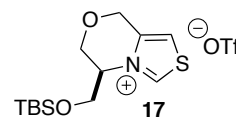
**35% yield
18% ee**

Enders and Teles 1996



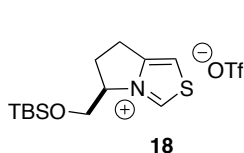
**66% yield
75% ee**

Leeper 1997



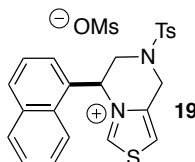
**34% yield
20% ee**

Leeper 1997



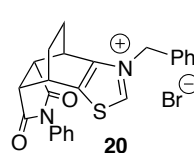
**50% yield
21% ee**

Rawal 1998



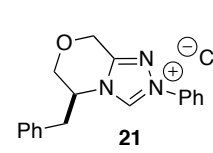
**18% yield
30% ee**

Leeper 1998



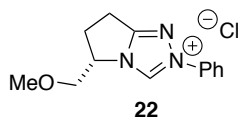
**18% yield
30% ee**

Leeper 1998



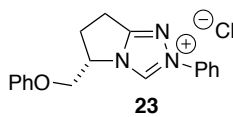
**45% yield
80% ee**

Leeper 1998



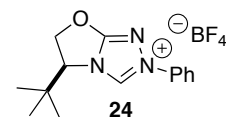
**47% yield
48% ee**

Leeper 1998



**22% yield
63% ee**

Enders 2002

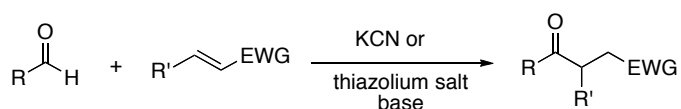


**83% yield
90% ee**

Further development of this bicyclic scaffold by Enders led to triazolium salt **24** that provides benzoin product in an impressive 83% yield and 90% ee.¹⁴

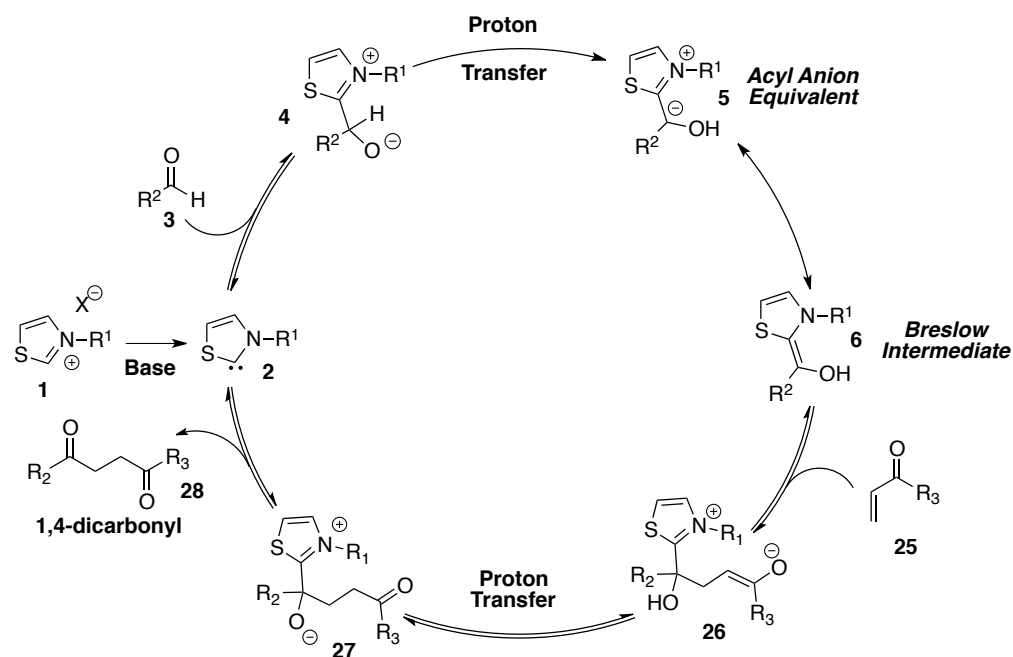
1.1.3 Development of the Asymmetric Stetter Reaction

In 1973, Stetter expanded the *umpolung* reactivity of aldehydes by addition of acyl anion equivalents to α,β -unsaturated Michael-acceptors, affording 1,4-dicarbonyl compounds.¹⁵ A thorough study of this reactivity was conducted by Stetter utilizing cyanide or thiazolyliidene carbenes as catalysts to couple aromatic and aliphatic aldehydes to a variety of Michael-acceptors including α,β -unsaturated ketones, esters, and nitriles (Scheme 1.2).¹⁶



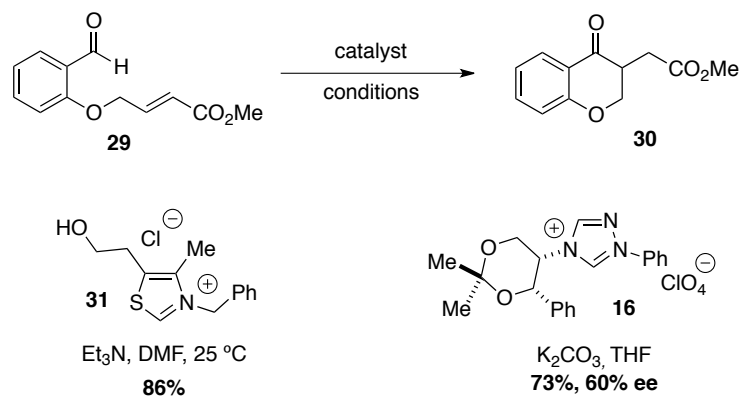
Scheme 1.2

Although the scope of this transformation was demonstrated to be broad, β -substituted Michael-acceptors imposed a major limitation. When R'=H, high yields of the desired Stetter product are obtained; however, a β -substituent on the Michael acceptor dramatically affects reactivity and only highly activated acceptors, such as fumarates, provide synthetically useful yields. The mechanism of the Stetter reaction was initially based on that of the benzoin reaction elucidated by Breslow. A recent study by Yates also supports the originally proposed mechanism.¹⁷ In identical fashion the carbene **2** is generated from a thiazolium salt **1** and base and undergoes nucleophilic addition to the aldehyde (**3**) forming tetrahedral intermediate **4**. After proton transfer, acyl anion equivalent **5** (or Breslow intermediate **6**) is generated and adds conjugately to the Michael-acceptor. After a second proton transfer, tetrahedral intermediate **27** is formed which collapses to yield the dicarbonyl product **28** and regenerates the thiazolyliidene carbene **2** (Scheme 1.3).



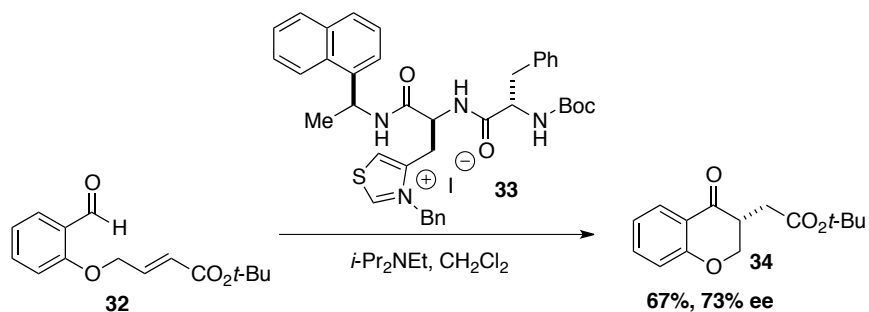
Scheme 1.3

The *intramolecular* Stetter reaction of salicylaldehyde derivatives was reported by Ciganek in 1995, almost 20 years after the initial discovery of the *intermolecular* reaction.¹⁸ Aldehyde **29** was treated with thiazolium salt **31** (thiamine) and Et₃N in DMF to afford the desired chromanone product **30** in 86% yield (Scheme 1.4). Enders reported the first asymmetric variant in 1996 utilizing triazolylidene precatalyst **16**, which displays high reactivity but only modest enantioselectivity.¹⁹



Scheme 1.4

Miller and coworkers have also shown that tethering a thiazolium moiety to a peptidic backbone can result in increased enantioselectivity while maintaining moderate reactivity (Scheme 1.5).²⁰



Scheme 1.5

The application of chiral triazolylidene carbenes demonstrated that this transformation could be rendered asymmetric but the development of a highly efficient and asymmetric Stetter reaction still remained a challenge.

Our group has developed a series of highly efficient and selective triazolylidene carbene catalysts for the asymmetric intramolecular Stetter reaction (Figure 1.2). The rigidity of the bicyclic framework allows for restricted rotation while the *N*-aryl substituent blocks the opposing side. Combined, this new scaffold leads to a catalyst with greater differentiation between

diastereomeric transition states than previously reported. Thiazolylidene carbenes developed by Leeper and Rawal only occupy one of the four quadrants of chemical space around the catalyst, whereas our bicyclic triazolylidene carbenes occupy three of four. This restricted access is believed to be the origin of the high selectivities obtained.²¹

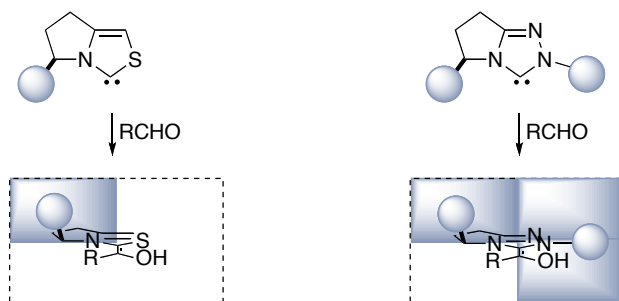
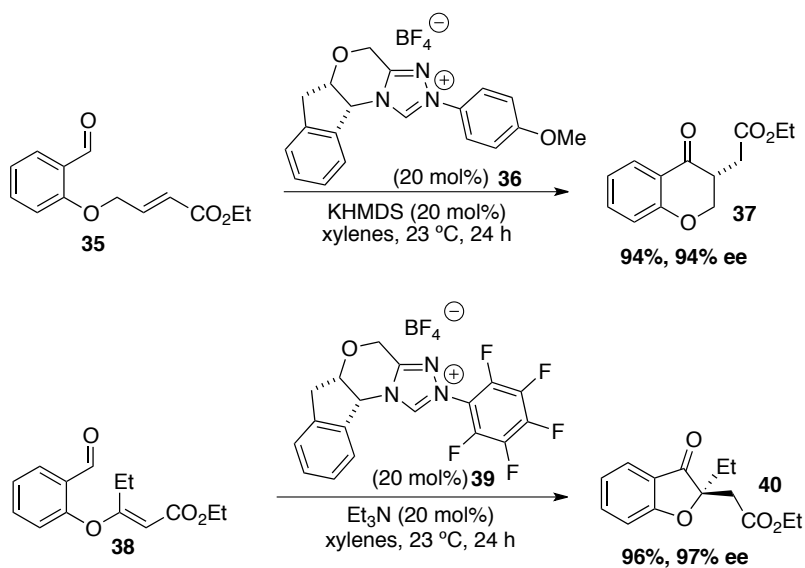


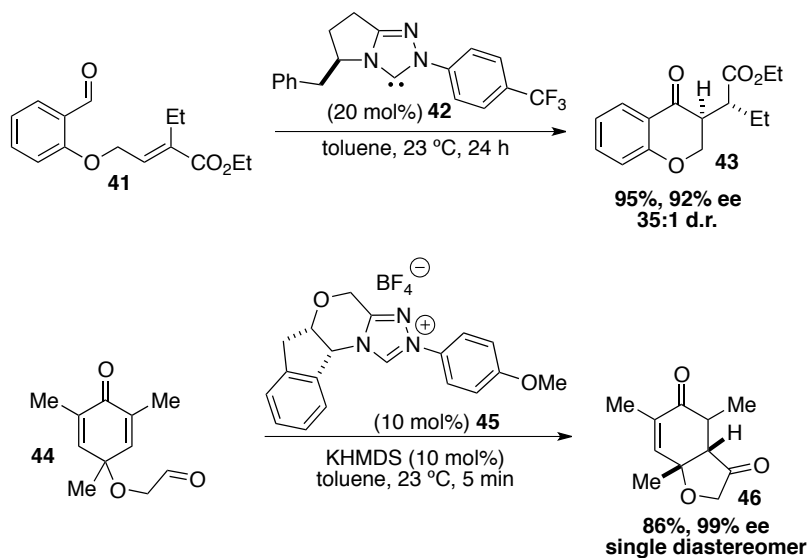
Figure 1.2

We have shown that by using a sterically encumbered bicyclic or tetracyclic triazolylidene carbene framework, high levels of enantioselectivity can be achieved in the intramolecular Stetter reaction (Scheme 1.6).²²



Scheme 1.6.

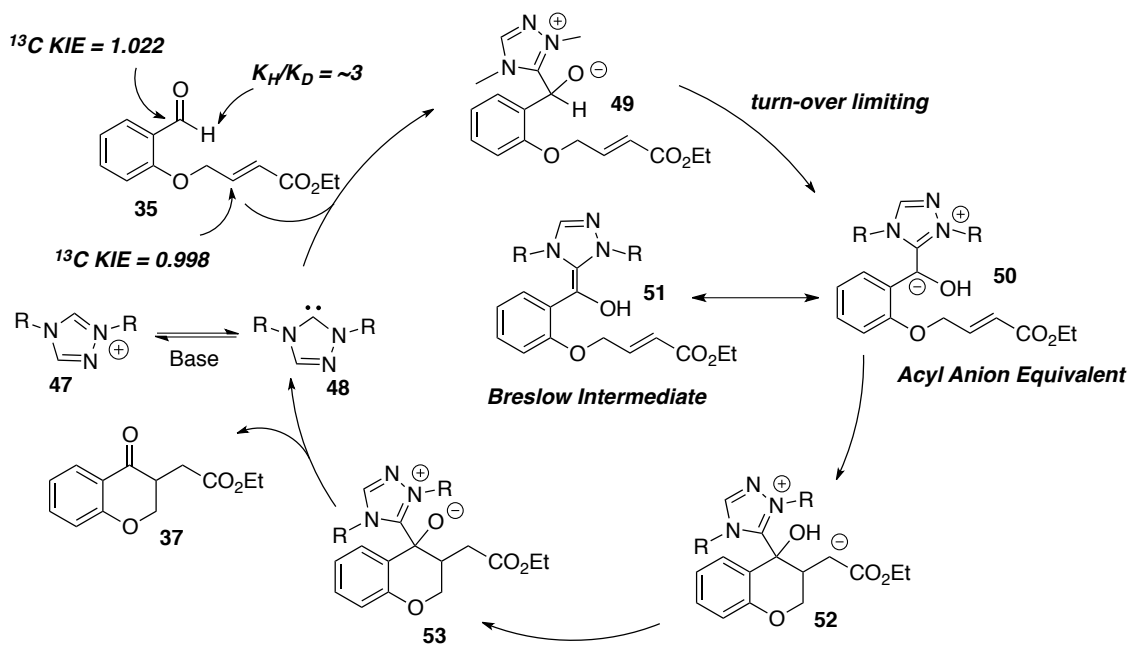
This transformation can also be highly diastereoselective, producing Stetter products in excellent yield, with high enantioselectivity and diastereoselectivity (Scheme 1.7).



Scheme 1.7

1.1.4 A Mechanistic Study of the Intramolecular Stetter Reaction

Although computational studies had made suggestions about the mechanism of the Stetter reaction, no experimental study of the mechanism had ever been conducted. In pursuit of the goal of rendering the asymmetric Stetter reaction a general and reliable method, we undertook an experimental study using our chiral triazolylidene carbene catalysts to better understand the factors that govern reactivity. Through a series of kinetic isotope effect and competition studies, sufficient evidence was provided to suggest that proton transfer of tetrahedral intermediate **49** is the turnover-limiting step (Scheme 1.8).²³

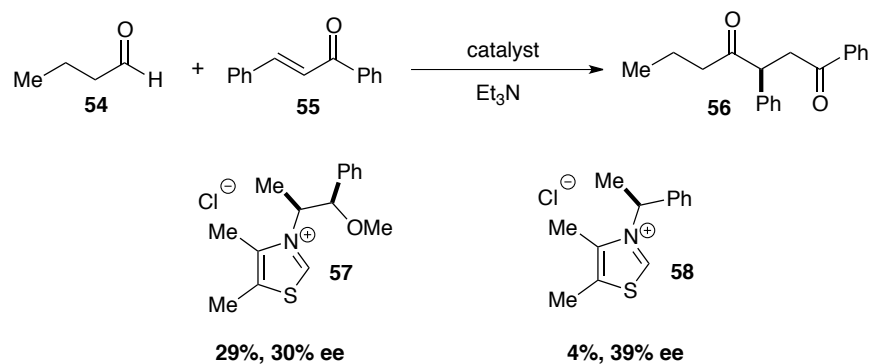


Scheme 1.8

Circumstantial evidence was also obtained to suggest the involvement of the ethereal tether in the proton transfer event. This mechanistic study has provided the impetus for rational catalyst design in solving challenging problems associated with the intermolecular variant.

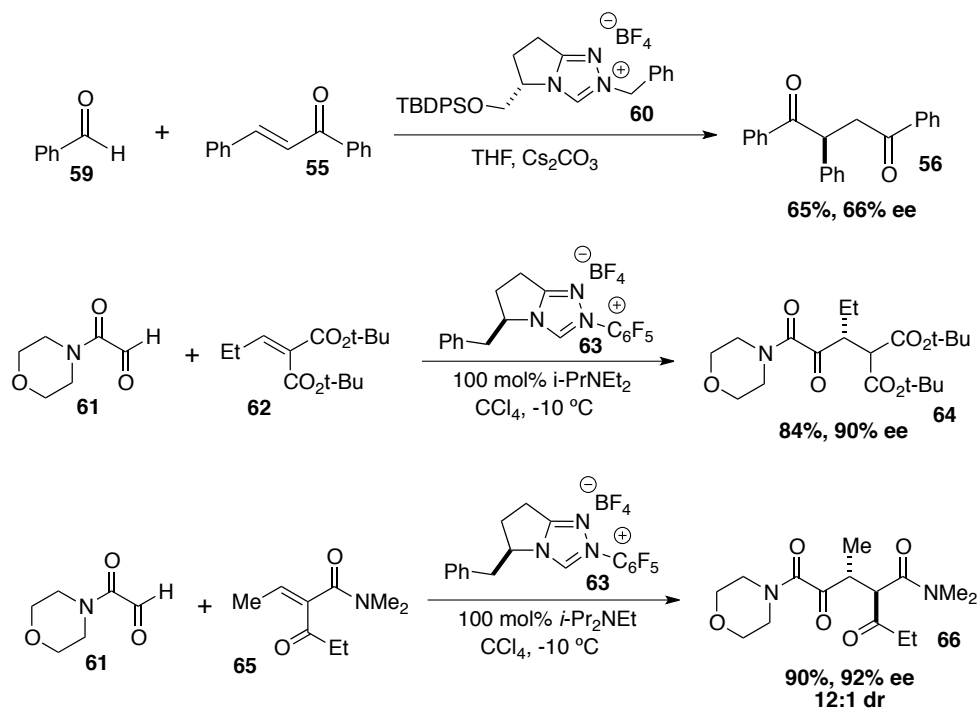
1.1.5 The Asymmetric Intermolecular Stetter Reaction

Although the intramolecular variant has been rendered highly enantioselective, advances in the asymmetric intermolecular Stetter reaction have only recently been reported. Enders described the first asymmetric intermolecular Stetter reaction utilizing *n*-butanal **54** and chalcone **55** with chiral thiazolium derived pre-catalysts (**57-58**) to give the corresponding 1,4-diketone **56** in poor yield and low enantioselectivity (Scheme 1.9).²⁴



Scheme 1.9

It was not until two recent examples of an asymmetric intermolecular Stetter reaction were reported in late 2008 that major advances in the area were made. Enders described utilizing triazolium precatalyst **60** with aryl aldehydes and chalcone (**55**) to form the 1,4-dicarbonyl compound in good yield and modest enantioselectivity (Scheme 1.10).²⁵ Concurrently and independently, we reported the use of glyoxamide **61** as the nucleophilic coupling partner with alkylidenemalonates to form the Stetter product in high yield and high enantioselectivity (Scheme 1.10).²⁶



Scheme 1.10

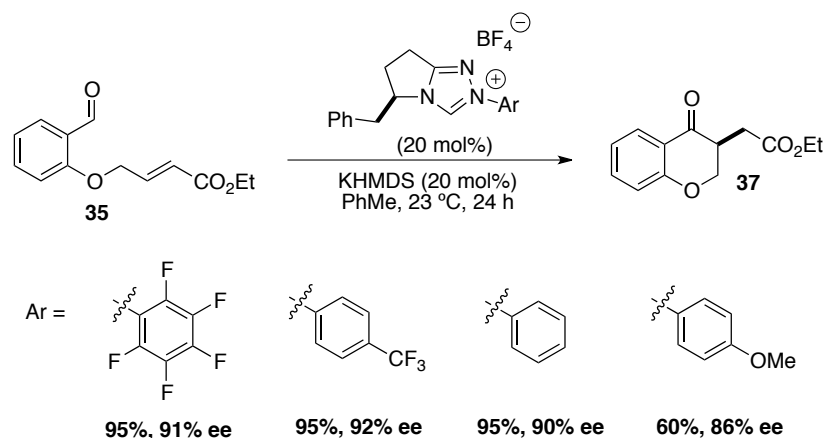
Our report was the first highly efficient asymmetric version of the intermolecular Stetter reaction, albeit with the obvious limitation of substrate scope. Through the rational design of new catalysts we aimed to improve this method by expanding the scope to different aldehydes and Michael-acceptors while maintaining high efficiency and selectivity, rendering this transformation a reliable and efficient means of preparing useful intermediates for the synthetic community.

1.2 Results

1.2.1 Catalyst Development and Application to the Asymmetric Intermolecular Stetter Reaction

Although the catalytic asymmetric *intramolecular* Stetter reaction is now well developed, the *intermolecular* variant has remained a challenge. The collective knowledge during the development of the asymmetric Stetter reaction suggested that significant advances in the efficiency and selectivity of the intermolecular transformation would ultimately come from the development of new catalysts. A screen of current catalysts with a variety of aldehydes and Michael-acceptors reveals that the limits of their utility have been reached and further development would be needed to advance this transformation.

We began with the development of new triazolylidene carbene based catalysts for the advancement of the asymmetric intermolecular Stetter reaction. The chromanone based intramolecular reaction has become a useful model system for testing and evaluating new catalysts. In general, we have observed that electron deficient triazolylidene carbenes are more reactive and give higher levels of enantioselectivity (Scheme 1.11).²⁷



Scheme 1.11

The reason that electron-deficient species are more reactive can be explained using the mechanistic insight obtained from the experimental study in our group. Foremost, we have revealed that the rate-determining step in the intramolecular Stetter reaction is initial proton transfer to generate the acyl anion equivalent. The acidity of the tetrahedral intermediate should play a role in the rate of the reaction. This hypothesis has been tested in our mechanistic study, which demonstrates that more electron deficient aldehydes are consumed preferentially in competition experiments. This observation should translate to a more electron deficient catalyst, with the assumption that proton transfer is still the turnover-limiting step in these systems. With regard to the marginal but reproducible increase in enantioselectivity, the most basic species in the reaction is generally the carbene. A less basic carbene would result in less catalyst-induced epimerization, leading to a higher observed enantioselectivity, although control studies have shown that catalyst induced epimerization is typically not observed. A DFT study of the Stetter reaction reported by Yates and coworkers has also provided evidence that the geometry of the Breslow intermediate can be modulated by controlling the electronic nature of the substituents on the triazolium moiety (Figure 1.3).²⁸

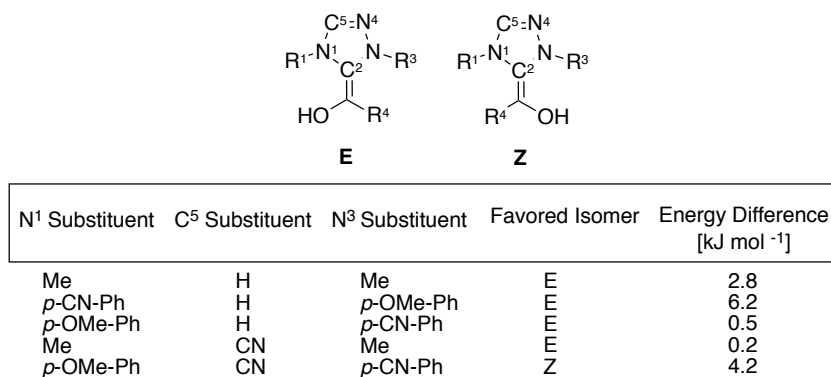


Figure 1.3

The geometry of the Breslow intermediate is not directly translated to the formed stereocenter, however it may influence the facial selectivity of the incoming electrophile.

With the goal of making a more electron deficient species, we first examined areas of the scaffold that would directly affect the electronic character of the triazolium moiety. Our group has developed two complimentary scaffolds, from which all of our catalysts are derived. The synthesis of these triazolium salts is highly modular, allowing for trivial derivatization (Figure 1.4). The morpholine-fused scaffold is derived from chiral amino alcohols and the pyrrolidine-fused scaffold from amino acids. The N-aryl substituent is the most obvious, and consequently the most trivial area to derivatize. We have already shown that a pentafluorophenyl substituent can be used with great results and is also the most electron-deficient species that is easily accessible. Although the steric modification of both of these scaffolds is straightforward, the pyrrolidine-fused platform would allow for easier electronic modification. We examined the synthesis of other enantioenriched, substituted γ -lactams to find that this particular area is fairly scarce. With the goal of modulating electronics without affecting the steric environment of the catalyst we considered synthesizing fluorinated analogues of the pyrrolidine scaffold. α -

Fluorination of γ -lactams has been reported by Coward, albeit in fairly poor yields with only modest diastereoselectivity.²⁹

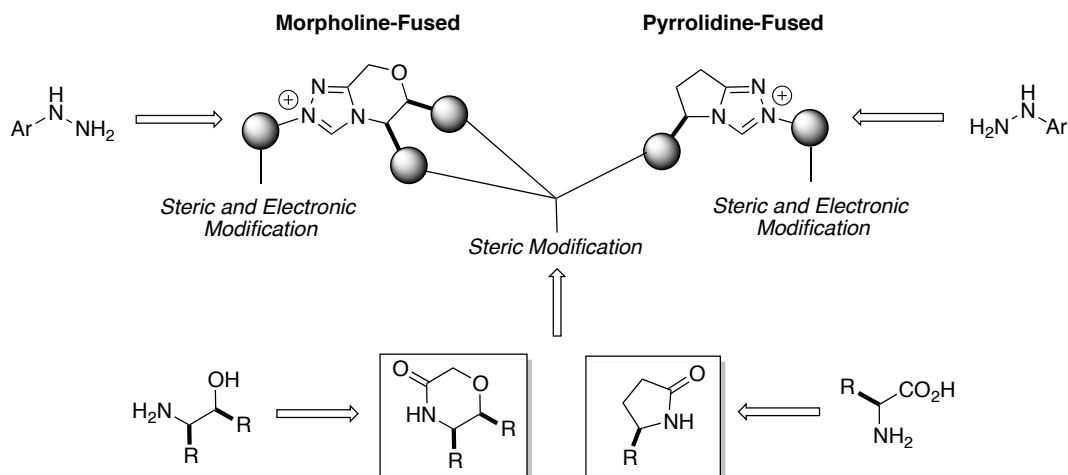
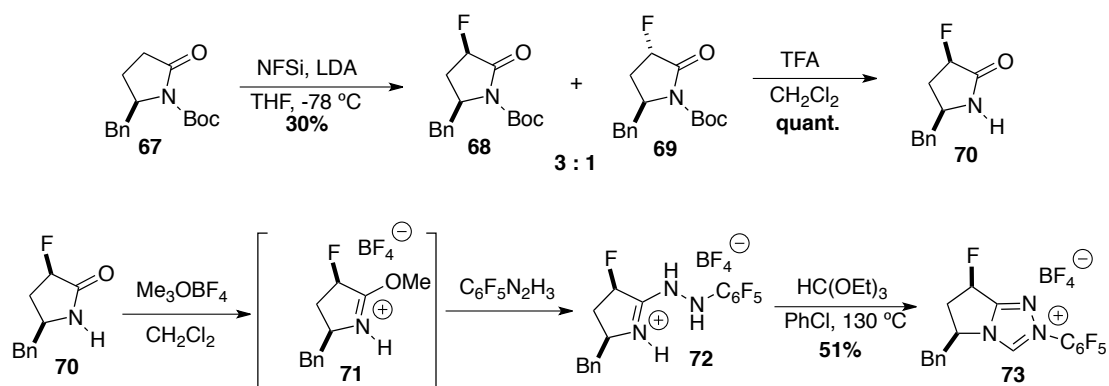


Figure 1.4

Enantioenriched γ -lactam **67** was synthesized from L-phenylalanine according to the method of Eissenstat.³⁰ The lactam was fluorinated via a procedure adapted from Coward to give the α -fluorolactam **68** as a separable 3:1 mixture of diastereomers. In this case we found that the fluorination was selective for the cis-stereochemistry, opposite that observed by Coward in his study of similar compounds. Boc-lactam **68** was then deprotected and subjected to the same one-pot procedure developed by our group for the synthesis of triazolium salts (Scheme 1.12).³¹ Treatment of lactam **70** with Meerwein's salt provides imidate **71** by ¹H NMR. Addition of pentafluorophenylhydrazine to this solution results in the formation of hydrazide **72** which could be elaborated to triazolium salt **73** by condensation with triethylorthoformate. In order to verify the relative stereochemistry of the fluorine atom with respect to the benzyl group, a sample of triazolium salt **73** was crystallized and subjected to x-ray analysis confirming the cis relative stereochemistry (Figure 1.5)



Scheme 1.12

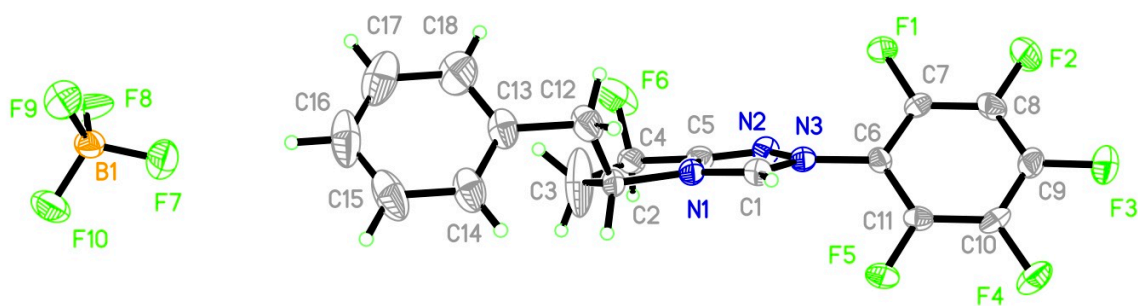
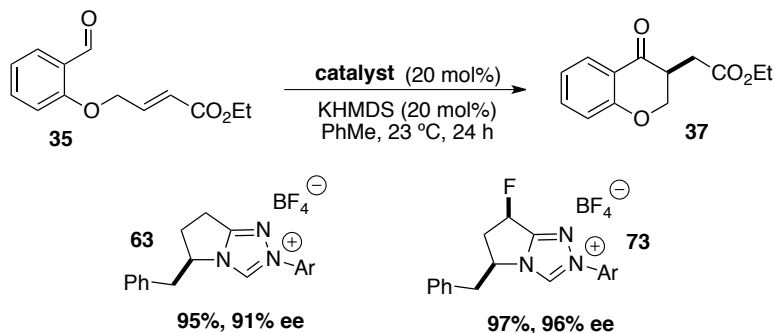


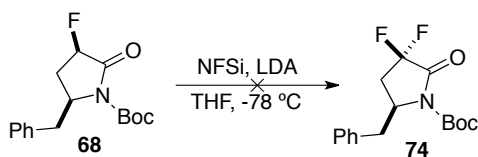
Figure 1.5

With the proposed catalyst in-hand we evaluated its reactivity in the intramolecular chromanone system. Although both catalysts provide high yield, a noticeable increase in reactivity was observed with fluorinated pre-catalyst **73** as well as a substantial increase in enantioselectivity (Scheme 1.13).



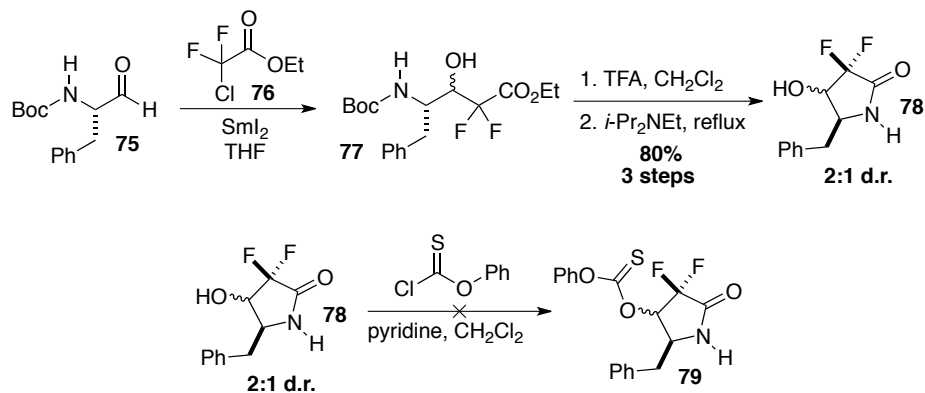
Scheme 13.

This result validated our original hypothesis and provided the impetus for synthesizing a difluorinated analogue. Unfortunately, all attempts to difluorinate lactam **68** failed to provide any of the desired product (Scheme 1.14).



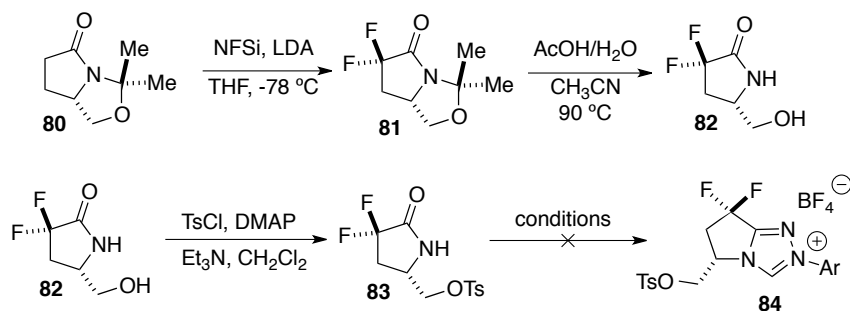
Scheme 1.14

An alternate approach to the synthesis of the difluorinated derivatives involves a Reformatsky addition of chloro-fluoro-ester **76** to phenylalanine derived aldehyde **75**. This reaction proceeds smoothly to afford amido-ester **77** and after subsequent removal of the Boc-group followed by intramolecular lactamization, yields the desired lactam in good yield as a mixture of diastereomers (Scheme 1.15). Unfortunately, formation of the Barton ester could not be accomplished and deoxygenation was not achieved.



Scheme 1.15

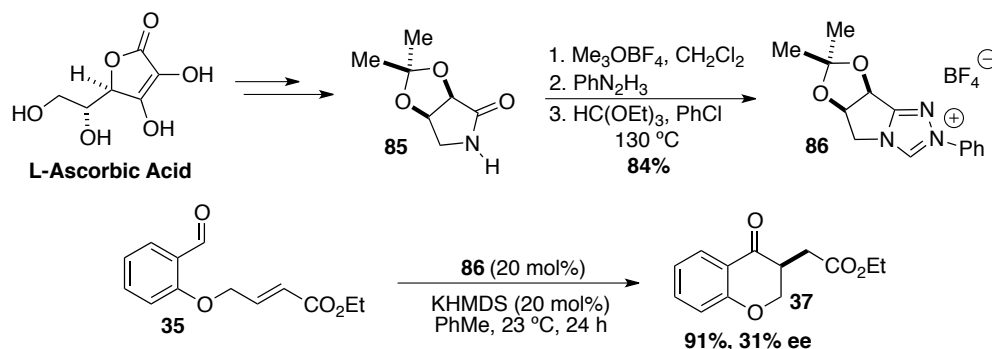
Lastly, it is known in the literature that bicyclic lactam **80** can be difluorinated by two successive iterations of the electrophilic fluorination procedure using NFSi. Deprotection of the aminal leads to formation of hydroxy lactam **82**, however, attempts to further elaborate this intermediate to triazolium salt **84** failed and led to decomposition (Scheme 1.16).



Scheme 1.16

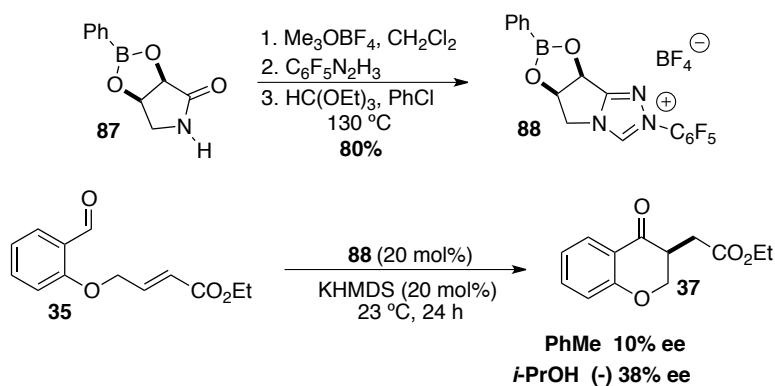
Aside from developing more electron deficient catalysts, we were also interested in changing the chiral manifold on which these catalysts are based. By moving steric bulk away from the reacting center we hoped to make a more reactive species while retaining good selectivity. Starting from L-ascorbic acid, lactam **85** was synthesized according to literature precedent.³² Lactam **85** was

converted to triazolium salt **86** in good yield and tested in the model system, which displays high reactivity but only modest enantioselectivity (Scheme 1.17).



Scheme 1.17

This scaffold allowed us to access boronate ester **87**, which was smoothly converted to the corresponding triazolium salt **88** (Scheme 1.18). We hypothesized that a boronate could act as an internal Lewis acid, potentially activating the Michael acceptor toward addition while also inducing asymmetry. Unfortunately, application to the chromanone system showed lower enantioselectivity for this scaffold. If the reaction is run in an alcoholic solvent the opposite major enantiomer is obtained in higher selectivity. This demonstrates the ability of **88** to act as a Lewis acid and the large effect that a coordinating alcoholic solvent can have on the transition state.



Scheme 1.18

From these results we can draw the conclusion that for high enantioselectivity in this reaction the stereodirecting group must be close to the reactive center. We have also shown that electron-withdrawing groups in proximity to the azolium moiety can have beneficial outcome on the reactivity and selectivity of the reaction. The main objective for developing new catalysts is to advance the current scope and limitations of the Stetter reaction. Since the *intramolecular* version has been rendered highly enantioselective with current catalysts, we planned to investigate the potential of new catalysts to advance the *intermolecular* reaction to the same state.

1.2.2 Development of an Asymmetric Intermolecular Stetter Reaction of Hetaryl Aldehydes and Nitroalkenes

Our aims at improving this reaction focused largely on increasing the generality of this method by expanding the scope while maintaining good reactivity and enantioselectivity. We envisioned that nitroalkenes might serve as viable Michael-acceptors in the Stetter reaction based on their high reactivity with other nucleophiles.³³ The corresponding β -nitro ketones derived from this

transformation are also highly attractive intermediates, which can be derivatized into a variety of synthetically useful compounds (Figure 1.6).³⁴

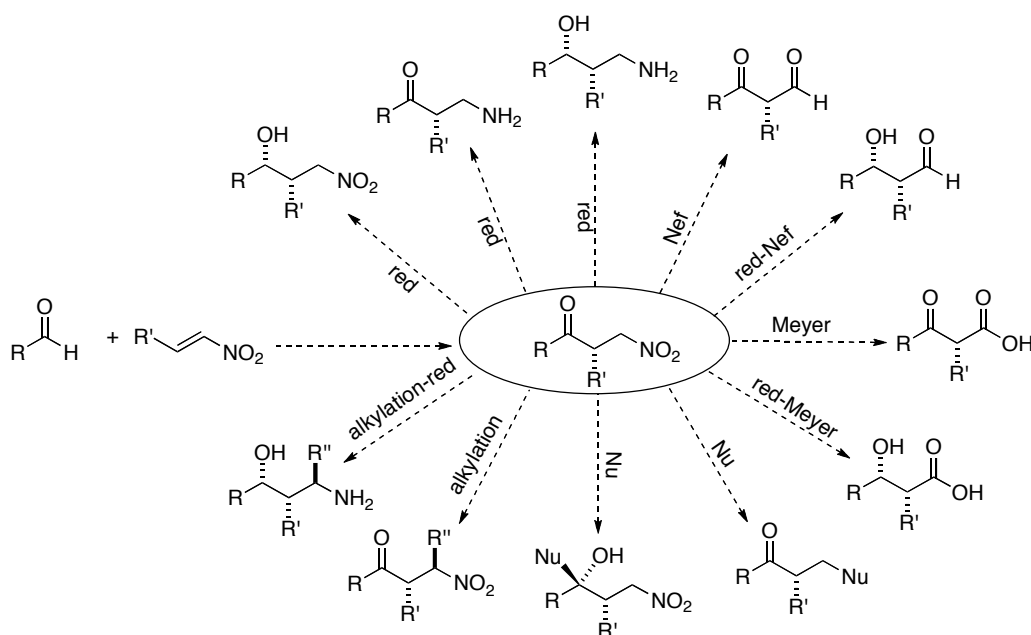
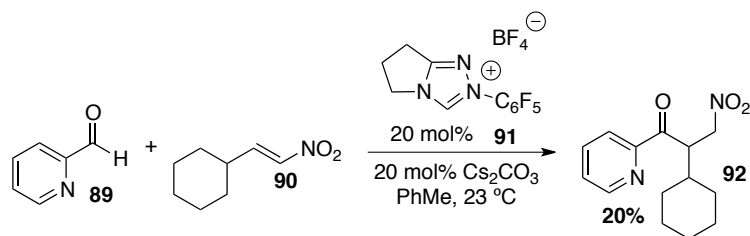


Figure 1.6

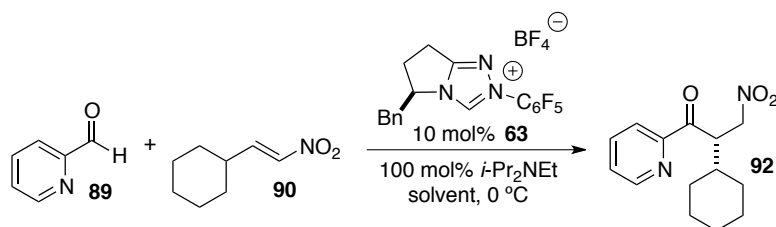
We started our investigation using picolinaldehyde **89** as the nucleophilic coupling partner, since it had been previously demonstrated to be a particularly reactive aldehyde,³⁵ with cyclohexyl-substituted nitroalkene **90** (Scheme 1.19). Initially inorganic bases were chosen in lieu of amines due to the sensitivity of nitroalkenes towards nucleophilic reagents. Using achiral triazolium salt **91**, 20% of the desired β -nitro ketone was obtained.



Scheme 1.19

In our extensive studies of the intramolecular reaction, non-polar solvents have always provided optimal reactivity and enantioselectivity. Recent studies on the intermolecular Stetter reaction of glyoxamides with alkylidene malonates has also shown the same trend, although traditional reaction conditions developed by Stetter employ amine bases and polar solvents. With this in mind, a variety of solvents were screened with amine bases revealing alcoholic solvents to be optimal, particularly methanol. Utilizing chiral triazolium pre-catalyst **63** under optimized conditions provides the desired product **92** in 82% yield and 74% ee (Table 1.2).

Table 1.2



Entry	Solvent	Yield (%) ^b	ee (%) ^c
1.	PhMe	<10%	—
2.	THF	<10%	—
3.	EtOH	59%	70%
4.	MeOH	82%	74%

^a Reactions conducted with 1.0 equiv **89** and 1.5 equiv **90**. ^b Isolated yield after chromatography. ^c Enantiomeric excess determined by HPLC on a chiral stationary phase.

After developing suitable conditions we evaluated a variety of aryl aldehydes as acyl anion precursors, revealing that only 2-heterocyclic derivatives participate efficiently under these conditions. Benzaldehyde does not provide any of the desired ketone product while more activated aldehydes show marginal reactivity, selectivities are poor (Table 1.3).

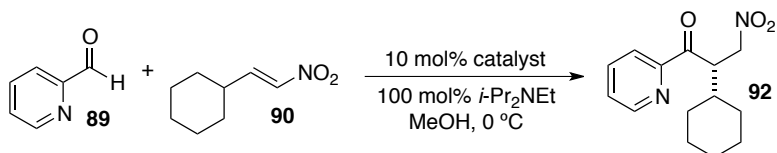
Table 1.3

Entry	Aldehyde	Yield (%) ^b	ee (%) ^c
1.		82%	74%
2.		17%	33%
3.		<5%	–
4.		28%	44%
5.		<5%	–

^a Reactions conducted with 1.0 equiv aldehyde and 1.5 equiv **90**. ^b Isolated yield after chromatography. ^c Enantiomeric excess determined by HPLC on a chiral stationary phase.

With an efficient intermolecular Stetter reaction identified we hoped to further improve selectivity by the development of new catalysts. We began by surveying an array of catalyst architectures containing varying *N*-aryl substituents (Table 1.4). Electron rich *N*-aryl substituents afford none of the desired product (catalyst **95**). While more electron

Table 1.4



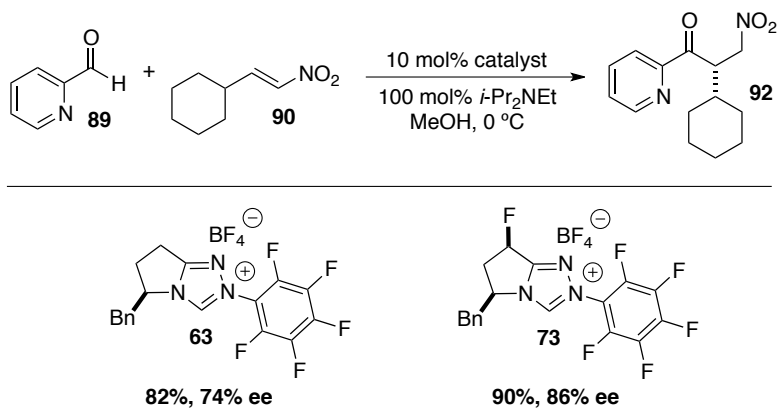
Entry	Catalyst	Yield (%) ^b	ee (%) ^c
1.		82%	74%
2.		<10%	42%
3.		21%	50%
4.		<5%	—
5.		<10%	44% ^d
6.		26%	50%

^a Reactions conducted with 1.0 equiv **89** and 1.5 equiv **90**. ^b Isolated yield after chromatography. ^c Enantiomeric excess determined by HPLC on a chiral stationary phase. ^d Opposite enantiomer obtained.

deficient groups provide modest reactivity, none offer an improvement in selectivity. Amino-indanol derived catalyst **97** as well as the very hindered pyroglutamic acid derived catalyst **96** both containing the pentafluorophenyl group show diminished selectivity. Having met with no

improvement in selectivity with known catalyst derivatives, we felt that a new catalyst scaffold must be developed.

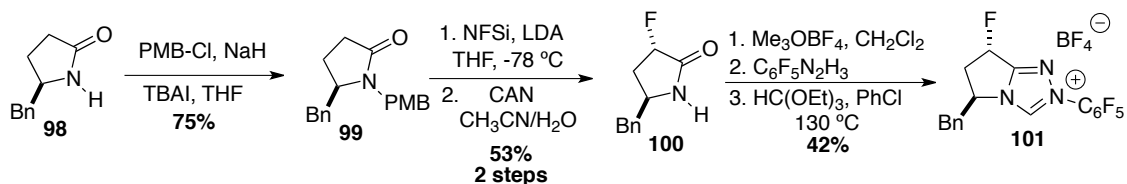
Catalyst **63** displays both high reactivity and moderate enantioselectivity, making this scaffold a candidate for further development. Since *cis*-fluorinated catalyst **73** provides increases in enantioselectivity relative to **63** in the intramolecular reaction of **35**, we sought to evaluate its efficacy in our newly developed *intermolecular* reaction. Using fluorinated catalyst **73** under identical conditions, we observe not only an increase in yield but also a dramatic increase in enantioselectivity (Scheme 1.19).



Scheme 1.19

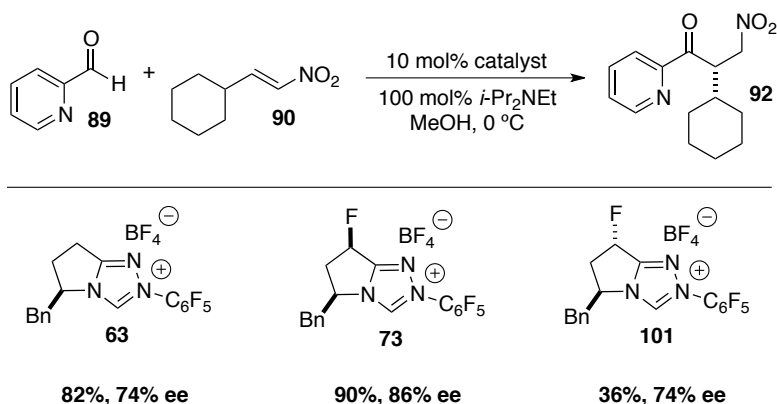
Given the beneficial impact that *cis*-fluorination of the catalyst scaffold has in both the *intra*- and *inter*-molecular variants we wanted to evaluate the opposite diastereomer to further probe this effect. Unfortunately, using electrophilic fluorination to install the fluorine stereocenter in the lactam precursor provides very small quantities of the *trans*-diastereomer. We were able to solve this problem by a simple switch of protecting groups. Lactam **98** was alkylated with 4-MeO-benzyl chloride to give **99** in good yield. The same electrophilic fluorination protocol performed on this substrate yields the *trans*-diastereomer as the major product in good yield after removal of

the PMB group with ceric ammonium nitrate. Azolium salt **101** was synthesized according to the general procedure (Scheme 1.20).



Scheme 1.20

Trans-fluorinated precatalyst **101** displays significantly lower reactivity than both the cis- and des-fluoro systems with no measurable increase in enantioselectivity. While the difference in reactivity was surprising, it became apparent that the impact of fluorine substitution was not merely an inductive effect and led us to the hypothesis that a stereoelectronic effect may be responsible (Scheme 1.21).

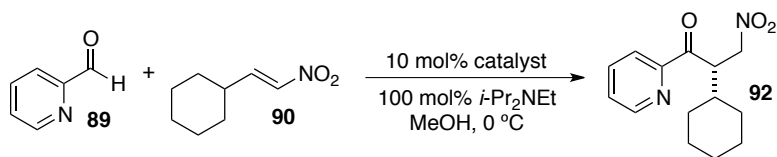


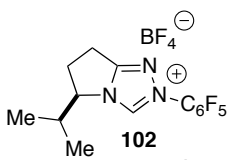
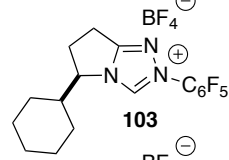
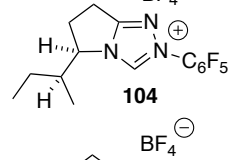
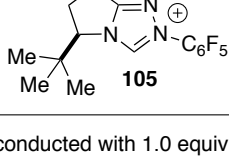
Scheme 1.21

Although catalyst **73** provides improved selectivities, there was still room for further optimization. We hypothesized that increasing the steric environment near the reactive center could give better enantioselection without a substantial loss in reactivity. Novel triazolium salt

102, derived from L-valine, was synthesized to test our hypothesis. Gratifyingly, under identical reaction conditions, triazolium salt **102** affords the desired product in 90% yield and 88% ee, a significant improvement from catalyst **63** (Table 1.5). Further manipulation of the stereodirecting group led to catalysts **103** and **104**, which display inferior results. Catalyst **105**, containing the bulky *t*-Bu substituent leads to almost complete loss of reactivity.

Table 1.5

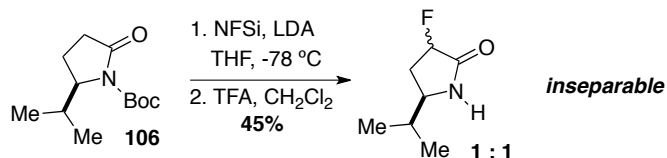


Entry	Catalyst	Yield (%) ^b	ee (%) ^c
1.		90%	88%
2.		90%	86%
3.		89%	86%
4.		<10%	90%

^a Reactions conducted with 1.0 equiv **89** and 1.5 equiv **90**. ^b Isolated yield after chromatography. ^c Enantiomeric excess determined by HPLC on a chiral stationary phase.

We hoped to translate the special reactivity observed upon *cis*-fluorination of the catalyst backbone to the more efficient valine derived scaffold. All attempts to synthesize the *cis* diastereomer of this scaffold proved difficult using electrophilic fluorination due to the presence of the bulkier directing group. Electrophilic fluorination of L-valine derived lactam **106** led to a

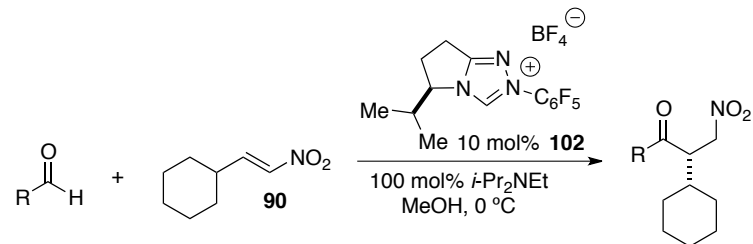
1:1 mixture of diastereomers, which proved inseparable by silica gel flash chromatography. This setback led us to examine the scope of this transformation with catalyst **102** (Scheme 1.22).



Scheme 1.22

Utilizing triazolium salt **102**, a variety of heterocyclic aldehydes were examined as potential partners for this transformation. Picolinaldehyde derivatives proceed smoothly with high enantioselectivity as do a variety of other heterocyclic aldehydes (Table 1.6). In general, 5-membered heterocyclic aldehydes provide lower enantioselectivity than 6-membered analogues.

Table 1.6



Entry	Aldehyde	Product	Yield (%) ^b	ee (%) ^c
1.		92	90%	88%
2.		107	99%	91%
3.		108	82%	90%
4.		109	73%	87%
5.		110	90%	70%
6.		111	71%	86%
7.		112	80%	82%
8.		113	84%	81%
9.		114	85%	79%

^a Reactions conducted with 1.0 equiv aldehyde and 1.5 equiv **90**. ^b Isolated yield after chromatography. ^c Enantiomeric excess determined by HPLC on a chiral stationary phase.

Absolute stereochemistry of the products were determined by X-ray analysis of **112** (Figure 1.7).

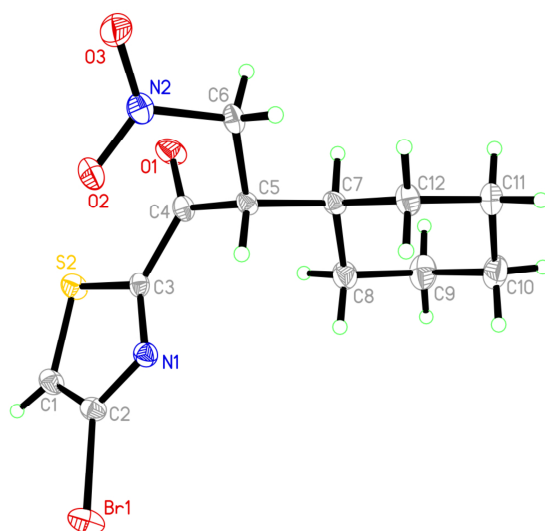
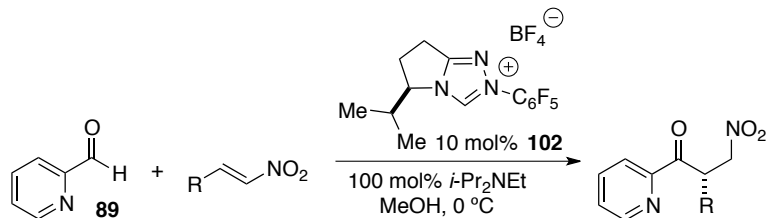


Figure 1.7

The scope of the nitroalkene was also examined by subjecting a variety of alkyl-substituted nitroalkenes to the optimized reaction conditions with picolinaldehyde **89** (Table 1.7). Secondary alkyl substituted nitroalkenes are well tolerated producing the desired β -nitro ketones in high yield and enantioselectivity. Primary alkyl substituted nitroalkenes also provide high yields of the desired product albeit with lower enantioselectivity. Cyclic disubstituted nitroalkenes such as 1-nitro-1-cyclohexene can also be used, which gives trans-substituted nitro-cyclohexane **122** as the major product in 74% yield, 5:1 dr and 89% ee. Acyclic disubstituted nitroalkenes do not participate. A 4 mmol scale experiment was performed, while reducing the catalyst loading to 5 mol% providing β -nitro ketone **62** in 99% yield (1.35 g) and 91% ee.

Table 1.7

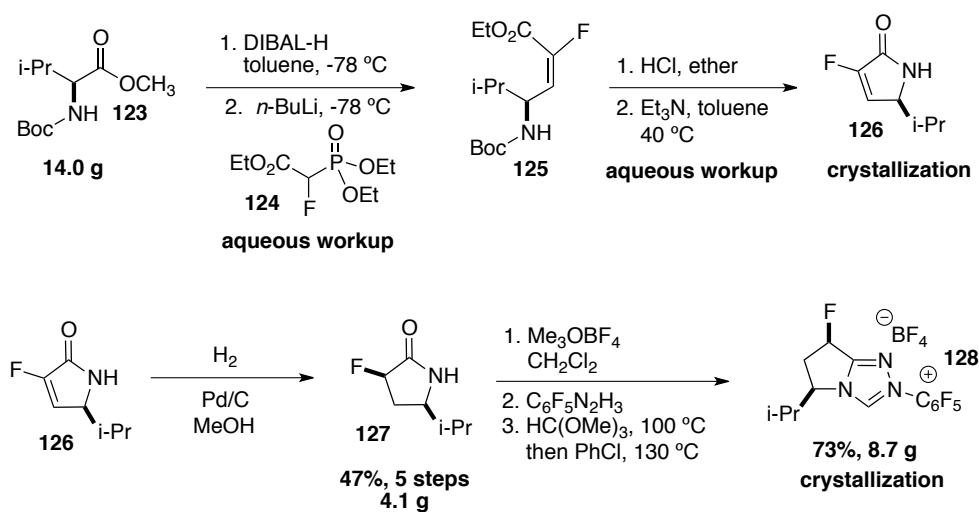


Entry	Nitroalkene	Product	Yield (%) ^b	ee (%) ^c
1.		92	90%	88%
2.		115	93%	88%
3.		116	65%	90%
4.		117	92%	89%
5.		118	84%	73%
6.		119	93%	74%
7.		120	76%	72%
8.		121	81%	71%
9.		122	74%	89% 5:1 dr

^a Reactions conducted with 1.0 equiv **89** and 1.5 equiv nitroalkene. ^b Isolated yield after chromatography. ^c Enantiomeric excess determined by HPLC on a chiral stationary phase.

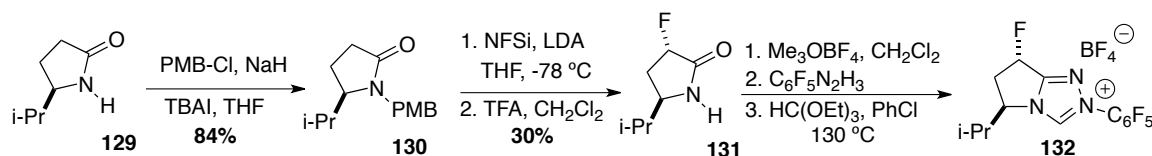
After investigating the scope of this transformation and realizing the limitations of selectivity with primary alkyl substituted nitroalkenes, our focus became the synthesis of a *cis*-fluorinated variant of pre-catalyst **102**. As shown previously (Scheme 1.22) direct fluorination of valine-derived lactam **106** provides an inseparable 1:1 mixture of diastereomers due to the large *trans*

directing effect observed for substituted lactams. We envisioned the *cis*-stereochemistry arising from a stereoselective hydrogenation of α,β -unsaturated lactams. This route was explored as a new way to access the desired enantioenriched lactam required for the synthesis of our triazolium pre-catalyst. Enantiopure Boc-valine methyl ester **123** is reduced with DIBAL-H to give the corresponding aldehyde, which is immediately treated with fluoro-phosphonate **124** yielding the desired *E*-olefin isomer **125**. Removal of the Boc group is accomplished by treatment with dry HCl in ether and upon addition of Et₃N the desired α,β -unsaturated lactam **126** is isolated via crystallization. Reduction of **126** with H₂-Pd/C in MeOH affords the desired *cis* substituted lactam **127** in 47% yield and >20:1 diastereoselectivity over the 5-step sequence. This procedure avoids all chromatographic purification and thus is amendable to large-scale preparation. Subjecting **127** to a modified version of our three-step one-pot procedure provides triazolium salt **128** (Scheme 1.23).



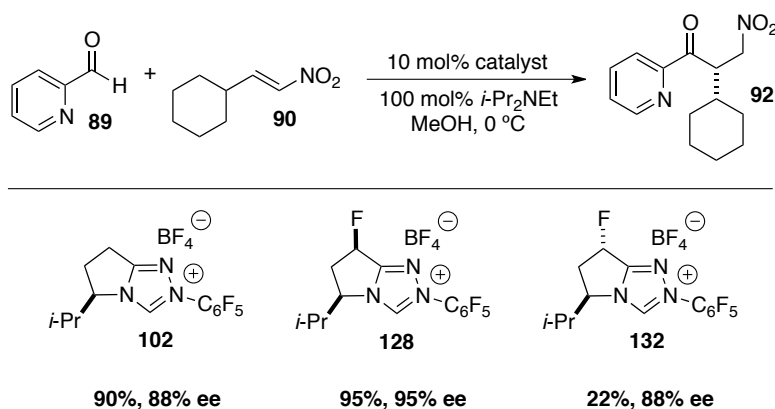
Scheme 1.23

We were also interested in evaluating the trans-diastereomer since using the protection group strategy demonstrated earlier provides a single diastereomer of trans-fluorinated lactam **131** (Scheme 1.24).



Scheme 1.24

This new route enabled the synthesis of the desired cis-fluorinated analogue of catalyst **102** which allowed its evaluation in the reaction to test our hypothesis. We were pleased to find that treatment of picolinaldehyde **89** and nitroalkene **90** with pre-catalyst **128** under identical conditions yields the desired Stetter product in 95% yield and 95% ee (Scheme 1.25). Precatalyst **132** provides no increase in selectivity with diminished yield as expected.

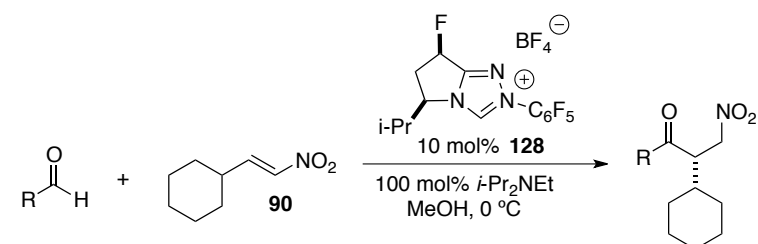


Scheme 1.25

After developing an efficient route to catalyst **128** and identifying its remarkable efficiency and selectivity, we began to reevaluate the scope of this transformation. 6-membered heterocyclic

aldehydes lead to exquisite selectivities. Smaller heterocycles such as furan, oxazole and isoxazole all participate with enantioselectivities in excess of 80% (Table 1.8).

Table 1.8

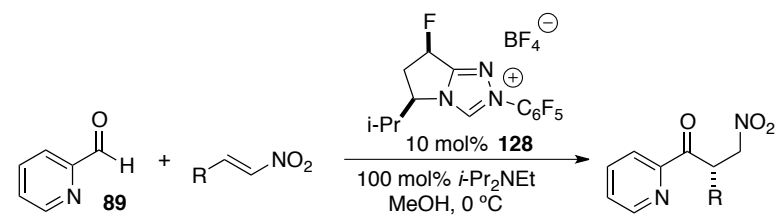


Entry	Aldehyde	Product	Yield (%) ^b	ee (%) ^c
1.		92	95%	95%
2.		107	95%	96%
3.		108	99%	96%
4.		109	88%	94%
5.		110	86%	84%
6.		111	70%	96%
7.		112	55%	95%
8.		113	75%	87%
9.		114	76%	86%

^a Reactions conducted with 1.0 equiv aldehyde and 1.5 equiv **90**. ^b Isolated yield after chromatography. ^c Enantiomeric excess determined by HPLC on a chiral stationary phase.

All secondary nitroalkenes now provide products with excellent enantioselectivity. Primary substitution leads to modest selectivities with des-fluoro catalyst **102**; however, with our improved catalyst, enantioselectivities in excess of 80% are routine (Table 1.9).

Table 1.9



Entry	Nitroalkene	Product	Yield (%) ^b	ee (%) ^c
1.		92	95%	95%
2.		115	85%	95%
3.		116	80%	96%
4.		117	98%	90%
5.		118	72%	87%
6.		119	99%	83%
7.		120	82%	83%
8.		121	72%	78%
9.		122	62%	96% 1:1 dr

^a Reactions conducted with 1.0 equiv **89** and 1.5 equiv nitroalkene. ^b Isolated yield after chromatography. ^c Enantiomeric excess determined by HPLC on a chiral stationary phase.

1.3 Investigation Into the Effect of Catalyst Fluorination

The remarkable effect that fluorination of our triazolium salt precatalysts has on reactivity and selectivity in the intermolecular Stetter reaction is notable; however, the origin of this effect was not well understood. In order to better understand these differences, we analyzed the triazolium salts by X-ray crystallography. Precatalyst **102** displays what is referred to as a C γ -endo ring pucker, placing the isopropyl group in a lower energy pseudoequatorial position thereby minimizing 1,3-diaxial interactions. X-ray analysis of precatalyst **128** shows a complete switch in conformational preference to the C γ -exo ring pucker in the solid state (Figure 1.7).

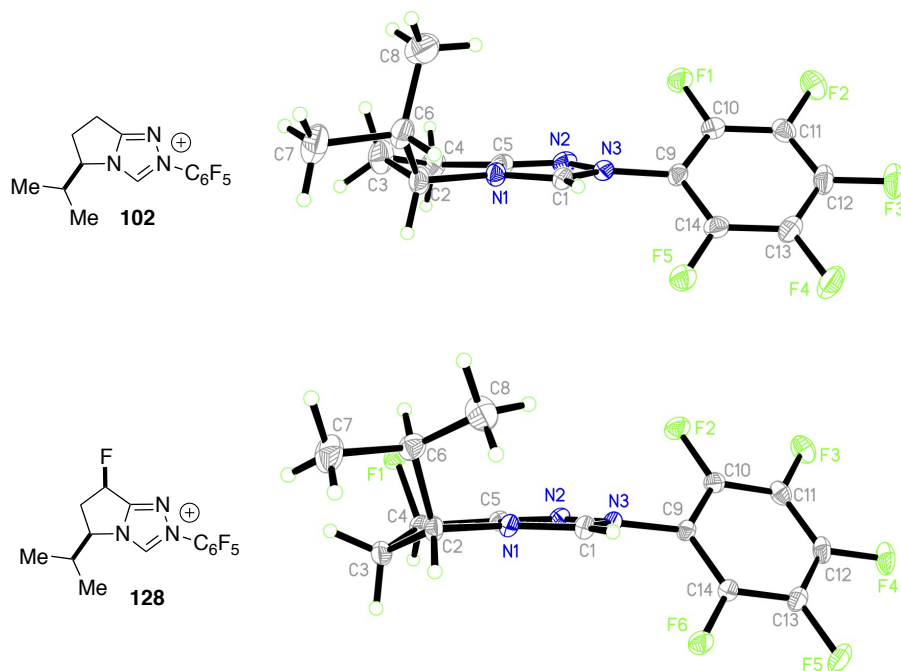


Figure 1.7

This conformation places both the bulky isopropyl group and fluorine in pseudoaxial positions, which would appear to be unfavorable in the ground state. We suggest that this contradiction arises from a stereoelectronic effect that overrides the inherent steric bias for the C γ -endo

conformation. Raines and coworkers have demonstrated that the *exo-endo* conformations of 3-fluoroprolines are stabilized by up to 3 kcal/mol due to a *gauche* effect.³⁶ The *gauche* effect is exemplified by the conformational preference of 1,2-difluoroethane. In 1,2-difluoroethane the *gauche* conformer is 2.4-3.4 kJ/mol more stable than the *anti* conformer.³⁷ This preference is proposed to arise from the hyperconjugative effect of donation of a σ_{C-H} bonding orbital into the low-lying σ^*_{C-F} antibonding orbital which is not available in the *anti* conformation (Figure 1.8).³⁸

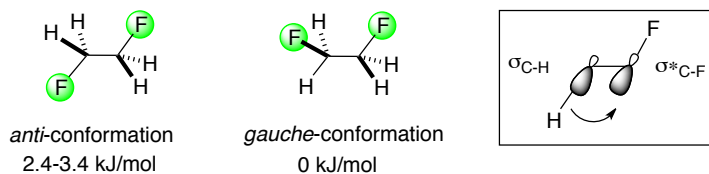


Figure 1.8

In our fluorinated triazolium salts there are two possible hyperconjugative interactions, the first being the σ_{C-H} to σ^*_{C-F} interaction present in fluoro-prolines as demonstrated by Raines. There is also the possibility of a σ_{C-H} to σ^*_{C-N} interaction between the pseudoequatorial C-H bond at C₄ and the σ^*_{C-N} antibonding orbital in the triazolium ring (Figure 1.9).

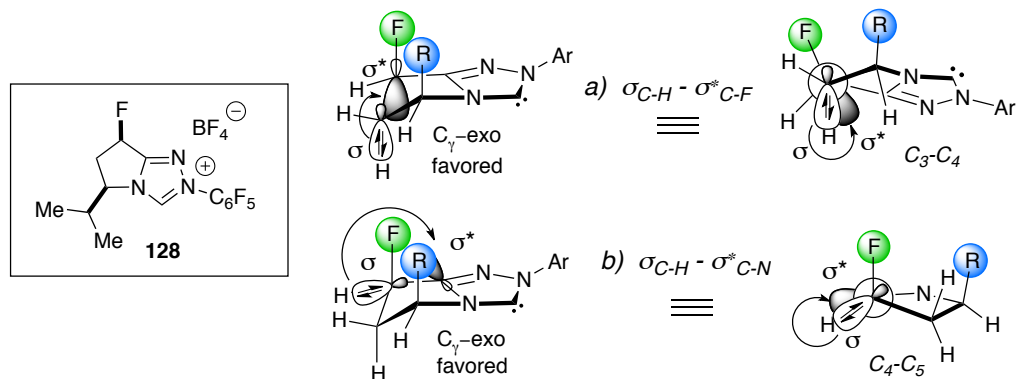


Figure 1.9

To gain further evidence for the gauche effect in the ground state of cis-fluorinated triazolium salt **128** we looked to analyze trans-fluorinated precatalyst **132**. If a gauche effect is responsible for the change in conformational preference then trans-fluorination of the catalyst architecture should not induce the said conformational change. Crystallization and X-ray analysis of precatalyst **132** confirms this hypothesis (Figure 1.10). The C γ -endo conformation is favored in the ground state of **132** and provides further support for the presence of a gauche effect in precatalyst **128**.

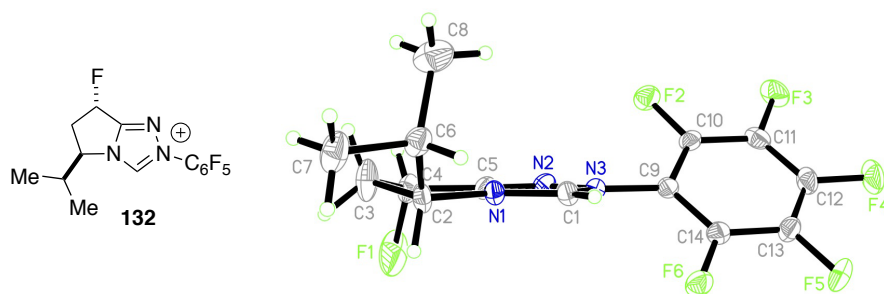
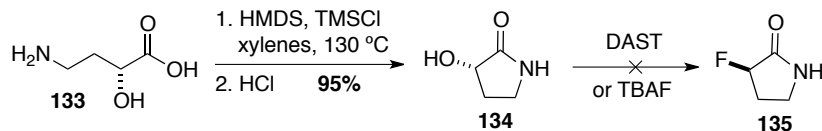


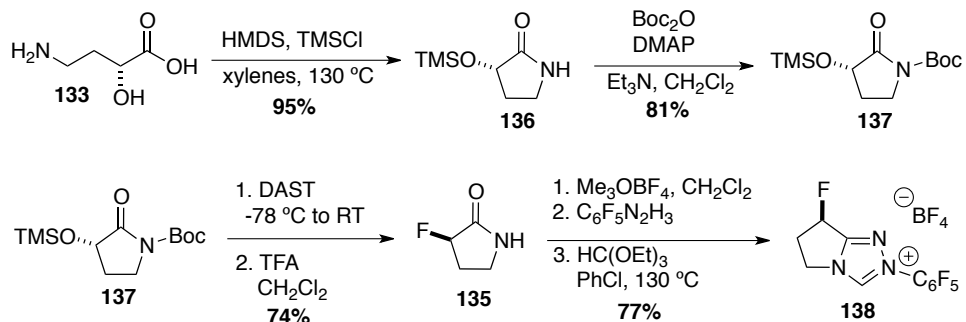
Figure 1.10

This may explain why fluorinated precatalyst **132** does not display an enhancement of selectivity. To probe the effect of fluorination alone, we sought to synthesize a catalyst that is chiral only at the fluorinated stereocenter, and does not contain a bulky directing group. We imagined that the requisite fluorinated lactam **135** could be accessed by treatment of α -hydroxy lactam **134** with a nucleophilic fluorination reagent. The synthesis of enantioenriched lactam **134** was preceded in a single step from commercially available L-(-)- α -hydroxy- γ -aminobutyric acid. Unfortunately, treatment of the hydroxy-lactam with nucleophilic fluorination reagents such as DAST (diethylaminosulfur trifluoride) or TBAF (tetrabutylammonium fluoride) results in decomposition of the starting material with no observed fluorination product (Scheme 1.26).



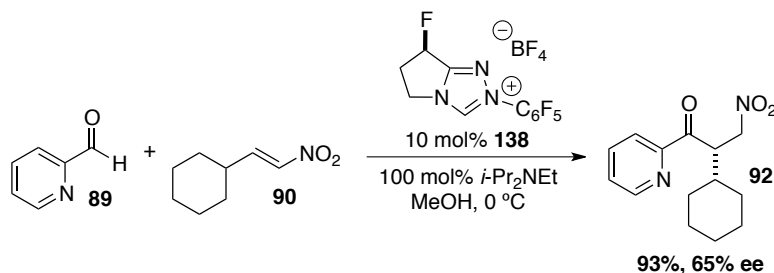
Scheme 1.26

Although fluorination of compounds with nitrogenous bases is preceded in the literature, we reasoned that the presence of a nitrogen base could pose a problem due to its potential nucleophilicity toward the reagent. Cyclization of **133** followed by treatment with aqueous HCl results in the formation of desilylated lactam **134**. Alternatively, the TMS protected hydroxy-lactam **136** can be isolated if the reaction is not exposed to acid.³⁹ Protection of the lactam is accomplished by treatment with Boc-anhydride to afford Boc-lactam **137** in good yield (Scheme 1.27). We envisioned that desilylation of the TMS group could be accomplished *in situ* by exposure to DAST, eliminating the need for re-isolation of this compound. To our delight, treatment of **137** with DAST leads to the clean formation of the fluoro-lactam and after deprotection of the Boc-group with trifluoroacetic acid catalyst, precursor **135** is isolated in high yield. Elaboration to the triazolium salt can be accomplished using our general procedure to provide precatalyst **138** (Scheme 1.27).



Scheme 1.27

With the proposed catalyst in-hand, we were able to delineate the effect of fluorination from sterics on selectivity. Under identical conditions, precatalyst **138** provides the ketone product in a surprising 65% ee (Scheme 1.28).



Scheme 1.28

Given that fluorine is used as an isostere to hydrogen due to its small size, it is unlikely that fluorine is influencing selectivity based on sterics.⁴⁰ Fluorine has an atomic radius of 1.47 Å, only 20% larger than hydrogen (1.20 Å), and less than 75% of the size of a methyl group (2.00 Å).⁴¹ Furthermore, the fluorine atom is 5 bonds away from the reacting center. It seems more likely that fluorine is responsible for asymmetric induction based on stereoelectronic effects alone and that the chiral conformation arising from these effects might lead to enantiofacial discrimination. X-ray analysis of precatalyst **138** confirms the presence of the C γ -exo ring pucker in this system (Figure 1.11).

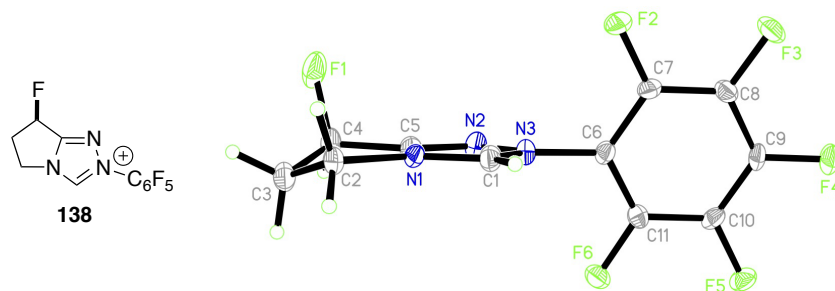


Figure 1.11

While the ground state analysis of the triazolium salt precatalysts is self-consistent, there is still no definitive proof that the conformation in these catalysts is responsible for the increase in selectivity. An alternate hypothesis involves an electrostatic interaction between the C-F dipole in the generated Breslow-intermediate and the developing nitronate in the transition state. This interaction could both activate and orient the incoming electrophile, resulting in higher selectivity. A DFT study was undertaken in collaboration with the Houk group to investigate the plausibility of each of these effects.⁴² Calculations were first performed on the triazolium salts to compare the observed ground state conformations to the theoretical predictions. As shown in the X-ray structure of **128** the lowest ground state conformation is predicted to be exo by 1.5 kcal/mol (Figure 1.12). Both trans-fluorinated precatalyst **132** as well as des-fluoro precatalyst **102**, which display a preference for the endo conformations in the X-ray structures, are also calculated to have lower energy endo conformers.

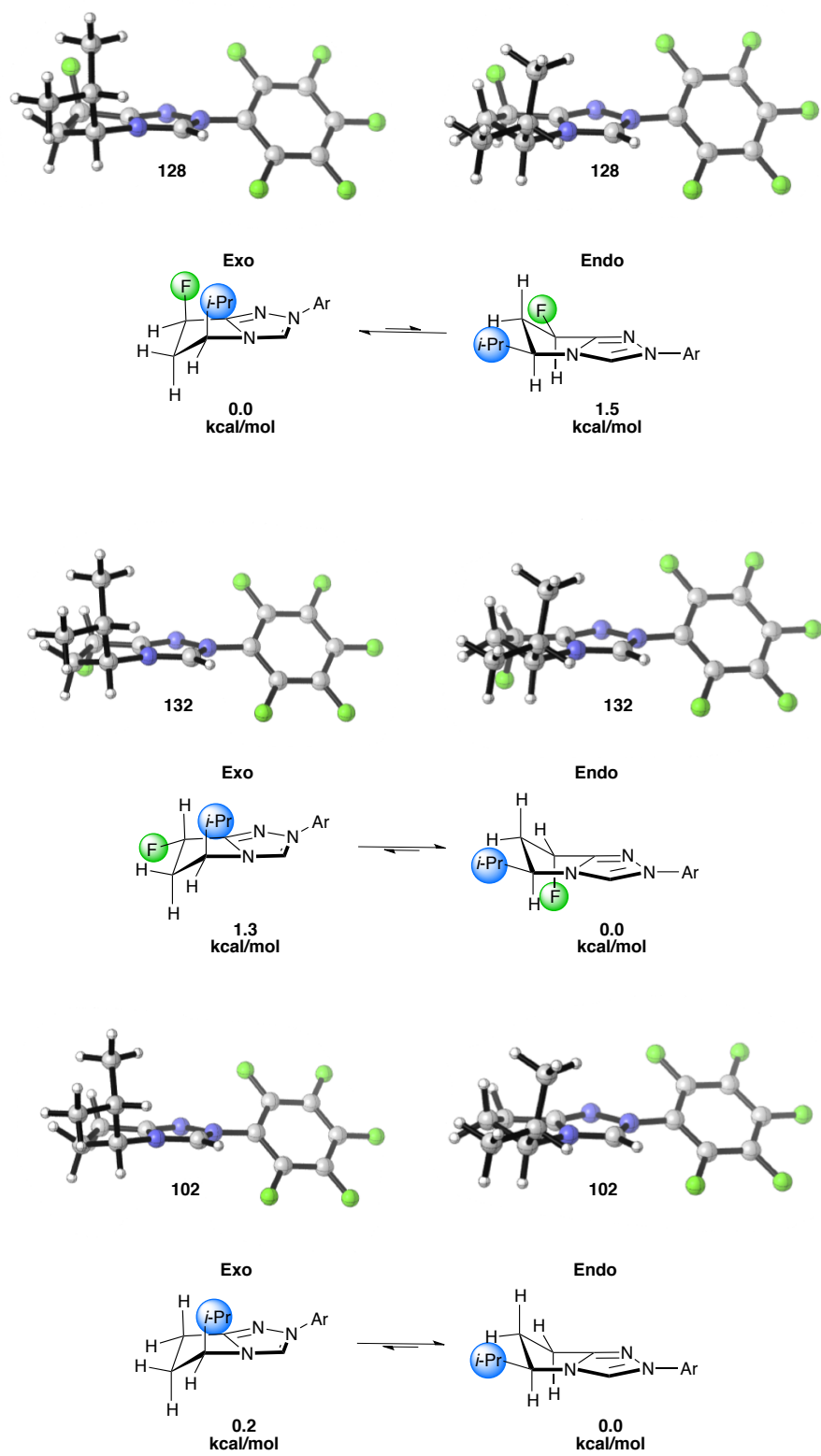


Figure 1.12

While calculations support the hypothesis that stereoelectronic effects favor the *exo*-conformers in the ground state of the triazolium salt precatalysts, the generated Breslow-intermediates do not share the same trends. All calculations of the *exo*-*endo* conformations of these intermediates converge to the *exo*, suggesting that the *endo* conformation is too high in energy to be accessible (Figure 1.13). This may be explained by a build up of $A_{1,3}$ strain between the isopropyl group and the enol as the conformation approaches *endo*, implying that the ground state argument may not be applicable to the transition state.

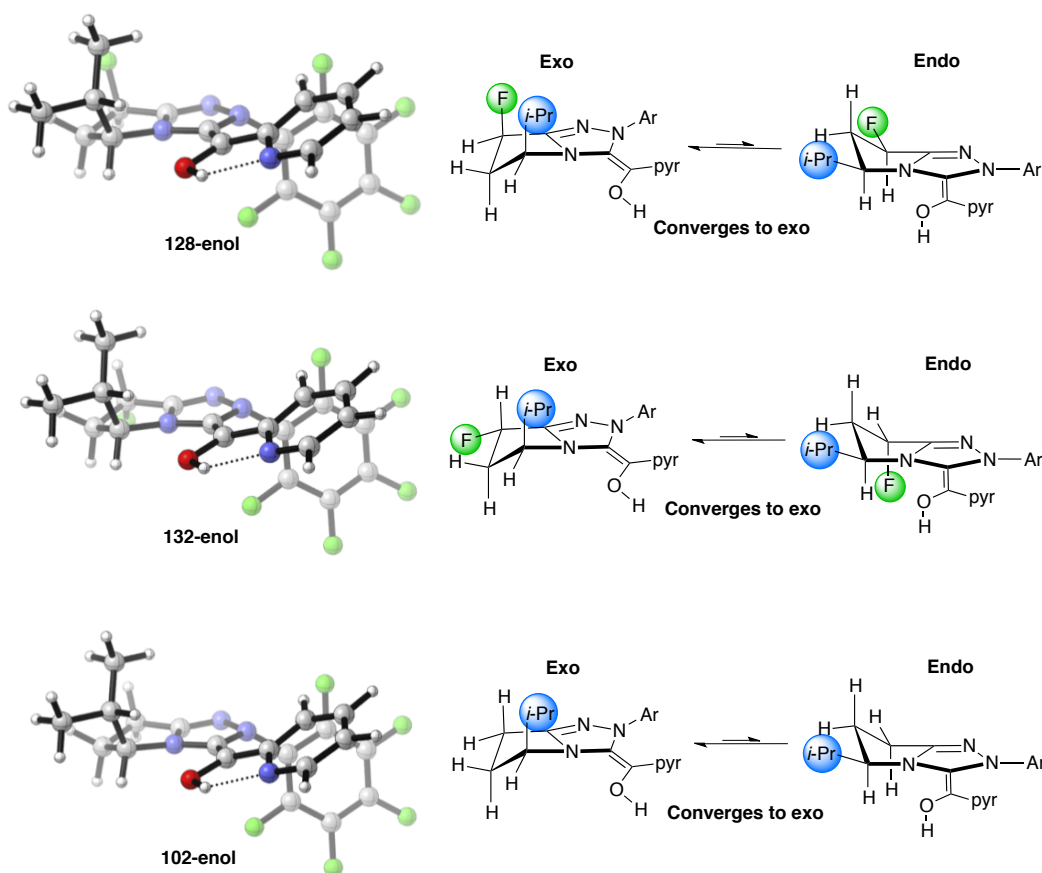


Figure 1.13

In the calculated transition states of precatalyst **128** in the gas phase, the improved selectivity is proposed to arise from a favorable electrostatic interaction between the nitro group and the C-F dipole (Figure 1.14). These calculations also predict the protonation event of the nitronate to be concerted with C-C bond formation, a hypothesis that our group suggested in earlier work.⁴³ The calculated value for enantioselectivity using this transition state in the gas phase was determined to be 98% ee, where the experimental value is 95% ee.

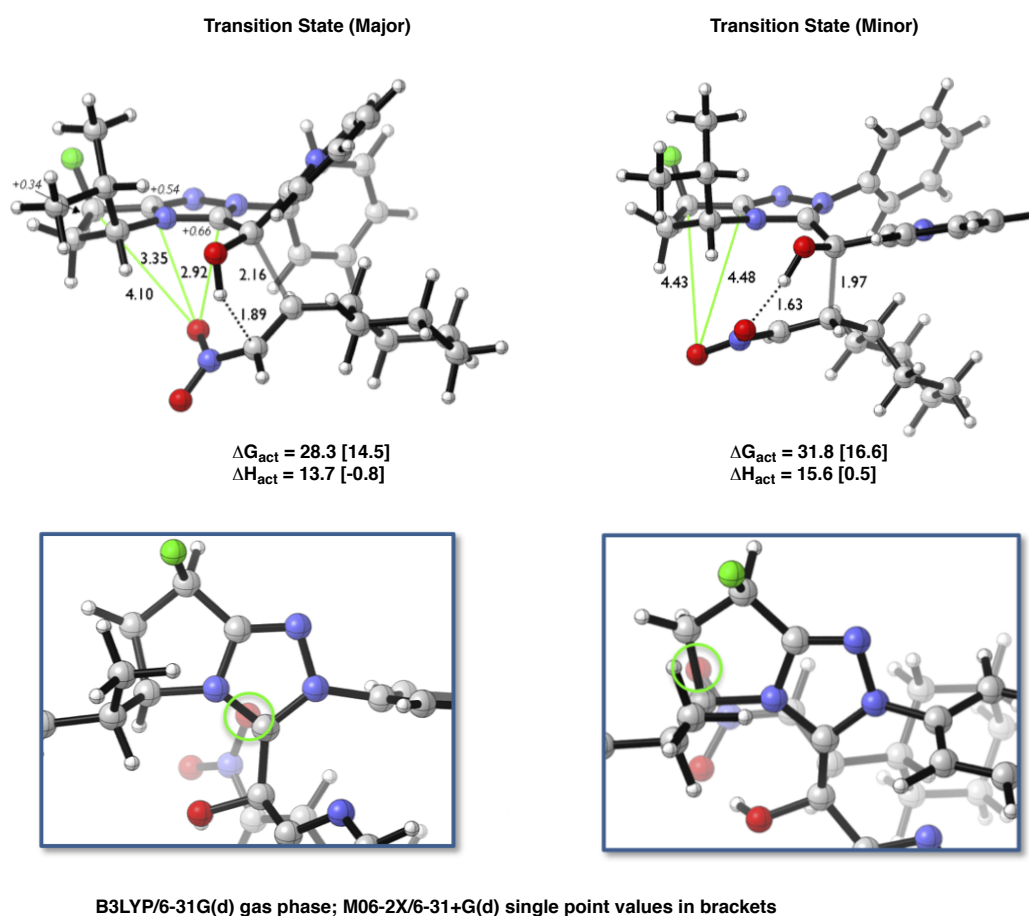


Figure 1.14

A variety of basis sets both in the gas phase as well as in MeOH were used to determine the best model for predicting selectivity. The results are summarized in Table 1.10. Although none of

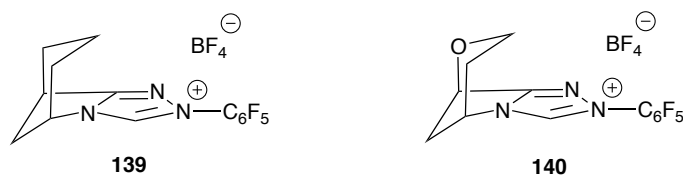
these methods correctly predict the experimental trends in selectivity they do provide evidence for the source of improved selectivity with cis-fluorinated precatalyst **128**.

Table 1.10

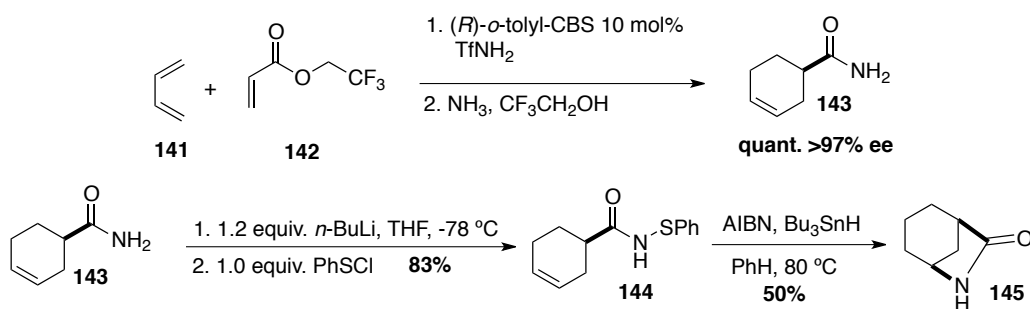
Catalyst	Experimental		B3LYP/6-31G(d) gas phase		M06-2X/6-31+G(d) gas phase		B3LYP/6-31+G(d) MeOH	
	er	$\Delta\Delta G_{\text{act}}$	er	$\Delta\Delta G_{\text{act}}$	er	$\Delta\Delta G_{\text{act}}$	er	$\Delta\Delta G_{\text{act}}$
128	97.5:2.5	2.2	99:1	2.9	98:2	2.3	93:7	1.6
132	94:6	1.6	98:2	2.2	86:14	1.1	86:14	1.1
102	94:6	1.6	97:3	2.1	91:9	1.3	93:7	1.6

While this study has provided good evidence that the source of increased selectivity with the fluorinated catalyst is an electrostatic interaction we were interested in designing an experimental method to distinguish between these two hypotheses. It seemed reasonable that a series of bicyclic catalyst could be synthesized that would allow for a direct comparison. We envisioned two unique bicyclic catalysts, **139** and **140**, both containing 3.2.1. bicyclic pyrrolidine units (Figure 1.15). Precatalyst **140** would be electronically different than **139**, containing oxygen at the same position as fluorine in **138**, but both should have similar transition-state conformations due to the bicyclic system. Evaluating them independently in the Stetter reaction should allow for direct experimental differentiation between the two hypotheses.

Figure 1.15

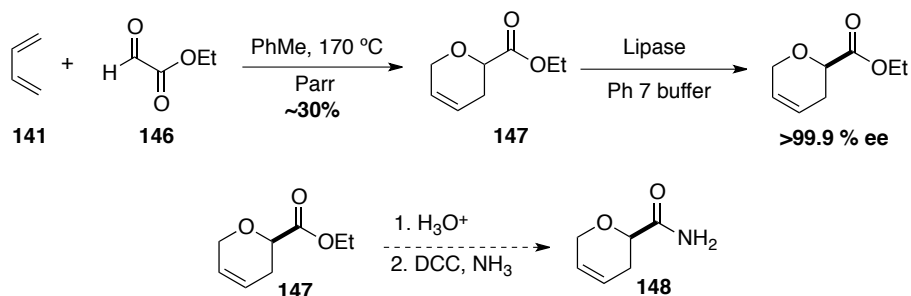


Both catalysts must be prepared as a single enantiomer for proper evaluation, so asymmetric syntheses of their precursors was mandatory. For the synthesis of **139** we envisioned an enantioselective Diels-Alder reaction of 1,3-butadiene **141** and trifluoroethyl acrylate **142** as the key C-C bond-forming step, based on literature precedent.⁴⁴ Amidation with liquid ammonia provides enantioenriched amide **143** in quantitative yield and 97% ee (Scheme 1.29). Conversion to the N-phenyl thioamide followed by treatment with Bu₃SnH initiates an intramolecular aminyl radical cyclization, forming the desired 3.2.1 bicyclic lactam **145** in good yield.⁴⁵



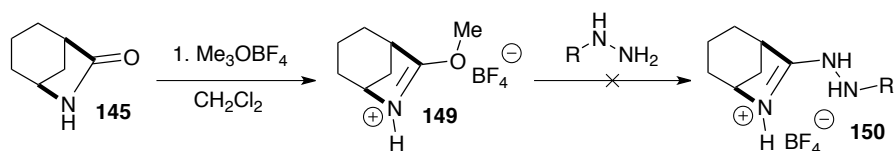
Scheme 1.29

The synthesis of **140** posed a larger challenge due to the presence of the pyran ring. No asymmetric syntheses of chiral pyrans containing an α -carboxylate are known; however, an enzyme catalyzed resolution of dihydropyran esters was precedented.⁴⁶ Thermal Diels-Alder cycloaddition between 1,3-butadiene and ethyl glyoxylate provides ester **147** upon distillation of the crude mixture. The ester can then be resolved using a lipase to afford the enantioenriched ester in >99.9 % ee (Scheme 1.30).⁴⁷ Hydrolysis of the ester followed by amidation should yield amide **148**.



Scheme 1.30

With a solidified asymmetric route to the starting materials, we attempted to elaborate lactam **145** to the triazolium salt. Unfortunately, all efforts to add hydrazines to the activated amide led to decomposition of the starting material, presumably through ring-opening of the strained bicyclic system (Scheme 1.31).



Scheme 1.31

For this reason, we were forced to abandon the preparation of oxygen containing precatalyst **140**.

1.4 Conclusion

In conclusion, we have identified an asymmetric intermolecular Stetter reaction of hetaryl aldehydes and nitroalkenes that proceeds in high efficiency with excellent enantioselectivity.⁴⁸ Previously reported catalysts lead to good yield, but only modest selectivity. The development of a fluorinated triazolylidene carbene scaffold has enabled a highly enantioselective reaction. Two

hypotheses are proposed to rationalize the improved selectivities. Solid-state crystallographic analysis of the fluorinated precatalysts reveals a conformational change due to a gauche effect induced by fluorine. The change in catalyst conformation may be responsible for improved enantiofacial discrimination. Based on DFT calculations, the ground state conformation of the precatalyst may not accurately reflect the transition state conformations due to the presence of $A_{1,3}$ strain in the Breslow intermediate. Furthermore, these calculations provide a new model for selectivity that implicates a positive electrostatic interaction of the C-F dipole and the developing nitronate in the transition state.⁴⁹ An experimental model was proposed to delineate the hypotheses in question; however, challenges associated with the synthesis of the required catalysts prohibited us from reaching a final conclusion.

REFERENCES

- ¹ Bourissou, D.; Guerret, O.; Gabbai, F. P.; Bertrand, G. *Chem. Rev.* **2000**, *100*, 39-91.
- ² H.-W. Wanzlick and E. Schikora. *Angew. Chem.* **1960**, *72*, 494.
- ³ Breslow, R. *Chem. & Ind.* **1957**, 893-894.
- ⁴ Igau, A.; Grutzmacher, H.; Baceiredo, A.; Bertrand, G. *J. Am. Chem. Soc.* **1988**, *110*, 6463–6466.
- ⁵ (a) Enders, D.; Breuer, K.; Raabe, G.; Runsink, J.; Teles, J. H.; Melder, J. P.; Ebel, K.; Brode, S. *Angew. Chem. Int. Ed.* **1995**, *34*, 1021-1023. (b) Enders, D.; Niemeier, O.; Henseler, A. *Chem. Rev.* **2007**, *107*, 5606-5655.
- ⁶ Wohler, F.; Liebig, J.; *Annalen der Pharmacie* **1832**, 249-282.
- ⁷ Lapworth, A. *J. Chem. Soc.* **1903**, *83*, 995-1005.
- ⁸ Ukai, T.; Tanaka, R.; Dokawa, T. *J. Pharm. Soc. Jpn.* **1943**, *63*, 296-300.
- ⁹ Breslow, R. *J. Chem. Soc.* **1958**, *80*, 995-1005.
- ¹⁰ Sheehan, J. C.; Hunneman, D. H. *J. Am. Chem. Soc.* **1966**, *88*, 3666-3667.
- ¹¹ (a) Sheehan J. C.; Hara, T. *J. Org. Chem.* **1974**, *39*, 1196-1199. (b) Tagaki, W.; Tamura, Y.; Yano, Y. *Bull. Chem. Soc. Jpn.* **1980**, *53*, 874-880. (c) Castells, J.; Lopez-Calahorra, F. *Tetrahedron Lett.* **1993**, *34*, 521-524. (d) Yamashita, K.; Sasaki, S.; Osaki, T.; Nango, M.; Tsuda, K. *Tetrahedron Lett.* **1995**, *36*, 4817-4820.
- ¹² Enders, D.; Breuer, K.; Teles, J. H. *Helv. Chim Acta* **1996**, *79*, 1217-1221.
- ¹³ Knight, R. L.; Leeper, F. J. *J. Chem. Soc., Perkin Trans. 1*, **1998**, 1891-1893.
- ¹⁴ Enders, D.; Kallfass, U. *Angew. Chem. Int. Ed.* **2002**, *41*, 1743-1745.
- ¹⁵ (a) Stetter, H.; Schreckenber, M. *Angew. Chem. Int. Ed. Engl.* **1973**, *12*, 81. (b) Stetter, H.; Kuhlmann, H. *Chem. Ber.* **1976**, *109*, 2890-2896.

- ¹⁶ Stetter, H.; Kuhlmann, H. *Organic Reactions*, Vol. 40; Paquette, L. A.; Ed.; Wiley: New York, **1991**, 407-496.
- ¹⁷ Hawkes, K. J.; Yates, B. F. *Eur. J. Org. Chem.* **2008**, *33*, 5563-5570.
- ¹⁸ Ciganek, E. *Synthesis*, **1995**, 1311-1314.
- ¹⁹ Enders, D.; Breuer, K.; Runsink, J.; Teles, J. H. *Helv. Chim Acta* **1996**, *79*, 1899-1902.
- ²⁰ Mennen, S. M.; Blank, J. T.; Tran-Dube, M. B.; Imbriglio, J. E.; Miller, S. J. *Chem. Commun.* **2005**, 195-197.
- ²¹ Rovis, T. *Chem. Lett.* **2008**, *37*, 2-7.
- ²² (a) Kerr, M.; Read de Alaniz, J.; Rovis, T. *J. Am. Chem. Soc.* **2002**, *124*, 10298-10299. (b) Kerr, M. S.; Rovis, T. *J. Am. Chem. Soc.* **2004**, *126*, 8876-8877. (c) Read de Alaniz, J.; Rovis, T. *J. Am. Chem. Soc.* **2005**, *127*, 6284-6289. (d) Liu, Q.; Rovis, T. *J. Am. Chem. Soc.* **2006**, *128*, 2552-2553. (e) Liu, Q.; Rovis, T. *Org. Process Res. Dev.* **2007**, *11*, 598-604. (f) Kerr, M.; Read de Alaniz, J.; Moore, J.; Rovis, T. *J. Org. Chem.* **2008**, *73*, 2033-2040.
- ²³ Moore, J. L.; Silvestri, A. P.; Read de Alaniz, J.; DiRocco, D. A.; Rovis, T. *Org. Lett.* **2011**, *13*, 1742-1745. and Singleton, D. A.; Rovis, T. *Unpublished Results*
- ²⁴ Enders, D.; Breuer, K. *Comprehensive Asymmetric Catalysis III*, Jacobsen, E. N.; Pfaltz, A.; Yamamoto, H.; Ed.; Springer: Heidelberg, **1999**, 1093.
- ²⁵ Enders, D. *Chem. Commun.* **2008**, 3989-3991.
- ²⁶ Liu, Q.; Perreault, S.; Rovis, T. *J. Am. Chem. Soc.* **2008**, *130*, 14066-14067.
- ²⁷ Javier Read de Alaniz Ph.D. Thesis Colorado State University **2006**.
- ²⁸ Hawkes, K. J.; Yates, B. F. *Eur. J. Org. Chem.* **2008**, *33*, 5563-5570.
- ²⁹ Konas, D. W.; Coward J. K. *J. Org. Chem.* **2001**, *66*, 8831-8842.

- ³⁰ Smrcina, M.; Majer, P.; Majerova, E.; Guerassina, T.; Eissenstat, M. A. *Tetrahedron*, **1997**, *53*, 12867-12874.
- ³¹ Kerr, M.; Read de Alaniz, J.; Rovis, T. *J. Org. Chem.* **2005**, *70*, 5725-5728.
- ³² For the synthesis of the lactone see: Cohen, H.; Banner, B. L.; Laurenzano, A. J.; Carozza, L. *Org. Synth.* **1985**, *63*, 127. For the synthesis of the lactam see: Hanessian, S. *J. Org. Chem.* **1969**, *34*, 675-681.
- ³³ (a) For a review, see: Berner, O. M.; Tedeschi, L.; Enders, D. *Eur. J. Org. Chem.* **2002**, 1877-1894. (b) Barrett, A. G. M.; Graboski, G. G. *Chem. Rev.* **1986**, *86*, 751-762. (c) Scheidt has reported the asymmetric conjugate addition of a stoichiometrically generated acyl anion equivalent to nitroalkenes mediated by a thiourea; see: Mattson, A. E.; Zuhl, A. M.; Reynolds, T. E.; Scheidt, K. A. *J. Am. Chem. Soc.* **2006**, *128*, 4932-4933.
- ³⁴ N. Ono, *The Nitro Group in Organic Synthesis*, Wiley-VCH, New York, **2001**.
- ³⁵ Javier Read de Alaniz, Ph.D. Thesis, Colorado State University **2006**.
- ³⁶ Hodges, J. A.; Raines, R. T. *J. Am. Chem. Soc.* **2005**, *127*, 15923-15932.
- ³⁷ Craig, N. C.; Chen, A.; Suh, K. H.; Klee, S.; Mellau, G. C.; Winnewisser, B. P.; Winnewisser, M. *J. Am. Chem. Soc.* **1997**, *119*, 4789-4790.
- ³⁸ Deslongchamps, P. *Stereoelectronic Effects in Organic Chemistry*; Pergamon Press: New York, 1983.
- ³⁹ Sarairi, D.; Maurey, G.; *Bull. Soc. Chim. Fr.* **1987**, 297-301.
- ⁴⁰ Böhm, H. J.; Banner, D.; Bendels, S.; Kansy, M.; Kuhn, B.; Müller, K.; Obst-Sander, U.; Stahl, M. *ChemBioChem* **2004**, *5*, 637-643.
- ⁴¹ Bondi, A. *J. Phys. Chem.* **1964**, *68*, 441-451.

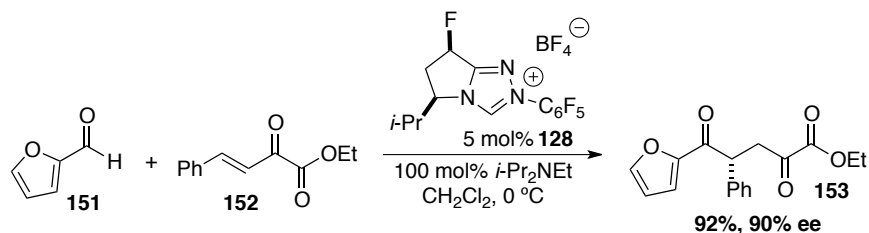
- ⁴² Um, J. M.; DiRocco, D. A.; Noey, E. L.; Rovis, T.; Houk, K. N. *J. Am. Chem. Soc.* **2011**, *133*, 11249-11254.
- ⁴³ (a) Read de Alaniz, J.; Rovis, T. *J. Am. Chem. Soc.* **2005**, *127*, 6284-6289. (b) DiRocco, D. A.; Rovis, T. *Angew. Chem. Int. Ed.* **2011**, *50*, 7982-7983.
- ⁴⁴ Yeung, Y-Y.; Hong, S.; Corey, E. J. *J. Am. Chem. Soc.* **2006**, *128*, 6310-6311.
- ⁴⁵ Gaudreault, P.; Drouin, C.; Lessard, J. *Can. J. Chem.* **2005**, *83*, 543-545.
- ⁴⁶ Caille, J.-C.; Govindan, C. K.; Junga, H.; Lalonde, J.; Yao, Y. *Org. Proc. Res. Dev.* **2002**, *6*, 471-476.
- ⁴⁷ We thank Greg Hughes and Matthew Truppo at Merck for performing these experiments.
- ⁴⁸ DiRocco, D. A.; Oberg, K. M.; Dalton, D. M.; Rovis, T. *J. Am. Chem. Soc.* **2009**, *131*, 10872-10874.
- ⁴⁹ Um, J. M.; DiRocco, D. A.; Noey, E. L.; Rovis, T.; Houk, K. N. *J. Am. Chem. Soc.* **2011**, *133*, 11249-11254.

Chapter 2

Expanding the Scope of the Asymmetric Intermolecular Stetter Reaction of Nitroalkenes

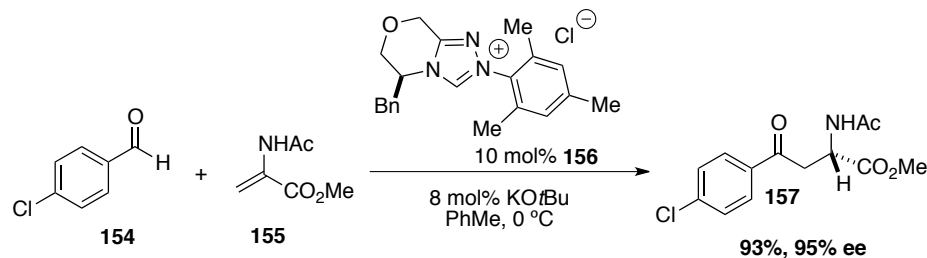
2.1 Introduction

With the advent of a highly efficient and selective catalyst for the asymmetric intermolecular Stetter reaction of heteraryl aldehydes and nitroalkenes, the Stetter reaction has found its niche as a mild and efficient method for asymmetric intermolecular C-C bond formation. Prior to the development of this new class of fluorinated triazolium salt precatalysts, only a few specific examples of asymmetric intermolecular reactions were known.¹ Since this work a few groups have reported advances in this area. The Gravel group has recently reported the use of our fluorinated triazolium salt as a competent precatalyst for the intermolecular Stetter reaction of heteraryl aldehydes and β,γ -unsaturated- α -ketoesters (Scheme 2.1).²



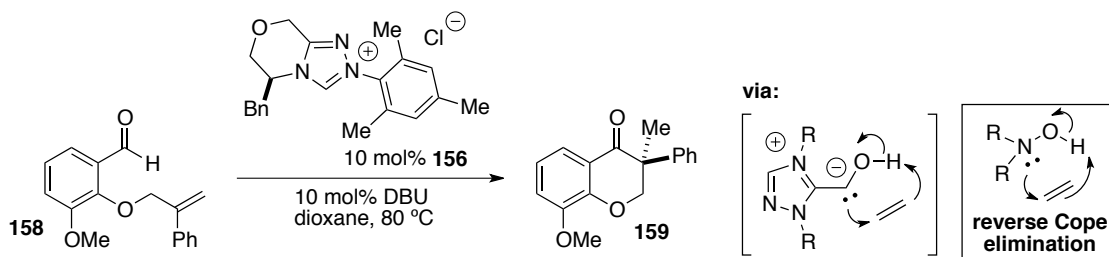
Scheme 2.1

Glorius and coworkers have developed an intermolecular Stetter reaction of β -unsubstituted dehydroaminoesters catalyzed by triazolium salt **156** that provides α -amino acid derivatives in high enantioselectivity after a diastereoselective protonation event (Scheme 2.2).³



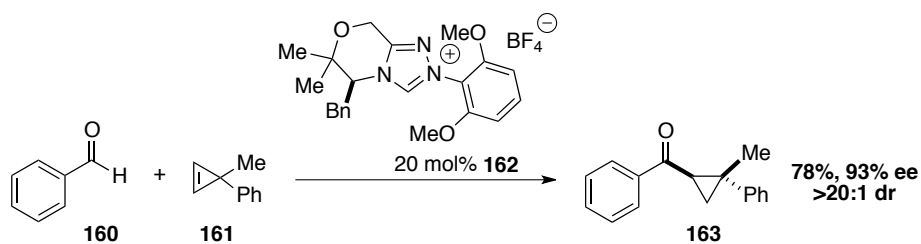
Scheme 2.2

Most interestingly, the same group has introduced a new system capable of hydroacylating unactivated olefins both *intra*- and *inter*-molecularly. Chromanone systems can undergo intramolecular hydroacylation in the presence of the same triazolium salt (**156**), in excellent enantioselectivity (Scheme 2.3).⁴ Due to the observed reactivity in the absence of a Michael acceptor, it is proposed that the Breslow intermediate reacts through a concerted transition state reminiscent of the reverse Cope elimination (Scheme 2.3).⁵



Scheme 2.3

This concept has also been applied to the intermolecular hydroacylation of cyclopropenes.⁶ Development of novel catalyst **162** containing the 2,6-dimethoxyphenyl group provides high enantioselectivity in the resulting acylcyclopropane product **163** (Scheme 2.4).



Scheme 2.4

Among the reports using chiral small molecule NHC catalysts, Müller and coworkers have also shown that enzymes can catalyze a highly enantioselective intermolecular Stetter reaction, albeit in low yields.⁷

2.2 Results

2.2.1 The Role of the α -Heteroatom

In our continuing efforts to expand the scope of this transformation, we questioned the unique reactivity of hetaryl aldehydes in our system. We have shown that, to date, only hetaryl aldehydes that contain heteroatoms at the 2-position react efficiently and with high selectivity. Given that the scope is rather invariant across a range of heterocycles with differing basicities, we speculated that the size of the aldehyde might be important. The smaller size of a nitrogen lone pair than a C-H bond is somewhat reflected in their A-values (methyl group 1.74, amino group 1.40).⁸ A more instructive comparison relates to the torsional barriers of substituted biaryl systems. Schlosser and coworkers have recently shown the rotational barrier in 2-(o-tolyl)pyridine to be ~ 4 kcal/mol higher than in 2-methyl-biphenyl (Figure 2.1).⁹ The lower barrier to rotation is proposed to be due to the compressibility of the lone pair relative to a C-H bond.

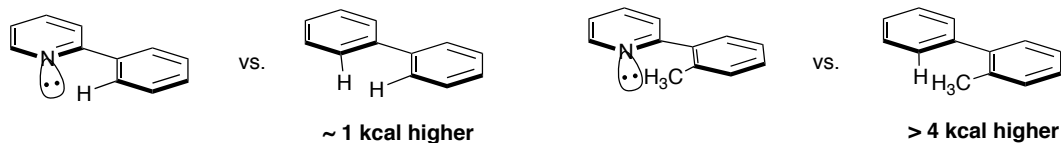
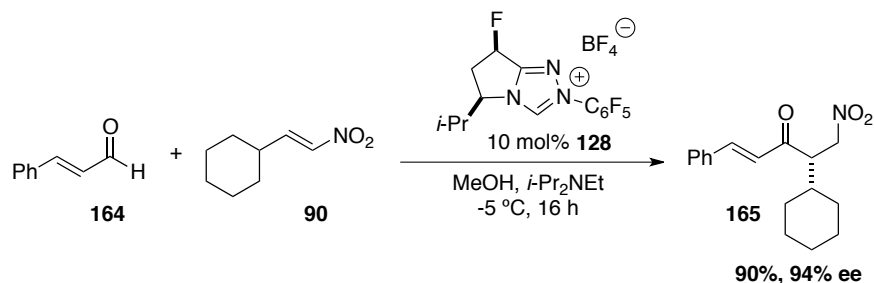


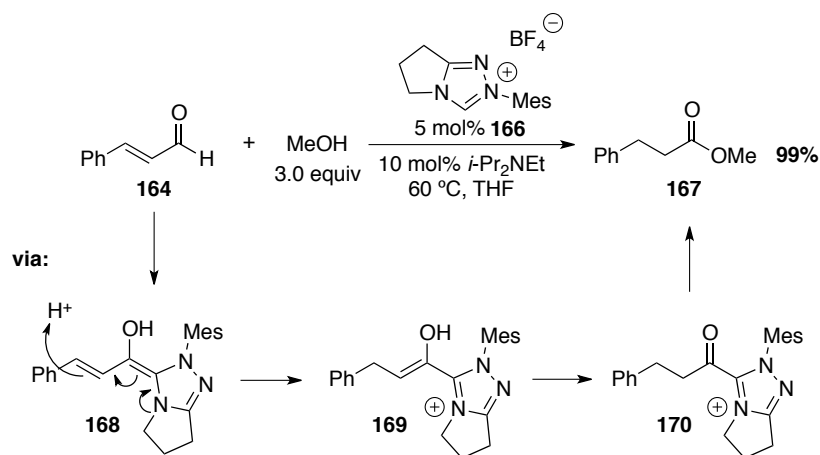
Figure 2.1

It stands to reason that in our system this compressibility might also be reflected in the transition state, leading to greater reactivity. We envisioned using enals to test this hypothesis due to their similar electronic nature yet smaller steric footprint. Subjection of cinnamaldehyde **164** to the standard conditions with cyclohexyl-nitroalkene **90** leads to good isolated yield and excellent enantioselectivity, albeit in longer reaction times (Scheme 2.5).



Scheme 2.5

This result demonstrated that a α -heteroatom was not required for reactivity or high enantioselectivity. Furthermore, we were surprised to find no appreciable amounts of the hydrocinnamate ester under these conditions. Bode and coworkers have shown that under conditions similar to that employed in our reaction, cinnamaldehyde **164** is converted to the hydrocinnamate ester **167** in quantitative yield (Scheme 2.6).¹⁰ This process involves rapid protonation of homoenolate **168** in the presence of a proton source to provide acyl azolium **170**. The acid chloride equivalent can then be displaced with a nucleophile such as methanol, delivering saturated ester **167**.

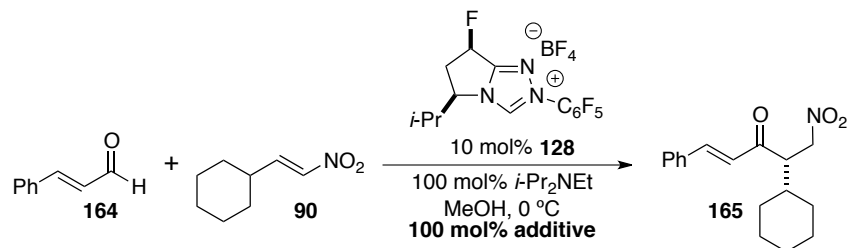


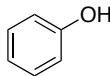
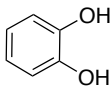
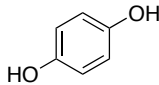
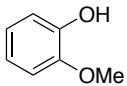
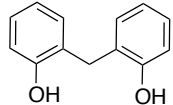
Scheme 2.6

With our catalyst, bearing the smaller more electron deficient *N*-aryl substituent, it is reasonable to assume that protonation might be slower due to decreased nucleophilicity of the homoenolate. Also, acyl anion addition should be more facile due to the smaller steric footprint of the pentafluorophenyl substituent.

We were pleased to see that the desired acyl anion reactivity was achievable with these substrates; however, long reaction times led to irreproducible results in many cases. With the hypothesis that the addition of oxygen scavengers to the reaction might lead to improved efficiency by prolonging catalyst lifetime, the reaction was run in the presence of hydroquinone, which showed a small but measurable increase in efficiency in a shorter timeframe (Table 2.1, entry 4). Given that protic solvents are requisite for this transformation, it seemed reasonable that the benefit of this additive may be due to its protic functionality. A variety of other phenolic additives were screened which revealed catechol as an extremely efficient co-catalyst (Table 2.1, entry 3), providing a surprising increase in rate and isolated yield. To probe the necessity for the bifunctional nature of catechol, guaicol (Table 2.1, entry 5) was evaluated which is electronically similar, yet lacks the bi-protic functionality, but showed no appreciable increase in rate.

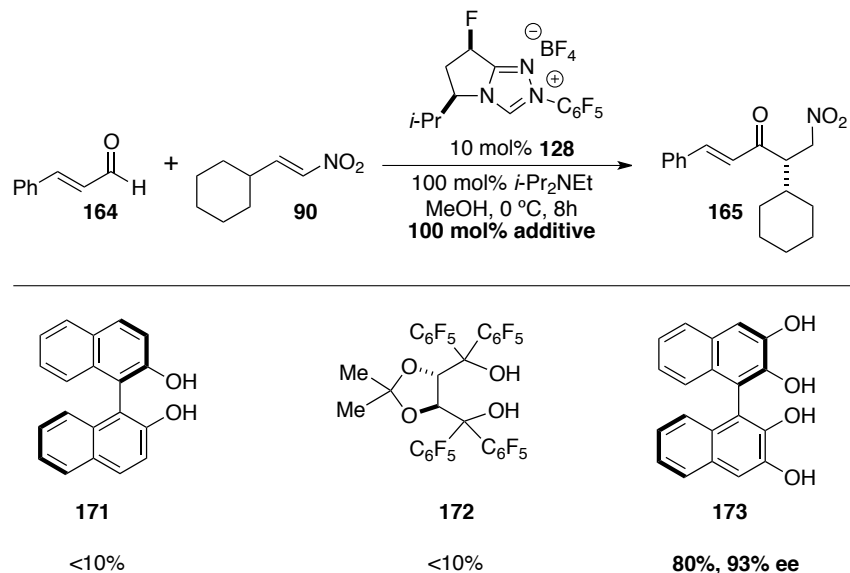
Table 2.1



Entry	Additive	Time (h)	Yield (%) ^b	ee (%) ^c
1.	none	8	5%	93%
2.		8	8%	93%
3.		2	80%	93%
4.		8	15%	93%
5.		8	9%	93%
6.		6	87%	93%

^a Reactions conducted with 1.0 equiv **164** and 1.5 equiv **90** and analyzed at the indicated time interval. ^b Isolated yield after chromatography. ^c Enantiomeric excess determined by HPLC analysis on a chiral stationary phase.

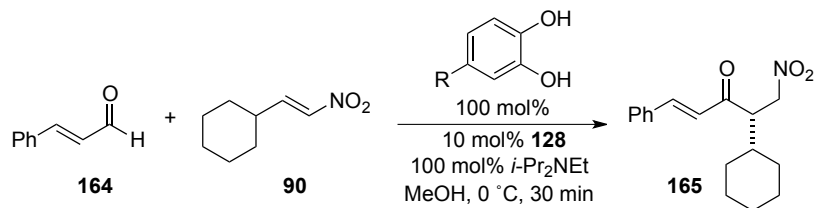
Bis-phenols (Table 2.1, entry 6) are also competent co-catalysts when they are ortho-substituted. We realized that the bifunctional nature of these additives is crucial to their function, yet the mechanism was unknown. Our initial hypothesis involved activation of the Michael acceptor through hydrogen bonding. We hoped that the use of chiral bifunctional phenols could both improve enantioselectivity as well as provide insight on the mode of activation. Unfortunately, binol **171** and taddol **172** were not competent co-catalysts in this reaction so we turned to the use of axially chiral catechol derivative **173** (Scheme 2.7).



Scheme 2.7

Although **173** provided the same rate enhancement as catechol itself, we observed no change in enantioselectivity. Furthermore, use of an achiral triazolium catalyst with **173** does not result in any asymmetric induction. These data suggest that the role of catechol is not in activation of the acceptor.

The impact of the electronic nature of catechol was also evaluated, in hope that a more efficient co-catalyst would be identified. Both electron rich and electron deficient derivatives were examined, which show only small differences in reactivity (Table 2.2). The best results are obtained with catechol and more electron-rich *t*-Bu-catechol. Given the low cost and wide availability of catechol, it was chosen as the optimal additive for further investigation.

Table 2.2

Entry	R	Yield (%) ^b	ee(%) ^c
1.	<i>t</i> -Bu	55%	93%
2.	H	48%	93%
3.	OMe	39%	93%
4.	CO ₂ Et	40%	93%
5.	CN	36%	93%

^a Reactions conducted with 1.0 equiv **164** and 1.5 equiv **90** and analyzed at the indicated time interval. ^b Isolated yield after chromatography. ^c Enantiomeric excess determined by HPLC analysis on a chiral stationary phase.

2.2.2 Mechanistic Study of the Effect of Catechol

Since our mechanistic study of the intramolecular Stetter reaction suggests that proton transfer to generate the acyl anion equivalent is turnover limiting, it seemed plausible that this could also be the slow step in the intermolecular reaction with a very reactive Michael acceptor. In order to test this hypothesis we initiated a mechanistic study of the intermolecular reaction, targeting identification of the turnover-limiting step. Monitoring the reaction by gas chromatography using TMB (trimethoxybenzene) as an internal standard demonstrates the dramatic effect that catechol has on the rate of reaction (Figure 2.2).

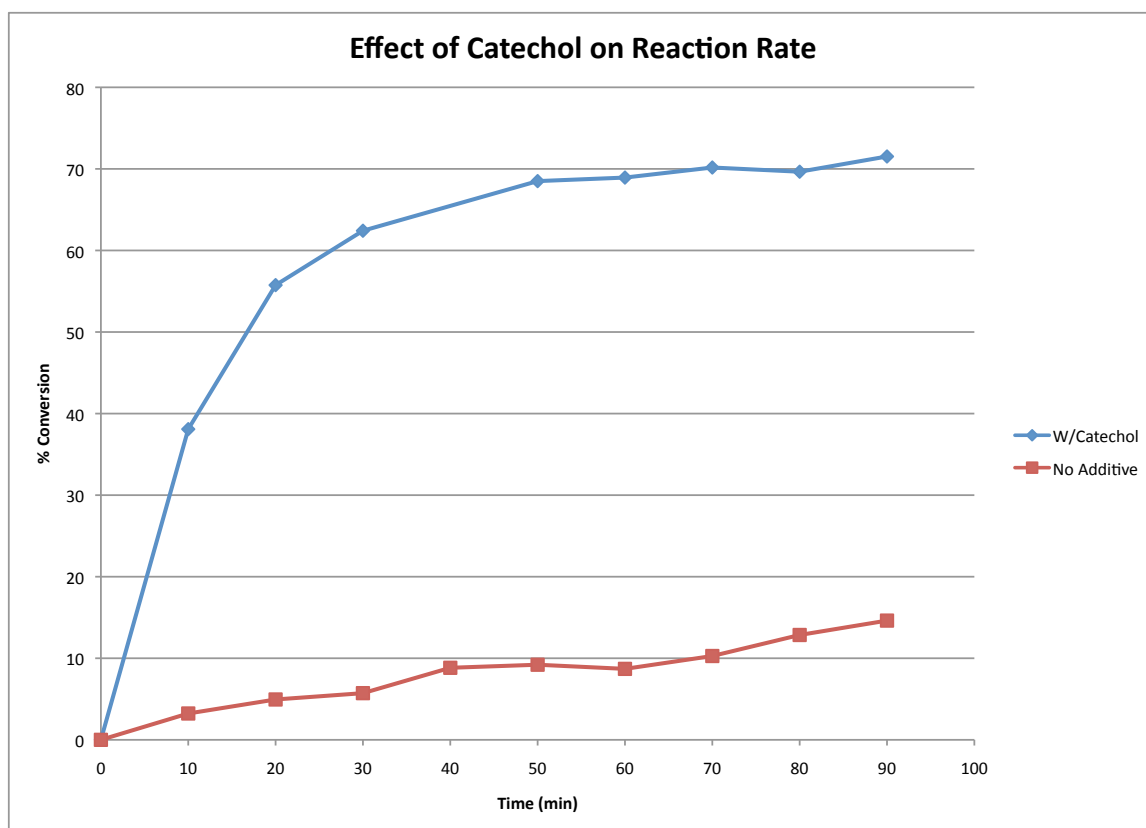


Figure 2.2

A series of ^2H KIE (kinetic isotope effect) studies of the aldehyde hydrogen were performed to determine if this bond was being broken in the turnover-limiting step in the presence of catechol. Using initial rate kinetics, we observe a $k_{\text{H}}/k_{\text{D}} = 2.7$ when the reaction is conducted in methanol and a $k_{\text{H}}/k_{\text{D}} = 4.2$ in methanol- d_4 (Figure 2.3). These data suggest that proton transfer to form the crucial acyl anion equivalent is also turnover-limiting in this transformation. Furthermore, a $k_{\text{H}}/k_{\text{D}} = 1.8$ is observed when ^1H -aldehyde is subjected to identical reaction conditions in methanol- d_4 , suggesting the participation of the phenolic proton in the slow step.

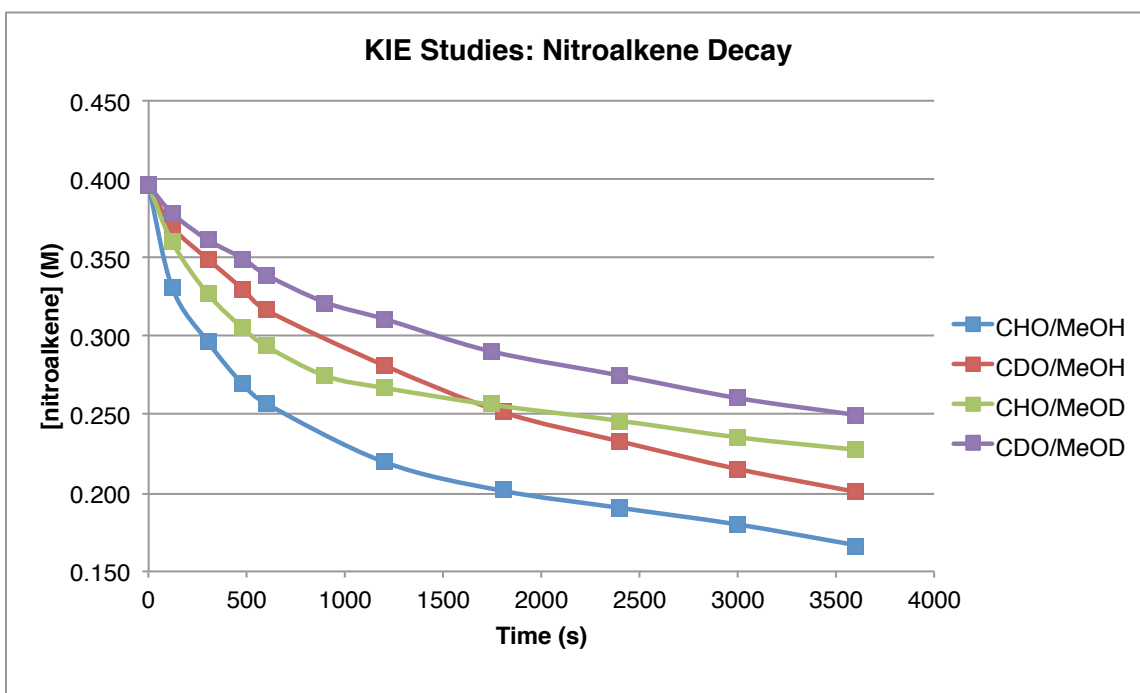
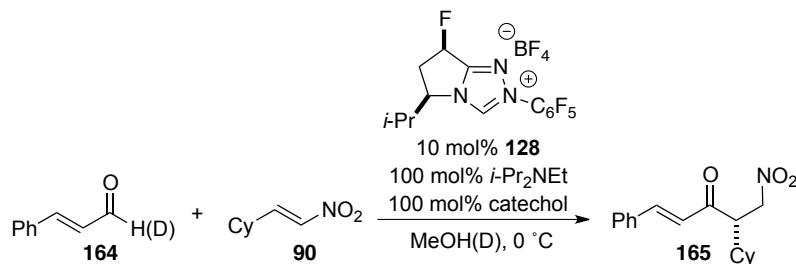


Figure 2.3

Based on this data we propose the following model: under basic reactions conditions, a catechol monoanion is likely the catalytically relevant species. It is known that 1,2-hydrogen shifts are prohibitively high in energy in symmetry-forbidden processes.¹¹ Catechol could facilitate proton transfer through a synchronous transition state, reminiscent of the familiar carboxylic acid dimer (Figure 2.4).

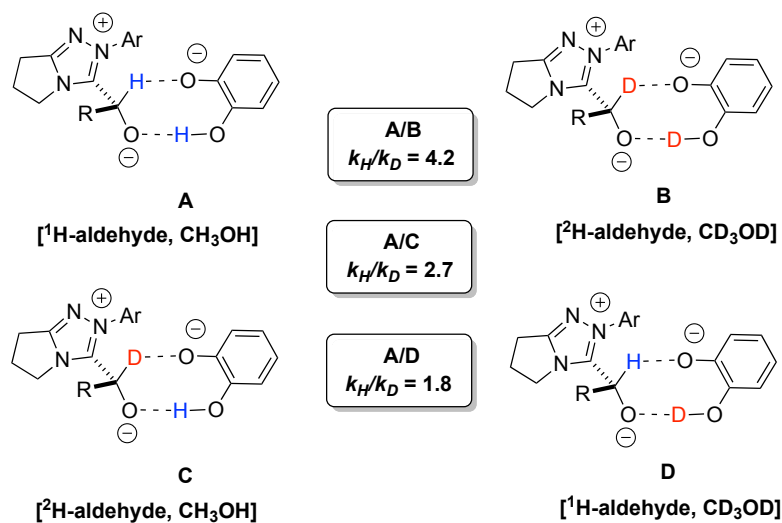
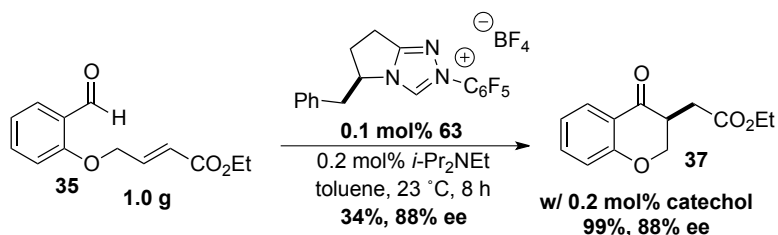


Figure 2.4

With good evidence that catechol assists in proton transfer, we wanted to evaluate its effect in other NHC catalyzed reactions. Since we were aware that the turnover-limiting step in the intramolecular Stetter reaction was undeniably proton transfer, we evaluated catechol as an additive in this context. After reducing catalyst loadings to unprecedented levels (0.1 mol%), we found that salicylaldehyde derivative **35** undergoes cyclization in 34% yield on a 1.0 g scale. After the incorporation of just 0.2 mol% of catechol, quantitative yield can be obtained under identical conditions (Scheme 2.8).

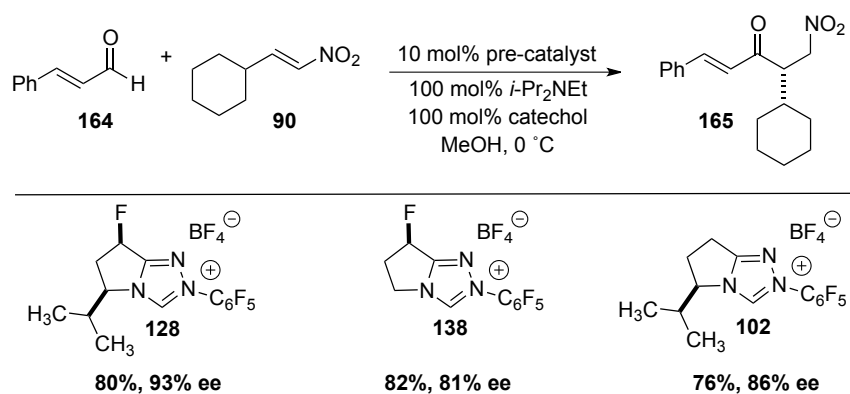


Scheme 2.8

This further substantiates our hypothesis that catechol's role in this transformation is to accelerate proton transfer. We looked to expand the utility of this additive to the intermolecular reaction of hetaryl aldehydes that we recently discovered; however, no improvement in rate was

observed in this case. Provided the high efficiency in this reaction, it seems likely the heteroatom may play a role in facilitating proton transfer.

Although precatalyst **128** proved to be highly selective, we were interested in probing the impact of catalyst fluorination with enals as substrates. As expected des-fluoro precatalyst **102** provides lower enantioselectivity than **128** but is still very efficient. Precatalyst **138**, which is chiral only at its fluorine stereocenter and lacks any bulky directing group, affords product in 81% ee, comparable to that of Valine-derived precatalyst **102**. This result shows the dramatic impact that fluorination has in this system as well, rivaling traditional catalyst manipulation of steric components (Scheme 2.9).



Scheme 2.9

With both an efficient and selective catalyst system developed, we began to examine the scope of this transformation.

2.2.3 The Scope of the Asymmetric Intermolecular Stetter Reaction of Enals and Nitroalkenes

Cinnamaldehyde derivatives undergo smooth addition to nitroalkene **90** in good yield and excellent enantioselectivity (Table 2.3, entries 1-3). Enals with β-heterocycles also provide high selectivity (Table 2.3, entry 4), whereas aliphatic substitution affords products in reduced yields

and lower selectivities (Table 2.3, entries 5-6). Furthermore, other functional groups such as protected aldehydes and dienes can be incorporated with equally good results.

Table 2.3

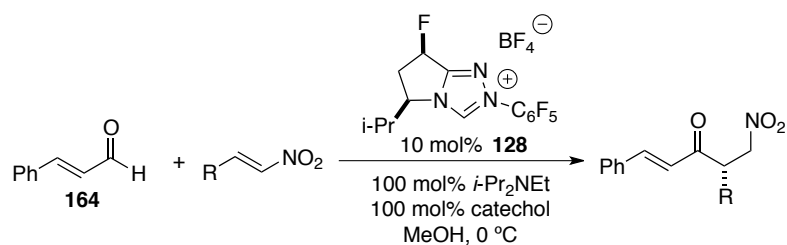
Entry	Aldehyde	Product	Yield (%) ^b	ee (%) ^c
1.		165	80%	93%
2.		166	97%	93%
3.		167	57%	98%
4.		168	98%	93%
5.		169	70%	83%
6.		170	67%	86%
7.		171	60%	82%
8.		172	90%	94%

^a Reactions conducted with 1.0 equiv aldehyde and 1.5 equiv **90**. ^b Isolated yield after chromatography. ^c Enantiomeric excess determined by HPLC analysis on a chiral stationary phase.

The scope of the nitroalkene is mainly limited to secondary alkyl substitution. Secondary cyclic and acyclic substitution provides the product in good yield and excellent enantioselectivity (Table

2.4, entries 1-3). Heteroatoms can also be incorporated into the substrates without deleterious impact on reactivity or selectivity. Unfortunately, primary alkyl substitution leads to lower yields as well as a significant loss in selectivity.

Table 2.4



Entry	Nitroalkene	Product	Yield (%) ^b	ee (%) ^c
1.		165	80%	93%
2.		173	75%	91%
3.		174	84%	88%
4.		175	82%	90%
5.		176	78%	90%
6. ^d		177	84%	43%
7. ^d		178	66%	52%
8.		179	<5%	—

^a Reactions conducted with 1.0 equiv **164** and 1.5 equiv nitroalkene. ^b Isolated yield after chromatography. ^c Enantiomeric excess determined by HPLC analysis on a chiral stationary phase. ^d 4-(ethoxycarbonyl)catechol was used.

Absolute stereochemistry of the Stetter products was determined by X-ray analysis of **167** (Figure 2.5).

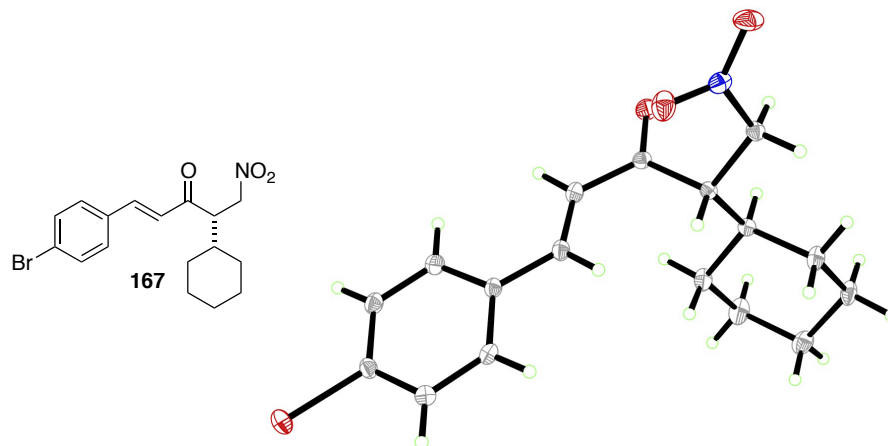
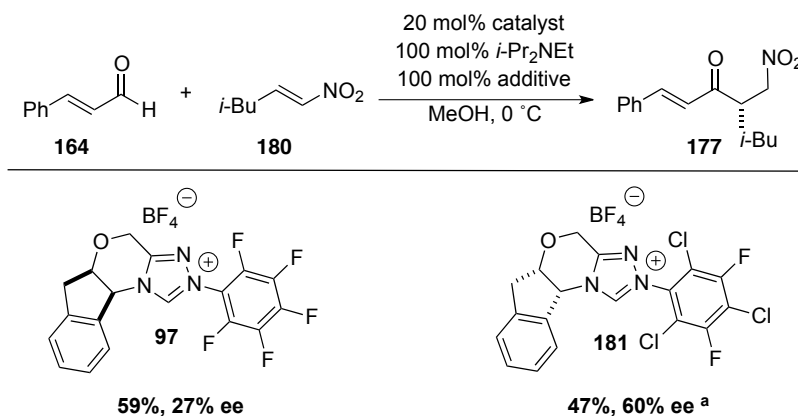


Figure 2.5

We found that selectivity could be remedied slightly by the use of bulkier electron deficient *N*-aryl substituents on the catalyst scaffold. Aminoindanol derived precatalyst **97** bearing the pentafluorophenyl substituent affords the product in poor enantioselectivity (Scheme 2.10). Introducing the larger 2,4,6-trichloro-3,5-difluorophenyl substituent on the catalyst scaffold results in significant improvement of selectivity.

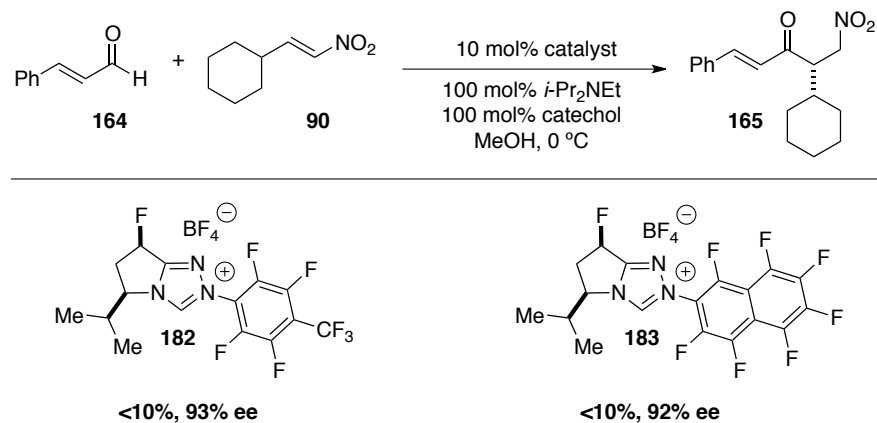


^a The opposite enantiomer was obtained.

Scheme 2.10

The synthesis of a precatalyst containing this substituent from the pyrrolidine-based scaffold was unsuccessful. Given the beneficial impact of bulky ortho substituents and electron withdrawing groups on the catalyst's *N*-aryl substituent, we were interested in exploring this space further.

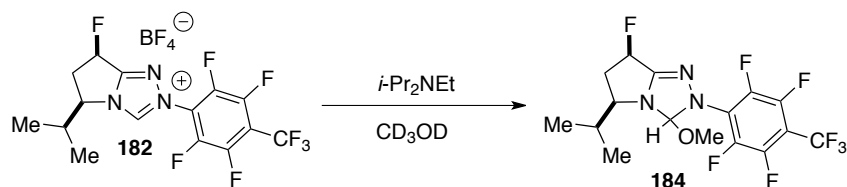
Synthesis of more electron-deficient catalysts proved non-trivial; however, small amounts were obtained and evaluated in the reaction. Hydrazines required for the synthesis of triazolium salts **182** and **183** were prepared by nucleophilic aromatic substitution of the corresponding aryl fluorides. Evaluation of these new precatalysts in the Stetter reaction show only poor reactivity with no benefit to enantioselectivity (Scheme 2.11).



Scheme 2.11

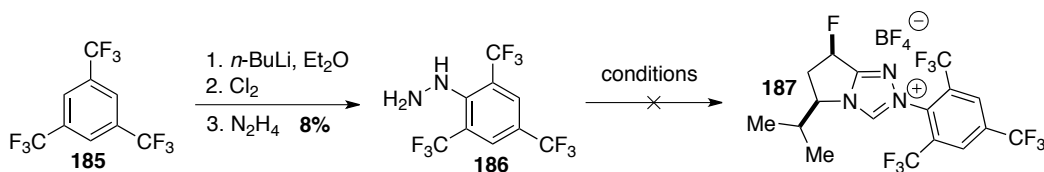
The reduction in reactivity with more electron deficient catalysts was puzzling at first. In most cases these catalysts outperform their more electron-rich counterparts. Since this electronic effect makes the azolium salts more electrophilic, we wondered if the nucleophilicity of the solvent was an issue. Using precatalyst **182** in the intramolecular Stetter reaction as an assay, we evaluated nucleophilic and non-nucleophilic solvents. Salicylaldehyde derivative **35** cyclizes to chromanone **37** in quantitative yield and high enantioselectivity in toluene; however, only trace amounts of product are observed in methanol. This result confirmed our suspicion about decomposition of the catalyst with nucleophilic solvents. To further study this decomposition pathway we monitored the fate of the precatalyst by ¹H NMR in methanol-*d*₄ in the presence of Hünig's base. With the addition of base, triazolium salt **182** is instantaneously converted to a

new species, which we propose to be **184** derived from the addition of methanol to the azolium (Scheme 2.12).



Scheme 2.12

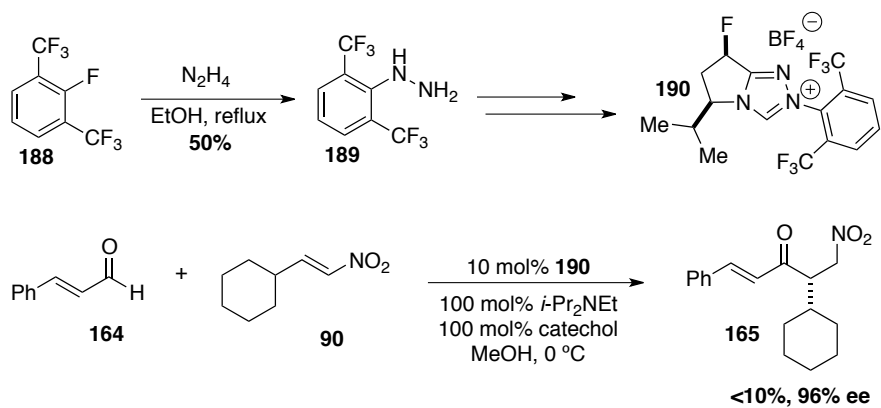
Evidence for the addition of water to azolium salts has also been noted in our group's work on the hydration of enals to form carboxylic acids.¹² Due to this issue, we abandoned the synthesis of more electron deficient systems and focused on incorporating bulky ortho-substitution in the aryl group. We knew from previous studies that the pentafluorophenyl substituent was important for reactivity and high selectivity so we targeted arenes that would be similar electronically but more sterically demanding. Our initial focus was on fluorinated mesityl derivative **186**, which was accessed in low yield by lithiation of the corresponding arene **185**, followed by quenching with liquid chlorine and nucleophilic aromatic substitution with hydrazine (Scheme 2.13). While we were able to make the desired hydrazine, all attempts to form the triazolium salt with this derivative proved unsuccessful due to its decreased nucleophilicity.



Scheme 2.13

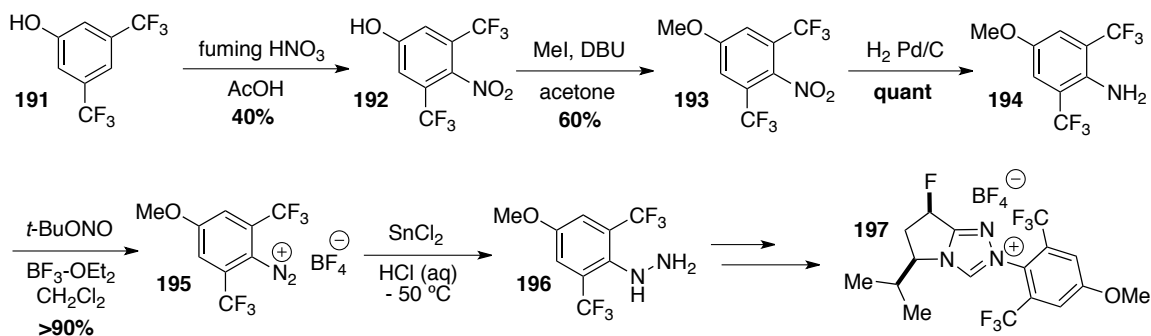
To remedy this problem, we thought to remove the para-substituent, which should increase the nucleophilicity of the hydrazine yet not affect its size. This hydrazine was prepared from commercially available aryl-fluoride **188** by nucleophilic aromatic substitution with hydrazine in

good yield. Elaboration to the desired triazolium salt **190** could be accomplished in this case, although isolation proved difficult and thus it was evaluated without purification in the Stetter reaction. We were delighted to find that precatalyst **190** provided improved enantioselectivity; however, electrophilicity of this catalyst also appeared to be a problem (Scheme 2.14).



Scheme 2.14

With the prospect that modulation of electrophilicity would lead to an efficient and highly selective catalyst we continued our efforts to tune the hydrazine. We hoped that modulation of the electrophilicity would be accomplished by the installation of a *p*-OMe group. Starting from 2,6-trifluoromethyl phenol **191**, nitration followed by alkylation and reduction provides aniline **194** (Scheme 2.15).¹³ Conversion of the aniline to the diazonium tetrafluoroborate salt **195** followed by reduction, affords the desired hydrazine **196**. The triazolium salt was prepared from this hydrazine as a crude mixture.

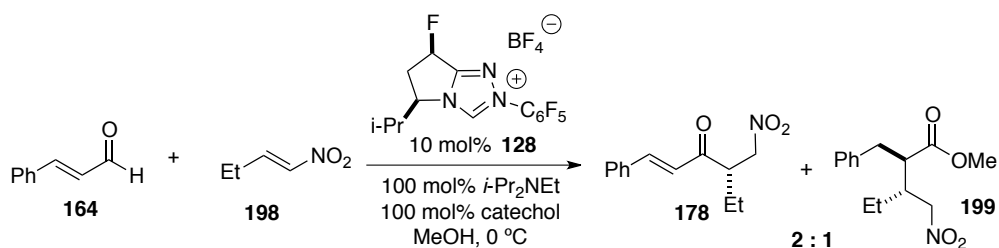


Scheme 2.15

Evaluation of crude precatalyst **197** showed none of the desired reactivity in the Stetter reaction. Problems associated with both the synthesis of more elaborate *N*-aryl substituents, as well as the lack of catalytic activity in these catalysts led us to abandon further optimization.

2.3 A [4+2] Cycloaddition of Enals and Nitroalkenes

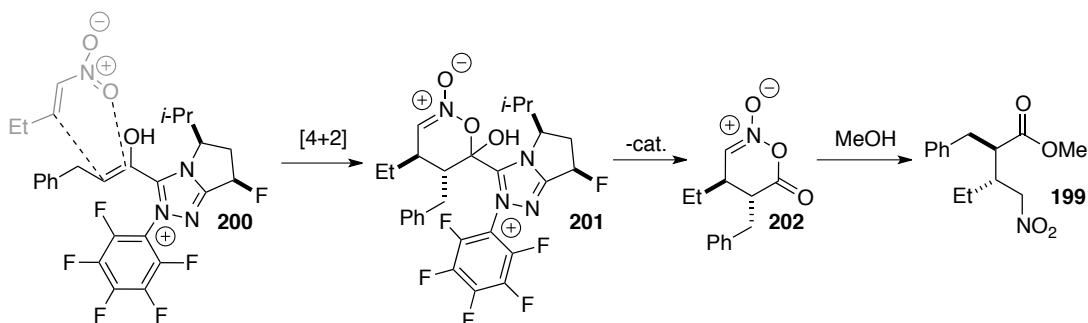
Although no significant amounts of esterification products are observed in most cases, the poor isolated yields obtained when primary alkyl substituted nitroalkenes are used as substrates is due to a competing side-reaction. Subjecting cinnamaldehyde **164** to ethyl nitroalkene **198** results in a 2:1 mixture of nitroketone **178** and nitroester **199** (Scheme 2.16).



Scheme 2.16

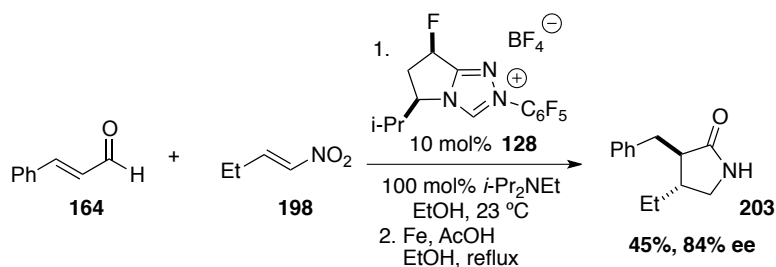
Nitroester **199** presumably comes from addition of the catalytically generated enol-azolium **200** to the nitroalkene. This process can be thought of as a concerted [4+2] between the enol and nitroalkene, providing cyclic nitronate **202** as a transient intermediate after elimination of the

carbene (Scheme 2.17). In the presence of methanol, this nitronate should undergo rapid decomposition to nitroester **199**.



Scheme 2.17

Initial studies to harness this reactivity show that at higher temperatures, protonation of the homoenolate is favored, providing moderate yield of the nitroester product **199**. Furthermore, this reaction proceeds with good enantioselectivity using precatalyst **128** and provides a single diastereomer of γ -lactam **203** after subsequent reduction in the same pot (Scheme 2.18).¹⁴



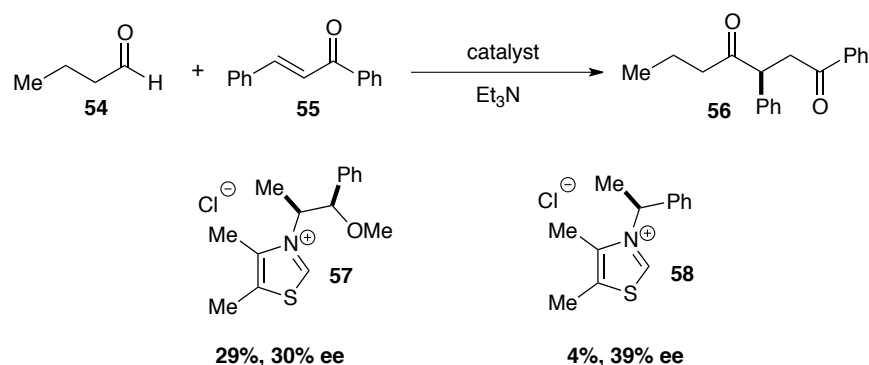
Scheme 2.18

Given the utility of enantioenriched γ -lactams, their synthesis in a stereospecific manner would be a highly valuable method. Studies are currently underway to optimize this transformation.

2.4 Aliphatic Aldehydes in the Asymmetric Intermolecular Stetter Reaction

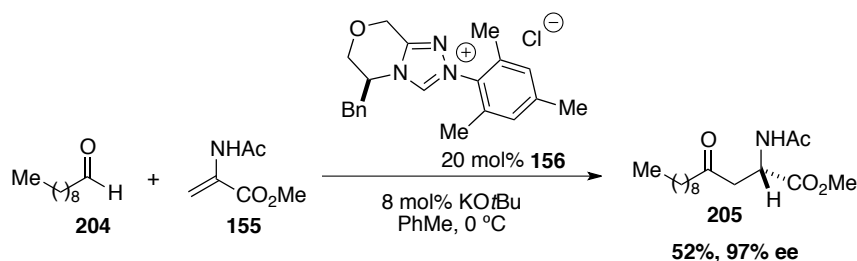
2.4.1 Introduction

With the development of new catalysts, the scope of the asymmetric intermolecular Stetter reaction has been dramatically increased; however, aliphatic aldehydes represent a particularly problematic class of substrates. Due to their lower electrophilicity, smaller steric footprint, and enolizable nature they have rarely been used successfully in the asymmetric reaction. Enders was the first to report the addition of butanal **54** to chalcone **55** in the presence of chiral thiazolium salts, which provides poor yield and low enantioselectivity in all cases (Scheme 2.19).¹⁵



Scheme 2.19

Glorius has recently shown a single example of aliphatic aldehyde **204** adding to β -unsubstituted Michael acceptor **155**, affording α -amino acid derivative **205** with high enantioselectivity after a diastereoselective protonation event (Scheme 2.20).¹⁶ Higher catalyst loading is required in this case, which also results in reduced yield compared to aromatic aldehydes.

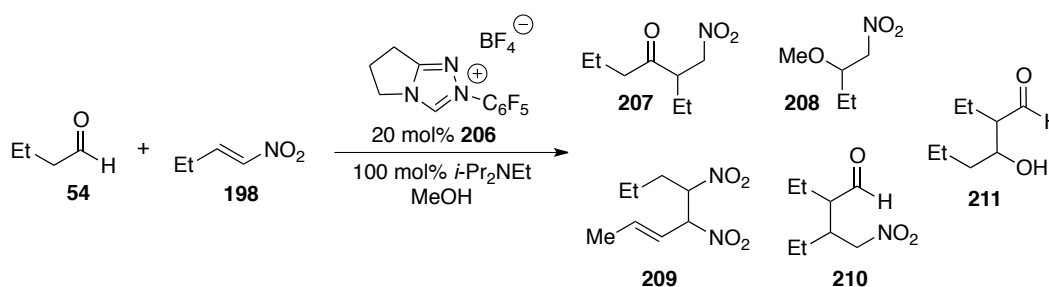


Scheme 2.20

In the enzyme catalyzed Stetter reaction reported by Müller and coworkers, products derived from acetaldehyde can be obtained in high selectivity but poor yield.¹⁷ Needless to say, the incorporation of aliphatic aldehydes has been a challenging problem in catalytic acyl anion chemistry.

2.4.2 Initial Studies and Catalyst Development

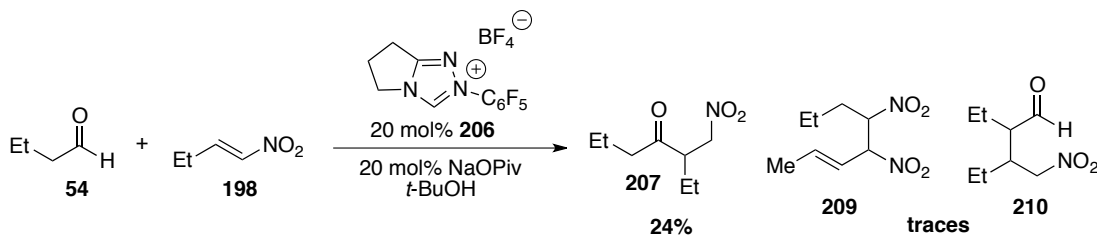
We approached this problem by evaluating the ability of aliphatic aldehydes to add to nitroalkenes with our improved catalysts. With the advent of fluorinated triazolium salt precatalysts that we have developed, we were confident that catalyst design would allow for the desired reactivity and enantioselectivity. Initial studies focused on the use of primary alkyl-substituted nitroalkenes as electrophiles given that they should be more reactive from a steric perspective. Subjecting butanal **54** and ethyl nitroalkene **198** to standard conditions with achiral precatalyst **206** leads to a variety of products (Scheme 2.21). Although desired nitroketone **207** was present in the crude reaction mixture, significant amounts of **208** were formed from based catalyzed addition of the solvent to the nitroalkene. Other products were also observed in smaller quantities, proposed to be the result of enolization of the aldehyde or nitroalkene.



Scheme 2.21

The greater sensitivity of both coupling partners mandated the development of milder and more effective conditions. Due to the nucleophilicity of the solvent, we chose to study tertiary alcohols

in place of methanol. Also, weaker bases are required to prevent by-products of self-condensation derived from the aldehyde and nitroalkene. Use of *tert*-butanol as solvent in combination with acetate bases proved the most effective at controlling the formation of by-products while promoting the Stetter reaction (Scheme 2.22). The use of non-protic solvents is unproductive, as has been well documented in this chemistry.



Scheme 2.22

While the desired nitroketone **207** could only be isolated in modest yield, we wanted to probe the enantioselectivity obtained using our chiral precatalysts. Under optimized conditions we screened our fluoro and des-fluoro pyrrolidine scaffold as well as the amino-indanol derivative. In this case, the pyrrolidine scaffold proved to be inferior. Promising selectivity (64% ee) is observed in the case of 2,4,6-trichlorophenyl amino-indanol derivative **212**; however, yields are poor in all cases (Table 2.5).

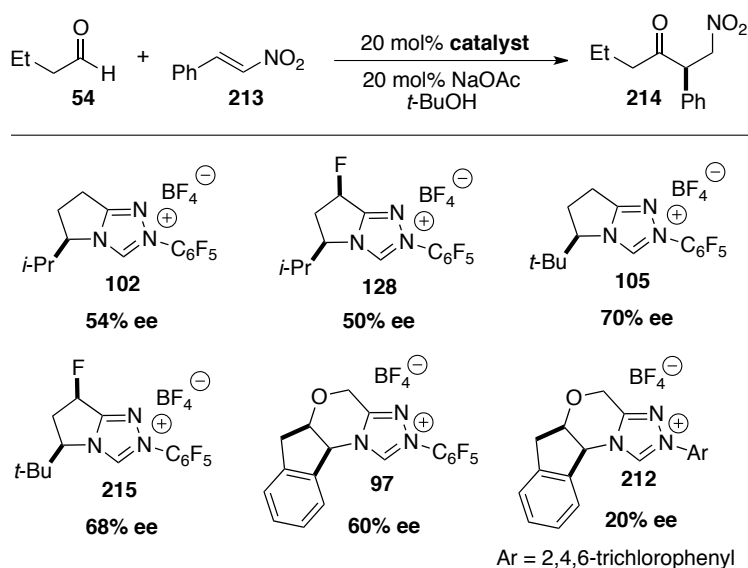
Table 2.5

Entry	Catalyst	Yield (%) ^b	ee (%) ^c
1.	 63	<10%	8%
2.	 128	<10%	16%
3.	 97	<10%	32%
4.	 212	<10%	64%

^a Reactions conducted with 1.5 equiv **54** and 1.0 equiv **198**. ^b Isolated yield after chromatography. ^c Enantiomeric excess determined by GC analysis on a chiral stationary phase.

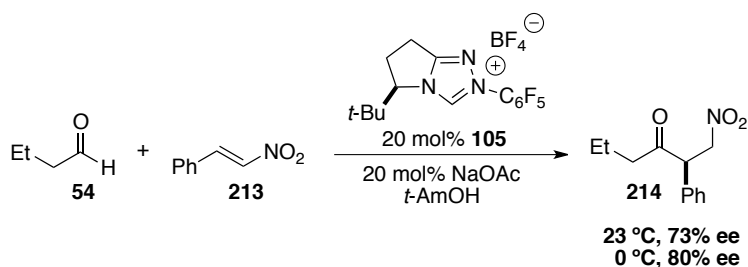
Due to the poor reactivity of alkyl nitroalkenes as well as the difficulty associated with analysis in the absence of a chromophore, we turned to the use of nitrostyrene derivatives. Under similar conditions found to be optimal for aliphatic nitroalkenes, nitrostyrenes react with high efficiency. We began a thorough investigation of our catalyst scaffolds, which showed promising selectivities. Valine-derived precatalyst **102** provides the nitroketone is 54% ee, but disappointingly our venerable fluorinated derivative **128** does not improve selectivity (Scheme 2.23). We were, however, excited to discover that, for the first time, *tert*-Leucine derived precatalyst **105** can be utilized with superior results. Again, synthesis of *cis*-fluorinated derivative **215** does not lead to improved selectivity. Based on the substantial reduction of

selectivity when switching *N*-aryl substituents, as in precatalyst **112**, we moved forward in optimizing the reaction with precatalyst **105**.



Scheme 2.23

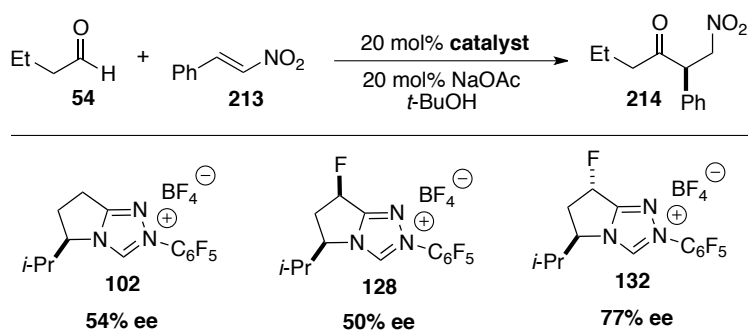
In order to lower the temperature of the reaction, a change in solvent was necessary due to the high freezing point of *tert*-butanol. Switching to *tert*-amyl alcohol, possessing a lower freezing point (-9 °C), allows for an increase in selectivity by lowering the temperature to 0 °C (Scheme 2.24).



Scheme 2.24

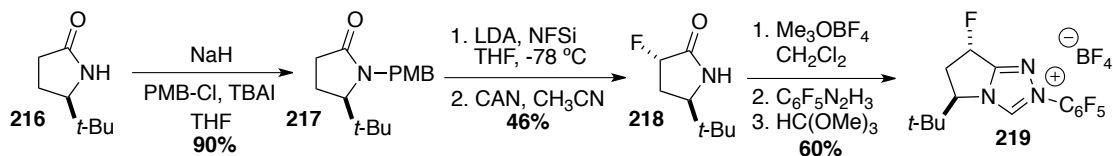
While manipulation of conditions provided modest improvements, our current catalyst system was unable to deliver enantioselectivities in excess of 80% ee. In our catalyst screen we noticed similarities in the results obtained using fluorinated catalysts in the Stetter reaction of hetaryl

aldehydes. The lower enantioselectivities obtained when *cis*-fluorinated precatalysts were used in this system encouraged us to evaluate the *trans*-fluorinated derivatives. After reexamining *trans*-fluorinated precatalyst **132** in this system, we were surprised to find a dramatic increase in selectivity compared to both the *des*- and *cis*-fluoro analogues (Scheme 2.25).



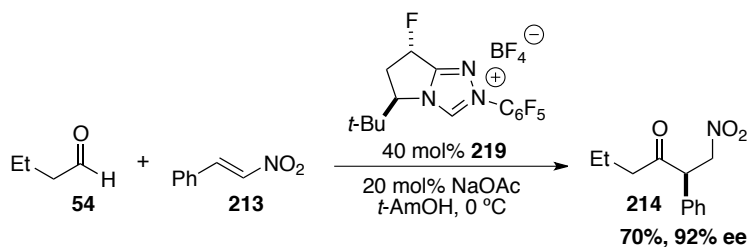
Scheme 2.25

Though we were uncertain of the reason for the sudden switch in optimal catalyst structure, this result prompted us to synthesize the bulkier and presumably more selective *trans*-fluorinated *tert*-leucine derived catalyst. Using the route previously employed to synthesize precatalyst **132** we commenced with lactam **216**, available in 5 steps from *L*-*tert*-leucine. Protection of the lactam with 4-MeO-benzyl chloride, followed by electrophilic fluorination using NFSi, provides the desired *trans*-fluorinated lactam **218** as a single diastereomer in good yield over the two-step sequence (Scheme 2.26). Triazolium salt **219** was prepared in good yield following our modified procedure.



Scheme 2.26

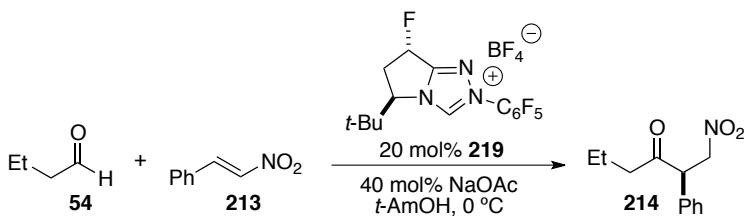
We were delighted to find that precatalyst **219** is not only incredibly selective (92% ee), but also provides good isolated yield (Scheme 2.27).



Scheme 2.27

To further optimize conditions using this new catalyst, we first evaluated the effect of concentration. Nitrostyrenes are remarkably insoluble in tertiary alcohols, especially at lower temperatures. Thus, we found concentrations around 0.1 M optimal for this transformation (Table 2.6).

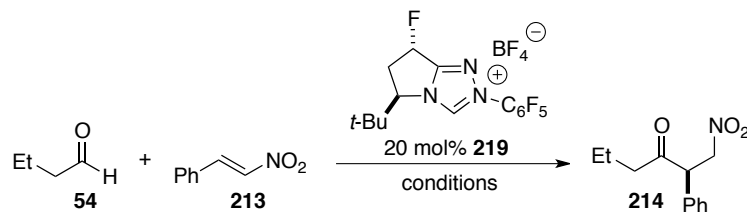
Table 2.6



Entry	Concentration (M)	Yield (%) ^b	ee (%) ^c
1.	1.0 M	49%	92%
2.	0.50 M	67%	93%
3.	0.25 M	78%	93%
4.	0.13 M	80%	93%
5.	0.06 M	65%	93%

^a Reactions conducted with 1.5 equiv **54** and 1.0 equiv **213**. ^b Isolated yield after chromatography. ^c Enantiomeric excess determined by HPLC analysis on a chiral stationary phase.

Also, a variety of solvents, bases and temperatures were screened at optimal concentration (Table 2.7). We found that acetate bases are crucial for the desired reactivity, as well protic solvents. THF and toluene both afford none of the nitroketone under these conditions. Temperature is also crucial; performing the reaction at ambient temperature results in drastically reduced yield (42%), as does lowering the temperature below 0 °C. The low efficiency of this reaction at lower temperatures is attributed to the poor solubility of the nitrostyrenes under the reaction conditions. Attempts were made to find tertiary alcohols that had better solvation properties, in which we identified 2-methyl-3-butenol (MBO). This somewhat uncommon solvent has all-around better properties than *tert*-amyl alcohol. The freezing point is significantly depressed creating a much lower viscosity, which ultimately leads to better solubility of the substrates. Furthermore, since MBO is a readily available terpene derived from the pine tree, the cost (\$44/kg) is significantly less than *tert*-amyl alcohol (\$100/kg). Using this solvent, we have observed better results in some cases (Table 2.7, entry 9) but ultimately *tert*-amyl alcohol was chosen out of convenience.

Table 2.7

Entry	Solvent	Base	Equiv.	Temp. (°C)	Yield (%) ^b	ee (%) ^c
1.	<i>t</i> -AmOH	NaOAc	0.4	0 °C	80%	93%
2.	<i>t</i> -AmOH	NaOAc	1.0	0 °C	78%	93%
3.	<i>t</i> -AmOH	<i>i</i> -Pr ₂ NEt	0.4	0 °C	< 5%	—
4.	<i>i</i> -PrOH	NaOAc	0.4	0 °C	42%	88%
5.	THF	NaOAc	0.4	0 °C	< 5%	—
6.	PhMe	NaOAc	0.4	0 °C	< 5%	—
7.	<i>t</i> -AmOH	NaOAc	0.4	23 °C	42%	90%
8.	<i>t</i> -AmOH	NaOAc	0.4	-10 °C	27%	93%
9. ^d	MBO	NaOAc	0.4	0 °C	84%	94%

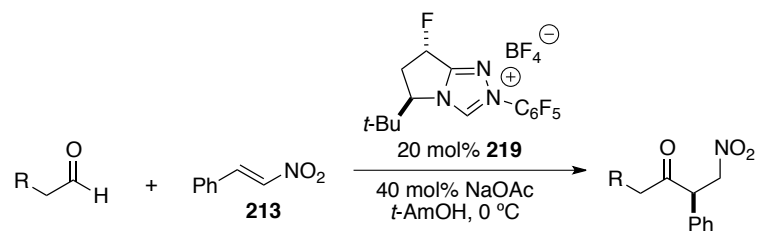
^a Reactions conducted with 1.5 equiv **54** and 1.0 equiv **213**. ^b Isolated yield after chromatography. ^c Enantiomeric excess determined by HPLC analysis on a chiral stationary phase. ^d MBO = 2-methyl-3-butenol

2.4.3 The Scope of the Asymmetric Intermolecular Stetter Reaction of Aliphatic Aldehydes and Nitrostyrenes

Using optimized conditions, we began evaluating the scope of this transformation starting with the aldehyde partner. Straight chain aliphatic aldehydes all participate in good yield with excellent enantioselectivities, with the exception of acetaldehyde, which reacts efficiently but is only modestly selective (Table 2.8, entry 3). Functional group tolerance is broad, allowing for the incorporation of silyl ethers, thioethers, alkyl halides and olefins (Table 2.8, entries 5-9). The major limitation lies in the use of bulkier α - and β -branched aldehydes. Isovaleraldehyde (Table

2.8, entry 4) provides the product in excellent enantioselectivity (95%), albeit in modest yield, where as isobutyraldehyde (Table 2.8, entry 10) does not participate.

Table 2.8



Entry	Aldehyde	Product	Yield (%) ^b	ee (%) ^c
1.		214	80%	93%
2.		220	87%	92%
3.		221	71%	62%
4.		222	32%	95%
5.		223	68%	87%
6.		224	67%	92%
7.		225	76%	93%
8.		226	83%	93%
9.		227	83%	93%
10.		228	< 5%	–

^a Reactions conducted with 1.5 equiv aldehyde and 1.0 equiv **213**. ^b Isolated yield after chromatography. ^c Enantiomeric excess determined by HPLC analysis on a chiral stationary phase.

With respect to the nitroalkene; although only nitrostyrene derivatives are competent, nearly all substitution patterns participate with equal facility (Table 2.9). Both activated and un-activated arenes are well tolerated. In the case of very activated systems, lower yields are obtained because of base-induced elimination of nitrous acid from the product resulting in the formation of an enone. On the opposite end of the spectrum, electron rich derivatives such as 4-MeO-phenyl are sluggish to react.

Table 2.9

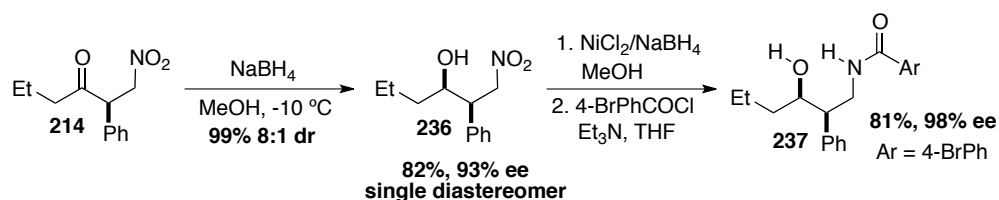
Reaction scheme: Ethyl acrylate (**54**) + Ar-CH=CH-NO₂ $\xrightarrow[40 \text{ mol\% NaOAc, } t\text{-AmOH, } 0 \text{ }^\circ\text{C}]{20 \text{ mol\% } \mathbf{219}}$ Product

Catalyst **219** structure: A chiral pyrrolidine derivative with a tert-butyl group, a fluorine atom, a C₆F₅ group, and a BF₄⁻ counterion.

Entry	Nitroalkene	Product	Yield (%) ^b	ee (%) ^c
1.		214	80%	93%
2.		229	70%	91%
3.		230	75%	93%
4.		231	83%	94%
5.		232	63%	91%
6.		233	50%	91%
7.		234	70%	92%
8.		235	81%	92%

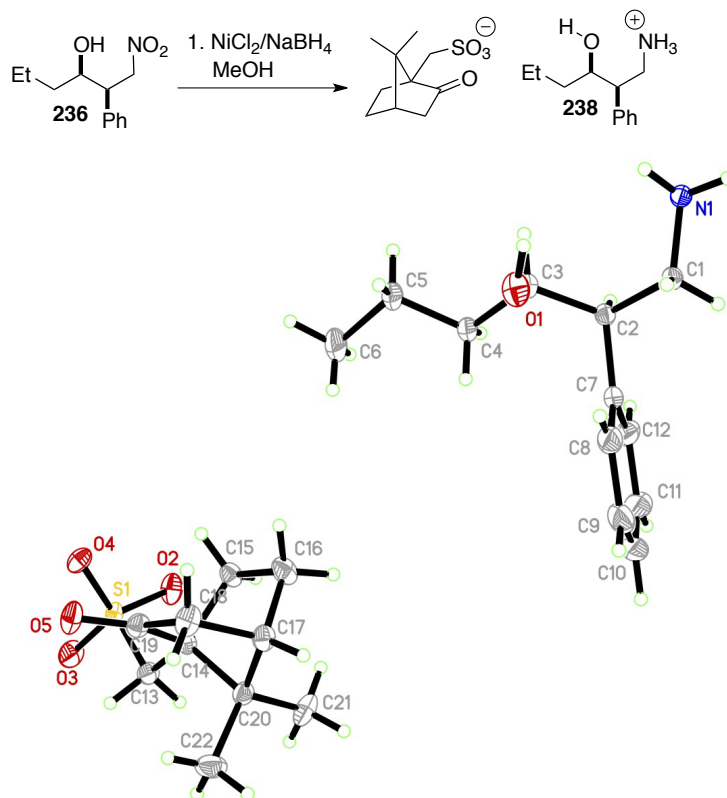
^a Reactions conducted with 1.5 equiv **54** and 1.0 equiv nitroalkene. ^b Isolated yield after chromatography. ^c Enantiomeric excess determined by HPLC analysis on a chiral stationary phase.

To demonstrate the utility of the β -nitroketone products, as well as determine their absolute stereochemistry, we synthesized an amino-alcohol derivative of **214**. The Stetter reaction was run on a 2.5 mmol scale using reduced catalyst loading (10 mol%), which provides product **214** in 84% yield and 93% ee (Scheme 2.28). Reduction of the ketone with NaBH_4 at $-10\text{ }^\circ\text{C}$ in methanol affords the syn nitro-alcohol **236** in quantitative yield as an 8:1 mixture of diastereomers. The major diastereomer can be isolated cleanly via chromatography, which can be reduced with $\text{NiCl}_2/\text{NaBH}_4$ and isolated as benzamide **237** in good yield over two steps (Scheme 2.28).



Scheme 2.28

Unfortunately, benzamide **237** was unable to provide suitable crystals for X-ray analysis. As an alternate approach we crystallized the amino alcohol directly from the reduction as the (*R*)-camphorsulfonic acid salt **238** (Scheme 2.29). This compound proved suitable for X-ray analysis and verified the absolute and relative stereochemistry.



Scheme 2.29

This assignment confirmed our suspicion that the opposite absolute stereochemistry was being obtained using the same antipode of catalyst as was used with heteryl and α,β -unsaturated aldehydes. We were intrigued by the switch in enantiomeric preference with these substrates and wondered if a much different effect is operable, given that the opposite relative stereochemistry of the fluorinated catalyst architecture is required.

To evaluate the relevance of our initial hypothesis of the effect of catalyst fluorination, we analyzed the fluorinated *tert*-leucine derived triazolium salts **215** and **219** by X-ray crystallography. Unexpectedly, *trans*-fluorinated precatalyst **219** displays a preference for the C_γ -exo conformation in the solid state, counterintuitive from a steric or stereoelectronic

perspective (Figure 2.6). Likewise, *cis*-fluorinated precatalyst **215** shows a preference for this same conformation, albeit with a much smaller torsional angle.

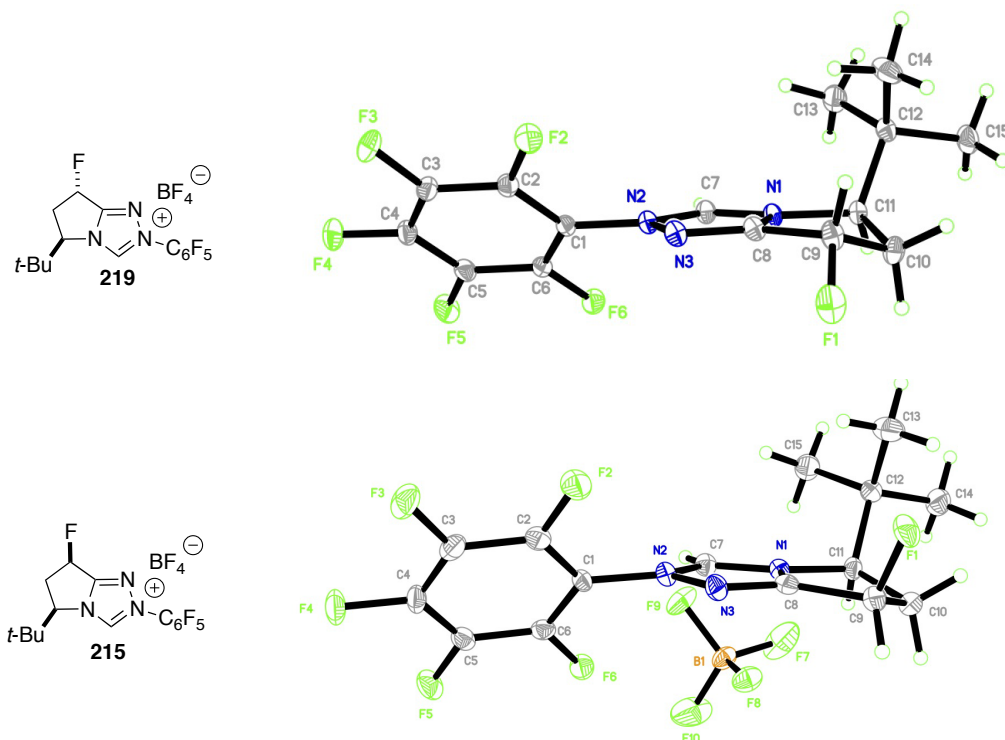


Figure 2.6

The conformational preferences in the ground states of these precatalysts are not well understood; however, the ground states may be irrelevant based on DFT calculations of the Breslow intermediate that we described previously. Not only are the selectivities much different between the *cis*- and *trans*-fluoro catalysts, but a large variation in reactivity also became apparent. A survey of both diastereomers of the fluorinated valine and *tert*-leucine derived precatalysts under our optimal conditions shows a remarkable difference in efficiency between them (Table 2.10). Catalysts **102** and **128** derived from L-valine are more competent than their *tert*-leucine derived counterparts, which is not surprising based on the difference in sterics between them. In both cases, the *trans*-fluorinated scaffold outperforms the *cis*, which is

increasingly noticeable in the *tert*-leucine scaffold. Precatalyst **215** provides the product in only 15% yield (Table 2.10, entry 5), where as diastereomer **219** under the same conditions is remarkably more efficient and affords product in 80% isolated yield (Table 2.10, entry 6).

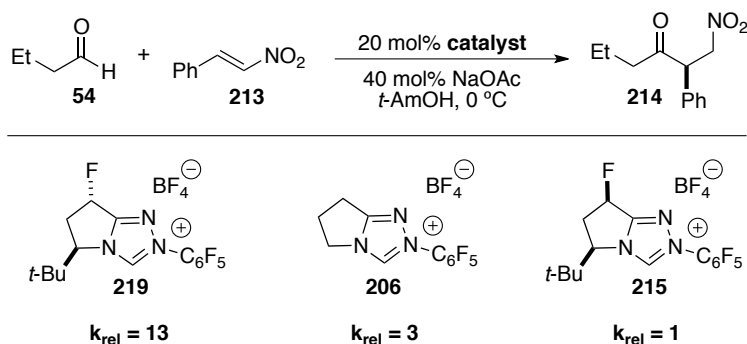
Table 2.10

Entry	Catalyst	Yield (%) ^b	ee (%) ^c
1.		49%	50%
2.		53%	48%
3.		78%	74%
4.		18%	80%
5.		15%	74%
6.		80%	93%

^a Reactions conducted with 1.5 equiv **54** and 1.0 equiv **213**. ^b Isolated yield after chromatography. ^c Enantiomeric excess determined by HPLC analysis on a chiral stationary phase.

To obtain a more quantitative comparison of the rate of product formation with these catalysts we performed several competition experiments with the assumption that the presence of two different catalysts will not alter their individual enantioselectivities. A competition experiment

between **215** and achiral precatalyst **206** provides product in 73% ee, while the same experiment between **219** and **206** provides product in only 18% ee. These enantioselectivities can be used to determine the relative rates of each catalyst separately, which shows that trans-fluorinated precatalyst **215** is approximately 13 fold more efficient than cis-fluorinated precatalyst **219** (Scheme 2.30). Furthermore, precatalyst **215** also outperforms achiral precatalyst **206** containing no bulky stereodirecting group.



Scheme 2.30

2.4.4 DFT Study of the Effect of Catalyst Fluorination

The difference in rates of these catalysts was surprising and our initial hypothesis did not seem to fit in this case, hence, we again turned to computational methods to provide a better understanding of the stereoelectronic effects governing selectivity and reactivity in this transformation. In collaboration with the Houk group, we undertook a DFT study, which examined both conformation in the Breslow intermediates derived from these catalysts, as well as the relevant transition states that explain the observed selectivity. Propionaldehyde was used as the model system to simplify calculations.

Catalysts **105**, **215**, and **219** react with propionaldehyde to form corresponding Breslow intermediates **239-241**. In all cases, no minima could be located for the endo conformations as all

optimizations from the endo conformations converge to exo (Figure 2.7). Freezing the triazolium ring system in the endo conformation predicts that these conformations are 5.2-7.5 kcal/mol higher in energy, thus the exo conformations were used to calculate the relevant transition states.

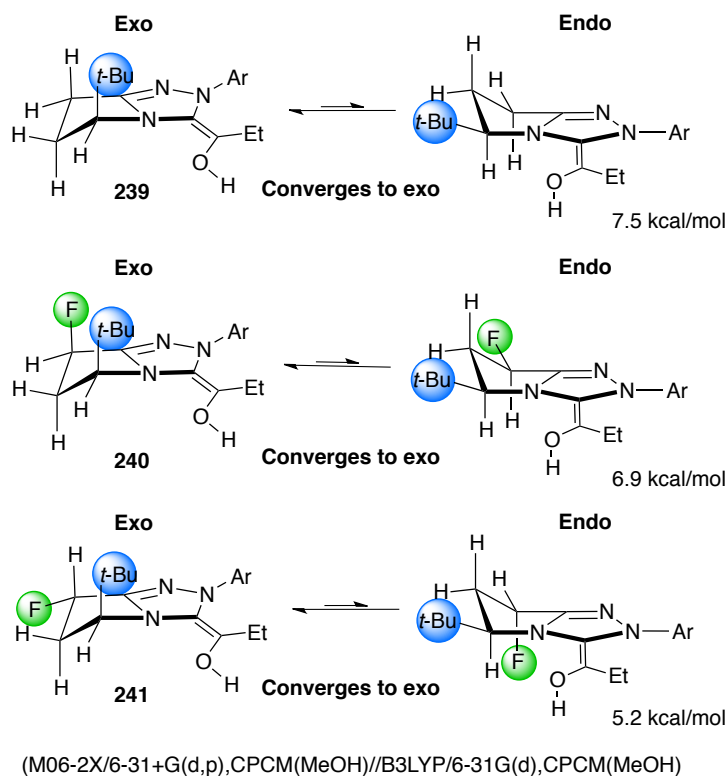


Figure 2.7

Addition of the Breslow intermediates to the *Re* face of the nitroalkene leads to the experimentally observed stereochemistry. In agreement with experiment, precatalyst **219** is computed to be the most selective. A gauche orientation in the *Si*-face attack is electrostatically favorable for precatalyst **215** in transition state **242** since the nitro group is placed under the fluorine atom, but not for precatalyst **219**, due to negative electrostatic interaction of the electronegative fluorine atom and the nitro group of the nitrostyrene (Figure 2.8). The anti conformation of the *Re*-face attack in both systems is favored due to a stabilizing interaction between the hydrogen of the hydroxyl group and the carbon α to the nitro group. This provides

further evidence that addition of the Breslow intermediate to the olefin is a concerted process. The additional source of selectivity of precatalyst **219** was found to be a favorable electrostatic interaction between the electronegative fluorine atom and the positive part of the phenyl ring in transition state **245** (Figure 2.8).

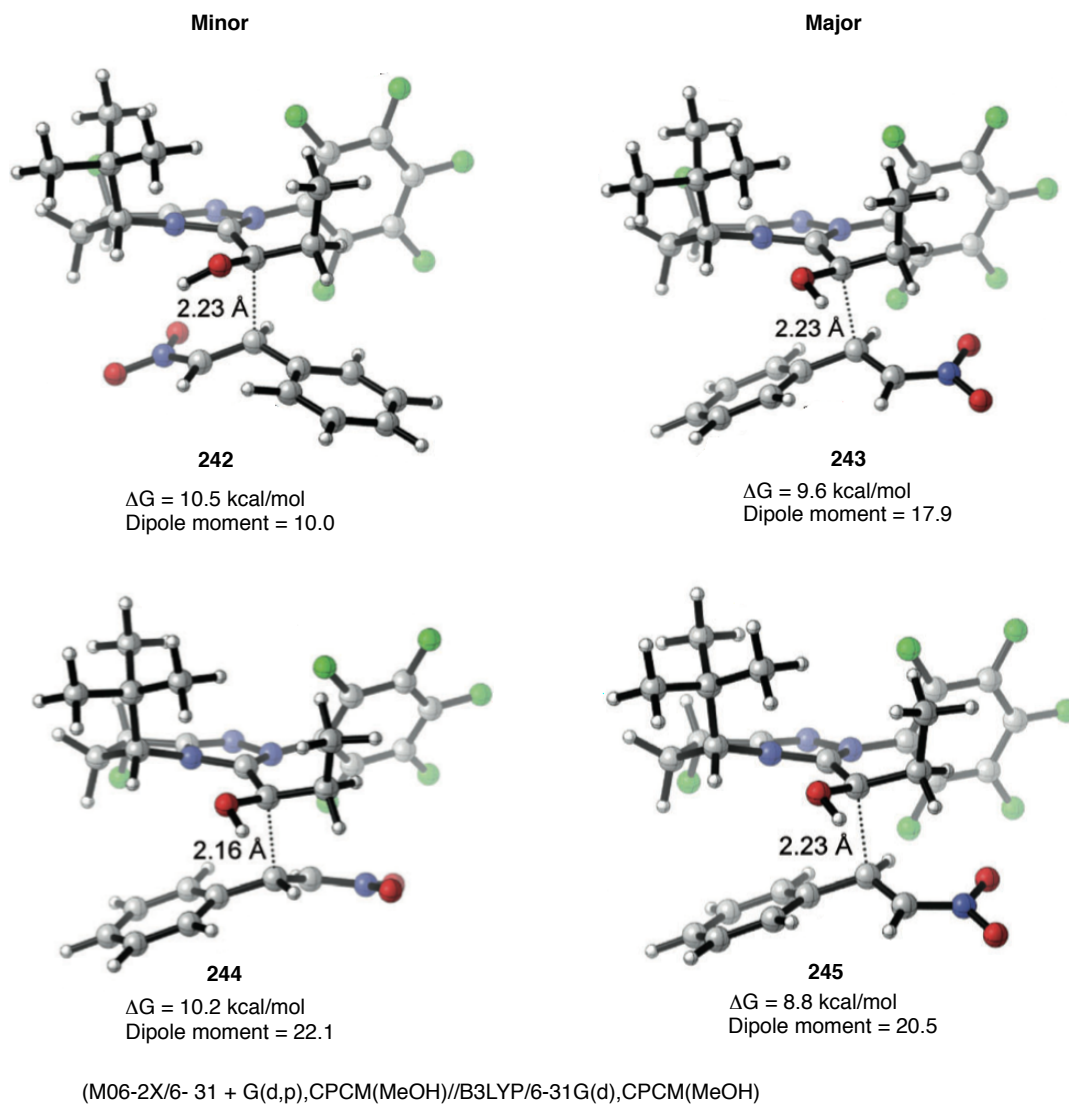
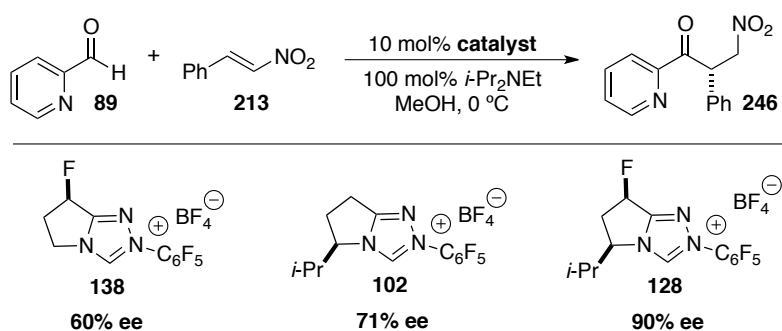


Figure 2.8

This type of fluorine to π interaction has been both observed and calculated in the literature when a very electron deficient π -system is present.¹⁸ Determining the source of increased reactivity was found to be non-trivial. Completing a complete study of the mechanism of this reaction was

out of our scope of interest, and would be necessary for a definitive answer. Based on these calculations, it seems reasonable that the large dipole moment in the transition states involving precatalyst **219** may be responsible for the increase in reactivity due to better solvation of the transition state.

With the insight of a new mode of catalyst control, we reevaluated the use of nitrostyrenes in the Stetter reaction with hetaryl aldehydes. We speculated that given the additional source of selectivity only observed with nitrostyrenes, due to the fluorine-arene interaction, selectivity may be reversed by using these substrates with other aldehydes. Initial studies of the addition of picolinaldehyde to β -nitrostyrene showed that the corresponding nitroketone was relatively unstable and underwent facile elimination of nitrous acid to form an enone. We hoped that we might be able to assess enantioselectivity early in the reaction to test our hypothesis. Subjecting picolinaldehyde **89** to β -nitrostyrene **213** with our fluorinated precatalyst shows a similar trend to what was observed previously using cyclohexyl-nitroalkene. We had wondered if precatalyst **128** would be less selective in this case than precatalyst **128**, due to the competing factors of sterics and electrostatics, however precatalyst **128** still provides a dramatic increase in selectivity over **102** (Scheme 2.31).



Scheme 2.31

2.5 Conclusion

In conclusion we have shown that size plays a major role in the reactivity of aldehydes for the asymmetric intermolecular Stetter reaction. Incorporation of enals as efficient coupling partners has been achieved by the use of bifunctional additives that accelerate the initial proton transfer event, leading to the acyl anion equivalent.¹⁹ Mechanistic studies were performed that support the hypothesis that proton transfer is the turnover-limiting step in the reaction. The use of these additives can be applied effectively to other systems where proton-transfer is also the slow step. Using catechol as an additive in the intramolecular Stetter reaction dramatically increases the efficiency in this system, and leads to dramatically reduced catalyst loadings.

Aliphatic aldehydes have also been shown to couple effectively with nitrostyrene derivatives in the presence of a newly developed precatalyst.²⁰ Trans-fluorination of the catalyst architecture in this case leads to both improved selectivity and improved reactivity. The reason for the switch in optimal catalyst structure was evaluated using DFT calculations that provide evidence for a new mode of catalyst control. Nitrostyrene derivatives are drawn to the electronegative fluorine atom in a F- π type interaction, which leads to improved selectivity. It has also been hypothesized that the observed increase in efficiency with this catalyst is due to a highly solvated transition state because of its large dipole moment.

REFERENCES

- ¹ See Chapter 1, ref 24-26.
- ² Sánchez-Larios, E.; Thai, K.; Bilodeau, F.; Gravel, Michel. *Org. Lett.* **2011**, *13*, 4942-4945.
- ³ Jousseau, T.; Wurz, N. E.; Glorius, F. *Angew. Chem. Int. Ed.* **2011**, *50*, 1410-1414.
- ⁴ Piel, I.; Steinmetz, M.; Hirano, K.; Fröhlich, R.; Grimme, S.; Glorius, F. *Angew. Chem. Int. Ed.* **2011**, *50*, 4983-4987.
- ⁵ DiRocco, D. A.; Rovis, T. *Angew. Chem. Int. Ed.* **2011**, *50*, 7982-7983.
- ⁶ (a) Bugaut, X.; Liu, F.; Glorius, F. *J. Am. Chem. Soc.* **2011**, *133*, 8130-8133. (b) Liu, F.; Bugaut, X.; Schedler, M.; Fröhlich, R.; Glorius, F. *Angew. Chem. Int. Ed.* **2011**, *50*, 12626-12630.
- ⁷ Dresen, C.; Richter, M.; Pohl, M.; Lüdeke, S.; Müller, M. *Angew. Chem. Int. Ed.* **2010**, *49*, 6600-6603.
- ⁸ Smith, M. B.; March, J. *March's Advanced Organic Chemistry: Reactions, Mechanisms and Structure*, 5th ed.; Wiley: New York, 2001.
- ⁹ Mazzanti, A.; Lunazzi, L.; Lepri, S.; Ruzziconi, R.; Schlosser, M. *Eur. J. Org. Chem.* **2011**, *33*, 6725-6731.
- ¹⁰ (a) Sohn, S. S.; Bode, J. W. *Org. Lett.* **2005**, *7*, 3873-3876. (b) For a review of redox pathways of α -reducible aldehydes catalyzed by NHCs see: Vora, H. U.; Rovis, T.; *Aldrichimica Acta* **2011**, *44*, 3-14.
- ¹¹ Kemp, D. S. *J. Org. Chem.* **1971**, *36*, 202-204.
- ¹² Vora, H. U.; Rovis, T. *J. Am. Chem. Soc.* **2010**, *132*, 2860-2861.
- ¹³ Shibuya, K.; Miura, T. Cyclic diamine compound and pharmaceutical containing the same. U.S. Patent 20,050,165,026, January 26, 2004.

- ¹⁴ Nick White, *Unpublished Results*, Colorado State University, **2012**
- ¹⁵ (a) Enders, D.; Bockstiegel, B.; Dyker, H.; Jegelka, U.; Kipphardt, H.; Kownatka, D.; Kuhlmann, H.; Mannes, D.; Tiebes, J.; Papadopoulos, K. in “Wege zu neuen Verfahren und Produkten der Biotechnologie”, DECHEMA-Monographie 1993, 129, 209. (b) Enders, D. in *Stereoselective Synthesis* (Eds.: E. Ottow, K. Schöllkopf, B.-G. Schulz), Springer, Berlin, 1994, p. 63. (c) Enders, D.; Breuer, K. *Comprehensive Asymmetric Catalysis*, Springer, Berlin, 1999, pp. 1093–1104. (d) Enders, D.; Balensiefer, T. *Acc. Chem. Res.* **2004**, *37*, 534 – 541.
- ¹⁶ See ref. 3.
- ¹⁷ Dresen, C.; Richter, M.; Pohl, M.; Lüdeke, S.; Müller, M. *Angew. Chem.* **2010**, *122*, 6750–6753; *Angew. Chem. Int. Ed.* **2010**, *49*, 6600 – 6603.
- ¹⁸ (a) Kawahara, S-I; Tsuzuki, S.; Uchimaru, T. *J. Phys. Chem. A* **2004**, *108*, 6744-6749. (b) Prasanna, M. D.; Row, T. N. G. *Crystal Engineering* **2000**, *3*, 135-154.
- ¹⁹ DiRocco, D. A.; Rovis, T. *J. Am. Chem. Soc.* **2011**, *133*, 10402-10405.
- ²⁰ DiRocco, D. A.; Noey, E. L.; Houk, K. N.; Rovis, T. *Angew. Chem. Int. Ed.* **2012**, *51*, 2391-2394.

Chapter 3

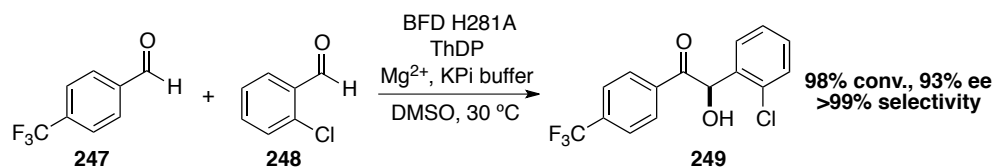
Addition of Catalytically Generated Acyl Anion Equivalents to Imines and Iminium Ions

3.1 Additions of Acyl Anion Equivalents to Imines

3.1.1 Introduction

The asymmetric addition of catalytically generated acyl anion equivalents to electrophiles other than Michael acceptors has received little attention in recent years. Although a highly enantioselective homo-benzoin reaction has been developed by Enders and coworkers,¹ no general methods for the asymmetric cross-benzoin reaction have been reported. The inherent challenge of this transformation lies in controlling chemoselectivity of the electrophilic partners. A few methods have addressed this problem, which makes the enantioenriched synthesis of cross-benzoin type products accessible.

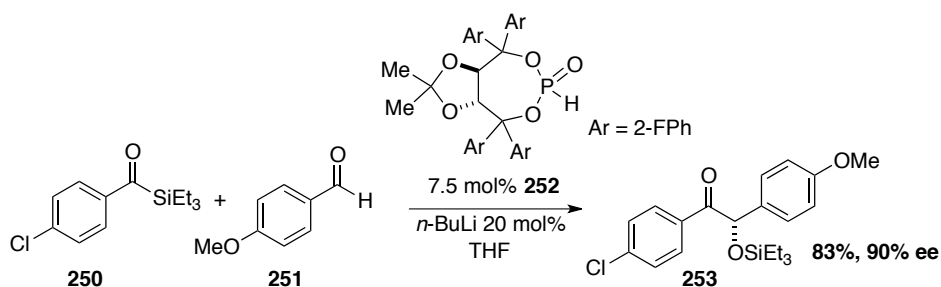
Müller and coworkers have effectively demonstrated a donor-acceptor concept utilizing thiaminediphosphate-dependent enzymes as catalysts for the asymmetric cross-benzoin reaction.² They found that 2-substituted aryl aldehydes do not undergo benzoin reaction with wild-type enzymes; thus, they could be suitable for use as a donor or acceptor in the presence a different aldehyde. Using this concept, a variety of aryl aldehydes can be coupled selectively, in good yield with high enantioselectivity (Scheme 3.1).



Scheme 3.1

The Johnson group has also developed a clever strategy that circumvents the problem of chemoselectivity using metallophosphites as umpolung catalysts. In this method, acyl silanes can

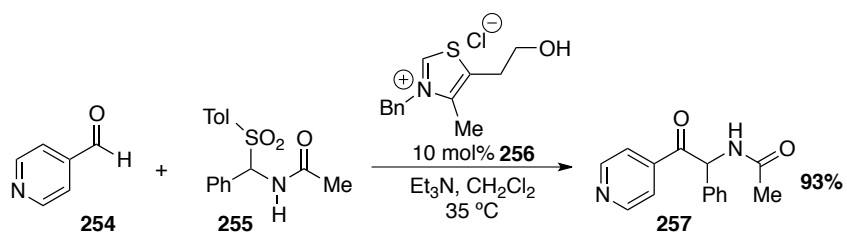
be added selectively to aldehydes to achieve silylated benzoin-type products in good enantioselectivity (Scheme 3.2).³



Scheme 3.2

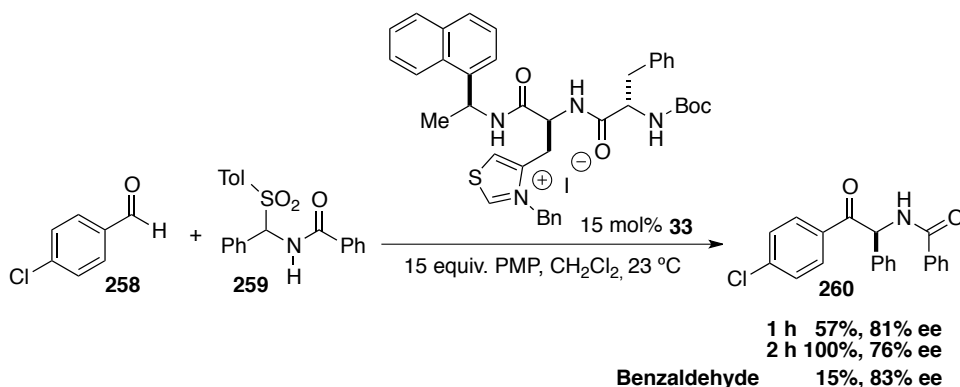
While these methods allow access to cross-benzoin products asymmetrically, the scope is still quite limited. For instance, aliphatic aldehydes and enals have still not been shown to participate efficiently.

A parallel strategy for the synthesis of differentiated benzoin-type products is the cross aza-benzoin reaction of aldehydes and imines. There are a variety of advantages to using imines as acceptors. First, the inherent difference in reactivity is greater, but it can also be easily tuned due to the trivalency of nitrogen. Furthermore, α -amido ketones are important biologically active compounds⁴ and are synthons for the ubiquitous 1,2-amino alcohol motif.⁵ The Merck group reported the first example of the aldehyde-imine aza-benzoin reaction using arylsulfonylamides as imine precursors.⁶ Under basic reaction conditions, these substrates eliminate sulfinic acid to unmask an acyl imine. A variety of aldehydes could be incorporated utilizing thiazolium salt **256** as the precatalyst (Scheme 3.3).



Scheme 3.3

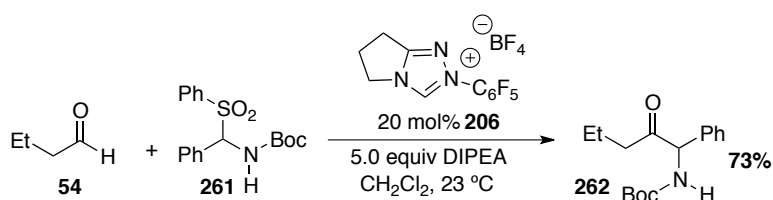
The scope of this transformation is broad and applicable to a variety of derivations of both substrates. Miller and coworkers have reported the first and only asymmetric reaction of this type, utilizing their peptide-derived thiazolium salt precatalyst **33**.⁷ Under conditions similar to that reported by the Merck group, aryl aldehydes can be coupled to aryl-acyl imines with modest enantioselectivity (Scheme 3.4). Although kinetic selectivity is moderate under these conditions, the lack of reactivity leads to extensive post-reaction epimerization, thus isolated yield and enantioselectivity are inversely proportional. Furthermore, only activated aryl aldehydes seem to participate efficiently as demonstrated by the inability to incorporate benzaldehyde effectively (Scheme 3.4).



Scheme 3.4

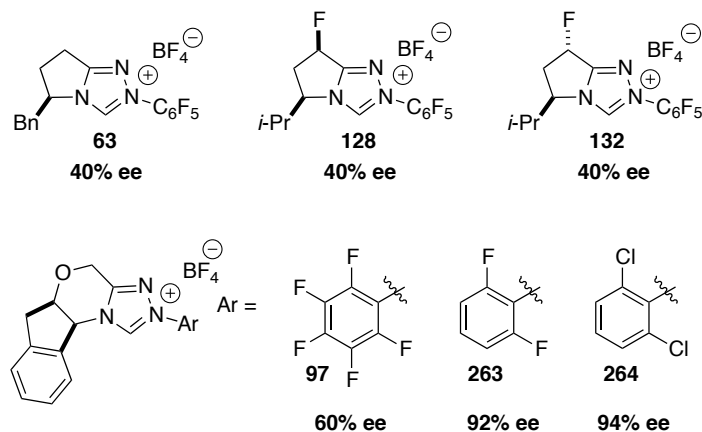
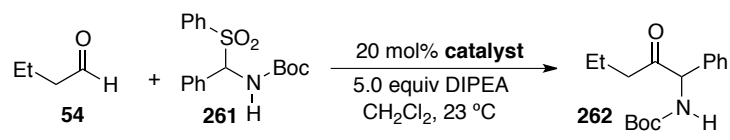
3.1.2 Catalytic Asymmetric Cross Aza-Benzoin Reactions of Aliphatic Aldehydes and *N*-Boc Imines

We envisioned that the use of aliphatic aldehydes in an aza-benzoin reaction with imines would result in α -amido ketone products that were less easily epimerized and also more synthetically useful. Initially, arylsulfonyl-carbamate **261** was used as the imine precursor with butanal **54**. Under conditions similar to that reported by the Merck group using achiral precatalyst **206**, we were able to obtain the desired amido ketone in 73% yield (Scheme 3.5).



Scheme 3.5

We were pleased to find that the desired reactivity could be obtained with *in situ* generated *N*-Boc imines since this leads to a less sensitive stereocenter in the product as well as an easily removable protecting group. An initial survey of our chiral triazolium salts revealed the pyrrolidine scaffold to be less selective in this case than the amino-indanol scaffold. All pyrrolidine based precatalysts that were examined provide kinetic selectivities of ~40% ee (Scheme 3.6). Precatalyst **97** containing the pentafluorophenyl substituent provides improved selectivities, and so this scaffold was evaluated further. By manipulating the electronics of the *N*-aryl substituent, we found that we can achieve high kinetic selectivity in the case of 2,6-difluorophenyl and 2,6-dichlorophenyl containing precatalysts **263** and **264** respectively (Scheme 3.6).

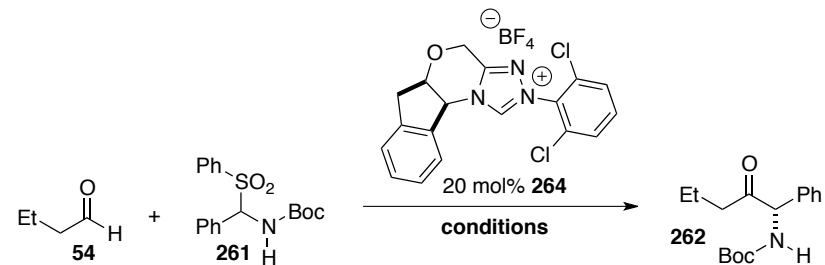


determined at ~30 min

Scheme 3.6

Unfortunately, significant erosion of enantioselectivity is observed over an extended time period, leading to 34% isolated yield in 66% ee at room temperature (Table 3.1, entry 1). Weaker bases such as sodium acetate are effective at reducing epimerization, but do not lead to an increase in yield. Lowering the temperature below 0 °C results in complete suppression of epimerization, while providing better isolated yield (Table 3.1, entry 4). Switching to a bulkier amine base (PMP) and further lowering the temperature produces higher enantioselectivity but at the expense of yield.

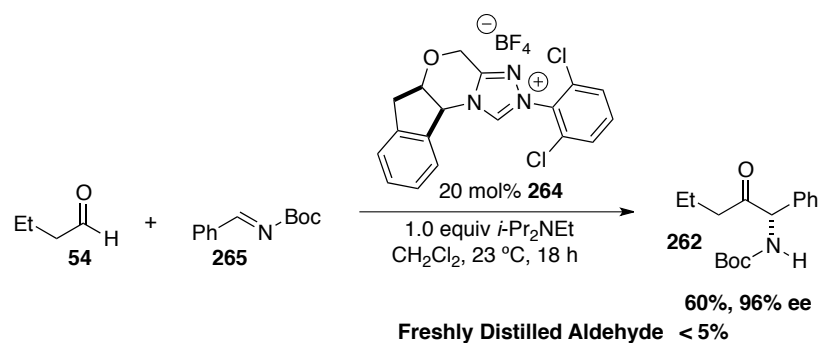
Table 3.1



Entry	Base	Equiv	Temp (°C)	Time	Yield (%) ^b	ee (%) ^c
1.	<i>i</i> -Pr ₂ NEt	2.0	23 °C	18 h	34%	66%
2.	NaOAc	2.0	23 °C	18 h	31%	86%
3.	<i>i</i> -Pr ₂ NEt	2.0	0 °C	45 min	28%	96%
4.	<i>i</i> -Pr ₂ NEt	2.0	-5 °C	18 h	60%	94%
5.	PMP	1.2	-10 °C	18 h	50%	97%
6.	PMP	2.5	-10 °C	40 h	65%	93%

^a Reactions conducted with 1.5 equiv **54** and 1.0 equiv **261**. ^b Isolated yield after chromatography. ^c Enantiomeric excess determined by HPLC analysis on a chiral stationary phase.

We recognized that epimerization was most likely base induced, but use of sulfonylamides precursors requires the addition of super stoichiometric amounts of base for *in situ* release of the imine. Literature precedent suggested that the use of the acylimine directly would result in decomposition or catalyst death. With this in mind, we decided to investigate use of the imine directly, which negated the requirement for super stoichiometric quantities of base. Subjecting imine **265** to the standard reaction conditions using just 1.0 equivalent of Hünig's base results in comparable results to that obtained with imine precursor **261** (Scheme 3.7). While we were pleased to find that the desired reactivity could be realized using the imine directly, we found the reaction to be irreproducible. The source of this irreproducibility was traced to the purity of the aldehyde. Using freshly distilled butanal under the same conditions provides only trace amounts of the desired product. Analysis of commercial butanal reveals butyric acid as the main impurity, which was then evaluated as an additive in the reaction



Scheme 3.7

Addition of just 20 mol% of acetic acid completely restores reactivity and provides the product in an improved 91% yield and 90% ee (Table 3.2, entry 1). Although we were unsure of the exact role of the acid it seemed necessary for catalyst turnover. We evaluated a variety of acid/base combinations to identify optimal conditions. Switching to the bulkier PMP as base and lowering the temperature led to better enantioselectivity, but at the cost of yield. Acid additives of varying acidity were examined which showed that acetic acid was most efficient. Other acids such as benzoic and pivalic were competent, but provided no improvement in yield.

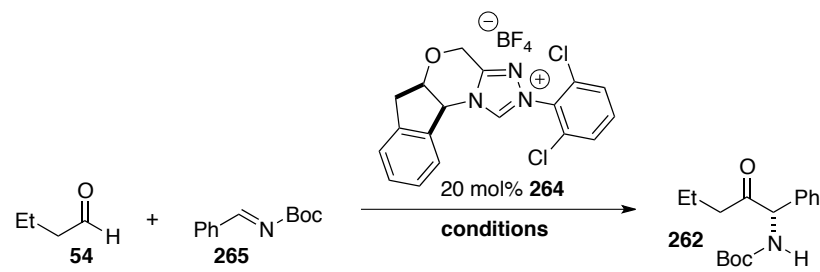
Table 3.2

Entry	Base	Equiv	Additive	Equiv	Temp (°C)	Time	Yield (%) ^b	ee (%) ^c
1.	<i>i</i> -Pr ₂ NEt	1.0	AcOH	0.2	-5 °C	18 h	91%	90%
2.	PMP	1.0	BzOH	0.2	-10 °C	18 h	53%	96%
3.	PMP	1.0	PivOH	0.2	-10 °C	18 h	93%	86%
4.	PMP	0.5	PivOH	0.5	-10 °C	18 h	70%	89%
5.	PMP	1.0	BzOH	1.0	-10 °C	18 h	45%	95%
6.	PMP	1.0	BzOH	0.5	-10 °C	18 h	45%	96%

^a Reactions conducted with 1.5 equiv **54** and 1.0 equiv **265**. ^b Isolated yield after chromatography. ^c Enantiomeric excess determined by HPLC analysis on a chiral stationary phase.

It was at this point that we began to examine to use of acetate bases, as deprotonation of the azolium salt would generate catalytic amounts of acid *in situ*. Sodium acetate proved to be effective at generating the product in excellent enantioselectivity (99% ee) albeit with only modest yield. Switching to a more soluble acetate source such as cesium acetate significantly improved reactivity when used in a stoichiometric quantity (Table 3.3, entry 4). Carbonate bases were also effective, but provided diminished results. It was later found that lowering the temperature to -20 °C while adding molecular sieves afforded the best combination of reactivity and enantioselectivity, hence, this was established as the optimal conditions (Table 3.3, entry 5). Further lowering the temperature leads to an observable increase in enantioselectivity, but at the expense of yield.

Table 3.3



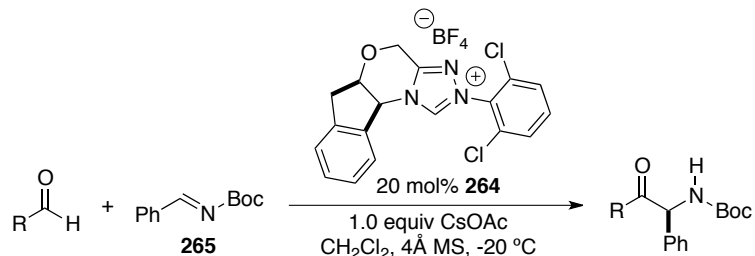
Entry	Base	Equiv	Temp (°C)	Time	Yield (%) ^b	ee (%) ^c
1.	NaOAc	1.0	0 °C	24 h	33%	99%
2.	CsOAc	0.2	-10 °C	24 h	55%	94%
3.	Cs ₂ CO ₃	0.2	-10 °C	24 h	45%	99%
4. ^d	CsOAc	1.0	-10 °C	24 h	83%	90%
5. ^d	CsOAc	1.0	-20 °C	24 h	89%	96%
6. ^d	CsOAc	1.0	-25 °C	24 h	68%	97%
7. ^d	CsOAc	1.0	-30 °C	24 h	61%	98%

^a Reactions conducted with 1.5 equiv **54** and 1.0 equiv **265**. ^b Isolated yield after chromatography. ^c Enantiomeric excess determined by HPLC analysis on a chiral stationary phase. ^d 4Å molecular sieves were added.

With optimized conditions in hand we began to evaluate the scope of this reaction. A variety of aliphatic aldehydes were examined, containing a diverse range of functionality. Straight-chain

aldehydes produce the desired products in high yield and excellent enantioselectivity. β -Branched aldehydes, such as isovaleraldehyde participate with high enantioselectivity, albeit in low yield (Table 3.4, entry 4). Heteroatoms can be incorporated into the tether without deleterious impact of yield or enantioselectivity, allowing for the incorporation of functionality such as thioethers, imides, and esters. Under these conditions we have found α -branched aldehydes to be unsuitable substrates. It should also be mentioned that only aliphatic aldehydes participate, enals and aryl aldehydes do not afford amido ketone products.

Table 3.4



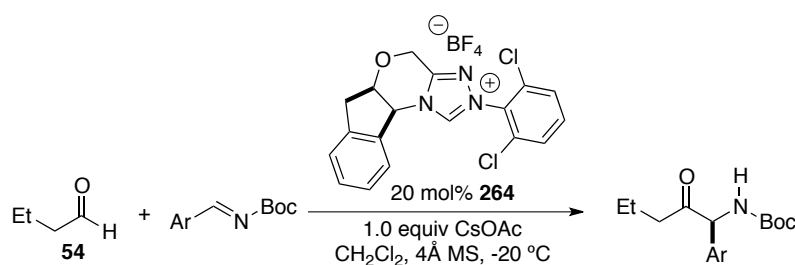
Entry	Aldehyde	Product	Yield (%) ^b	ee (%) ^c
1.		262	89%	96%
2.		266	90%	96%
3.		267	86%	84%
4.		268	33%	98%
5.		269	62%	91%
6.		270	83%	88%
7.		271	71%	92%
8.		272	72%	96%
9.		273	93%	93%
10.		274	< 5%	–

^a Reactions conducted with 1.5 equiv aldehyde and 1.0 equiv **265**. ^b Isolated yield after chromatography. ^c Enantiomeric excess determined by HPLC analysis on a chiral stationary phase.

The scope of the *N*-acyl imine electrophile is limited to aryl substitution but leads to fairly invariant results thereof. Electron rich and electron poor arenes provide both high yield and

excellent enantioselectivity (Table 3.5). The methylenedioxy motif, common to many biologically relevant molecules, can be incorporated with good results. Heterocycles, such as furan are tolerated; however, low enantioselectivity is observed in this case, most likely due to rapid epimerization in the presence of an internal hydrogen bond acceptor. A surprising limitation is that the use of ortho-substituted arenes leads to an almost complete loss of reactivity.

Table 3.5

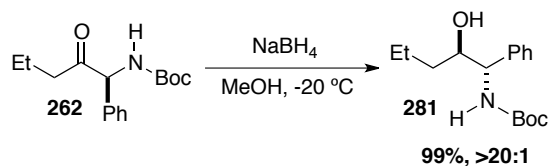


Entry	Imine	Product	Yield (%) ^b	ee (%) ^c
1.		262	89%	96%
2.		275	74%	90%
3.		276	84%	96%
4.		277	83%	96%
5.		278	72%	94%
6.		279	<5%	—
7.		280	66%	60%

^a Reactions conducted with 1.5 equiv **54** and 1.0 equiv imine. ^b Isolated yield after chromatography. ^c Enantiomeric excess determined by HPLC analysis on a chiral stationary phase.

Absolute stereochemistry of the amido ketone products has been assigned based on analogy to those reported in the literature.⁸

To demonstrate the utility of these products we sought to reduce the ketone selectively. Reduction of **262** with NaBH₄ in methanol provides the anti-aminoalcohol **281** in quantitative yield as a single diastereomer (Scheme 3.8).

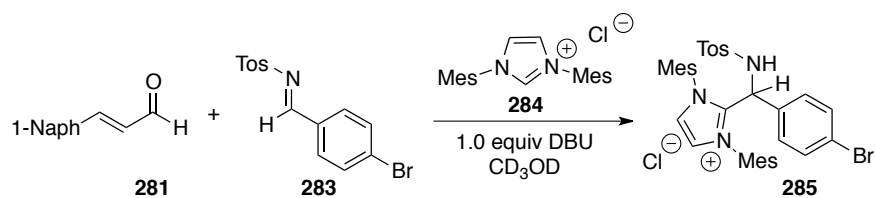


Scheme 3.8

We attempted to use bulkier reducing agents with non-labile groups in hopes of obtaining the syn-diastereomer selectively. Unfortunately, only a 1:1 diastereomeric ratio of the syn/anti products could be obtained.

3.1.3 The Role of the Carboxylic Acid

We were initially unsure of the role of the carboxylic acid additive in providing better catalyst turnover. Initially we hypothesized that the acid might be activating the acyl imine toward nucleophilic addition, based on precedent from our own group⁹ and others.¹⁰ However, we were unable to observe any enantioselectivity in the presence of chiral acids. A second hypothesis involved the reactivity of our carbene catalyst toward imines. Evidence for the addition of nucleophilic carbenes to imines has been reported in the literature. Bode and coworkers demonstrated that the combination of *N*-tosyl imine **283** and imidazolium salt precatalyst **284** results in complete conversion to species **285**, a protonated Breslow intermediate (Scheme 3.9). In this case, this interaction leads to catalyst death and is not shown to be reversible.



Scheme 3.9

We realized this type of adduct may be formed under our reaction conditions and wondered if acid could be a source of catalyst turnover (*vide infra*). With a more electron deficient triazolylidene carbene this protonated intermediate could eliminate the carbene, reforming the imine (Figure 3.1).

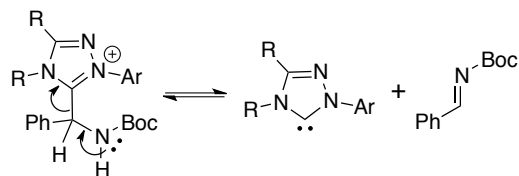
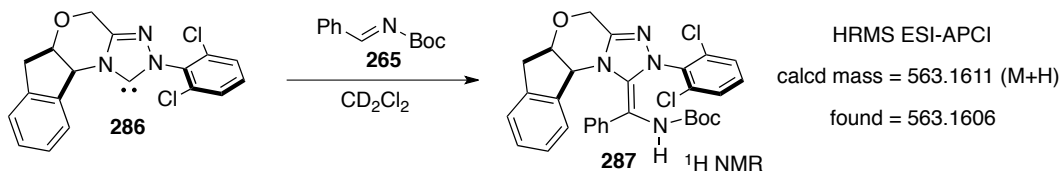


Figure 3.1

We performed an NMR experiment to investigate the interaction of our carbene derived from triazolium salt **264**, and *N*-Boc imine **265**. Triazolium salt precatalyst **264** was deprotonated with excess KO^tBu in dichloromethane-*d*₄ to provide free carbene **286**, observable by ¹H NMR. The addition of a solution of imine **265** in dichloromethane-*d*₄ immediately affords a bright-yellow solution, with complete disappearance of carbene **286**. Both ¹H NMR and HRMS analysis of this solution suggest the species to be aza-Breslow intermediate **287** (Scheme 3.10).



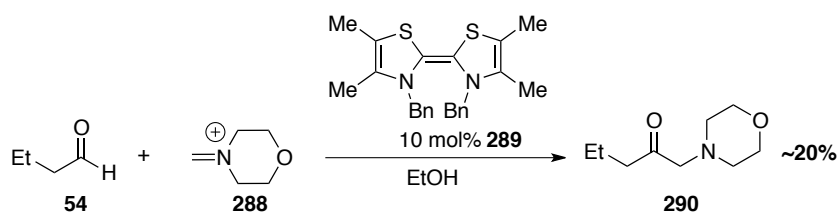
Scheme 3.10

Furthermore, addition of excess acetic acid instantly regenerates a colorless solution with complete disappearance of **287** by NMR. This experiment provides strong evidence that aza-Breslow intermediates are the resting state of the catalyst in this system and that catalytic acid is allowing for its regeneration.

3.2 Addition of Acyl Anion Equivalents to Iminium Salts

3.2.1 Introduction

During our investigation of the aza-Benzoin reaction of aliphatic aldehydes and *N*-Boc imines, we wondered if other electrophiles such as iminium ions could be used instead. The use of these intermediates poses a potential liability due to their high electrophilicity in comparison to aldehydes. This being said, a thiazolylidene carbene-catalyzed synthesis of α -amino ketones from aldehydes and iminium salts has been reported in the literature.¹¹ In this study, iminium salts derived from formaldehyde are used as electrophiles, with aryl and aliphatic aldehydes as the nucleophilic coupling partners. Exposing butanal **54** to a pregenerated solution of iminium salt **288** in the presence of bis-thiazolylidene **289** provides the desired α -amino ketone in modest yield (Scheme 3.11). No subsequent studies of this transformation have been reported.

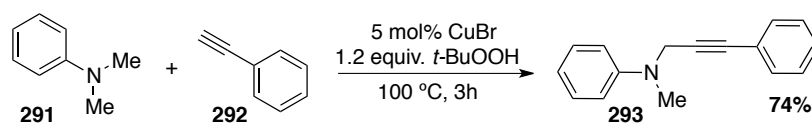


Scheme 3.11

We were interested in the use of α -substituted iminium salts, as to set a stereocenter during the C-C bond-forming event. Given the low yields obtained in the previous report it seemed

reasonable that catalyst turnover may be a problematic; hence, we sought to find a parallel method for slow generation of iminium ions *in situ*.

A convenient and reliable method for the generation of iminium ions *in situ* directly from amines is by SET (single electron transfer). Many methods rely on the use of a transition-metal catalyst in combination with a stoichiometric oxidant to afford the desired oxidation. This method has proven useful in the development of cross-dehydrogenative coupling reactions of amines, pioneered by the Li group.¹² In a seminal example, dimethyl aniline **291** is coupled directly with a terminal alkyne in the presence of CuBr and *t*-BuOOH as the stoichiometric oxidant (Scheme 3.12).

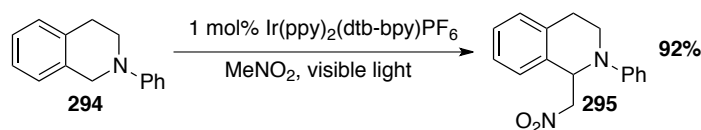


Scheme 3.12

Although much work has been done in this area to develop asymmetric variants, only recently has a highly enantioselective example been reported.¹³ Given the need for a strong oxidant, a transition-metal catalyst and high temperatures, we were concerned that these conditions would not be amenable to carbene catalysis.

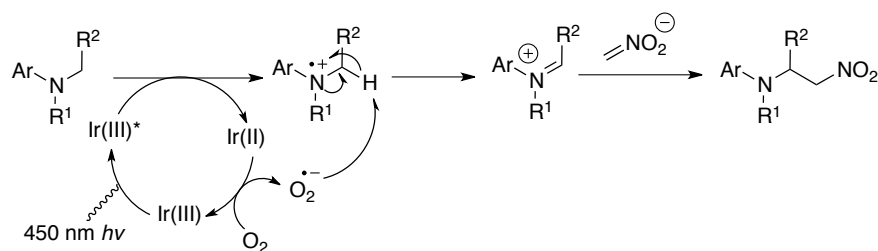
A milder alternative for the generation of iminium ions from tertiary amines is by means of photoredox catalysis. The concept of using light for chemical synthesis has been realized since the early 20th century.¹⁴ Photoredox catalysis, which takes advantage of the unique photophysical properties of organic molecules and organometallic complexes, has been used for decades, but only recently have chemists taken advantage of these properties to solve long-standing problems in organic synthesis.¹⁵ An initial report by Stephenson and coworkers shows that tertiary amines can be activated using a combination of a metal photocatalyst, in this case Ru(bpy)₃Cl₂ or

$\text{Ir}(\text{ppy})_2(\text{dtb-bpy})\text{PF}_6$, and visible light.¹⁶ This manifold generates iminium ions *in situ*, which are trapped with nitroalkanes in an oxidative aza-Henry type process (Scheme 3.13).



Scheme 3.13

The mechanism of amine oxidation is generally proposed to proceed as follows: first excitation of $[\text{Ir}(\text{ppy})_2(\text{dtb-bpy})]^+$ by visible light irradiation, populates the $[\text{Ir}(\text{ppy})_2(\text{dtb-bpy})]^{+*}$ excited state via metal to ligand charge transfer (MLCT). This excited state complex is a sufficient oxidant (+ 0.66 V vs SCE) to oxidize a tertiary amine amine (+ 0.73 V vs SCE for Et_3N) leading to an amine radical cation. Hydrogen atom abstraction reveals an iminium ion that is trapped with a suitable nucleophile (Scheme 3.14).¹⁷



Scheme 3.14

The authors note in this report that the reaction can be run without the presence of oxygen, as long as nitromethane is used as solvent. This provides evidence that nitro compounds may also play a role in catalyst turnover by functioning as the terminal oxidant. The use of visible light photoredox catalysis to generate these reactive species is attractive in the sense that no pre-activation of the substrate is required and reaction conditions are mild, thereby allowing for potential compatibility between multiple catalytic pathways.

3.2.2 Results

We envisioned the union of chiral *N*-heterocyclic carbene catalysis of aldehydes with visible light photoredox catalysis of tertiary amines could be achieved, resulting in a direct asymmetric α -acylation of tertiary amines (Figure 3.2).

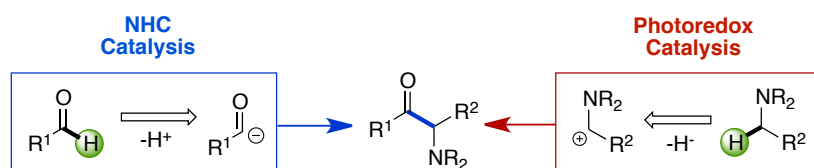


Figure 3.2

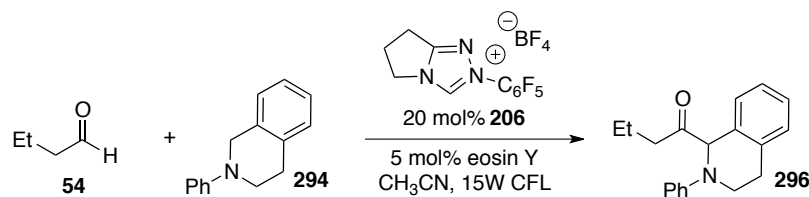
The anticipated coupling reaction would rely on two chemically distinct activation pathways, forming a C-C bond asymmetrically while producing H_2 (in the form of H_2O in the presence of a weak oxidant) as the only byproduct. The biological relevance of these products as well as the synthetic utility of the derived 1,2-aminoalcohols makes this a desirable transformation.

At the onset of this investigation we realized a few caveats of this approach. First, oxidation of a tertiary amine would be in direct competition with oxidation of our triazolylidene carbenes, containing three nitrogen atoms, a likely pathway for catalyst decomposition. Also, these highly reactive iminium ions could interfere with catalyst turnover, as mentioned earlier. Despite these potential complications we began to investigate the direct coupling of aliphatic aldehydes with tertiary amines.

Our studies focused on tetrahydroisoquinoline **294** as the amine substrate due to its proven ability to be oxidized using visible light photoredox catalysis, with butanal **54**. Organic photocatalysts were chosen initially out of concern for the potential compatibility issues of NHC's with transition metals complexes. Exposing butanal **54** and tetrahydroisoquinoline **294** to 5 mol% of eosin Y in the presence of achiral NHC precatalyst **206** and light showed trace amounts of product when stoichiometric amine bases were used (Table 3.6). We were pleased to

find that decreasing the stoichiometry of the base significantly improved conversion to the desired amino ketone **296**. Inorganic bases such as cesium carbonate were not effective.

Table 3.6

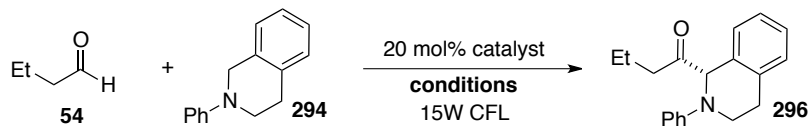


Entry	Base	Equiv	Conversion ^b
1.	<i>i</i> -Pr ₂ NEt	1.0	< 5%
2.	<i>i</i> -Pr ₂ NEt	0.2	35%
3.	Cs ₂ CO ₃	0.2	< 5%

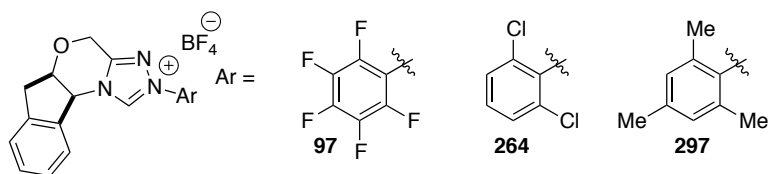
^a Reactions conducted with 1.5 equiv **54** and 1.0 equiv **294**. ^b Conversion based on ¹H NMR.

With conditions that allowed for the formation of amino ketone **296** in hand, we were interested in evaluating the prospect of an asymmetric transformation. The use of aminoindanol-derived precatalyst **97** provides the product in low yield and a modest 40% ee (Table 3.7). Precatalyst **264** containing the 2,6-dichlorophenyl substituent leads to better yield and promising enantioselectivity. More electron-rich catalysts such as **297**, do not provide any of the desired product. Acetate bases can be employed which leads to improved reactivity, while changing to a less polar solvent (DCE) has almost no effect on the outcome of the reaction. At this point we wanted to evaluate more efficient photocatalysts in hopes of attaining better yields, as the amine was not being completely consumed under the reaction conditions. Use of Ru(bpy)₃Cl₂ as the photocatalyst did provide a slight increase in yield but with a substantial increase in enantioselectivity (Table 3.7, entry 6).

Table 3.7



Entry	Catalyst	Base	Solvent	Photocat.	Yield (%) ^b	ee (%) ^c
1.	97	<i>i</i> -Pr ₂ NEt	CH ₃ CN	Eosin Y	14%	40%
2.	264	<i>i</i> -Pr ₂ NEt	CH ₃ CN	Eosin Y	30%	68%
3.	297	<i>i</i> -Pr ₂ NEt	CH ₃ CN	Eosin Y	< 5%	–
4.	264	NaOAc	CH ₃ CN	Eosin Y	36%	66%
5.	264	<i>i</i> -Pr ₂ NEt	DCE	Eosin Y	32%	68%
6.	264	<i>i</i> -Pr ₂ NEt	CH ₃ CN	Ru(bpy) ₃ Cl ₂	43%	78%

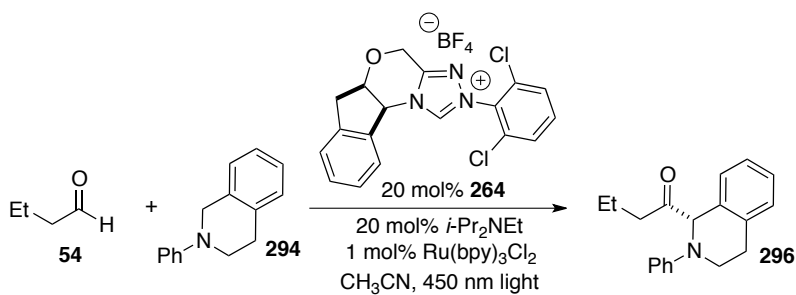


^a Reactions conducted with 1.5 equiv **54** and 1.0 equiv **294**. ^b Isolated yield after chromatography. ^c Enantiomeric excess determined by HPLC analysis on a chiral stationary phase.

We were pleased with the higher enantioselectivity obtained using Ru(bpy)₃Cl₂ as the photocatalyst but unfortunately this transformation still suffered from low yield. Given that Ru(bpy)₃Cl₂ is known to be a competent photocatalyst in this system, we focused on the choice of oxidant. Until this point all reactions had been run open to the atmosphere using oxygen as the terminal oxidant. In the oxidative aza-Henry reaction reported by Stephenson and coworkers, aliphatic nitro compounds were proposed to be involved in the oxidative regeneration of [Ru(bpy)]²⁺. We knew that introduction of a nitroalkane to our system would likely produce aza-Henry products, consuming our starting material. Nitroarenes are better oxidants and non-nucleophilic sources of the nitro group; therefore, we examined them as additives in our system. We also began using a blue LED lamp (~450 nm) as the light source since Ru(bpy)₃Cl₂ absorbs strongly at this wavelength. In a closed system, 4-nitrotoluene (E_{ox} = -0.50 V vs SCE) was first

evaluated as an additive, which provides improved results and validated our hypothesis (Table 8).¹⁸ Addition of the stronger oxidant 1,3-dinitrobenzene (*m*-DNB) ($E_{\text{ox}} = -0.345 \text{ V vs SCE}$) leads to the best results and affords good isolated yield of the desired product (Table 3.8, entry 4). Even catalytic amounts of *m*-DNB in combination with ambient oxygen can affect the desired reactivity.

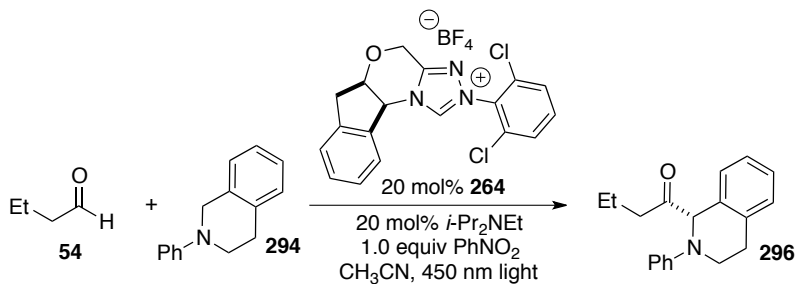
Table 3.8



Entry	Additive	Equiv.	Temp (°C)	Yield (%) ^b	ee (%) ^c
1.	none	–	23 °C	43%	78%
2.	4-nitrotoluene	2.0	23 °C	64%	78%
3.	1,3-dinitrobenzene	1.0	23 °C	75%	78%
4.	1,3-dinitrobenzene	1.2	0 °C	84%	78%
5. ^d	1,3-dinitrobenzene	1.0	23 °C	67%	75%
6. ^d	1,3-dinitrobenzene	0.1	23 °C	72%	72%

^a Reactions conducted with 1.5 equiv **54** and 1.0 equiv **294**. ^b Isolated yield after chromatography. ^c Enantiomeric excess determined by HPLC analysis on a chiral stationary phase. ^d run open to the atmosphere

While good yields can be obtained using this catalyst system, we were still not achieving complete consumption of starting material and we thought that using a more active photocatalyst might be advantageous. The cyclometalated iridium (III) catalyst $[\text{Ir}(\text{ppy})_2(\text{dtb-bpy})]\text{PF}_6$ was prepared and examined in our reaction. Using nitrobenzene as the oxidant in the presence of $\text{Ru}(\text{bpy})_3\text{Cl}_2$ we observe ~70% conversion by NMR with 72% of the desired product present (Table 3.9). Use of $[\text{Ir}(\text{ppy})_2(\text{dtb-bpy})]\text{PF}_6$ results in complete consumption of starting material, however with no benefit to the yield of desired product.

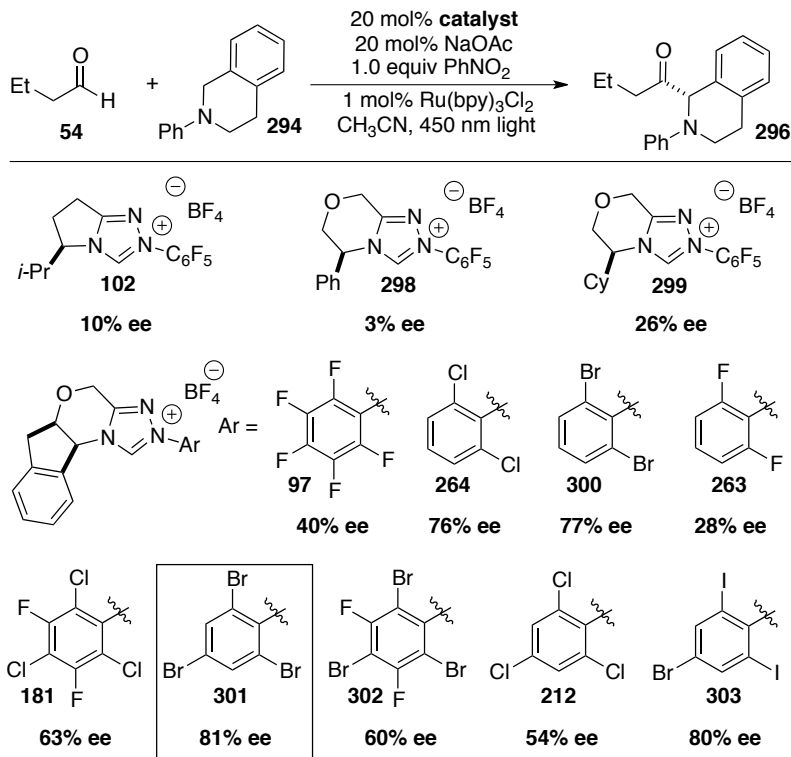
Table 3.9

Entry	Photocatalyst	Conversion (%) ^b	Yield (%) ^c	ee (%) ^d
1.	Ru(bpy) ₃ Cl ₂	70%	72%	74%
2.	[Ir(ppy) ₂ (dtb-bpy)]PF ₆	> 95%	73%	70%

^a Reactions conducted with 1.5 equiv **54** and 1.0 equiv **294**. ^b Conversion determined by ¹H NMR using an internal standard ^c Isolated yield after chromatography. ^d Enantiomeric excess determined by HPLC analysis on a chiral stationary phase.

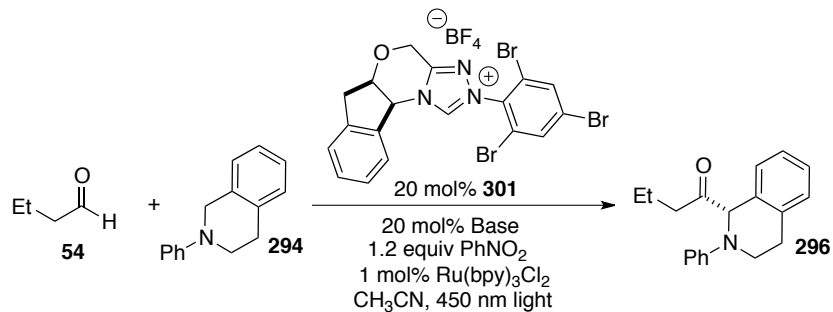
With yields at a satisfactory level we turned our attention to the problem of selectivity. Optimal precatalyst **264** only delivers the product in a modest 78% ee under ideal conditions. This prompted us to perform an extensive catalyst study, using all scaffolds currently known, as well as exhaustive derivatization of the amino-indanol derived catalyst's *N*-aryl substituent. Since the amino acid based precatalysts **102**, **298**, and **299** provide poor selectivities in all cases (Chart 3.1), it seemed that further development of the amino-indanol scaffold would be necessary. After our initial investigation, a sensitive balance between sterics and electronics of the *N*-aryl substituent became apparent. Merely changing the 2,6-dichlorinated derivative **264**, which was previously the most selective, to the smaller 2,6-difluorinated precatalyst **263** leads to almost complete loss of selectivity. To further investigate aryl derivatives containing bulkier halogen substituents, we examined precatalyst **181**, previously employed in the Stetter reaction. Although this catalyst does contain *ortho*-chloro substituents the increased electron deficiency leads to a decrease in selectivity. We eventually identified the 2,4,6-tribromophenyl derivative **301** to be optimal, albeit providing only marginally better selectivity (81% ee).

Chart 3.1



^a Enantioselectivity determined by HPLC analysis on a chiral stationary phase of the crude reaction mixture.

Using this optimal catalyst we also examined the effect that base has on enantioselectivity. Acetate bases provided lower selectivities than amine bases in initial studies, so a variety of amine bases were screened. All tertiary amines show a beneficial impact on selectivity, while HMDS provides somewhat inferior results (Table 3.10).

Table 3.10

Entry	Base	ee (%)
1.	NaOAc	81%
2.	Et ₃ N	85%
3.	<i>i</i> -Pr ₂ NEt	85%
4.	PMP	85%
5.	HMDS	78%

^a Enantioselectivity determined by HPLC analysis on a chiral stationary phase of the crude reaction mixture.

In all cases, less than 10% conversion is observed using precatalyst **301** under optimized conditions. Although reactions using precatalyst **301** are homogenous after a few minutes, small amounts of a yellow precipitate are observed over the course of the reaction, accompanied by noticeable stalling of the reaction. This precipitate was presumed to be a catalyst decomposition pathway, possibly from oxidation by the photocatalyst. Initial isolation and characterization by ¹H NMR confirmed our suspicion that it was catalyst derived; however, the exact structure was unable to be determined via this method. Crystallization and analysis by X-ray crystallography reveals the species to be aza-Breslow intermediate **304** derived from the addition of the active catalyst to the *in situ* formed iminium ion (Figure 3.3).

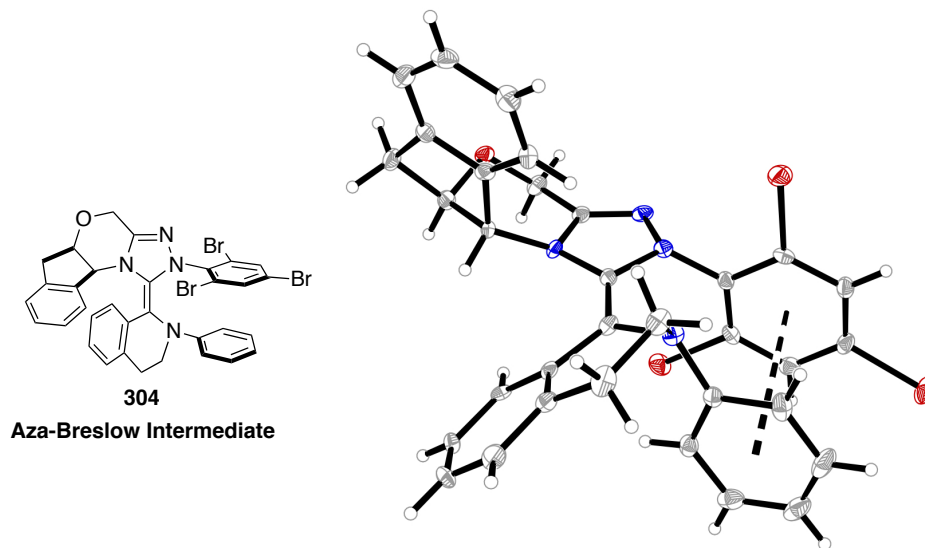
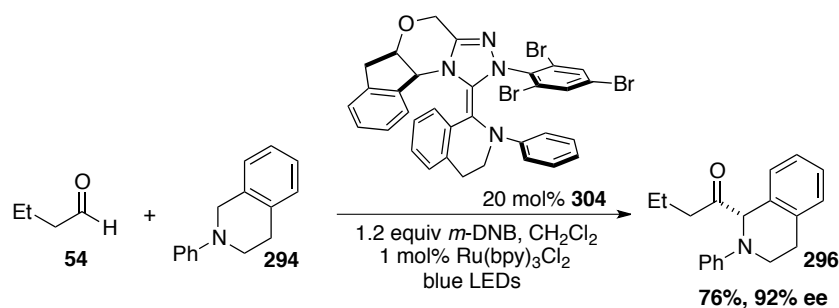


Figure 3.3

While the isolation of this type of intermediate is interesting from a theoretical standpoint, we were unsure if this is a catalyst deactivation pathway that is ultimately prohibiting the productive pathway. To test this hypothesis, we resubjected a catalytic amount of aza-Breslow intermediate **304** to the reaction conditions but using dichloromethane as the solvent to increase its solubility. We were delighted to find that not only is aza-Breslow intermediate **304** a competent precatalyst, it also provides excellent enantioselectivity under the modified conditions (Scheme 3.15).

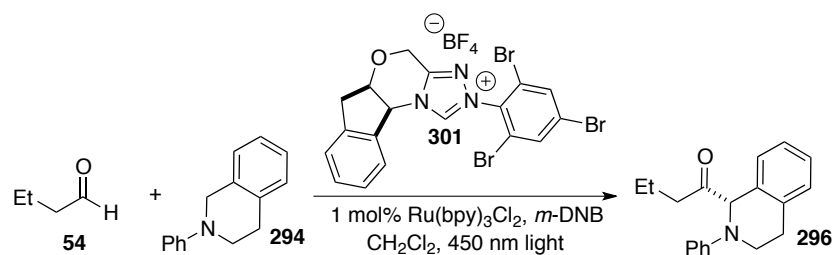


Scheme 3.15

It should be noted that our original solvent screen ruled out chlorinated solvents as superior for previous catalysts.

Using dichloromethane as the solvent we began a reoptimization study to find suitable conditions in the new solvent. Both sodium acetate and Hünig's base provide better yields and higher selectivities than were obtained earlier in acetonitrile (Table 3.11). Employing free carbene conditions, by first deprotonating the azolium salt with sodium hydride, leads to optimal enantioselectivity. Furthermore, extending the reaction time was found to provide full conversion of the amine, and leads to greatly improved yields. The relatively high catalyst loading of triazolium salt used for preliminary studies can also be reduced to 5 mol% without deleterious impact on reaction efficiency.

Table 3.11



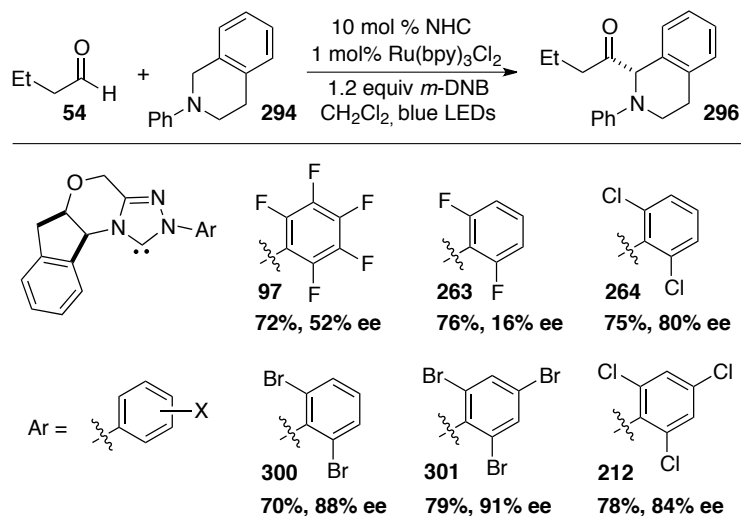
Entry	mol % Cat.	Base	Equiv <i>m</i> -DNB	Time	Conv. ^b	Yield (%) ^c	ee (%) ^d
1.	20 %	NaOAc	1.2	24 h	88%	66%	90%
2.	20 %	<i>i</i> -Pr ₂ NEt	1.2	24 h	80%	41%	90%
3.	20 %	NaH	1.2	24 h	89%	65%	92%
4.	20 %	NaH	0.1	24 h	85%	60%	90%
5.	20 %	NaH	1.2	40 h	100%	84%	91%
6.	10 %	NaH	1.2	40 h	100%	79%	91%
7.	5 %	NaH	1.2	40 h	100%	80%	92%

^a Reactions conducted with 1.5 equiv **54** and 1.0 equiv **294**. ^b Conversion determined by ¹H NMR using an internal standard ^c Isolated yield after chromatography. ^d Enantiomeric excess determined by HPLC analysis on a chiral stationary phase.

To ensure that precatalyst **301** was in fact the best catalyst under these conditions, we reevaluated a variety of other precatalysts. In this case, 2,6-dibromo-derivative **300** and 2,4,6-trichloro-derivative **212** turned out to be competent precatalysts; however, precatalyst **301** is still optimal (Table 3.12). Control experiments show the necessity for both *m*-DNB and Ru(bpy)₃Cl₂ to be present. Exclusion of *m*-DNB from the reaction mixture results in only trace amounts of

product. Removal of Ru(bpy)₃Cl₂, although deleterious, does not completely shutdown reactivity. In this case it is possible that *m*-DNB is acting as a weak sensitizer.¹⁹ While use of a 15 W fluorescent light results in a slight decrease in yield, rigorous exclusion of light results in only 5% of the desired product.

Table 3.12



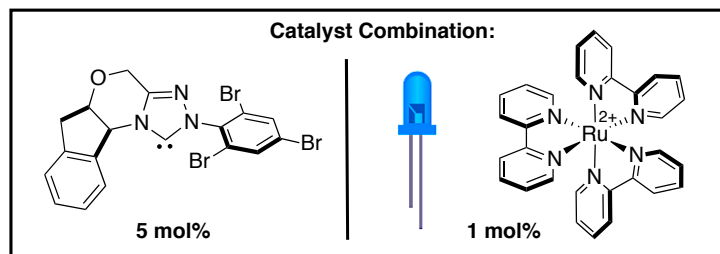
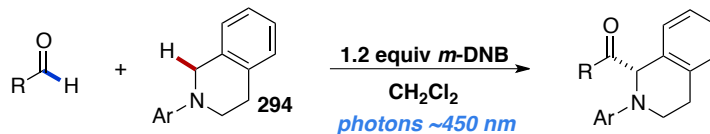
Entry	dev. from standard conditions	conv % ^a	yield % ^b	ee % ^c
1.	No Ru(bpy) ₃ Cl ₂	47%	32%	90%
2.	No <i>m</i> -DNB	46%	13%	88%
3.	No light	19%	5%	90%
4.	15 W fluorescent light	89%	63%	90%
5.	CH ₃ CN as solvent	>95%	12%	70%
6.	Precatalyst w/ no base	>95%	78%	88%
7.	Degassed (Ar)	>95%	75%	87%
8.	Open to air	>95%	46%	92%

^a Reactions conducted with 1.5 equiv **54** and 1.0 equiv **294**. ^b Conversion determined by ¹H NMR using an internal standard ^c Isolated yield after chromatography. ^d Enantiomeric excess determined by HPLC analysis on a chiral stationary phase.

Under the optimized conditions, a variety of aliphatic aldehydes react efficiently, affording the desired α -amino ketones in good yield and high enantioselectivity (Table 3.13). Like we have previously observed, α -branched aldehydes do not participate, while smaller aldehydes such as

acetaldehyde (Table 3.13, entry 3) and cyclopropane carboxaldehyde (Table 3.13, entry 4) react efficiently but with only modest selectivity.

Table 3.13



Entry	Aldehyde	Product	Yield (%) ^b	ee (%) ^c
1.		296	81%	92%
2.		305	67%	91%
3.		306	72%	62%
4.		307	61%	59%
5.		308	88%	92%
6.		309	61%	87%
7.		310	91%	92%
8.		311	79%	88%
9.		312	75%	92%
10.		313	< 5%	–

^a Reactions conducted with 1.5 equiv aldehyde and 1.0 equiv **294**. ^b Isolated yield after chromatography. ^c Enantiomeric excess determined by HPLC analysis on a chiral stationary phase.

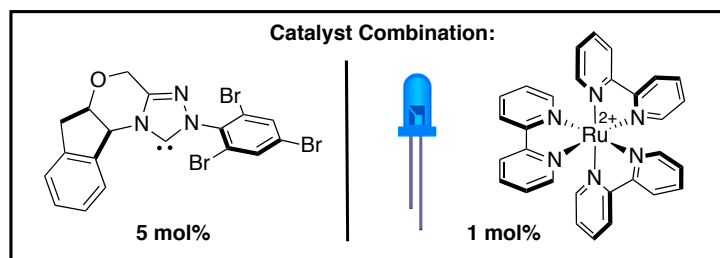
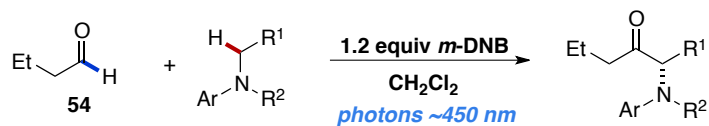
Additional functionality can also be incorporated into the aldehyde tether without deleterious effect to either efficiency or enantioselectivity, such as thioethers, esters, and protected amines.

Aryl aldehydes and enals do not provide the desired product under these conditions.

Unfortunately, the scope of the amine is more specific. This reactivity seems to be unique to tetrahydroisoquinoline derivatives. The *N*-aryl substituent can be modified slightly, to more electron releasing and electron deficient, without significant loss of reactivity (Table 3.14). Very electron-deficient groups such as 4-CF₃-phenyl provide products of competing radical dimerization products (Table 3.14, entry 5), likely due to increased acidity of the α -hydrogen.²⁰

Attempts to access simpler products derived from tetrahydropyridines, pyrrolidines, or acyclic benzylic amines, were unsuccessful (Table 3.14, entries 7-9).

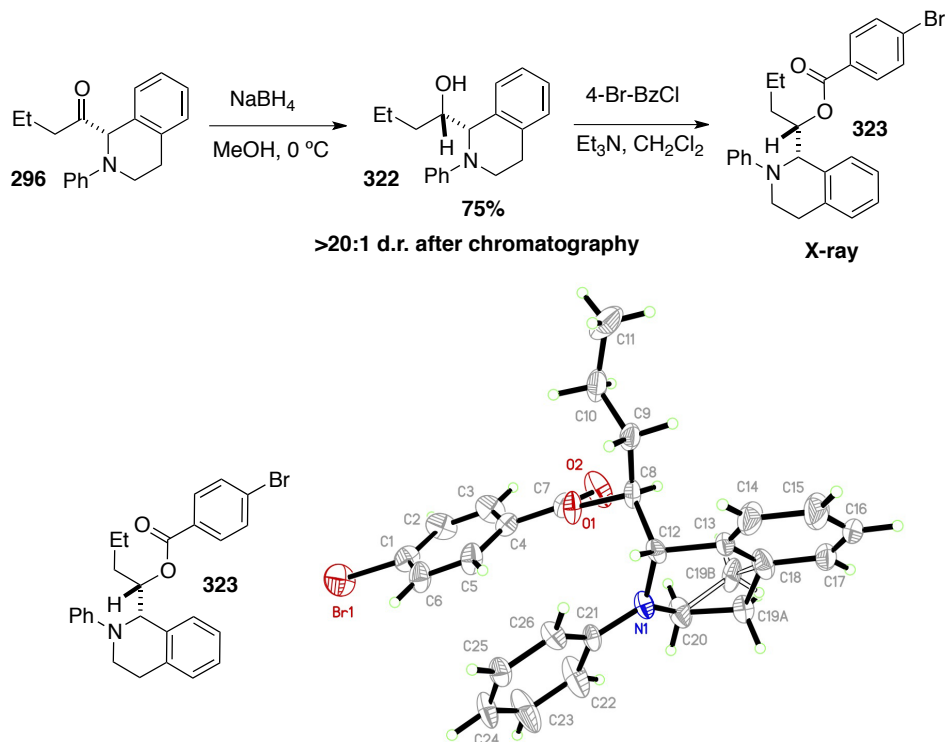
Table 3.14



Entry	Amine	Product	Yield (%) ^b	ee (%) ^c
1.		296	81%	92%
2.		314	84%	92%
3.		315	51%	90%
4.		316	54%	91%
5.		317	< 5%	—
6.		318	94%	90%
7.		319	< 5%	—
8.		320	< 5%	—
9.		321	< 5%	—

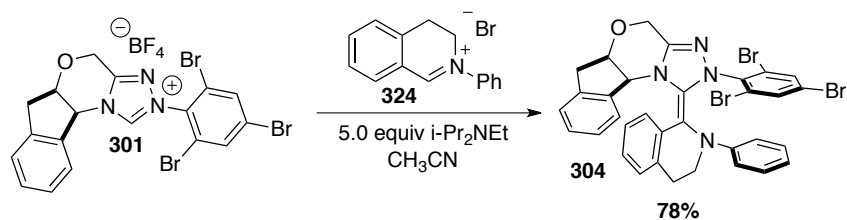
^a Reactions conducted with 1.5 equiv **54** and 1.0 equiv amine. ^b Isolated yield after chromatography. ^c Enantiomeric excess determined by HPLC analysis on a chiral stationary phase.

Further derivatization of ketone product **296** was accomplished by first reduction with NaBH₄, leading to a single diastereomer of the corresponding amino alcohol **322** after chromatography. Acylation of the alcohol with 4-Br-benzoyl chloride furnishes bromo-benzoate **323**, which was analyzed by X-ray crystallography to determine both the relative and absolute stereochemistry of these products (Scheme 3.16).



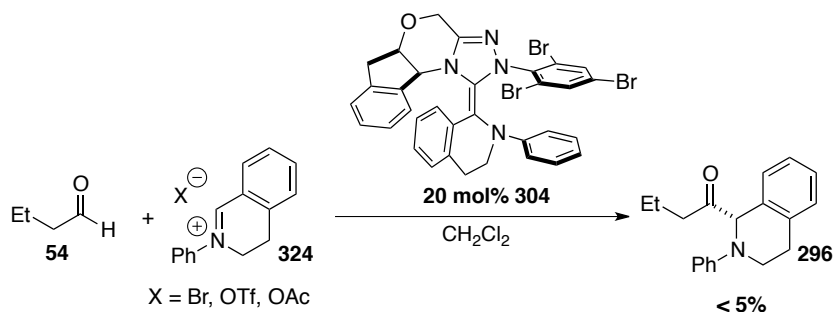
Scheme 3.16

With the initial scope of this transformation evaluated, we were interested in further understanding the mechanistic implications of isolated aza-Breslow intermediate **301**. In order to confirm that this intermediate was being generated from addition of the carbene to an iminum salt, we pregenerated iminum salt **324** and subjected it to a solution containing precatalyst **301** and Hünig's base. Under these conditions, aza-Breslow intermediate **304** crystallizes from the reaction mixture in good yield (Scheme 3.17).



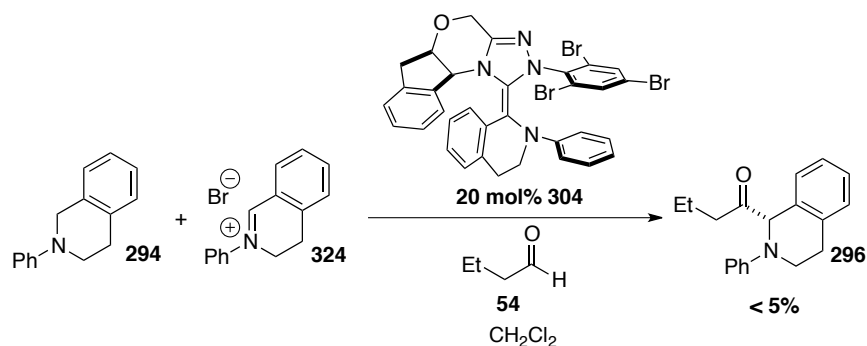
Scheme 3.17

While we had shown that this intermediate was a competent precatalyst under the reaction conditions, we were unsure of the exact mechanism of catalyst release. Subjecting aza-Breslow intermediate **304** to butanal **54** and pregenerated iminium salt, **324**, does not lead to significant formation of amino ketone **296** (Scheme 3.18), suggesting a role for the photocatalyst.



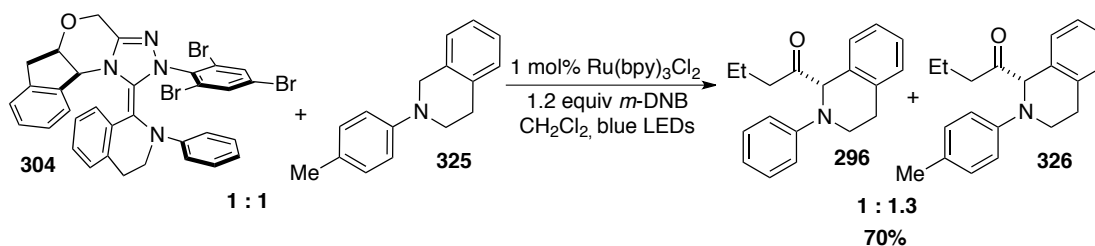
Scheme 3.18

We realized that in this experiment there is no amine starting material present. Since the presence of a base may be key in catalyst turnover, we ran the same experiment with the addition of tetrahydroisoquinoline **294**. Again, no appreciable amounts of the desired product were observed (Scheme 3.19).



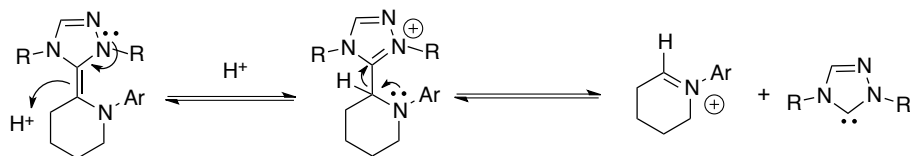
Scheme 3.19

Since exposure of the aza-Breslow intermediate to conditions containing the photoredox catalyst and light seemed to be required, we were interested in the fate of the amine derived from the Breslow intermediate. If the release were based on decomposition of this substrate we would not see any product derived from this iminium ion in a crossover experiment. Subjecting equimolar ratios of the aza-Breslow intermediate **304** and tolyl-labeled amine **325** to the reaction conditions provided a 1:1.3 ratio of the desired products in good yield, demonstrating that the fate of the amine is not decomposition (Scheme 3.20).



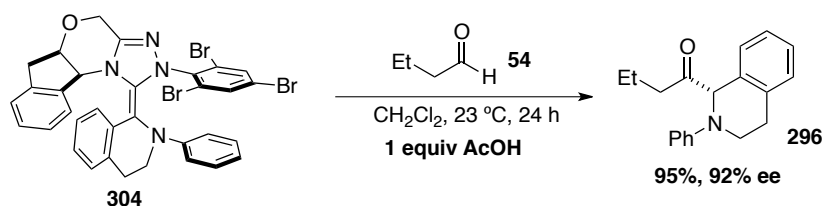
Scheme 3.20.

If the aza-Breslow intermediate is generating an iminium ion as part of its release mechanism, than it stands to reason that the active carbene is generated concurrently. It seemed reasonable that protonation of the Breslow intermediate could lead to reversibility of this event, regenerating the iminium ion and the free carbene as products (Scheme 3.21).



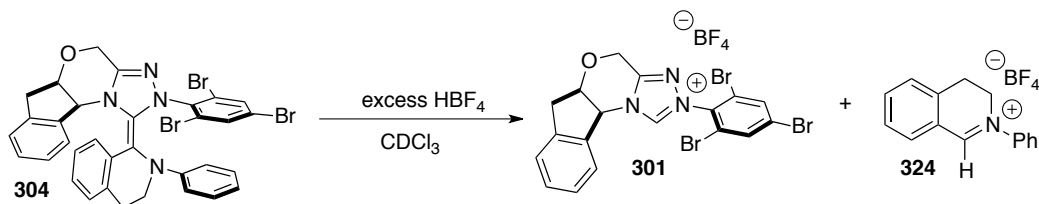
Scheme 3.21

To test this hypothesis, aza-Breslow intermediate **301** and butanal **54** were exposed to 1.0 equivalent of acetic acid in dichloromethane (Scheme 3.22). After 24 h, 95% of the desired amino ketone was obtained in excellent enantioselectivity, consistent with our hypothesis.



Scheme 3.22

Furthermore, addition of excess HBF_4 to a solution of **304** in CDCl_3 results in the formation of azolium salt **301** and iminium salt **324** by ^1H NMR (Scheme 3.23).

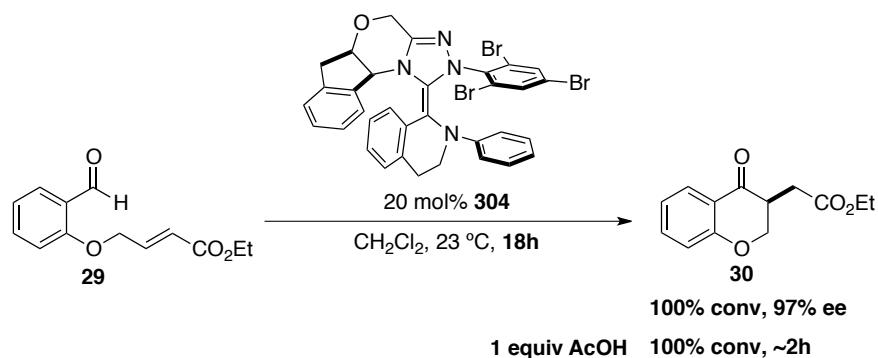


Scheme 3.23

Under the oxidative conditions employed in the α -acylation of amines using NHC and photoredox catalysis, we suggest that small amounts of carboxylic acid impurities are generated *in situ*, leading to the desired reactivity. We wondered if this type of intermediate could be used as a precatalyst in other carbene catalyzed reactions. Many NHC catalyzed reactions form stereocenters with acidic hydrogens, which in some cases leads to poor selectivity due to catalyst or base-induced epimerization. Since aza-Breslow intermediate **304** is a competent precatalyst

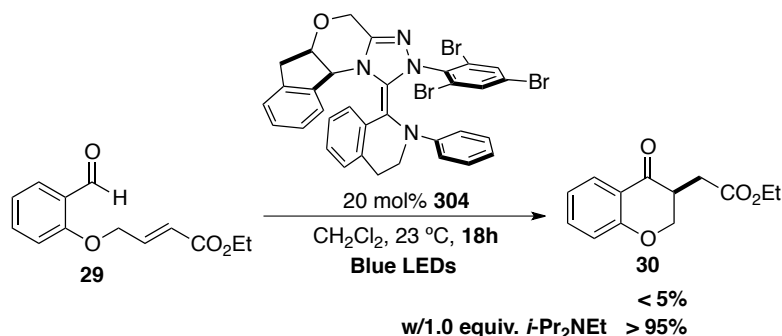
under acidic conditions, this may be a solution to the problems associated with the formation of base sensitive substrates.

The intramolecular Stetter reaction of salicylaldehyde derivatives has proven to be a reliable testing ground for the efficiency of NHC catalysts. With this in mind, we evaluated the use of aza-Breslow intermediate **304** as a precatalyst in this manifold. In the presence of 20 mol% of **304**, salicylaldehyde derivative **29**, undergoes smooth cyclization to afford chromanone product **30** in excellent enantioselectivity (Scheme 3.24). Although **304** is a competent precatalyst in the absence of acid in this case, the addition of acetic acid dramatically increase the rate of product formation. We attribute the reactivity observed in the absence of acetic acid to residual quantities of salicylic acid in the starting material.



Scheme 3.24

Interestingly, when the same transformation is run under irradiation with blue light (450 nm), none of the desired product is obtained. Since the combination of photoredox and NHC catalysis to generate amino ketones is efficient under these conditions we were puzzled by the fact that light inhibits the reactivity of the NHC catalyst in this case. To better recreate the conditions used in the photoredox manifold, we added an external amine base (Hünig's base). With base added, visible light irradiation promotes the desired reactivity more efficiently than with added base alone (Scheme 3.25).



Scheme 3.25

Although the exact mechanism in which light seems to affect the efficiency of these reactions is unknown, it undoubtedly plays a role.

Given the aforementioned results, we propose the following mechanism for the α -acylation of tertiary amines via photoredox/NHC catalysis (Figure 3.4). Irradiation of $[\text{Ru}(\text{bpy})_3]^{2+}$ with visible light should populate the $[\text{Ru}(\text{bpy})_3]^{2+*}$ excited state through metal-to-ligand charge transfer. In the presence of a suitable oxidative quencher (in this case *m*-DNB)²¹ $[\text{Ru}(\text{bpy})_3]^{2+*}$ becomes oxidized to generate the powerful oxidant $[\text{Ru}(\text{bpy})_3]^{3+}$ (1.29 V vs SCE).²² Single-electron oxidation of the tertiary amine followed by hydrogen-atom abstraction generates iminium ion **I**, returning $[\text{Ru}(\text{bpy})_3]^{2+}$ to the catalytic cycle. Interaction of the NHC with an aldehyde generates the nucleophilic Breslow intermediate **II** that can intercept the generated iminium ion **I**, forging a new C-C bond. Elimination of the NHC from **III** leads to the formation of the desired amino ketone **IV**, with concomitant regeneration of the NHC catalyst. Furthermore, we have identified an aza-Breslow intermediate as the resting state in this transformation arising from addition of the NHC catalyst to the generated iminium ion preferentially. This process has been shown to be reversible in the presence of acid or light, which allows the NHC to re-enter the productive pathway in the catalytic cycle.

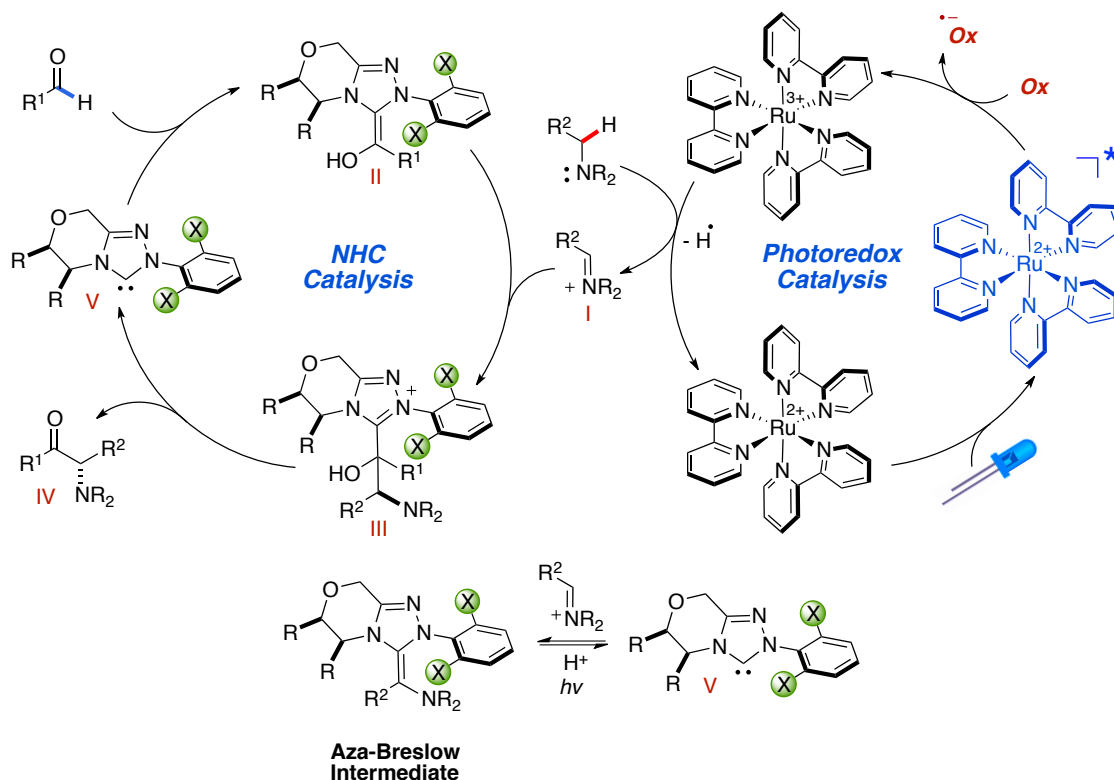
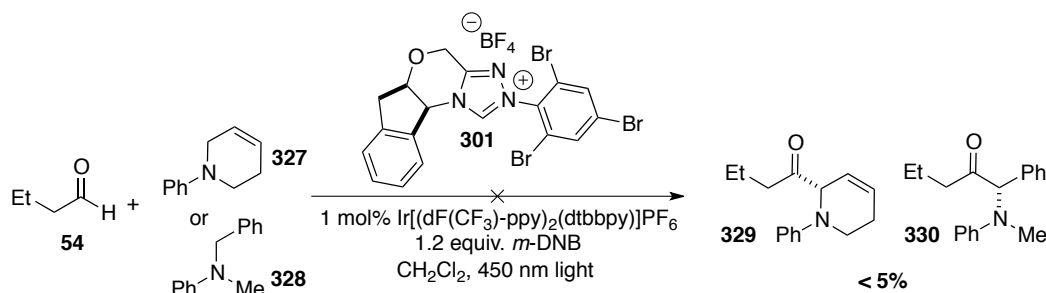


Figure 3.4

With respect to the oxidant, although *m*-DNB is used in stoichiometric quantities no reduction products are observed during the course of the reaction. It is known that nitrosobenzenes, arising from the reduction of nitrobenzenes, can be reoxidized in the presence of air and light. In this case oxygen is likely the terminal oxidant with *m*-DNB being a more efficient oxidative quencher of $[\text{Ru}(\text{bpy})_3]^{2+*}$.

In an attempt to expand the scope of the α -acylation of tertiary amines via photoredox/NHC catalysis, we evaluated the use of a new photocatalyst possessing an even more positive oxidation potential, along with better oxidants. $\text{Ir}[(\text{dF}(\text{CF}_3)\text{-ppy})_2(\text{dtbbpy})]\text{PF}_6$ displays a more negative reduction potential in its $\text{Ir}[(\text{dF}(\text{CF}_3)\text{-ppy})_2(\text{dtbbpy})]^{+*}$ excited state (-1.21 V vs SCE) and a more positive oxidation potential of the resultant oxidized $\text{Ir}[(\text{dF}(\text{CF}_3)\text{-ppy})_2(\text{dtbbpy})]^{2+}$ (+1.69 V vs SCE). We hoped that the more positive oxidation potential of $\text{Ir}[(\text{dF}(\text{CF}_3)\text{-$

ppy)₂(dtbbpy)]²⁺ would allow for the successful implementation of a variety of amines in the said coupling reaction. Subjecting either tetrahydropyridines **327** or acyclic benzyl amine **328** to the reaction conditions containing Ir[(dF(CF₃)-ppy)₂(dtbbpy)]PF₆ does not lead to any of the desired products, with recovery of both starting materials (Scheme 3.26).



Scheme 3.26

Since this photocatalyst should be capable of oxidizing these tertiary amines we wondered if our choice of oxidant was insufficient. Bromotrichloromethane has been shown to be an extremely efficient oxidant in this chemistry, generating chloroform as the only byproduct.²³ Replacing *m*-DNB with BrCCl₃ leads to facile oxidation of both amines; however, with none of the desired amino ketone product. It seems likely that use of stronger oxidants decompose the active NHC catalyst, rendering this pathway unattainable, thus judicious choice of the oxidant is crucial.

3.3 Conclusion

In conclusion, we have developed a highly enantioselective aza-benzoin reaction of aliphatic aldehydes and *N*-Boc imines.²⁴ The combination of a new amino-indanol derived NHC precatalyst leads to generation of α -amido ketone products in high enantioselectivity, while mild conditions allow for suppression of epimerization in otherwise sensitive products. The requirement for acid additives in these processes has been elucidated and overcome by the implementation of acetate bases. These additives are proposed to catalyze the reversibility of

addition of the active carbene species to the electrophilic acyl-imine. Circumstantial evidence for the generation of aza-Breslow intermediates in this system was also provided.

The successful inclusion of highly electrophilic acyl-imines in catalytic acyl anion chemistry has led to the development of a dual-catalysis mode, allowing for the direct α -acylation of tertiary amines.²⁵ This method takes advantage of a photoredox manifold to activate amines toward nucleophilic addition by a catalytically generated acyl anion equivalent. Aliphatic aldehydes can be coupled to tetrahydroisoquinoline frameworks in good yield and with high enantioselectivity. Importantly, an aza-Breslow intermediate was identified as the catalyst resting state in this process, which has provided the opportunity for further study of this intermediate.

REFERENCES

- ¹ Enders, D.; Kallfass, U. *Angew. Chem. Int. Ed.* **2002**, *41*, 1743-1745.
- ² Dünkemann, P.; Kolter-Jung, D.; Nitsche, A.; Demir, A. S.; Siegert, P.; Lingen, B.; Baumann, M.; Pohl, M.; Müller, M. *J. Am. Chem. Soc.* **2002**, *124*, 12084-12085.
- ³ Linghu, X.; Potnick, J. R.; Johnson, J. S. *J. Am. Chem. Soc.* **2004**, *126*, 3070-3071.
- ⁴ Lee, A.; Huang, L.; Ellman, J. *J. Am. Chem. Soc.* **1999**, *121*, 9907-9914.
- ⁵ Ager, D. J.; Prakash, I.; Schaad, D. R. *Chem. Rev.* **1996**, *96*, 835-876.
- ⁶ Murry, J. A.; Frantz, D. E.; Soheili, A.; Tillyer, R.; Grabowski, E. J. J.; Reider, P. J. *J. Am. Chem. Soc.* **2001**, *123*, 9696-9697.
- ⁷ Mennen, S. M.; Gipson, J. D.; Kim, Y. R.; Miller, S. J. *J. Am. Chem. Soc.* **2005**, *127*, 1654-1655.
- ⁸ Ghorai, M. K.; Kumar, A.; Tiwari, D. P. *J. Org. Chem.* **2010**, *75*, 137-151.
- ⁹ Zhao, X.; DiRocco, D. A.; Rovis, T. *J. Am. Chem. Soc.* **2011**, *133*, 12466-12469.
- ¹⁰ (a) Nugent, B. M.; Yoder, R. A.; Johnston, J. N. *J. Am. Chem. Soc.* **2004**, *126*, 3418-3419. (b) Uruguchi, D.; Terada, M. *J. Am. Chem. Soc.* **2004**, *126*, 5356-5357. (c) Uruguchi, D.; Sorimachi, K.; Terada, M. *J. Am. Chem. Soc.* **2004**, *126*, 11804-11805.
- ¹¹ Castells, J.; López-Calahorra, F.; Bassedas, M.; Urrios, P. *Synthesis*, **1988**, 314-315.
- ¹² Li, C.-J. *Acc. Chem. Res.* **2009**, *42*, 335-344.
- ¹³ (a) Zhang, J.; Tiwari, B.; Xing, C.; Chen, K.; Chi, Y. R. *Angew. Chem. Int. Ed.* **2012**, *51*, 3649-3652. (b) Baslé, O.; Li, C.-J. *Org. Lett.* **2008**, *10*, 3661-3663. (c) Li, Z.; Li, C.-J. *Org. Lett.* **2004**, *6*, 4997-4999.
- ¹⁴ Ciamician, G. *Science*, **1912**, *36*, 385-394.
- ¹⁵ Narayanam, J. M. R.; Stephenson, C. R. J. *Chem. Soc. Rev.* **2011**, *40*, 102-113.

- ¹⁶ Condie, A. G.; González-Gómez, J. C.; Stephenson, C. R. J. *J. Am. Chem. Soc.* **2010**, *132*, 1464-1465.
- ¹⁷ For excited state properties of iridium complexes see: Lowry, M. S.; Goldsmith, J. I.; Slinker, J. D.; Rohl, R.; Pascal, R. A. Jr.; Malliaras, G. G.; Bernhard, S. *Chem. Mater.* **2005**, *17*, 5712-5719.
- ¹⁸ For redox potentials of nitroaromatics see: Uchimiya, M.; Gorb, L.; Qasim, M. M.; Leszczynski, J. *Environ. Pollut.* **2010**, *158*, 3048-3053.
- ¹⁹ It is known that amines form electron-donor acceptor (EDA) complexes with *m*-dinitrobenzene that absorb in the visible spectrum; see: Siddiqi, Z. M.; Pathania, D. *Talanta*, **2003**, *60*, 1197-1203.
- ²⁰ Lohmann, J.-J.; Seebach, D.; Syfrig, M. A.; Yoshifuji, M. *Angew. Chem. Int. Ed. Engl.* **1981**, *20*, 128-129.
- ²¹ Bock, C. R.; Connor, J. A.; Guitierrez, A. R.; Meyer, T. J.; Whitten, D. G.; Sullivan, B. P.; Nagle, J. K. *J. Am. Chem. Soc.* **1979**, *101*, 4815-4824.
- ²² Campagna, S.; Puntoriero, F.; Nastasi, F.; Bergamini G.; Balzani, V. *Top. Curr. Chem.* **2007**, *280*, 117-214.
- ²³ Freeman, D. B.; Furst, L.; Condie, A. G.; Stephenson, C. R. J. *Org. Lett.* **2012**, *14*, 94-97.
- ²⁴ DiRocco, D. A.; Rovis, T. *Angew. Chem. Int. Ed.* **2012**, *51*, 5904-5906.
- ²⁵ DiRocco, D. A.; Rovis, T. *J. Am. Chem. Soc.* **2012**, *134*, 6143-6145.

Chapter 4

Isolation and Characterization of Aza-Breslow Intermediates

4.1 Introduction

In 1958 Breslow proposed the currently accepted mechanism of carbene catalyzed reactions, namely the benzoin reaction, while investigating the thiamine mode of action.¹ In this initial report he showed the thiazolium moiety to be responsible for thiamine's distinct mode of action, not the pendant amino group that had been initially proposed. On the basis of his mechanistic studies, Breslow described that the thiazolium salt could be deprotonated under relatively mild conditions, leading to the generation of an ylide or carbene. Reacting this species with a pyruvic acid moiety in biological systems, or an aldehyde, would lead to a nucleophilic enaminol now commonly referred to as the Breslow intermediate (Figure 4.1).

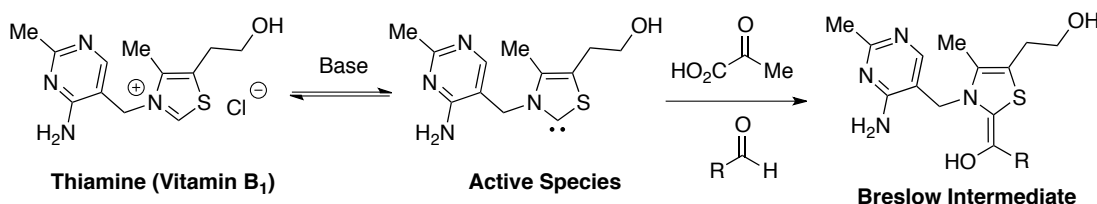
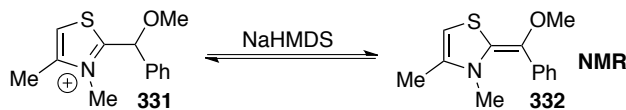


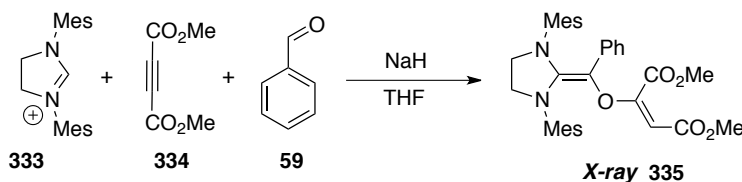
Figure 4.1

With a renaissance in azolyidene catalysis of organic reactions in recent years, much effort has been expended searching for this intermediate, and until recently no structural information had been disclosed. The first successful generation of structures related to the Breslow intermediate were reported by Jordan and coworkers. In their work, thiazolium acetals such as **331** could be deprotonated to yield the related enaminol **332**, which was observed by ¹H NMR (Scheme 4.1).²



Scheme 4.1

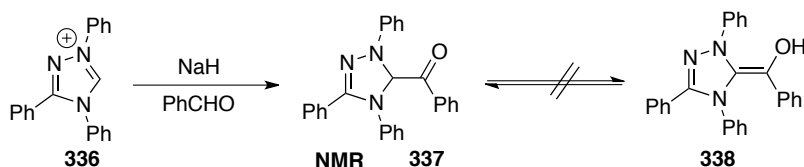
It wasn't until Nair and coworkers isolated a Breslow type intermediate in the context of their work in 2003 that any structural data was obtained.³ These workers found that SIMes **333** forms an alkylate enaminal **335** from benzaldehyde in the presence of dimethylacetylenedicarboxylate (**334**) (Scheme 4.2). This product presumably arises from *O*-alkylation of the Breslow intermediate, due to its high nucleophilicity.



Scheme 4.2

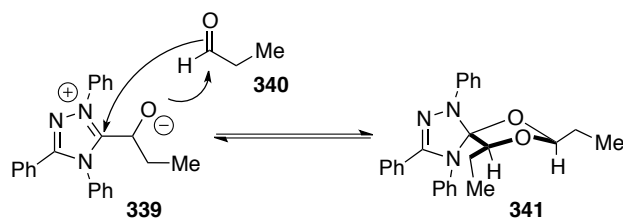
A thorough study of the interaction of a triphenyl-triazolylidene carbene with aliphatic and aromatic aldehydes has recently been reported by Teles and coworkers.⁴ In this study they report that deprotonation of triazolium salt **336** followed by addition of benzaldehyde yields the keto-form of the Breslow intermediate **337**, which was characterized by NMR. Treatment of the keto-form with acid or base failed to result in the detectable formation of enol **338**

(Scheme 4.3).



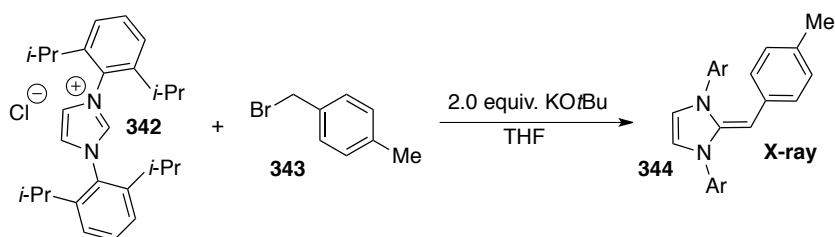
Scheme 4.3

In the case of aliphatic aldehydes, they report the formation of spirocycle **341** from propanal **340** and precatalyst **336** (Scheme 4.4). They also propose these intermediates to be the resting state under these conditions based on DFT calculations.



Scheme 4.4

Arguably the most relevant example of the isolation of a Breslow-type intermediate was recently published by Jacobi von Wangelin and coworkers.⁵ In their study, deoxy-Breslow intermediates could be isolated from the reaction of imidazolylidene carbenes with alkyl halides. Imidazolium salt **341** in the presence of base reacts with 4-tolyl-benzyl bromide **343** to provide enediamine **344** (Scheme 4.5).

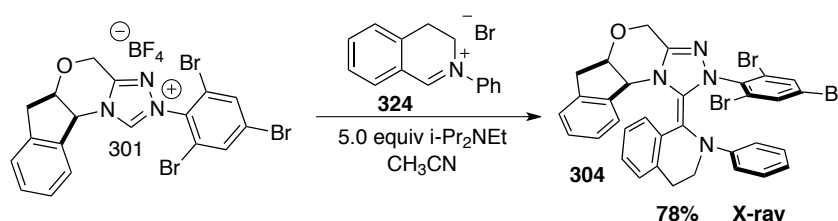


Scheme 4.5

These intermediates proved isolable and their structures determined by X-ray crystallography. NMR studies of these compounds show formal rotation about the exocyclic double bond, speaking to their nucleophilic nature and partial single bond character.

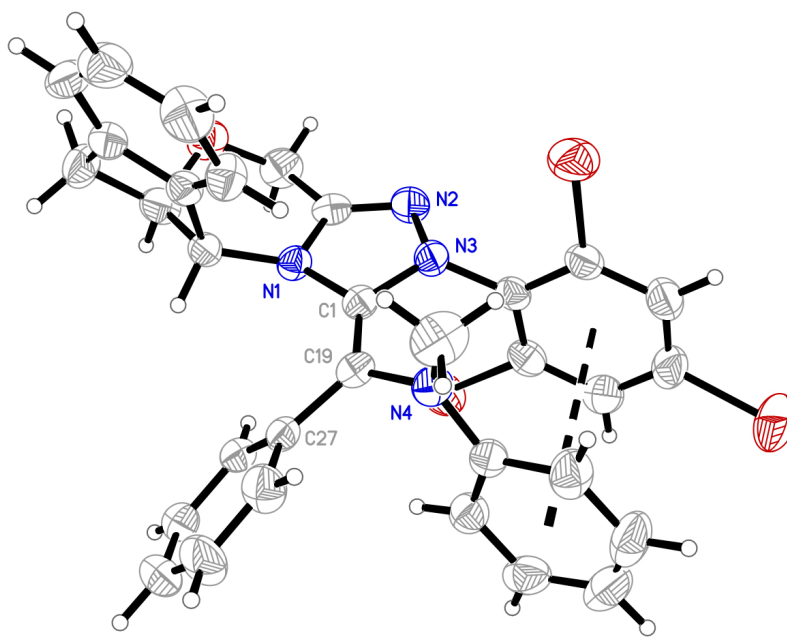
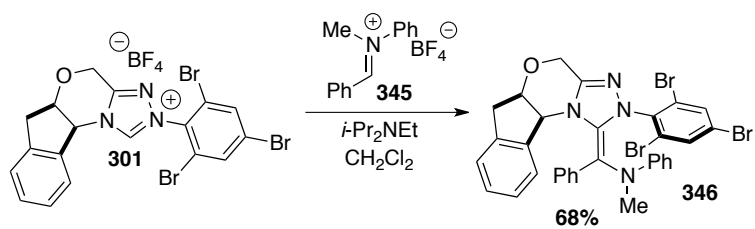
4.2 Results

During the course of our studies of the aza-Benzoin reaction of aliphatic aldehydes with *N*-Boc imines and iminium ions, we have gained significant insight into the formation of aza-Breslow intermediates as the catalyst resting states in these systems. NMR and HRMS data suggest the formation of these intermediates from *N*-Boc imines; however, during our study of iminium ions as electrophiles, a stable crystalline aza-Breslow intermediate was isolated and fully characterized by NMR and X-ray crystallography (Scheme 4.6).



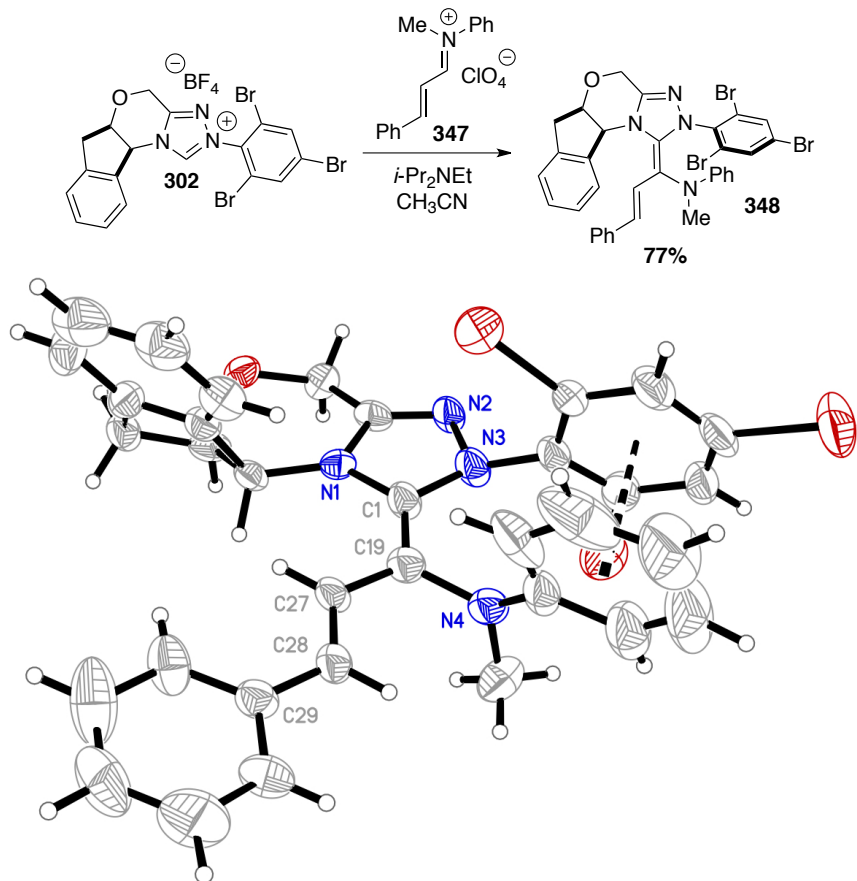
Scheme 4.6

Since aza-Breslow intermediate **304** was isolable, we wondered if other more general aza-Breslow intermediates could be generated in simpler systems. Aza-analogues of the Breslow intermediate would be an important tool in studying the fundamental reactivity of this type of intermediate. Given the similar electronic nature between the amino and hydroxyl groups,⁶ these intermediates would be the most closely related structures ever studied. Initially, we targeted the use of iminium salt **345** due to its relevance to the NHC catalysis of aryl aldehydes. Subjecting triazolium salt precatalyst **301** to basic conditions containing iminium salt **345** in acetonitrile leads to facile generation of the acyclic aza-Breslow intermediate **346** as a yellow, crystalline solid (Scheme 4.7). We were delighted to see that the synthesis of these intermediates would not be limited to the very specific tetrahydroisoquinoline scaffold we initially discovered. This intermediate was analyzed by X-ray crystallography, which confirmed the structure to be aza-Breslow intermediate **346** as was originally proposed.



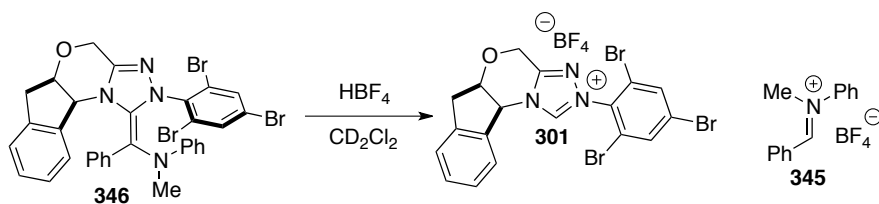
Scheme 4.7

While this intermediate would allow for the study of acyl-anion processes, we were also interested in studying Breslow intermediates displaying homoenolate-type reactivity. With this in mind we evaluated the use of an enal-derived iminium salt to generate a conjugated system. Again, pre-catalyst **301** in the presence of base and iminium salt **347** affords a yellow, crystalline solid, which was analyzed by X-ray crystallography and determined to be aza-Breslow intermediate **348** (Scheme 4.8).



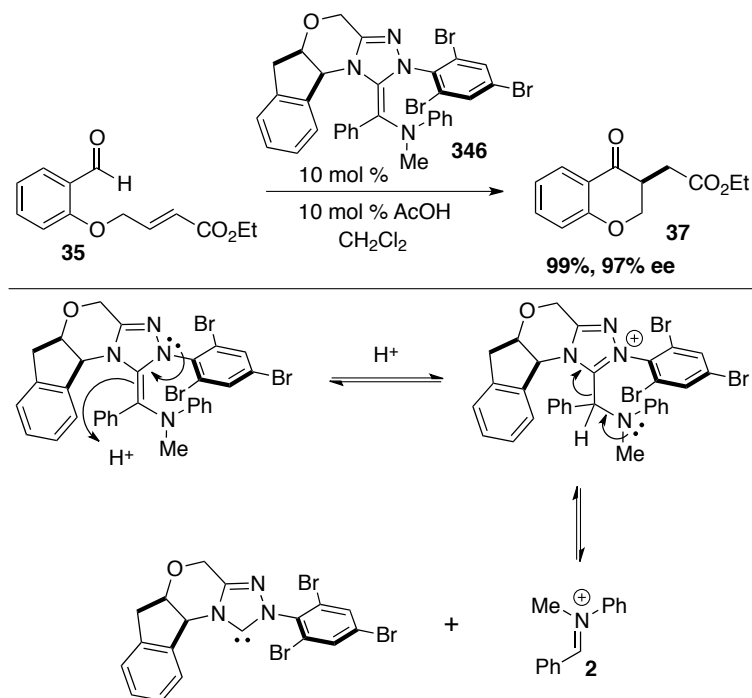
Scheme 4.8

With good model systems for both acyl anion reactivity and homoenolate reactivity in-hand, we began to study these systems more closely. As we had demonstrated previously with intermediate **304**, addition of excess HBF_4 to **346** results in complete conversion to triazolium salt **301** and iminium salt **345** (Scheme 4.9), demonstrating its reversible formation in the presence of acid.



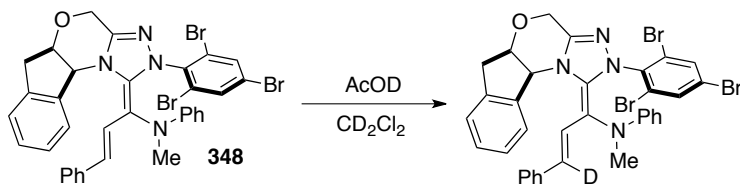
Scheme 4.9

To further demonstrate the catalytic relevance of **346**, we aimed to use it as a precatalyst in the intramolecular Stetter reaction of salicylaldehyde derivatives. Subjecting aldehyde **35** to aza-Breslow intermediate **346** in the presence of a catalytic amount of acetic acid provides smooth conversion to chromanone derivative **37** in excellent enantioselectivity (Scheme 4.10).



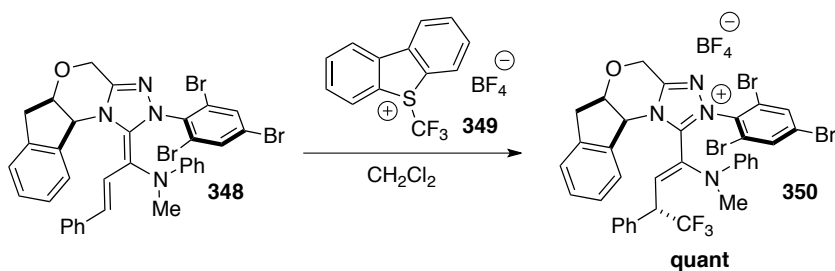
Scheme 4.10

With the catalytic activity of **346** confirmed we wanted to evaluate the nucleophilicity of homoenolate equivalent **348** at the γ -position. An NMR experiment shows selective and complete deuterium incorporation at the λ -position in the presence of acetic acid-*d*₄ (Scheme 4.11).



Scheme 4.11

Furthermore, homoenolate equivalent **345** reacts rapidly with trifluoromethylating reagent **346** to provide what is proposed to be salt **347**, in quantitative yield (Scheme 4.12). Unfortunately, all attempts to decompose **347** to the trifluoromethylated aldehyde were unsuccessful.



Scheme 4.12

DFT studies have suggested the E-olefin geometry to be favored in aldehyde-derived systems.⁷ Solid-state analysis of both isolated aza-Breslow intermediates indicates a preferred Z-olefin geometry as seen in the X-ray structures. This contradiction may arise from π -stacking interactions exhibited by the electron rich/electron deficient aryl substituents present in these analogues, as well as a greater steric influence of the aniline unit in relation to a hydroxyl group. Since the geometry of this nucleophilic olefin likely plays a significant role in determining the stereochemical outcome of NHC catalyzed processes, we were interested in probing these intermediates in solution.

The ^1H NMR of intermediate **346** is relatively complicated, showing at least 3 major species at room temperature in toluene- d_8 (Figure 4.2). A variable temperature ^1H NMR experiment shows coalescence of two of the species at approximately 60 °C, likely rotamers around the C19-N4

single bond. The resultant species are proposed to be the E/Z olefin isomers of the C1-C19 double bond. Coalescence of the isomers is not observed at temperatures of up to 100 °C; thus, the barrier to rotation around the double bond likely exceeds 18 kcal/mol.

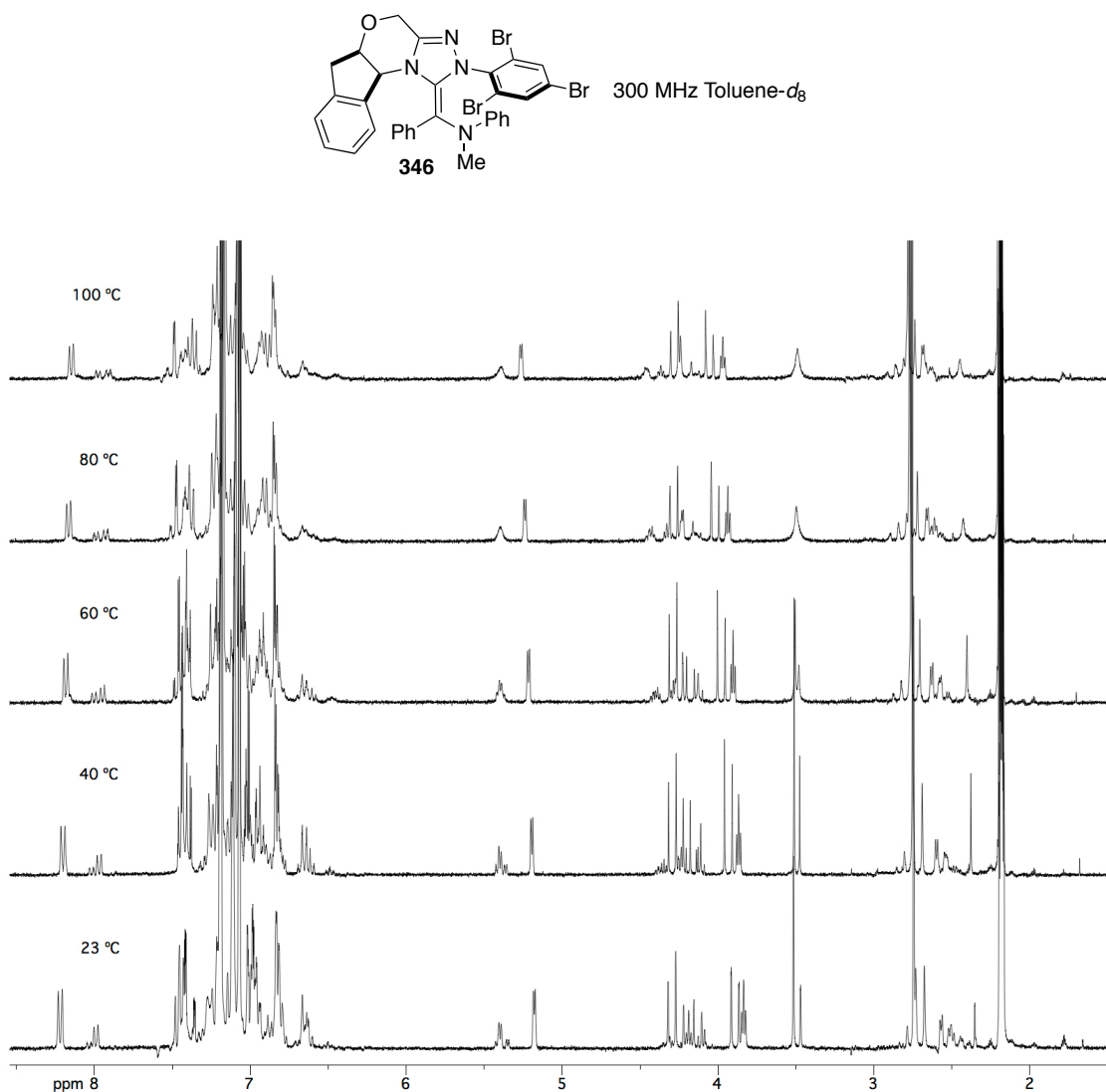


Figure 4.2

We wondered if we could still observe interconversion of these isomers at elevated temperatures using EXSY NMR. At 100 °C the EXSY-NOESY spectrum of **346** shows cross peaks for the two olefin isomers, demonstrating their interconversion on the NMR timescale (Figure 4.3).

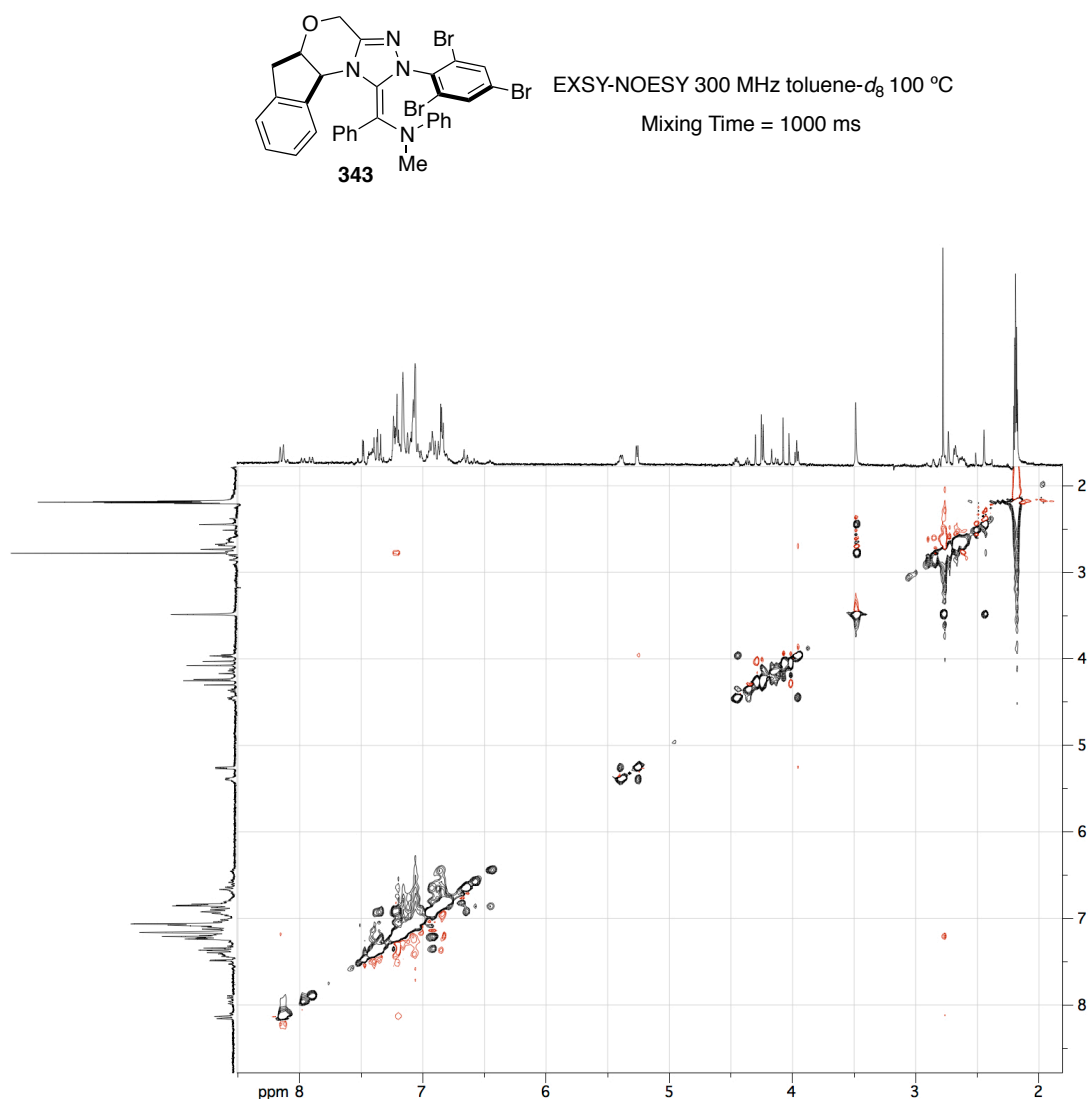


Figure 4.3

We analyzed homoenolate equivalent **348** in a similar manner. The ¹H NMR spectrum of **348** in toluene-*d*₈ indicates the presence of rotamers around the C19-N4 bond as well as isomers of the C1-C19 double bond. Variable temperature experiments show coalescence of two of them at approximately 60 °C, presumably the C19-N4 rotamers (Figure 4.4). While the spectrum continues to become simpler at higher temperatures, all isomers do not coalesce.

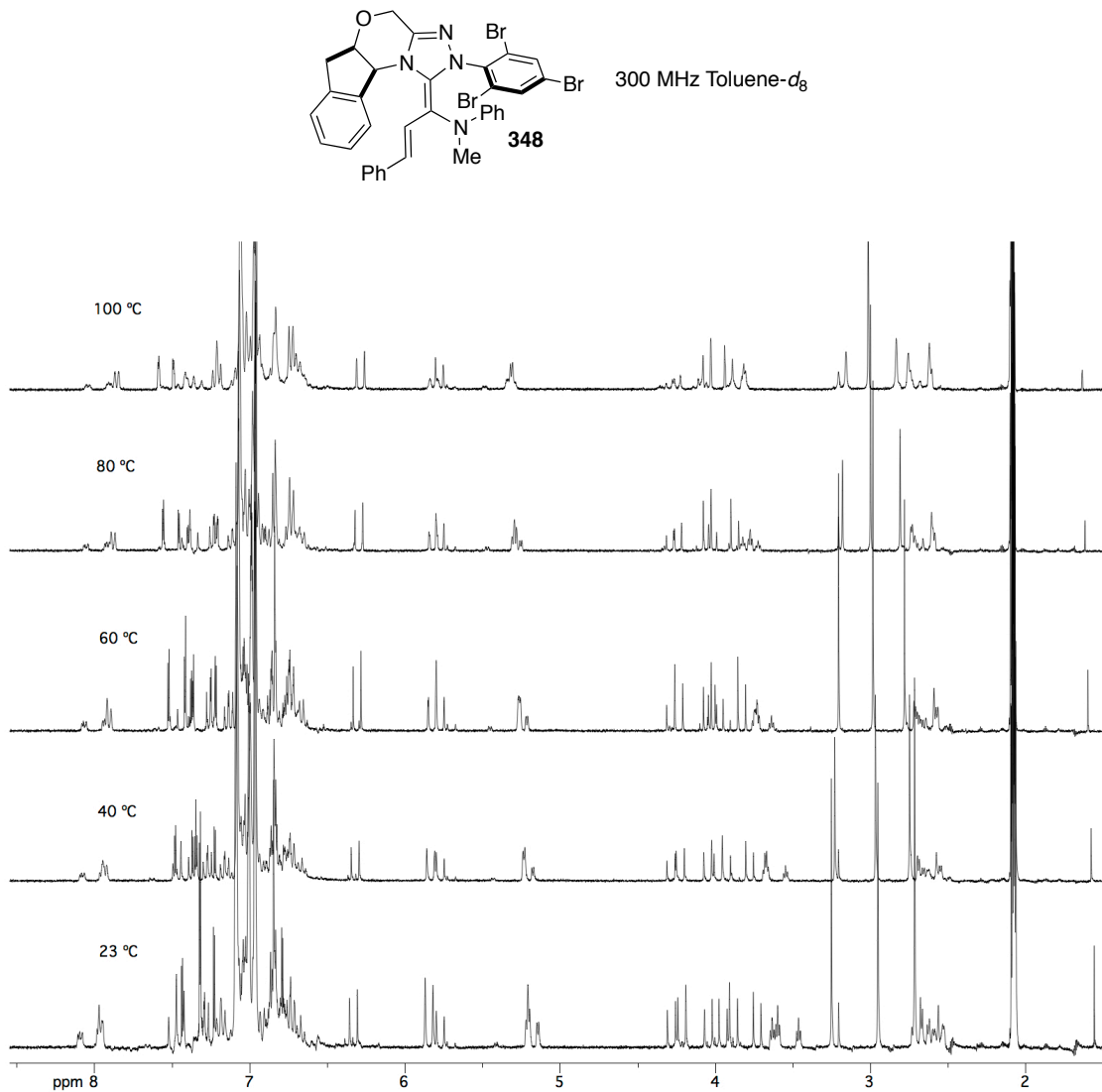


Figure 4.4

Again, the EXSY-NOESY spectrum of **348** at 100 °C shows interconversion of the remaining species on the NMR timescale (Figure 4.5).

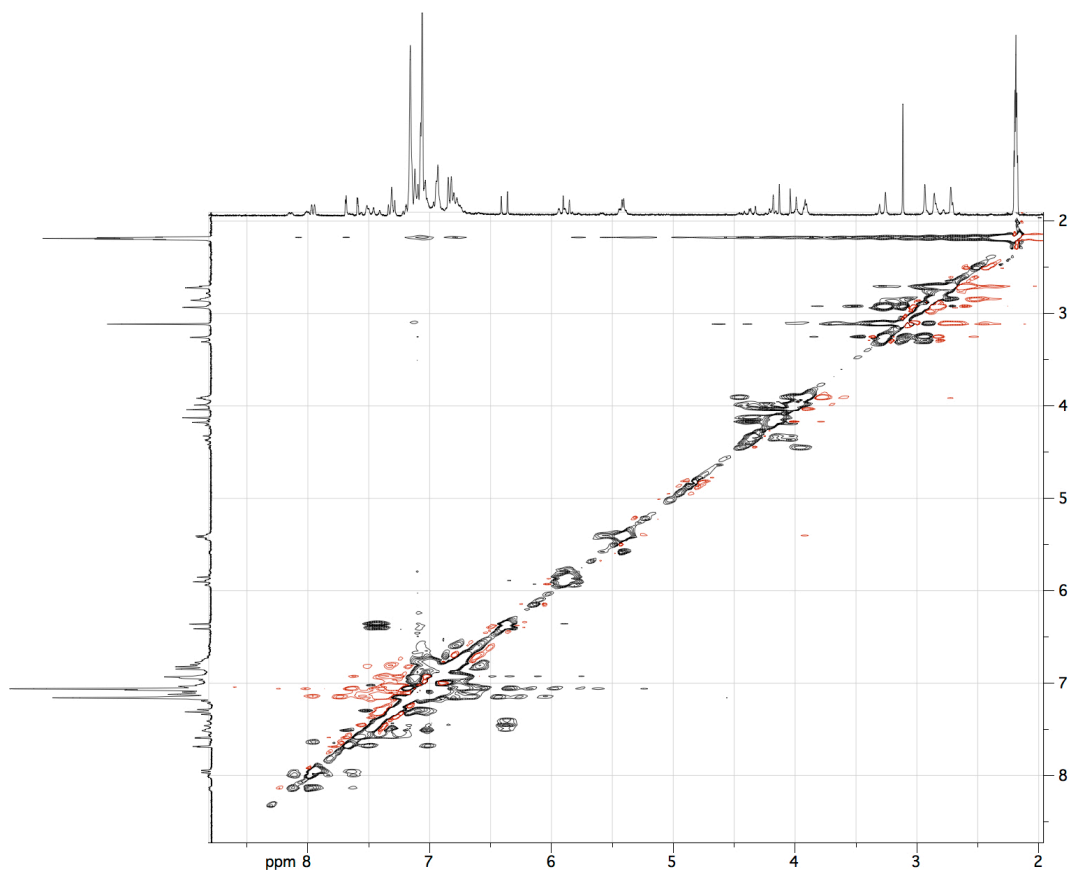
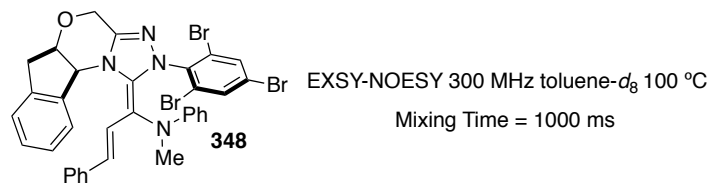


Figure 4.5

With these data we propose that interconversion can occur through a formal rotation of the double bond in these intermediates. This is a situation also observed by Jacobi von Wangelin and coworkers in their study of deoxy-Breslow type intermediates. Further data suggests that interconversion can also occur through a bond breaking/bond forming mechanism in which H^+ acts as a catalyst.

Finally, we wanted to measure the oxidation potential of these intermediates as their structures are the most closely related to those involved in NHC catalysis to date. Given the numerous

examples of oxidative NHC catalyzed transformations, direct information about the oxidation potential of the Breslow intermediate is useful in the judicious choice of oxidants.⁸ Aza-Breslow intermediate **346** undergoes a highly reversible oxidation at +0.17 V (vs SSCE in CH₂Cl₂), while homoenolate equivalent **348** is oxidized irreversibly at +0.49 V (vs SSCE in CH₂Cl₂) (Figure 4.6).

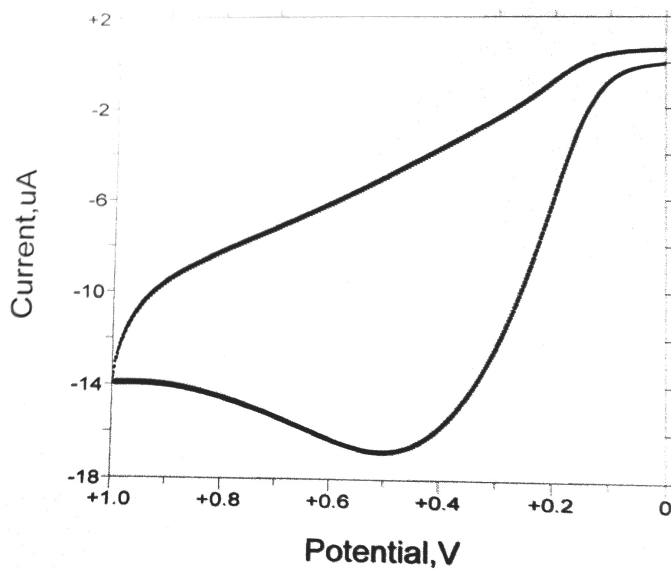
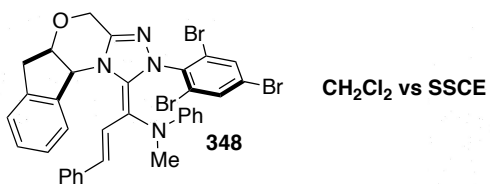
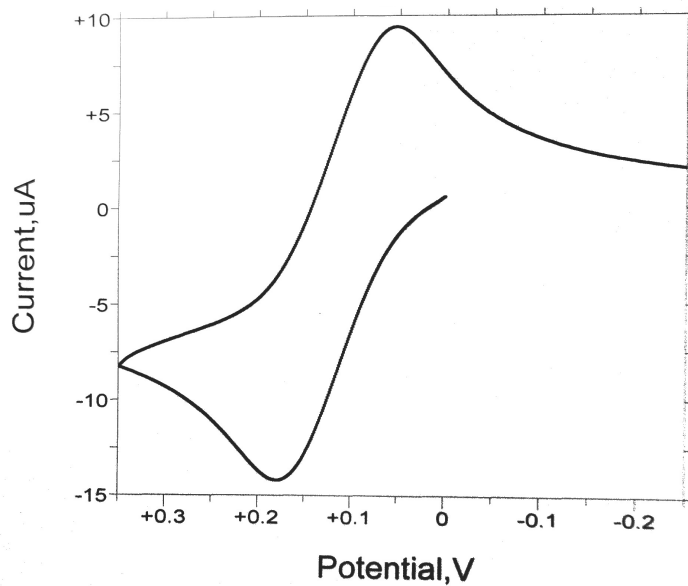
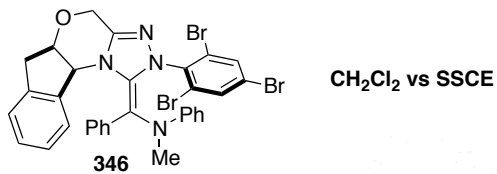


Figure 4.6

The irreversible oxidation of **348** is most likely due to dimerization or other degradation pathways.⁹

4.3 Conclusion

In conclusion, we have successfully synthesized, isolated and fully characterized aza-analogues of the Breslow intermediate derived from our series of chiral triazolylidene carbenes.¹⁰ The use of iminium salts as aldehyde surrogates has allowed for the formation and isolation of catalytically relevant acyl anion and homoenolate equivalents. Protonation of these intermediates leads to the reversible formation of the active carbene catalyst and allows for their use as precatalysts in other NHC catalyzed reactions. NMR studies suggest that both olefin isomers are present which can interconvert by bond rotation at elevated temperatures. Finally, measurement of their oxidation potentials by cyclic voltammetry has been accomplished which provides the first experimental redox data on such systems.

REFERENCES

- ¹ Breslow, R. *J. Am. Chem. Soc.* **1958**, *80*, 3719-3726.
- ² Jordan, F.; Kudzin, Z. H.; Rios, C. B. *J. Am. Chem. Soc.* **1987**, *109*, 4415-4416.
- ³ Nair, V.; Bindu, S.; Sreekumar, V.; Rath, N. P. *Org. Lett.* **2003**, *5*, 665-667.
- ⁴ Berkessel, A.; Elfert, S.; Etzenbach-Effers, K.; Teles, J. H. *Angew. Chem. Int. Ed.* **2010**, *49*, 7120-7124.
- ⁵ (a) Knappke, C. E. I.; Neudörfl, J. M.; Jacobi von Wangelin, A. *Org. Biomol. Chem.* **2010**, *8*, 1695-1705. (b) Knappke, C. E. I.; Arduengo, A. J. III; Jiao, H.; Neudörfl, J.-M. *Synthesis*, **2011**, *23*, 3784-3795.
- ⁶ The electronic character of the OH should be analogous to a NPh group. Witness the respective pKa's of H₂O (31.2) and PhNH₂ (30.6) in DMSO; Bordwell, F. G. *Acc. Chem. Res.* **1988**, *21*, 456-463.
- ⁷ (a) Hawkes, K. J.; Yates, B. R. *Eur. J. Org. Chem.* **2008**, 5563-5570. (b) Dudding, T.; Houk, K. N. *Proc. Natl. Acad. Sci. U.S.A.* **2004**, *101*, 5770-5775.
- ⁸ a) Guin, J.; De Sarkar, S.; Grimme, S.; Studer, A. *Angew. Chem. Int. Ed.* **2008**, *47*, 8727-8730. (b) De Sarkar, S.; Studer, A. *Angew. Chem. Int. Ed.* **2010**, *49*, 9266-9269.
- ⁹ Barletta, G.; Chung, A. C.; Rios, C. B.; Jordan, F.; Schlegel, J. M. *J. Am. Chem. Soc.* **1990**, *112*, 8144-8149.
- ¹⁰ DiRocco, D. A.; Oberg, K. M.; Rovis, T. *J. Am. Chem. Soc.* **2012**, *134*, 6143-6145.

Appendix 1

***N*-Heterocyclic Carbene Catalysis and the Development of Chiral Triazolylidene Carbenes for the Asymmetric Intermolecular Stetter Reaction**

Materials and Methods

All reactions were carried out under an atmosphere of argon in flame-dried glassware with magnetic stirring. Tetrahydrofuran and dichloromethane were degassed with argon and passed through two columns of neutral alumina. Toluene was degassed with argon and passed through one column of neutral alumina and one column of Q5 reactant. Methanol was purchased from Fisher Scientific and used without further purification. *N,N*-Diisopropylethylamine was purchased from Aldrich and used without further purification. Column chromatography was performed on SiliCycle®SilicaFlash® P60, 40-63µm 60A. Thin layer chromatography was performed on SiliCycle® 250µm 60A plates. Visualization was accomplished with UV light or KMnO₄ stain followed by heating.

¹H NMR spectra were recorded on Varian 300 or 400 MHz spectrometers at ambient temperature. Data is reported as follows: chemical shift in parts per million (δ, ppm) from CDCl₃ (7.26 ppm) or acetone-*d*₆ (2.03 ppm), multiplicity (s = singlet, bs = broad singlet, d = doublet, t = triplet, q = quartet, and m = multiplet), coupling constants (Hz). ¹³C NMR were recorded Varian 300 or 400 MHz spectrometers (at 75 or 100 MHz) at ambient temperature. Chemical shifts are reported in ppm from CDCl₃ (77.2 ppm) or acetone-*d*₆ (205.6, 29.1 ppm).

Aldehydes were either purchased from Aldrich or prepared via literature procedures. Nitroalkenes were prepared according to the general procedure as described within.¹

General Procedure for the Synthesis of Nitroalkenes

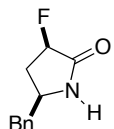
To a dry round bottom flask was added cyclopentane carboxaldehyde (1.02 g, 10.4 mmol), nitromethane (840 μ l, 15.6 mmol), and 1:1 THF/*t*-BuOH (10 mL). This solution was cooled to 0 °C and potassium tert-butoxide (0.233 g, 2.08 mmol) added in one portion. The reaction was then stirred at 0 °C for 1 h then warmed to room temperature and stirred for 12 h. After completion, saturated aqueous NH₄Cl solution (20 mL) was added to quench the reaction and then extracted with CH₂Cl₂ (3 x 20 mL). The combined organic extracts were then dried over anhydrous Na₂SO₄ and concentrated *in vacuo*. After drying the crude residue under vacuum (4 mm) for 1 h, CH₂Cl₂ (20 mL) was added followed by cooling to 0 °C. Trifluoroacetic anhydride (1.52 mL, 10.9 mmol) was added followed by the slow dropwise addition of Et₃N (3.04 mL, 21.8 mmol). After stirring for 1 h at 0 °C the reaction was allowed to warm to room temperature and stirred an additional 2 h. The reaction was diluted with CH₂Cl₂ (20 mL) followed by the addition of water (20 mL). The organic layer was separated and washed with saturated aqueous NH₄Cl solution (3 x 20 mL), dried (Na₂SO₄) and concentrated *in vacuo* to give a yellow oil that was purified by column chromatography (20:1 hexanes:ether) yielding 0.779 g (53%) of (*E*)-(2-nitrovinyl)cyclopentane as a pale yellow oil.

General Procedure for the Asymmetric Intermolecular Stetter Reaction

To a dry 4 mL vial, with a magnetic stir bar, was added triazolium salt (**128**) (16 mg, 0.037 mmol, 0.1 equiv), aldehyde (0.371 mmol, 1.0 equiv), nitroalkene (0.556 mmol, 1.5 equiv), and methanol (1 mL). The vial was then cooled to 0 °C in an ice/water bath with stirring. *N,N*-diisopropylethylamine (64 μ l, 0.371 mmol) was added dropwise and the reaction was stirred at 0 °C for 2 h. AcOH (100 μ l) was then added to quench the reaction followed by concentration *in*

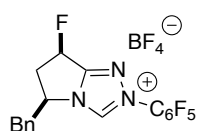
vacuo. Column chromatography (hexanes:ether) of the resulting dark red residue gave the desired β -nitro ketone.

Experimental Procedures and Characterization Data



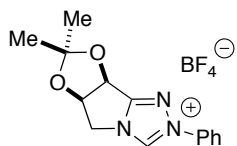
(3R,5S)-5-benzyl-3-fluoropyrrolidin-2-one (70): To a freshly prepared solution of LDA (1.1 equiv) in THF (100 mL) at $-78\text{ }^{\circ}\text{C}$ was added a solution of (*R*)-*tert*-butyl 2-benzyl-5-oxopyrrolidine-1-carboxylate (**67**) (2.50 g, 9.08 mmol, 1.0 equiv) in THF (10 mL) and stirred for 90 min at $-78\text{ }^{\circ}\text{C}$. A solution of N-fluorobenzenesulfonamide (3.72 g, 11.8 mmol, 1.3 equiv) in THF (20 mL) was added dropwise, stirred for 1 h at $-78\text{ }^{\circ}\text{C}$ and then warmed to r.t. slowly by removing the dry ice/acetone bath. The reaction was quenched by the addition of $\text{NH}_4\text{Cl}_{(\text{sat})}$ (20 mL), concentrated *in vacuo*, and extracted with DCM (3 X 200 mL). The combined organic extracts were dried (Na_2SO_4) and concentrated to yield a crude solid. To this solid (mainly consisting of unreacted N-fluorobenzenesulfonamide and benzenesulfonamide) was added ether (30 mL) while stirring vigorously. The slurry was filtered through a sintered glass funnel and washed continuously with ether (200 mL). Concentration of the filtrate *in vacuo* provided the crude lactam, which was immediately used in the next step without further purification. To a cooled ($0\text{ }^{\circ}\text{C}$) solution of the crude lactam in CH_2Cl_2 (50 mL) was added trifluoroacetic anhydride (5.0 equiv) dropwise. After stirring for 1 h the reaction was quenched by the addition of $\text{NaHCO}_{3(\text{aq})}$ and extracted with CH_2Cl_2 . The combined extracts were dried (Na_2SO_4), and concentrated *in vacuo* to yield a crude oil. The solid was purified via flash chromatography on silica gel to yield the desired compound. $^1\text{H NMR}$ (300 MHz, CDCl_3): δ 7.37-7.25 (m, 3H), 7.20-7.17 (m, 2H), 6.27 (s, 1H), 5.05 (ddd, $J = 52.4, 8.0, 7.0\text{ Hz}$, 1H), 3.84-

3.74 (m, 1H), 2.92 (dd, $J = 13.5, 5.9$ Hz, 1H), 2.81 (dd, $J = 13.5, 8.1$ Hz, 1H), 2.74-2.60 (m, 1H), 2.03 (ddt, $J = 26.3, 13.6, 6.8$ Hz, 1H); ^{13}C NMR (75 MHz, CDCl_3): δ 136.7, 129.1, 129.0, 127.3, 88.3 (d, $J = 186$ Hz), 52.2 (d, $J = 3.7$ Hz), 43.4, 34.7 (d, $J = 19.5$ Hz).



(5*S*,7*R*)-5-benzyl-7-fluoro-2-(perfluorophenyl)-6,7-dihydro-5*H*-pyrrolo[2,1-*c*][1,2,4]triazol-2-ium tetrafluoroborate (73): To a flame-dried round-

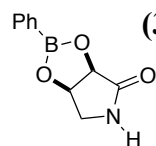
bottomed flask was added (3*R*,5*S*)-5-benzyl-3-fluoropyrrolidin-2-one (**70**) (219 mg, 1.13 mmol, 1.0 equiv) and dichloromethane (15 mL). The mixture was stirred until homogeneous then trimethyloxonium tetrafluoroborate (168 mg, 1.13 mmol, 1.0 equiv) was added in one portion. After stirring for 18 h, pentafluorophenyl hydrazine (224 mg, 1.13 mmol, 1.0 equiv) was added and the reaction was allowed to stir an additional 24 h. Concentration of the solution gave a solid that was triturated with ether and dried under vacuum (4 mm) for 1 h. After installing a reflux condenser, chlorobenzene (15 mL) and triethyl orthoformate (0.47 mL, 2.83 mmol, 2.5 equiv) were added and the mixture was heated to reflux in an oil bath for 18 h. The solution was concentrated *in vacuo* and crystallized with ether to yield the desired product as a tan solid (273 mg, 51%). ^1H NMR (300 MHz, acetone- d_6): δ 10.18 (s, 1H), 7.46-7.34 (m, 5H), 6.55 (ddd, $J = 53.9, 7.2, 2.8$ Hz, 1H), 5.58-5.52 (m, 1H), 3.90-3.83 (m, 1H), 3.66 (dd, $J = 13.7, 7.1$ Hz, 1H), 3.61-3.46 (m, 1H), 3.04-2.90 (m, 1H).



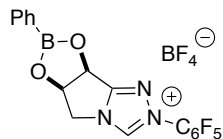
(5*aR*,8*aS*)-7,7-dimethyl-2-phenyl-5*a*,8*a*-dihydro-5*H*-

[1,3]dioxolo[4',5':3,4]pyrrolo[2,1-*c*][1,2,4]triazol-2-ium tetrafluoroborate (86): Prepared in analogous fashion to (**73**) from (3*aR*,6*aR*)-2,2-dimethyldihydro-3*aH*-[1,3]dioxolo[4,5-*c*]pyrrol-4(5*H*)-one **85**. ^1H NMR (300 MHz, acetone- d_6): δ 10.47 (s, 1H), 7.99-

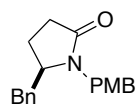
7.96 (m, 2H), 7.75-7.69 (m, 3H), 6.02 (d, $J = 5.6$ Hz, 1H), 5.75 (td, $J = 5.2, 0.9$ Hz, 1H), 4.95 (dd, $J = 13.7, 4.8$ Hz, 1H), 4.84-4.79 (m, 1H), 1.49 (s, 3H), 1.40 (s, 3H).

 **(3aR,6aR)-2-phenyldihydro-3aH-[1,3,2]dioxaborolo[4,5-c]pyrrol-4(5H)-one (87):** Prepared from (3aR,6aR)-2,2-dimethyldihydro-3aH-[1,3]dioxolo[4,5-c]pyrrol-4(5H)-one (85) by hydrolysis followed by treatment with phenyl boronic acid in toluene. ¹H

NMR (300 MHz, acetone-*d*₆): δ 7.81-7.78 (m, 2H), 7.55-7.49 (m, 1H), 7.41 (m, 2H), 7.13 (s, 1H), 5.34-5.30 (m, 1H), 4.90 (dd, $J = 7.0, 1.6$ Hz, 1H), 3.86 (ddd, $J = 11.5, 6.0, 1.0$ Hz, 1H), 3.53 (ddd, $J = 11.6, 1.7, 1.0$ Hz, 1H).

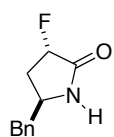


(3aS,8aR)-2,5-diphenyl-8,8a-dihydro-3aH-[1,3,2]dioxaborolo[4',5':3,4]pyrrolo[2,1-c][1,2,4]triazol-5-ium tetrafluoroborate (88): Prepared from (3aR,6aR)-2-phenyldihydro-3aH-[1,3,2]dioxaborolo[4,5-c]pyrrol-4(5H)-one (87) analogously to (73). ¹H NMR (300 MHz, acetone-*d*₆): δ 7.81-7.78 (m, 2H), 7.55-7.49 (m, 1H), 7.41 (m, 2H), 7.13 (s, 1H), 5.34-5.30 (m, 1H), 4.90 (dd, $J = 7.0, 1.6$ Hz, 1H), 3.86 (ddd, $J = 11.5, 6.0, 1.0$ Hz, 1H), 3.53 (ddd, $J = 11.6, 1.7, 1.0$ Hz, 1H).



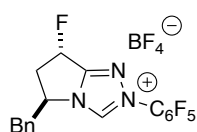
(R)-5-benzyl-1-(4-methoxybenzyl)pyrrolidin-2-one (99): To a solution of (*R*)-5-benzylpyrrolidin-2-one³ (1.81 g, 10.3 mmol, 1.0 equiv) in THF (150 mL) was added sodium hydride (0.298 g, 12.4 mmol, 1.2 equiv) 4-methoxy-benzylchloride (1.62 g, 10.3 mmol, 1.0 equiv) and tetrabutylammonium iodide (0.38 g, 1.03 mmol, 0.10 equiv). After stirring for 24 h at room temperature the reaction was quenched by the addition of NH₄Cl_(sat) (50 mL) and

concentrated to approximately half the original volume then extracted with dichloromethane (3 x 50 mL). The combined extracts were dried (Na₂SO₄) and concentrated *in vacuo* to leave a crude residue that was purified by column chromatography (9:1 EtOAc:hex), providing the desired product as a colorless oil (2.28 g, 75%). ¹H NMR (300 MHz, CDCl₃): δ 7.30-7.22 (m, 3H), 7.19-7.15 (m, 2H), 7.08-7.05 (m, 2H), 6.89-6.85 (m, 2H), 5.05 (d, *J* = 14.8 Hz, 1H), 3.93 (d, *J* = 14.9 Hz, 1H), 3.81 (s, 3H), 3.64 (m, 1H), 3.02 (dd, *J* = 13.4, 4.3 Hz, 1H), 2.55 (dd, *J* = 13.3, 8.6 Hz, 1H), 2.26 (t, *J* = 8.1 Hz, 2H), 1.94-1.82 (m, 1H), 1.78-1.67 (m, 1H).



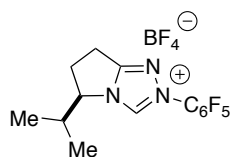
(3*S*,5*S*)-5-benzyl-3-fluoropyrrolidin-2-one (100): To a freshly prepared solution of LDA (1.1 equiv) in THF (50 mL) at -78 °C was added a solution of (*R*)-5-benzyl-1-(4-methoxybenzyl)pyrrolidin-2-one (**99**) (2.28 g, 7.71 mmol, 1.0 equiv) in THF (10 mL) and stirred for 90 min at -78° C. A solution of N-fluorobenzenesulfonamide (3.25 g, 10.03 mmol, 1.3 equiv) in THF (10 mL) was added dropwise, stirred for 1 h at -78 °C and then warmed to r.t. slowly by removing the dry ice/acetone bath. The reaction was quenched by the addition of NH₄Cl_(sat) (20 mL), concentrated *in vacuo*, and extracted with DCM (3 X 50 mL). The combined organic extracts were dried (Na₂SO₄) and concentrated to yield a crude solid. To this solid (mainly consisting of unreacted N-fluorobenzenesulfonamide and benzenesulfonamide) was added ether (20 mL) while stirring vigorously. The slurry was filtered through a sintered glass funnel and washed continuously with ether (100 mL). Concentration of the filtrate *in vacuo* provided the crude PMB-lactam, which was purified by flash chromatography (8:2 hex:EtOAc) to yield predominantly the *trans*-diastereomer (1.10 g). To a cooled (0 °C) solution of the PMB-lactam in CH₃CN (5 mL) and water (1 mL) was added ceric ammonium nitrate (4.81 g, 8.76 mmol, 2.5 equiv) portionwise. After stirring for 30 min at 0 °C the reaction was warmed to r.t., stirred an

additional 1 h at r.t., and concentrated to approximately 1/3 of its original volume. Water was then added (20 mL), and the mixture extracted with DCM (3 X 25 mL). The combined extracts were dried (Na₂SO₄), and concentrated *in vacuo* to yield a crude solid. The solid was purified via flash chromatography on silica gel (20% EtOAc/hexanes) to yield the desired compound (258 mg, 53%) as an off-white crystalline solid. ¹H NMR (300 MHz, CDCl₃): δ 7.36-7.24 (m, 3H), 7.18-7.15 (m, 2H), 4.78 (ddd, *J* = 52.7, 7.4, 5.2 Hz, 1H), 4.07-4.01 (m, 1H), 2.87-2.73 (m, 2H), 2.46-2.16 (m, 2H); ¹³C NMR (75 MHz, CDCl₃): δ 172.5 (*J*_{C-F} = 20.6 Hz), 136.3, 129.4, 128.9, 127.3, 88.4 (*J*_{C-F} = 182.2 Hz), 53.0, 42.5, 33.8 (*J*_{C-F} = 19.8 Hz).



(5*S*,7*S*)-5-benzyl-7-fluoro-2-(perfluorophenyl)-6,7-dihydro-5*H*-pyrrolo[2,1-*c*][1,2,4]triazol-2-ium tetrafluoroborate (101): Prepared analogously to (73)

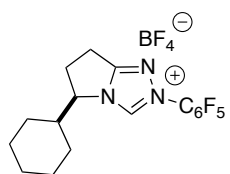
using (3*S*,5*S*)-5-benzyl-3-fluoropyrrolidin-2-one (100). ¹H NMR (300 MHz, CDCl₃): δ 10.21 (s, 1H), 7.46-7.28 (m, 5H), 6.50 (ddd, *J* = 53.9, 6.7, 2.5 Hz, 1H), 3.71 (dd, *J* = 13.7, 6.8 Hz, 1H), 3.45 (dd, *J* = 13.7, 7.7 Hz, 1H), 3.38-3.08 (m, 2H), 3.05-2.80 (m, 2H).



(*R*)-5-isopropyl-2-(perfluorophenyl)-6,7-dihydro-5*H*-pyrrolo[2,1-*c*][1,2,4]triazol-2-ium tetrafluoroborate (102): To a flame-dried flask with

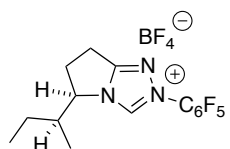
magnetic stir bar was added (*R*)-5-isopropylpyrrolidin-2-one² (3.28 g, 25.8 mmol). The flask was then evacuated and back-filled with argon. Dichloromethane (125 mL) and trimethyloxonium tetrafluoroborate (3.82 g, 25.8 mmol) were then added via powder funnel. The heterogeneous mixture was stirred at room temperature until the reaction was homogeneous (about 6 hours). Pentafluorophenyl hydrazine (5.12 g, 25.8 mmol) was added in one portion and the mixture was refluxed for 18 hours at which point dichloromethane was removed *in vacuo*.

Triethylorthoformate (20.0 mL, 120.2 mmol) was then added and the solution transferred to a 75 mL pressure flask and heated in a 130 °C oil bath for 6 h. The resulting dark brown solution was then concentrated *in vacuo* to leave a semi-solid, which was then triturated with ethyl acetate, filtered and washed with cold ethyl acetate. The resulting off-white powder was dried under vacuum for 12 h to give triazolium salt **102** (3.21 g, 30%) as an off-white solid. $[\alpha]_D^{21} = +30.0$ (c = 0.010 g/ml, MeOH); **m.p.** (°C): 158-162; **¹H NMR** (300 MHz, acetone-*d*₆) δ 10.39 (s, 1H), 5.03 (m, 1H), 3.44 (m, 2H), 3.09 (m, 1H), 2.82 (m, 1H), 2.51 (m, *J* = 6.6 Hz, 1H), 1.14 (d, *J* = 6.8 Hz, 3H), 1.05 (d, *J* = 6.8 Hz, 3H); **¹³C NMR** (75 MHz, acetone-*d*₆) δ 164.6, 145.1 (m), 143.8, 141.9 (m), 140.1 (m), 136.8 (m), 67.9, 31.2, 21.7, 18.0, 16.7; **IR** (NaCl, neat) 3125, 2979, 1600, 1527, 1061 cm⁻¹; **HRMS** (ESI+) calcd for C₁₄H₁₃F₅N₃, 318.1024. Found 318.1016.



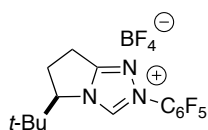
(R)-5-cyclohexyl-2-(perfluorophenyl)-6,7-dihydro-5H-pyrrolo[2,1-c][1,2,4]triazol-2-ium tetrafluoroborate (103): Prepared analogously to **(102)** using (*R*)-5-cyclohexylpyrrolidin-2-one². White solid. $[\alpha]_D^{21} = +43.6$ (c = 0.005 g/mL, MeOH); **m.p.** (°C): 180-181; **¹H NMR** (300 MHz, CDCl₃) δ 10.37 (s, 1H), 5.00

(td, *J* = 5.9, 8.1 Hz, 1H), 3.51-3.36 (m, 2H), 3.14-3.04 (m, 1H), 2.91-2.84 (m, 1H), 2.21-2.13 (m, 1H), 1.94-1.91 (m, 1H), 1.82-1.79 (m, 2H), 1.75-1.67 (m, 2H), 1.38-1.17 (m, 4H); **¹³C NMR** (100 MHz, CDCl₃) δ 164.2, 143.5, 67.0, 40.3, 29.9, 28.5, 27.3, 25.6, 25.4, 25.3, 21.4 **HRMS** (ESI+) calcd for C₁₇H₁₇F₅N₃, 358.1337. Found 358.1355.



(R)-5-((S)-sec-butyl)-2-(perfluorophenyl)-6,7-dihydro-5H-pyrrolo[2,1-c][1,2,4]triazol-2-ium tetrafluoroborate (104): To a flame-dried flask with magnetic stir bar was added (*R*)-5-((*S*)-sec-butyl)pyrrolidin-2-one² (1.0 g,

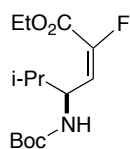
7.08 mmol). The flask was then evacuated and back-filled with argon. Dichloromethane (35 mL) and trimethyloxonium tetrafluoroborate (1.05 g, 7.08 mmol) were then added via powder funnel. The heterogeneous mixture was stirred at room temperature until the reaction was homogeneous (about 6 hours). Pentafluorophenyl hydrazine (1.40 g, 7.08 mmol) was added in one portion and the mixture was stirred for 18 hours at which point dichloromethane was removed *in vacuo*. Triethylorthoformate (20.0 mL) was then added and the solution transferred to a 75 mL pressure flask and heated in a 130 °C oil bath for 12 h. The resulting dark brown solution was then concentrated *in vacuo* to leave a semi-solid, which was then triturated with diethyl ether, filtered and washed with diethyl ether. The resulting off-white powder was dried under vacuum for 12 h to give triazolium salt (**104**) (1.04 g, 35%) as an off-white solid. $[\alpha]_D^{21} = +35.6$ (c = 0.005 g/ml, MeOH); **m.p.** (°C): 176-178; **¹H NMR** (400 MHz, CDCl₃) δ 10.41 (s, 1H), 5.20-5.15 (m, 2H), 3.46 (ddd, J = 4.0, 6.6, 8.5 Hz, 2H), 3.06 (dtd, J = 6.5, 8.5, 13.5 Hz, 1H), 2.89-2.82 (m, 1H), 2.46-2.36 (m, 1H), 1.71-1.60 (m, 1H), 1.46-1.35 (m, 1H), 1.03-0.99 (m, 6H); **¹³C NMR** (100 MHz, CDCl₃) δ 164.2, 143.4, 66.2, 36.9, 28.5, 25.3, 21.6, 12.5, 10.6; **HRMS** (ESI+) calcd for C₁₅H₁₅F₅N₃, 332.1181. Found 332.1171.



(R)-5-(tert-butyl)-2-(perfluorophenyl)-6,7-dihydro-5H-pyrrolo[2,1-

c][1,2,4]triazol-2-ium tetrafluoroborate (105): To a flame-dried flask with magnetic stir bar was added (*R*)-5-*tert*-butylpyrrolidin-2-one² (1.00 g, 7.08 mmol, 1.0 equiv). The flask was then evacuated and back-filled with argon. Dichloromethane (35 mL) and trimethyloxonium tetrafluoroborate (1.05 g, 7.08 mmol, 1.0 equiv) were then added via powder funnel. The heterogeneous mixture was stirred at room temperature until the reaction was homogeneous (about 6 hours). Pentafluorophenyl hydrazine (1.40 g, 7.08 mmol, 1.0 equiv) was

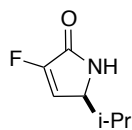
added in one portion and the mixture was stirred for 18 hours at which point dichloromethane was removed *in vacuo*. Triethylorthoformate (20.0 mL) was then added and the solution transferred to a 75 mL pressure flask and heated in a 130 °C oil bath for 4 h. After cooling to room temperature, the reaction was filtered and the resultant solid was washed with ether and dried under vacuum for 12 h to give triazolium salt (**105**) (1.60 g, 54%) as an off-white solid. $[\alpha]_D^{21} = +28.3$ (c = 0.010 g/ml, MeOH); **m.p.** (°C): 200-202; **¹H NMR** (400 MHz, acetone-*d*₆) δ 10.37 (s, 1H), 4.98 (dd, *J* = 8.7, 4.8 Hz, 1H), 3.42 (m, 2H), 3.09 (m, 1H), 2.91 (m, 1H), 1.14 (s, 9H); **¹³C NMR** (100 MHz, acetone-*d*₆) δ 164.9, 144.3, 142.1 (m), 139.5 (m), 138.3 (m), 137.3 (m), 71.9, 34.6, 25.1, 21.8; **IR** (NaCl, neat) 3134, 2958, 2882, 1587, 1518, 1480, 1410, 1366, 1069, 1006 cm⁻¹; **HRMS** (ESI+) calcd for C₁₅H₁₅F₅N₃, 332.1186. Found 332.1188.



(*S,E*)-ethyl 4-(*tert*-butoxycarbonylamino)-2-fluoro-5-methylhex-2-enoate (125**):**

Synthesized via a modified literature procedure.⁴ A solution of (*S*)-methyl 2-(*tert*-butoxycarbonylamino)-3-methylbutanoate (3.24 g, 14.00 mmol, 1.0 equiv) in toluene (60 mL) at -78 °C was added a 1.0 M solution of diisobutylaluminum hydride in hexanes (28.0 mL, 28.00 mmol, 2.0 equiv) dropwise. The reaction was then allowed to stir for 3 h at -78 °C at which point it was quenched with AcOH (10 mL) and then warmed slowly to room temperature. The mixture was diluted with EtOAc (100 mL) and poured into a separatory funnel containing a 10% aqueous tartaric acid solution (100 mL). The organic layer was separated and washed with water (2 x 100 mL) and brine (100 mL), dried over anhydrous Na₂SO₄, and concentrated *in vacuo*. The crude aldehyde was dried under vacuum (4 mm) for 1 h and then used in the next step without further purification. To a solution of triethyl 2-fluoro-2-phosphonoacetate (3.56 g, 14.70 mmol, 1.05 equiv) in THF (100 mL) at room temperature was added a 1.6 M solution of *n*-

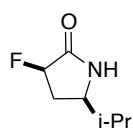
BuLi in hexanes (9.19 mL, 14.70 mmol, 1.05 equiv) and stirred for 30 min. This solution was then cooled to -78 °C at which point a solution of the crude aldehyde (described previously) in THF (50 mL) was added dropwise via cannula over 30 min. The reaction was stirred at this temperature for 3 h and then quenched by the addition of saturated aqueous NH₄Cl (50 mL). The THF was evaporated *in vacuo*, and to the residue was added water (100 mL) and EtOAc (150 mL). The organic layer was washed with water (2 x 100 mL), dried over anhydrous Na₂SO₄, and concentrated *in vacuo*. The crude residue was purified by silica gel chromatography (5:1 hexanes:EtOAc) to yield the desired product as a white solid (3.34 g, 83%); R_f = 0.43 (5:1 hexanes:EtOAc); [α]_D²¹ = +112.4 (c = 0.010 g/ml, CH₂Cl₂); **m.p.** (°C): 49-50; **¹H NMR** (400 MHz, CDCl₃) δ 5.73 (dd, *J* = 21.1, 9.7 Hz, 1H), 4.83 (m, 1H), 4.63 (bs, 1H), 4.29 (m, 2H), 1.85 (bs, 1H), 1.40 (s, 9H), 0.92 (m, 6H); **¹³C NMR** (100 MHz, CDCl₃) δ 169.1, 160.6 (*J*_{C-F} = 35.3 Hz), 155.3, 149.0, 122.8 (m), 79.6, 61.9, 52.0, 33.1, 28.5, 19.0, 18.3, 14.3; **IR** (NaCl, neat) 3370, 2959, 2931, 1737, 1693, 1501, 1370 cm⁻¹; **HRMS** (ESI+) calcd for C₁₄H₂₄FNO₄, 289.1689. Found 289.1692.



(S)-3-fluoro-5-isopropyl-1H-pyrrol-2(5H)-one (126): A stream of dry HCl gas was slowly bubbled through a solution of **(125)** (3.34 g, 11.54 mmol, 1.0 equiv) in ether (150 mL) until TLC indicated complete consumption of the starting material.

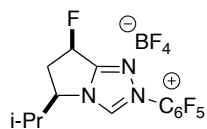
The solution was then concentrated *in vacuo*, dissolved in toluene (150 mL), and warmed to 40 °C in a water bath. Triethylamine (4.02 mL, 28.86 mmol, 2.5 equiv) was then added dropwise over 30 min. The heterogeneous mixture was allowed to stir for an additional 30 min at which point saturated aqueous NH₄Cl_(aq) (100 ml) was added. The layers were separated and the aqueous layer was then extracted with EtOAc (2 x 50 mL). The combined organic layers were

dried over anhydrous Na₂SO₄, and concentrated *in vacuo*. The crude residue was then purified by silica gel chromatography (EtOAc) to yield the desired product as a white solid (1.15 g, 69%). R_f = 0.55 (EtOAc); [α]_D²¹ = +156.1 (c = 0.010 g/ml, CH₂Cl₂); **m.p.** (°C): 89-90; **¹H NMR** (400 MHz, CDCl₃) δ 8.15 (bs, 1H), 6.26 (s, 1H), 3.90 (m, 1H), 1.88 (m, *J* = 6.7 Hz, 1H), 0.95 (dd, *J* = 5.7, 5.7 Hz, 6H); **¹³C NMR** δ (100 MHz, CDCl₃) δ 166.2 (*J*_{C-F} = 40.0 Hz), 153.1 (*J*_{C-F} = 278.0 Hz), 118.6 (*J*_{C-F} = 3.5 Hz), 59.1 (*J*_{C-F} = 5.0 Hz), 31.5, 18.5, 18.4; **IR** (NaCl, neat) 3201, 3125, 2954, 2927, 2868, 1698, 1655, 1462, 1194 cm⁻¹; **HRMS** (ESI+) calcd for C₇H₁₁FNO, 143.0747. Found 143.0746.



(3R,5R)-3-fluoro-5-isopropylpyrrolidin-2-one (127): To a solution of (126)

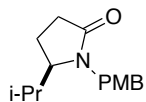
(1.135 g, 7.93 mmol) in methanol (100 mL) was added 10% Pd/C (0.20 g) and exposed to a hydrogen atmosphere (balloon). The mixture was stirred for 12 h then filtered and concentrated *in vacuo* to yield the desired compound as a white solid (1.12 g, 97%). R_f = 0.53 (EtOAc); [α]_D²¹ = +92.4 (c = 0.010 g/ml, CH₂Cl₂); **m.p.** (°C): 92-93; **¹H NMR** (400 MHz, CDCl₃) δ 7.89 (bs, 1H) 5.02 (ddd, *J* = 52.7, 7.2, 7.2 Hz, 1H), 3.26 (m, 1H), 2.56 (m, 1H), 1.85 (m, 1H), 1.67 (m, *J* = 6.6 Hz, 1H), 0.96 (d, *J* = 6.6 Hz, 3H), 0.89 (d, *J* = 6.6 Hz, 3H); **¹³C NMR** δ (100 MHz, CDCl₃) δ 173.0 (*J*_{C-F} = 20.9 Hz), 88.8 (*J*_{C-F} = 185.7 Hz), 32.4 (*J*_{C-F} = 18.5 Hz), 18.9, 18.0; **IR** (NaCl, neat) 3217, 3104, 2975, 2863, 1709, 1698, 1473, 1328, 1296, 1081 cm⁻¹; **HRMS** (ESI+) calcd for C₇H₁₂FNO, 145.093. Found 145.092.



(5R,7R)-7-fluoro-5-isopropyl-2-(perfluorophenyl)-6,7-dihydro-5H-pyrrolo[2,1-c][1,2,4]triazol-2-ium tetrafluoroborate (128): To a flame-dried

flask with magnetic stir bar was added (127) (1.00 g, 6.88 mmol, 1.0 equiv). The flask was then evacuated and back-filled with argon. Dichloromethane (50 mL) and trimethyloxonium

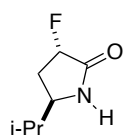
tetrafluoroborate (1.06 g, 6.88 mmol, 1.0 equiv) were then added via powder funnel. The heterogeneous mixture was stirred at room temperature until the reaction was homogeneous (about 6 hours). Pentafluorophenyl hydrazine (1.40 g, 6.88 mmol, 1.0 equiv) was added in one portion and the mixture was refluxed for 18 hours at which point dichloromethane was removed *in vacuo*. Trimethylorthoformate (30.0 mL) was then added and the solution was refluxed for 6 h, concentrated and refluxed again in trimethylorthoformate (30.0 mL). After concentration *in vacuo* the residue was dissolved in chlorobenzene (30 ml) and heated to 130 °C for 2h. Following cooling to room temperature an off-white solid precipitated which was filtered and washed with ether and dried to yield triazolium salt (**128**) (2.12 g, 73%) as an off-white solid. $[\alpha]_D^{21} = +22.8$ (c = 0.010 g/ml, MeOH); **m.p.** (°C): 154-155; **¹H NMR** (400 MHz, acetone-*d*₆) δ 10.62 (s, 1H), 6.51 (ddd, *J* = 54.4, 7.4, 2.3 Hz, 1H), 5.12 (m, 1H), 3.61 (dddd, *J* = 27.2, 15.7, 8.4, 7.5 Hz, 1H), 2.96 (dddd, 27.2, 15.6, 3.6, 2.3 Hz, 1H), 2.51 (m, *J* = 6.8 Hz, 1H), 1.17 (d, *J* = 6.8 Hz, 3H), 1.09 (d, *J* = 6.8 Hz, 3H); **¹³C NMR** (100 MHz, acetone-*d*₆) δ 160.3 (*J*_{C-F} = 23.1 Hz), 144.7, 144.5 (m), 141.9 (m), 139.7 (m), 137.0 (m), 83.5 (*J*_{C-F} = 183.9 Hz), 67.3, 37.7 (*J*_{C-F} = 21.9 Hz), 31.8, 18.0, 16.8; **IR** (NaCl, neat) 3136, 2965, 1704, 1607, 1543, 1478, 1065 cm⁻¹; **HRMS** (ESI+) calcd for C₁₄H₁₂F₆N₃, 336.0935. Found 336.0942.



(R)-5-isopropyl-1-(4-methoxybenzyl)pyrrolidin-2-one (130): To a dry round

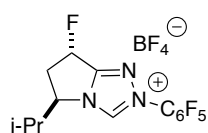
bottomed flask was added (*R*)-5-isopropylpyrrolidin-2-one (1.50 g, 11.8 mmol, 1.0 equiv) and anhydrous THF (20 mL). Sodium hydride (0.34 g, 14.2 mmol, 1.2 equiv) was added portionwise and the mixture was stirred for 30 min followed by the addition of 4-methoxybenzylchloride (2.21 g, 14.2 mmol, 1.2 equiv) and tetrabutylammonium iodide (0.436 g, 1.18 mmol, 0.1 equiv). After 18 h the reaction was quenched with NH₄Cl_(sat) (20 mL), extracted

with dichloromethane (3 X 20 mL), and dried (Na₂SO₄). Concentration of the combined organic extracts left a crude oil which was purified by flash chromatography (9:1 EtOAc:Hex) to provide the desired product (2.44 g, 84%) as a colorless oil. ¹H NMR (300 MHz, CDCl₃): δ 7.17-7.14 (m, 2H), 6.85-6.82 (m, 2H), 5.02 (d, *J* = 14.8 Hz, 1H), 3.79 (s, 3H), 3.77 (d, *J* = 18.3 Hz), 3.37 (ddd, *J* = 8.5, 5.1, 3.5 Hz, 1H), 2.42-2.35 (m, 2H), 2.10 (m, 1H), 1.85-1.71 (m, 2H), 0.83 (d, *J* = 6.9 Hz, 3H), 0.74 (d, *J* = 6.8 Hz, 3H).



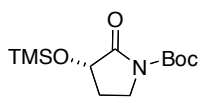
(3*S*,5*R*)-3-fluoro-5-isopropylpyrrolidin-2-one (131): To a freshly prepared solution of LDA (1.1 equiv) in THF (10 mL) at -78 °C was added a solution of (*R*)-5-isopropyl-1-(4-methoxybenzyl)pyrrolidin-2-one (**130**) (2.44 g, 9.87 mmol, 1.0 equiv) in THF (10 mL) and stirred for 90 min at -78° C. A solution of N-fluorobenzenesulfonamide (4.05 g, 12.84 mmol, 1.3 equiv) in THF (10 mL) was added dropwise, stirred for 1 h at -78 °C and then warmed to room temperature slowly by removing the dry ice/acetone bath. The reaction was quenched by the addition of NH₄Cl_(sat) (20 mL), concentrated *in vacuo*, and extracted with DCM (3 X 50 mL). The combined organic extracts were dried (Na₂SO₄) and concentrated to yield a crude solid. To this solid (mainly consisting of unreacted N-fluorobenzenesulfonamide and benzenesulfonamide) was added ether (20 mL) while stirring vigorously. The slurry was filtered through a sintered glass funnel and washed continuously with ether (100 mL). Concentration of the filtrate *in vacuo* provided the crude PMB-lactam, which was used in the next step without further purification. To a cooled (0 °C) solution of the PMB-lactam in CH₃CN (5 mL) and water (1 mL) was added ceric ammonium nitrate (13.54 g, 24.7 mmol, 2.5 equiv) portionwise. After stirring for 30 min at 0 °C the reaction was warmed to r.t., stirred an additional 1 h at r.t., and concentrated to approximately 1/3 of its original volume. Water was then added (20 mL), and the

mixture extracted with DCM (3 X 25 mL). The combined extracts were dried (Na₂SO₄), and concentrated *in vacuo* to yield a crude solid. The solid was purified via flash chromatography on silica gel (40% EtOAc/hexanes) to yield the desired compound (0.43 g, 30%) as an off-white crystalline solid. ¹H NMR (300 MHz, CDCl₃): δ 7.84 (s, 1H), 5.04 (ddd, *J* = 52.8, 7.5, 4.5 Hz, 1H), 3.55 (q, *J* = 5.9 Hz, 1H), 2.43-2.03 (m, 2H), 1.64 (m, 1H), 0.92 (dd, *J* = 11.8, 6.7 Hz, 6H).



(5*R*,7*S*)-7-fluoro-5-isopropyl-2-(perfluorophenyl)-6,7-dihydro-5*H*-pyrrolo[2,1-*c*][1,2,4]triazol-2-ium tetrafluoroborate (132): Prepared

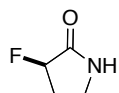
analogously to (73) using (3*S*,5*R*)-3-fluoro-5-isopropylpyrrolidin-2-one (131). [α]_D²¹ = +33.5 (*c* = 0.010 g/ml, MeOH); **m.p.** (°C): 179-181; ¹H NMR (400 MHz, acetone-*d*₆) δ 10.65 (s, 1H), 6.61 (ddd, *J* = 53.9, 6.7, 2.8 Hz, 1H), 5.30 (dt, 6.9, 6.8 Hz, 1H), 3.27 (m, 2H), 2.58 (m, *J* = 6.7 Hz, 1H), 1.19 (d, *J* = 6.8 Hz, 3H), 1.05 (d, *J* = 6.8 Hz, 3H); ¹³C NMR (100 MHz, acetone-*d*₆) δ 160.3 (*J*_{C-F} = 23.4 Hz), 144.8, 144.6 (m), 139.7 (m), 137.2 (m), 83.9 (*J*_{C-F} = 184.9 Hz), 67.5, 38.4 (*J*_{C-F} = 22.0 Hz), 30.7, 18.1, 16.6; **IR** (NaCl, neat) 3142, 2975, 1709, 1591, 1527, 1478, 1071 cm⁻¹; **HRMS** (ESI+) calcd for C₁₄H₁₂F₆N₃, 336.0935. Found 336.0935.



(*S*)-tert-butyl 2-oxo-3-(trimethylsilyloxy)pyrrolidine-1-carboxylate (137):

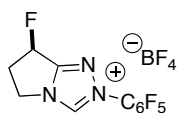
To a solution of (*S*)-3-(trimethylsilyloxy)pyrrolidin-2-one⁵ (6.00 g, 34.62 mmol, 1.0 equiv) in CH₂Cl₂ (150 mL) was added di-*tert*-butyl dicarbonate (15.11 g, 69.24 mmol, 2.0 equiv), triethylamine (4.82 mL, 34.62 mmol, 1.0 equiv), and dimethylamino pyridine (4.23 g, 34.62 mmol, 1.0 equiv). The mixture was stirred overnight at room temperature then 1N HCl (100 mL) was added, and the layers were separated. The organic layer was washed with 1N HCl (2 x 50 mL), and brine (1 x 50 mL) then dried over anhydrous Na₂SO₄. The solution was

concentrated *in vacuo* to leave a crude oil which was purified by silica gel chromatography (19:1 hexanes:EtOAc) to yield the desired compound as a clear viscous oil (7.62 g, 81%). $R_f = 0.40$ (5:1, hexanes:EtOAc) $[\alpha]_D^{21} = -50.9$ ($c = 0.010$ g/ml, CH_2Cl_2); $^1\text{H NMR}$ (400 MHz, CDCl_3) δ 4.27 (dd, $J = 4.3, 4.3$ Hz, 1H), 3.77 (dd, $J = 10.8, 9.0$ Hz, 1H), 3.44 (m, 1H), 2.25 (m, 1H), 1.89 (m, 1H), 1.49 (s, 9H), 0.16 (s, 9H); $^{13}\text{C NMR}$ δ (100 MHz, CDCl_3) δ 172.9, 150.5, 83.2, 71.5, 42.0, 28.2, 0.3; **IR** (NaCl, neat) 2991, 2884, 1780, 1757, 1709, 1371, 1322, 1242, 1140 cm^{-1} ; **HRMS** (ESI+) calcd for $\text{C}_{12}\text{H}_{23}\text{NO}_4\text{Si}$, 273.1396. Found 273.1393.



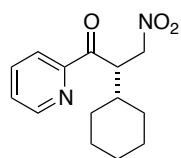
(R)-3-fluoropyrrolidin-2-one (135): A solution of (*S*)-3-(trimethylsilyloxy)pyrrolidin-2-one (**137**) (7.62 g, 27.87 mmol, 1.0 equiv) in CH_2Cl_2 was cooled to -78 °C at which point diethylaminosulfur trifluoride (7.43 mL, 55.74 mmol, 2.0 equiv) was added dropwise. The solution was then allowed to warm to room temperature slowly and saturated aqueous NaHCO_3 (100 mL) was then added to quench the reaction. The layers were separated and the organic layer was then washed with saturated NH_4Cl (2 x 50 mL), dried over anhydrous Na_2SO_4 , and concentrated *in vacuo* to yield a crude solid. This crude material was then dissolved in CH_2Cl_2 (100 mL) and trifluoroacetic acid (6.7 mL, 86.95 mmol, 3.0 equiv) was added. The solution was stirred for 3 h at which point the evolution of gas had subsided. Concentration *in vacuo*, then purification of the crude residue by silica gel chromatography (99:1, EtOAc:MeOH) yielded the desired product as a white solid (2.21 g, 74%). $R_f = 0.20$ (EtOAc); $[\alpha]_D^{21} = +118.7$ ($c = 0.010$ g/ml, CH_2Cl_2); **m.p.** (°C): 76-78; $^1\text{H NMR}$ (400 MHz, CDCl_3) δ 7.70 (bs, 1H), 5.00 (ddd, $J = 52.7, 6.8, 6.8$ Hz, 1H), 3.46 (ddd, $J = 9.5, 9.5, 3.6$ Hz, 1H), 3.31 (m, 1H), 2.48 (m, 1H), 2.24 (m, 1H); $^{13}\text{C NMR}$ δ (100 MHz, CDCl_3) δ 173.5 ($J_{\text{C-F}} = 19.9$ Hz), 88.5 ($J_{\text{C-F}} = 183.3$ Hz), 38.9 ($J_{\text{C-F}} = 3.7$ Hz), 28.4 ($J_{\text{C-F}} = 20.2$ Hz); **IR** (NaCl,

neat) 3455, 3395, 3204, 3139, 2910, 1685, 1462, 1310, 1070 cm^{-1} ; **HRMS** (ESI+) calcd for $\text{C}_4\text{H}_6\text{FNO}$, 103.0433. Found 103.0439.

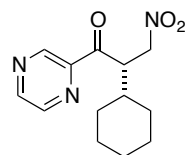


(R)-7-fluoro-2-(perfluorophenyl)-6,7-dihydro-5H-pyrrolo[2,1-c][1,2,4]triazol-2-ium tetrafluoroborate (138): To a flame-dried flask with magnetic stir bar was added (*R*)-3-fluoropyrrolidin-2-one (**135**) (1.00 g, 9.70 mmol, 1.0 equiv). The flask was then evacuated and back-filled with argon. Dichloromethane (50 mL) and trimethyloxonium tetrafluoroborate (1.51 g, 9.70 mmol, 1.0 equiv) were then added via powder funnel. The heterogeneous mixture was stirred at room temperature until the reaction was homogeneous (about 12 hours). Pentafluorophenyl hydrazine (1.92 g, 9.70 mmol, 1.0 equiv) was added in one portion and the mixture was refluxed for 18 hours at which point dichloromethane was removed *in vacuo*. Chlorobenzene (40 mL) and triethylorthoformate (10.0 mL) was then added and the solution heated in a 130 °C oil bath for 12 h. The dark brown solution was then cooled to 0 °C in an ice bath and filtered. The resultant brown solid was washed with cold ethyl acetate and dried under vacuum for 12 h to give triazolium salt (**138**) (2.84 g, 77%) as an off-white solid. $[\alpha]_{\text{D}}^{21} = -1.8$ ($c = 0.010$ g/ml, MeOH); **m.p.** (°C): 214-216; **$^1\text{H NMR}$** (400 MHz, acetone- d_6) δ 10.36 (s, 1H), 6.54 (ddd, 54.2, 7.1, 2.8 Hz, 1H), 4.97 (m, 1H), 4.87 (m, 1H), 3.50 (m, 1H), 3.11 (m, 1H); **$^{13}\text{C NMR}$** (100 MHz, acetone- d_6) δ 160.8 ($J_{\text{C-F}} = 23.3$ Hz), 144.9, 144.7 (m), 142.2 (m), 139.7 (m), 137.1 (m), 84.2 ($J_{\text{C-F}} = 184.8$ Hz), 47.8, 35.2 ($J_{\text{C-F}} = 22.2$ Hz); **IR** (NaCl, neat) 3136, 3099, 1703, 1591, 1521, 1296, 1076, 1022 cm^{-1} ; **HRMS** (ESI+) calcd for $\text{C}_{11}\text{H}_6\text{F}_6\text{N}_3$, 294.0466. Found 294.0467.

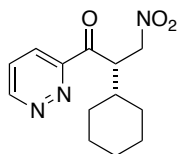
Characterization of Stetter Products



(S)-2-cyclohexyl-3-nitro-1-(pyridin-2-yl)propan-1-one (92): White solid; $R_f = 0.30$ (1:1 ether:hexanes) 95% yield, 95% ee; $[\alpha]_D^{21} = -68.0$ ($c = 0.010$ g/ml, CH_2Cl_2); HPLC analysis – Chiracel OD-H column, 90:10 hexanes/*iso*-propanol, 1.0 mL/min. Major: 7.74 min, minor: 6.90 min. **m.p.** ($^\circ\text{C}$): 128-130; **^1H NMR** (300 MHz, CDCl_3) δ 8.72 (dm, $J = 4.8$ Hz, 1H), 8.08 (d, $J = 7.9$ Hz, 1H), 7.86 (ddd, $J = 7.8, 7.8, 1.8$ Hz, 1H), 7.50 (ddd, $J = 7.8, 4.8, 1.1$ Hz, 1H), 5.06 (dd, $J = 14.3, 10.9$ Hz, 1H), 4.80 (m, 1H), 4.59 (dd, $J = 14.3, 3.2$ Hz, 1H), 1.85 (m, 1H), 1.65 (m, 5H), 1.15 (m, 4H), 0.93 (m, 1H); **^{13}C NMR** (75 MHz, CDCl_3) δ 200.9, 152.7, 149.3, 137.3, 127.7, 122.7, 73.9, 47.3, 39.0, 31.5, 29.6, 26.6, 26.5, 26.2; **IR** (NaCl, neat) 3070, 3003, 2924, 2856, 1696, 1544, 1448, 1392 cm^{-1} ; **HRMS** (ESI+) calcd for $\text{C}_{14}\text{H}_{19}\text{N}_2\text{O}_3$, 263.1390. Found 263.1393.



(S)-2-cyclohexyl-3-nitro-1-(pyrazin-2-yl)propan-1-one (108): White solid; $R_f = 0.33$ (1:1 ether:hexanes); 99% yield, 96% ee; $[\alpha]_D^{21} = -75.8$ ($c = 0.010$ g/ml, CH_2Cl_2); HPLC analysis – Chiracel OD-H column, 90:10 hexanes/*iso*-propanol, 1.0 mL/min. Major: 10.69 min, minor: 9.67 min. **m.p.** ($^\circ\text{C}$): 102-105; **^1H NMR** (300 MHz, CDCl_3) δ 9.29 (m, 1H), 8.81 (dm, $J = 2.4$ Hz, 1H), 8.71 (m, 1H), 5.08 (dd, $J = 14.6, 11.0$ Hz, 1H), 4.78 (m, 1H), 4.61 (dd, $J = 14.6, 3.2$ Hz, 1H), 1.72 (m, 6H), 1.18 (m, 4H), 0.97 (m, 1H); **^{13}C NMR** (75 MHz, CDCl_3) δ 200.5, 148.4, 147.0, 144.5, 143.9, 73.8, 47.4, 39.0, 31.5, 29.8, 26.6, 26.4, 26.1. **IR** (NaCl, neat) 3058, 2919, 2848, 1685, 1557, 1383, 1020 cm^{-1} ; **HRMS** (ESI+) calcd for $\text{C}_{13}\text{H}_{18}\text{N}_3\text{O}_3$, 264.1343. Found 264.1344.

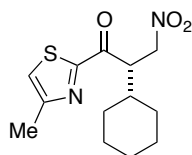


(S)-2-cyclohexyl-3-nitro-1-(pyridazin-3-yl)propan-1-one (109): Yellow solid;

$R_f = 0.08$ (1:1 ether:hexanes); 88% yield, 94% ee; $[\alpha]_D^{21} = -73.2$. (c = 0.010 g/ml,

CH_2Cl_2); HPLC analysis – Chiracel OD-H column, 80:20 hexanes/*iso*-propanol,

1.0 mL/min. Major: 15.15 min, minor: 13.10 min. **m.p.** ($^\circ\text{C}$): 82-84; **^1H NMR** (300 MHz, CDCl_3) δ 9.38 (dd, $J = 5.0, 1.7$ Hz, 1H), 8.20 (dd, $J = 8.5, 1.7$ Hz, 1H), 7.71 (dd, $J = 8.5, 5.0$ Hz, 1H), 5.08 (m, 2H), 4.67 (dd, $J = 14.0, 2.6$ Hz, 1H), 1.97 (m, 1H), 1.68 (m, 5H), 1.13 (m, 5H); **^{13}C NMR** (75 MHz, CDCl_3) δ 155.2, 153.6, 127.7, 125.6, 73.8, 48.0, 39.0, 31.6, 29.7, 26.5, 26.4, 26.1; **IR** (NaCl, neat) 2923, 2862, 1697, 1549, 1450, 1422, 1378 cm^{-1} ; **HRMS** (ESI+) calcd for $\text{C}_{13}\text{H}_{17}\text{N}_3\text{O}_3$, 263.1270. Found 263.1274.

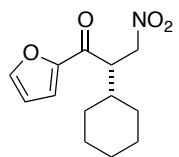


(S)-2-cyclohexyl-1-(4-methylthiazol-2-yl)-3-nitropropan-1-one (111):

White solid; $R_f = 0.65$ (1:1 ether:hexanes); 70% yield, 96% ee; $[\alpha]_D^{21} = -76.4$ (c

= 0.010 g/ml, CH_2Cl_2); HPLC analysis – Chiracel OD-H column, 90:10

hexanes/*iso*-propanol, 1.0 mL/min. Major: 7.62 min, minor: 6.97 min. **m.p.** ($^\circ\text{C}$): 124-126; **^1H NMR** (300 MHz, CDCl_3) δ 7.29 (m, 1H), 5.05 (dd, $J = 14.6, 11.0$ Hz, 1H), 4.58 (dd, $J = 14.6, 3.3$ Hz, 1H), 4.49 (m, 1H), 2.54 (s, 3H), 1.87 (m, 1H), 1.66 (m, 5H), 1.18 (m, 4H), 0.97 (m, 1H); **^{13}C NMR** δ (75 MHz, CDCl_3) δ 193.0, 165.4, 155.9, 122.5, 73.7, 49.5, 39.2, 31.4, 29.9, 26.5, 26.4, 26.1, 17.5; **IR** (NaCl, neat) 3105, 2923, 2836, 1661, 1548, 1424, 1370 cm^{-1} ; **HRMS** (ESI+) calcd for $\text{C}_{13}\text{H}_{19}\text{N}_2\text{O}_3\text{S}$, 283.1111. Found 283.1114.

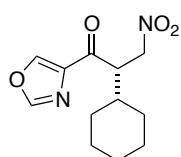


(S)-2-cyclohexyl-1-(furan-2-yl)-3-nitropropan-1-one (113): Clear oil; $R_f = 0.28$

(1:1 ether:hexanes); 75% yield, 87% ee; $[\alpha]_D^{21} = -88.0$ (c = 0.010 g/ml, CH_2Cl_2);

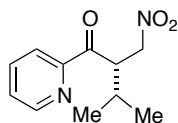
HPLC analysis – Chiracel OD-H column, 90:10 hexanes/*iso*-propanol, 1.0

mL/min. Major: 10.43 min, minor: 8.82 min; $^1\text{H NMR}$ (300 MHz, CDCl_3) δ 7.64 (m, 1H), 7.29 (dm, $J = 3.6$ Hz, 1H), 6.60 (dd, $J = 3.6, 1.7$ Hz, 1H), 5.02 (dd, $J = 14.6, 10.5$ Hz, 1H), 4.51 (dd, $J = 14.6, 3.6$ Hz, 1H), 3.95 (m, 1H), 1.71 (m, 6H), 1.17 (m, 4H), 0.95 (m, 1H); $^{13}\text{C NMR}$ (75 MHz, CDCl_3) δ 188.4, 152.8, 147.2, 118.5, 112.9, 73.5, 49.9, 39.5, 31.3, 30.1, 26.5, 26.4, 26.1; **IR** (NaCl, neat) 3128, 2933, 2846, 1669, 1554, 1467, 1375, 1277 cm^{-1} ; **HRMS** (ESI+) calcd for $\text{C}_{13}\text{H}_{18}\text{N}_2\text{O}_4$, 252.1230. Found 252.1238.



(S)-2-cyclohexyl-3-nitro-1-(oxazol-4-yl)propan-1-one (114): White solid; $R_f = 0.25$ (1:1 ether:hexanes); 76% yield; $[\alpha]_D^{21} = -83.6$ ($c = 0.010$ g/ml, CH_2Cl_2)
HPLC analysis – Chiracel OD-H column, 90:10 hexanes/*iso*-propanol, 1.0

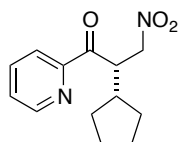
mL/min. Major: 12.08 min, minor: 10.50 min; **m.p.** ($^\circ\text{C}$): 65-68; $^1\text{H NMR}$ (300 MHz, CDCl_3) δ 8.33 (s, 1H), 7.96 (s, 1H), 5.05 (ddd, $J = 14.7, 10.9, 0.7$ Hz, 1H), 4.53 (ddd, $J = 14.7, 3.3, 0.7$ Hz, 1H), 4.17 (m, 1H), 1.87 (m, 1H), 1.70 (m, 5H), 1.18 (m, 4H), 0.96 (m, 1H); $^{13}\text{C NMR}$ (75 MHz, CDCl_3) δ 194.4, 151.2, 143.3, 140.2, 73.2, 50.5, 38.8, 31.4, 29.7, 26.5, 26.4, 26.1; **IR** (NaCl, neat) 2921, 2843, 1675, 1557, 1372, 1096, 1057, 905 cm^{-1} ; **HRMS** (ESI+) calcd for $\text{C}_{12}\text{H}_{16}\text{N}_2\text{O}_4$, 252.1110. Found 252.1108.



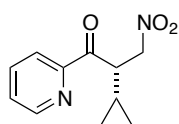
(S)-3-methyl-2-(nitromethyl)-1-(pyridin-2-yl)butan-1-one (115): White solid, $R_f = 0.35$ (1:1 ether:hexanes) 85% yield, 95% ee; $[\alpha]_D^{21} = -78.0$ ($c = 0.010$

g/ml, CH_2Cl_2); HPLC analysis – Chiracel OD-H column, 90:10 hexanes/*iso*-propanol, 1.0 mL/min. Major: 8.52 min, minor: 7.22 min; **m.p.** ($^\circ\text{C}$): 58-62; $^1\text{H NMR}$ (300 MHz, CDCl_3) δ 8.72 (m, 1H), 8.09 (ddd, $J = 7.9, 7.9, 0.9$ Hz, 1H), 7.86 (ddd, $J = 7.7, 7.7, 1.7$ Hz, 1H), 7.51 (dd, $J = 7.5, 1.1$ Hz, 1H), 5.08 (dd, $J = 14.4, 10.8$ Hz, 1H), 4.87 (ddd, $J = 13.9, 10.8, 5.1$ Hz, 1H),

4.57 (dd, $J = 14.4, 3.2$ Hz, 1H), 2.26 (oct, $J = 6.9$ Hz, 1H), 1.04 (d, $J = 6.9$ Hz, 3H), 0.88 (d, $J = 6.9$ Hz, 3H); $^{13}\text{C NMR}$ (75 MHz, CDCl_3) δ 200.7, 152.5, 149.3, 137.3, 127.7, 122.8, 73.3, 47.8, 29.0, 21.2, 18.8; **IR** (NaCl, neat) 3058, 3022, 2961, 2929, 2886, 1691, 1578, 1557, 1385 cm^{-1} ; **HRMS** (ESI+) calcd for $\text{C}_{11}\text{H}_{15}\text{N}_2\text{O}_3$, 223.1077. Found 223.1073.

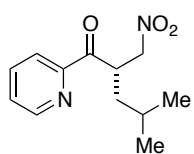


(S)-2-cyclopentyl-3-nitro-1-(pyridin-2-yl)propan-1-one (117): White solid; $R_f = 0.35$ (1:1 ether:hexanes); 98% yield, 90% ee; $[\alpha]_D^{21} = -51.6$ ($c = 0.010$ g/ml, CH_2Cl_2) HPLC analysis – Chiracel OD-H column, 90:10 hexanes/*iso*-propanol, 1.0 mL/min. Major: 8.86 min, minor: 8.11 min; **m.p.** ($^\circ\text{C}$): 92-94; $^1\text{H NMR}$ (300 MHz, CDCl_3) δ 8.72 (dm, $J = 4.8$ Hz, 1H), 8.11 (dm, $J = 7.8$ Hz, 1H), 7.87 (ddd, $J = 7.7, 7.7, 1.8$ Hz, 1H), 7.50 (ddd, $J = 7.7, 4.8, 1.2$ Hz, 1H), 5.08 (dd, $J = 14.2, 10.7$ Hz, 1H), 4.89 (ddd, $J = 11.8, 8.6, 3.2$, 1H), 4.63 (dd, $J = 14.2, 3.2$ Hz, 1H), 2.06 (m, 1H), 1.78 (m, 1H), 1.54 (m, 5H), 1.28 (m, 2H); $^{13}\text{C NMR}$ (75 MHz, CDCl_3) δ 201.2, 152.9, 149.2, 137.3, 127.7, 122.8, 75.8, 46.1, 41.0, 30.7, 30.5, 25.1, 24.7; **IR** (NaCl, neat) 3057, 3013, 2948, 2856, 1690, 1549, 1425, 1381 cm^{-1} ; **HRMS** (ESI+) calcd for $\text{C}_{13}\text{H}_{17}\text{N}_2\text{O}_3$, 249.1234. Found 249.1237.



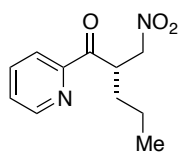
(S)-2-cyclopropyl-3-nitro-1-(pyridin-2-yl)propan-1-one (118): Amorphous solid; $R_f = 0.33$ (1:1 ether:hexanes); 72% yield, 87% ee; $[\alpha]_D^{21} = -86.3$ ($c = 0.006$ g/ml, CH_2Cl_2) HPLC analysis – Chiracel OD-H column, 90:10 hexanes/*iso*-propanol, 1.0 mL/min. Major: 9.28 min, minor: 8.53 min; $^1\text{H NMR}$ (300 MHz, CDCl_3) δ 8.72 (dm, $J = 4.7$ Hz, 1H), 8.14 (dm, $J = 8.7$ Hz, 1H), 7.88 (dddd, $J = 7.9, 7.9, 1.7, 0.4$ Hz, 1H), 7.53 (dddd, $J = 7.6, 4.8, 1.3, 0.4$ Hz, 1H), 5.15 (dd, $J = 14.3, 10.1$ Hz, 1H), 4.72 (dd, $J = 14.3, 4.5$ Hz, 1H), 4.25 (ddd, $J = 10.1, 10.1, 4.5$ Hz, 1H), 0.81 (m, 1H), 0.63 (m, 2H), 0.41 (m, 2H); $^{13}\text{C NMR}$ (75 MHz,

CDCl₃) δ 199.9, 149.2, 137.3, 127.8, 123.2, 120.3, 76.2, 46.1, 11.4, 4.8, 4.4; **IR** (NaCl, neat) 3053, 3001, 2909, 1690, 1552, 1378, 1358 cm⁻¹; **HRMS** (ESI+) calcd for C₁₁H₁₃N₂O₃, 221.0921. Found 221.0923.



(S)-4-methyl-2-(nitromethyl)-1-(pyridin-2-yl)pentan-1-one (119):

Amorphous solid; R_f = 0.40 (1:1 ether:hexanes); 99% yield, 83% ee; $[\alpha]_D^{21} = -20.0$ (c = 0.010 g/ml, CH₂Cl₂) HPLC analysis – Chiracel OD-H column, 90:10 hexanes/*iso*-propanol, 1.0 mL/min. Major: 7.35 min, minor: 6.93 min; **¹H NMR** (300 MHz, CDCl₃) δ 8.72 (d, *J* = 4.7 Hz, 1H), 8.09 (dm, *J* = 7.9 Hz, 1H), 7.87 (ddd, *J* = 7.7, 7.7, 1.5 Hz, 1H), 7.51 (ddd, *J* = 4.8, 4.8, 1.3 Hz, 1H), 4.98 (m, 2H), 4.57 (m, 1H), 1.63 (m, 2H), 1.34 (m, 1H), 0.99 (d, *J* = 6.4 Hz, 3H), 0.93 (d, *J* = 6.4 Hz, 3H); **¹³C NMR** (75 MHz, CDCl₃) δ 201.5, 152.2, 149.3, 137.3, 127.8, 122.9, 75.8, 41.0, 38.7, 26.3, 23.1, 22.4; **IR** (NaCl, neat) 3059, 3020, 2952, 2924, 1690, 1583, 1544, 1380 cm⁻¹; **HRMS** (ESI+) calcd for C₁₂H₁₇N₂O₃, 237.1234. Found 237.1233.

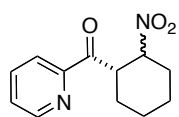


(S)-2-(nitromethyl)-1-(pyridin-2-yl)pentan-1-one (120): Clear oil; R_f = 0.25

(1:1 ether:hexanes); 82% yield, 83% ee; $[\alpha]_D^{21} = -29.9$. (c = 0.013 g/ml, CH₂Cl₂); HPLC analysis – Chiracel OD-H column, 90:10 hexanes/*iso*-propanol, 1.0 mL/min. Major: 8.30 min, minor: 7.68 min; **¹H NMR** (300 MHz, CDCl₃) δ 8.70 (dm, *J* = 4.2 Hz, 1H), 8.07 (dm, *J* = 7.9 Hz, 1H), 7.86 (ddd, *J* = 7.7, 7.7, 1.7 Hz, 1H), 7.50 (ddd, *J* = 7.5, 4.7, 1.2 Hz, 1H), 5.01 (dd, *J* = 13.8, 9.7 Hz, 1H), 4.89 (m, 1H), 4.57 (dd, *J* = 13.8, 4.0 Hz, 1H), 1.76 (m, 1H), 1.54 (m, 1H), 1.33 (m, 2H), 0.89 (t, *J* = 7.3 Hz, 3H); **¹³C NMR** (75 MHz, CDCl₃) δ 200.8, 152.2, 149.3, 137.3, 127.8, 122.9, 75.4, 42.6, 31.8, 20.3, 14.2; **IR** (NaCl, neat) 3054,

2952, 2930, 2868, 1696, 1549, 1386 cm^{-1} ; **HRMS** (ESI+) calcd for $\text{C}_{11}\text{H}_{15}\text{N}_2\text{O}_3$, 223.1077.

Found 223.1077.



((1S)-2-nitrocyclohexyl)(pyridin-2-yl)methanone (122): Clear oil; $R_f = 0.20$

(1:1 ether:hexanes) 62% yield, 96% ee $[\alpha]_D^{21} = -4.0, -20.3$. (c = 0.010 g/ml, CH_2Cl_2) HPLC analysis – Chiracel AC column, 80:20 hexanes/*iso*-propanol, 1.0 mL/min. Major:

13.55, 14.74 min, minor: 18.47, 16.52 min; $^1\text{H NMR}$ (300 MHz, CDCl_3) δ 8.72 (dm, $J = 4.8$ Hz,

1H), 8.03 (dt, $J = 7.8, 1.1$ Hz, 1H), 7.85 (ddd, $J = 7.7, 7.7, 1.8$ Hz, 1H), 7.49 (ddd, $J = 7.7, 4.8,$

1.3 Hz, 1H), 4.95 (ddd, $J = 12.3, 10.9, 4.3$ Hz, 1H), 4.61 (ddd, $J = 12.3, 10.9, 3.8$ Hz, 1H), 2.61

(m, 1H), 2.32 (m, 1H), 1.99 (m, 1H), 1.82 (m, 2H), 1.48 (m, 2H), 1.24 (m, 1H); δ 8.63 (dm, $J =$

4.8 Hz, 1H), 8.04 (dm, $J = 7.8$ Hz, 1H), 7.86 (m, 1H), 7.48 (m, 1H), 5.25 (m, 1H), 4.35 (m, 1H),

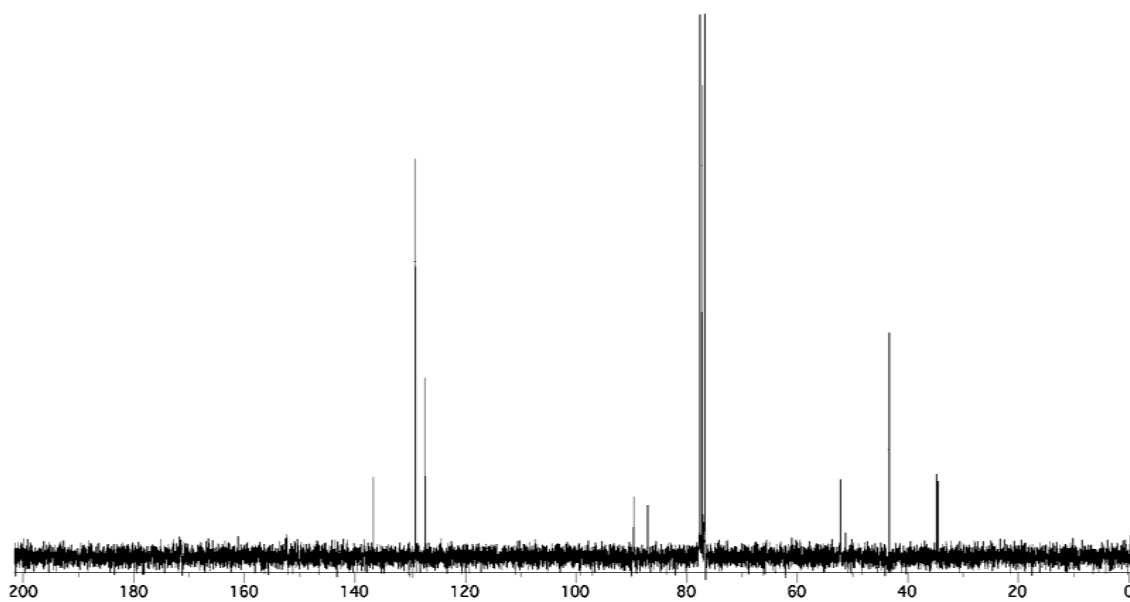
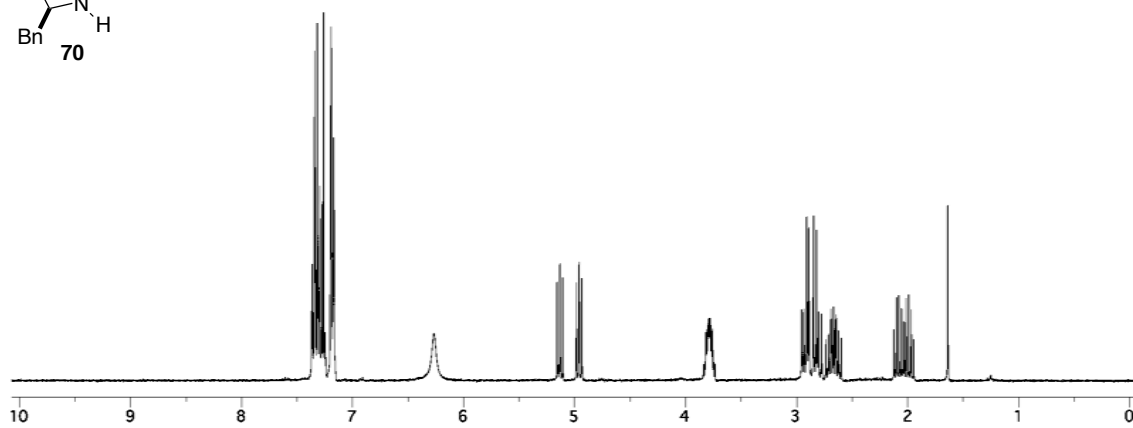
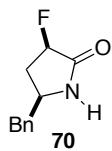
2.64 (m, 1H), 2.15 (m, 1H), 1.98 (m, 2H), 1.61 (m, 4H); $^{13}\text{C NMR}$ (75 MHz, CDCl_3) δ 201.0,

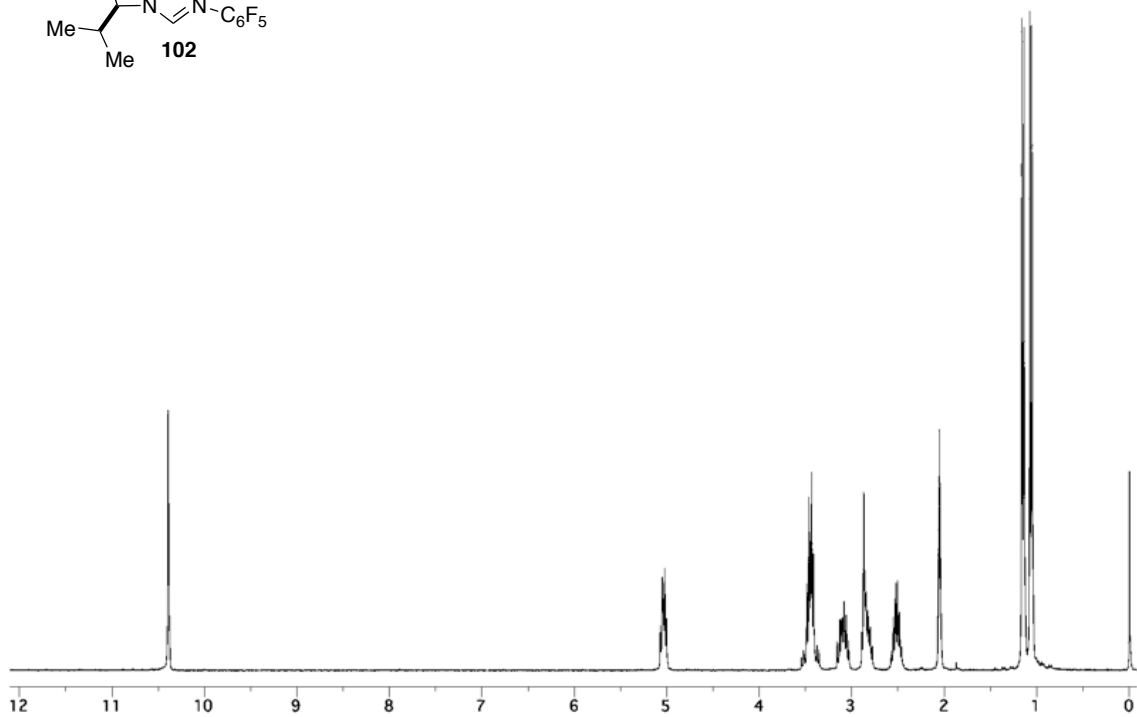
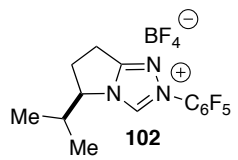
151.9, 149.3, 137.3, 127.8, 122.9, 84.9, 46.7, 31.7, 29.1, 25.1, 25.0; δ 199.6, 169.1, 152.9, 148.7,

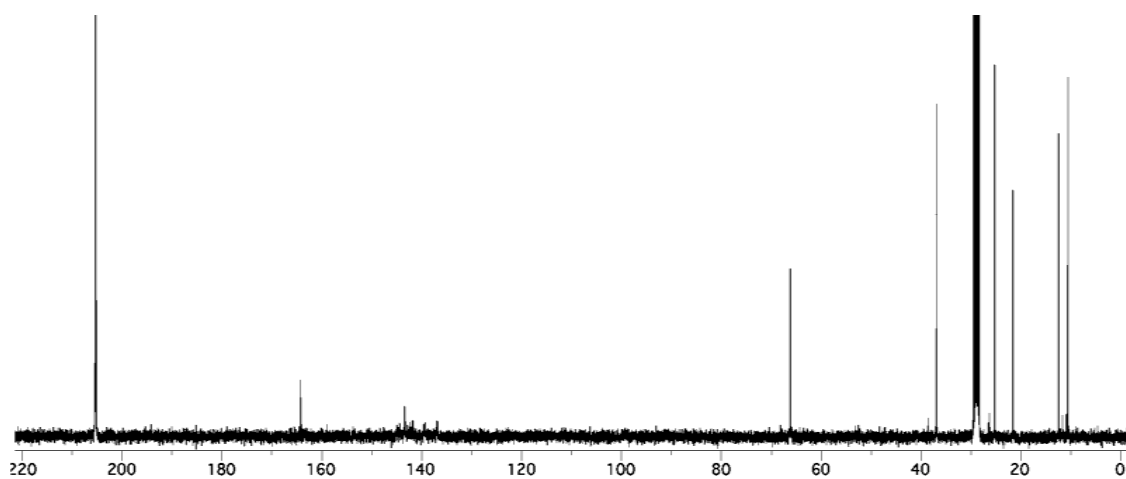
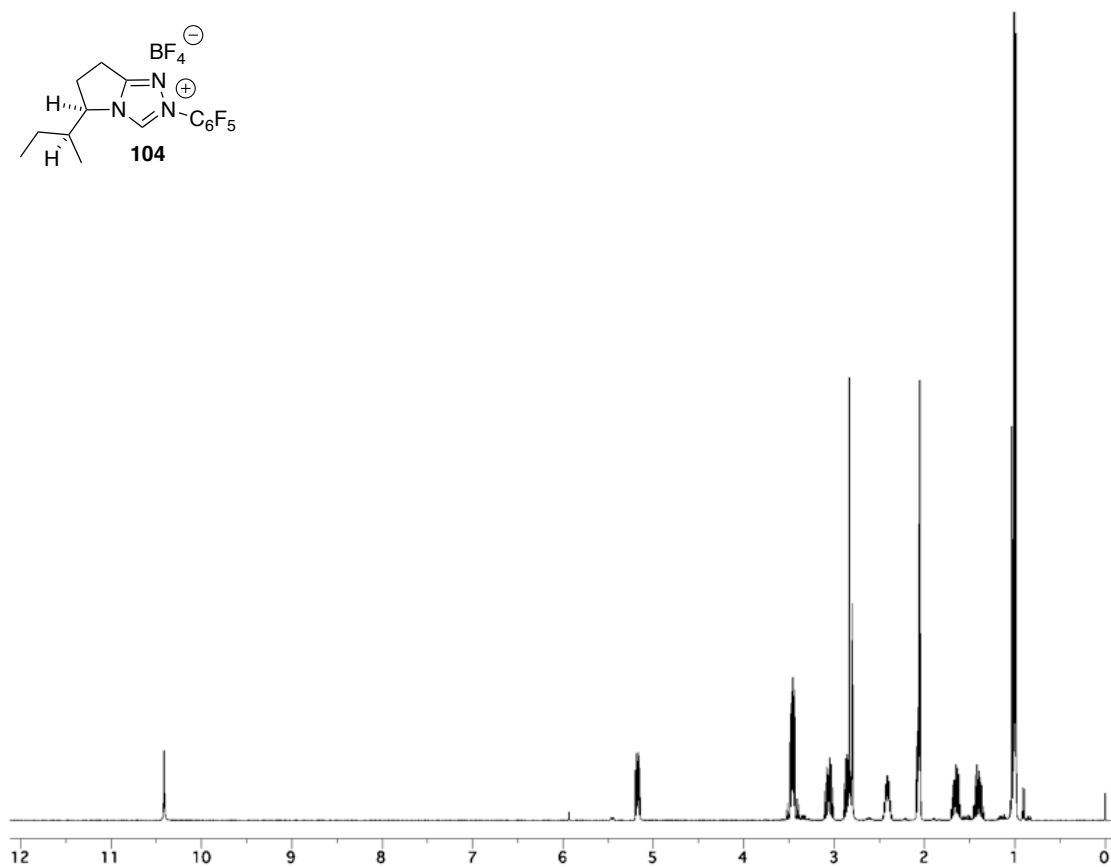
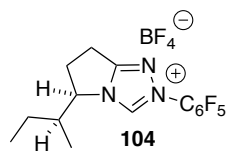
137.5, 127.3, 123.0, 84.2, 45.4, 28.3, 24.4, 23.1, 22.3; **IR** (NaCl, neat) 3045, 2941, 2859, 1684,

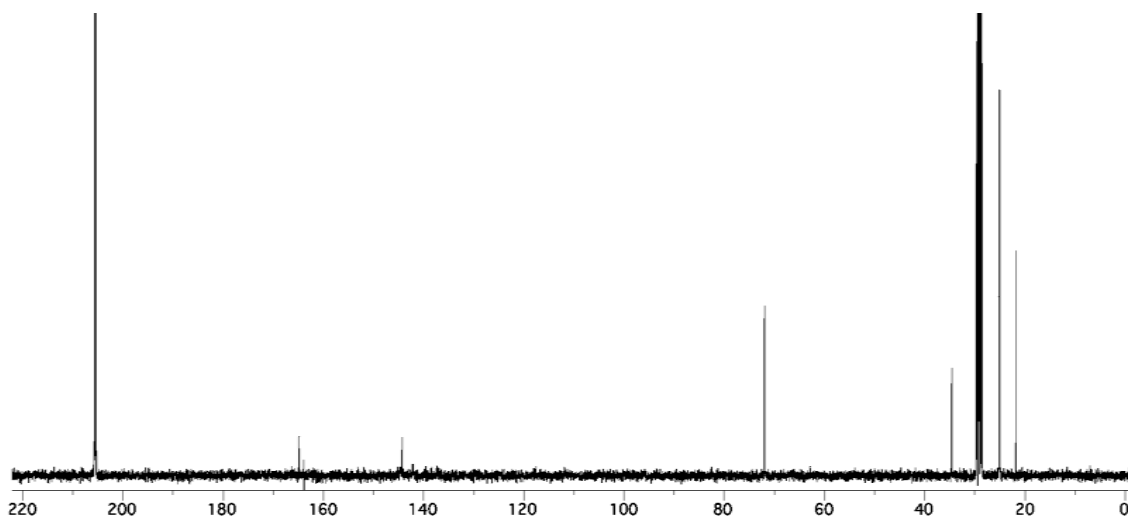
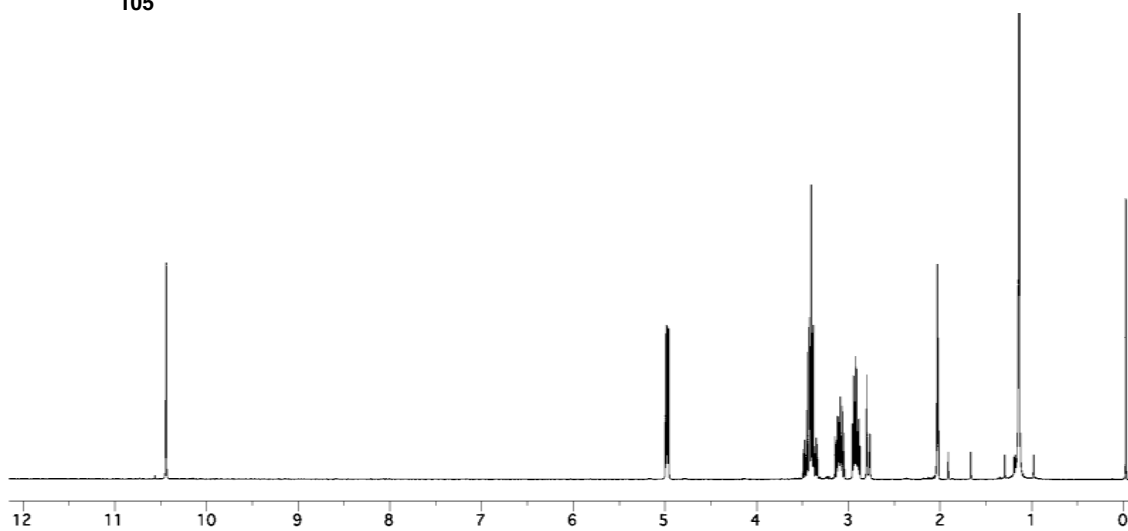
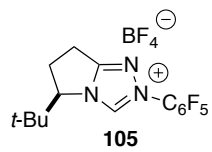
1541, 1431, 1377 cm^{-1} ; **HRMS** (ESI+) calcd for $\text{C}_{12}\text{H}_{15}\text{N}_2\text{O}_3$, 235.1077. Found 235.1077.

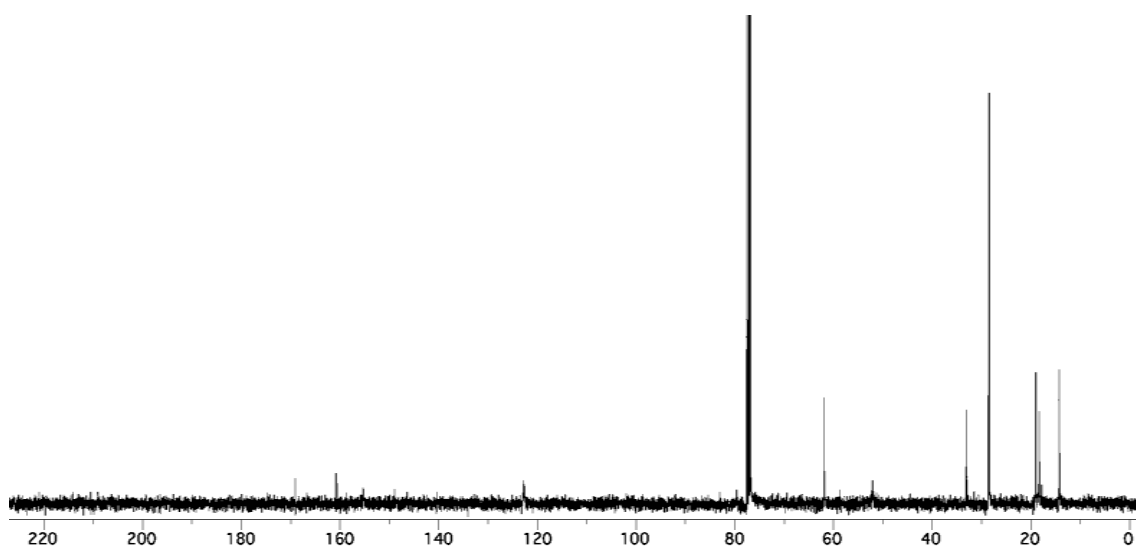
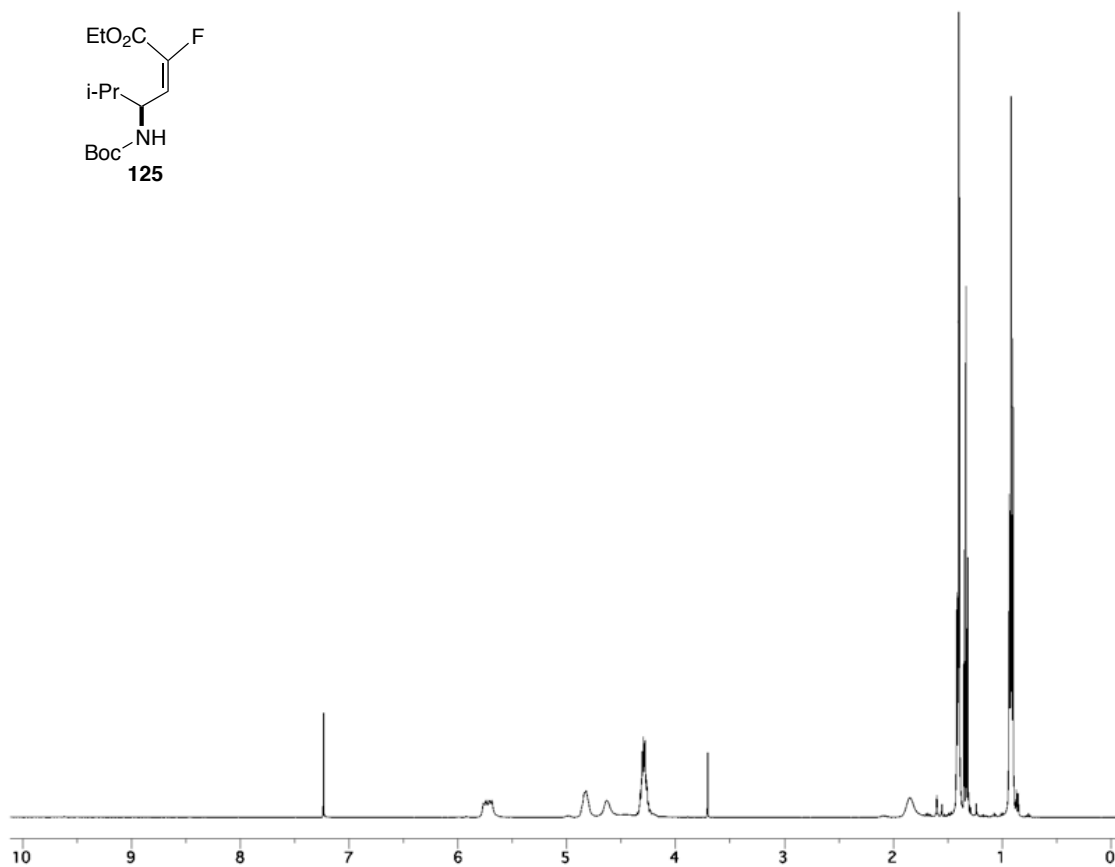
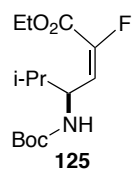
^1H and ^{13}C NMR Spectra

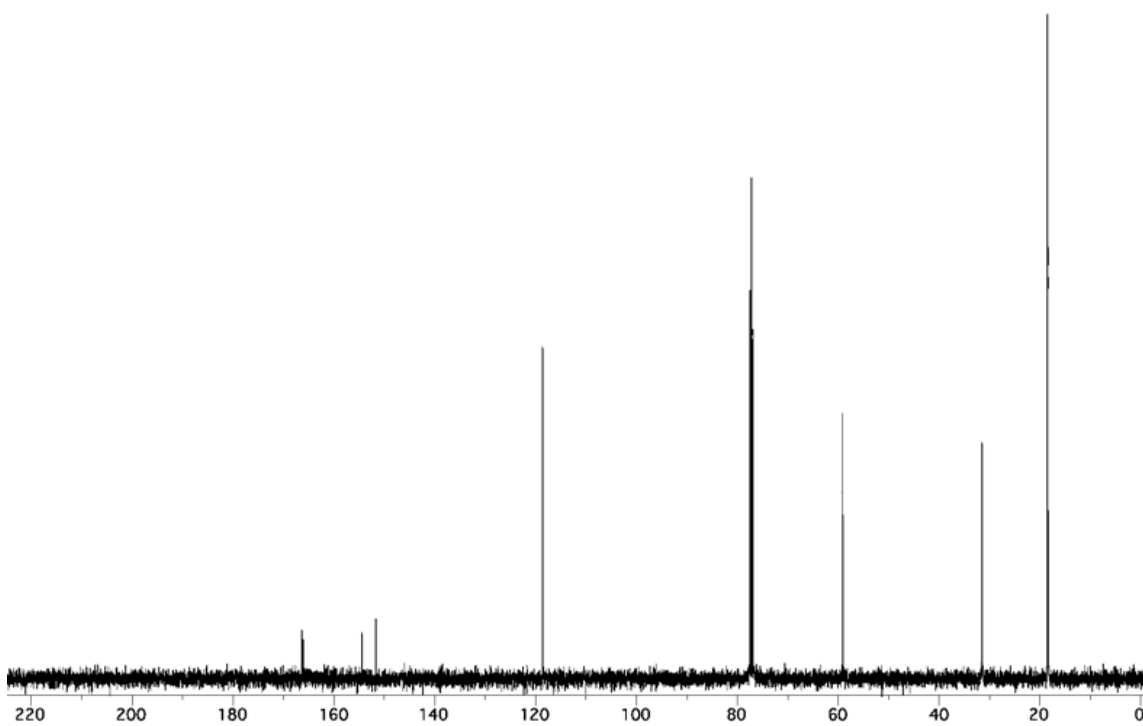
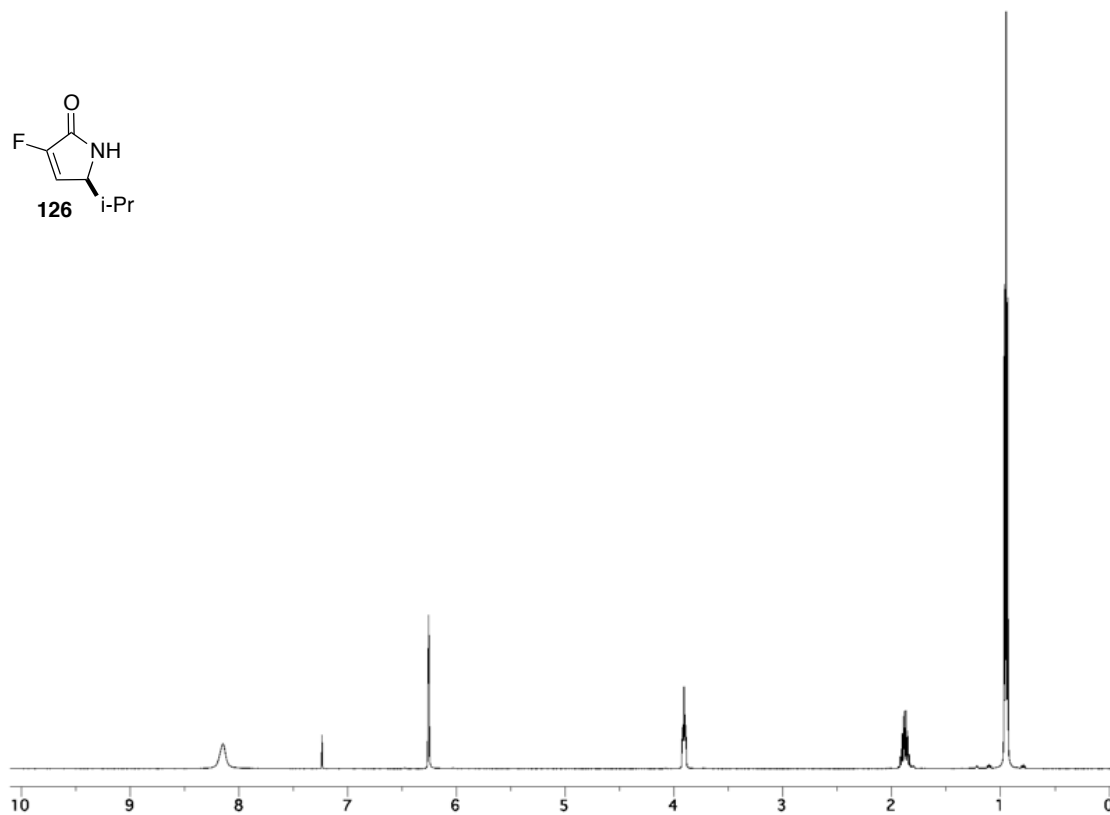
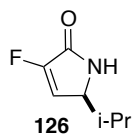


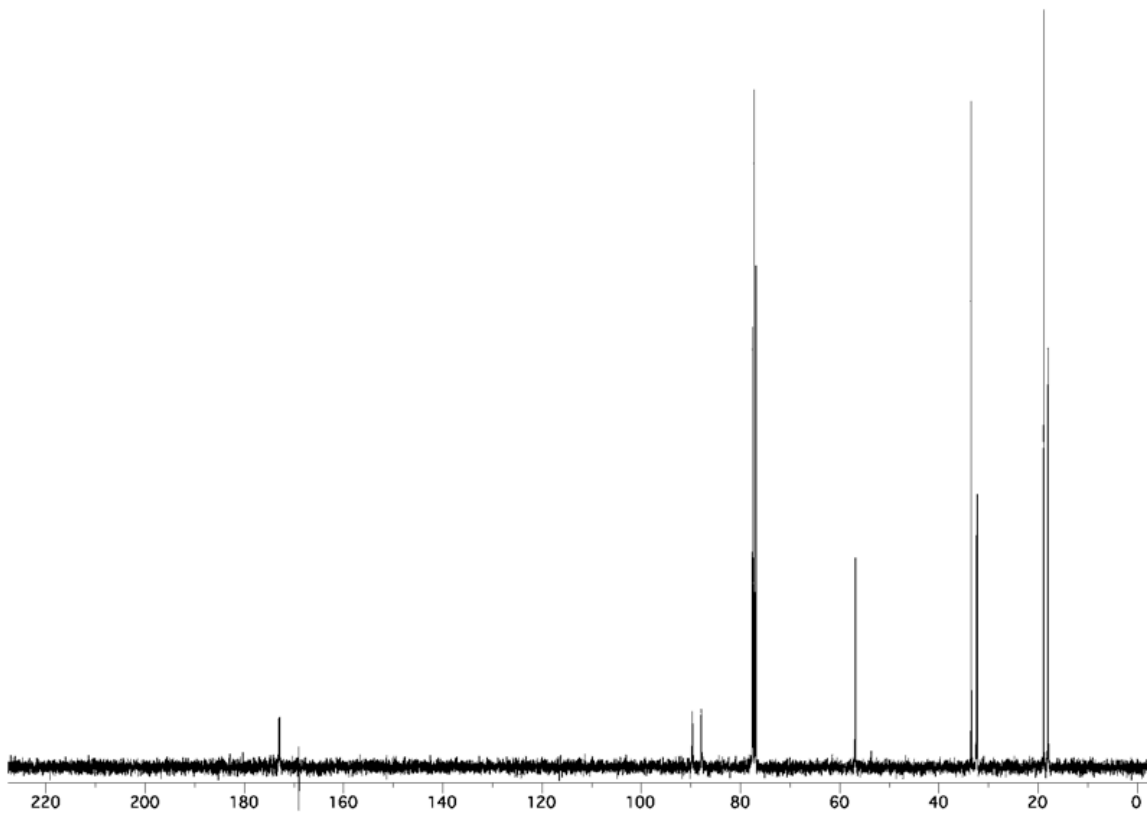
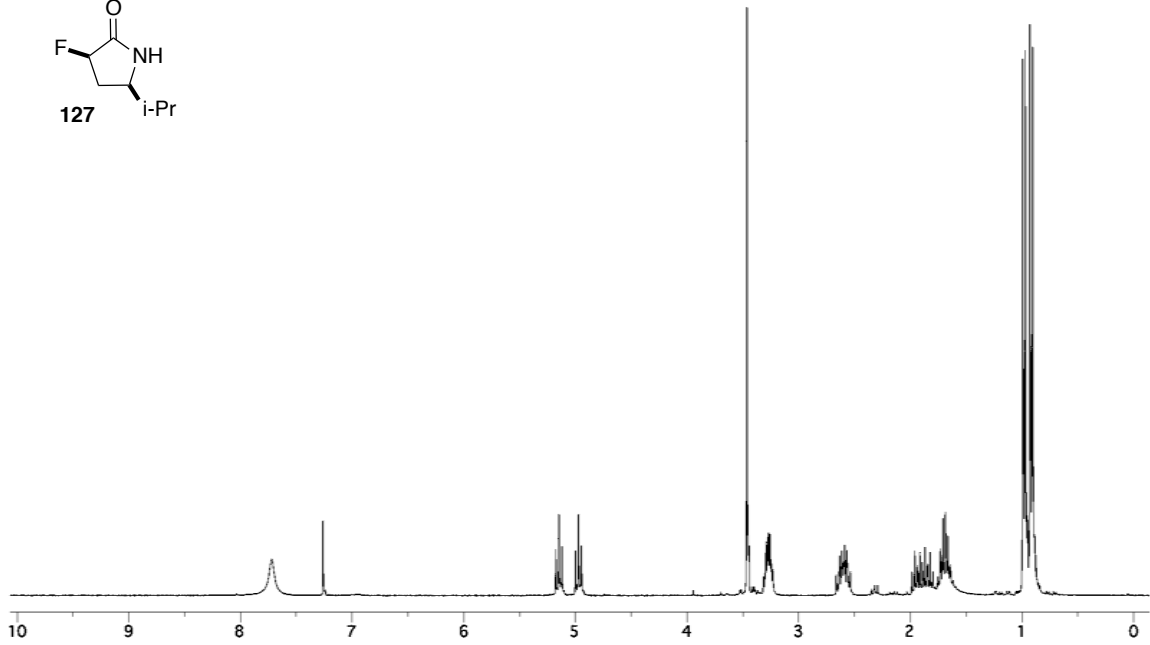
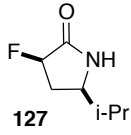


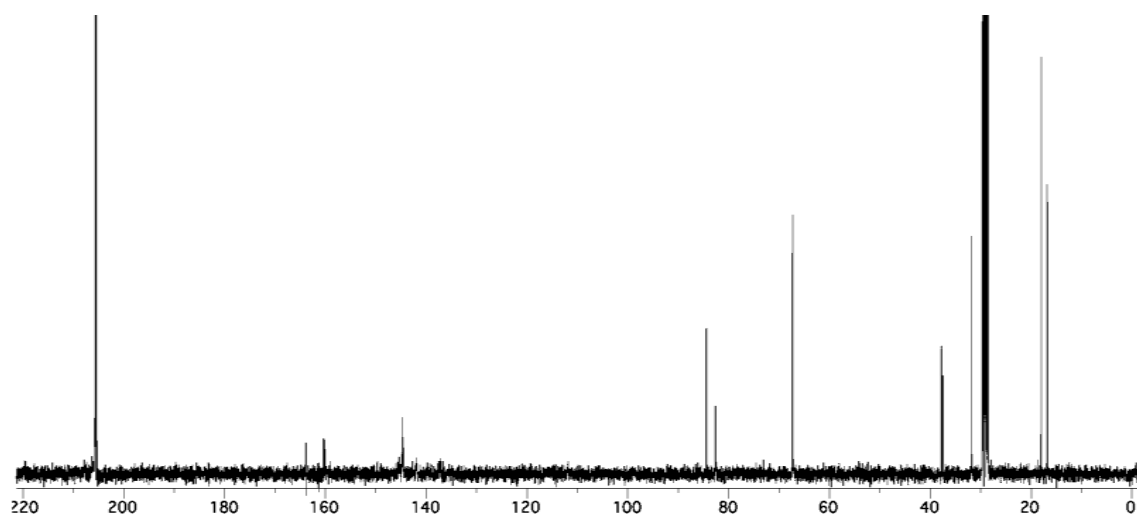
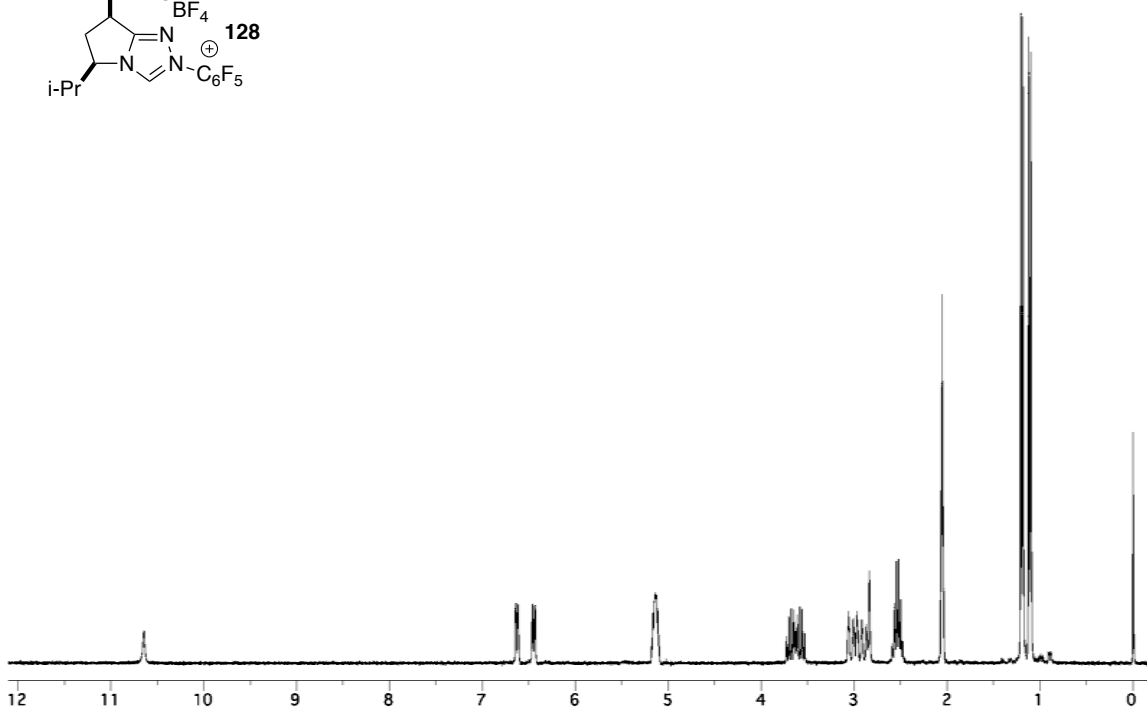
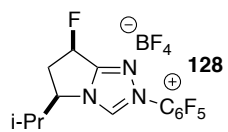


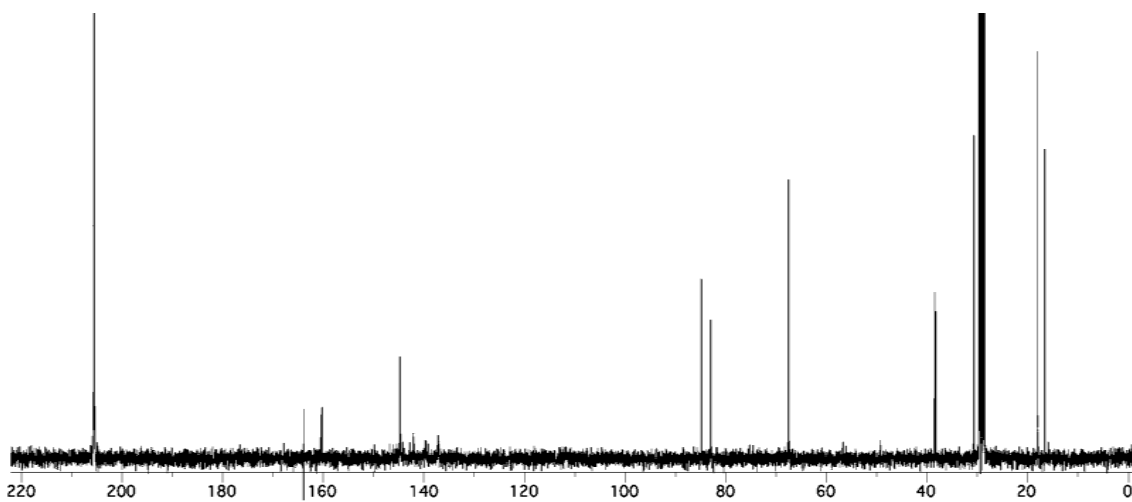
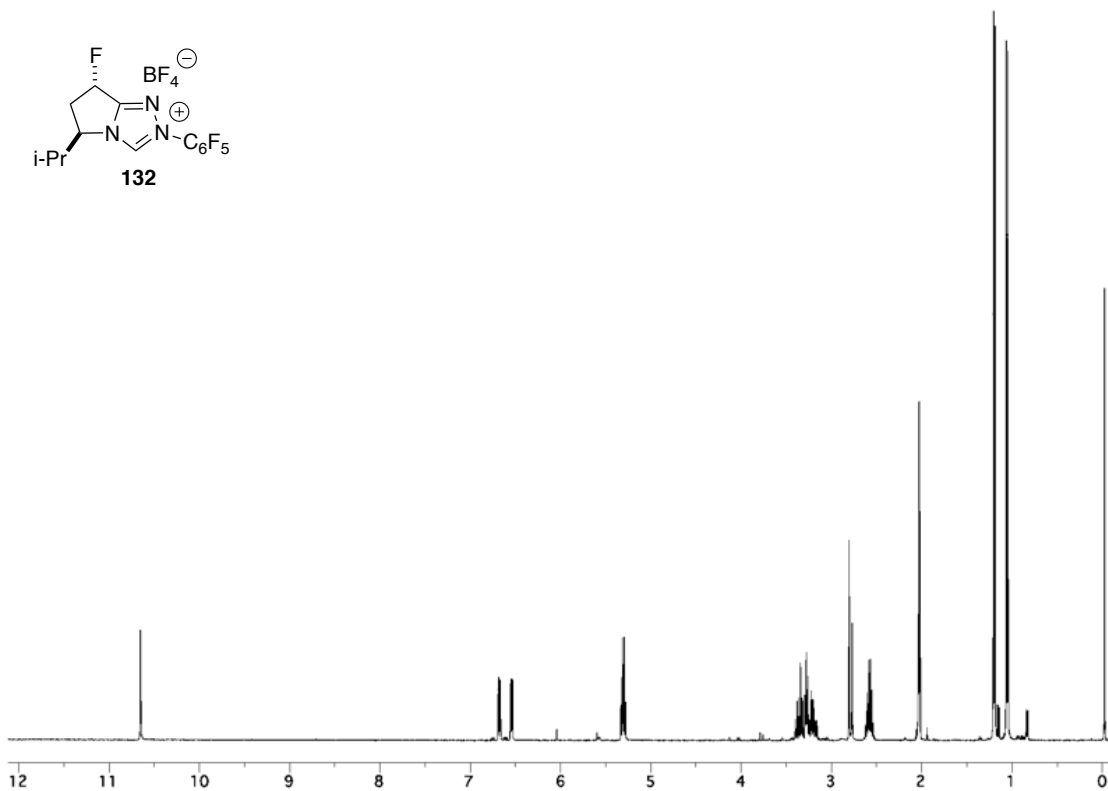
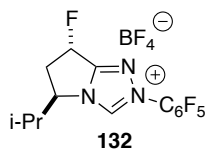


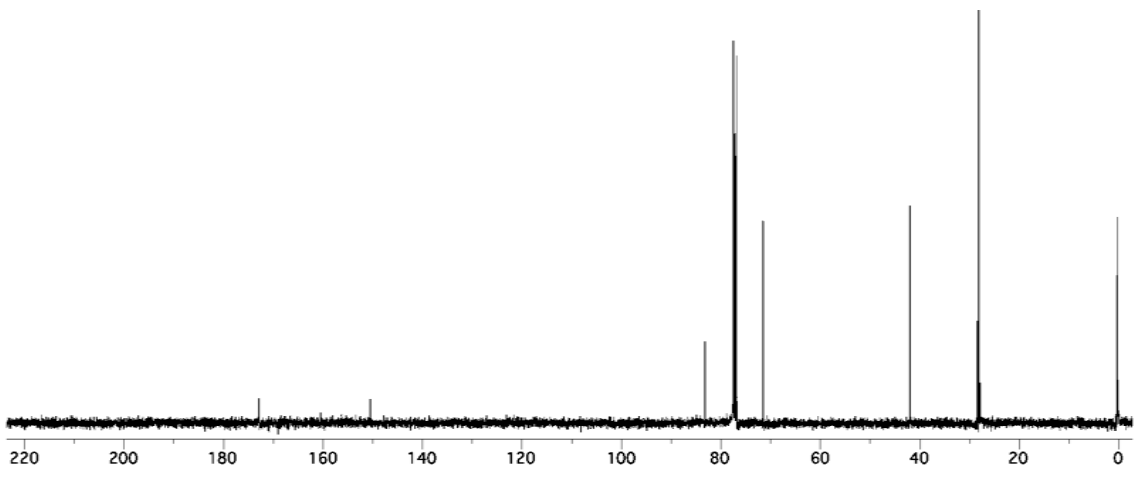
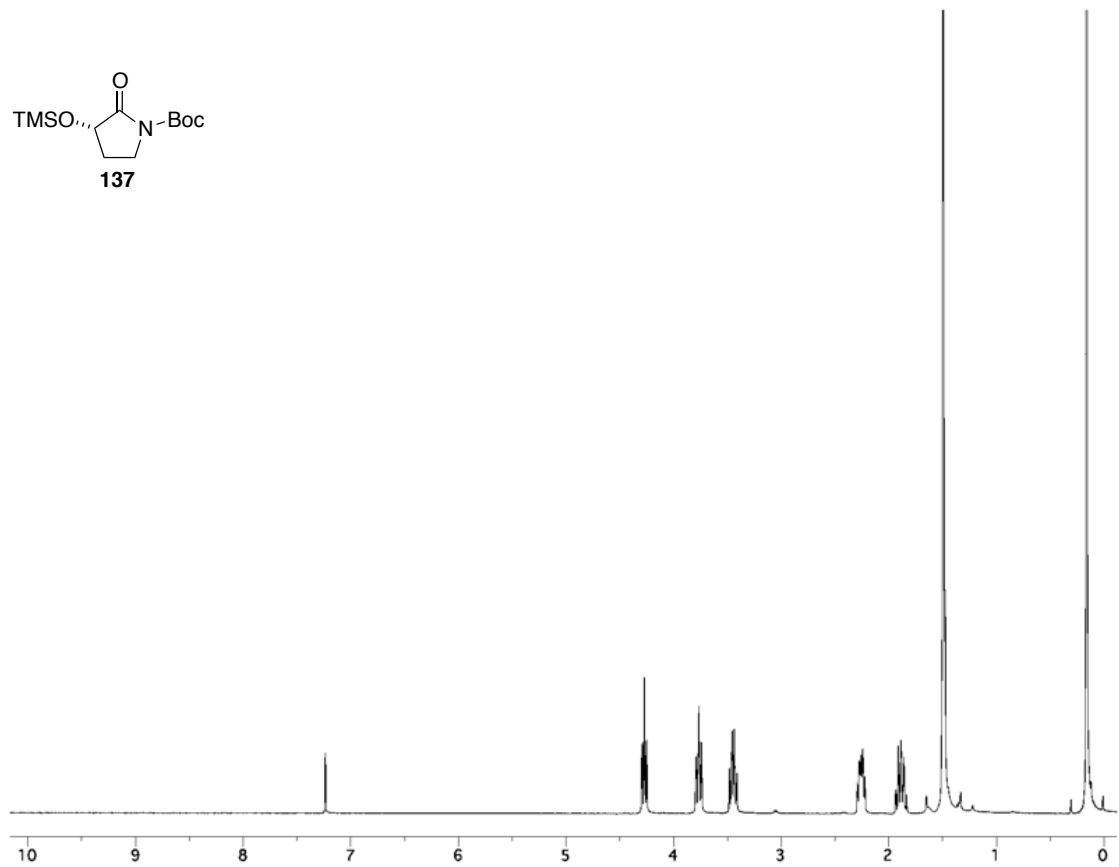
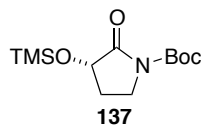


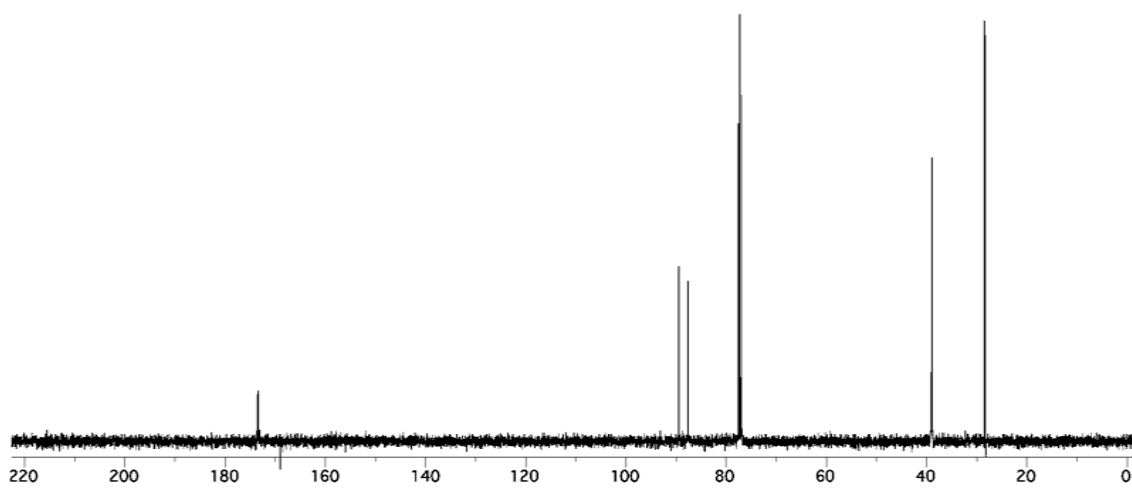
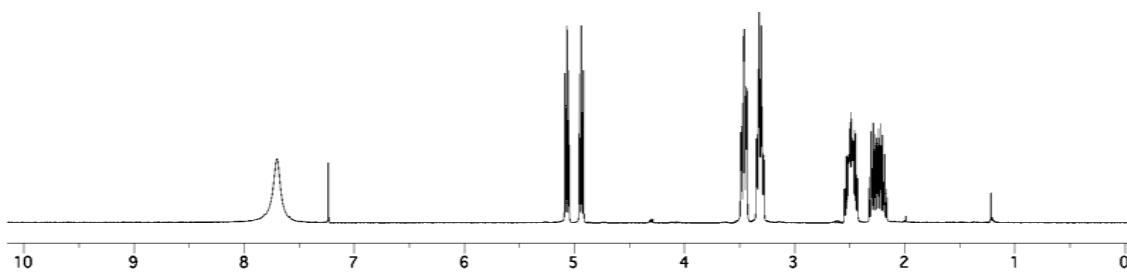
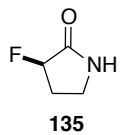


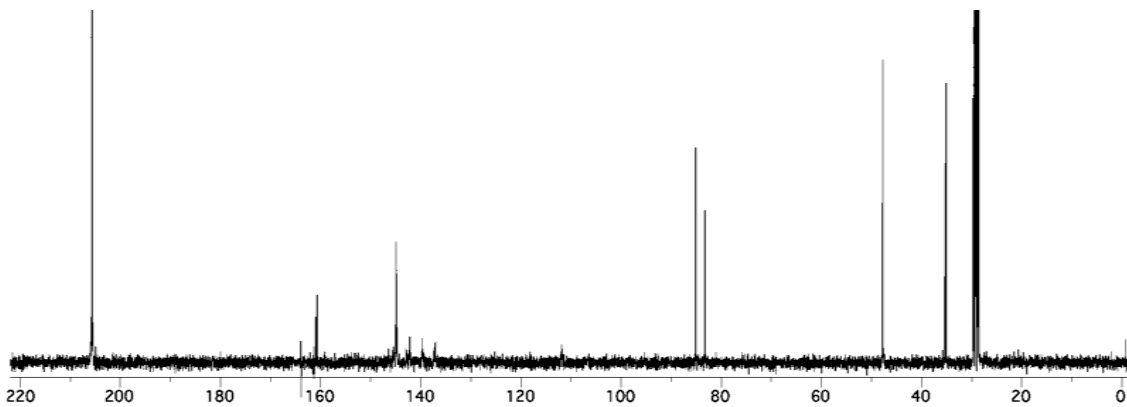
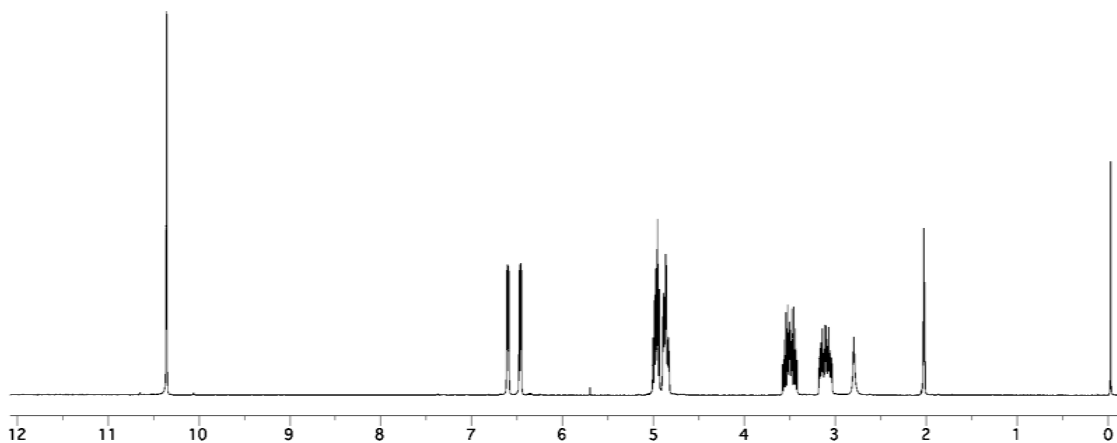
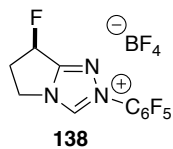


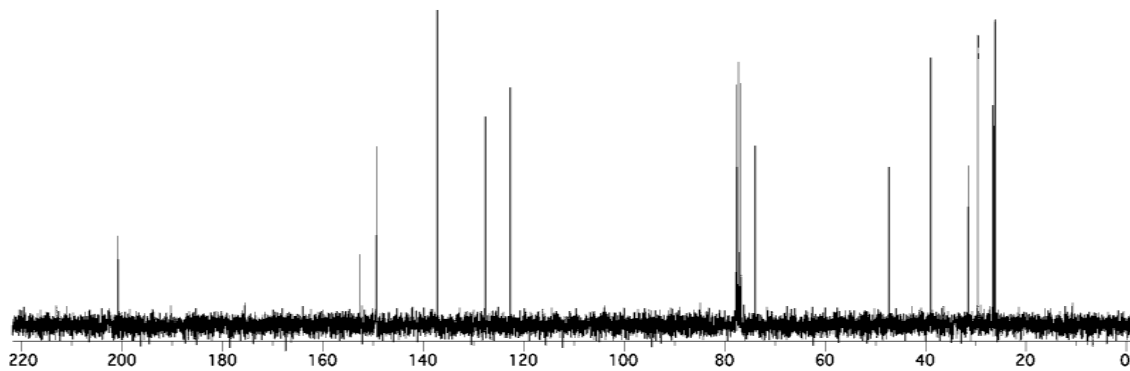
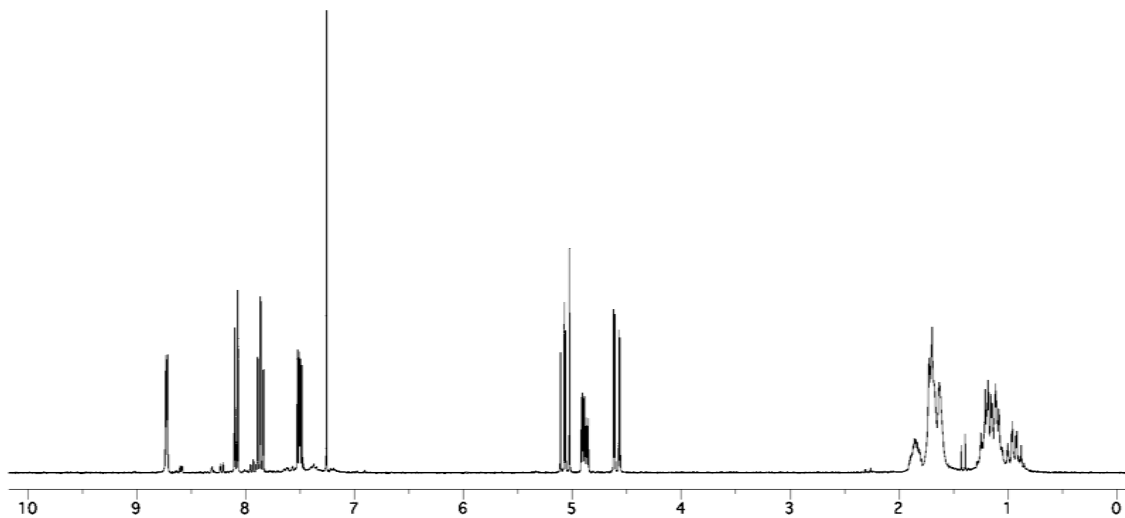
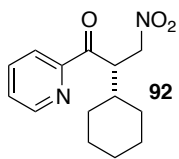












Crystallographic Data

Table A1.1 Crystal data and structure refinement for (73).

Identification code	rovis50	
Empirical formula	$C_{18}H_{12}BF_{10}N_3$	
Formula weight	471.12	
Temperature	120(2) K	
Wavelength	0.71073 Å	
Crystal system	Monoclinic	
Space group	$P2_1$	
Unit cell dimensions	$a = 9.8672(8)$ Å	$\alpha = 90^\circ$.
	$b = 7.3492(5)$ Å	$\beta = 94.526(2)^\circ$.
	$c = 13.0804(8)$ Å	$\gamma = 90^\circ$.
Volume	$945.58(12)$ Å ³	
Z	2	
Density (calculated)	1.655 Mg/m ³	
Absorption coefficient	0.168 mm ⁻¹	
F(000)	472	
Crystal size	0.15 x 0.13 x 0.06 mm ³	
Theta range for data collection	2.07 to 24.11°.	
Index ranges	$-10 \leq h \leq 11$, $-8 \leq k \leq 8$, $-15 \leq l \leq 13$	
Reflections collected	7591	
Independent reflections	2997 [R(int) = 0.0462]	
Completeness to theta = 24.11°	99.9 %	
Absorption correction	Semi-empirical from equivalents	
Max. and min. transmission	0.9895 and 0.9757	
Refinement method	Full-matrix least-squares on F ²	
Data / restraints / parameters	2997 / 1 / 289	
Goodness-of-fit on F ²	1.019	
Final R indices [I > 2σ(I)]	R1 = 0.0489, wR2 = 0.0905	
R indices (all data)	R1 = 0.0766, wR2 = 0.1018	
Absolute structure parameter	0.1(10)	
Largest diff. peak and hole	0.352 and -0.344 e.Å ⁻³	

Table A1.2 Atomic coordinates ($\times 10^4$) and equivalent isotropic displacement parameters ($\text{\AA}^2 \times 10^3$) for (73). $U(\text{eq})$ is defined as one third of the trace of the orthogonalized U^{ij} tensor.

	x	y	z	$U(\text{eq})$
B(1)	8160(5)	9815(7)	8915(4)	33(1)
C(1)	2002(4)	10164(6)	147(3)	25(1)
C(2)	3319(4)	10523(5)	1969(3)	25(1)
C(3)	4804(5)	9943(11)	2123(4)	76(2)
C(4)	5224(4)	8859(6)	1218(3)	31(1)
C(5)	4018(4)	9051(6)	459(3)	26(1)
C(6)	1756(4)	9320(6)	-1683(3)	23(1)
C(7)	1586(4)	7723(6)	-2226(3)	24(1)
C(8)	959(5)	7695(6)	-3191(3)	29(1)
C(9)	456(4)	9274(7)	-3627(3)	30(1)
C(10)	598(4)	10894(6)	-3099(3)	29(1)
C(11)	1261(4)	10910(6)	-2132(3)	23(1)
C(12)	2355(5)	9629(7)	2654(3)	44(1)
C(13)	2789(4)	9969(7)	3771(3)	37(1)
C(14)	2742(5)	11700(7)	4193(4)	45(1)
C(15)	3169(5)	11997(9)	5212(4)	61(2)
C(16)	3654(6)	10571(11)	5824(4)	63(2)
C(17)	3688(5)	8848(10)	5415(4)	62(2)
C(18)	3250(5)	8538(8)	4394(4)	55(2)
F(1)	2031(3)	6144(3)	-1792(2)	36(1)
F(2)	838(3)	6126(3)	-3714(2)	46(1)
F(3)	-152(3)	9258(4)	-4578(2)	47(1)
F(4)	112(3)	12429(3)	-3526(2)	42(1)
F(5)	1410(2)	12498(3)	-1632(2)	34(1)
F(6)	5407(4)	7062(4)	1478(3)	95(2)
F(7)	7768(3)	10045(4)	7885(2)	62(1)
F(8)	9120(3)	8404(4)	8984(3)	62(1)
F(9)	7077(2)	9306(4)	9444(2)	46(1)
F(10)	8778(3)	11385(3)	9308(2)	52(1)
N(1)	3007(3)	9990(5)	871(2)	24(1)
N(2)	3720(3)	8629(5)	-506(3)	26(1)

N(3) 2420(3) 9359(5) -683(2) 24(1)

Table A1.3 Bond lengths [\AA] and angles [$^\circ$] for (73).

B(1)-F(9)	1.370(6)	C(15)-C(16)	1.382(8)
B(1)-F(7)	1.382(6)	C(16)-C(17)	1.376(8)
B(1)-F(10)	1.385(6)	C(17)-C(18)	1.390(7)
B(1)-F(8)	1.403(6)	N(2)-N(3)	1.393(4)
C(1)-N(1)	1.323(5)	F(9)-B(1)-F(7)	110.9(4)
C(1)-N(3)	1.330(5)	F(9)-B(1)-F(10)	112.2(4)
C(2)-N(1)	1.497(5)	F(7)-B(1)-F(10)	110.0(4)
C(2)-C(12)	1.508(6)	F(9)-B(1)-F(8)	108.4(4)
C(2)-C(3)	1.524(6)	F(7)-B(1)-F(8)	106.8(4)
C(3)-C(4)	1.512(6)	F(10)-B(1)-F(8)	108.4(4)
C(4)-F(6)	1.373(5)	N(1)-C(1)-N(3)	106.2(4)
C(4)-C(5)	1.495(5)	N(1)-C(2)-C(12)	111.4(3)
C(5)-N(2)	1.310(5)	N(1)-C(2)-C(3)	100.1(3)
C(5)-N(1)	1.360(5)	C(12)-C(2)-C(3)	116.4(4)
C(6)-C(7)	1.375(6)	C(4)-C(3)-C(2)	111.4(4)
C(6)-C(11)	1.381(6)	F(6)-C(4)-C(5)	109.8(3)
C(6)-N(3)	1.416(5)	F(6)-C(4)-C(3)	110.6(4)
C(7)-F(1)	1.350(5)	C(5)-C(4)-C(3)	102.5(4)
C(7)-C(8)	1.362(6)	N(2)-C(5)-N(1)	112.7(3)
C(8)-F(2)	1.342(5)	N(2)-C(5)-C(4)	136.4(4)
C(8)-C(9)	1.368(6)	N(1)-C(5)-C(4)	110.8(3)
C(9)-F(3)	1.338(4)	C(7)-C(6)-C(11)	118.5(3)
C(9)-C(10)	1.379(6)	C(7)-C(6)-N(3)	121.5(4)
C(10)-F(4)	1.331(5)	C(11)-C(6)-N(3)	119.9(4)
C(10)-C(11)	1.376(6)	F(1)-C(7)-C(8)	119.1(4)
C(11)-F(5)	1.340(5)	F(1)-C(7)-C(6)	119.6(4)
C(12)-C(13)	1.510(6)	C(8)-C(7)-C(6)	121.3(4)
C(13)-C(18)	1.384(7)	F(2)-C(8)-C(7)	120.1(4)
C(13)-C(14)	1.389(7)	F(2)-C(8)-C(9)	120.1(4)
C(14)-C(15)	1.383(7)	C(7)-C(8)-C(9)	119.8(4)

F(3)-C(9)-C(8)	120.1(4)	C(15)-C(14)-C(13)	120.7(5)
F(3)-C(9)-C(10)	119.6(4)	C(16)-C(15)-C(14)	120.3(6)
C(8)-C(9)-C(10)	120.3(3)	C(17)-C(16)-C(15)	119.4(5)
F(4)-C(10)-C(11)	120.5(4)	C(16)-C(17)-C(18)	120.6(6)
F(4)-C(10)-C(9)	120.1(4)	C(13)-C(18)-C(17)	120.3(6)
C(11)-C(10)-C(9)	119.3(4)	C(1)-N(1)-C(5)	107.3(3)
F(5)-C(11)-C(10)	118.8(4)	C(1)-N(1)-C(2)	138.4(3)
F(5)-C(11)-C(6)	120.5(3)	C(5)-N(1)-C(2)	114.3(3)
C(10)-C(11)-C(6)	120.7(4)	C(5)-N(2)-N(3)	101.7(3)
C(2)-C(12)-C(13)	111.0(4)	C(1)-N(3)-N(2)	112.1(3)
C(18)-C(13)-C(14)	118.8(4)	C(1)-N(3)-C(6)	127.7(4)
C(18)-C(13)-C(12)	119.9(5)	N(2)-N(3)-C(6)	119.9(3)
C(14)-C(13)-C(12)	121.3(5)		

Symmetry transformations used to generate equivalent atoms:

Table A1.4 Anisotropic displacement parameters ($\text{\AA}^2 \times 10^3$) for (73). The anisotropic displacement factor exponent takes the form: $-2\pi^2 [h^2 a^{*2} U^{11} + \dots + 2 h k a^* b^* U^{12}]$

	U^{11}	U^{22}	U^{33}	U^{23}	U^{13}	U^{12}
B(1)	37(3)	30(3)	34(3)	-2(2)	9(3)	-5(3)
C(1)	24(2)	24(2)	27(2)	-1(2)	7(2)	0(2)
C(2)	32(3)	24(2)	19(2)	-2(2)	-2(2)	0(2)
C(3)	36(3)	163(7)	29(3)	-24(4)	1(2)	36(4)
C(4)	31(3)	25(3)	36(3)	1(2)	-7(2)	0(2)
C(5)	29(2)	21(2)	28(2)	-1(2)	3(2)	2(2)
C(6)	26(2)	23(2)	19(2)	-2(2)	1(2)	-3(2)
C(7)	27(2)	19(2)	26(3)	4(2)	2(2)	4(2)
C(8)	37(3)	23(2)	28(3)	-10(2)	5(2)	-2(2)
C(9)	33(3)	37(3)	19(2)	4(2)	4(2)	-4(2)
C(10)	32(3)	26(3)	29(3)	13(2)	6(2)	3(2)
C(11)	26(2)	18(2)	26(3)	-3(2)	7(2)	1(2)
C(12)	48(3)	58(4)	28(3)	-8(2)	11(2)	-22(3)
C(13)	27(3)	57(3)	27(3)	-8(3)	10(2)	-5(3)
C(14)	38(3)	66(4)	31(3)	-13(3)	11(2)	-7(3)

C(15)	53(4)	91(5)	41(4)	-32(3)	19(3)	-26(4)
C(16)	36(3)	127(7)	28(3)	-10(4)	5(2)	-20(4)
C(17)	43(3)	109(6)	36(4)	12(4)	20(3)	7(4)
C(18)	57(4)	71(4)	40(3)	-3(3)	24(3)	-4(3)
F(1)	50(2)	17(1)	40(2)	1(1)	-8(1)	4(1)
F(2)	66(2)	34(2)	38(2)	-13(1)	-6(1)	-4(2)
F(3)	61(2)	53(2)	25(2)	2(1)	-8(1)	-2(2)
F(4)	53(2)	33(2)	41(2)	15(1)	1(1)	12(1)
F(5)	48(2)	15(1)	38(2)	-6(1)	1(1)	3(1)
F(6)	101(3)	33(2)	136(3)	6(2)	-86(3)	1(2)
F(7)	78(2)	73(2)	36(2)	5(2)	2(2)	-22(2)
F(8)	48(2)	32(2)	110(3)	23(2)	40(2)	8(1)
F(9)	35(2)	58(2)	45(2)	-2(2)	19(1)	-4(1)
F(10)	64(2)	35(2)	60(2)	-13(1)	7(2)	-9(1)
N(1)	26(2)	22(2)	23(2)	0(2)	0(2)	2(2)
N(2)	20(2)	30(2)	28(2)	1(2)	2(2)	1(2)
N(3)	26(2)	19(2)	25(2)	0(2)	1(2)	2(2)

Table A1.5 Hydrogen coordinates ($\times 10^4$) and isotropic displacement parameters ($\text{\AA}^2 \times 10^{-3}$) for (73).

	x	y	z	U(eq)
H(7)	1152	10746	207	30
H(11)	3254	11875	2036	30
H(10A)	5386	11037	2215	91
H(10B)	4941	9196	2752	91
H(9)	6059	9382	945	37
H(12A)	2330	8303	2522	53
H(12B)	1427	10116	2494	53
H(14)	2412	12689	3777	54
H(15)	3129	13187	5492	73
H(16)	3962	10777	6521	76
H(17)	4013	7861	5834	74

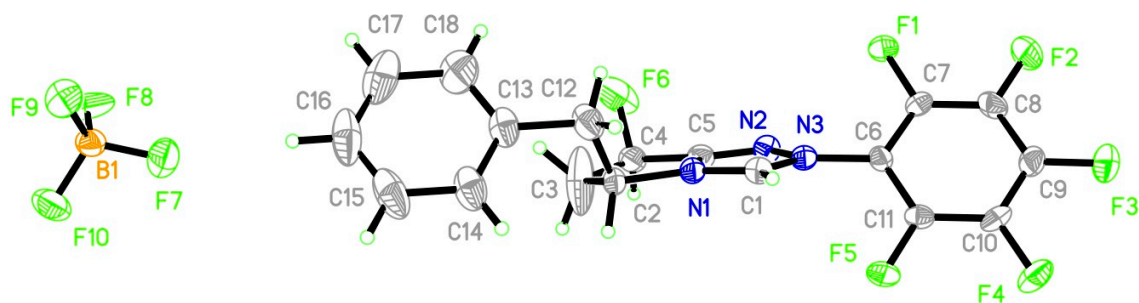


Figure A1.1 Thermal plot of triazolium salt (**73**). Ellipsoids drawn at the 50% probability level.

Table A1.6 Crystal data and structure refinement for triazolium salt (**102**).

Identification code	rovis58_0m	
Empirical formula	$C_{14}H_{13}BF_9N_3$	
Formula weight	405.08	
Temperature	120 K	
Wavelength	0.71073 Å	
Crystal system	Monoclinic	
Space group	$P2_1$	
Unit cell dimensions	$a = 9.9143(3)$ Å	$\alpha = 90^\circ$.
	$b = 7.5803(2)$ Å	$\beta = 107.6080(10)^\circ$.
	$c = 11.2293(3)$ Å	$\gamma = 90^\circ$.
Volume	$804.38(4)$ Å ³	
Z	2	
Density (calculated)	1.672 Mg/m ³	
Absorption coefficient	0.174 mm ⁻¹	
F(000)	408	
Crystal size	0.19 x 0.18 x 0.05 mm ³	
Theta range for data collection	2.41 to 32.58°.	
Index ranges	-15 ≤ h ≤ 15, -11 ≤ k ≤ 9, -17 ≤ l ≤ 14	
Reflections collected	14071	
Independent reflections	5310 [R(int) = 0.0369]	
Completeness to theta = 32.58°	99.9 %	
Absorption correction	Semi-empirical from equivalents	

Max. and min. transmission	0.9909 and 0.9683
Refinement method	Full-matrix least-squares on F ²
Data / restraints / parameters	5310 / 1 / 246
Goodness-of-fit on F ²	1.013
Final R indices [I>2sigma(I)]	R1 = 0.0464, wR2 = 0.0778
R indices (all data)	R1 = 0.0863, wR2 = 0.0906
Absolute structure parameter	-0.1(5)
Largest diff. peak and hole	0.282 and -0.253 e.Å ⁻³

Table A1.7 Atomic coordinates (x 10⁴) and equivalent isotropic displacement parameters (Å²x 10³) for triazolium salt (**102**). U(eq) is defined as one third of the trace of the orthogonalized U^{ij} tensor.

	x	y	z	U(eq)
B(1)	4041(2)	6227(3)	1434(2)	26(1)
C(1)	6614(2)	5724(2)	9771(2)	17(1)
C(2)	8209(2)	6812(3)	11954(2)	23(1)
C(3)	9642(2)	7720(3)	12080(2)	32(1)
C(4)	9595(2)	8465(3)	10790(2)	26(1)
C(5)	8428(2)	7415(3)	9928(2)	19(1)
C(6)	8265(2)	5075(3)	12676(2)	25(1)
C(7)	8786(2)	5478(4)	14079(2)	38(1)
C(8)	9150(2)	3634(3)	12326(2)	37(1)
C(9)	5805(2)	5586(3)	7478(2)	18(1)
C(10)	6308(2)	4969(3)	6537(2)	21(1)
C(11)	5395(2)	4408(3)	5411(2)	23(1)
C(12)	3953(2)	4442(3)	5222(2)	26(1)
C(13)	3443(2)	5069(3)	6154(2)	24(1)
C(14)	4356(2)	5642(3)	7270(2)	21(1)
F(1)	7697(1)	4834(2)	6714(1)	29(1)
F(2)	5917(1)	3755(2)	4537(1)	35(1)
F(3)	3057(1)	3848(2)	4161(1)	35(1)
F(4)	2043(1)	5120(2)	5972(1)	35(1)
F(5)	3823(1)	6215(2)	8156(1)	27(1)
F(6)	4241(2)	6228(2)	2694(1)	66(1)
F(7)	4953(1)	7458(1)	1163(1)	28(1)

F(8)	2668(1)	6712(2)	805(2)	61(1)
F(9)	4340(1)	4578(2)	1044(1)	38(1)
N(1)	7679(1)	6546(2)	10582(1)	18(1)
N(2)	7898(2)	7185(2)	8731(1)	21(1)
N(3)	6748(1)	6092(2)	8653(1)	17(1)

Table A1.8 Bond lengths [\AA] and angles [$^\circ$] for triazolium salt (**102**).

B(1)-F(6)	1.368(3)	N(2)-N(3)	1.391(2)
B(1)-F(8)	1.380(3)	F(6)-B(1)-F(8)	109.92(19)
B(1)-F(9)	1.386(3)	F(6)-B(1)-F(9)	110.45(18)
B(1)-F(7)	1.396(3)	F(8)-B(1)-F(9)	110.54(18)
C(1)-N(1)	1.324(2)	F(6)-B(1)-F(7)	108.93(18)
C(1)-N(3)	1.331(2)	F(8)-B(1)-F(7)	108.33(18)
C(2)-N(1)	1.483(2)	F(9)-B(1)-F(7)	108.61(16)
C(2)-C(6)	1.538(3)	N(1)-C(1)-N(3)	105.29(15)
C(2)-C(3)	1.546(3)	N(1)-C(2)-C(6)	112.06(16)
C(3)-C(4)	1.542(3)	N(1)-C(2)-C(3)	100.49(14)
C(4)-C(5)	1.494(3)	C(6)-C(2)-C(3)	116.61(16)
C(5)-N(2)	1.298(2)	C(4)-C(3)-C(2)	108.17(16)
C(5)-N(1)	1.362(2)	C(5)-C(4)-C(3)	102.18(15)
C(6)-C(8)	1.525(3)	N(2)-C(5)-N(1)	112.20(15)
C(6)-C(7)	1.533(3)	N(2)-C(5)-C(4)	137.22(17)
C(9)-C(10)	1.379(3)	N(1)-C(5)-C(4)	110.46(15)
C(9)-C(14)	1.385(2)	C(8)-C(6)-C(7)	111.48(17)
C(9)-N(3)	1.420(2)	C(8)-C(6)-C(2)	114.13(17)
C(10)-F(1)	1.335(2)	C(7)-C(6)-C(2)	108.53(18)
C(10)-C(11)	1.380(3)	C(10)-C(9)-C(14)	118.55(16)
C(11)-F(2)	1.336(2)	C(10)-C(9)-N(3)	121.02(15)
C(11)-C(12)	1.381(3)	C(14)-C(9)-N(3)	120.39(16)
C(12)-F(3)	1.331(2)	F(1)-C(10)-C(9)	120.48(16)
C(12)-C(13)	1.377(3)	F(1)-C(10)-C(11)	118.28(16)
C(13)-F(4)	1.341(2)	C(9)-C(10)-C(11)	121.18(16)
C(13)-C(14)	1.375(3)	F(2)-C(11)-C(10)	119.66(16)
C(14)-F(5)	1.333(2)	F(2)-C(11)-C(12)	120.49(17)

C(10)-C(11)-C(12)	119.76(17)	C(13)-C(14)-C(9)	120.47(17)
F(3)-C(12)-C(13)	119.90(17)	C(1)-N(1)-C(5)	107.94(15)
F(3)-C(12)-C(11)	120.72(18)	C(1)-N(1)-C(2)	137.47(15)
C(13)-C(12)-C(11)	119.37(17)	C(5)-N(1)-C(2)	114.53(14)
F(4)-C(13)-C(14)	119.68(17)	C(5)-N(2)-N(3)	102.27(14)
F(4)-C(13)-C(12)	119.67(17)	C(1)-N(3)-N(2)	112.29(14)
C(14)-C(13)-C(12)	120.65(17)	C(1)-N(3)-C(9)	126.48(15)
F(5)-C(14)-C(13)	118.86(15)	N(2)-N(3)-C(9)	121.06(14)
F(5)-C(14)-C(9)	120.65(16)		

Symmetry transformations used to generate equivalent atoms:

Table A1.9 Anisotropic displacement parameters ($\text{\AA}^2 \times 10^3$) for triazolium salt (**102**). The anisotropic displacement factor exponent takes the form: $-2\pi^2 [h^2 a^{*2} U^{11} + \dots + 2 h k a^* b^* U^{12}]$

	U^{11}	U^{22}	U^{33}	U^{23}	U^{13}	U^{12}
B(1)	28(1)	20(1)	32(1)	0(1)	14(1)	0(1)
C(1)	14(1)	18(1)	19(1)	-2(1)	3(1)	0(1)
C(2)	17(1)	29(1)	19(1)	-6(1)	2(1)	-4(1)
C(3)	24(1)	38(1)	31(1)	-5(1)	5(1)	-12(1)
C(4)	17(1)	29(1)	31(1)	-3(1)	6(1)	-6(1)
C(5)	14(1)	19(1)	25(1)	0(1)	6(1)	-1(1)
C(6)	19(1)	34(1)	20(1)	0(1)	3(1)	-2(1)
C(7)	32(1)	56(2)	22(1)	3(1)	2(1)	-2(1)
C(8)	35(1)	39(1)	35(1)	6(1)	11(1)	8(1)
C(9)	18(1)	16(1)	16(1)	2(1)	0(1)	1(1)
C(10)	20(1)	20(1)	23(1)	2(1)	6(1)	2(1)
C(11)	31(1)	19(1)	19(1)	0(1)	7(1)	3(1)
C(12)	29(1)	24(1)	18(1)	0(1)	-2(1)	-4(1)
C(13)	18(1)	24(1)	26(1)	4(1)	1(1)	-1(1)
C(14)	21(1)	20(1)	22(1)	3(1)	6(1)	4(1)
F(1)	21(1)	40(1)	26(1)	-5(1)	7(1)	7(1)
F(2)	42(1)	41(1)	23(1)	-9(1)	11(1)	3(1)
F(3)	37(1)	39(1)	22(1)	-5(1)	-5(1)	-7(1)
F(4)	18(1)	46(1)	34(1)	0(1)	-1(1)	-1(1)

F(5)	21(1)	35(1)	25(1)	-3(1)	7(1)	3(1)
F(6)	131(2)	39(1)	39(1)	3(1)	42(1)	-3(1)
F(7)	28(1)	20(1)	38(1)	-2(1)	12(1)	-4(1)
F(8)	21(1)	48(1)	108(1)	4(1)	11(1)	4(1)
F(9)	40(1)	19(1)	66(1)	-10(1)	30(1)	-6(1)
N(1)	15(1)	21(1)	17(1)	-2(1)	3(1)	-2(1)
N(2)	16(1)	21(1)	26(1)	1(1)	7(1)	1(1)
N(3)	14(1)	18(1)	19(1)	-2(1)	4(1)	1(1)

Table A1.10 Hydrogen coordinates ($\times 10^4$) and isotropic displacement parameters ($\text{\AA}^2 \times 10^3$) for triazolium salt (**102**).

	x	y	z	U(eq)
H(1)	5920	5036	9945	21
H(2)	7587	7645	12202	27
H(3A)	9801	8666	12688	38
H(3B)	10407	6875	12358	38
H(4A)	9377	9715	10732	31
H(4B)	10484	8275	10616	31
H(6)	7294	4631	12481	30
H(7A)	8786	4413	14541	57
H(7B)	8170	6327	14279	57
H(7C)	9729	5946	14295	57
H(8A)	8780	3387	11448	55
H(8B)	9114	2584	12793	55
H(8C)	10113	4025	12515	55

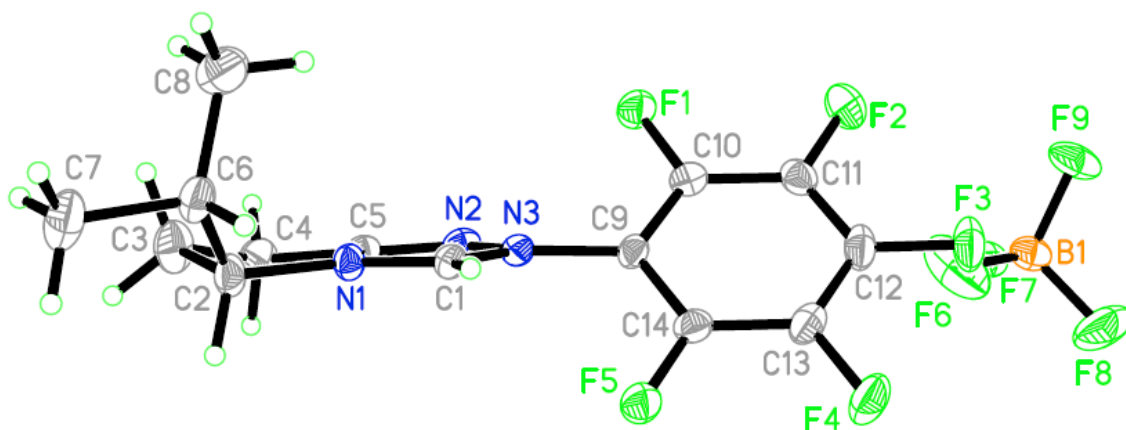


Figure A1.2 Thermal plot of triazolium salt (**102**). Ellipsoids drawn at the 50% probability level.

Table A1.11 Crystal data and structure refinement for triazolium salt (**128**).

Identification code	rovis56_0m	
Empirical formula	$C_{14}H_{12}BF_{10}N_3$	
Formula weight	423.08	
Temperature	120 K	
Wavelength	0.71073 Å	
Crystal system	Monoclinic	
Space group	$P2_1$	
Unit cell dimensions	$a = 9.9726(3)$ Å	$\alpha = 90^\circ$.
	$b = 7.6892(2)$ Å	$\beta = 102.604(2)^\circ$.
	$c = 11.0520(4)$ Å	$\gamma = 90^\circ$.
Volume	$827.06(4)$ Å ³	
Z	2	
Density (calculated)	1.699 Mg/m ³	
Absorption coefficient	0.181 mm ⁻¹	
F(000)	424	
Crystal size	0.24 x 0.15 x 0.12 mm ³	
Theta range for data collection	1.89 to 36.36°.	
Index ranges	-16 ≤ h ≤ 16, -12 ≤ k ≤ 12, -18 ≤ l ≤ 18	
Reflections collected	26473	
Independent reflections	7828 [R(int) = 0.0303]	
Completeness to theta = 36.36°	99.7 %	
Absorption correction	Semi-empirical from equivalents	

Max. and min. transmission	0.9782 and 0.9585
Refinement method	Full-matrix least-squares on F ²
Data / restraints / parameters	7828 / 1 / 255
Goodness-of-fit on F ²	1.018
Final R indices [I>2sigma(I)]	R1 = 0.0388, wR2 = 0.0899
R indices (all data)	R1 = 0.0543, wR2 = 0.1026
Absolute structure parameter	0.1(3)
Largest diff. peak and hole	0.495 and -0.418 e.Å ⁻³

Table A1.12 Atomic coordinates (x 10⁴) and equivalent isotropic displacement parameters (Å²x 10³) for triazolium salt (**128**). U(eq) is defined as one third of the trace of the orthogonalized U^{ij} tensor.

	x	y	z	U(eq)
B(1)	4311(1)	8900(2)	6628(1)	17(1)
C(1)	3214(1)	3495(1)	5334(1)	15(1)
C(2)	1910(1)	5059(1)	3290(1)	16(1)
C(3)	1295(1)	6881(2)	3432(1)	18(1)
C(4)	817(1)	6896(1)	4661(1)	17(1)
C(5)	1718(1)	5529(1)	5383(1)	14(1)
C(6)	901(1)	3724(2)	2561(1)	21(1)
C(7)	569(2)	4229(2)	1190(1)	31(1)
C(8)	1487(2)	1877(2)	2713(1)	29(1)
C(9)	3869(1)	3110(1)	7599(1)	14(1)
C(10)	3252(1)	2445(1)	8516(1)	17(1)
C(11)	4042(1)	1873(1)	9630(1)	19(1)
C(12)	5465(1)	1939(1)	9830(1)	20(1)
C(13)	6081(1)	2581(1)	8920(1)	19(1)
C(14)	5284(1)	3185(1)	7818(1)	15(1)
F(1)	-555(1)	6381(1)	4491(1)	22(1)
F(2)	1890(1)	2358(1)	8333(1)	24(1)
F(3)	3432(1)	1231(1)	10489(1)	26(1)
F(4)	6238(1)	1341(1)	10881(1)	28(1)
F(5)	7451(1)	2646(1)	9111(1)	27(1)
F(6)	5893(1)	3845(1)	6960(1)	21(1)

F(7)	4459(1)	7299(1)	6076(1)	30(1)
F(8)	4812(1)	10212(1)	5958(1)	25(1)
F(9)	2944(1)	9215(1)	6618(1)	39(1)
F(10)	5089(1)	8924(1)	7835(1)	32(1)
N(1)	2349(1)	4577(1)	4619(1)	14(1)
N(2)	2117(1)	5088(1)	6540(1)	15(1)
N(3)	3061(1)	3793(1)	6485(1)	14(1)

Table A1.13 Bond lengths [Å] and angles [°] for triazolium salt (**128**).

B(1)-F(9)	1.3830(15)	C(13)-F(5)	1.3371(14)
B(1)-F(10)	1.3892(17)	C(13)-C(14)	1.3814(16)
B(1)-F(7)	1.3960(14)	C(14)-F(6)	1.3333(13)
B(1)-F(8)	1.4059(15)	N(2)-N(3)	1.3807(13)
C(1)-N(1)	1.3290(14)	F(9)-B(1)-F(10)	110.36(11)
C(1)-N(3)	1.3335(16)	F(9)-B(1)-F(7)	110.44(10)
C(2)-N(1)	1.4847(16)	F(10)-B(1)-F(7)	109.94(10)
C(2)-C(6)	1.5370(17)	F(9)-B(1)-F(8)	109.46(10)
C(2)-C(3)	1.5510(16)	F(10)-B(1)-F(8)	107.96(10)
C(3)-C(4)	1.5343(18)	F(7)-B(1)-F(8)	108.62(10)
C(4)-F(1)	1.3971(13)	N(1)-C(1)-N(3)	105.40(10)
C(4)-C(5)	1.4953(15)	N(1)-C(2)-C(6)	111.69(9)
C(5)-N(2)	1.2985(16)	N(1)-C(2)-C(3)	99.39(9)
C(5)-N(1)	1.3701(14)	C(6)-C(2)-C(3)	115.36(9)
C(6)-C(7)	1.529(2)	C(4)-C(3)-C(2)	107.58(9)
C(6)-C(8)	1.5306(19)	F(1)-C(4)-C(5)	109.19(9)
C(9)-C(14)	1.3802(15)	F(1)-C(4)-C(3)	111.28(10)
C(9)-C(10)	1.3919(16)	C(5)-C(4)-C(3)	101.62(9)
C(9)-N(3)	1.4167(15)	N(2)-C(5)-N(1)	112.59(9)
C(10)-F(2)	1.3310(14)	N(2)-C(5)-C(4)	136.79(10)
C(10)-C(11)	1.3810(17)	N(1)-C(5)-C(4)	110.43(10)
C(11)-F(3)	1.3295(15)	C(7)-C(6)-C(8)	109.86(11)
C(11)-C(12)	1.3883(18)	C(7)-C(6)-C(2)	108.98(11)
C(12)-F(4)	1.3282(14)	C(8)-C(6)-C(2)	111.81(10)
C(12)-C(13)	1.3794(18)	C(14)-C(9)-C(10)	119.01(10)

C(14)-C(9)-N(3)	120.14(10)	F(5)-C(13)-C(14)	119.87(11)
C(10)-C(9)-N(3)	120.75(10)	C(12)-C(13)-C(14)	120.03(11)
F(2)-C(10)-C(11)	118.98(10)	F(6)-C(14)-C(9)	119.92(10)
F(2)-C(10)-C(9)	120.39(10)	F(6)-C(14)-C(13)	119.39(10)
C(11)-C(10)-C(9)	120.63(11)	C(9)-C(14)-C(13)	120.69(11)
F(3)-C(11)-C(10)	119.61(11)	C(1)-N(1)-C(5)	107.06(10)
F(3)-C(11)-C(12)	120.75(11)	C(1)-N(1)-C(2)	139.29(10)
C(10)-C(11)-C(12)	119.63(11)	C(5)-N(1)-C(2)	113.63(9)
F(4)-C(12)-C(13)	119.70(11)	C(5)-N(2)-N(3)	102.18(9)
F(4)-C(12)-C(11)	120.29(12)	C(1)-N(3)-N(2)	112.75(9)
C(13)-C(12)-C(11)	119.99(11)	C(1)-N(3)-C(9)	127.16(10)
F(5)-C(13)-C(12)	120.09(11)	N(2)-N(3)-C(9)	119.50(9)

Symmetry transformations used to generate equivalent atoms:

Table A1.14 Anisotropic displacement parameters ($\text{\AA}^2 \times 10^3$) for triazolium salt (**128**). The anisotropic displacement factor exponent takes the form: $-2\pi^2 [h^2 a^{*2} U^{11} + \dots + 2 h k a^* b^* U^{12}]$

	U^{11}	U^{22}	U^{33}	U^{23}	U^{13}	U^{12}
B(1)	16(1)	16(1)	21(1)	-2(1)	4(1)	-1(1)
C(1)	14(1)	16(1)	14(1)	0(1)	2(1)	2(1)
C(2)	16(1)	19(1)	12(1)	4(1)	3(1)	2(1)
C(3)	16(1)	19(1)	20(1)	5(1)	3(1)	2(1)
C(4)	12(1)	16(1)	21(1)	1(1)	2(1)	2(1)
C(5)	12(1)	15(1)	16(1)	-1(1)	3(1)	0(1)
C(6)	21(1)	24(1)	16(1)	-2(1)	3(1)	-2(1)
C(7)	36(1)	37(1)	16(1)	-2(1)	-2(1)	1(1)
C(8)	42(1)	23(1)	22(1)	-4(1)	5(1)	0(1)
C(9)	14(1)	16(1)	12(1)	-1(1)	1(1)	0(1)
C(10)	17(1)	18(1)	17(1)	1(1)	3(1)	-2(1)
C(11)	26(1)	16(1)	14(1)	1(1)	5(1)	1(1)
C(12)	26(1)	16(1)	14(1)	0(1)	-3(1)	4(1)
C(13)	16(1)	18(1)	20(1)	-2(1)	-1(1)	3(1)
C(14)	15(1)	16(1)	15(1)	0(1)	3(1)	1(1)
F(1)	11(1)	30(1)	26(1)	4(1)	4(1)	3(1)

F(2)	16(1)	33(1)	24(1)	4(1)	5(1)	-4(1)
F(3)	35(1)	26(1)	19(1)	7(1)	10(1)	0(1)
F(4)	35(1)	27(1)	18(1)	5(1)	-5(1)	8(1)
F(5)	15(1)	32(1)	30(1)	0(1)	-3(1)	4(1)
F(6)	15(1)	27(1)	23(1)	4(1)	6(1)	0(1)
F(7)	35(1)	18(1)	40(1)	-10(1)	17(1)	-4(1)
F(8)	33(1)	19(1)	26(1)	4(1)	10(1)	2(1)
F(9)	18(1)	35(1)	64(1)	-13(1)	12(1)	0(1)
F(10)	42(1)	28(1)	22(1)	3(1)	1(1)	-1(1)
N(1)	12(1)	16(1)	13(1)	1(1)	2(1)	2(1)
N(2)	13(1)	17(1)	16(1)	-2(1)	3(1)	1(1)
N(3)	13(1)	16(1)	13(1)	0(1)	1(1)	1(1)

Table A1.15 Hydrogen coordinates ($\times 10^4$) and isotropic displacement parameters ($\text{\AA}^2 \times 10^3$) for triazolium salt (**128**).

	x	y	z	U(eq)
H(1)	3802	2698	5085	18
H(2)	2715	5170	2921	19
H(3A)	1983	7774	3437	22
H(3B)	525	7106	2746	22
H(4)	972	8033	5069	20
H(6)	50	3752	2868	25
H(7A)	1390	4174	872	46
H(7B)	209	5392	1100	46
H(7C)	-102	3440	735	46
H(8A)	872	1099	2182	44
H(8B)	1590	1515	3560	44
H(8C)	2366	1859	2493	44

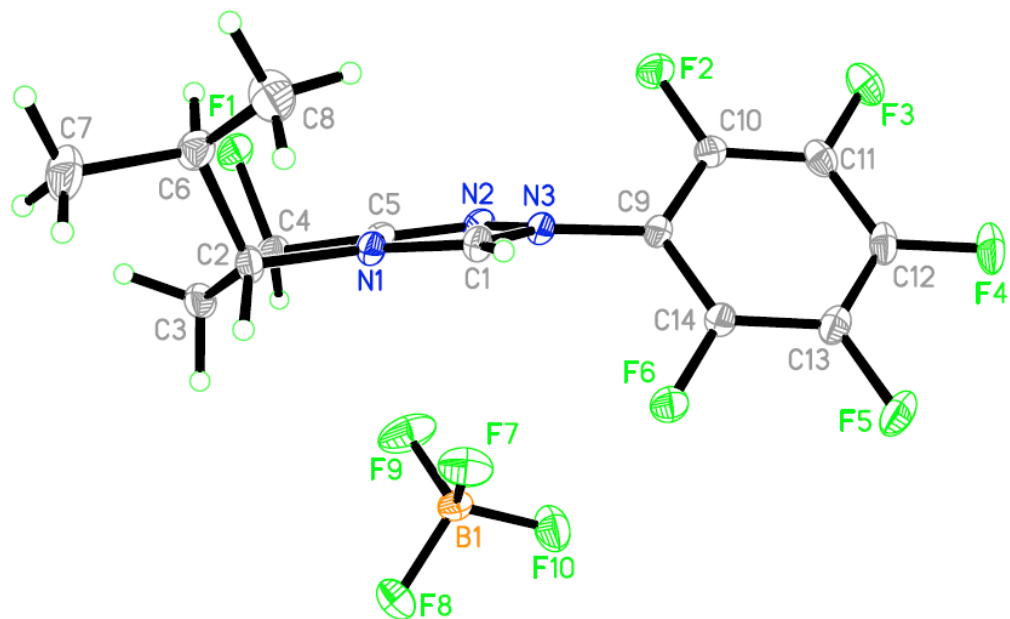


Figure A1.3 Thermal plot of triazolium salt (**128**). Ellipsoids drawn at the 50% probability level.

Table A1.16 Crystal data and structure refinement for triazolium salt (**132**).

Identification code	rovis57_0m	
Empirical formula	$C_{14}H_{12}BF_{10}N_3$	
Formula weight	423.08	
Temperature	120 K	
Wavelength	0.71073 Å	
Crystal system	Monoclinic	
Space group	$P2_1$	
Unit cell dimensions	$a = 9.9082(3)$ Å	$\alpha = 90^\circ$.
	$b = 7.7653(3)$ Å	$\beta = 106.157(2)^\circ$.
	$c = 11.0984(4)$ Å	$\gamma = 90^\circ$.
Volume	$820.19(5)$ Å ³	
Z	2	
Density (calculated)	1.713 Mg/m ³	
Absorption coefficient	0.183 mm ⁻¹	
F(000)	424	
Crystal size	0.23 x 0.05 x 0.02 mm ³	
Theta range for data collection	1.91 to 32.58°.	

Index ranges	-15<=h<=14, -11<=k<=11, -16<=l<=16
Reflections collected	13190
Independent reflections	5480 [R(int) = 0.0339]
Completeness to theta = 32.58°	99.9 %
Absorption correction	Semi-empirical from equivalents
Max. and min. transmission	0.9956 and 0.9585
Refinement method	Full-matrix least-squares on F ²
Data / restraints / parameters	5480 / 1 / 255
Goodness-of-fit on F ²	1.044
Final R indices [I>2sigma(I)]	R1 = 0.0518, wR2 = 0.1283
R indices (all data)	R1 = 0.0753, wR2 = 0.1502
Absolute structure parameter	0.0(6)
Largest diff. peak and hole	0.693 and -0.556 e.Å ⁻³

Table A1.17 Atomic coordinates (x 10⁴) and equivalent isotropic displacement parameters (Å²x 10³) for triazolium salt (**132**). U(eq) is defined as one third of the trace of the orthogonalized U^{ij} tensor.

	x	y	z	U(eq)
B(1)	5838(3)	5625(4)	8378(3)	27(1)
C(1)	3461(2)	5052(3)	234(2)	18(1)
C(2)	1817(2)	6030(3)	-1954(2)	22(1)
C(3)	359(3)	6857(4)	-2031(3)	36(1)
C(4)	361(3)	7487(3)	-736(2)	25(1)
C(5)	1596(2)	6585(3)	117(2)	19(1)
C(6)	1762(2)	4354(3)	-2671(2)	25(1)
C(7)	1216(3)	4742(4)	-4073(2)	35(1)
C(8)	925(3)	2918(5)	-2270(3)	41(1)
C(9)	4221(2)	4876(3)	2535(2)	18(1)
C(10)	3686(2)	4196(3)	3468(2)	19(1)
C(11)	4574(3)	3624(3)	4583(2)	23(1)
C(12)	6006(3)	3692(3)	4781(2)	26(1)
C(13)	6557(2)	4351(3)	3863(2)	24(1)
C(14)	5664(2)	4943(3)	2748(2)	21(1)
F(1)	620(3)	9256(3)	-633(2)	68(1)
F(2)	2307(2)	4042(2)	3283(1)	28(1)

F(3)	4022(2)	2912(2)	5438(1)	33(1)
F(4)	6874(2)	3092(2)	5841(1)	37(1)
F(5)	7948(2)	4430(2)	4048(2)	36(1)
F(6)	6219(2)	5567(2)	1870(1)	28(1)
F(7)	5187(3)	5566(3)	7098(2)	61(1)
F(8)	5054(2)	6798(2)	8868(2)	35(1)
F(9)	7173(2)	6215(3)	8601(3)	76(1)
F(10)	5762(2)	4033(2)	8927(2)	39(1)
N(1)	2368(2)	5800(2)	-569(2)	17(1)
N(2)	2135(2)	6377(3)	1313(2)	21(1)
N(3)	3315(2)	5401(2)	1366(2)	16(1)

Table A1.18 Bond lengths [\AA] and angles [$^\circ$] for triazolium salt (**132**).

B(1)-F(9)	1.357(3)	C(11)-F(3)	1.339(3)
B(1)-F(7)	1.387(4)	C(11)-C(12)	1.376(4)
B(1)-F(10)	1.389(3)	C(12)-F(4)	1.334(3)
B(1)-F(8)	1.401(3)	C(12)-C(13)	1.381(4)
C(1)-N(1)	1.330(3)	C(13)-F(5)	1.337(3)
C(1)-N(3)	1.332(3)	C(13)-C(14)	1.384(3)
C(2)-N(1)	1.492(3)	C(14)-F(6)	1.336(3)
C(2)-C(6)	1.519(4)	N(2)-N(3)	1.381(3)
C(2)-C(3)	1.561(3)	F(9)-B(1)-F(7)	110.5(2)
C(3)-C(4)	1.518(4)	F(9)-B(1)-F(10)	112.9(2)
C(4)-F(1)	1.396(3)	F(7)-B(1)-F(10)	110.7(2)
C(4)-C(5)	1.497(3)	F(9)-B(1)-F(8)	109.1(3)
C(5)-N(2)	1.296(3)	F(7)-B(1)-F(8)	105.6(2)
C(5)-N(1)	1.364(3)	F(10)-B(1)-F(8)	107.7(2)
C(6)-C(8)	1.527(4)	N(1)-C(1)-N(3)	105.14(19)
C(6)-C(7)	1.529(4)	N(1)-C(2)-C(6)	112.74(19)
C(9)-C(14)	1.384(3)	N(1)-C(2)-C(3)	100.00(18)
C(9)-C(10)	1.393(3)	C(6)-C(2)-C(3)	115.2(2)
C(9)-N(3)	1.416(3)	C(4)-C(3)-C(2)	108.9(2)
C(10)-F(2)	1.329(3)	F(1)-C(4)-C(5)	108.0(2)
C(10)-C(11)	1.377(3)	F(1)-C(4)-C(3)	110.2(3)

C(5)-C(4)-C(3)	103.49(19)	F(4)-C(12)-C(11)	120.7(2)
N(2)-C(5)-N(1)	112.39(19)	F(4)-C(12)-C(13)	119.4(2)
N(2)-C(5)-C(4)	137.5(2)	C(11)-C(12)-C(13)	119.9(2)
N(1)-C(5)-C(4)	110.1(2)	F(5)-C(13)-C(12)	120.4(2)
C(2)-C(6)-C(8)	114.6(2)	F(5)-C(13)-C(14)	119.8(2)
C(2)-C(6)-C(7)	108.4(2)	C(12)-C(13)-C(14)	119.8(2)
C(8)-C(6)-C(7)	111.9(2)	F(6)-C(14)-C(9)	120.3(2)
C(14)-C(9)-C(10)	118.4(2)	F(6)-C(14)-C(13)	118.8(2)
C(14)-C(9)-N(3)	120.49(19)	C(9)-C(14)-C(13)	120.9(2)
C(10)-C(9)-N(3)	121.0(2)	C(1)-N(1)-C(5)	107.45(18)
F(2)-C(10)-C(11)	118.8(2)	C(1)-N(1)-C(2)	137.69(19)
F(2)-C(10)-C(9)	120.5(2)	C(5)-N(1)-C(2)	114.84(18)
C(11)-C(10)-C(9)	120.7(2)	C(5)-N(2)-N(3)	102.39(17)
F(3)-C(11)-C(12)	120.7(2)	C(1)-N(3)-N(2)	112.64(18)
F(3)-C(11)-C(10)	119.0(2)	C(1)-N(3)-C(9)	126.67(19)
C(12)-C(11)-C(10)	120.2(2)	N(2)-N(3)-C(9)	120.69(18)

Symmetry transformations used to generate equivalent atoms:

Table A1.19 Anisotropic displacement parameters ($\text{\AA}^2 \times 10^3$) for triazolium salt (**132**). The anisotropic displacement factor exponent takes the form: $-2\pi^2 [h^2 a^{*2} U^{11} + \dots + 2 h k a^* b^* U^{12}]$

	U^{11}	U^{22}	U^{33}	U^{23}	U^{13}	U^{12}
B(1)	29(1)	20(1)	36(2)	3(1)	17(1)	0(1)
C(1)	18(1)	19(1)	18(1)	2(1)	4(1)	2(1)
C(2)	21(1)	28(1)	15(1)	7(1)	2(1)	5(1)
C(3)	28(1)	49(2)	28(1)	4(1)	0(1)	20(1)
C(4)	19(1)	28(1)	26(1)	0(1)	0(1)	7(1)
C(5)	14(1)	20(1)	23(1)	-1(1)	3(1)	1(1)
C(6)	20(1)	33(1)	20(1)	0(1)	6(1)	-2(1)
C(7)	30(1)	54(2)	19(1)	-1(1)	3(1)	3(1)
C(8)	41(2)	47(2)	39(2)	-7(1)	16(1)	-14(1)
C(9)	20(1)	15(1)	16(1)	-1(1)	2(1)	-2(1)
C(10)	19(1)	19(1)	18(1)	-2(1)	3(1)	-4(1)
C(11)	35(1)	17(1)	16(1)	0(1)	6(1)	-4(1)

C(12)	32(1)	21(1)	18(1)	-1(1)	-5(1)	2(1)
C(13)	19(1)	24(1)	25(1)	-2(1)	-2(1)	-1(1)
C(14)	22(1)	19(1)	21(1)	0(1)	4(1)	-2(1)
F(1)	69(1)	28(1)	76(2)	-11(1)	-30(1)	23(1)
F(2)	23(1)	36(1)	25(1)	4(1)	8(1)	-6(1)
F(3)	46(1)	34(1)	20(1)	9(1)	10(1)	-5(1)
F(4)	43(1)	37(1)	22(1)	6(1)	-7(1)	6(1)
F(5)	17(1)	46(1)	37(1)	3(1)	-5(1)	0(1)
F(6)	20(1)	37(1)	26(1)	5(1)	7(1)	-5(1)
F(7)	116(2)	39(1)	33(1)	-8(1)	28(1)	-18(1)
F(8)	47(1)	22(1)	42(1)	2(1)	22(1)	3(1)
F(9)	22(1)	66(2)	138(2)	52(2)	21(1)	2(1)
F(10)	45(1)	22(1)	64(1)	14(1)	35(1)	9(1)
N(1)	16(1)	19(1)	16(1)	3(1)	4(1)	3(1)
N(2)	16(1)	24(1)	22(1)	-2(1)	6(1)	1(1)
N(3)	15(1)	16(1)	16(1)	1(1)	3(1)	0(1)

Table A1.20 Hydrogen coordinates ($\times 10^4$) and isotropic displacement parameters ($\text{\AA}^2 \times 10^3$) for triazolium salt (**132**).

	x	y	z	U(eq)
H(1)	4174	4420	47	22
H(2)	2403	6863	-2241	26
H(3A)	185	7814	-2616	44
H(3B)	-381	6013	-2327	44
H(4)	-515	7190	-539	30
H(6)	2731	3943	-2515	29
H(7A)	272	5170	-4258	53
H(7B)	1229	3707	-4543	53
H(7C)	1805	5593	-4299	53
H(8A)	1355	2632	-1407	62
H(8B)	915	1920	-2783	62
H(8C)	-21	3300	-2369	62

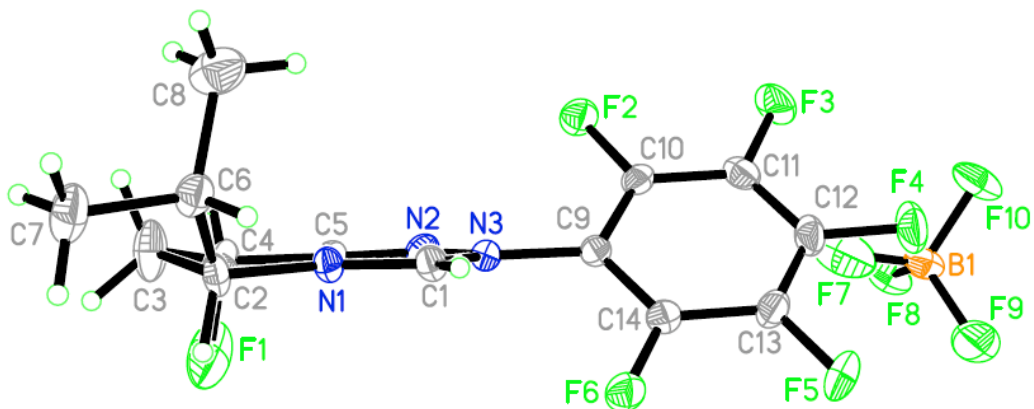


Figure A1.4 Thermal plot of triazolium salt (**132**). Ellipsoids drawn at the 50% probability level.

Table 21. Crystal data and structure refinement for triazolium salt (**138**).

Identification code	rovis65_0m	
Empirical formula	$C_{11}H_6BF_{10}N_3$	
Formula weight	381.00	
Temperature	120 K	
Wavelength	0.71073 Å	
Crystal system	Monoclinic	
Space group	$P2_1$	
Unit cell dimensions	$a = 10.8932(8)$ Å	$\alpha = 90^\circ$.
	$b = 7.6975(5)$ Å	$\beta = 98.254(4)^\circ$.
	$c = 16.1350(14)$ Å	$\gamma = 90^\circ$.
Volume	$1338.91(18)$ Å ³	
Z	4	
Density (calculated)	1.890 Mg/m ³	
Absorption coefficient	0.212 mm ⁻¹	
F(000)	752	
Crystal size	0.30 x 0.13 x 0.11 mm ³	
Theta range for data collection	1.89 to 32.58°.	
Index ranges	$-16 \leq h \leq 16$, $-10 \leq k \leq 11$, $-24 \leq l \leq 16$	
Reflections collected	19989	
Independent reflections	8762 [R(int) = 0.0305]	

Completeness to theta = 32.58°	99.9 %
Absorption correction	Semi-empirical from equivalents
Max. and min. transmission	0.9781 and 0.9394
Refinement method	Full-matrix least-squares on F ²
Data / restraints / parameters	8762 / 1 / 451
Goodness-of-fit on F ²	0.998
Final R indices [I>2sigma(I)]	R1 = 0.0468, wR2 = 0.1013
R indices (all data)	R1 = 0.0810, wR2 = 0.1230
Absolute structure parameter	0.0(4)
Largest diff. peak and hole	0.346 and -0.337 e.Å ⁻³

Table A1.22 Atomic coordinates (x 10⁴) and equivalent isotropic displacement parameters (Å²x 10³) for triazolium salt (**138**). U(eq) is defined as one third of the trace of the orthogonalized U^{ij} tensor.

	x	y	z	U(eq)
B(1)	7284(2)	7566(4)	4772(2)	23(1)
B(2)	2678(2)	1892(4)	303(2)	21(1)
C(1)	4174(2)	7421(3)	5369(2)	18(1)
C(2)	1951(2)	7452(3)	4504(2)	20(1)
C(3)	898(2)	8394(3)	4854(2)	23(1)
C(4)	1175(2)	8218(4)	5809(2)	25(1)
C(5)	2564(2)	8056(3)	5944(2)	18(1)
C(6)	5721(2)	7787(3)	6633(1)	17(1)
C(7)	6318(2)	6236(3)	6866(2)	19(1)
C(8)	7533(2)	6229(3)	7245(2)	18(1)
C(9)	8163(2)	7784(3)	7402(1)	18(1)
C(10)	7576(2)	9334(3)	7178(2)	18(1)
C(11)	6353(2)	9328(3)	6789(2)	17(1)
C(12)	5802(2)	1842(3)	9691(2)	19(1)
C(13)	8050(2)	1756(3)	10531(1)	21(1)
C(14)	9105(2)	2591(3)	10134(2)	23(1)
C(15)	8805(2)	2273(3)	9194(2)	22(1)
C(16)	7414(2)	2204(3)	9073(2)	18(1)
C(17)	4244(2)	2191(3)	8424(2)	18(1)
C(18)	3736(2)	3789(3)	8182(2)	20(1)

C(19)	2529(2)	3903(3)	7781(2)	22(1)
C(20)	1830(2)	2427(3)	7621(2)	21(1)
C(21)	2339(2)	836(3)	7857(2)	20(1)
C(22)	3545(2)	716(3)	8253(2)	18(1)
F(1)	692(1)	6684(2)	6070(1)	39(1)
F(2)	5727(1)	4728(2)	6698(1)	27(1)
F(3)	8125(1)	4728(2)	7436(1)	26(1)
F(4)	9343(1)	7769(2)	7747(1)	25(1)
F(5)	8196(1)	10832(2)	7294(1)	25(1)
F(6)	5805(1)	10829(2)	6536(1)	24(1)
F(7)	6647(1)	6127(2)	5035(1)	30(1)
F(8)	8150(1)	8138(2)	5428(1)	33(1)
F(9)	7870(2)	7077(2)	4108(1)	38(1)
F(10)	6421(1)	8864(2)	4550(1)	53(1)
F(11)	9232(1)	652(2)	8986(1)	32(1)
F(12)	4400(1)	5249(2)	8361(1)	29(1)
F(13)	2040(1)	5465(2)	7561(1)	32(1)
F(14)	663(1)	2537(2)	7253(1)	30(1)
F(15)	1649(1)	-607(2)	7713(1)	27(1)
F(16)	4026(1)	-838(2)	8487(1)	24(1)
F(17)	3490(2)	3199(2)	609(1)	48(1)
F(18)	1872(1)	2499(2)	-386(1)	33(1)
F(19)	3372(1)	503(2)	46(1)	29(1)
F(20)	2007(1)	1297(2)	908(1)	29(1)
N(1)	2959(2)	7589(2)	5218(1)	16(1)
N(2)	3473(2)	8190(3)	6564(1)	21(1)
N(3)	4490(2)	7782(3)	6180(1)	17(1)
N(4)	7019(2)	1889(2)	9823(1)	17(1)
N(5)	6493(2)	2324(3)	8464(1)	21(1)
N(6)	5480(2)	2096(2)	8872(1)	18(1)

Table A1.23 Bond lengths [Å] and angles [°] for triazolium salt (**138**).

B(1)-F(9)	1.376(3)	C(15)-F(11)	1.390(3)
B(1)-F(10)	1.383(3)	C(15)-C(16)	1.500(3)
B(1)-F(8)	1.385(3)	C(16)-N(5)	1.303(3)
B(1)-F(7)	1.405(3)	C(16)-N(4)	1.363(3)
B(2)-F(20)	1.380(3)	C(17)-C(22)	1.372(3)
B(2)-F(17)	1.383(3)	C(17)-C(18)	1.382(3)
B(2)-F(18)	1.394(3)	C(17)-N(6)	1.435(3)
B(2)-F(19)	1.405(3)	C(18)-F(12)	1.345(3)
C(1)-N(1)	1.317(3)	C(18)-C(19)	1.383(3)
C(1)-N(3)	1.333(3)	C(19)-F(13)	1.342(3)
C(2)-N(1)	1.476(3)	C(19)-C(20)	1.371(4)
C(2)-C(3)	1.532(3)	C(20)-F(14)	1.326(2)
C(3)-C(4)	1.533(3)	C(20)-C(21)	1.375(4)
C(4)-F(1)	1.383(3)	C(21)-F(15)	1.343(3)
C(4)-C(5)	1.502(3)	C(21)-C(22)	1.379(3)
C(5)-N(2)	1.307(3)	C(22)-F(16)	1.339(3)
C(5)-N(1)	1.354(3)	N(2)-N(3)	1.381(3)
C(6)-C(11)	1.376(3)	N(5)-N(6)	1.375(3)
C(6)-C(7)	1.386(3)	F(9)-B(1)-F(10)	111.8(2)
C(6)-N(3)	1.432(3)	F(9)-B(1)-F(8)	109.9(2)
C(7)-F(2)	1.336(3)	F(10)-B(1)-F(8)	109.3(2)
C(7)-C(8)	1.376(3)	F(9)-B(1)-F(7)	108.9(2)
C(8)-F(3)	1.338(3)	F(10)-B(1)-F(7)	107.5(2)
C(8)-C(9)	1.385(3)	F(8)-B(1)-F(7)	109.4(2)
C(9)-F(4)	1.325(2)	F(20)-B(2)-F(17)	111.4(2)
C(9)-C(10)	1.377(3)	F(20)-B(2)-F(18)	109.74(19)
C(10)-F(5)	1.336(3)	F(17)-B(2)-F(18)	109.8(2)
C(10)-C(11)	1.389(3)	F(20)-B(2)-F(19)	108.6(2)
C(11)-F(6)	1.337(3)	F(17)-B(2)-F(19)	108.39(19)
C(12)-N(4)	1.313(3)	F(18)-B(2)-F(19)	108.9(2)
C(12)-N(6)	1.333(3)	N(1)-C(1)-N(3)	105.9(2)
C(13)-N(4)	1.486(3)	N(1)-C(2)-C(3)	101.05(18)
C(13)-C(14)	1.535(3)	C(2)-C(3)-C(4)	106.15(18)
C(14)-C(15)	1.524(3)	F(1)-C(4)-C(5)	107.69(19)

F(1)-C(4)-C(3)	110.7(2)	C(22)-C(17)-C(18)	119.5(2)
C(5)-C(4)-C(3)	101.73(19)	C(22)-C(17)-N(6)	120.8(2)
N(2)-C(5)-N(1)	112.56(19)	C(18)-C(17)-N(6)	119.7(2)
N(2)-C(5)-C(4)	137.9(2)	F(12)-C(18)-C(19)	119.6(2)
N(1)-C(5)-C(4)	109.5(2)	F(12)-C(18)-C(17)	120.16(19)
C(11)-C(6)-C(7)	119.34(19)	C(19)-C(18)-C(17)	120.2(2)
C(11)-C(6)-N(3)	120.2(2)	F(13)-C(19)-C(20)	120.3(2)
C(7)-C(6)-N(3)	120.3(2)	F(13)-C(19)-C(18)	119.7(2)
F(2)-C(7)-C(8)	119.5(2)	C(20)-C(19)-C(18)	120.1(2)
F(2)-C(7)-C(6)	119.96(19)	F(14)-C(20)-C(21)	120.2(2)
C(8)-C(7)-C(6)	120.5(2)	F(14)-C(20)-C(19)	120.1(2)
F(3)-C(8)-C(7)	120.5(2)	C(21)-C(20)-C(19)	119.6(2)
F(3)-C(8)-C(9)	119.6(2)	F(15)-C(21)-C(20)	119.7(2)
C(7)-C(8)-C(9)	119.9(2)	F(15)-C(21)-C(22)	119.8(2)
F(4)-C(9)-C(10)	120.3(2)	C(20)-C(21)-C(22)	120.5(2)
F(4)-C(9)-C(8)	119.6(2)	F(16)-C(22)-C(17)	119.96(18)
C(10)-C(9)-C(8)	120.07(19)	F(16)-C(22)-C(21)	119.9(2)
F(5)-C(10)-C(9)	120.29(19)	C(17)-C(22)-C(21)	120.1(2)
F(5)-C(10)-C(11)	119.9(2)	C(1)-N(1)-C(5)	107.50(19)
C(9)-C(10)-C(11)	119.71(19)	C(1)-N(1)-C(2)	138.8(2)
F(6)-C(11)-C(6)	119.90(19)	C(5)-N(1)-C(2)	113.64(18)
F(6)-C(11)-C(10)	119.55(19)	C(5)-N(2)-N(3)	101.92(19)
C(6)-C(11)-C(10)	120.5(2)	C(1)-N(3)-N(2)	112.14(17)
N(4)-C(12)-N(6)	105.8(2)	C(1)-N(3)-C(6)	126.36(19)
N(4)-C(13)-C(14)	100.29(18)	N(2)-N(3)-C(6)	121.50(19)
C(15)-C(14)-C(13)	106.35(19)	C(12)-N(4)-C(16)	107.54(19)
F(11)-C(15)-C(16)	107.65(19)	C(12)-N(4)-C(13)	139.2(2)
F(11)-C(15)-C(14)	110.68(19)	C(16)-N(4)-C(13)	113.25(18)
C(16)-C(15)-C(14)	101.79(19)	C(16)-N(5)-N(6)	102.4(2)
N(5)-C(16)-N(4)	112.0(2)	C(12)-N(6)-N(5)	112.22(18)
N(5)-C(16)-C(15)	138.6(2)	C(12)-N(6)-C(17)	127.0(2)
N(4)-C(16)-C(15)	109.4(2)	N(5)-N(6)-C(17)	120.8(2)

Symmetry transformations used to generate equivalent atoms:

Table A1.24 Anisotropic displacement parameters ($\text{\AA}^2 \times 10^3$) for triazolium salt (**138**). The anisotropic displacement factor exponent takes the form: $-2\pi^2 [h^2 a^{*2} U^{11} + \dots + 2 h k a^* b^* U^{12}]$

	U ¹¹	U ²²	U ³³	U ²³	U ¹³	U ¹²
B(1)	19(1)	21(1)	29(2)	-2(1)	2(1)	1(1)
B(2)	15(1)	17(1)	32(2)	-3(1)	4(1)	-1(1)
C(1)	14(1)	18(1)	22(1)	-2(1)	1(1)	1(1)
C(2)	16(1)	22(1)	20(1)	1(1)	-5(1)	-1(1)
C(3)	17(1)	28(1)	23(1)	2(1)	-2(1)	0(1)
C(4)	14(1)	35(1)	25(1)	0(1)	0(1)	1(1)
C(5)	16(1)	21(1)	17(1)	1(1)	2(1)	0(1)
C(6)	14(1)	18(1)	18(1)	-1(1)	0(1)	-2(1)
C(7)	20(1)	14(1)	22(1)	1(1)	0(1)	-4(1)
C(8)	19(1)	17(1)	18(1)	3(1)	0(1)	3(1)
C(9)	10(1)	28(1)	16(1)	1(1)	-1(1)	-1(1)
C(10)	18(1)	19(1)	17(1)	-1(1)	1(1)	-7(1)
C(11)	16(1)	19(1)	16(1)	0(1)	0(1)	2(1)
C(12)	15(1)	21(1)	20(1)	0(1)	1(1)	-3(1)
C(13)	19(1)	25(1)	16(1)	-4(1)	-4(1)	3(1)
C(14)	14(1)	26(1)	27(1)	-4(1)	-4(1)	0(1)
C(15)	14(1)	26(1)	25(1)	2(1)	0(1)	4(1)
C(16)	15(1)	16(1)	23(1)	1(1)	2(1)	-1(1)
C(17)	12(1)	22(1)	18(1)	-1(1)	-2(1)	1(1)
C(18)	18(1)	20(1)	21(1)	-1(1)	0(1)	-2(1)
C(19)	22(1)	22(1)	19(1)	2(1)	-1(1)	5(1)
C(20)	13(1)	34(2)	16(1)	2(1)	0(1)	2(1)
C(21)	16(1)	23(1)	19(1)	-3(1)	3(1)	-6(1)
C(22)	16(1)	20(1)	18(1)	-3(1)	0(1)	2(1)
F(1)	21(1)	62(1)	31(1)	18(1)	-2(1)	-14(1)
F(2)	26(1)	16(1)	36(1)	1(1)	-6(1)	-6(1)
F(3)	27(1)	18(1)	32(1)	1(1)	-2(1)	9(1)
F(4)	13(1)	33(1)	26(1)	0(1)	-3(1)	-1(1)
F(5)	25(1)	22(1)	25(1)	1(1)	-3(1)	-10(1)
F(6)	25(1)	17(1)	28(1)	2(1)	-5(1)	2(1)
F(7)	29(1)	19(1)	44(1)	-2(1)	15(1)	-1(1)

F(8)	26(1)	44(1)	29(1)	-10(1)	4(1)	-5(1)
F(9)	41(1)	51(1)	24(1)	-5(1)	10(1)	-14(1)
F(10)	27(1)	25(1)	101(2)	14(1)	-8(1)	5(1)
F(11)	24(1)	42(1)	29(1)	-7(1)	-1(1)	15(1)
F(12)	28(1)	20(1)	36(1)	2(1)	-5(1)	-5(1)
F(13)	31(1)	29(1)	33(1)	8(1)	-6(1)	8(1)
F(14)	13(1)	47(1)	28(1)	4(1)	-4(1)	1(1)
F(15)	21(1)	29(1)	31(1)	-3(1)	-1(1)	-10(1)
F(16)	23(1)	17(1)	31(1)	-1(1)	-1(1)	2(1)
F(17)	30(1)	23(1)	88(2)	-12(1)	-4(1)	-6(1)
F(18)	33(1)	39(1)	29(1)	10(1)	8(1)	9(1)
F(19)	27(1)	21(1)	41(1)	2(1)	15(1)	3(1)
F(20)	27(1)	39(1)	23(1)	3(1)	7(1)	6(1)
N(1)	13(1)	15(1)	19(1)	-2(1)	-1(1)	-2(1)
N(2)	16(1)	28(1)	19(1)	-1(1)	2(1)	-2(1)
N(3)	12(1)	20(1)	18(1)	-1(1)	1(1)	1(1)
N(4)	14(1)	15(1)	19(1)	-1(1)	-2(1)	0(1)
N(5)	14(1)	26(1)	21(1)	2(1)	2(1)	2(1)
N(6)	13(1)	19(1)	21(1)	1(1)	1(1)	-1(1)

Table A1.25 Hydrogen coordinates ($\times 10^4$) and isotropic displacement parameters ($\text{\AA}^2 \times 10^3$) for triazolium salt (**138**).

	x	y	z	U(eq)
H(1)	4702	7113	4989	22
H(2A)	1740	6250	4371	24
H(2B)	2166	8029	4010	24
H(3A)	105	7867	4645	28
H(3B)	873	9608	4692	28
H(4)	892	9232	6096	30
H(12)	5273	1667	10088	22
H(13A)	8232	557	10688	25
H(13B)	7873	2401	11016	25

H(14A)	9151	3827	10251	28
H(14B)	9894	2064	10354	28
H(15)	9115	3208	8868	26

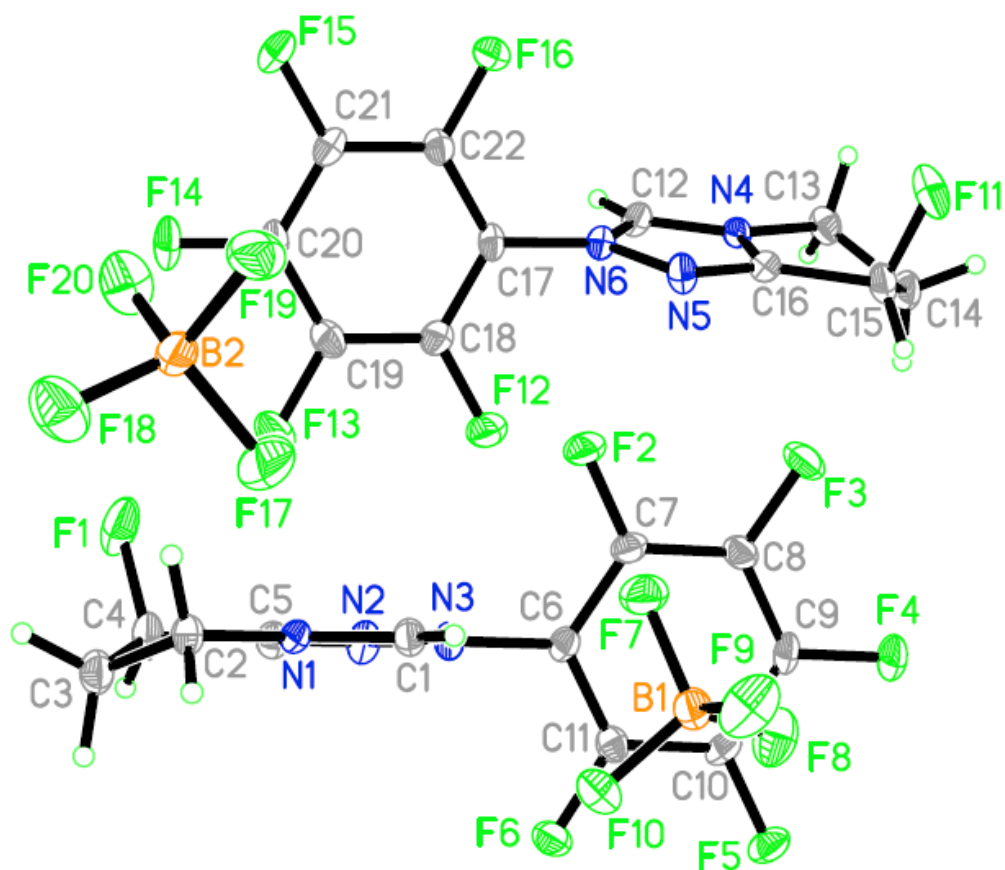


Figure A1.5 Thermal plot of triazolium salt (**138**). Ellipsoids drawn at the 50% probability level.

Table 26. Crystal data and structure refinement for (**112**).

Identification code	rovis46	
Empirical formula	C ₁₂ H ₁₅ BrN ₂ O ₃ S	
Formula weight	347.23	
Temperature	120 K	
Wavelength	0.71073 Å	
Crystal system	Orthorhombic	
Space group	P2 ₁ 2 ₁ 2 ₁	
Unit cell dimensions	$a = 5.6745(3)$ Å	$\alpha = 90^\circ$.

	$b = 13.5498(6) \text{ \AA}$	$\beta = 90^\circ$.
	$c = 17.9944(8) \text{ \AA}$	$\gamma = 90^\circ$.
Volume	1383.56(11) \AA^3	
Z	4	
Density (calculated)	1.667 Mg/m ³	
Absorption coefficient	3.127 mm ⁻¹	
F(000)	704	
Crystal size	0.48 x 0.45 x 0.40 mm ³	
Theta range for data collection	2.26 to 30.60°.	
Index ranges	-8 ≤ h ≤ 7, -14 ≤ k ≤ 19, -24 ≤ l ≤ 25	
Reflections collected	9320	
Independent reflections	4112 [R(int) = 0.0334]	
Completeness to theta = 30.60°	98.9 %	
Absorption correction	Semi-empirical from equivalents	
Max. and min. transmission	0.3692 and 0.3141	
Refinement method	Full-matrix least-squares on F ²	
Data / restraints / parameters	4112 / 0 / 173	
Goodness-of-fit on F ²	0.876	
Final R indices [I > 2σ(I)]	R1 = 0.0317, wR2 = 0.0543	
R indices (all data)	R1 = 0.0455, wR2 = 0.0577	
Absolute structure parameter	0.012(7)	
Largest diff. peak and hole	0.490 and -0.794 e.Å ⁻³	

Table A1.27 Atomic coordinates (x 10⁴) and equivalent isotropic displacement parameters (Å²x 10³) for (112). U(eq) is defined as one third of the trace of the orthogonalized U^{ij} tensor.

	x	y	z	U(eq)
Br(1)	7108(1)	7210(1)	2089(1)	26(1)
C(1)	3017(5)	6017(2)	2351(1)	19(1)
C(2)	5191(4)	6294(2)	2589(1)	18(1)
C(3)	4386(4)	5268(2)	3482(1)	14(1)
C(4)	4612(4)	4645(2)	4153(1)	16(1)
C(5)	6863(4)	4709(2)	4610(1)	14(1)
C(6)	7739(5)	3671(1)	4772(1)	17(1)
C(7)	6341(4)	5252(2)	5358(1)	16(1)

C(8)	5219(5)	6267(2)	5236(1)	23(1)
C(9)	4715(5)	6786(2)	5970(1)	29(1)
C(10)	6949(5)	6888(2)	6438(1)	28(1)
C(11)	8077(5)	5884(2)	6564(1)	24(1)
C(12)	8576(4)	5354(2)	5827(1)	21(1)
N(1)	5987(3)	5879(1)	3231(1)	17(1)
N(2)	8037(4)	3073(1)	4080(1)	18(1)
O(1)	3011(3)	4088(1)	4326(1)	24(1)
O(2)	8316(3)	2176(1)	4165(1)	30(1)
O(3)	8026(4)	3477(1)	3473(1)	24(1)
S(2)	1850(1)	5181(1)	2955(1)	20(1)

Table A1.28 Bond lengths [\AA] and angles [$^\circ$] for **(112)**.

Br(1)-C(2)	1.879(2)	C(2)-C(1)-S(2)	109.66(17)
C(1)-C(2)	1.359(4)	C(1)-C(2)-N(1)	117.0(2)
C(1)-S(2)	1.703(2)	C(1)-C(2)-Br(1)	123.90(18)
C(2)-N(1)	1.363(3)	N(1)-C(2)-Br(1)	119.09(18)
C(3)-N(1)	1.310(3)	N(1)-C(3)-C(4)	125.5(2)
C(3)-C(4)	1.480(3)	N(1)-C(3)-S(2)	115.61(16)
C(3)-S(2)	1.727(2)	C(4)-C(3)-S(2)	118.83(17)
C(4)-O(1)	1.222(3)	O(1)-C(4)-C(3)	119.7(2)
C(4)-C(5)	1.521(3)	O(1)-C(4)-C(5)	121.49(19)
C(5)-C(6)	1.521(3)	C(3)-C(4)-C(5)	118.8(2)
C(5)-C(7)	1.562(3)	C(6)-C(5)-C(4)	108.97(19)
C(6)-N(2)	1.496(2)	C(6)-C(5)-C(7)	109.44(15)
C(7)-C(12)	1.530(3)	C(4)-C(5)-C(7)	109.44(18)
C(7)-C(8)	1.530(3)	N(2)-C(6)-C(5)	112.22(16)
C(8)-C(9)	1.523(3)	C(12)-C(7)-C(8)	110.0(2)
C(9)-C(10)	1.528(4)	C(12)-C(7)-C(5)	111.14(18)
C(10)-C(11)	1.521(3)	C(8)-C(7)-C(5)	112.26(17)
C(11)-C(12)	1.533(3)	C(9)-C(8)-C(7)	111.6(2)
N(2)-O(3)	1.221(2)	C(8)-C(9)-C(10)	111.3(2)
N(2)-O(2)	1.235(2)	C(11)-C(10)-C(9)	110.5(2)
		C(10)-C(11)-C(12)	111.56(18)

C(7)-C(12)-C(11)	111.5(2)	O(3)-N(2)-C(6)	120.06(17)
C(3)-N(1)-C(2)	108.8(2)	O(2)-N(2)-C(6)	116.32(16)
O(3)-N(2)-O(2)	123.62(17)	C(1)-S(2)-C(3)	88.91(12)

Symmetry transformations used to generate equivalent atoms:

Table A1.29 Anisotropic displacement parameters ($\text{\AA}^2 \times 10^3$) for **(112)**. The anisotropic displacement factor exponent takes the form: $-2\pi^2 [h^2 a^{*2} U^{11} + \dots + 2 h k a^* b^* U^{12}]$

	U ¹¹	U ²²	U ³³	U ²³	U ¹³	U ¹²
Br(1)	22(1)	28(1)	27(1)	12(1)	3(1)	-1(1)
C(1)	22(1)	20(1)	16(1)	3(1)	-2(1)	5(1)
C(2)	18(1)	18(1)	18(1)	2(1)	2(1)	2(1)
C(3)	14(1)	15(1)	13(1)	-2(1)	-1(1)	2(1)
C(4)	16(1)	20(1)	13(1)	-1(1)	1(1)	1(1)
C(5)	12(1)	18(1)	12(1)	2(1)	-1(1)	-2(1)
C(6)	17(1)	22(1)	11(1)	-2(1)	1(1)	0(1)
C(7)	15(1)	20(1)	14(1)	1(1)	2(1)	-2(1)
C(8)	26(1)	22(1)	20(1)	-1(1)	-4(1)	3(1)
C(9)	29(1)	30(1)	28(1)	-8(1)	-4(1)	10(1)
C(10)	32(1)	28(1)	23(1)	-8(1)	-2(1)	-2(1)
C(11)	25(1)	28(1)	18(1)	-5(1)	-4(1)	-1(1)
C(12)	20(1)	26(1)	18(1)	-2(1)	-3(1)	2(1)
N(1)	18(1)	17(1)	15(1)	0(1)	1(1)	1(1)
N(2)	14(1)	22(1)	18(1)	0(1)	-4(1)	1(1)
O(1)	18(1)	31(1)	23(1)	9(1)	-2(1)	-9(1)
O(2)	46(1)	19(1)	26(1)	-2(1)	-8(1)	10(1)
O(3)	31(1)	27(1)	13(1)	0(1)	1(1)	-3(1)
S(2)	15(1)	25(1)	19(1)	4(1)	-4(1)	-2(1)

Table A1.30 Hydrogen coordinates ($\times 10^4$) and isotropic displacement parameters ($\text{\AA}^2 \times 10^3$) for (112).

	x	y	z	U(eq)
H(1)	2278	6248	1924	23
H(5)	8065	5073	4331	17
H(6A)	9238	3709	5030	20
H(6B)	6626	3342	5098	20
H(7)	5218	4849	5638	19
H(8A)	6271	6671	4940	27
H(8B)	3759	6189	4962	27
H(9A)	3547	6413	6246	35
H(9B)	4070	7436	5871	35
H(10A)	8057	7319	6186	33
H(10B)	6560	7185	6913	33
H(11A)	7034	5480	6864	28
H(11B)	9541	5967	6834	28
H(12A)	9748	5722	5550	26
H(12B)	9213	4704	5929	26

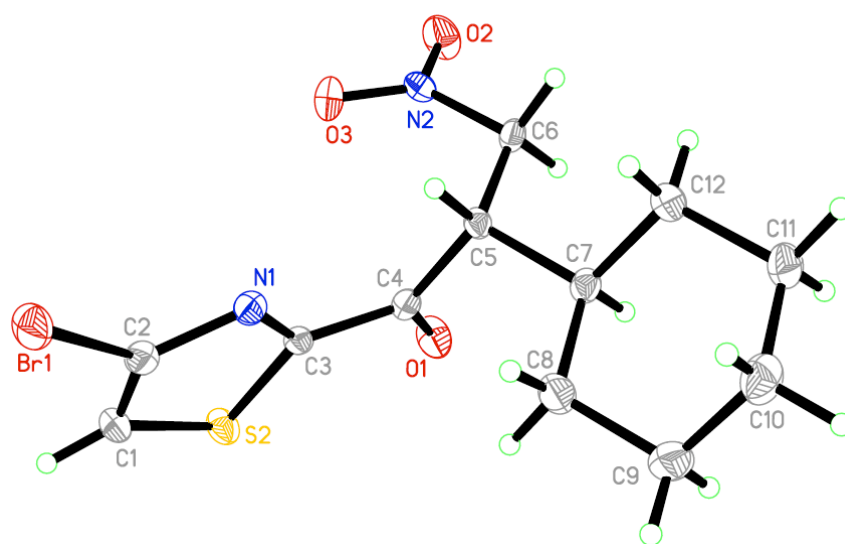


Figure A1.6 Thermal plot of triazolium salt (**112**). Ellipsoids drawn at the 50% probability level

REFERENCES

¹ For the synthesis of nitroalkenes see: Duursma, A.; Minnaard, A. J.; Feringa, B. L. *Tetrahedron* **2002**, *58*, 5773-5778.

² For the synthesis of the lactone see: Cohen, H.; Banner, B. L.; Laurenzano, A. J.; Carozza, L. *Org. Synth.* **1985**, *63*, 127. For the synthesis of the lactam see: Hanessian, S. *J. Org. Chem.* **1969**, *34*, 675-681.

³ For the synthesis of pyrrolidinones from amino acids see: Smrcina, M.; Majer, P.; Majerová, E.; Guerassina, T.; Eissenstat, M. A. *Tetrahedron* **1997**, *53*, 12867-12874.

⁴ Synthesized via a procedure similar to: Grison, C.; Genève, S.; Coutrot, P. *Tetrahedron Lett.* **2001**, *42*, 3831-3834.

⁵ Harris, B. D.; Krishna, L.; Joullie, M. M. *Synth. Commun.* **1986**, *14*, 1815-1822.

Appendix 2

Expanding the Scope of the Asymmetric Intermolecular Stetter Reaction of Nitroalkenes

Materials and Methods

All reactions were carried out under an atmosphere of argon in flame-dried glassware with magnetic stirring. Dichloromethane was degassed with argon and passed through two columns of neutral alumina. Toluene was degassed with argon and passed through one column of neutral alumina and one column of Q5 reactant. Methanol was purchased from Fisher Scientific and dried with activated 3Å molecular sieves. N,N-Diisopropylethylamine was purchased from Aldrich and distilled from Calcium hydride prior to use. Column chromatography was performed on SiliCycle®SilicaFlash® P60, 40-63µm 60A. Thin layer chromatography was performed on SiliCycle® 250µm 60A plates. Visualization was accomplished with UV light or KMnO₄ stain followed by heating.

¹H NMR spectra were recorded on Varian 300 or 400 MHz spectrometers at ambient temperature. Data is reported as follows: chemical shift in parts per million (δ, ppm) from CDCl₃ (7.26 ppm) or acetone-*d*₆ (2.03 ppm), multiplicity (s = singlet, bs = broad singlet, d = doublet, t = triplet, q = quartet, and m = multiplet), coupling constants (Hz). ¹³C NMR were recorded Varian 300 or 400 MHz spectrometers (at 75 or 100 MHz) at ambient temperature. Chemical shifts are reported in ppm from CDCl₃ (77.36 ppm) or acetone-*d*₆ (205.87, 30.6 ppm). Aldehydes were either purchased from Aldrich or prepared via literature procedures. Nitroalkenes were prepared according to the general procedure as described in Chapter 1.¹

General Procedure for the Asymmetric Intermolecular Stetter Reaction of Enals with Nitroalkenes

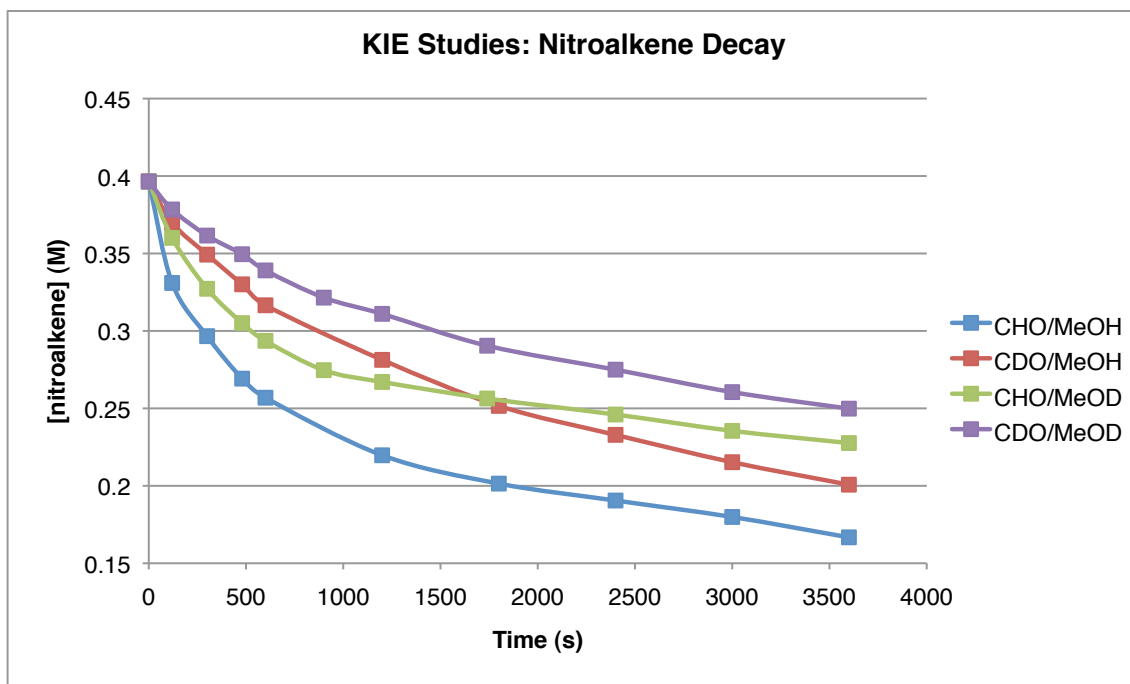
To a dry 4 mL vial, with a magnetic stir bar, was added triazolium salt (**128**) (16 mg, 0.0378 mmol, 0.1 equiv), catechol (42 mg, 0.378 mmol, 1.0 equiv) and anhydrous methanol (0.8 mL). The vial was cooled to 0 °C in an ice/water bath with stirring under argon. N,N-diisopropylethylamine (66 μ l, 0.378 mmol) was added dropwise and the reaction was stirred at 0 °C for 5 min. A solution of the aldehyde (0.378 mmol, 1.0 equiv), and nitroalkene (0.567 mmol, 1.5 equiv), in methanol (0.2 mL) was then added dropwise. After approximately 4 h, or complete consumption of aldehyde, as indicated by TLC, AcOH (100 μ l) was added to quench the reaction followed by concentration *in vacuo*. Column chromatography (hexanes:ether) of the resulting residue gave the desired β -nitro ketone.

Kinetic Isotope Effect Experiments:

General Procedure for the Asymmetric Intermolecular Stetter Reaction of Enals and Nitroalkenes Monitored by Gas Chromatography:

To a dry 4 mL vial, with a magnetic stir bar, was added triazolium salt (**128**) (32 mg, 0.0756 mmol, 0.1 equiv), catechol (83 mg, 0.756 mmol, 1.0 equiv), trimethoxy benzene (25.4 mg, 0.151 mmol, 0.2 equiv) (internal standard) and anhydrous methanol (1.6 mL). The vial was cooled to 0 °C in an ice/water bath with stirring under argon. N,N-diisopropylethylamine (132 μ l, 0.756 mmol) was added dropwise and the reaction was stirred at 0 °C for 5 min. A cooled (0 °C) solution of the aldehyde (0.756 mmol, 1.0 equiv), and nitroalkene (0.794 mmol, 1.05 equiv), in methanol (0.4 mL) was then added via syringe. The reaction was stirred at 0 °C, and aliquots (50 μ l) were removed from the reactions at the indicated time intervals and quenched by placing

them directly into 1.5 mL vials containing DCM (1 mL) and AcOH (50 μ L). GC analysis – CP Wax 52CB column 80 $^{\circ}$ C at 1mL/min for 5 min ramp to 110 $^{\circ}$ C at 20 $^{\circ}$ C/min. Nitroalkene (**90**) 5.0 min, trimethoxy benzene (internal standard): 6.1 min.



Initial rates were extrapolated from the slopes at low conversion.

CHO/MeOH		CDO/MeOH		CHO/MeOD		CDO/MeOD	
[alkene]M	Time (s)	[alkene]M	Time (s)	[alkene]M	Time (s)	[alkene]M	Time (s)
0.397	0	0.397	0	0.397	0	0.397	0
0.331	120	0.370	120	0.360	120	0.378	120
0.297	300	0.349	300	0.327	300	0.362	300
0.269	480	0.330	480	0.305	480	0.350	480
0.257	600	0.317	600	0.294	600	0.339	600
0.220	1200	0.281	1200	0.275	900	0.322	900
0.201	1800	0.252	1800	0.267	1200	0.311	1200
0.191	2400	0.233	2400	0.256	1740	0.290	1740
0.180	3000	0.215	3000	0.246	2400	0.275	2400
0.167	3600	0.201	3600	0.235	3000	0.261	3000
				0.228	3600	0.250	3600

Substrate/Solvent	kobs(M s ⁻¹)
-------------------	--------------------------

CHO/MeOH	5.20E-04
CDO/MeOH	1.92E-04
CHO/MeOD	2.95E-04
CDO/MeOD	1.23E-04

$k_{\text{obs}}(\text{CHO/MeOH})/k_{\text{obs}}(\text{CDO/MeOD}) = 4.2$
$k_{\text{obs}}(\text{CHO/MeOH})/k_{\text{obs}}(\text{CDO/MeOH}) = 2.7$
$k_{\text{obs}}(\text{CHO/MeOH})/k_{\text{obs}}(\text{CHO/MeOD}) = 1.8$

General Procedure for the Asymmetric Intermolecular Stetter Reaction of Aliphatic Aldehydes with Nitrostyrenes

To a dry 4 mL vial, with a magnetic stir bar, was added triazolium salt (**219**) (22 mg, 0.05 mmol, 0.2 equiv), β -nitrostyrene (38 mg, 0.25 mmol, 1.0 equiv), sodium acetate (8 mg, 0.10 mmol, 0.4 equiv) and *tert*-amyl alcohol (2 mL, 0.125 M). The vial was cooled to 0 °C in a cooling bath with stirring and purged with argon. Butyraldehyde (34 μ l, 0.375 mmol, 1.5 equiv) was added dropwise and the reaction was stirred at 0 °C until TLC indicated consumption of the nitrostyrene (24-48 h), at which point the reaction was concentrated *in vacuo*. The residue was purified by flash chromatography (hexanes:ether) which provided the desired β -nitro ketone as a colorless oil.

Catalyst Competition Experiments

Competition experiments between catalysts (**219**)/(**206**) and (**215**)/(**206**) were used to determine k_{rel} data. Catalysts (**219**)/(**206**) or (**215**)/(**206**) were added to the standard reaction conditions at 20 mol % loading each. After completion of the reaction, enantioselectivity of the product was

determined by chiral HPLC analysis. The competition experiment between (219)/(206) provided the product with 73% ee and (215)/(206) with 18% ee. Furthermore, the competition experiment between (219)/(215) provided product with 92% ee. Based on the enantioselectivity obtained under otherwise identical conditions with each catalyst separately, the relative rates of each catalyst were extrapolated.

Achiral catalyst (206) delivers 0% ee or equal amounts of R and S

Chiral catalyst (219) delivers 93% ee or 26.5 ratio of R to S

Let x = S fraction delivered by Achiral catalyst (206)

Let y = S fraction delivered by Catalyst (219)

The competition experiment between (219)/(206) provides material in 73% ee or 86.5% R and 13.5% S.

Therefore,

$$0.135 = x + y$$

$$0.865 = x + 26.5y$$

Solving for y provides

$$y = 0.0286$$

then solving for x provides

$$x = 0.1064$$

Rate ratio:

$$\frac{\text{Chiral Catalyst (219)}}{\text{Achiral Catalyst (206)}} = \frac{27.5(0.0286)}{0.1064 \cdot 2} = 3.696$$

Achiral Catalyst (206) delivers 0% ee or equal amounts of R and S.

Chiral Catalyst (215) delivers 74% ee or 6.69 ratio of R to S.

Let x = S fraction delivered by achiral catalyst (206)

Let y = S fraction delivered by Catalyst (215).

The competition experiment between (215)/(206) provides material in 18% ee or 59% R and 41% S.

Therefore,

$$0.41 = x + y$$

$$0.59 = x + 6.69y$$

Solving for y provides

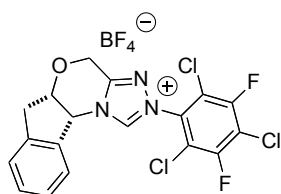
$$y = 0.0316$$

then for x provides
 $x = 0.3784$

Rate ratio:

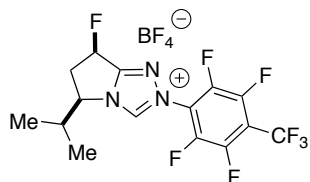
$$\frac{\text{Chiral Catalyst (215)}}{\text{Achiral Catalyst (206)}} = \frac{6.69(0.0316)}{0.3784^*} = 0.279$$

Experimental Procedures and Characterization Data



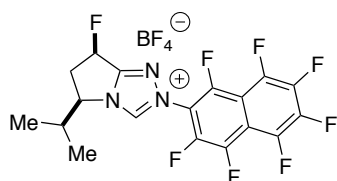
(5*a*S,10*b*R)-2-(2,4,6-trichloro-3,5-difluorophenyl)-4,5*a*,6,10*b*-tetrahydroindeno[2,1-*b*][1,2,4]triazolo[4,3-*d*][1,4]oxazin-2-ium tetrafluoroborate (181). Prepared according to the general procedure

outlined in Chapter 1. White solid; **m.p.** (°C): 267-269; $[\alpha]_D^{21} = -79.1$ ($c = 0.005$ g/ml, acetone/DMSO); **¹H NMR** (400 MHz, acetone-*d*₆+10% DMSO-*d*₆) δ 11.53 (s, 1H), 7.61 (d, $J = 7.5$ Hz, 1H), 7.42 (ddt, $J = 20.3, 13.1, 6.8$ Hz, 3H), 6.36 (d, $J = 4.1$ Hz, 1H), 5.40-5.22 (m, 2H), 5.18 (t, $J = 4.5$ Hz, 1H), 3.56 (dd, $J = 17.1, 4.9$ Hz, 1H), 3.24 (m, 1H); **¹³C NMR** (100 MHz, acetone-*d*₆+10% DMSO-*d*₆) δ 156.3, 153.8, 152.6, 147.9, 141.8, 131.6, 130.5, 128.3, 126.6, 124.9, 78.2, 63.6, 60.9, 38.1; **IR** (NaCl, neat) 3133, 3101, 2951, 2907, 1678, 1587, 1531, 1483, 1080 cm^{-1} ; **HRMS** (ESI+) calcd for C₁₈H₁₁Cl₃F₂N₃O, 427.9936. Found 427.9948.



(5*R*,7*R*)-7-fluoro-5-isopropyl-2-(2,3,5,6-tetrafluoro-4-(trifluoromethyl)phenyl)-6,7-dihydro-5*H*-pyrrolo[2,1-*c*][1,2,4]triazol-2-ium tetrafluoroborate (181): Prepared according to

the general procedure. $^1\text{H NMR}$ (400 MHz, acetone- d_6) δ 10.69 (s, 1H), 6.55 (ddd, $J = 54.3, 7.4, 2.2$ Hz, 1H), 5.18-5.12 (m, 1H), 3.74-3.54 (m, 1H), 3.08-2.92 (m, 1H), 2.60-2.49 (m, 1H), 1.20 (d, $J = 6.8$ Hz, 3H), 1.11 (d, $J = 6.8$ Hz, 3H).

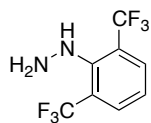


(5R,7R)-7-fluoro-5-isopropyl-2-(perfluoronaphthalen-2-yl)-6,7-dihydro-5H-pyrrolo[2,1-c][1,2,4]triazol-2-ium tetrafluoroborate (183): Prepared according to the general procedure. $^1\text{H NMR}$ (300

MHz, acetone- d_6) δ 10.67 (s, 1H), 6.55 (ddd, $J = 54.5, 7.4, 2.2$ Hz, 1H), 5.17 (m, 1H), 3.77-3.50 (m, 1H), 3.07-2.91 (m, 1H), 2.56 (m, 1H), 1.21 (d, $J = 6.8$ Hz, 3H), 1.13 (d, $J = 6.8$ Hz, 3H).

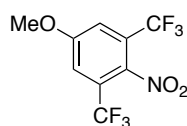


(2,4,6-tris(trifluoromethyl)phenyl)hydrazine (186): *n*-butyl lithium (1.6 M in hexanes) (9.72 mL, 15.6 mmol, 1.10 equiv) was added to a solution of 1,3,5-tris(trifluoromethyl)benzene (4.0 g, 14.18 mmol, 1.0 equiv) in diethyl ether (10 mL) at room temperature and stirred for 45 min. After cooling in a liquid N_2 bath, chlorine $_{(g)}$ (654 mL) was added via separatory funnel and allowed to condense into the flask, followed by warming to room temperature. This process was repeated a second time and then quenched with water (20 mL) and extracted with diethyl ether (3 X 20 mL). The combined organic extracts were concentrated *in vacuo* and then dissolved in ethanol (20 mL). Hydrazine hydrate (3.44 mL, 70.9 mmol, 5.0 equiv) was added and the mixture was refluxed until the starting material was consumed. The mixture was then concentrated *in vacuo* and directly purified by flash chromatography (9:1, hex:EtOAc) to yield the desired compound (0.329 g, 9%) as a colorless oil. $^1\text{H NMR}$ (300 MHz, CDCl_3) δ 7.59 (s, 2H), 6.06 (bs, 1H), 4.09 (bs, 2H).



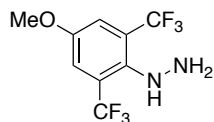
(2,6-bis(trifluoromethyl)phenyl)hydrazine (189): To a solution of 2-fluoro-1,3-bis(trifluoromethyl)benzene (4.0 g, 17.23 mmol, 1.0 equiv) in ethanol (50 mL)

was added hydrazine hydrate (2.09 mL, 43.08 mmol, 2.5 equiv) and the mixture refluxed overnight. Water (100 mL) was added and the mixture extracted with CH₂Cl₂ (3 x 50 mL). The combined organic extracts were concentrated *in vacuo* followed by Kugelrohr distillation (75 °C, 4 mm) to yield the hydrazine as a clear oil (2.08 g, 50%). ¹H NMR (300 MHz, CDCl₃) δ 7.76 (d, *J* = 7.9 Hz, 2H), 7.17-7.11 (m, 1H), 5.47 (bs, 1H), 3.99 (bs, 2H).



5-methoxy-2-nitro-1,3-bis(trifluoromethyl)benzene (193): To a solution of 4-nitro-3,5-bis(trifluoromethyl)phenol² (9.5 g, 34.53 mmol, 1.0 equiv) in acetone

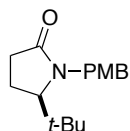
(180 mL) was added DBU (10.32 mL, 69.0 mmol, 2.0 equiv) and methyl iodide (12.88 mL, 207 mmol, 6.0 equiv). The reaction was stirred at room temperature for 4 h at which point it was concentrated *in vacuo*. Water (100 mL) was added followed by extraction with EtOAc (3 x 100 mL) and concentration of the combined organic extracts. Flash chromatography (20:1, hex:EtOAc) of the crude residue provided the desired product as a white solid (7.53 g, 60%). ¹H NMR (300 MHz, CDCl₃) δ 7.39 (s, 2H), 3.97 (s, 3H).



4-methoxy-2,6-bis(trifluoromethyl)hydrazine (196): A solution of 5-methoxy-2-nitro-1,3-bis(trifluoromethyl)benzene (193) (1.0 g, 3.46 mmol,

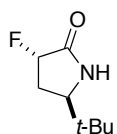
1.0 equiv) in methanol was added 10% Pd/C (100 mg) and the mixture exposed to a hydrogen atmosphere (balloon) and stirred overnight. The reaction was filtered through celite and concentrated to yield the aniline in quantitative yield and used in the next step without further

purification. To a solution of the aniline in dichloromethane (7 ml) at -15 °C was added BF₃-OEt₂ (0.64 mL, 5.19 mmol, 1.5 equiv). The solution was allowed to stir for 15 min followed by the addition of *t*-butyl nitrite (0.495 mL, 4.15 mmol, 1.2 equiv) dropwise. After stirring for 10 min pentanes (10 mL) was added and the mixture filtered to yield a white solid that was filtered, washed with pentanes (10 mL) and dried. A portion of the diazonium salt (1.0 g, 2.79 mmol, 1.0 equiv) thus obtained was added to a solution of tin(II)chloride hydrate (1.89 g, 8.37 mmol, 3.0 equiv) in HCl_(conc) at -50 °C portionwise. After addition was complete the reaction was allowed to warm to room temperature at which point the whole mixture was added to 2N NaOH (150 mL) and extracted with CH₂Cl₂ (3 X 50 mL). The combined organic extracts were concentrated *in vacuo* to yield the desired hydrazine without further purification. ¹H NMR (300 MHz, CDCl₃) δ 7.32 (s, 2H), 4.90 (bs, 1H), 3.86 (s, 3H), 3.82 (bs, 2H).



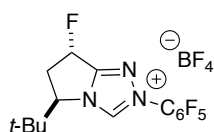
(R)-5-(*tert*-butyl)-1-(4-methoxybenzyl)pyrrolidin-2-one (217): To a dry round bottomed flask was added (*R*)-5-(*tert*-butyl)pyrrolidin-2-one³ (10.42 g, 73.8 mmol, 1.0 equiv) and anhydrous THF (150 mL). Sodium hydride (2.13 g, 88.6 mmol, 1.2 equiv) was added portionwise and the mixture was stirred for 30 min followed by the addition of 4-methoxybenzyl chloride (13.87 g, 88.6 mmol, 1.2 equiv) and tetrabutylammonium iodide (2.73 g, 7.38 mmol, 0.1 equiv). After 18 h a reflux condenser was installed and the reaction refluxed for 30 min. After cooling to r.t. the reaction was quenched with NH₄Cl_(sat)(100 mL), extracted with dichloromethane (3 X 200 mL), and dried (Na₂SO₄). Concentration of the combined organic extracts left a crude oil which was purified by flash chromatography (1:1 EtOAc:Hex) to provide the desired product (17.35 g, 90%) as a colorless oil. R_f= 0.32 (1:1 hexanes:EtOAc); [α]_D²¹ = -80.0 (c = 0.007 g/ml, CHCl₃); ¹H NMR (400 MHz, CDCl₃): δ 7.12-7.08 (m, 2H), 6.87-6.83 (m,

2H), 5.26 (d, $J = 15.1$ Hz, 1H), 4.00 (d, $J = 15.1$ Hz, 1H), 3.80 (s, 3H), 3.17-3.15 (m, 1H), 2.55-2.56 (m, 1H), 2.35-2.27 (m, 1H), 1.94-1.86 (m, 2H), 0.93 (s, 9H); ^{13}C NMR (100 MHz, CDCl_3): δ 177.4, 159.0, 129.2, 114.1, 65.7, 55.4, 46.9, 36.9, 30.9, 27.2, 22.2; IR (NaCl, neat) 2958, 2836, 1687, 1612, 1513, 1441, 1301, 1245, 1175, 1034 cm^{-1} ; HRMS (ESI+) calcd for $\text{C}_{16}\text{H}_{24}\text{NO}_2$ (M+H), 262.1802. Found 262.1659.



(3S,5R)-5-(tert-butyl)-3-fluoropyrrolidin-2-one (218): To a freshly prepared solution of LDA (1.1 equiv) in THF (300 mL) at -78°C was added a solution of (*R*)-5-(tert-butyl)-1-(4-methoxybenzyl)pyrrolidin-2-one (**217**) (17.13 g, 65.92 mmol, 1.0 equiv) in THF (100 mL) and stirred for 90 min at -78°C . A solution of N-fluorobenzenesulfonamide (27.03 g, 85.7 mmol, 1.3 equiv) in THF (100 mL) was added dropwise, stirred for 1 h at -78°C and then warmed to r.t. slowly by removing the dry ice/acetone bath. The reaction was quenched by the addition of $\text{NH}_4\text{Cl}_{(\text{sat})}$ (50 mL), concentrated *in vacuo*, and extracted with DCM (3 X 200 mL). The combined organic extracts were dried (Na_2SO_4) and concentrated to yield a crude solid. To this solid (mainly consisting of unreacted N-fluorobenzenesulfonamide and benzenesulfonamide) was added ether (100 mL) while stirring vigorously. The slurry was filtered through a sintered glass funnel and washed continuously with ether (500 mL). Concentration of the filtrate *in vacuo* provided the crude PMB-lactam, which was immediately used in the next step without further purification. To a cooled (0°C) solution of the crude PMB-lactam in CH_3CN (300 mL) and water (100 mL) was added ceric ammonium nitrate (90.35 g, 164.88 mmol, 2.5 equiv) portionwise. After stirring for 30 min at 0°C the reaction was warmed to r.t., stirred an additional 1 h at r.t., and concentrated to approximately 1/3 of its original volume. Water was then added (200 mL), and the mixture extracted with DCM (3 X 150 mL).

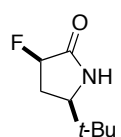
The combined extracts were dried (Na₂SO₄), and concentrated *in vacuo* to yield a crude solid. The solid was purified via flash chromatography on silica gel (20% EtOAc/hexanes) then triturated with pentanes and ether and filtered to yield the desired compound (4.85 g, 46%) as a white crystalline solid. $R_f = 0.46$ (1:1 EtOAc:hex); $[\alpha]_D^{21} = -47.0$ (c = 0.010 g/ml, CHCl₃); **m.p.** (°C): 113-115; **¹H NMR** (400 MHz, CDCl₃): δ 7.73 (bs, 1H), 5.05 (ddd, $J = 53.0, 7.2, 5.5$ Hz, 1H), 3.53 (m, 1H), 2.27 (t, $J = 6.3$ Hz, 1H), 2.21 (m, 1H), 0.89 (s, 9H); **¹³C NMR** (100 MHz, CDCl₃): δ 173.0 ($J_{C-F} = 19.9, 2.1$ Hz), 88.9 ($J_{C-F} = 181.2$ Hz), 61.6, 33.8, 30.2 ($J_{C-F} = 20.8$ Hz), 25.5; **IR** (NaCl, neat) 3215, 3112, 2964, 2874, 1717, 1478, 1370, 1304, 1282, 1082 cm⁻¹; **HRMS** (ESI+) calcd for C₈H₁₅FNO, 159.1059. Found 159.1060.



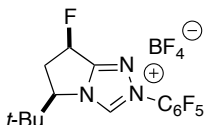
(5R,7S)-5-(tert-butyl)-7-fluoro-2-(perfluorophenyl)-6,7-dihydro-5H-pyrrolo[2,1-c][1,2,4]triazol-2-ium tetrafluoroborate (219): To a flame-

dried round-bottomed flask was added (3*S*,5*R*)-5-(tert-butyl)-3-fluoropyrrolidin-2-one (**218**) (2.0 g, 12.56 mmol, 1.0 equiv) and dichloromethane (75 mL). The mixture was stirred until homogeneous then trimethyloxonium tetrafluoroborate (1.86 g, 12.56 mmol, 1.0 equiv) was added in one portion. After stirring for 18 h, pentafluorophenyl hydrazine (2.49 g, 12.56 mmol, 1.0 equiv) was added and the reaction was allowed to stir an additional 24 h. Concentration of the solution gave a solid that was triturated with ether and dried under vacuum (4 mm) for 1 h. After installing a reflux condenser, trimethyl orthoformate (20 mL) was added and the mixture was heated to reflux in an oil bath for 8 h. The solution was concentrated *in vacuo* and more trimethyl orthoformate (20 mL) was added. After refluxing for 18 h, this procedure was repeated once more. Finally, concentration of the solution provided a gum that was crystallized with ether to yield a tan solid. The solid was filtered, washed with cold (0 °C) dichloromethane and dried to

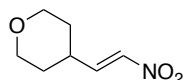
yield the desired triazolium salt (3.33 g, 60 %) as a white solid. $[\alpha]_D^{21} = +50.0$ ($c = 0.008$ g/ml, acetone); **m.p.** (°C): 198-199; **¹H NMR** (400 MHz, acetone-*d*₆): δ 10.73 (s, 1H), 6.67 (ddd, $J = 54.0, 7.0, 3.5$ Hz, 1H), 5.32 (dd, $J = 7.4, 6.3$ Hz, 1H), 3.46 (dddd, $J = 22.5, 15.3, 7.1, 6.1$ Hz, 1H), 3.23 (dddd, $J = 26.8, 15.2, 7.8, 3.6$ Hz, 1H), 1.20 (s, 9H); **¹³C NMR** (100 MHz, acetone): δ 161.0 (d, $J = 22.9$ Hz), 145.0 (m), 142.5 (m), 140.1 (m), 137.4 (m), 84.2 ($J_{C-F} = 185.2$ Hz), 72.2, 38.3 ($J_{C-F} = 21.9$ Hz), 34.3, 25.5; **IR** (NaCl, neat) 3126, 2972, 2880, 1598, 1530, 1485, 1418, 1377, 1074, 1005 cm^{-1} ; **HRMS** (ESI+) calcd for C₁₅H₁₄F₆N₃, 350.1092. Found 350.1089.



(3R,5R)-5-(tert-butyl)-3-fluoropyrrolidin-2-one: Prepared analogously to **(127)** see chapter 1. **¹H NMR** (300 MHz, CDCl₃) δ 7.30 (s, 1H), 5.08 (ddd, $J = 52.9, 8.2$ Hz, 8.2 Hz, 1H), 3.35-3.29 (m, 1H), 2.58-2.45 (m, 1H), 1.95 (m, 1H), 0.93 (s, 10H).

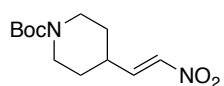


(5R,7R)-5-(tert-butyl)-7-fluoro-2-(perfluorophenyl)-6,7-dihydro-5H-pyrrolo[2,1-c][1,2,4]triazol-2-ium tetrafluoroborate (215): Prepared analogously to **(128)** see chapter 1. White solid. $[\alpha]_D^{21} = -3.5$ ($c = 0.010$ g/ml, acetone); **m.p.** (°C): 203-204; **¹H NMR** (400 MHz, acetone-*d*₆): δ 10.71 (s, 1H), 6.51 (ddd, $J = 54.8, 7.7, 1.8$ Hz, 1H), 5.12 (ddd, $J = 8.9, 4.3, 3.4$ Hz, 1H), 3.65 (dddd, $J = 28.0, 16.0, 8.9, 7.7$ Hz, 1H), 3.07 (dddd, $J = 27.5, 16.0, 3.4, 1.9$ Hz, 1H), 1.20 (s, 9H); **¹³C NMR** (100 MHz, acetone): δ 161.0 (d, 22.7 Hz), 145.1 (m), 143.4 (m), 140.2 (m), 137.6 (m), 83.4 (d, $J = 184.5$ Hz), 71.9, 37.5 (d, $J = 21.7$ Hz), 34.6, 25.6; **IR** (NaCl, neat) 3134, 2974, 1598, 1530, 1485, 1418, 1377, 1228, 1075, 1057, 1019, 1006 cm^{-1} ; **HRMS** (ESI+) calcd for C₁₅H₁₄F₆N₃, 350.1092. Found 350.1092.



(E)-4-(2-nitrovinyl)tetrahydro-2H-pyran: Prepared according to the general

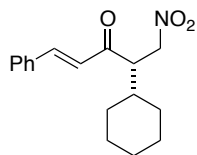
procedure outline in chapter 1. Amorphous solid; $R_f = 0.30$ (1:1 hexanes:ether); 31% yield; $^1\text{H NMR}$ (300 MHz, CDCl_3) δ 7.20 (dd, $J = 13.5, 6.9$ Hz, 1H), 6.95 (dd, $J = 13.5, 1.4$ Hz, 1H), 4.04-3.98 (m, 2H), 3.45 (td, $J = 11.7, 2.4$ Hz, 2H), 2.57-2.46 (m, 1H), 1.74-1.68 (m, 2H), 1.64-1.50 (m, 2H); $^{13}\text{C NMR}$ (100 MHz, CDCl_3) δ 145.1, 138.9, 67.1, 34.9, 31.1; IR (NaCl, neat) 3107, 2944, 2849, 1648, 1524, 1389, 1352, 1239, 1146, 1122, 1093 cm^{-1} ; HRMS ESI/APCI or APCI failed to produce the parent or related ions.



(E)-tert-butyl 4-(2-nitrovinyl)piperidine-1-carboxylate: Prepared according to the general procedure outlined in chapter 1. Amorphous solid; $R_f = 0.35$

(1:1 hexanes:ether); 40% yield; $^1\text{H NMR}$ (300 MHz, CDCl_3) δ 7.20 (dd, $J = 13.5, 7.1$ Hz, 1H), 6.95 (dd, $J = 13.5, 1.3$ Hz, 1H), 4.16 (m, 2H), 2.82-2.72 (m, 2H), 2.47-2.35 (m, 1H), 1.79-1.74 (m, 2H), 1.45 (s, 9H), 1.54-1.24 (m, 2H); $^{13}\text{C NMR}$ (100 MHz, CDCl_3) δ 154.7, 145.0, 139.1, 79.9, 36.0, 30.5, 28.5; IR (NaCl, neat) 2977, 2934, 2858, 1690, 1648, 1525, 1424, 1366, 1351, 1234, 1171 cm^{-1} ; HRMS (ESI+) calcd for $\text{C}_7\text{H}_{13}\text{N}_2\text{O}_2$ (-Boc), 157.0977. Found 157.0971.

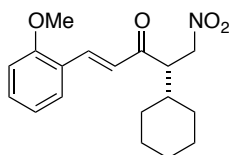
Characterization of Stetter Products



(S,E)-4-cyclohexyl-5-nitro-1-phenylpent-1-en-3-one (165): Prepared according to the general procedure: White solid; $R_f = 0.29$ (4:1 hexanes:ether); 80% yield, 93% ee; $[\alpha]_D^{21} = -106.7$ ($c = 0.006$ g/ml, CH_2Cl_2); HPLC analysis –

Chiracel IC column, 70:30 hexanes/*iso*-propanol, 1.0 mL/min. Major: 15.17 min, minor: 10.66 min; **m.p.** ($^\circ\text{C}$): 94-97; $^1\text{H NMR}$ (300 MHz, CDCl_3) δ 7.66 (d, $J = 16.0$ Hz, 1H), 7.61-7.58 (m, 2H), 7.44-7.41 (m, 3H), 6.86 (d, $J = 16.0$ Hz, 1H), 4.99 (dd, $J = 14.6, 10.2$ Hz, 1H), 4.45 (dd, $J =$

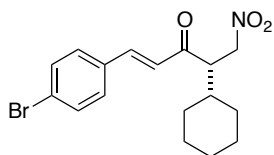
14.6, 3.6 Hz, 1H), 3.58 (ddd, $J = 10.2, 5.1, 3.7$ Hz, 1H), 1.79-1.59 (m, 6H), 1.32-0.93 (m, 5H); $^{13}\text{C NMR}$ (100 MHz, CDCl_3) δ 198.9, 144.3, 134.7, 131.3, 129.4, 129.0, 125.7, 73.9, 53.2, 39.3, 31.7, 30.3, 26.8, 26.7, 26.3; **IR** (NaCl, neat) 2929, 2854, 1685, 1657, 1608, 1576, 1450, 1375 cm^{-1} ; **HRMS** (ESI+) calcd for $\text{C}_{17}\text{H}_{22}\text{NO}_3$, 287.1521. Found 287.1515.



(*S,E*)-4-cyclohexyl-1-(2-methoxyphenyl)-5-nitropent-1-en-3-one (166):

Prepared according to the general procedure: Amorphous solid; $R_f = 0.25$ (4:1 hexanes:ether); 97% yield, 93% ee; $[\alpha]_D^{21} = -64.1$ ($c = 0.013$ g/ml,

CH_2Cl_2); HPLC analysis – Chiracel IC column, 70:30 hexanes/*iso*-propanol, 1.0 mL/min. Major: 16.24 min, minor: 13.62 min; $^1\text{H NMR}$ (300 MHz, CDCl_3) δ 8.00 (d, $J = 16.2$ Hz, 1H), 7.58 (dd, $J = 7.7, 1.7$ Hz, 1H), 7.39 (ddd, $J = 8.3, 7.4, 1.7$ Hz, 1H), 7.01-6.90 (m, 3H), 4.98 (dd, $J = 14.4, 10.1$ Hz, 1H), 4.45 (dd, $J = 14.4, 3.8$ Hz, 1H), 3.91 (s, 1H), 3.66-3.58 (m, 1H), 1.80-1.64 (m, 6H), 1.32-0.93 (m, 5H); $^{13}\text{C NMR}$ (100 MHz, CDCl_3) δ 199.0, 158.9, 139.3, 132.2, 129.0, 125.8, 123.2, 120.8, 111.3, 73.6, 55.6, 52.5, 39.0, 31.2, 29.9, 26.4, 26.4, 26.0; **IR** (NaCl, neat) 2930, 2864, 1682, 1654, 1598, 1555, 1465, 1419, 1375, 1316, 1248 cm^{-1} ; **HRMS** (ESI+) calcd for $\text{C}_{18}\text{H}_{24}\text{NO}_4$, 317.1627. Found 317.1628.

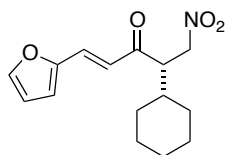


(*S,E*)-1-(4-bromophenyl)-4-cyclohexyl-5-nitropent-1-en-3-one (167):

Prepared according to the general procedure: Off-white solid; $R_f = 0.27$ (4:1 hexanes:ether); 57% yield, 98% ee; $[\alpha]_D^{21} = -84.1$ ($c = 0.011$ g/ml,

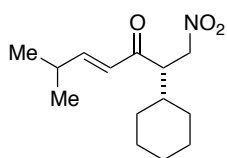
CH_2Cl_2); HPLC analysis – Chiracel IC column, 70:30 hexanes/*iso*-propanol, 1.0 mL/min. Major: 15.95 min, minor: 11.55 min; **m.p.** ($^\circ\text{C}$): 141-143; $^1\text{H NMR}$ (300 MHz, CDCl_3) δ 7.61-7.53 (m, 3H), 7.46-7.44 (m, 2H), 6.84 (d, $J = 16.0$ Hz, 1H), 4.98 (dd, $J = 14.6, 10.4$ Hz, 1H), 4.45 (dd, $J =$

14.6, 3.5 Hz, 1H), 3.55 (ddd, $J = 10.3, 5.2, 3.6$ Hz, 1H), 1.80-1.63 (m, 6H), 1.33-0.92 (m, 5H); ^{13}C NMR (100 MHz, CDCl_3) δ 198.4, 142.6, 133.3, 132.4, 130.1, 125.8, 125.3, 73.5, 53.0, 39.0, 31.4, 29.9, 26.5, 26.4, 26.0; IR (NaCl, neat) 2929, 2854, 1686, 1658, 1608, 1554, 1487, 1449, 1402, 1375, 1063, 1009; HRMS (ESI+) calcd for $\text{C}_{17}\text{H}_{21}\text{BrNO}_3$, 365.0627. Found 365.0629.



(*S,E*)-4-cyclohexyl-1-(furan-2-yl)-5-nitropent-1-en-3-one (168): Prepared according to the general procedure: Colorless oil; $R_f = 0.28$ (4:1 hexanes:ether); 98% yield, 93% ee; $[\alpha]_D^{21} = -82.7$ ($c = 0.009$ g/ml, CH_2Cl_2);

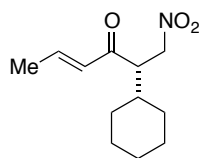
HPLC analysis – Chiracel IC column, 70:30 hexanes/*iso*-propanol, 1.0 mL/min. Major: 16.30 min, minor: 11.39 min; ^1H NMR (300 MHz, CDCl_3) δ 7.52 (dd, $J = 1.8, 0.5$ Hz, 1H), 7.41 (d, $J = 15.6$ Hz, 1H), 6.78-6.72 (m, 2H), 6.51 (dd, $J = 3.5, 1.8$ Hz, 1H), 4.97 (dd, $J = 14.5, 10.3$ Hz, 1H), 4.43 (dd, $J = 14.5, 3.6$ Hz, 1H), 3.48 (ddd, $J = 10.2, 5.1, 3.7$ Hz, 1H), 1.81-1.58 (m, 6H), 1.33-0.92 (m, 5H); ^{13}C NMR (100 MHz, CDCl_3) δ 198.1, 151.1, 145.4, 129.8, 122.6, 117.0, 112.9, 73.5, 53.2, 39.0, 31.3, 29.9, 26.5, 26.4, 26.0; IR (NaCl, neat) 2930, 2855, 1682, 1655, 1608, 1555, 1376, 1018 cm^{-1} ; HRMS (ESI+) calcd for $\text{C}_{15}\text{H}_{20}\text{NO}_4$, 277.1314. Found 277.1318.



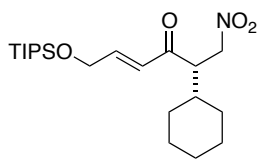
(*S,E*)-2-cyclohexyl-6-methyl-1-nitrohept-4-en-3-one (169): Prepared according to the general procedure: Colorless oil; $R_f = 0.41$ (4:1 hexanes:ether); 70% yield, 83% ee; $[\alpha]_D^{21} = -90.1$ ($c = 0.008$ g/ml, CH_2Cl_2);

HPLC analysis – Chiracel IC column, 70:30 hexanes/*iso*-propanol, 1.0 mL/min. Major: 9.98 min, minor: 7.62 min; ^1H NMR (300 MHz, CDCl_3) δ 6.91 (dd, $J = 15.8, 6.6$ Hz, 1H), 6.16 (dd, $J = 15.8, 1.4$ Hz, 1H), 4.90 (dd, $J = 14.4, 10.2$ Hz, 1H), 4.39 (dd, $J = 14.4, 3.7$ Hz, 1H), 3.47 (ddd, $J = 10.2, 4.9, 3.8$ Hz, 1H), 2.56-2.44 (m, 1H), 1.78-1.57 (m, 6H), 1.09 (d, $J = 6.8$ Hz, 6H), 1.27-

0.87 (m, 5H); ^{13}C NMR (100 MHz, CDCl_3) δ 199.1, 155.3, 126.8, 73.6, 52.0, 38.9, 31.3, 31.2, 29.8, 26.5, 26.4, 26.0, 21.3, 21.3; IR (NaCl, neat) 2963, 2930, 2856, 1692, 1667, 1625, 1450, 1420, 1375 cm^{-1} ; HRMS (ESI+) calcd for $\text{C}_{14}\text{H}_{23}\text{NNaO}_3$, 253.1678. Found 253.1675.

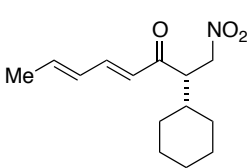


(S,E)-2-cyclohexyl-1-nitrohex-4-en-3-one (170): Prepared according to the general procedure: Colorless oil; $R_f = 0.35$ (4:1 hexanes:ether); 67% yield, 86% ee; $[\alpha]_D^{21} = -100.3$ ($c = 0.007$ g/ml, CH_2Cl_2); HPLC analysis – Chiracel IC column, 70:30 hexanes/*iso*-propanol, 1.0 mL/min. Major: 14.00 min, minor: 10.91 min; ^1H NMR (300 MHz, CDCl_3) δ 6.97 (dq, $J = 15.6, 6.9$ Hz, 1H), 6.26 (dq, $J = 15.6, 1.7$ Hz, 1H), 4.91 (dd, $J = 14.5, 10.3$ Hz, 1H), 4.39 (dd, $J = 14.5, 3.6$ Hz, 1H), 3.45 (ddd, $J = 10.3, 4.9, 3.7$ Hz, 1H), 1.95 (dd, $J = 6.9, 1.7$ Hz, 3H), 1.80-1.57 (m, 6H), 1.31-0.87 (m, 5H); ^{13}C NMR (100 MHz, CDCl_3) δ 198.5, 144.5, 131.2, 73.5, 52.0, 38.9, 31.3, 29.8, 26.5, 26.4, 26.0, 18.5; IR (NaCl, neat) 2928, 2855, 1692, 1665, 1629, 1553, 1444, 1375, 1286, 1201, 1065 cm^{-1} ; HRMS (ESI+) calcd for $\text{C}_{12}\text{H}_{20}\text{NO}_3$, 225.1365. Found 253.1397.



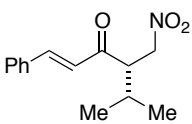
(S,E)-2-cyclohexyl-1-nitro-6-((triisopropylsilyloxy)hex-4-en-3-one (171): Prepared according to the general procedure: Colorless oil; $R_f = 0.42$ (4:1 hexanes:ether); 60% yield, 82% ee; $[\alpha]_D^{21} = -24.0$ ($c = 0.006$ g/ml, CH_2Cl_2); HPLC analysis – Chiracel IC column, 70:30 hexanes/*iso*-propanol, 1.0 mL/min. Major: 9.74 min, minor: 7.44 min; ^1H NMR (300 MHz, CDCl_3) δ 6.99 (dt, $J = 15.5, 3.2$ Hz, 1H), 6.60 (dt, $J = 15.4, 2.3$ Hz, 1H), 4.92 (dd, $J = 14.5, 10.1$ Hz, 1H), 4.49 (dd, $J = 3.2, 2.3$ Hz, 2H), 4.39 (dd, $J = 14.5, 3.8$ Hz, 1H), 3.48 (ddd, $J = 10.1, 5.0, 3.9$ Hz, 1H), 1.82-1.58 (m, 6H), 1.33-0.86 (m, 26H); ^{13}C NMR (100 MHz, CDCl_3) δ 198.5, 147.3, 126.9, 73.5, 62.8, 52.7, 38.9, 31.3, 30.0,

26.5, 26.5, 26.1, 18.1, 12.1; **IR** (NaCl, neat) 2932, 2866, 1737, 1694, 1671, 1556, 1463, 1450, 1420, 1375, 1267, 1138, 1069 cm^{-1} ; **HRMS** ESI/APCI or APCI failed to produce the parent or related ions.



(S,4E,6E)-2-cyclohexyl-1-nitroocta-4,6-dien-3-one (172): Prepared according to the general procedure: Colorless oil; $R_f = 0.28$ (4:1 hexanes:ether); 90% yield, 94% ee; $[\alpha]_D^{21} = -124.8$ ($c = 0.005$ g/ml,

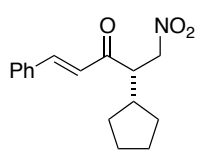
CH_2Cl_2); HPLC analysis – Chiracel IC column, 70:30 hexanes/*iso*-propanol, 1.0 mL/min. Major: 17.33 min, minor: 12.05 min; **^1H NMR** (300 MHz, CDCl_3) δ 7.23 (m, 1H), 6.33-6.11 (m, 3H), 4.91 (dd, $J = 14.4, 10.2$ Hz, 1H), 4.39 (dd, $J = 14.4, 3.7$ Hz, 1H), 3.44 (ddd, $J = 10.1, 5.0, 3.8$ Hz, 1H), 1.89 (d, $J = 5.3$ Hz, 3H), 1.81-1.54 (m, 6H), 1.30-0.86 (m, 5H); **^{13}C NMR** (100 MHz, CDCl_3) δ 198.9, 144.4, 142.1, 130.3, 126.9, 73.7, 52.5, 39.1, 31.3, 30.0, 26.5, 26.4, 26.1, 19.0; **IR** (NaCl, neat) 2930, 2855, 1683, 1657, 1636, 1594, 1555, 1449, 1419, 1375, 1058 cm^{-1} ; **HRMS** (ESI+) calcd for $\text{C}_{14}\text{H}_{22}\text{NO}_3$, 251.1521. Found 251.1524.



(S,E)-5-methyl-4-(nitromethyl)-1-phenylhex-1-en-3-one (173): Prepared according to the general procedure: Colorless oil; $R_f = 0.25$ (4:1 hexanes:ether);

75% yield, 91% ee; $[\alpha]_D^{21} = -108.5$ ($c = 0.010$ g/ml, CH_2Cl_2); HPLC analysis – Chiracel IC column, 70:30 hexanes/*iso*-propanol, 1.0 mL/min. Major: 15.98 min, minor: 10.31 min; **^1H NMR** (300 MHz, CDCl_3) δ 7.67 (d, $J = 16.0$ Hz, 1H), 7.61-7.57 (m, 2H), 7.43-7.40 (m, 2H), 6.87 (d, $J = 16.0$ Hz, 1H), 4.99 (dd, $J = 14.6, 10.2$ Hz, 1H), 4.43 (dd, $J = 14.6, 3.6$ Hz, 1H), 3.58 (ddd, $J = 10.2, 5.1, 3.6$ Hz, 1H), 2.24-2.09 (m, 1H), 1.07 (d, $J = 6.9$ Hz, 3H), 0.94 (d, $J = 6.9$ Hz, 3H); **^{13}C NMR** (100 MHz, CDCl_3) δ 198.4, 144.1, 134.3, 131.0, 129.1, 128.7, 125.1, 73.0, 53.1,

29.0, 20.8, 19.1; **IR** (NaCl, neat) 2967, 1686, 1658, 1608, 1556, 1450, 1419, 1375, 1332, 1193, 1077 cm^{-1} ; **HRMS** (ESI+) calcd for $\text{C}_{14}\text{H}_{18}\text{NO}_3$, 247.1208. Found 247.1211.



(S,E)-4-cyclopentyl-5-nitro-1-phenylpent-1-en-3-one (174): Prepared

according to the general procedure: Colorless oil; $R_f = 0.24$ (4:1 hexanes:ether);

84% yield, 88% ee; $[\alpha]_D^{21} = -90.7$ ($c = 0.009$ g/ml, CH_2Cl_2); HPLC analysis –

Chiracel IC column, 70:30 hexanes/*iso*-propanol, 1.0 mL/min. Major: 15.24 min, minor: 11.60

min; **$^1\text{H NMR}$** (300 MHz, CDCl_3) δ 7.66 (d, $J = 16.0$ Hz, 1H), 7.61-7.58 (m, 2H), 7.43-7.40 (m,

3H), 6.88 (d, $J = 16.0$ Hz, 1H), 4.99 (dd, $J = 14.6, 10.5$ Hz, 1H), 4.47 (dd, $J = 14.6, 3.5$ Hz, 1H),

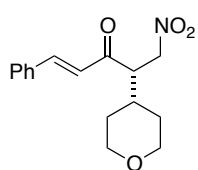
3.59 (ddd, $J = 10.4, 8.6, 3.5$ Hz, 1H), 2.05-1.91 (m, 1H), 1.85-1.72 (m, 2H), 1.71-1.60 (m, 2H),

1.59-1.49 (m, 2H), 1.38-1.22 (m, 2H); **$^{13}\text{C NMR}$** (100 MHz, CDCl_3) δ 199.2, 144.1, 134.4,

131.0, 129.1, 128.7, 125.8, 75.2, 51.7, 41.0, 31.0, 30.5, 24.9, 24.5; **IR** (NaCl, neat) 2948, 2871,

1690, 1656, 1555, 1451, 1412, 1378, 1196 cm^{-1} ; **HRMS** (ESI+) calcd for $\text{C}_{16}\text{H}_{20}\text{NO}_3$, 273.1365.

Found 273.1365.



(S,E)-5-nitro-1-phenyl-4-(tetrahydro-2H-pyran-4-yl)pent-1-en-3-one (175):

Prepared according to the general procedure: Amorphous solid; $R_f = 0.13$ (1:1

hexanes:ether); 82% yield, 90% ee; $[\alpha]_D^{21} = -100.2$ ($c = 0.011$ g/ml, CH_2Cl_2);

HPLC analysis – Chiracel IC column, 60:40 hexanes/*iso*-propanol, 1.0 mL/min. Major: 22.68

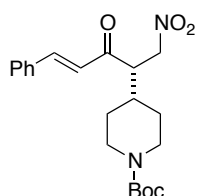
min, minor: 20.04 min; **$^1\text{H NMR}$** (300 MHz, CDCl_3) δ 7.68 (d, $J = 16.0$ Hz, 1H), 7.62-7.59 (m,

2H), 7.43 (dd, $J = 5.0, 2.0$ Hz, 3H), 6.87 (d, $J = 16.0$ Hz, 1H), 4.98 (dd, $J = 14.5, 10.1$ Hz, 1H),

4.49 (dd, $J = 14.5, 3.8$ Hz, 1H), 4.00-3.95 (m, 2H), 3.62 (ddd, $J = 10.1, 6.2, 3.8$ Hz, 1H), 3.39-

3.29 (m, 2H), 2.00-1.93 (m, 1H), 1.60-1.40 (m, 4H); **$^{13}\text{C NMR}$** (100 MHz, CDCl_3) δ 198.2,

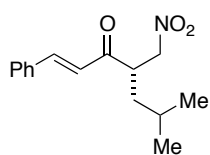
144.7, 134.1, 131.2, 129.2, 128.8, 125.3, 73.5, 67.8, 67.7, 52.0, 36.3, 30.9, 30.0; **IR** (NaCl, neat) 2941, 2848, 1685, 1656, 1607, 1554, 1450, 1375, 1183, 1151, 1090 cm^{-1} ; **HRMS** (ESI+) calcd for $\text{C}_{16}\text{H}_{20}\text{NO}_4$, 289.1314. Found 289.1314.



(S,E)-tert-butyl 4-(1-nitro-3-oxo-5-phenylpent-4-en-2-yl)piperidine-1-

carboxylate (176): Prepared according to the general procedure: Amorphous solid; $R_f = 0.23$ (3:2 hexanes:ether); 78% yield, 90% ee; $[\alpha]_D^{21} = -50.4$ (c =

0.008 g/ml, CH_2Cl_2); HPLC analysis – Chiracel IC column, 60:40 hexanes/*iso*-propanol, 1.0 mL/min. Major: 36.28 min, minor: 22.87 min; **$^1\text{H NMR}$** (300 MHz, CDCl_3) δ 7.68 (d, $J = 16.0$ Hz, 1H), 7.62-7.59 (m, 2H), 7.43 (dd, $J = 5.1, 1.9$ Hz, 3H), 6.87 (d, $J = 16.0$ Hz, 1H), 4.98 (dd, $J = 14.5, 10.1$ Hz, 1H), 4.47 (dd, $J = 14.5, 3.8$ Hz, 1H), 4.18-4.14 (m, 2H), 3.63 (ddd, $J = 10.0, 6.0, 3.9$ Hz, 1H), 2.69-2.57 (m, 2H), 1.94-1.81 (m, 1H), 1.70-1.58 (m, 2H), 1.44 (s, 9H), 1.40-1.14 (m, 2H); **$^{13}\text{C NMR}$** (100 MHz, CDCl_3) δ 198.1, 154.5, 144.6, 134.1, 131.2, 129.1, 128.8, 125.2, 79.8, 73.5, 51.8, 37.3, 30.1, 29.1, 28.5; **IR** (NaCl, neat) 2933, 2860, 1684, 1607, 1558, 1426, 1367, 1250, 1170, 1066 cm^{-1} ; **HRMS** (ESI+) calcd for $\text{C}_{21}\text{H}_{28}\text{N}_2\text{NaO}_5$, 388.1998. Found 388.1997.

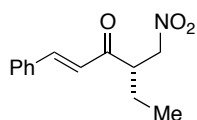


(S,E)-6-methyl-4-(nitromethyl)-1-phenylhept-1-en-3-one (177): Prepared

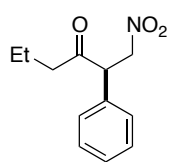
according to the general procedure: Colorless oil; $R_f = 0.26$ (9:1 hexanes:EtOAc); 84% yield, 42% ee; $[\alpha]_D^{21} = -28.6$ (c = 0.019 g/ml, CHCl_3);

HPLC analysis – Chiracel IC column, 70:30 hexanes/*iso*-propanol, 1.0 mL/min. Major: 11.24 min, minor: 8.95 min; **$^1\text{H NMR}$** (300 MHz, CDCl_3) δ 7.69 (d, $J = 16.0$ Hz, 1H), 7.59 (dd, $J = 6.5, 3.1$ Hz, 2H), 7.42 (dd, $J = 5.0, 1.8$ Hz, 3H), 6.84 (d, $J = 16.0$ Hz, 1H), 4.90 (dd, $J = 14.4, 9.6$

Hz, 1H), 4.39 (dd, $J = 14.4, 4.3$ Hz, 1H), 3.76-3.70 (m, 1H), 1.68-1.57 (m, 2H), 1.37-1.26 (m, 1H), 1.01-0.88 (m, 6H); ^{13}C NMR (100 MHz, CDCl_3) δ 198.9, 144.5, 134.3, 131.1, 129.2, 128.7, 124.6, 75.3, 45.5, 38.9, 26.0, 22.9, 22.5; IR (NaCl, neat) 3028, 2959, 2872, 1687, 1662, 1610, 1554, 1450, 1376, 1204, 1054 cm^{-1} ; HRMS (ESI+) calcd for $\text{C}_{15}\text{H}_{19}\text{NO}_3$, 261.1365. Found 261.1361.

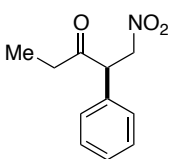


(*S,E*)-4-(nitromethyl)-1-phenylhex-1-en-3-one (178): Prepared according to the general procedure: Colorless oil; $R_f = 0.18$ (9:1 hexanes:EtOAc); 66% yield, 52% ee; $[\alpha]_D^{21} = -34.2$ ($c = 0.011$ g/ml, CH_2Cl_2); HPLC analysis – Chiracel IC column, 70:30 hexanes/*iso*-propanol, 1.0 mL/min. Major: 12.66 min, minor: 9.56 min; ^1H NMR (400 MHz, CDCl_3) δ 7.61 (d, $J = 16.0$ Hz, 1H), 7.52 (dd, $J = 6.5, 3.1$ Hz, 2H), 7.35 (m, 3H), 6.79 (d, $J = 16.0$ Hz, 1H), 4.85 (dd, $J = 14.3, 9.1$ Hz, 1H), 4.36 (dd, $J = 14.3, 4.9$ Hz, 1H), 3.59 (m, 1H), 1.76-1.68 (m, 1H), 1.60 (m, 1H), 0.91 (t, $J = 7.5$ Hz, 3H); ^{13}C NMR (100 MHz, CDCl_3) δ 198.6, 144.5, 134.2, 131.1, 129.2, 128.7, 124.5, 74.7, 48.4, 22.9, 11.1; IR (NaCl, neat) 2922, 1736, 1687, 1657, 1608, 1549, 1415, 1157, 1074 cm^{-1} . HRMS (ESI+) calcd for $\text{C}_{13}\text{H}_{15}\text{NO}_3$, 233.1052. Found 233.1051.

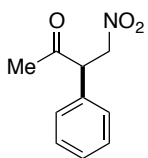


(*R*)-1-nitro-2-phenylhexan-3-one (214): Prepared according to the general procedure: 80% yield; 93% ee; colorless oil; $R_f = 0.24$ (9:1 hex:Et₂O); $[\alpha]_D^{21} = +299.0$ ($c = 0.007$ g/ml, CHCl_3); HPLC analysis – Chiracel IC column, 70:30 hexanes/*iso*-propanol, 1.0 mL/min. Major: 5.79 min, minor: 8.72 min; ^1H NMR (400 MHz, CDCl_3): δ 7.40-7.33 (m, 3H), 7.21-7.19 (m, 3H), 5.16 (dd, $J = 14.4, 9.2$ Hz, 1H), 4.52 (dd, $J = 9.2, 5.2$ Hz, 1H), 4.45 (dd, $J = 14.4, 5.2$ Hz, 1H), 2.52-2.35 (m, 2H), 1.65-1.48 (m, 2H), 0.81 (t, J

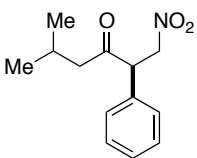
= 7.4 Hz, 3H); ^{13}C NMR (100 MHz, CDCl_3): δ 206.5, 133.1, 129.7, 128.9, 128.5, 75.4, 55.3, 43.4, 17.1, 13.6; IR (NaCl, neat) 3031, 2965, 2935, 2878, 1716, 1554, 1495, 1455, 1415, 1376, 1128, 1003 cm^{-1} ; HRMS (DART) (M^+NH_4) $^+$ calcd for $\text{C}_{12}\text{H}_{19}\text{N}_2\text{O}_3$, 221.1052. Found 221.1058.



(R)-1-nitro-2-phenylpentan-3-one (220): Prepared according to the general procedure: 87% yield; 92% ee; colorless oil; R_f = 0.16 (9:1 hex:Et₂O); $[\alpha]_D^{21}$ = +379.0 (c = 0.010 g/ml, CHCl_3); HPLC analysis – Chiracel IC column, 70:30 hexanes/*iso*-propanol, 1.0 mL/min. Major: 6.73 min, minor: 9.83 min; ^1H NMR (400 MHz, CDCl_3): δ 7.40-7.32 (m, 3H), 7.21-7.19 (m, 2H), 5.16 (dd, J = 14.4, 9.3 Hz, 1H), 4.54 (dd, J = 9.3, 5.2 Hz, 1H), 4.46 (dd, J = 14.5, 5.2 Hz, 1H), 2.57-2.41 (m, 2H), 1.02 (t, J = 7.3 Hz, 3H); ^{13}C NMR (100 MHz, CDCl_3): δ 207.1, 133.3, 129.7, 128.9, 128.5, 75.5, 55.1, 34.9, 7.8; IR (NaCl, neat) 3032, 2980, 2941, 1717, 1555, 1495, 1456, 1415, 1377, 1125, 1031 cm^{-1} ; HRMS (DART) (M^+NH_4) $^+$ calcd for $\text{C}_{11}\text{H}_{17}\text{N}_2\text{O}_3$, 207.0895. Found 207.0900.



(R)-4-nitro-3-phenylbutan-2-one (221): Prepared according to the general procedure: 71% yield; 62% ee; colorless oil; R_f = 0.10 (9:1 hex:Et₂O); $[\alpha]_D^{21}$ = +230.6 (c = 0.012 g/ml, CHCl_3); HPLC analysis – Chiracel IC column, 70:30 hexanes/*iso*-propanol, 1.0 mL/min. Major: 8.49 min, minor: 9.92 min; ^1H NMR (400 MHz, CDCl_3): δ 7.42-7.34 (m, 3H), 7.22-7.20 (m, 2H), 5.14 (dd, J = 14.5, 9.2 Hz, 1H), 4.54 (dd, J = 9.1, 5.3 Hz, 1H), 4.45 (dd, J = 14.5, 5.3 Hz, 1H), 2.17 (s, 3H); ^{13}C NMR (100 MHz, CDCl_3): δ 204.2, 133.0, 129.8, 129.0, 128.5, 75.3, 56.0, 28.8; IR (NaCl, neat) 3030, 2959, 2922, 2852, 1712, 1551, 1494, 1454, 1376, 1224, 1163 cm^{-1} ; HRMS (DART) (M^+NH_4) $^+$ calcd for $\text{C}_{10}\text{H}_{15}\text{N}_2\text{O}_3$, 193.0739. Found 193.0740.

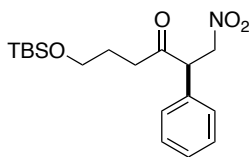


(R)-5-methyl-1-nitro-2-phenylhexan-3-one (222): Prepared according to the

general procedure: 32% yield; 95% ee; colorless oil; $R_f = 0.27$ (9:1 hex:Et₂O);

$[\alpha]_D^{21} = +276.3$ ($c = 0.008$ g/ml, CHCl₃); HPLC analysis – Chiracel IC

column, 70:30 hexanes/*iso*-propanol, 1.0 mL/min. Major: 5.28 min, minor: 8.13 min; **¹H NMR** (400 MHz, CDCl₃): δ 7.40-7.33 (m, 3H), 7.19 (m, 2H), 5.15 (dd, $J = 14.0, 8.9$ Hz, 1H), 4.51-4.42 (m, 2H), 2.40 (dd, $J = 16.6, 6.2$ Hz, 1H), 2.25 (dd, $J = 16.6, 7.5$ Hz, 1H), 2.13 (m, 1H), 0.88 (d, $J = 6.6$ Hz, 3H), 0.74 (d, $J = 6.6$ Hz, 3H); **¹³C NMR** (100 MHz, CDCl₃): δ 206.0, 133.0, 129.7, 128.9, 128.6, 75.3, 55.7, 50.4, 24.3, 22.7, 22.2; **IR** (NaCl, neat) 3064, 3031, 2960, 2934, 2873, 1716, 1556, 1495, 1467, 1455, 1416, 1376, 1034 cm⁻¹; **HRMS** (DART) ($M^+NH_4^+$) calcd for C₁₃H₂₁N₂O₃, 235.1208. Found 235.1206.

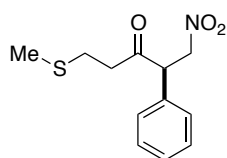


(R)-6-((*tert*-butyldimethylsilyloxy)-1-nitro-2-phenylhexan-3-one (223):

Prepared according to the general procedure: 68% yield; 87% ee; colorless

oil; $R_f = 0.23$ (9:1 hex:Et₂O); $[\alpha]_D^{21} = +161.5$ ($c = 0.015$ g/ml, CHCl₃);

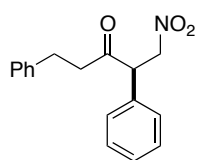
HPLC analysis – Chiracel IC column, 70:30 hexanes/*iso*-propanol, 1.0 mL/min. Major: 4.70 min, minor: 6.01 min; **¹H NMR** (400 MHz, CDCl₃): δ 7.39-7.32 (m, 3H), 7.21-7.19 (m, 2H), 5.15 (dd, $J = 14.4, 9.1$ Hz, 1H), 4.54 (dd, $J = 9.1, 5.4$ Hz, 1H), 4.46 (dd, $J = 14.4, 5.4$ Hz, 1H), 3.57-3.46 (m, 2H), 2.63-2.46 (m, 3H), 1.89-1.63 (m, 3H), 0.82 (s, 9H), -0.02 (s, 3H), -0.04 (s, 3H); **¹³C NMR** (100 MHz, CDCl₃): δ 206.6, 133.2, 129.8, 128.9, 128.5, 75.4, 61.8, 55.4, 37.9, 26.8, 26.0, 18.4, 5.3; **IR** (NaCl, neat) 2956, 2930, 2858, 1718, 1557, 1495, 1572, 1415, 1376, 1256, 1103 cm⁻¹; **HRMS** (DART) ($M+H$) calcd for C₁₈H₃₀NO₄Si, 351.1866. Found 351.1868.



(R)-5-(methylthio)-1-nitro-2-phenylpentan-3-one (224): Prepared

according to the general procedure: 67% yield; 92% ee; colorless oil; $R_f = 0.1$ (9:1 hex:Et₂O); $[\alpha]_D^{21} = +224.5$ (c = 0.011 g/ml, CHCl₃); HPLC analysis

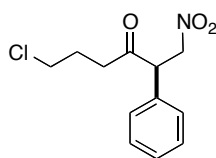
– Chiracel IC column, 70:30 hexanes/*iso*-propanol, 1.0 mL/min. Major: 7.96 min, minor: 10.55 min; **¹H NMR** (400 MHz, CDCl₃): δ 7.41-7.34 (m, 3H), 7.22-7.20 (m, 2H), 5.16 (dd, $J = 14.3, 9.0$ Hz, 1H), 4.56-4.45 (m, 2H), 2.83-2.60 (m, 4H), 1.99 (s, 3H); **¹³C NMR** (100 MHz, CDCl₃): δ 204.7, 132.6, 129.9, 129.1, 128.6, 75.3, 55.5, 41.2, 27.8, 15.7; **IR** (NaCl, neat) 3030, 2964, 2920, 1715, 1552, 1494, 1414, 1375, 1111 cm⁻¹; **HRMS** (DART) (M⁺NH₄)⁺ calcd for C₁₂H₁₉N₂O₃S, 253.0773. Found 253.0778.



(R)-1-nitro-2,5-diphenylpentan-3-one (225): Prepared according to the general procedure: 76% yield; 93% ee; colorless oil; $R_f = 0.15$ (9:1 hex:Et₂O);

$[\alpha]_D^{21} = +176.8$ (c = 0.019 g/ml, CHCl₃); HPLC analysis – Chiracel IC column,

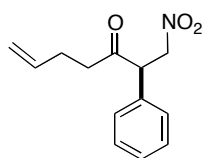
70:30 hexanes/*iso*-propanol, 1.0 mL/min. Major: 6.56 min, minor: 9.60 min; **¹H NMR** (400 MHz, CDCl₃): δ 7.33-7.29 (m, 3H), 7.23-7.09 (m, 5H), 7.04-7.02 (m, 2H), 5.12 (dd, $J = 14.0, 8.8$ Hz, 1H), 4.50-4.40 (m, 2H), 2.90-2.70 (m, 4H); **¹³C NMR** (100 MHz, CDCl₃): δ 205.5, 140.4, 132.8, 129.8, 128.9, 128.6, 128.5, 128.3, 126.3, 75.3, 55.5, 43.0, 29.6; **IR** (NaCl, neat) 3087, 3063, 3029, 2923, 1717, 1602, 1555, 1495, 1454, 1415, 1376, 1117, 1030 cm⁻¹; **HRMS** (DART) (M⁺NH₄)⁺ calcd for C₁₇H₂₁N₂O₃, 283.1208. Found 283.1209.



(R)-6-chloro-1-nitro-2-phenylhexan-3-one (226): Prepared according to the general procedure: 83% yield; 93% ee; colorless oil; $R_f = 0.10$ (9:1 hex:Et₂O);

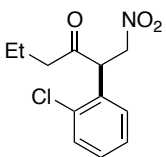
$[\alpha]_D^{21} = +216.1$ (c = 0.012 g/ml, CHCl₃); HPLC analysis – Chiracel IC

column, 70:30 hexanes/*iso*-propanol, 1.0 mL/min. Major: 6.36 min, minor: 8.71 min; **¹H NMR** (400 MHz, CDCl₃): δ 7.42-7.36 (m, 3H), 7.22-7.19 (m, 2H), 5.17 (dd, *J* = 14.6, 9.5 Hz, 1H), 4.55 (dd, *J* = 9.5, 5.0 Hz, 1H), 4.46 (dd, *J* = 14.6, 5.0 Hz, 1H), 3.54-3.41 (m, 2H), 2.76-2.58 (m, 2H), 2.10-1.92 (m, 2H); **¹³C NMR** (100 MHz, CDCl₃): δ 205.6, 132.7, 129.9, 129.1, 128.5, 75.2, 55.4, 44.1, 38.3, 26.4; **IR** (NaCl, neat) 3030, 2961, 2921, 1717, 1553, 1495, 1454, 1415, 1376, 1309, 1116 cm⁻¹; **HRMS** (DART) (M⁺NH₄)⁺ calcd for C₁₂H₁₈ClN₂O₃, 255.0662. Found 255.0665.



(*R*)-1-nitro-2-phenylhept-6-en-3-one (3i): Prepared according to the general procedure: 83% yield; 93% ee; colorless oil; *R*_f = 0.18 (9:1 hex:Et₂O); [α]_D²¹ = +279.4 (*c* = 0.007 g/ml, CHCl₃); HPLC analysis – Chiracel IC column, 70:30

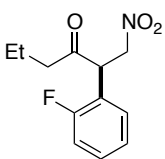
hexanes/*iso*-propanol, 1.0 mL/min. Major: 5.81 min, minor: 8.47 min; **¹H NMR** (400 MHz, CDCl₃): δ 7.41-7.33 (m, 3H), 7.19 (m, 2H), 5.73-5.63 (m, 1H), 5.16 (ddd, *J* = 14.4, 9.3, 1.3 Hz, 1H), 4.96-4.91 (m, 2H), 4.55-4.43 (m, 2H), 2.65-2.49 (m, 2H), 2.37-2.21 (m, 2H); **¹³C NMR** (100 MHz, CDCl₃): δ 205.7, 136.5, 133.0, 129.8, 129.0, 128.6, 115.6, 75.4, 55.4, 40.6, 27.5; **IR** (NaCl, neat) 3067, 3031, 2921, 1717, 1642, 1555, 1495, 1416, 1376, 1227, 1119 cm⁻¹; **HRMS** (DART) (M⁺NH₄)⁺ calcd for C₁₃H₁₉N₂O₃, 233.1052. Found 233.1061.



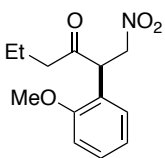
(*R*)-2-(2-chlorophenyl)-1-nitrohexan-3-one (229): Prepared according to the general procedure: 70% yield; 91% ee; colorless oil; *R*_f = 0.22 (9:1 hex:Et₂O); [α]_D²¹ = +232.0 (*c* = 0.009 g/ml, CHCl₃); HPLC analysis – Chiracel IC column,

70:30 hexanes/*iso*-propanol, 1.0 mL/min. Major: 5.74 min, minor: 7.78 min; **¹H NMR** (400 MHz, CDCl₃): δ 7.46 (dd, *J* = 7.8, 1.6 Hz, 1H), 7.30-7.22 (m, 2H), 7.07 (dd, *J* = 7.5, 1.9 Hz, 1H),

5.14-5.04 (m, 2H), 4.43 (dd, $J = 13.4, 3.6$ Hz, 1H), 2.47 (ddd, $J = 17.3, 8.0, 6.3$ Hz, 1H), 2.33 (ddd, $J = 17.3, 7.9, 6.9$ Hz, 1H), 1.64-1.49 (m, 2H), 0.81 (t, $J = 7.4$ Hz, 3H); ^{13}C NMR (100 MHz, CDCl_3): δ 205.9, 134.5, 131.1, 130.8, 130.2, 129.4, 128.0, 74.0, 51.4, 43.6, 17.1, 13.6; IR (NaCl, neat) 2966, 2934, 2878, 1719, 1556, 1475, 1416, 1376, 1130, 1052 cm^{-1} ; HRMS (DART) (M^+NH_4) $^+$ calcd for $\text{C}_{12}\text{H}_{18}\text{ClN}_2\text{O}_3$, 255.0662. Found 255.0670.

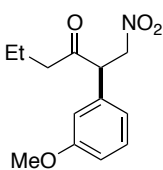


(R)-2-(2-fluorophenyl)-1-nitrohexan-3-one (230): Prepared according to the general procedure: 75% yield; 93% ee; colorless oil; $R_f = 0.24$ (9:1 hex:Et₂O); $[\alpha]_D^{21} = +252.1$ ($c = 0.011$ g/ml, CHCl_3); HPLC analysis – Chiracel IC column, 70:30 hexanes/*iso*-propanol, 1.0 mL/min. Major: 5.50 min, minor: 7.52 min; ^1H NMR (400 MHz, CDCl_3): δ 7.38-7.33 (m, 1H), 7.18-7.10 (m, 3H), 5.18 (dd, $J = 14.7, 9.2$ Hz, 1H), 4.83 (dd, $J = 9.2, 5.2$ Hz, 1H), 4.46 (dd, $J = 14.6, 5.2$ Hz, 1H), 2.52-2.33 (m, 2H), 1.64-1.53 (m, 2H), 0.83 (t, $J = 7.4$ Hz, 3H); ^{13}C NMR (100 MHz, CDCl_3): δ 205.6, 160.6 (d, $J = 247.7$ Hz), 130.8 (d, $J = 8.5$ Hz), 129.7 (d, $J = 3.1$ Hz), 125.3 (d, $J = 3.6$ Hz), 120.6 (d, $J = 15.0$ Hz), 116.6 (d, $J = 22.1$ Hz), 74.2, 48.1, 43.2, 17.1, 13.6; IR (NaCl, neat) 2963, 2926, 1719, 1586, 1554, 1493, 1457, 1417, 1377, 1287, 1130, 1109, 1035, 1018 cm^{-1} ; HRMS (DART) (M^+NH_4) $^+$ calcd for $\text{C}_{12}\text{H}_{18}\text{FN}_2\text{O}_3$, 239.0958. Found 239.0963



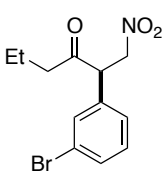
(R)-2-(2-methoxyphenyl)-1-nitrohexan-3-one (231): Prepared according to the general procedure: 83% yield; 94% ee; colorless oil; $R_f = 0.16$ (9:1 hex:Et₂O); $[\alpha]_D^{21} = +271.5$ ($c = 0.011$ g/ml, CHCl_3); HPLC analysis – Chiracel IC column, 70:30 hexanes/*iso*-propanol, 1.0 mL/min. Major: 6.50 min, minor: 8.53 min; ^1H NMR (400 MHz, CDCl_3): δ 7.35-7.30 (m, 1H), 7.05 (d, $J = 7.6$ Hz, 1H), 6.96-6.92 (m, 2H), 5.14 (dd, $J =$

14.3, 8.7 Hz, 1H), 4.80 (dd, $J = 8.7, 5.4$ Hz, 1H), 4.42 (dd, $J = 14.4, 5.4$ Hz, 1H), 3.85 (s, 3H), 2.43-2.25 (m, 2H), 1.56 (m, 2H), 0.82 (t, $J = 7.4$ Hz, 3H); ^{13}C NMR (100 MHz, CDCl_3): δ 207.0, 157.0, 130.1, 129.9, 122.1, 121.4, 111.3, 74.4, 55.6, 49.9, 42.8, 17.2, 13.7; IR (NaCl, neat) 3008, 2965, 2938, 2877, 2842, 1716, 1600, 1554, 1494, 1464, 1377, 1292, 1251, 1026 cm^{-1} ; HRMS (DART) (M^+NH_4) $^+$ calcd for $\text{C}_{13}\text{H}_{21}\text{N}_2\text{O}_4$, 251.1158. Found 251.1167.



(R)-2-(3-methoxyphenyl)-1-nitrohexan-3-one (232): Prepared according to the general procedure: 63% yield; 91% ee; colorless oil; $R_f = 0.13$ (9:1 hex:Et₂O); $[\alpha]_D^{21} = +274.7$ ($c = 0.006$ g/ml, CHCl_3); HPLC analysis – Chiracel IC column,

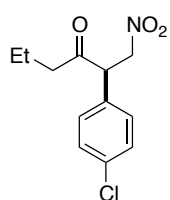
70:30 hexanes/*iso*-propanol, 1.0 mL/min. Major: 6.56 min, minor: 9.17 min; ^1H NMR (400 MHz, CDCl_3): δ 7.28 (m, 1H), 6.88 (dd, $J = 8.3, 2.5$ Hz, 1H), 6.77 (d, $J = 7.6$ Hz, 1H), 6.71 (t, $J = 2.0$ Hz, 1H), 5.14 (dd, $J = 14.0, 8.8$ Hz, 1H), 4.46 (ddd, $J = 18.0, 13.6, 4.8$ Hz, 2H), 3.80 (s, 3H), 2.52-2.36 (m, 2H), 1.57 (m, 2H), 0.82 (t, $J = 7.4$ Hz, 3H); ^{13}C NMR (100 MHz, CDCl_3): δ 206.4, 160.5, 134.5, 130.8, 120.7, 114.3, 114.2, 75.3, 55.5, 55.3, 43.4, 17.2, 13.6; IR (NaCl, neat) 2965, 2938, 2877, 2840, 1716, 1600, 1586, 1555, 1491, 1377, 1299, 1265, 1154, 1046 cm^{-1} ; HRMS (DART) (M^+NH_4) $^+$ calcd for $\text{C}_{13}\text{H}_{21}\text{N}_2\text{O}_4$, 251.1158. Found 251.1163.



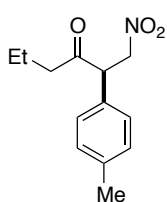
(R)-2-(3-bromophenyl)-1-nitrohexan-3-one (233): Prepared according to the general procedure: 50% yield; 91% ee; colorless oil; $R_f = 0.17$ (9:1 hex:Et₂O); $[\alpha]_D^{21} = +244.3$ ($c = 0.008$ g/ml, CHCl_3); HPLC analysis – Chiracel IC column,

70:30 hexanes/*iso*-propanol, 1.0 mL/min. Major: 5.73 min, minor: 7.41 min; ^1H NMR (400 MHz, CDCl_3): δ 7.47 (ddd, $J = 8.0, 1.9, 1.0$ Hz, 1H), 7.35 (t, $J = 1.8$ Hz, 1H), 7.23 (t, $J = 7.9$ Hz, 1H), 7.11 (dt, $J = 7.7, 1.4$ Hz, 1H), 5.11 (dd, $J = 13.7, 8.4$ Hz, 1H), 4.48-4.39 (m, 2H), 2.52-2.33

(m, 2H), 1.62-1.49 (m, 2H), 0.81 (t, $J = 7.4$ Hz, 3H); ^{13}C NMR (100 MHz, CDCl_3): δ 205.8, 135.3, 132.2, 131.6, 131.2, 127.1, 123.8, 75.2, 54.8, 43.7, 17.1, 13.6; IR (NaCl, neat) 2964, 2922, 1714, 1590, 1553, 1475, 1415, 1375, 1186, 1127, 1075, 1018 cm^{-1} ; HRMS (DART) (M^+NH_4) $^+$ calcd for $\text{C}_{12}\text{H}_{18}\text{BrN}_2\text{O}_3$, 299.0157. Found 299.0162.

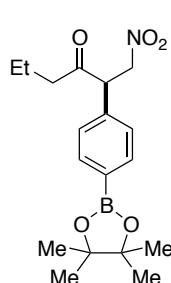


(R)-2-(4-chlorophenyl)-1-nitrohexan-3-one (234): Prepared according to the general procedure: 70% yield; 92% ee; colorless oil; $R_f = 0.16$ (9:1 hex:Et₂O); $[\alpha]_D^{21} = +285.4$ ($c = 0.010$ g/ml, CHCl_3); HPLC analysis – Chiracel IC column, 70:30 hexanes/*iso*-propanol, 1.0 mL/min. Major: 5.58 min, minor: 8.58 min; ^1H NMR (400 MHz, CDCl_3): δ 7.36 (d, $J = 8.5$ Hz, 2H), 7.15 (d, $J = 8.4$ Hz, 2H), 5.12 (dd, $J = 14.2, 8.9$ Hz, 1H), 4.52-4.41 (m, 2H), 2.52-2.34 (m, 2H), 1.56 (m, 2H), 0.82 (t, $J = 7.4$ Hz, 3H); ^{13}C NMR (100 MHz, CDCl_3): δ 206.1, 135.1, 131.6, 130.0, 129.8, 75.3, 54.6, 43.6, 17.1, 13.6; IR (NaCl, neat) 2966, 2935, 2878, 1716, 1556, 1491, 1413, 1377, 1127, 1094, 1015 cm^{-1} ; HRMS (DART) (M^+NH_4) $^+$ calcd for $\text{C}_{12}\text{H}_{18}\text{ClN}_2\text{O}_3$, 255.0662. Found 255.0661.



(R)-1-nitro-2-(*p*-tolyl)hexan-3-one (235): Prepared according to the general procedure: 81% yield; 92% ee; colorless oil; $R_f = 0.27$ (9:1 hex:Et₂O); $[\alpha]_D^{21} = +328.4$ ($c = 0.012$ g/ml, CHCl_3); HPLC analysis – Chiracel IC column, 70:30 hexanes/*iso*-propanol, 1.0 mL/min. Major: 5.84 min, minor: 8.93 min; ^1H NMR (400 MHz, CDCl_3): δ 7.18 (m, 2H), 7.08 (m, 2H), 5.13 (dd, $J = 14.2, 9.0$ Hz, 1H), 4.50-4.40 (m, 2H), 2.51-2.36 (m, 2H), 2.34 (s, 3H), 1.63-1.49 (m, 2H), 0.81 (t, $J = 7.4$ Hz, 3H); ^{13}C NMR (100 MHz, CDCl_3): δ 206.7, 138.8, 130.4, 130.1, 128.4, 75.5, 55.0, 43.3, 21.2, 17.2, 13.6; IR (NaCl, neat)

2965, 2934, 2877, 1716, 1556, 1514, 1458, 1416, 1377, 1129, 1021 cm^{-1} ; **HRMS** (DART) (M^+NH_4)⁺ calcd for $\text{C}_{13}\text{H}_{21}\text{N}_2\text{O}_3$, 235.1208. Found 235.1213.

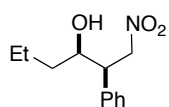


(R)-1-nitro-2-(4-(4,4,5,5-tetramethyl-1,3,2-dioxaborolan-2-yl)phenyl)hexan-

3-one: Prepared according to the general procedure: 62% yield; 91% ee; colorless oil; $R_f=0.10$ (9:1 hex:Et₂O); $[\alpha]_D^{21} = +213.3$ ($c = 0.009$ g/ml, CHCl₃);

HPLC analysis – Chiracel IC column, 70:30 hexanes/*iso*-propanol, 1.0 mL/min.

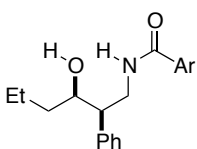
Major: 5.32 min, minor: 6.84 min; **¹H NMR** (400 MHz, CDCl₃): δ 7.81 (d, $J = 8.1$ Hz, 2H), 7.20 (d, $J = 8.2$ Hz, 2H), 5.16 (dd, $J = 14.5, 9.3$ Hz, 1H), 4.53 (dd, $J = 9.3, 5.1$ Hz, 1H), 4.43 (dd, $J = 14.5, 5.2$ Hz, 1H), 2.50-2.32 (m, 2H), 1.62-1.48 (m, 2H), 1.34 (s, 12H), 0.80 (t, $J = 7.4$ Hz, 3H); **¹³C NMR** (100 MHz, CDCl₃): δ 206.3, 136.1, 136.0, 127.9, 84.2, 75.3, 55.5, 43.5, 25.0, 17.1, 13.6; **IR** (NaCl, neat) 2977, 2934, 1717, 1611, 1557, 1400, 1361, 1329, 1273, 1144, 1090, 1021 cm^{-1} ; **HRMS** (DART) (M^+NH_4)⁺ calcd for $\text{C}_{18}\text{H}_{30}\text{BN}_2\text{O}_3$, 346.1940. Found 346.1944.



(2R,3R)-1-nitro-2-phenylhexan-3-ol (236): To a solution of (*R*)-1-nitro-2-phenylhexan-3-one (**214** (200 mg, 0.903 mmol, 1.0 equiv) in anhydrous methanol

(9 mL) at -10 °C was added sodium borohydride (86 mg, 2.26 mmol, 2.5 equiv) portionwise. The reaction was stirred for 2 h at this temperature and then quenched by the addition of 10% HCl (1 mL). After stirring for 30 min the reaction was concentrated and 10% HCl (10 mL) was added. The mixture was extracted with dichloromethane (3 X 20 mL) and the combined organic extracts dried (Na₂SO₄) and concentrated *in vacuo* to yield the desired product (201 mg, 99%) in 8:1 dr. The major diastereomer was isolated by flash chromatography (15% Et₂O in hex) yielding the nitro-alcohol in >20:1 dr as a colorless oil (87%). $R_f=0.61$ (1:1 EtOAc:hex); 93% ee; $[\alpha]_D^{21} =$

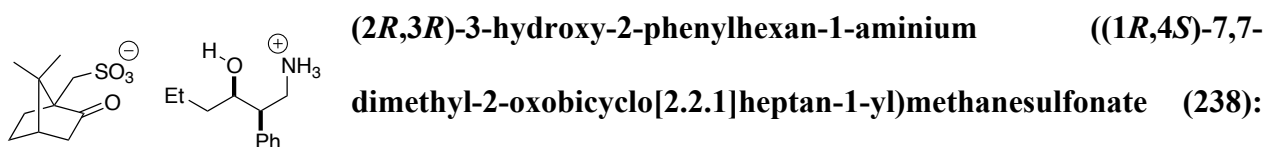
+17.1 (c = 0.014 g/ml, CHCl₃); HPLC analysis – Chiracel IA column, 90:10 hexanes/*iso*-propanol, 1.0 mL/min. Major: 6.60 min, minor: 8.36 min; ¹H NMR (400 MHz, CDCl₃): δ 7.85-7.74 (m, 5H), 5.40 (dd, *J* = 12.7, 7.4 Hz, 1H), 5.24 (dd, *J* = 12.7, 8.0 Hz, 1H), 4.37 (m, 1H), 4.03 (td, *J* = 7.7, 3.4 Hz, 1H), 1.98-1.89 (m, 2H), 1.89-1.77 (m, 2H), 1.71-1.61 (m, 1H), 1.39-1.33 (t, *J* = 7.1 Hz, 3H); ¹³C NMR (100 MHz, CDCl₃): δ 135.7, 129.1, 128.9, 128.1, 77.7, 71.7, 49.2, 37.5, 19.2, 14.0; IR (NaCl, neat) 3565, 3451, 3064, 3031, 2960, 2934, 2874, 1552, 1496, 1455, 1433, 1380, 1122, 1082 cm⁻¹; HRMS (DART) (M⁺NH₄)⁺ calcd for C₁₂H₂₁N₂O₃, 223.1208. Found 223.1205.



4-bromo-*N*-((2*R*,3*R*)-3-hydroxy-2-phenylhexyl)benzamide (237): To a solution of NiCl₂·6H₂O (160 mg, 0.672 mmol, 1.5 equiv) in MeOH (5 mL) was added sodium borohydride (76 mg, 2.02 mmol, 4.5 equiv) in portions.

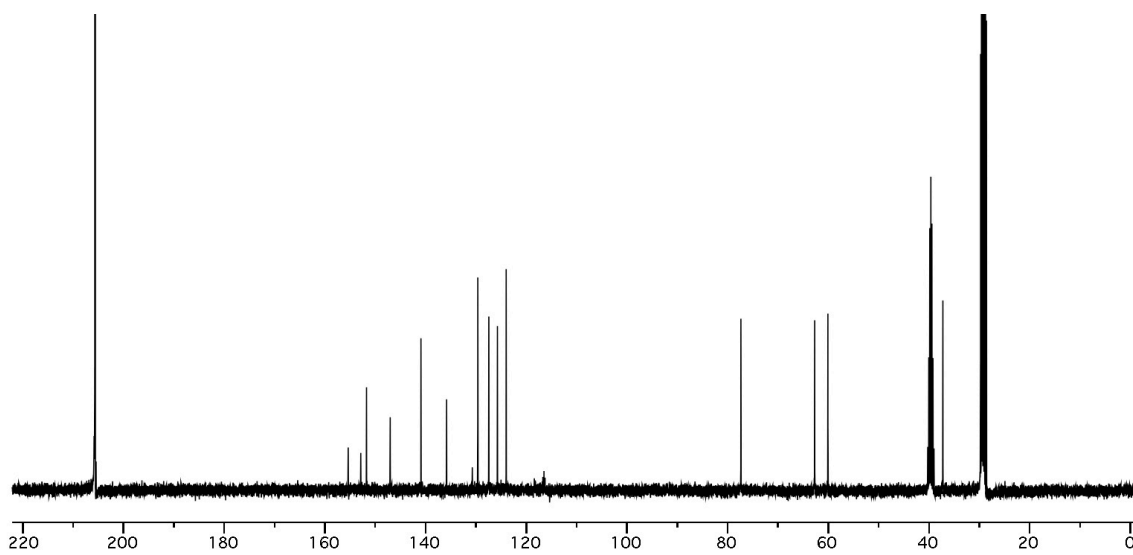
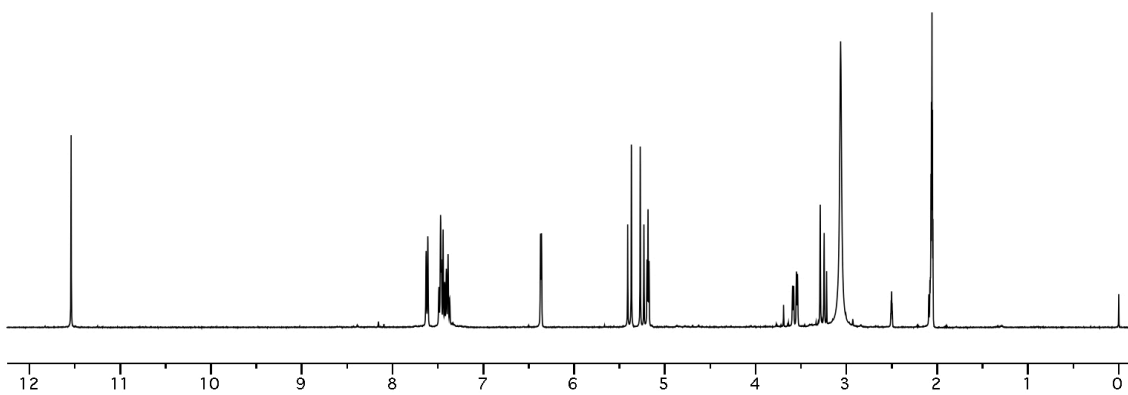
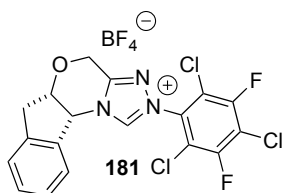
After 30 min a solution of (2*R*,3*R*)-1-nitro-2-phenylhexan-3-ol (**236**) (100 mg, 0.448 mmol, 1.0 equiv) in MeOH (1 mL) was added slowly, followed by additional sodium borohydride (60 mg, 1.56 mmol, 3.5 equiv). The heterogeneous mixture was stirred for 1 h then filtered through celite and concentrated *in vacuo*. The crude solid was dissolved in dichloromethane (20 mL), washed with 10% NaOH, dried and concentrated. This crude residue was then dissolved in THF (5 mL) and triethylamine (0.156 mL, 1.12 mmol, 2.5 equiv) was added. The solution was cooled to 0 °C at which point 4-bromobenzoyl chloride (103 mg, 0.470 mmol, 1.05 equiv) was added. After allowing the reaction to warm to room temperature, water (10 mL) and dichloromethane (10 mL) were added and the organic layer separated. The aqueous layer was extracted with dichloromethane (2 x 10 mL) and the combined organic extracts dried (Na₂SO₄) and concentrated to yield a solid. Trituration with ether, yielded the desired product (136 mg, 81%)

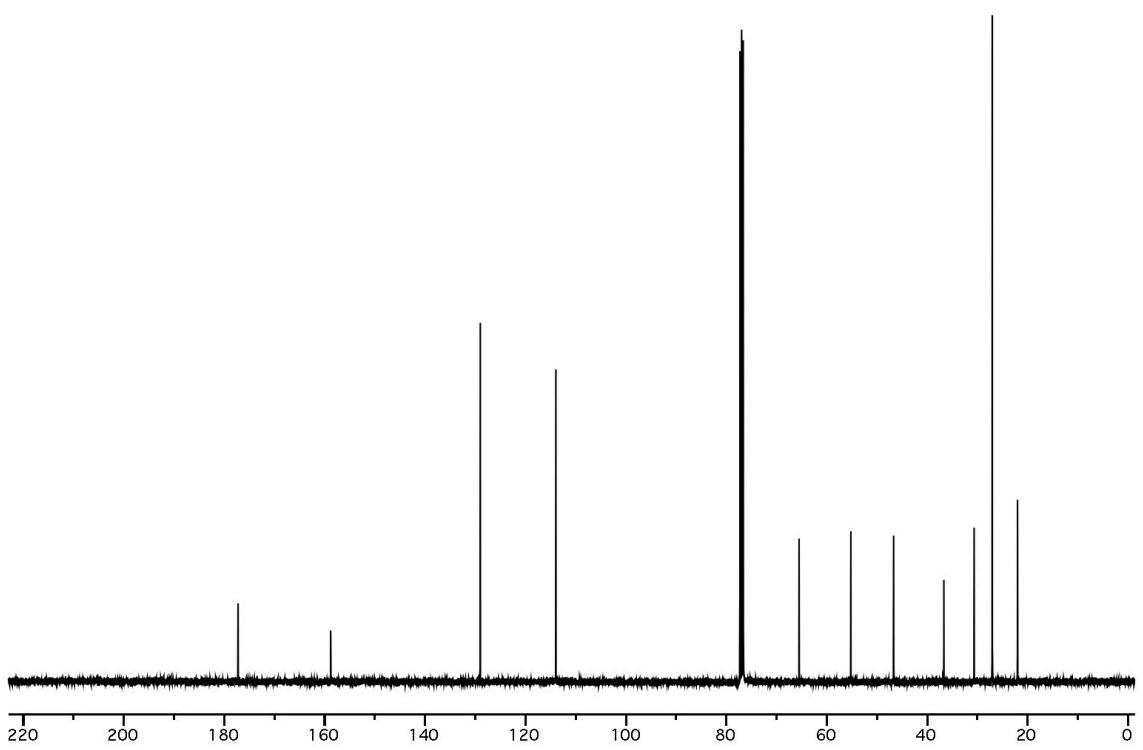
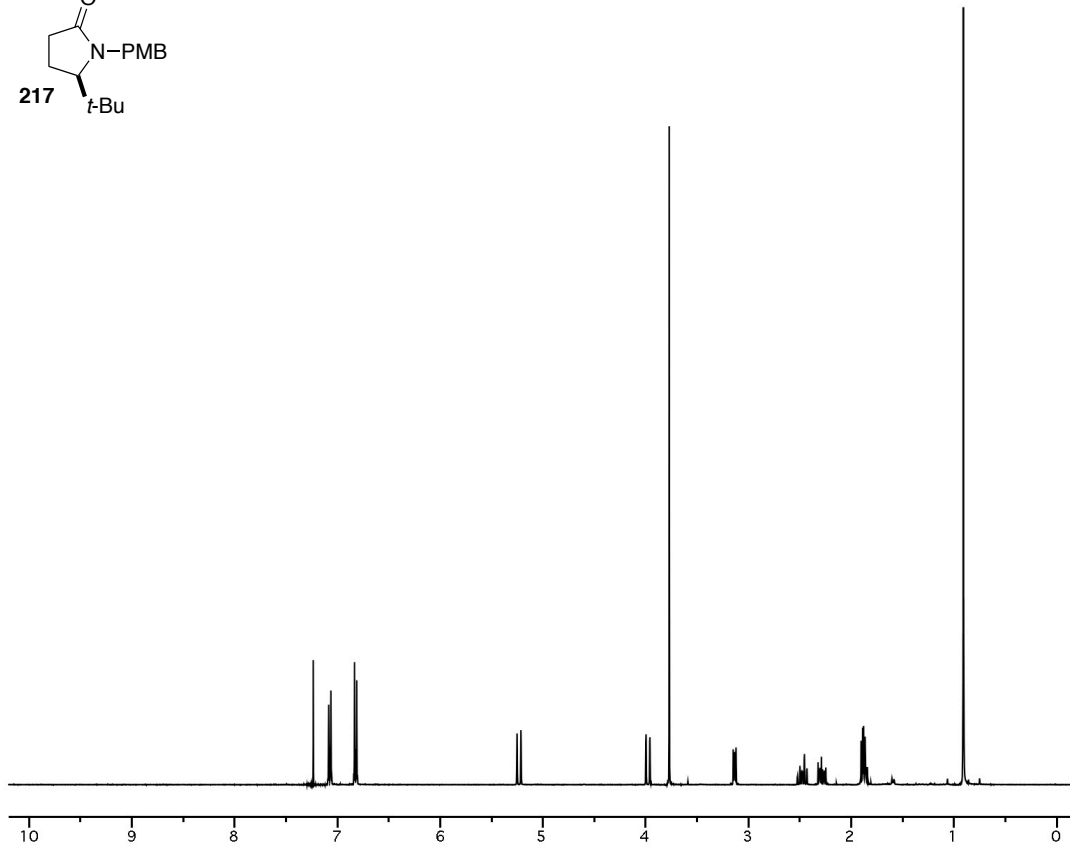
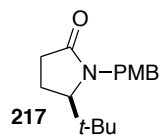
as a white solid. $R_f = 0.17$ (1:1 EtOAc:hex); 98% ee; $[\alpha]_D^{21} = +17.0$ ($c = 0.005$ g/ml, acetone); HPLC analysis – Chiracel IA column, 90:10 hexanes/*iso*-propanol, 1.0 mL/min. Major: 12.92 min, minor: 25.34 min; **m.p.** (°C): 149-151; **^1H NMR** (400 MHz, acetone): δ 8.11 (bs, 1H), 7.81 (m, 2H), 7.65 (m, 2H), 7.40 (m, 2H), 7.28 (m, 2H), 7.21 (m, 1H), 4.07 (dd, $J = 13.5, 9.6$ Hz, 1H), 3.90 (m, 1H), 3.47 (dd, $J = 13.5, 9.6$ Hz, 1H), 2.92 (ddd, $J = 9.5, 6.2, 3.2$ Hz, 1H), 2.84 (bs, 1H), 1.44 (m, 1H), 1.28 (m, 1H), 1.16 (m, 2H), 0.78 (t, $J = 7.3$ Hz, 3H); **^{13}C NMR** (100 MHz, CDCl_3): δ 167.3, 141.0, 134.4, 132.1, 130.1, 129.8, 128.5, 127.1, 125.9, 70.6, 51.8, 43.1, 37.6, 19.9, 14.1; **IR** (NaCl, neat) 3181, 3025, 2948, 2930, 2467, 2364, 1624, 1563, 1456, 1348, 1071 cm^{-1} ; **HRMS** (ESI+) calcd for $\text{C}_{19}\text{H}_{23}\text{BrNO}_2$, 375.0834. Found 375.0830.

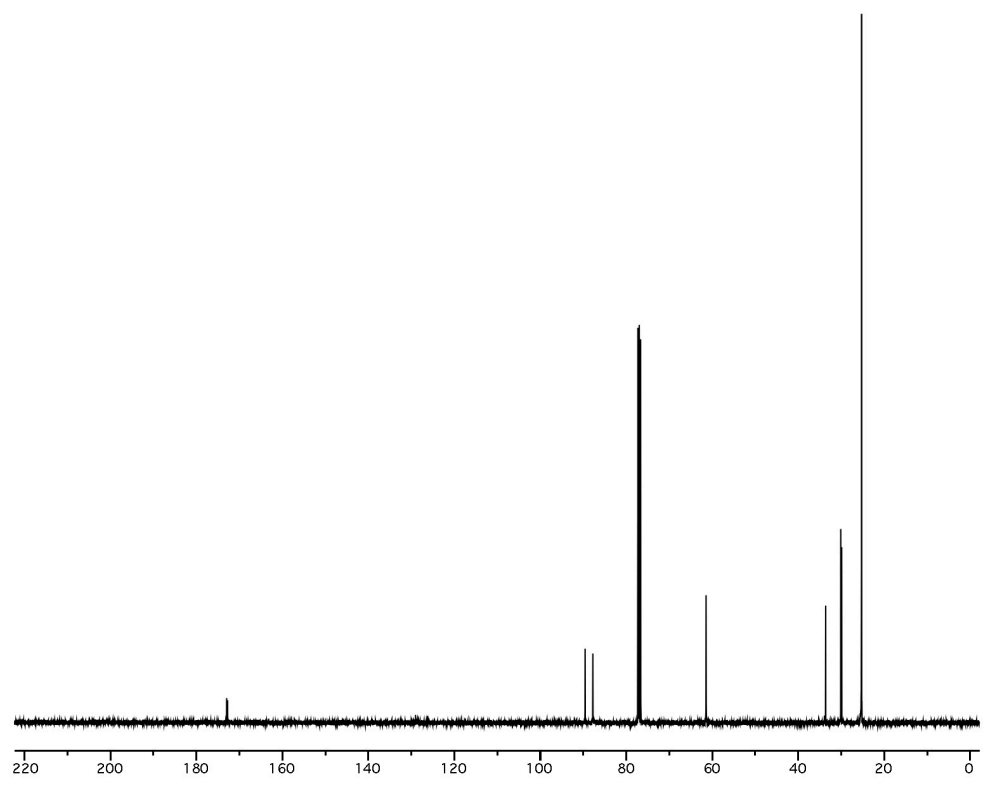
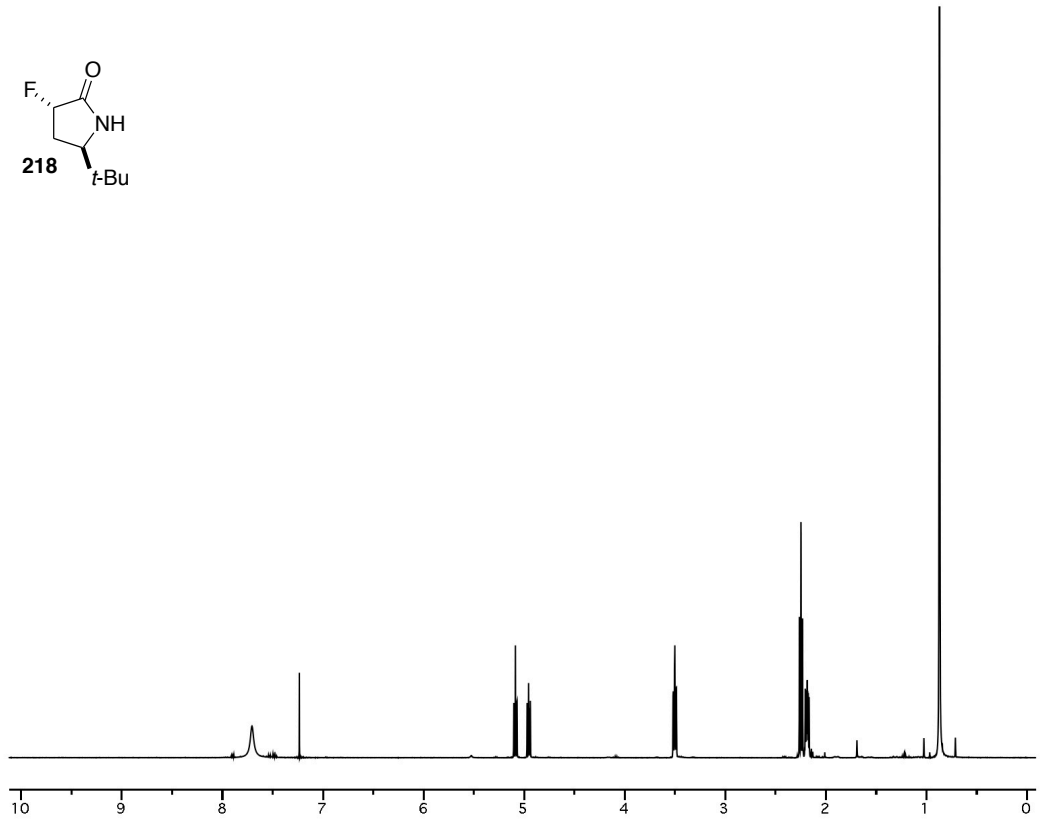
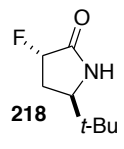


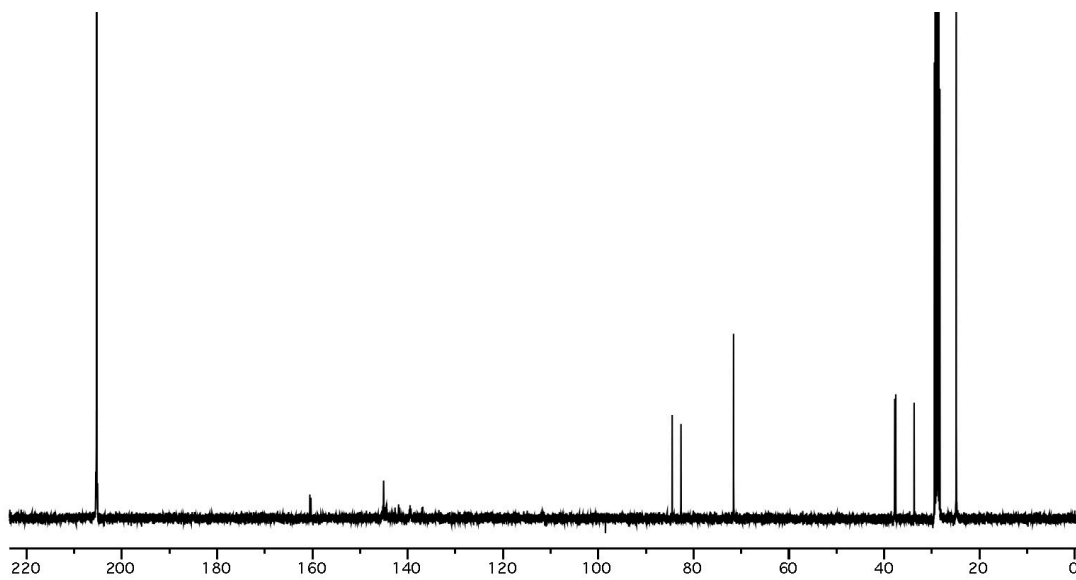
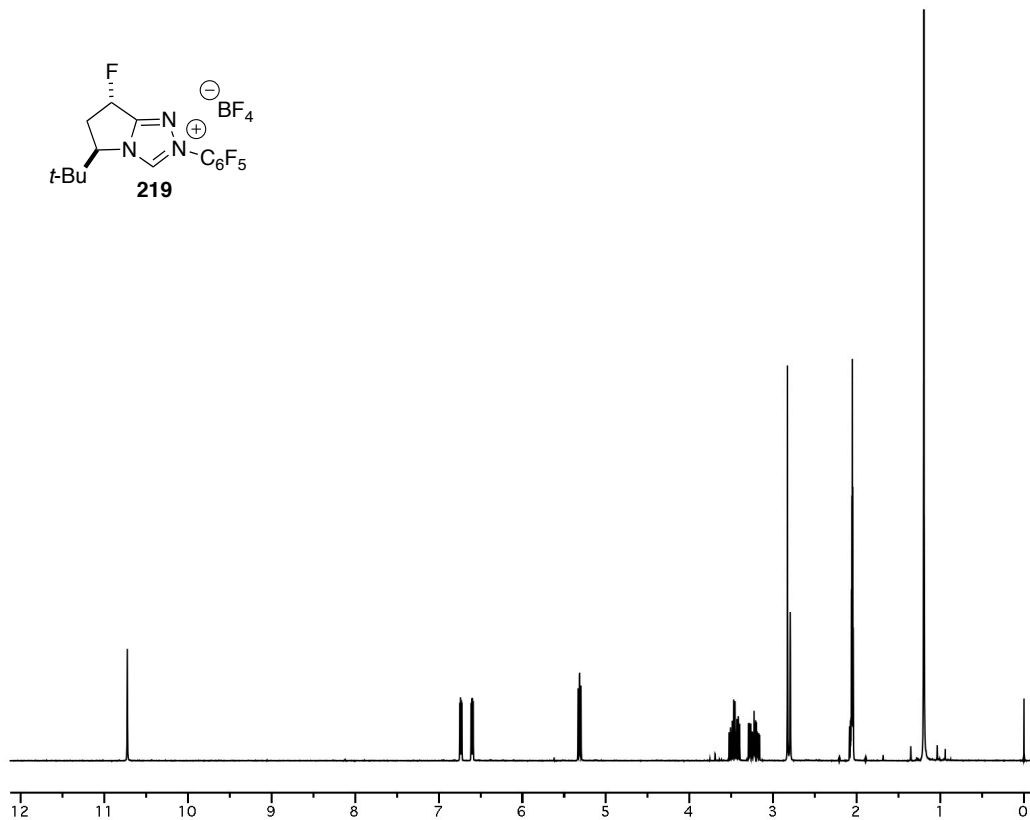
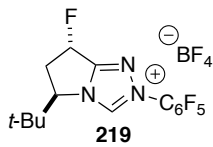
To a solution of the crude amino alcohol in dichloromethane (as described above) was added (–)-Camphor-10-sulfonic acid (0.90 equiv). Slow evaporation of the solvent provided the salt as colorless needles.

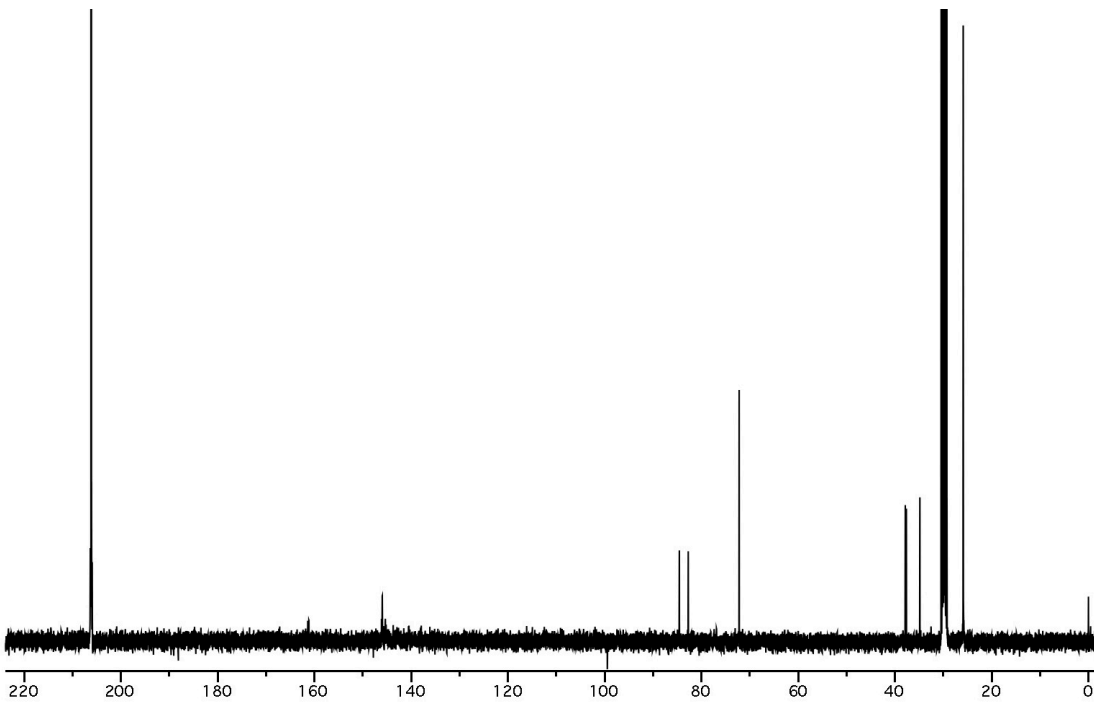
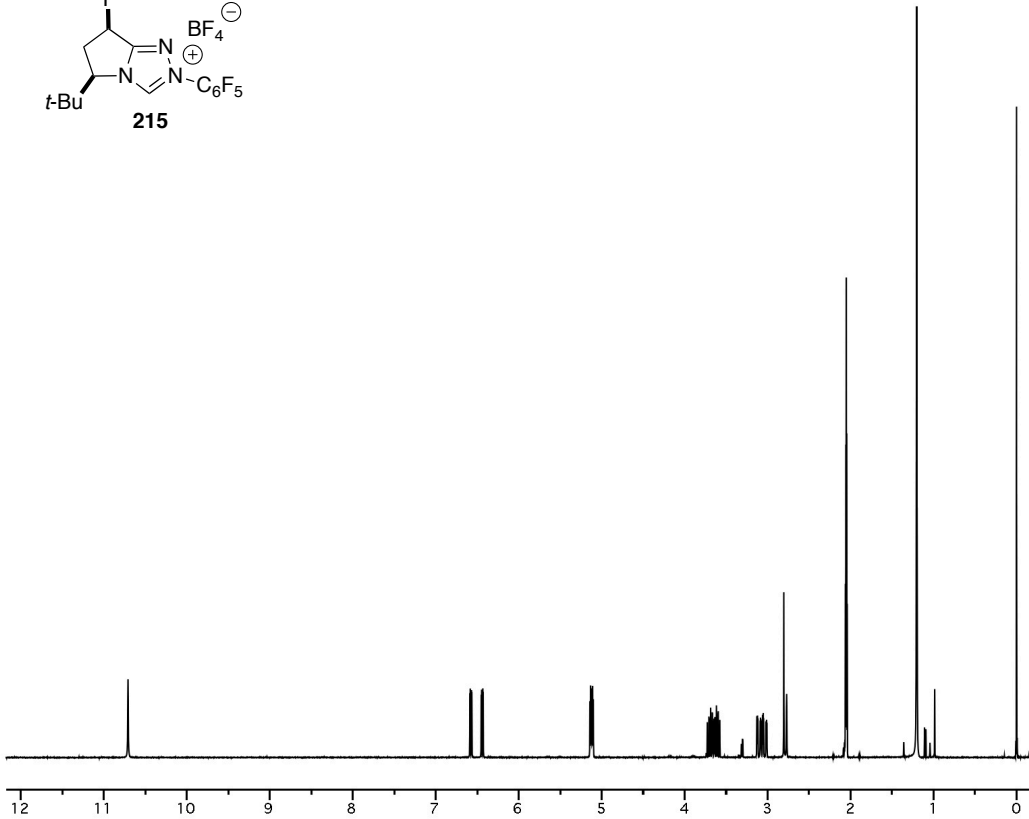
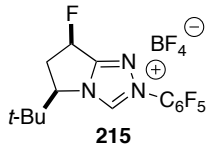
^1H and ^{13}C NMR Spectra

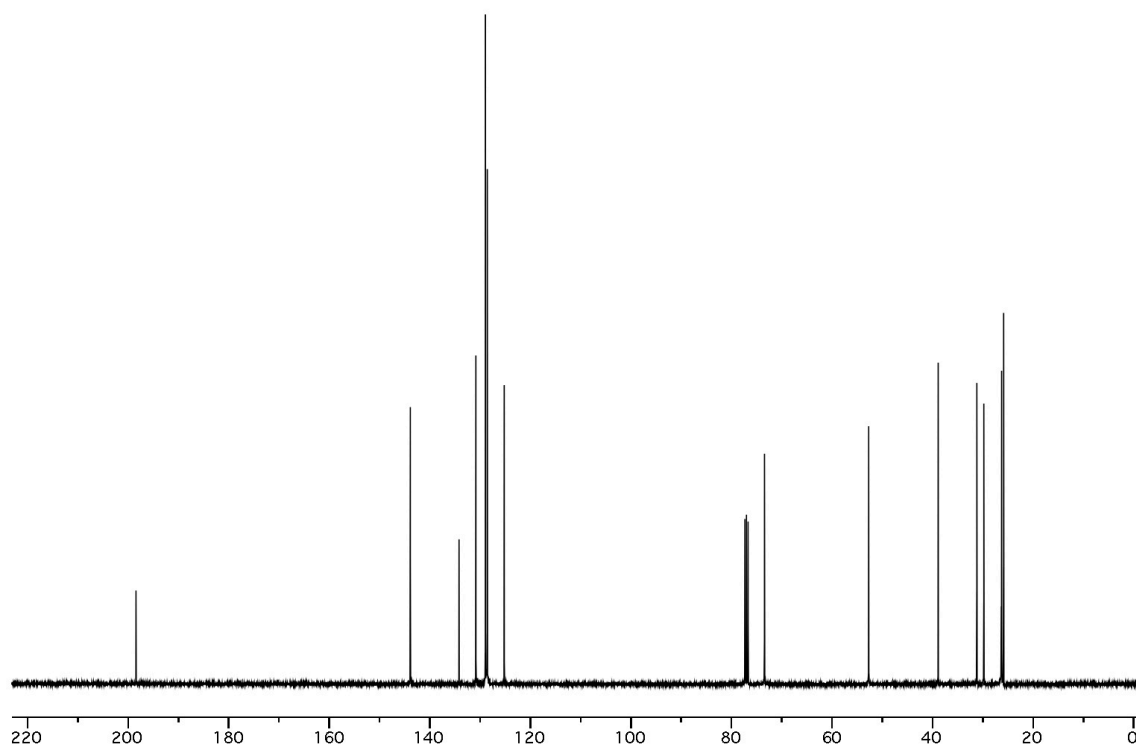
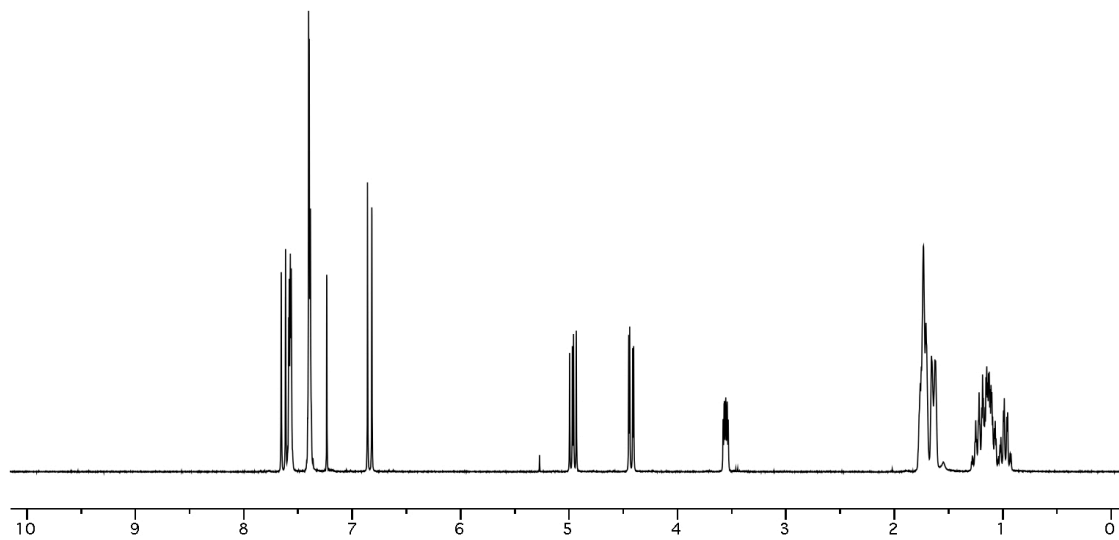
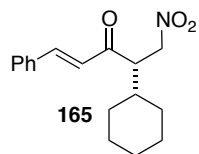


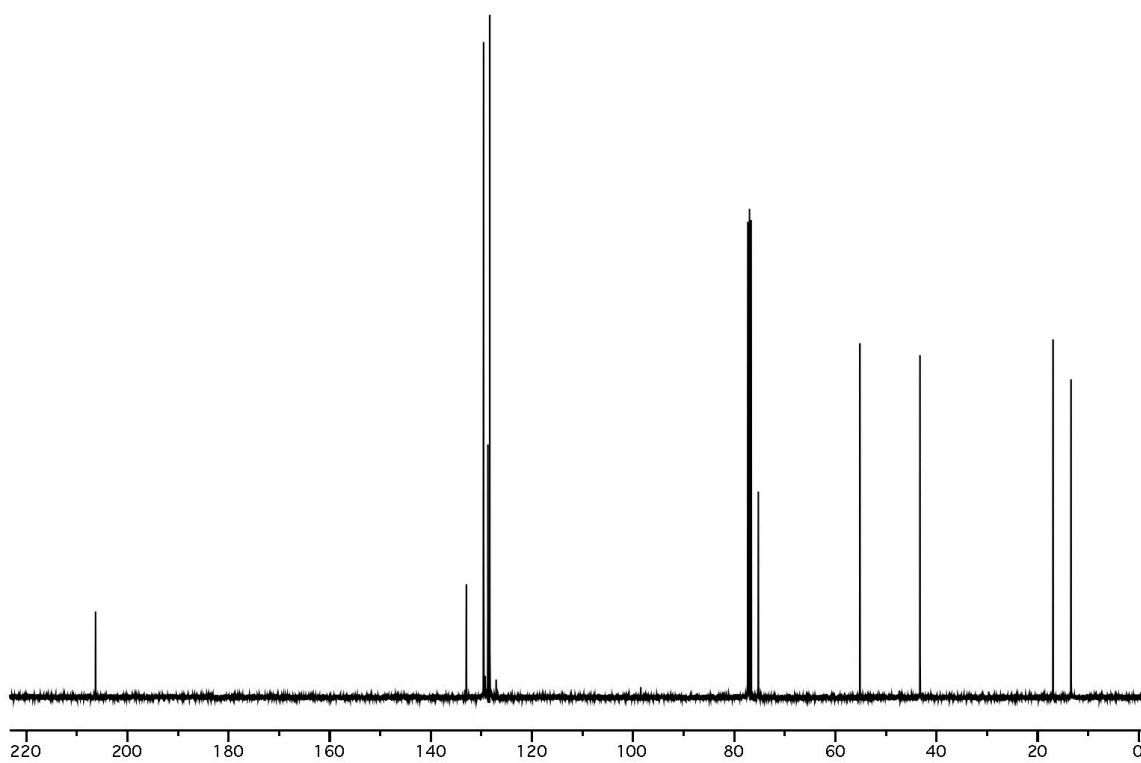
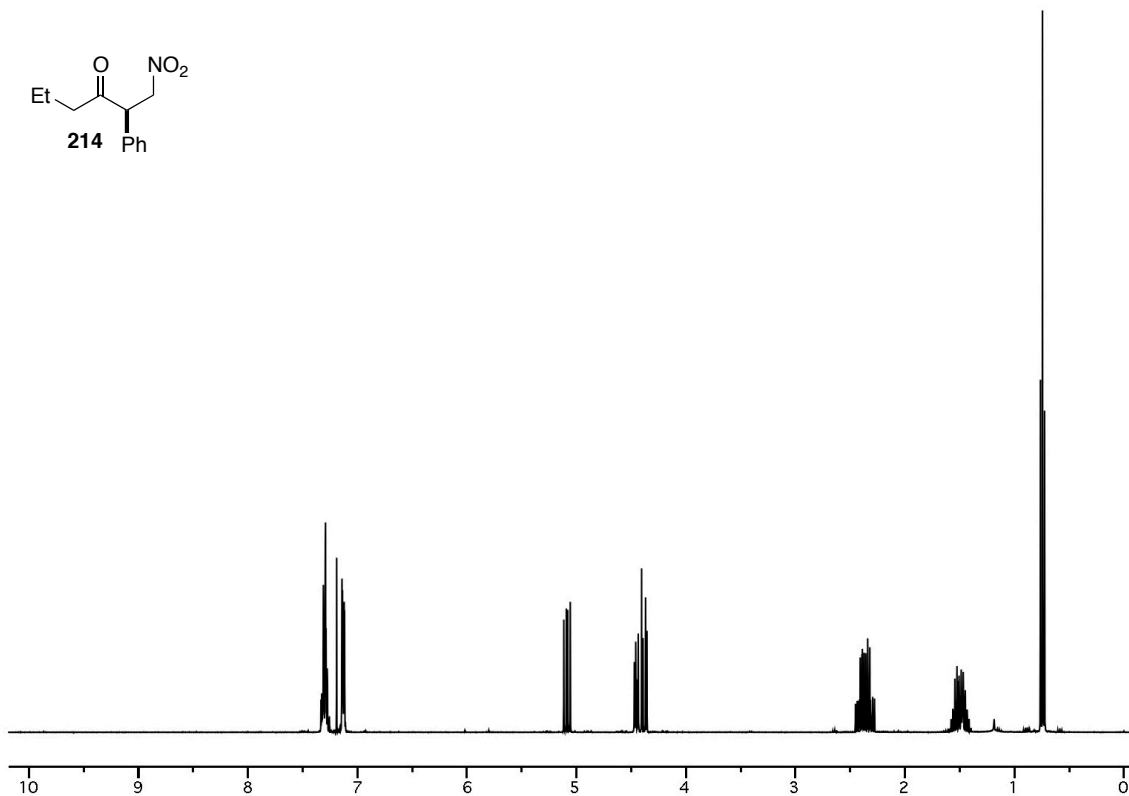
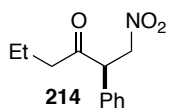


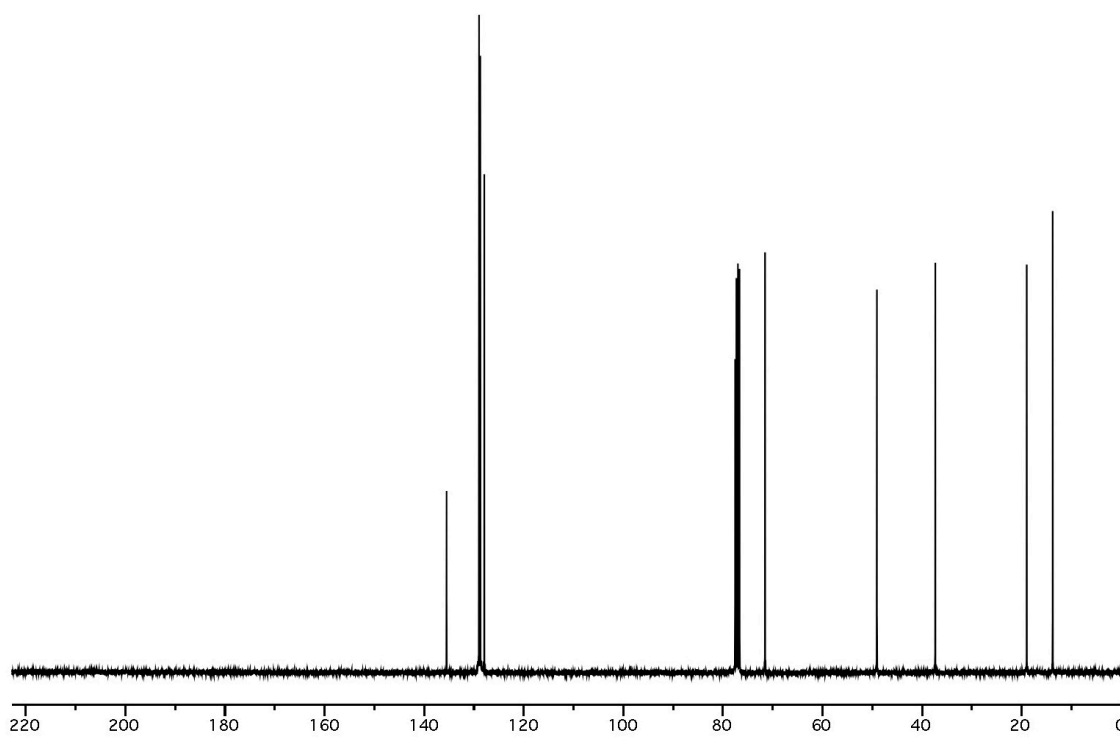
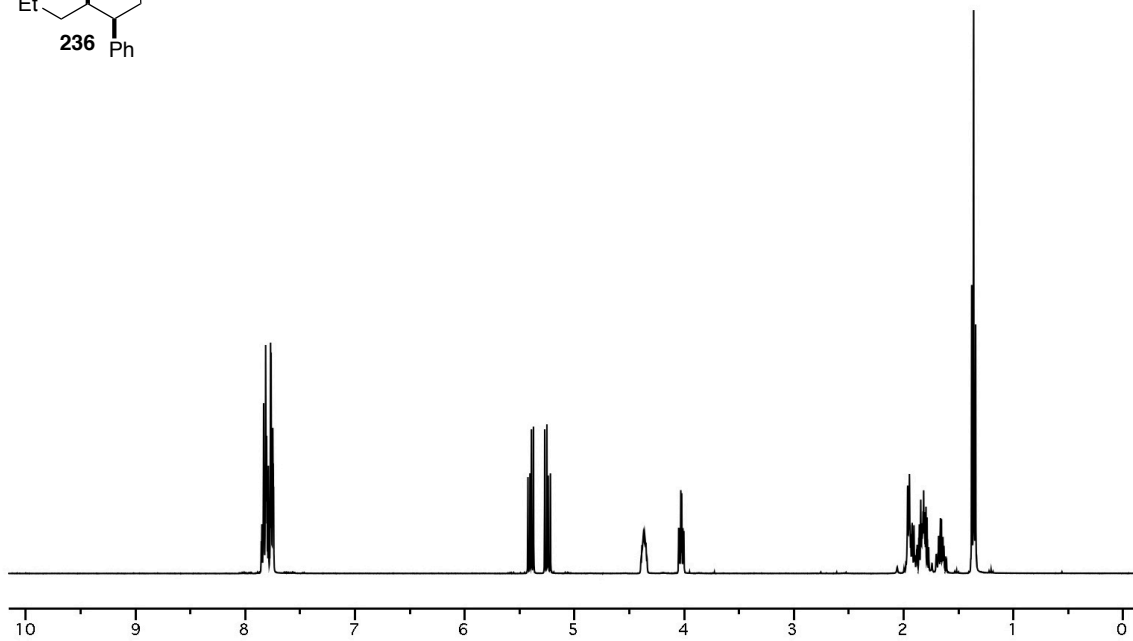
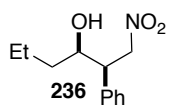


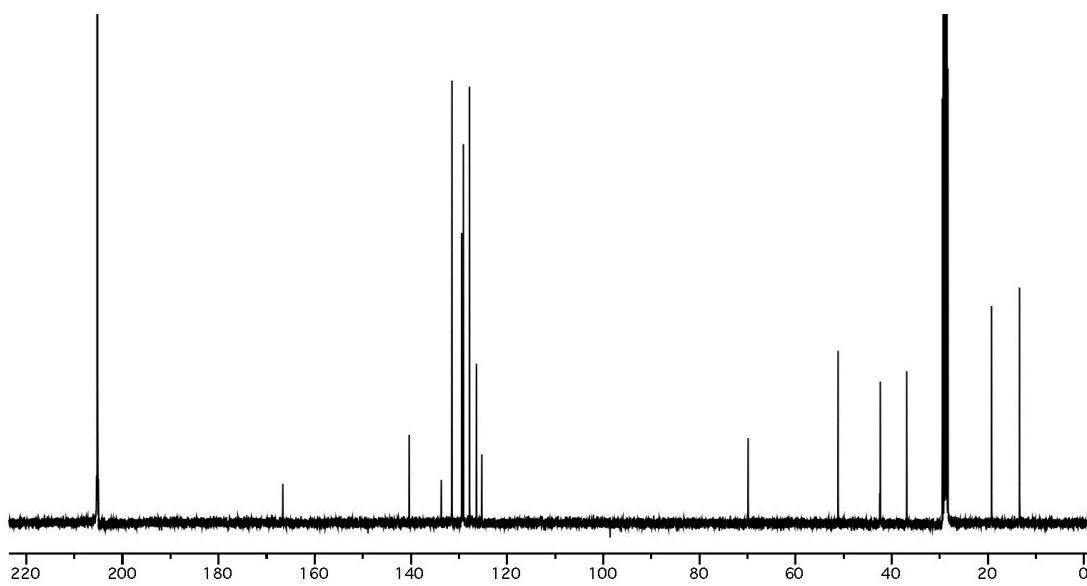
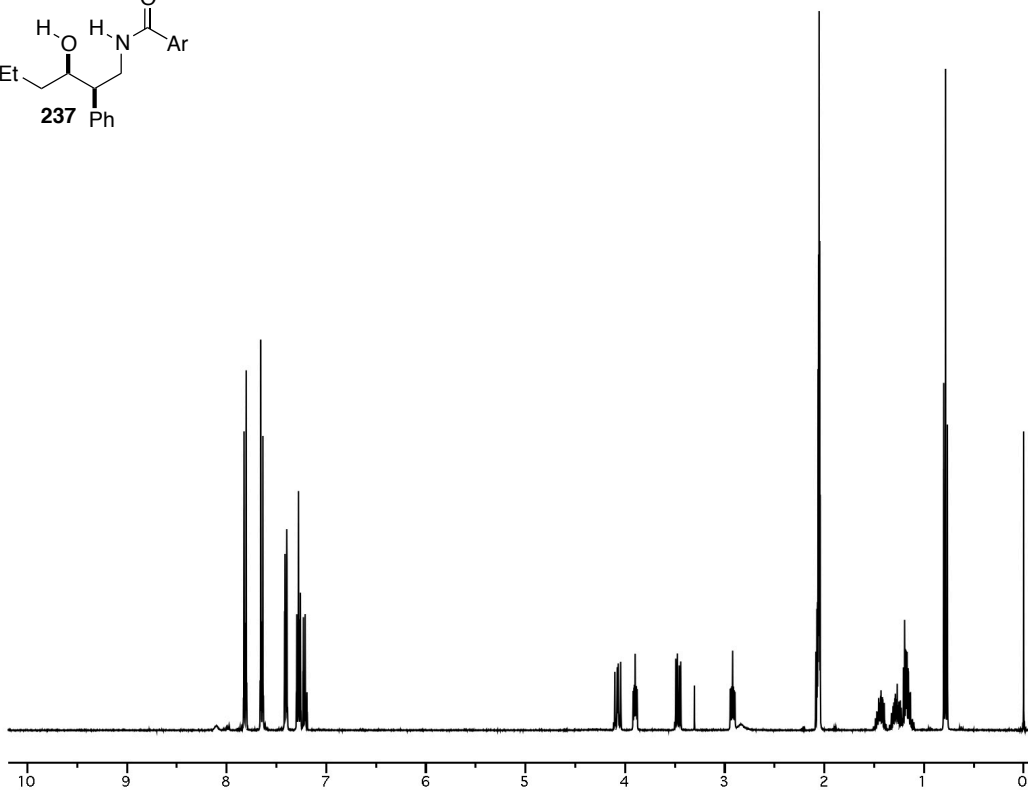
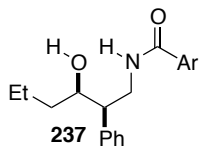












Crystallographic Data

Table A2.1 Crystal data and structure refinement for (167).

Identification code	rovis101_0m	
Empirical formula	C ₁₇ H ₂₀ BrNO ₃	
Formula weight	366.25	
Temperature	120 K	
Wavelength	0.71073 Å	
Crystal system	Orthorhombic	
Space group	<i>P</i> 2 ₁ 2 ₁ 2 ₁	
Unit cell dimensions	<i>a</i> = 5.8072(3) Å	α = 90°
	<i>b</i> = 12.3826(5) Å	β = 90°
	<i>c</i> = 22.3700(9) Å	γ = 90°
Volume	1608.59(12) Å ³	
<i>Z</i>	4	
Density (calculated)	1.512 Mg/m ³	
Absorption coefficient	2.567 mm ⁻¹	
F(000)	752	
Crystal size	0.25 x 0.22 x 0.08 mm ³	
Theta range for data collection	1.82 to 33.31°	
Index ranges	-8 ≤ <i>h</i> ≤ 8, -19 ≤ <i>k</i> ≤ 19, -34 ≤ <i>l</i> ≤ 34	
Reflections collected	43252	
Independent reflections	6182 [R(int) = 0.0569]	
Completeness to theta = 33.31°	99.8 %	
Absorption correction	Semi-empirical from equivalents	
Max. and min. transmission	0.8209 and 0.5628	
Refinement method	Full-matrix least-squares on F ²	
Data / restraints / parameters	6182 / 0 / 200	
Goodness-of-fit on F ²	1.179	
Final R indices [I > 2σ(I)]	R1 = 0.0379, wR2 = 0.0931	
R indices (all data)	R1 = 0.0619, wR2 = 0.1594	
Absolute structure parameter	-0.003(11)	
Largest diff. peak and hole	1.320 and -1.802 e.Å ⁻³	

Table A2.2 Atomic coordinates ($\times 10^4$) and equivalent isotropic displacement parameters ($\text{\AA}^2 \times 10^3$) for (167). $U(\text{eq})$ is defined as one third of the trace of the orthogonalized U^{ij} tensor.

x	y	z	U(eq)	
Br(1)	7169(1)	254(1)	-374(1)	24(1)
C(1)	6344(6)	1143(2)	280(1)	15(1)
C(2)	4216(6)	992(3)	560(1)	17(1)
C(3)	3635(6)	1669(2)	1032(1)	16(1)
C(4)	5115(5)	2489(2)	1226(1)	13(1)
C(5)	7239(6)	2625(2)	932(1)	16(1)
C(6)	7857(6)	1954(2)	459(1)	16(1)
C(7)	4390(6)	3138(2)	1742(1)	15(1)
C(8)	5602(6)	3918(2)	2011(1)	15(1)
C(9)	4865(5)	4510(2)	2547(1)	13(1)
C(10)	2629(5)	4230(2)	2875(1)	12(1)
C(11)	3196(5)	3571(2)	3448(1)	13(1)
C(12)	998(6)	3288(3)	3799(1)	18(1)
C(13)	1541(6)	2617(3)	4354(2)	20(1)
C(14)	2896(7)	1601(3)	4198(1)	22(1)
C(15)	5087(7)	1887(3)	3858(2)	24(1)
C(16)	4551(6)	2545(3)	3296(2)	18(1)
C(17)	1415(5)	5262(2)	3056(1)	14(1)
N(1)	942(5)	5999(2)	2543(1)	16(1)
O(1)	6083(4)	5231(2)	2746(1)	19(1)
O(2)	999(5)	5633(2)	2032(1)	24(1)
O(3)	471(5)	6943(2)	2660(1)	24(1)

Table A2.3 Bond lengths [\AA] and angles [$^\circ$] for (**167**).

Br(1)-C(1)	1.893(3)	C(7)-C(8)-C(9)	125.0(3)
C(1)-C(6)	1.393(5)	O(1)-C(9)-C(8)	119.5(3)
C(1)-C(2)	1.398(5)	O(1)-C(9)-C(10)	118.8(3)
C(2)-C(3)	1.391(4)	C(8)-C(9)-C(10)	121.7(3)
C(3)-C(4)	1.399(4)	C(17)-C(10)-C(9)	109.4(2)
C(4)-C(5)	1.408(5)	C(17)-C(10)-C(11)	108.8(2)
C(4)-C(7)	1.468(4)	C(9)-C(10)-C(11)	109.5(2)
C(5)-C(6)	1.392(4)	C(16)-C(11)-C(12)	110.5(2)
C(7)-C(8)	1.338(4)	C(16)-C(11)-C(10)	111.2(2)
C(8)-C(9)	1.470(4)	C(12)-C(11)-C(10)	111.4(2)
C(9)-O(1)	1.223(4)	C(13)-C(12)-C(11)	111.6(3)
C(9)-C(10)	1.531(4)	C(14)-C(13)-C(12)	111.6(3)
C(10)-C(17)	1.514(4)	C(15)-C(14)-C(13)	110.7(3)
C(10)-C(11)	1.554(4)	C(14)-C(15)-C(16)	111.3(3)
C(11)-C(16)	1.532(4)	C(15)-C(16)-C(11)	111.3(3)
C(11)-C(12)	1.539(4)	N(1)-C(17)-C(10)	113.4(2)
C(12)-C(13)	1.528(5)	O(3)-N(1)-O(2)	123.7(3)
C(13)-C(14)	1.524(5)	O(3)-N(1)-C(17)	117.3(3)
C(14)-C(15)	1.524(5)	O(2)-N(1)-C(17)	119.0(3)
C(15)-C(16)	1.530(5)		
C(17)-N(1)	1.492(4)		
N(1)-O(3)	1.228(3)		
N(1)-O(2)	1.230(4)		
C(6)-C(1)-C(2)	121.7(3)		
C(6)-C(1)-Br(1)	118.8(2)		
C(2)-C(1)-Br(1)	119.5(2)		
C(3)-C(2)-C(1)	118.3(3)		
C(2)-C(3)-C(4)	121.6(3)		
C(3)-C(4)-C(5)	118.7(3)		
C(3)-C(4)-C(7)	117.7(3)		
C(5)-C(4)-C(7)	123.5(3)		
C(6)-C(5)-C(4)	120.6(3)		
C(5)-C(6)-C(1)	119.1(3)		
C(8)-C(7)-C(4)	126.7(3)		

Symmetry transformations used to generate equivalent atoms:

Table A2.4 Anisotropic displacement parameters ($\text{\AA}^2 \times 10^3$) for (167). The anisotropic displacement factor exponent takes the form: $-2\pi^2 [h^2 a^{*2} U^{11} + \dots + 2 h k a^* b^* U^{12}]$

	U^{11}	U^{22}	U^{33}	U^{23}	U^{13}	U^{12}
Br(1)	30(1)	20(1)	22(1)	-7(1)	8(1)	2(1)
C(1)	19(1)	14(1)	13(1)	0(1)	2(1)	4(1)
C(2)	19(2)	16(1)	17(1)	-1(1)	2(1)	-2(1)
C(3)	16(1)	17(1)	14(1)	2(1)	4(1)	-2(1)
C(4)	12(1)	14(1)	12(1)	1(1)	1(1)	2(1)
C(5)	15(1)	17(1)	16(1)	0(1)	2(1)	0(1)
C(6)	15(1)	17(1)	16(1)	2(1)	4(1)	1(1)
C(7)	14(1)	16(1)	13(1)	1(1)	2(1)	2(1)
C(8)	13(1)	18(1)	14(1)	1(1)	2(1)	0(1)
C(9)	10(1)	13(1)	16(1)	1(1)	0(1)	-1(1)
C(10)	10(1)	12(1)	13(1)	-1(1)	0(1)	1(1)
C(11)	13(1)	13(1)	12(1)	1(1)	-1(1)	1(1)
C(12)	15(2)	23(1)	16(1)	4(1)	3(1)	4(1)
C(13)	22(2)	25(2)	13(1)	6(1)	6(1)	3(1)
C(14)	23(2)	22(1)	20(1)	9(1)	1(1)	2(1)
C(15)	21(2)	28(2)	23(2)	11(1)	4(1)	11(1)
C(16)	18(2)	19(1)	16(1)	4(1)	3(1)	7(1)
C(17)	14(1)	14(1)	13(1)	0(1)	0(1)	2(1)
N(1)	11(1)	16(1)	22(1)	4(1)	0(1)	1(1)
O(1)	16(1)	21(1)	22(1)	-4(1)	1(1)	-6(1)
O(2)	25(1)	29(1)	17(1)	5(1)	2(1)	6(1)
O(3)	21(1)	14(1)	37(1)	4(1)	-1(1)	3(1)

Table A2.5 Hydrogen coordinates ($\times 10^4$) and isotropic displacement parameters ($\text{\AA}^2 \times 10^3$) for (167).

	x	y	z	U(eq)
H(2)	3214	452	433	21
H(3)	2229	1574	1224	19
H(5)	8238	3168	1055	19
H(6)	9261	2046	266	19
H(7)	2939	2991	1898	18
H(8)	7019	4099	1846	18
H(10)	1628	3805	2613	14
H(11)	4167	4021	3705	15
H(12A)	228	3949	3918	21
H(12B)	-42	2886	3542	21
H(13A)	2427	3050	4633	24
H(13B)	114	2413	4549	24
H(14A)	3293	1218	4562	26
H(14B)	1949	1129	3955	26
H(15A)	5883	1229	3746	29
H(15B)	6099	2301	4116	29
H(16A)	3661	2106	3021	21
H(16B)	5980	2741	3100	21
H(17A)	-32	5079	3247	17
H(17B)	2356	5641	3346	17

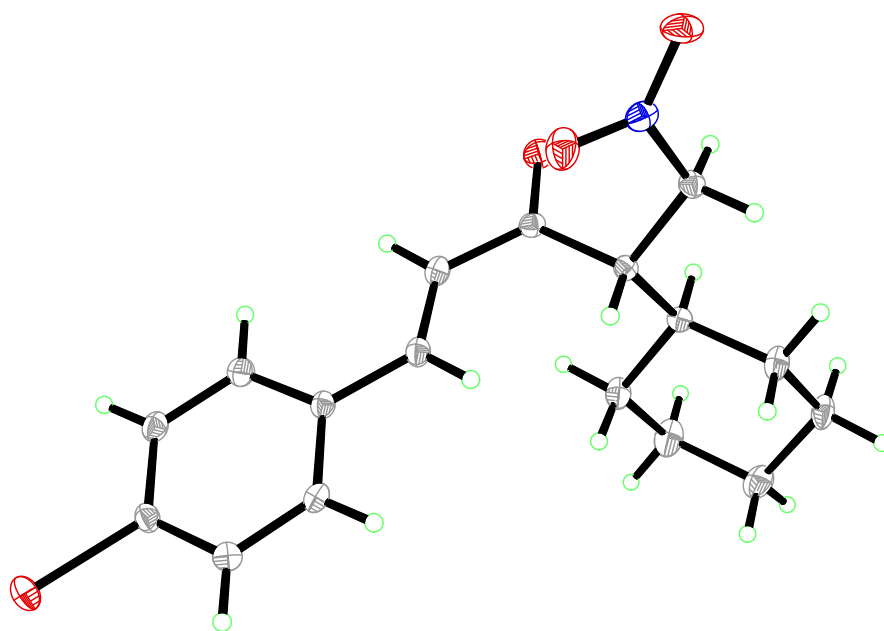


Figure A2.1 Thermal plot of (167). Ellipsoids drawn at the 50% probability level.

Table A2.6 Crystal data and structure refinement for (237).

Identification code	rovis126	
Empirical formula	$C_{22}H_{35}NO_5S$	
Formula weight	425.57	
Temperature	120 K	
Wavelength	0.71073 Å	
Crystal system	Monoclinic	
Space group	$P2_1$	
Unit cell dimensions	$a = 9.2006(6)$ Å	$\alpha = 90^\circ$.
	$b = 7.7075(5)$ Å	$\beta = 98.189(3)^\circ$.
	$c = 16.4397(10)$ Å	$\gamma = 90^\circ$.
Volume	1153.91(13) Å ³	
Z	2	

Density (calculated)	1.225 Mg/m ³
Absorption coefficient	0.171 mm ⁻¹
F(000)	460
Crystal size	0.24 x 0.19 x 0.06 mm ³
Theta range for data collection	2.24 to 33.25°.
Index ranges	-14<=h<=14, -11<=k<=11, -25<=l<=25
Reflections collected	32074
Independent reflections	8539 [R(int) = 0.0400]
Completeness to theta = 33.25°	99.8 %
Absorption correction	Semi-empirical from equivalents
Max. and min. transmission	0.9903 and 0.9607
Refinement method	Full-matrix least-squares on F ²
Data / restraints / parameters	8539 / 1 / 268
Goodness-of-fit on F ²	1.082
Final R indices [I>2sigma(I)]	R1 = 0.0428, wR2 = 0.0989
R indices (all data)	R1 = 0.0590, wR2 = 0.1160
Absolute structure parameter	0.02(5)
Largest diff. peak and hole	0.403 and -0.333 e.Å ⁻³

Table A2.7 Atomic coordinates (x 10⁴) and equivalent isotropic displacement parameters (Å²x 10³) for (237). U(eq) is defined as one third of the trace of the orthogonalized U^{ij} tensor.

	x	y	z	U(eq)
C(1)	5465(2)	8219(2)	1796(1)	16(1)
C(2)	6573(2)	8609(2)	2560(1)	16(1)
C(3)	7577(2)	7058(2)	2860(1)	17(1)
C(4)	8525(2)	7452(2)	3674(1)	20(1)
C(5)	9739(2)	6139(3)	3919(1)	27(1)
C(6)	10526(2)	6449(3)	4785(1)	35(1)
C(7)	5742(2)	9376(2)	3210(1)	23(1)
C(8)	4714(2)	8414(3)	3561(1)	33(1)
C(9)	3939(2)	9209(4)	4139(1)	50(1)
C(10)	4196(3)	10921(4)	4357(1)	53(1)
C(11)	5205(3)	11889(4)	4007(1)	47(1)
C(12)	5974(2)	11113(3)	3437(1)	30(1)

C(13)	10955(2)	7831(2)	9280(1)	20(1)
C(14)	9965(2)	7084(2)	8547(1)	15(1)
C(15)	10301(2)	7538(2)	7666(1)	20(1)
C(16)	8848(2)	7119(2)	7097(1)	25(1)
C(17)	7859(2)	6422(2)	7698(1)	20(1)
C(18)	8461(2)	4631(2)	7978(1)	24(1)
C(19)	9859(2)	5113(2)	8543(1)	19(1)
C(20)	8300(2)	7569(2)	8471(1)	18(1)
C(21)	7977(2)	9501(3)	8314(1)	31(1)
C(22)	7599(2)	7021(3)	9220(1)	31(1)
N(1)	6176(1)	7896(2)	1050(1)	16(1)
O(1)	6747(1)	5517(2)	2957(1)	26(1)
O(2)	12983(1)	9497(2)	8645(1)	26(1)
O(3)	13573(1)	8350(2)	10024(1)	29(1)
O(4)	13333(1)	6419(1)	8844(1)	22(1)
O(5)	10698(1)	4093(2)	8930(1)	26(1)
S(1)	12866(1)	8011(1)	9191(1)	16(1)

Table A2.8 Bond lengths [Å] and angles [°] for (237).

C(1)-N(1)	1.4901(17)	C(13)-C(14)	1.5168(19)
C(1)-C(2)	1.5307(19)	C(13)-S(1)	1.7906(16)
C(2)-C(7)	1.519(2)	C(14)-C(19)	1.522(2)
C(2)-C(3)	1.548(2)	C(14)-C(15)	1.5631(19)
C(3)-O(1)	1.4333(19)	C(14)-C(20)	1.564(2)
C(3)-C(4)	1.521(2)	C(15)-C(16)	1.552(2)
C(4)-C(5)	1.519(2)	C(16)-C(17)	1.533(2)
C(5)-C(6)	1.522(2)	C(17)-C(18)	1.534(2)
C(7)-C(8)	1.391(3)	C(17)-C(20)	1.554(2)
C(7)-C(12)	1.398(3)	C(18)-C(19)	1.521(2)
C(8)-C(9)	1.407(3)	C(19)-O(5)	1.2155(19)
C(9)-C(10)	1.379(4)	C(20)-C(22)	1.528(2)
C(10)-C(11)	1.379(4)	C(20)-C(21)	1.533(2)
C(11)-C(12)	1.387(3)	O(2)-S(1)	1.4685(12)

O(3)-S(1)	1.4532(11)	C(19)-C(14)-C(20)	100.19(12)
O(4)-S(1)	1.4440(12)	C(15)-C(14)-C(20)	101.17(11)
N(1)-C(1)-C(2)	112.92(12)	C(16)-C(15)-C(14)	104.13(12)
C(7)-C(2)-C(1)	108.13(12)	C(17)-C(16)-C(15)	102.97(12)
C(7)-C(2)-C(3)	114.49(12)	C(16)-C(17)-C(18)	106.65(14)
C(1)-C(2)-C(3)	113.98(12)	C(16)-C(17)-C(20)	102.56(13)
O(1)-C(3)-C(4)	108.37(12)	C(18)-C(17)-C(20)	103.01(12)
O(1)-C(3)-C(2)	111.83(13)	C(19)-C(18)-C(17)	101.63(13)
C(4)-C(3)-C(2)	111.53(12)	O(5)-C(19)-C(18)	125.42(15)
C(5)-C(4)-C(3)	114.11(13)	O(5)-C(19)-C(14)	127.46(15)
C(4)-C(5)-C(6)	112.21(14)	C(18)-C(19)-C(14)	107.09(13)
C(8)-C(7)-C(12)	119.13(16)	C(22)-C(20)-C(21)	108.04(15)
C(8)-C(7)-C(2)	121.64(16)	C(22)-C(20)-C(17)	114.22(14)
C(12)-C(7)-C(2)	119.19(16)	C(21)-C(20)-C(17)	113.13(13)
C(7)-C(8)-C(9)	119.2(2)	C(22)-C(20)-C(14)	113.03(12)
C(10)-C(9)-C(8)	120.5(2)	C(21)-C(20)-C(14)	114.19(14)
C(9)-C(10)-C(11)	120.64(19)	C(17)-C(20)-C(14)	93.91(11)
C(10)-C(11)-C(12)	119.1(2)	O(4)-S(1)-O(3)	114.00(7)
C(11)-C(12)-C(7)	121.4(2)	O(4)-S(1)-O(2)	111.69(7)
C(14)-C(13)-S(1)	116.77(10)	O(3)-S(1)-O(2)	111.92(7)
C(13)-C(14)-C(19)	114.38(13)	O(4)-S(1)-C(13)	108.51(8)
C(13)-C(14)-C(15)	118.38(12)	O(3)-S(1)-C(13)	104.50(7)
C(19)-C(14)-C(15)	103.93(12)	O(2)-S(1)-C(13)	105.53(8)
C(13)-C(14)-C(20)	116.28(12)		

Symmetry transformations used to generate equivalent atoms:

Table A2.9 Anisotropic displacement parameters ($\text{\AA}^2 \times 10^3$) for (**237**). The anisotropic displacement factor exponent takes the form: $-2\pi^2 [h^2 a^{*2} U^{11} + \dots + 2 h k a^* b^* U^{12}]$

	U ¹¹	U ²²	U ³³	U ²³	U ¹³	U ¹²
C(1)	14(1)	18(1)	16(1)	1(1)	1(1)	0(1)
C(2)	17(1)	15(1)	15(1)	1(1)	1(1)	1(1)
C(3)	17(1)	16(1)	18(1)	2(1)	0(1)	0(1)
C(4)	20(1)	22(1)	17(1)	1(1)	-1(1)	4(1)

C(5)	26(1)	30(1)	22(1)	1(1)	-5(1)	8(1)
C(6)	32(1)	42(1)	28(1)	5(1)	-9(1)	8(1)
C(7)	20(1)	33(1)	15(1)	1(1)	-1(1)	10(1)
C(8)	27(1)	48(1)	25(1)	15(1)	9(1)	12(1)
C(9)	31(1)	95(2)	24(1)	22(1)	10(1)	20(1)
C(10)	42(1)	96(2)	19(1)	-12(1)	-2(1)	34(1)
C(11)	39(1)	67(2)	30(1)	-25(1)	-9(1)	23(1)
C(12)	24(1)	38(1)	26(1)	-12(1)	-5(1)	10(1)
C(13)	17(1)	24(1)	17(1)	-3(1)	-1(1)	1(1)
C(14)	14(1)	16(1)	15(1)	0(1)	-1(1)	-1(1)
C(15)	17(1)	25(1)	17(1)	2(1)	0(1)	-4(1)
C(16)	20(1)	34(1)	18(1)	1(1)	-2(1)	-6(1)
C(17)	14(1)	22(1)	22(1)	0(1)	-2(1)	-2(1)
C(18)	17(1)	20(1)	33(1)	-1(1)	-2(1)	-3(1)
C(19)	15(1)	20(1)	22(1)	2(1)	3(1)	-1(1)
C(20)	15(1)	20(1)	19(1)	0(1)	1(1)	2(1)
C(21)	23(1)	24(1)	44(1)	-3(1)	-4(1)	9(1)
C(22)	21(1)	49(1)	25(1)	-2(1)	7(1)	1(1)
N(1)	16(1)	14(1)	16(1)	-2(1)	0(1)	1(1)
O(1)	31(1)	16(1)	30(1)	5(1)	0(1)	-4(1)
O(2)	26(1)	14(1)	37(1)	5(1)	-3(1)	-4(1)
O(3)	21(1)	38(1)	25(1)	-10(1)	-9(1)	5(1)
O(4)	22(1)	13(1)	32(1)	-4(1)	5(1)	1(1)
O(5)	19(1)	20(1)	39(1)	10(1)	2(1)	2(1)
S(1)	15(1)	12(1)	19(1)	-2(1)	-4(1)	1(1)

Table A2.10 Hydrogen coordinates ($\times 10^4$) and isotropic displacement parameters ($\text{\AA}^2 \times 10^3$) for (237).

	x	y	z	U(eq)
H(1D)	4894	7207	1902	20
H(1E)	4795	9191	1691	20
H(2)	7217	9528	2405	19

H(3)	8226	6829	2448	21
H(4A)	8964	8589	3640	24
H(4B)	7901	7499	4102	24
H(5A)	10445	6203	3535	33
H(5B)	9322	4981	3887	33
H(6A)	10929	7600	4823	52
H(6B)	11305	5619	4908	52
H(6C)	9843	6323	5171	52
H(8)	4540	7259	3415	39
H(9)	3248	8575	4376	59
H(10)	3683	11428	4744	63
H(11)	5368	13047	4151	56
H(12)	6657	11761	3202	36
H(13A)	10860	7115	9755	24
H(13B)	10594	8978	9389	24
H(15A)	10556	8753	7628	24
H(15B)	11102	6835	7523	24
H(16A)	8432	8153	6819	30
H(16B)	9001	6252	6690	30
H(17)	6808	6437	7486	24
H(18A)	7783	4006	8272	29
H(18B)	8673	3937	7517	29
H(21A)	6943	9659	8143	47
H(21B)	8510	9909	7891	47
H(21C)	8274	10144	8810	47
H(22A)	7982	7724	9683	47
H(22B)	7819	5824	9342	47
H(22C)	6554	7172	9104	47
H(1A)	6840	8718	1007	23
H(1B)	5498	7912	607	23
H(1C)	6615	6864	1092	23
H(1)	6749	4892	2554	39

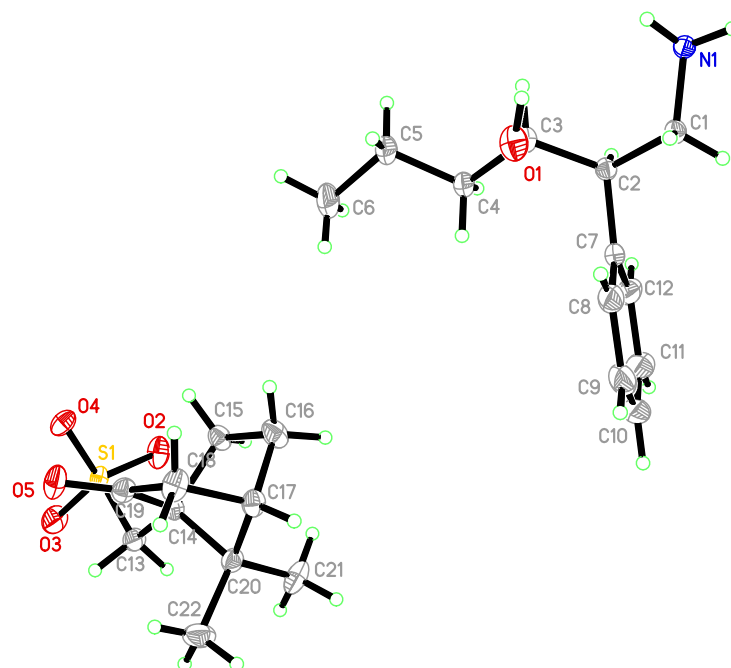


Figure A2.2 Thermal plot of (237). Ellipsoids drawn at the 50% probability level.

REFERENCES

¹ For the synthesis of nitroalkenes see: Duursma, A.; Minnaard, A. J.; Feringa, B. L. *Tetrahedron* **2002**, *58*, 5773-5778.

² Shibuya, K.; Miura, T. Cyclic diamine compound and pharmaceutical containing the same.
U.S. Patent 20,050,165,026, January 26, 2004.

³ For the synthesis of pyrrolidinones from amino acids see: Smrcina, M.; Majer, P.; Majerová, E.; Guerassina, T.; Eissenstat, M. A. *Tetrahedron* **1997**, *53*, 12867-12874.

Appendix 3

Addition of Catalytically Generated Acyl Anion Equivalents to Imines and Iminium Ions

Materials and Methods

Dichloromethane was degassed with argon and passed through two columns of neutral alumina. Molecular sieves were purchased from Mallinckrodt chemicals and activated prior to use using standard procedures. Aldehydes were purchased from Aldrich or prepared via previous literature procedures. Imines were prepared according to literature procedures.¹ Tris(2,2'-bipyridyl)dichlororuthenium(II) hexahydrate was purchased from Aldrich and used without further purification. N-aryl tetrahydroisoquinolines were prepared via literature procedures.² A 32W Kessil H150 Blue LED lamp was used as the light source. Column chromatography was performed on SiliCycle®SilicaFlash® P60, 40-63µm 60A. Thin layer chromatography was performed on SiliCycle® 250µm 60A plates. Visualization was accomplished with UV light, Seebach's stain or KMnO₄ stain followed by heating.

¹H NMR spectra were recorded on Varian 300 or 400 MHz spectrometers at ambient temperature. Data is reported as follows: chemical shift in parts per million (δ , ppm) from CDCl₃ (7.26 ppm), acetone-*d*₆ (2.03 ppm), or CD₂Cl₂ (5.32 ppm) multiplicity (s = singlet, bs = broad singlet, d = doublet, t = triplet, q = quartet, and m = multiplet), coupling constants (Hz).

¹³C NMR spectra were recorded on Varian 300 or 400 MHz spectrometers (at 75 or 100 MHz) at ambient temperature. Chemical shifts are reported in ppm from CDCl₃ (77.36 ppm), acetone-D₆ (205.87, 30.6 ppm), or CD₂Cl₂ (53.84 ppm). Mass spectra were recorded on an Agilent 6130 Quadrupole LC/MS.

Absolute stereochemistry of aza-benzoin products was assigned by analogy to an identical series of compounds in the literature.³

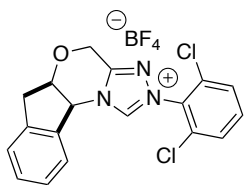
General Procedure for the Asymmetric Aza-Benzoin Reaction of Aliphatic Aldehydes and *N*-Boc imines

To a dry 4 mL vial with a magnetic stir bar, was added triazolium salt pre-catalyst (**264**) (26 mg, 0.058 mmol, 0.2 equiv), cesium acetate (55 mg, 0.29 mmol, 1.0 equiv), activated 4Å molecular sieves (8-12 mesh) (5-10 beads) and dichloromethane (1.5 mL). The vial was then placed in a -20 °C cooling bath with constant stirring and purged with argon. After 5 min the aldehyde (0.43 mmol, 1.5 equiv) was added via syringe followed by a solution of the imine (0.28 mmol, 1.0 equiv) in dichloromethane (0.5 mL). The reaction was stirred at -20 °C for 24 h at which point acetic acid (50 µL) was added and the whole mixture placed directly on a silica gel column and eluted with a hexanes:EtOAc mixture (typically 20:1). After chromatography the desired amino-ketone was obtained as a white amorphous solid.

General Procedure for the Asymmetric α -Acylation of Tertiary Amines with Aliphatic Aldehydes

To a dry 4 mL vial with a magnetic stir bar, was added triazolium salt pre-catalyst (**301**) (7.3 mg, 0.012 mmol, 0.05 equiv), dichloromethane (2 mL) and sodium hydride (excess, ~20 equiv). After stirring this heterogeneous mixture for ~5 min, it was filtered through a 0.45 micron nylon syringe filter into another 4 mL vial containing the *N*-aryl tetrahydroisoquinoline (0.238 mmol, 1.0 equiv), aldehyde (0.357 mmol, 1.5 equiv), tris(2,2'-bipyridyl)dichlororuthenium(II) hexahydrate (1.7 mg, 0.002 mmol, 0.01 equiv), and 1,3-dinitrobenzene (48 mg, 0.286 mmol, 1.2 equiv). The vial is capped and stirred at ambient temperature ~ 12 inches from a 32W Kessil H150 Blue LED lamp for 48 h, at which point it is purified directly by flash chromatography on silica gel, yielding the pure amino ketone.

Experimental Procedures and Characterization Data

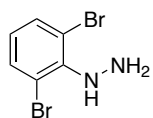


(5aR,10bS)-2-(2,6-dichlorophenyl)-4,5a,6,10b-tetrahydro-2H-

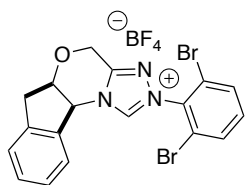
indeno[2,1-*b*][1,2,4]triazolo[4,3-*d*][1,4]oxazin-11-ium tetrafluoroborate (264): To a flame-dried round-bottomed flask was added (4a*S*,9a*R*)-

4,4a,9,9a-tetrahydroindeno[2,1-*b*][1,4]oxazin-3(2*H*)-one (5.0 g, 26.4 mmol, 1.0 equiv) and dichloromethane (150 mL). The mixture was stirred until homogeneous then trimethyloxonium tetrafluoroborate (3.91 g, 26.4 mmol, 1.0 equiv) was added in one portion. After stirring for 18 h, (2,6-dichlorophenyl)hydrazine (4.68 g, 26.4 mmol, 1.0 equiv) was added and the reaction was allowed to stir an additional 24 h at which point a slurry formed that was filtered, washed with ether and dried under vacuum (4 mm) for 1 h. After installing a reflux condenser, triethyl orthoformate (22 mL, 132 mmol, 5.0 equiv), chlorobenzene (150 mL) and a few drops of tetrafluoroboric acid diethyl ether complex were added and the mixture was heated to reflux in an oil bath for 16 h. The solution was cooled to 0° C in an ice bath at which point the precipitated solid was filtered and washed with EtOAc providing the desired triazolium salt as a tan solid (1.55 g, 29%). The filtrate was concentrated, dried and refluxed in chlorobenzene for an additional 18 h, at which point concentration and trituration with ethyl acetate yielded another portion of the triazolium salt as a tan solid (4.64 g, 39%). $[\alpha]_D^{21} = +70.5$ ($c = 0.010$ g/ml, acetone); **m.p.** (°C): 198-200; **¹H NMR** (400 MHz, acetone-*d*₆): δ 11.16 (s, 1H), 7.89-7.86 (m, 3H), 7.67 (d, $J = 7.6$ Hz, 1H), 7.46 (dt, $J = 13.7, 7.0$ Hz, 2H), 7.37 (t, $J = 7.4$ Hz, 1H), 6.39 (d, $J = 4.1$ Hz, 1H), 5.35 (q, $J = 19.5$ Hz, 2H), 5.25 (t, $J = 4.5$ Hz, 1H), 3.57 (dd, $J = 17.2, 4.9$ Hz, 1H), 3.30 (d, $J = 17.2$ Hz, 1H); **¹³C NMR** (100 MHz, acetone-*d*₆): δ 153.2, 147.4, 142.7, 137.5, 136.4, 135.0, 132.6, 131.5, 131.4, 129.3, 127.5, 125.5, 79.2, 64.4, 61.8, 39.0; **IR** (NaCl, neat) 3128,

3093, 3052, 1591, 1575, 1536, 1447, 1365, 1214, 1062 (broad) cm^{-1} ; **LRMS** (ESI+) calcd for $\text{C}_{18}\text{H}_{14}\text{Cl}_2\text{N}_3\text{O}$, 358.05. Found 358.1.

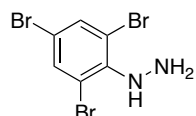


(2,6-dibromophenyl)hydrazine: To a solution of 2,6-dibromoaniline (2.0 g, 7.97 mmol, 1.0 equiv) in CH_2Cl_2 (40 mL) at $-15\text{ }^\circ\text{C}$ was added borontrifluoride diethyletherate (1.48 mL, 11.96 mmol, 1.5 equiv) dropwise. After stirring for 15 min, *t*-butyl nitrite (1.14 mL, 9.56 mmol, 1.2 equiv) was added slowly and the reaction stirred for an additional 30 min. Pentanes was added (40 mL) and the reaction filtered to yield a white solid that was washed with pentanes (50 mL) and dried, providing the corresponding diazonium salt which was used in the next step without further purification. To a cooled solution of tin(II) chloride hydrate (3.52 g, 15.6 mmol, 2.0 equiv) in $\text{HCl}_{(\text{conc})}$ (60 mL) at $0\text{ }^\circ\text{C}$ was added a quantity of the diazonium salt (2.73 g, 7.81 mmol, 1.0 equiv) portionwise. After stirring at $0\text{ }^\circ\text{C}$ for 1 h the reaction was basified to pH 10 with 10% NaOH, extracted with CH_2Cl_2 (3 X 50 mL) and the combined organic extracts dried (Na_2SO_4) and concentrated to yield the hydrazine as an off-white solid (1.5 g, 52%). Further purification was accomplished by trituration with pentanes. **^1H NMR** (300 MHz, CDCl_3): δ 7.49 (d, $J = 8.0$ Hz, 2H), 6.79 (t, $J = 8.0$ Hz, 1H), 5.53 (s, 1H), 3.94 (s, 2H).



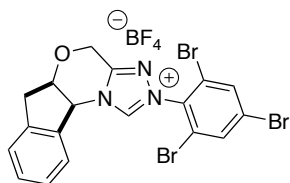
(5aR,10bS)-2-(2,6-dibromophenyl)-4,5a,6,10b-tetrahydro-2H-indeno[2,1-*b*][1,2,4]triazolo[4,3-*d*][1,4]oxazin-11-ium tetrafluoroborate (300): Prepared according to the general procedure using (2,6-dibromophenyl)hydrazine. $[\alpha]_{\text{D}}^{21} = +21.4$ ($c = 0.009$ g/ml, acetone); **m.p.** ($^\circ\text{C}$): 176-180; **^1H NMR** (400 MHz, acetone- d_6): δ 11.19 (s, 1H), 8.05 (dd, $J = 7.2, 3.3$ Hz, 2H), 7.73-7.68 (m, 2H), 7.46 (m, 2H), 7.38 (q, $J = 6.8$ Hz, 1H), 6.43 (d, $J = 4.1$ Hz, 1H), 5.36 (q, $J = 18.9$ Hz, 2H), 5.27

(t, $J = 4.5$ Hz, 1H), 3.58 (dd, $J = 17.1, 4.9$ Hz, 1H), 3.30 (d, $J = 17.2$ Hz, 1H); ^{13}C NMR (100 MHz, acetone- d_6): δ 152.1, 146.2, 141.8, 136.7, 136.2, 134.6, 134.5, 134.3, 130.5, 128.4, 126.7, 124.5; IR (NaCl, neat) 3127, 3092, 3048, 1589, 1565, 1440, 1322, 1214, 1062 (broad) cm^{-1} ; LRMS (ESI+) calcd for $\text{C}_{18}\text{H}_{14}\text{Br}_2\text{N}_3\text{O}$, 447.95. Found 448.0.



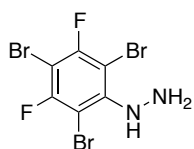
(2,4,6-tribromophenyl)hydrazine: To a solution of 2,4,6-tribromoaniline (20.0 g, 60.6 mmol, 1.0 equiv) in CH_2Cl_2 (300 mL) at -15 °C was added

borontrifluoride diethyletherate (11.23 mL, 90.96 mmol, 1.5 equiv) dropwise. After stirring for 15 min, *t*-butyl nitrite (8.68 mL, 72.77 mmol, 1.2 equiv) was added slowly and the reaction stirred for an additional 30 min. Pentanes was added (300 mL) and the reaction filtered to yield a white solid that was washed with pentanes (200 mL) and dried, providing the corresponding diazonium salt in quantitative yield which was used in the next step without further purification. To a cooled solution of tin(II) chloride hydrate (31.3 g, 138.6 mmol, 2.2 equiv) in $\text{HCl}_{(\text{Conc})}$ (100 mL) at 0 °C was added the diazonium salt portionwise with vigorous stirring. After 30 min the reaction was filtered and the solid washed with water (100 mL) and transferred to a flask containing 10% NaOH (100 mL). After stirring vigorously for 10 min, the solid was filtered, washed with water, and dried. Recrystallization from hot ethanol (1000 mL) yielded the hydrazine as a pink solid (9.8 g, 67%). ^1H NMR (300 MHz, CDCl_3): δ 7.63 (s, 2H), 5.49 (bs, 1H), 3.93 (bs, 2H).

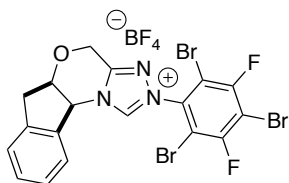


(5a*R*,10b*S*)-2-(2,4,6-tribromophenyl)-4,5a,6,10b-tetrahydro-2*H*-indeno[2,1-*b*][1,2,4]triazolo[4,3-*d*][1,4]oxazin-11-ium tetrafluoroborate (301): To a flame-dried round-bottomed flask was

added (4a*S*,9a*R*)-4,4a,9,9a-tetrahydroindeno[2,1-*b*][1,4]oxazin-3(2*H*)-one (1.64 g, 8.69 mmol, 1.0 equiv) and dichloromethane (50 mL). The mixture was stirred until homogeneous then trimethyloxonium tetrafluoroborate (1.29 g, 8.69 mmol, 1.0 equiv) was added in one portion. After stirring for 18 h, (2,4,6-tribromophenyl)hydrazine (3.00 g, 8.69 mmol, 1.0 equiv) was added and the reaction was allowed to stir an additional 24 h. Concentration of the solution gave a solid that was triturated with ether and dried under vacuum (4 mm) for 1 h. After installing a reflux condenser, triethyl orthoformate (3.61 mL, 21.7 mmol, 2.5 equiv) and chlorobenzene (50 mL) were added and the mixture was heated to reflux in an oil bath for 16 h. The solution was concentrated *in vacuo* and ethyl acetate was added to precipitate the product. After filtration the triazolium salt was obtained as a white solid (1.55 g, 29%). The filtrate was concentrated, dried and refluxed in chlorobenzene for an additional 18 h, at which point concentration and trituration with ethyl acetate yielded another portion of the triazolium salt as a tan solid (1.80 g, 3.35 g total, 63%). $[\alpha]_D^{21} = +28.4$ ($c = 0.010$ g/ml, methanol); **m.p.** (°C): 240-242; **¹H NMR** (400 MHz, acetone-*d*₆): δ 11.20 (s, 1H), 8.30 (s, 2H), 7.66 (d, $J = 7.6$ Hz, 1H), 7.46 (dt, $J = 14.3, 7.3$ Hz, 2H), 7.37 (t, $J = 7.4$ Hz, 1H), 6.42 (d, $J = 4.1$ Hz, 1H), 5.36 (q, $J = 21.2$ Hz, 2H), 5.25 (t, $J = 4.5$ Hz, 1H), 3.58 (dd, $J = 17.1, 4.9$ Hz, 1H), 3.30 (d, $J = 17.2$ Hz, 1H); **¹³C NMR** (100 MHz, acetone-*d*₆): δ 152.3, 148.2, 147.2, 146.3, 141.8, 136.6 (m), 134.1, 130.6, 128.4, 128.3, 126.7, 124.5, 78.4, 63.7, 60.9, 38.1; **IR** (NaCl, neat) 3123, 3083, 3048, 1590, 1561, 1407, 1376, 1217, 1102 cm^{-1} ; **LRMS** (ESI+) calcd for C₁₈H₁₃Br₃N₃O, 525.85. Found 525.9.

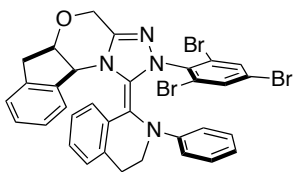


(2,4,6-tribromo-3,5-difluorophenyl)hydrazine: Prepared according to the procedure described previously using 2,4,6-tribromo-3,5-difluoroaniline (96%). **¹H NMR** (300 MHz, CDCl₃): δ 5.76 (bs, 1H), 4.04 (bs, 2H).



(5aR,10bS)-2-(2,4,6-tribromo-3,5-difluorophenyl)-4,5a,6,10b-tetrahydroindeno[2,1-*b*][1,2,4]triazolo[4,3-*d*][1,4]oxazin-2-ium tetrafluoroborate (302): Prepared according to the general procedure.

¹H NMR (400 MHz, acetone-*d*₆): δ 11.24 (s, 1H), 7.64 (d, *J* = 7.6 Hz, 1H), 7.46 (dt, *J* = 13.7, 7.1 Hz, 2H), 7.37 (t, *J* = 7.4 Hz, 1H), 6.44 (d, *J* = 4.1 Hz, 1H), 5.44 (d, *J* = 16.3 Hz, 1H), 5.33 (d, *J* = 16.4 Hz, 1H), 5.25 (t, *J* = 4.5 Hz, 1H), 3.58 (dd, *J* = 17.2, 4.8 Hz, 1H), 3.31 (d, *J* = 17.2 Hz, 1H); **¹³C NMR** (100 MHz, acetone-*d*₆): δ 152.7, 146.6, 141.8, 136.5, 130.6, 128.5, 126.7, 124.6, 78.4, 63.8, 61.0, 38.1.

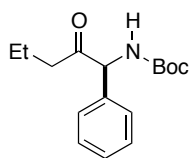


(5aR,10bS,Z)-1-(2-phenyl-3,4-dihydroisoquinolin-1(2H)-ylidene)-2-(2,4,6-tribromophenyl)-1,2,4,5a,6,10b-hexahydroindeno[2,1-*b*][1,2,4]triazolo[4,3-*d*][1,4]oxazine (304): A flask was charged with

triazolium salt (**301**) (200 mg, 0.324 mmol, 1.0 equiv), 2-phenyl-3,4-dihydroisoquinolin-2-ium bromide (**324**) (96 mg, 0.324 mmol, 1.0 equiv), and acetonitrile (4 mL). The resultant mixture was stirred until homogeneous at which point *N,N*-Diisopropylethylamine (284 μL, 1.62 mmol, 5.0 equiv) was added dropwise. After addition was complete the flask was left undisturbed for 1 h during which time the desired product crystallized from the reaction mixture. Filtration of the solid followed by washing with acetonitrile (3 X 2 mL) provided the aza-Breslow intermediate (**298**) as a bright yellow solid (184 mg, 78%). $[\alpha]_D^{21} = +266.9$ (*c* = 0.012 g/mL, acetone); **m.p.** (°C): 213-216; **¹H NMR** (mixture of isomers) (400 MHz, CD₂Cl₂): δ 7.93 (d, *J* = 7.3 Hz, 0.49 H), 7.80 (d, *J* = 2.2 Hz, 0.40H), 7.70-7.68 (m, 1H), 7.56 (d, *J* = 2.1 Hz, 1H), 7.37-7.33 (m, 1.59H), 7.31-7.20 (m, 1.31H), 7.20-7.03 (m, 5.18H), 6.89-6.79 (m, 5H), 6.74 (td, *J* = 7.4, 1.3 Hz,

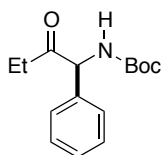
0.48H), 6.66-6.57 (m, 3.48H), 5.57 (d, $J = 3.8$ Hz, 1H), 5.21 (d, $J = 3.9$ Hz, 0.44H), 4.78 (t, $J = 3.9$ Hz, 1H), 4.57-4.51 (m, 2.44H), 4.34 (td, $J = 3.7, 1.1$ Hz, 0.49H), 4.15-4.08 (m, 1.45H), 3.97-3.89 (m, 1.17H), 3.66 (dt, $J = 12.3, 6.2$ Hz, 0.58H), 3.14 (dd, $J = 16.5, 4.2$ Hz, 1.19H), 3.06-2.99 (m, 1.61H), 2.93 (d, $J = 5.8$ Hz, 0.76H), 2.86-2.74 (m, 1.72H), 2.66 (ddd, $J = 17.2, 5.7, 1.6$ Hz, 1.20H); ^{13}C NMR (100 MHz, CD_2Cl_2): δ 152.7, 150.1, 145.4, 144.6, 143.5, 141.5, 140.8, 140.35, 140.25, 138.5, 136.0, 135.44, 135.32, 134.97, 134.83, 134.4, 134.1, 133.7, 129.5, 129.2, 129.0, 128.34, 128.22, 128.0, 127.5, 127.1, 126.85, 126.79, 125.72, 125.60, 125.47, 125.34, 125.22, 125.11, 124.94, 124.19, 124.18, 124.04, 123.5, 122.1, 121.7, 119.1, 118.5, 117.4, 115.5, 90.2, 89.5, 79.1, 78.5, 61.11, 61.06, 61.01, 50.84, 50.65, 37.61, 37.52, 27.8, 26.6; **IR** (NaCl, neat) 3060, 2957, 1639, 1615, 1559, 1489, 1419, 1369, 1164, 1075 cm^{-1} ; **LRMS** (ESI+) calcd for $\text{C}_{33}\text{H}_{26}\text{Br}_3\text{N}_4\text{O}$, 732.96. Found 733.0.

Characterization of α -Amido and α -Amino Ketones



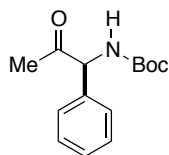
(S)-tert-butyl (2-oxo-1-phenylpentyl)carbamate (262): Prepared according to the general procedure: 89% yield; 96% ee; white amorphous solid; $R_f = 0.22$ (9:1 hex:EtOAc); $[\alpha]_D^{21} = +249$ ($c = 0.021$ g/ml, CHCl_3); HPLC analysis –

Chiracel IA column, 95:5 hexanes/*iso*-propanol, 1.0 mL/min. Major: 6.34 min, minor: 7.65 min; ^1H NMR (400 MHz, CDCl_3): 7.38-7.28 (m, 5H), 5.92-5.91 (m, 1H), 5.26 (d, $J = 6.3$ Hz, 1H), 2.41-2.26 (m, 2H), 1.60-1.57 (m, 2H), 1.40 (s, 9H), 0.77 (t, $J = 7.4$ Hz, 3H); ^{13}C NMR (100 MHz, CDCl_3): δ 206.1, 155.0, 137.2, 129.39, 129.24, 128.5, 128.12, 128.02, 79.9, 64.3, 41.6, 28.5, 17.3, 13.6; **IR** (NaCl, neat) 3426, 3356, 3031, 2968, 2876, 1709, 1491, 1391, 1247, 1169, 1011 cm^{-1} ; **LRMS** (ESI+) ($\text{M}+\text{Na}$) calcd for $\text{C}_{16}\text{H}_{23}\text{NNaO}_3$, 300.16. Found 300.2.



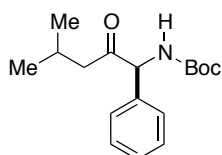
(S)-tert-butyl (2-oxo-1-phenylbutyl)carbamate (266): Prepared according to the general procedure: 90% yield; 96% ee; white amorphous solid; $R_f = 0.19$ (9:1 hex:EtOAc); $[\alpha]_D^{21} = +254$ (c = 0.011 g/ml, CHCl₃); HPLC analysis – Chiracel

IA column, 95:5 hexanes/*iso*-propanol, 1.0 mL/min. Major: 7.03 min, minor: 8.55 min; **¹H NMR** (400 MHz, CDCl₃): δ 7.38-7.28 (m, 5H), 5.91-5.90 (m, 1H), 5.29 (d, $J = 6.3$ Hz, 1H), 2.39 (dt, $J = 7.0, 3.5$ Hz, 2H), 1.40 (s, 9H), 0.98 (t, $J = 7.3$ Hz, 3H); **¹³C NMR** (100 MHz, CDCl₃): δ 206.7, 155.0, 137.4, 129.3, 128.5, 127.9, 80.0, 64.1, 33.1, 28.5, 7.9; **IR** (NaCl, neat) 3422, 3335, 2978, 2938, 1710, 1492, 1456, 1366, 1246, 1168, 1029 cm⁻¹; **LRMS** (ESI+) (M+Na) calcd for C₁₅H₂₁NNaO₃, 286.14. Found 286.2.



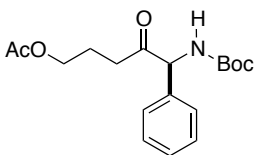
(S)-tert-butyl (2-oxo-1-phenylpropyl)carbamate (267): Prepared according to the general procedure: 86% yield; 84% ee; white amorphous solid; $R_f = 0.14$ (9:1 hex:EtOAc); $[\alpha]_D^{21} = +196$ (c = 0.021 g/ml, CHCl₃); HPLC analysis – Chiracel

IA column, 95:5 hexanes/*iso*-propanol, 1.0 mL/min. Major: 7.41 min, minor: 8.88 min; **¹H NMR** (400 MHz, CDCl₃): δ 7.39-7.30 (m, 5H), 5.88-5.87 (m, 1H), 5.28 (d, $J = 6.2$ Hz, 1H), 2.08 (s, 3H), 1.40 (s, 9H); **¹³C NMR** (100 MHz, CDCl₃): δ 203.72, 203.70, 155.0, 137.0, 129.3, 128.6, 128.0, 80.0, 64.9, 28.46, 28.37, 27.2; **IR** (NaCl, neat) 3423, 3265, 3063, 2978, 2929, 1709, 1492, 1365, 1247, 1166, 1027 cm⁻¹; **LRMS** (ESI+) (M+Na) calcd for C₁₄H₁₉NNaO₃, 272.13. Found 272.2.



(S)-tert-butyl (4-methyl-2-oxo-1-phenylpentyl)carbamate (268): Prepared according to the general procedure: 33% yield; 98% ee; white amorphous

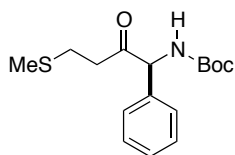
solid; $R_f = 0.22$ (9:1 hex:EtOAc); $[\alpha]_D^{21} = +250$ ($c = 0.013$ g/ml, CHCl_3); HPLC analysis – Chiracel IA column, 95:5 hexanes/*iso*-propanol, 1.0 mL/min. Major: 5.99 min, minor: 6.67 min; $^1\text{H NMR}$ (400 MHz, CDCl_3): 7.38-7.26 (m, 5H), 5.93-5.91 (m, 1H), 5.23 (d, $J = 6.5$ Hz, 1H), 2.32-2.25 (m, 1H), 2.20-2.06 (m, 3H), 1.40 (s, 9H), 0.87 (d, $J = 6.5$ Hz, 2H), 0.70 (d, $J = 6.5$ Hz, 3H); $^{13}\text{C NMR}$ (100 MHz, CDCl_3): δ 205.6, 155.0, 137.0, 129.2, 128.5, 128.1, 79.9, 64.6, 48.6, 28.47, 28.41, 24.6, 22.7, 22.2; **IR** (NaCl, neat) 3428, 2959, 2931, 2872, 1709, 1486, 1391, 1247, 1168, 1017 cm^{-1} ; **LRMS** (ESI+) ($\text{M}+\text{Na}$) calcd for $\text{C}_{17}\text{H}_{25}\text{NNaO}_3$, 314.17. Found 314.2.



(S)-5-((tert-butoxycarbonyl)amino)-4-oxo-5-phenylpentyl acetate

(269): Prepared according to the general procedure: 62% yield; 91% ee; white amorphous solid; $R_f = 0.33$ (7:3 hex:EtOAc); $[\alpha]_D^{21} = +94$ ($c =$

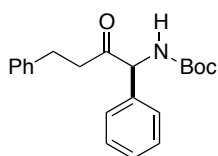
0.020 g/ml, CHCl_3); HPLC analysis – Chiracel IA column, 90:10 hexanes/*iso*-propanol, 1.0 mL/min. Major: 8.11 min, minor: 9.66 min; $^1\text{H NMR}$ (400 MHz, CDCl_3): 7.38-7.26 (m, 5H), 5.86 (d, $J = 5.4$ Hz, 1H), 5.28 (d, $J = 6.4$ Hz, 1H), 3.96 (dt, $J = 11.3, 5.8$ Hz, 1H), 3.88 (ddd, $J = 11.0, 7.3, 5.7$ Hz, 1H), 2.48-2.40 (m, 2H), 1.93 (s, 3H), 1.91-1.76 (m, 2H), 1.40 (s, 9H); $^{13}\text{C NMR}$ (100 MHz, CDCl_3): 205.2, 171.0, 155.0, 136.9, 132.8, 129.35, 129.20, 128.9, 128.7, 128.0, 127.6, 80.1, 64.3, 63.3, 36.0, 28.4, 28.2, 22.7, 20.9; **IR** (NaCl, neat) 3355, 2977, 2933, 1710, 1492, 1366, 1244, 1167, 1042 cm^{-1} ; **LRMS** (ESI+) ($\text{M}+\text{Na}$) calcd for $\text{C}_{18}\text{H}_{25}\text{NNaO}_5$, 358.16. Found 358.2.



(S)-tert-butyl(4-(methylthio)-2-oxo-1-phenylbutyl)carbamate **(270)**:

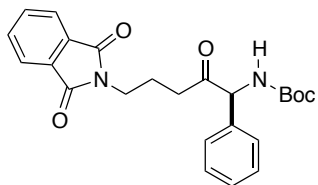
Prepared according to the general procedure: 83% yield; 88% ee; white amorphous solid; $R_f = 0.46$ (7:3 hex:EtOAc); $[\alpha]_D^{21} = +147$ ($c = 0.018$ g/ml,

CHCl₃); HPLC analysis – Chiracel IA column, 95:5 hexanes/*iso*-propanol, 1.0 mL/min. Major: 9.74 min, minor: 10.76 min; ¹H NMR (400 MHz, CDCl₃): 7.38-7.26 (m, 5H), 5.86 (d, *J* = 4.9 Hz, 1H), 5.28 (d, *J* = 6.3 Hz, 1H), 2.69-2.55 (m, 4H), 1.95 (s, 3H), 1.39 (s, 9H); ¹³C NMR (100 MHz, CDCl₃): δ 204.3, 155.0, 136.6, 129.3, 128.7, 128.1, 80.1, 64.5, 39.4, 28.41, 28.34, 28.23, 27.9, 15.6; IR (NaCl, neat) 3418, 3265, 3031, 2977, 2919, 1709, 1493, 1366, 1247, 1168, 1028 cm⁻¹; LRMS (ESI+) (M+Na) calcd for C₁₆H₂₃NNaO₃S, 332.13. Found 332.2.



(*S*)-tert-butyl (4-methyl-2-oxo-1-phenylpentyl)carbamate (271): Prepared according to the general procedure: 71% yield; 92% ee; white amorphous solid; R_f = 0.22 (9:1 hex:EtOAc); [α]_D²¹ = +121 (c = 0.023 g/ml, CHCl₃);

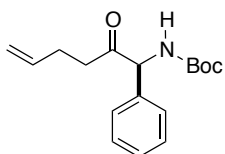
HPLC analysis – Chiracel IA column, 95:5 hexanes/*iso*-propanol, 1.0 mL/min. Major: 9.09 min, minor: 9.53 min; ¹H NMR (400 MHz, CDCl₃): 7.38-7.12 (m, 8H), 7.07-6.98 (m, 2H), 5.91-5.79 (m, 1H), 5.30-5.22 (m, 1H), 2.93-2.81 (m, 1H), 2.81-2.59 (m, 3H), 1.48-1.31 (m, 9H); ¹³C NMR (100 MHz, CDCl₃): δ 205.1, 155.0, 140.5, 136.8, 129.3, 128.6, 128.3, 128.0, 126.3, 80.0, 64.5, 41.3, 29.8, 28.46, 28.37; IR (NaCl, neat) 3426, 3332, 3063, 3029, 2977, 2933, 1709, 1494, 1454, 1366, 1247, 1167 cm⁻¹; LRMS (ESI+) (M+Na) calcd for C₂₁H₂₅NNaO₃, 362.17. Found 362.3.



(*S*)-tert-butyl (5-(1,3-dioxoisindolin-2-yl)-2-oxo-1-phenylpentyl)carbamate (272): Prepared according to the general procedure: 72% yield; 96% ee; white amorphous solid; R_f = 0.23 (7:3

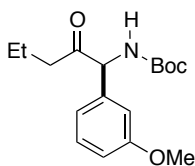
hex:EtOAc); [α]_D²¹ = +168 (c = 0.018 g/ml, CHCl₃); HPLC analysis – Chiracel IA column, 80:20 hexanes/*iso*-propanol, 1.0 mL/min. Major: 14.54 min, minor: 13.78 min; ¹H NMR (400 MHz, CDCl₃): 7.79 (dd, *J* = 5.4, 3.1 Hz, 2H), 7.68 (dd, *J* = 5.4, 3.1 Hz, 2H), 7.31-7.23 (m, 5H),

5.85 (d, $J = 5.7$ Hz, 1H), 5.25 (d, $J = 6.0$ Hz, 1H), 3.56 (t, $J = 7.0$ Hz, 2H), 2.50-2.32 (m, 2H), 1.97 (qt, $J = 15.0, 7.7$ Hz, 1H), 1.79-1.72 (m, 1H), 1.36 (s, 9H); $^{13}\text{C NMR}$ (100 MHz, CDCl_3): 205.0, 176.0, 168.47, 168.35, 155.0, 137.0, 134.1, 132.1, 129.3, 128.6, 127.9, 123.4, 80.0, 64.3, 37.25, 37.12, 36.8, 31.2, 28.4, 23.9, 22.8; **IR** (NaCl, neat) 3466, 3377, 3062, 2976, 2934, 1771, 1714, 1492, 1438, 1397, 1365, 1169, 1044 cm^{-1} ; **LRMS** (ESI+) ($\text{M}+\text{Na}$) calcd for $\text{C}_{24}\text{H}_{26}\text{N}_2\text{NaO}_5$, 445.17. Found 445.3.



(S)-tert-butyl (2-oxo-1-phenylhex-5-en-1-yl)carbamate (273): Prepared according to the general procedure: 93% yield; 93% ee; white amorphous solid; $R_f = 0.46$ (9:1 hex:EtOAc); $[\alpha]_D^{21} = +168$ ($c = 0.018$ g/ml, CHCl_3);

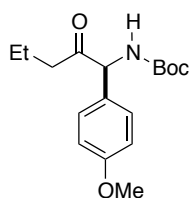
HPLC analysis – Chiracel IA column, 95:5 hexanes/*iso*-propanol, 1.0 mL/min. Major: 6.90 min, minor: 8.35 min; $^1\text{H NMR}$ (400 MHz, CDCl_3): 7.38-7.26 (m, 5H), 5.90-5.88 (m, 1H), 5.69-5.59 (m, 1H), 5.28 (d, $J = 6.3$ Hz, 1H), 4.91 (dq, $J = 6.7, 1.5$ Hz, 1H), 4.88 (t, $J = 1.4$ Hz, 1H), 2.46 (8, $J = 8.2$ Hz, 2H), 2.33-2.15 (m, 2H), 1.40 (s, 9H); $^{13}\text{C NMR}$ (100 MHz, CDCl_3): 205.3, 155.0, 137.0, 136.5, 129.3, 128.6, 128.0, 115.6, 80.0, 64.4, 38.9, 28.4, 27.6; **IR** (NaCl, neat) 3421, 3331, 3064, 2978, 2933, 1709, 1491, 1391, 1247, 1168, 1048 cm^{-1} ; **LRMS** (ESI+) ($\text{M}+\text{Na}$) calcd for $\text{C}_{17}\text{H}_{23}\text{NNaO}_3$, 312.16. Found 312.2.



(S)-tert-butyl (1-(3-methoxyphenyl)-2-oxopentyl)carbamate (275): Prepared according to the general procedure: 74% yield; 90% ee; white amorphous solid; $R_f = 0.18$ (9:1 hex:EtOAc); $[\alpha]_D^{21} = +59$ ($c = 0.028$ g/ml, CHCl_3); HPLC

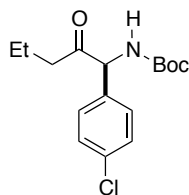
analysis – Chiracel IA column, 95:5 hexanes/*iso*-propanol, 1.0 mL/min. Major: 6.74 min, minor: 9.42 min; $^1\text{H NMR}$ (400 MHz, CDCl_3): 7.29-7.25 (m, 1H), 6.90-6.81 (m, 3H), 5.89 (m, 1H),

5.23 (d, $J = 6.4$ Hz, 1H), 3.79 (s, 3H), 2.42-2.28 (m, 2H), 1.52 (m, 2H), 1.41 (s, 9H), 0.79 (t, $J = 7.4$ Hz, 3H); ^{13}C NMR (100 MHz, CDCl_3): 206.0, 160.2, 155.0, 130.3, 120.4, 114.1, 113.4, 80.0, 64.2, 55.4, 41.6, 28.5, 17.3, 13.6; IR (NaCl, neat) 3331, 2967, 2935, 2877, 1709, 1600, 1489, 1366, 1263, 1168, 1044, 1012 cm^{-1} ; LRMS (ESI+) ($\text{M}+\text{Na}$) calcd for $\text{C}_{17}\text{H}_{25}\text{NNaO}_4$, 330.17. Found 330.2.



(S)-tert-butyl (1-(4-methoxyphenyl)-2-oxopentyl)carbamate (276): Prepared according to the general procedure: 84% yield; 96% ee; white amorphous solid;

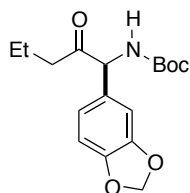
$R_f = 0.21$ (9:1 hex:EtOAc); $[\alpha]_D^{21} = +186$ ($c = 0.013$ g/ml, CHCl_3); HPLC analysis – Chiracel IA column, 95:5 hexanes/*iso*-propanol, 1.0 mL/min. Major: 8.86 min, minor: 11.12 min; ^1H NMR (400 MHz, CDCl_3): 7.19 (d, $J = 8.4$ Hz, 2H), 6.87-6.85 (m, 2H), 5.85 (d, $J = 5.5$ Hz, 1H), 5.20 (d, $J = 6.3$ Hz, 1H), 3.78 (s, 3H), 2.31 (t, $J = 7.1$ Hz, 2H), 1.51 (m, 2H), 1.38 (s, 9H), 0.77 (t, $J = 7.4$ Hz, 3H); ^{13}C NMR (100 MHz, CDCl_3): 206.3, 159.7, 155.0, 129.2, 114.6, 79.8, 63.6, 55.4, 41.5, 28.4, 17.3, 13.6; IR (NaCl, neat) 3425, 2967, 2935, 1709, 1610, 1511, 1366, 1303, 1253, 1169, 1034 cm^{-1} ; LRMS (ESI+) ($\text{M}+\text{Na}$) calcd for $\text{C}_{17}\text{H}_{25}\text{NNaO}_4$, 330.17. Found 330.1.



(S)-tert-butyl (1-(4-chlorophenyl)-2-oxopentyl)carbamate (277): Prepared according to the general procedure: 83% yield; 96% ee; white amorphous solid;

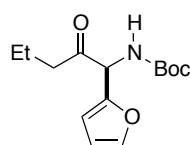
$R_f = 0.15$ (9:1 hex:EtOAc); $[\alpha]_D^{21} = +231$ ($c = 0.009$ g/ml, CHCl_3); HPLC analysis – Chiracel IA column, 95:5 hexanes/*iso*-propanol, 1.0 mL/min. Major: 7.56 min, minor: 9.64 min; ^1H NMR (400 MHz, CDCl_3): 7.34-7.32 (m, 2H), 7.25 (q, $J = 5.8$ Hz, 2H), 5.96 (dd, $J = 3.7, 0.7$ Hz, 1H), 5.22 (d, $J = 5.9$ Hz, 1H), 2.32 (dt, $J = 13.9, 7.1$ Hz, 2H), 1.59-1.47 (m, 2H),

1.39 (s, 9H), 0.78 (t, $J = 7.4$ Hz, 3H); ^{13}C NMR (100 MHz, CDCl_3): 205.5, 154.9, 135.9, 134.5, 129.45, 129.34, 80.2, 63.7, 41.6, 28.4, 17.2, 13.6; IR (NaCl, neat) 3418, 2967, 2934, 2877, 1709, 1490, 1366, 1246, 1167, 1015 cm^{-1} ; LRMS (ESI+) ($\text{M}+\text{Na}$) calcd for $\text{C}_{16}\text{H}_{22}\text{ClNNaO}_3$, 334.12. Found 334.2.



(S)-tert-butyl (1-(benzo[d][1,3]dioxol-5-yl)-2-oxopentyl)carbamate (278):

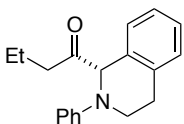
Prepared according to the general procedure: 72% yield; 94% ee; white amorphous solid; $R_f = 0.56$ (7:3 hex:EtOAc); $[\alpha]_D^{21} = +221$ ($c = 0.017$ g/ml, CHCl_3); HPLC analysis – Chiracel IA column, 95:5 hexanes/*iso*-propanol, 1.0 mL/min. Major: 9.58 min, minor: 11.67 min; ^1H NMR (400 MHz, CDCl_3): 6.77 (s, 2H), 6.72 (s, 1H), 5.94 (d, $J = 0.9$ Hz, 2H), 5.89 (d, $J = 5.3$ Hz, 1H), 5.15 (d, $J = 6.2$ Hz, 1H), 2.33 (t, $J = 7.2$ Hz, 2H), 1.53 (m, 2H), 1.39 (s, 9H), 0.79 (t, $J = 7.4$ Hz, 3H); ^{13}C NMR (100 MHz, CDCl_3): 205.9, 155.0, 148.3, 147.8, 131.0, 121.8, 108.8, 108.1, 101.4, 79.9, 63.8, 41.5, 28.4, 17.3, 13.6; IR (NaCl, neat) 3417, 2970, 1708, 1487, 1444, 1367, 1249, 1168, 1039 cm^{-1} ; LRMS (ESI+) ($\text{M}+\text{Na}$) calcd for $\text{C}_{17}\text{H}_{23}\text{NNaO}_5$, 344.15. Found 344.2.



(S)-tert-butyl (1-(furan-2-yl)-2-oxopentyl)carbamate (280):

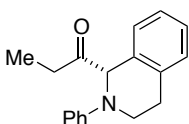
Prepared according to the general procedure: 66% yield; 60% ee; clear oil; $R_f = 0.26$ (9:1 hex:EtOAc); $[\alpha]_D^{21} = +63$ ($c = 0.008$ g/ml, CHCl_3); HPLC analysis – Chiracel IA column, 95:5 hexanes/*iso*-propanol, 1.0 mL/min. Major: 7.19 min, minor: 8.02 min; ^1H NMR (400 MHz, CDCl_3): 7.37 (t, $J = 1.3$ Hz, 1H), 6.36 (s, 2H), 5.70 (dd, $J = 5.0, 0.4$ Hz, 1H), 5.41 (d, $J = 7.0$ Hz, 1H), 2.40 (td, $J = 7.3, 1.9$ Hz, 2H), 1.58 (m, 2H), 1.42 (s, 9H), 0.84 (t, $J = 7.4$ Hz, 3H); ^{13}C NMR (100 MHz, CDCl_3): 203.9, 155.1, 149.5, 143.1, 111.0, 109.2, 80.2, 57.9, 41.5,

28.4, 17.2, 13.7; **IR** (NaCl, neat) 3428, 2970, 2935, 1714, 1498, 1367, 1248, 1168, 1010 cm^{-1} ;
LRMS (ESI+) ($\text{M}+\text{Na}$) calcd for $\text{C}_{14}\text{H}_{21}\text{NNaO}_4$, 290.14. Found 290.2.



(S)-1-(2-phenyl-1,2,3,4-tetrahydroisoquinolin-1-yl)butan-1-one (296):

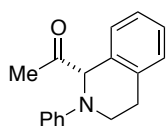
Prepared according to the general procedure: 81% yield; 92% ee; yellow oil;
 $R_f = 0.39$ (20:1 hex:EtOAc); $[\alpha]_D^{21} = -48.2$ ($c = 0.010$ g/ml, CHCl_3); HPLC analysis – Chiracel
IC column, 98:2 hexanes/*iso*-propanol, 1.0 mL/min. Major: 10.48 min, minor: 9.30 min; ^1H
NMR (400 MHz, CDCl_3): δ 7.26 (dd, $J = 5.8, 2.9$ Hz, 1H), 7.22-7.11 (m, 5H), 6.75-6.72 (m,
3H), 5.07 (s, 1H), 3.80 (dt, $J = 11.2, 4.9$ Hz, 1H), 3.34 (ddd, $J = 11.1, 10.0, 4.1$ Hz, 1H), 3.08
(ddd, $J = 15.5, 10.1, 5.2$ Hz, 1H), 2.91 (dt, $J = 15.6, 4.3$ Hz, 1H), 2.53-2.31 (m, 2H), 0.83 (t, $J =$
7.2 Hz, 3H); ^{13}C **NMR** (100 MHz, CDCl_3): δ 211.6, 149.3, 135.5, 131.5, 129.5, 128.5, 128.1,
127.7, 126.8, 118.5, 113.9, 70.2, 44.4, 39.7, 29.3, 17.0, 13.7; **IR** (NaCl, neat) 3061, 2960, 2930,
2871, 1716, 1660, 1599, 1504, 1457, 1324 cm^{-1} ; **LRMS** (ESI+) calcd for $\text{C}_{19}\text{H}_{22}\text{NO}$, 280.17.
Found 280.2.



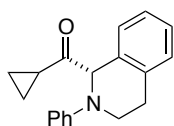
(S)-1-(2-phenyl-1,2,3,4-tetrahydroisoquinolin-1-yl)propan-1-one (305):

Prepared according to the general procedure: 67% yield; 91% ee; yellow oil;
 $R_f = 0.29$ (20:1 hex:EtOAc); $[\alpha]_D^{21} = -25.5$ ($c = 0.013$ g/ml, CHCl_3); HPLC analysis – Chiracel
IC column, 98:2 hexanes/*iso*-propanol, 1.0 mL/min. Major: 10.17 min, minor: 8.74 min; ^1H
NMR (400 MHz, CDCl_3): δ 7.26 (m, 1H), 7.22-7.11 (m, 5H), 6.75-6.72 (m, 3H), 5.07 (s, 1H),
3.80 (dt, $J = 11.2, 4.9$ Hz, 1H), 3.34 (ddd, $J = 11.1, 10.0, 4.1$ Hz, 1H), 3.08 (ddd, $J = 15.5, 10.1,$
5.2 Hz, 1H), 2.91 (dt, $J = 15.6, 4.3$ Hz, 1H), 2.53-2.31 (m, 2H), 0.83 (t, $J = 7.2$ Hz, 3H); ^{13}C
NMR (100 MHz, CDCl_3): δ

212.5 149.3, 135.5, 131.7, 129.5, 128.5, 128.0, 127.7, 126.9, 118.5, 113.8, 98.8, 69.9, 44.3, 31.1, 29.3, 7.8; **IR** (NaCl, neat) 3028, 2972, 2937, 1711, 1598, 1504, 1456, 1384, 1343, 1227 cm^{-1} ; **LRMS** (ESI+) calcd for $\text{C}_{18}\text{H}_{20}\text{NO}$, 266.15. Found 266.2.

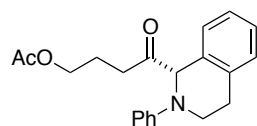


(S)-1-(2-phenyl-1,2,3,4-tetrahydroisoquinolin-1-yl)ethanone (306): Prepared according to the general procedure: 72% yield; 62% ee; yellow oil; $R_f = 0.19$ (20:1 hex:EtOAc); $[\alpha]_D^{21} = -42.4$ ($c = 0.014$ g/ml, CHCl_3); HPLC analysis – Chiracel IC column, 98:2 hexanes/*iso*-propanol, 1.0 mL/min. Major: 19.19 min, minor: 14.26 min; **^1H NMR** (400 MHz, CDCl_3): δ 7.28-7.13 (m, 6H), 6.78-6.74 (m, 3H), 5.05 (s, 1H), 3.81 (dt, $J = 11.2, 4.9$ Hz, 1H), 3.35 (ddd, $J = 11.2, 9.9, 4.1$ Hz, 1H), 3.09 (ddd, $J = 15.5, 10.0, 5.2$ Hz, 1H), 2.92 (dt, $J = 15.7, 4.4$ Hz, 1H), 2.03 (s, 3H); **^{13}C NMR** (100 MHz, CDCl_3): δ 209.8, 149.2, 135.5, 131.3, 129.5, 128.5, 128.1, 127.9, 126.9, 118.7, 113.9, 70.3, 44.4, 29.3, 25.9; **IR** (NaCl, neat) 3061, 2923, 2852, 1711, 1597, 1504, 1385, 1350, 1228, 1154 cm^{-1} ; **LRMS** (ESI+) calcd for $\text{C}_{17}\text{H}_{18}\text{NO}$, 252.14. Found 252.2.



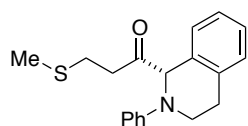
(S)-cyclopropyl(2-phenyl-1,2,3,4-tetrahydroisoquinolin-1-yl)methanone (307): Prepared according to the general procedure: 61% yield; 59% ee; yellow oil; $R_f = 0.24$ (20:1 hex:EtOAc); $[\alpha]_D^{21} = -37.2$ ($c = 0.011$ g/ml, CHCl_3); HPLC analysis – Chiracel IC column, 98:2 hexanes/*iso*-propanol, 1.0 mL/min. Major: 14.74 min, minor: 13.06 min; **^1H NMR** (400 MHz, CDCl_3): δ 7.29-7.27 (m, 1H), 7.22-7.11 (m, 5H), 6.79-6.72 (m, 3H), 5.17 (s, 1H), 3.79 (dt, $J = 10.9, 5.3$ Hz, 1H), 3.43 (ddd, $J = 11.2, 9.8, 4.3$ Hz, 1H), 3.08 (ddd, $J = 15.4, 9.9, 5.3$ Hz, 1H), 2.91 (dt, $J = 15.6, 4.5$ Hz, 1H), 2.25 (m, 1H), 0.89-0.81 (m, 2H), 0.77-0.65 (m, 2H); **^{13}C NMR** (100 MHz, CDCl_3): δ 211.1, 149.3, 135.7, 132.1, 129.4, 128.3, 127.7,

126.7, 118.4, 113.9, 70.0, 44.65, 29.1, 17.4, 11.9, 11.7; **IR** (NaCl, neat) 3061, 2922, 2844, 1703, 1599, 1504, 1376, 1229, 1063 cm^{-1} ; **LRMS** (ESI+) calcd for $\text{C}_{19}\text{H}_{20}\text{NO}$, 278.15. Found 278.2.



(S)-4-oxo-4-(2-phenyl-1,2,3,4-tetrahydroisoquinolin-1-yl)butyl acetate

(308): Prepared according to the general procedure: 88% yield; 92% ee; yellow oil; $R_f = 0.44$ (7:3 hex:EtOAc); $[\alpha]_D^{21} = -35.4$ ($c = 0.014$ g/ml, CHCl_3); HPLC analysis – Chiracel OJ-H column, 70:30 hexanes/*iso*-propanol, 1.0 mL/min. Major: 16.0 min, minor: 17.9 min; **$^1\text{H NMR}$** (400 MHz, CDCl_3): δ 7.26-7.12 (m, 6H), 6.77-6.74 (m, 3H), 5.08 (s, 1H), 3.80 (m, 3H), 3.34 (ddd, $J = 11.2, 9.9, 4.1$ Hz, 1H), 3.08 (ddd, $J = 15.5, 10.0, 5.2$ Hz, 1H), 2.92 (dt, $J = 15.7, 4.3$ Hz, 1H), 2.47 (m, 2H), 1.83 (s, 3H), 1.69 (m, 2H); **$^{13}\text{C NMR}$** (100 MHz, CDCl_3): δ 210.8, 171.0, 149.2, 135.4, 131.3, 129.6, 128.6, 128.0, 127.9, 126.9, 118.9, 114.1, 70.1, 63.5, 44.5, 33.9, 29.3, 22.6, 20.9; **IR** (NaCl, neat) 3060, 2958, 2925, 2851, 1737, 1598, 1504, 1386, 1364, 1239, 1038 cm^{-1} ; **LRMS** (ESI+) calcd for $\text{C}_{21}\text{H}_{24}\text{NO}_3$, 338.18. Found 338.2.

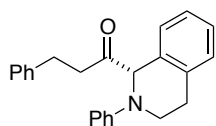


(S)-3-(methylthio)-1-(2-phenyl-1,2,3,4-tetrahydroisoquinolin-1-

yl)propan-1-one (309): Prepared according to the general procedure: 61%

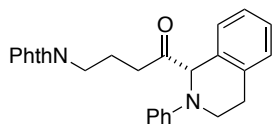
yield; 87% ee; yellow oil; $R_f = 0.39$ (9:1 hex:EtOAc); $[\alpha]_D^{21} = -57.9$ ($c = 0.009$ g/ml, CHCl_3); HPLC analysis – Chiracel IC column, 98:2 hexanes/*iso*-propanol, 1.0 mL/min. Major: 15.24 min, minor: 14.34 min; **$^1\text{H NMR}$** (400 MHz, CDCl_3): δ 7.32-7.18 (m, 6H), 6.86-6.81 (m, 3H), 5.15 (s, 1H), 3.87 (dt, $J = 10.9, 5.3$ Hz, 1H), 3.40 (ddd, $J = 11.3, 9.8, 4.1$ Hz, 1H), 3.14 (ddd, $J = 15.5, 10.0, 5.3$ Hz, 1H), 2.98 (dt, $J = 15.8, 4.4$ Hz, 1H), 2.85-2.66 (m, 2H), 2.61-2.52 (m, 2H), 1.92 (s, 3H); **$^{13}\text{C NMR}$** (100 MHz, CDCl_3): δ 209.9, 135.5, 131.0, 129.7, 129.6, 128.6, 128.1, 127.9, 126.9, 119.0, 114.3, 70.1, 44.6, 37.8, 29.2, 28.1, 15.8; **IR** (NaCl, neat) 3061, 2915, 2834, 1717,

1598, 1504, 1386, 1344, 1324, 1229 cm^{-1} ; **LRMS** (ESI+) calcd for $\text{C}_{19}\text{H}_{22}\text{NOS}$, 312.14. Found 312.2.



(S)-3-phenyl-1-(2-phenyl-1,2,3,4-tetrahydroisoquinolin-1-yl)propan-1-

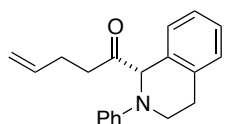
one (310): Prepared according to the general procedure: 91% yield; 92% ee; yellow oil; $R_f = 0.27$ (20:1 hex:EtOAc); $[\alpha]_D^{21} = -7.9$ ($c = 0.023$ g/ml, CHCl_3); HPLC analysis – Chiracel IC column, 98:2 hexanes/*iso*-propanol, 1.0 mL/min. Major: 10.19 min, minor: 9.18 min; **$^1\text{H NMR}$** (400 MHz, CDCl_3): δ 7.22-7.03 (m, 9H), 6.94-6.92 (m, 2H), 6.76-6.69 (m, 3H), 5.05 (s, 1H), 3.75 (dt, $J = 11.2, 4.9$ Hz, 1H), 3.31 (ddd, $J = 11.2, 9.9, 4.2$ Hz, 1H), 3.02 (ddd, $J = 15.5, 10.0, 5.3$ Hz, 1H), 2.88 (dt, $J = 15.7, 4.4$ Hz, 1H), 2.80-2.63 (m, 4H); **$^{13}\text{C NMR}$** (100 MHz, CDCl_3): δ 210.6, 149.2, 141.1, 135.5, 131.3, 129.5, 128.5, 128.4, 128.1, 127.8, 126.9, 126.1, 118.7, 114.0; **IR** (NaCl, neat) 3061, 3027, 2924, 2852, 1713, 1598, 1504, 1473, 1386, 1229 cm^{-1} ; **LRMS** (ESI+) calcd for $\text{C}_{24}\text{H}_{24}\text{NO}$, 342.19. Found 342.2.



((S)-2-(4-oxo-4-(2-phenyl-1,2,3,4-tetrahydroisoquinolin-1-

yl)butyl)isoindoline-1,3-dione (311): Prepared according to the general procedure: 79% yield; 88% ee; yellow oil; $R_f = 0.33$ (7:3 hex:EtOAc); $[\alpha]_D^{21} = -30.8$ ($c = 0.029$ g/ml, CHCl_3); HPLC analysis – Chiracel IC column, 70:30 hexanes/*iso*-propanol, 1.0 mL/min. Major: 16.25 min, minor: 19.23 min; **$^1\text{H NMR}$** (400 MHz, CDCl_3): δ 7.80 (dd, $J = 5.4, 3.1$ Hz, 2H), 7.69 (dd, $J = 5.5, 3.0$ Hz, 2H), 7.30-7.16 (m, 6H), 6.83-6.76 (m, 3H), 5.17 (s, 1H), 3.82 (dt, $J = 11.0, 5.3$ Hz, 1H), 3.55 (td, $J = 7.0, 2.0$ Hz, 2H), 3.42 (ddd, $J = 11.3, 9.4, 4.3$ Hz, 1H), 3.17-3.06 (m, 1H), 2.97 (dt, $J = 15.8, 4.7$ Hz, 1H), 2.65-2.47 (m, 2H), 1.82 (m, 2H); **$^{13}\text{C NMR}$** (100 MHz, CDCl_3): δ 210.2, 168.4, 149.1, 135.5, 134.0, 132.2, 131.4, 129.5, 128.5, 128.1, 127.8,

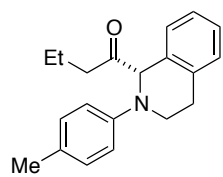
126.8, 123.3, 118.7, 113.9, 69.8, 44.4, 37.3, 35.3, 29.0, 22.8; **IR** (NaCl, neat) 3062, 2935, 2853, 1771, 1713, 1598, 1504, 1396, 1360, 1229 cm^{-1} ; **LRMS** (ESI+) calcd for $\text{C}_{27}\text{H}_{25}\text{N}_2\text{O}_3$, 425.19. Found 425.2.



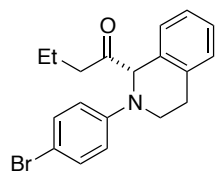
(S)-1-(2-phenyl-1,2,3,4-tetrahydroisoquinolin-1-yl)pent-4-en-1-one (312):

Prepared according to the general procedure: 75% yield; 92% ee; yellow oil; $R_f = 0.34$ (20:1 hex:EtOAc); $[\alpha]_D^{21} = -28.2$ ($c = 0.020$ g/ml, CHCl_3); HPLC analysis – Chiracel IC column, 98:2 hexanes/*iso*-propanol, 1.0 mL/min. Major: 10.01 min, minor: 8.46 min; **^1H NMR** (400 MHz, CDCl_3): δ 7.26-7.11 (m, 6H), 6.76-6.73 (m, 3H), 5.60-5.50 (m, 1H), 5.07 (s, 1H), 4.81-4.75 (m, 2H), 3.79 (dt, $J = 11.2, 4.9$ Hz, 1H), 3.34 (ddd, $J = 11.2, 10.0, 4.1$ Hz, 1H), 3.07 (ddd, $J = 15.5, 10.0, 5.2$ Hz, 1H), 2.91 (dt, $J = 15.7, 4.3$ Hz, 1H), 2.59-2.40 (m, 2H), 2.13-2.07 (m, 2H); **^{13}C NMR** (100 MHz, CDCl_3): δ 210.8, 149.2, 137.2, 135.5, 131.4, 129.5, 128.5, 128.1, 127.8, 126.9, 118.7, 115.2, 113.9, 70.1, 44.4, 37.0, 29.2, 27.6; **IR** (NaCl, neat) 3063, 2922, 2844, 1715, 1599, 1504, 1386, 1229 cm^{-1} ; **LRMS** (ESI+) calcd for $\text{C}_{20}\text{H}_{22}\text{NO}$, 292.17. Found 292.2.

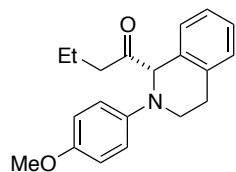
(S)-1-(2-(*p*-tolyl)-1,2,3,4-tetrahydroisoquinolin-1-yl)butan-1-one (314): Prepared according to the general procedure: 84% yield; 92% ee; yellow oil; $R_f = 0.34$ (20:1 hex:EtOAc); $[\alpha]_D^{21} = -38.6$ ($c = 0.025$ g/ml, CHCl_3); HPLC analysis – Chiracel IC column, 98:2 hexanes/*iso*-propanol, 1.0 mL/min. Major: 11.4 min, minor: 8.1 min; **^1H NMR** (400 MHz, CDCl_3): δ 7.32-7.30 (m, 1H), 7.26-7.19 (m, 3H), 7.08 (ddd, $J = 9.2, 2.5, 0.7$ Hz, 2H), 6.80-6.77 (m, 2H), 5.09 (s, 1H), 3.85 (dt, $J = 11.3, 4.9$ Hz, 1H), 3.38 (ddd, $J = 11.3, 9.6, 4.1$ Hz, 1H), 3.16 (ddd, $J = 15.4, 9.9, 5.3$ Hz, 1H), 2.98 (dt, $J = 15.7, 4.4$ Hz, 1H), 2.52-2.34 (m, 2H), 2.27 (s, 3H), 1.49-1.40 (m, 2H), 0.72 (t, $J =$



7.4 Hz, 3H); ^{13}C NMR (100 MHz, CDCl_3): δ 211.9, 147.2, 135.4, 131.5, 130.0, 128.6, 128.3, 128.0, 127.6, 126.7, 114.6, 70.4, 44.9, 39.8, 29.3, 20.4, 17.0, 13.7; IR (NaCl, neat) 3028, 2962, 2927, 2873, 1713, 1618, 1519, 1495, 1455, 1384, 1354, 1322, 1296, 1136 cm^{-1} ; LRMS (ESI+) calcd for $\text{C}_{20}\text{H}_{24}\text{NO}$, 294.19. Found 294.2.

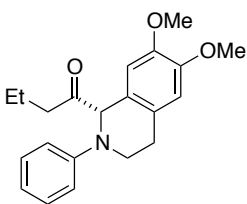


(S)-1-(2-(4-bromophenyl)-1,2,3,4-tetrahydroisoquinolin-1-yl)butan-1-one (315): Prepared according to the general procedure: 51% yield; 90% ee; yellow oil; $R_f = 0.29$ (20:1 hex:EtOAc); $[\alpha]_D^{21} = -14.7$ ($c = 0.019$ g/ml, CHCl_3); HPLC analysis – Chiracel IC column, 98:2 hexanes/*iso*-propanol, 1.0 mL/min. Major: 12.2 min, minor: 8.5 min; ^1H NMR (400 MHz, CDCl_3): δ 7.28-7.24 (m, 3H), 7.20-7.12 (m, 3H), 6.61-6.57 (m, 2H), 5.01 (s, 1H), 3.75 (dt, $J = 10.9, 4.8$ Hz, 1H), 3.30 (td, $J = 10.6, 4.2$ Hz, 1H), 3.07 (ddd, $J = 15.5, 10.2, 5.2$ Hz, 1H), 2.89 (dt, $J = 15.6, 4.2$ Hz, 1H), 2.42-2.26 (m, 2H), 1.38 (m, 2H), 0.66 (t, $J = 7.4$ Hz, 3H); ^{13}C NMR (100 MHz, CDCl_3): δ 210.8, 148.2, 135.4, 132.2, 131.3, 128.5, 128.1, 127.9, 127.0, 115.2, 110.4, 70.0, 44.4, 39.7, 29.1, 17.0, 13.7; IR (NaCl, neat) 3062, 2973, 2935, 2852, 1718, 1589, 1494, 1385, 1299, 1228 cm^{-1} ; LRMS (ESI+) calcd for $\text{C}_{19}\text{H}_{21}\text{BrNO}$, 358.08. Found 358.1.



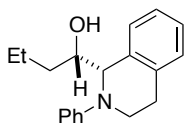
(S)-1-(2-(4-methoxyphenyl)-1,2,3,4-tetrahydroisoquinolin-1-yl)butan-1-one (316): Prepared according to the general procedure: 54% yield; 91% ee; yellow oil; $R_f = 0.41$ (9:1 hex:EtOAc); $[\alpha]_D^{21} = -68.6$ ($c = 0.007$ g/ml, CHCl_3); HPLC analysis – Chiracel IC column, 98:2 hexanes/*iso*-propanol, 1.0 mL/min. Major: 16.8 min, minor: 15.4 min; ^1H NMR (400 MHz, CDCl_3): δ 7.27-7.18 (m, 5H), 6.85 (s, 3H), 5.04

(s, 1H), 3.77 (m, 4H), 3.32 (ddd, $J = 11.4, 9.5, 3.9$ Hz, 1H), 3.16 (ddd, $J = 15.4, 9.7, 5.2$ Hz, 1H), 2.94 (dt, $J = 15.7, 4.3$ Hz, 1H), 2.40 (m, 2H), 1.42 (m, 2H), 0.70 (t, $J = 7.4$ Hz, 3H); ^{13}C NMR (100 MHz, CDCl_3): δ 212.0, 153.4, 143.9, 135.3, 131.5, 128.8, 127.8, 127.5, 127.3, 126.8, 126.6, 117.0, 114.4, 70.8, 55.8, 46.2, 39.7, 29.5, 17.0, 13.7; **IR** (NaCl, neat) 2961, 2933, 2834, 1711, 1657, 1604, 1511, 1463, 1246, 1037 cm^{-1} ; **LRMS** (ESI+) calcd for $\text{C}_{20}\text{H}_{24}\text{NO}_2$, 310.18. Found 310.2.



(S)-1-(6,7-dimethoxy-2-phenyl-1,2,3,4-tetrahydroisoquinolin-1-yl)butan-1-one (318): Prepared according to the general procedure: 94% yield; 90% ee; yellow oil; $R_f = 0.40$ (7:3 hex:EtOAc); $[\alpha]_D^{21} = -25.8$ ($c =$

0.011 g/mL, CHCl_3); HPLC analysis – Chiracel IC column, 90:10 hexanes/*iso*-propanol, 1.0 mL/min. Major: 16.4 min, minor: 26.9 min; ^1H NMR (400 MHz, CDCl_3): δ 7.29-7.25 (m, 2H), 6.86-6.79 (m, 4H), 6.68 (s, 1H), 5.01 (s, 1H), 3.87 (d, $J = 8.0$ Hz, 6H), 3.39 (ddd, $J = 11.4, 9.6, 4.1$ Hz, 1H), 3.09 (ddd, $J = 15.3, 9.8, 5.2$ Hz, 1H), 2.91 (dt, $J = 15.6, 4.4$ Hz, 1H), 2.48-2.32 (m, 2H), 1.48-1.39 (m, 2H), 0.71 (t, $J = 7.4$ Hz, 3H); ^{13}C NMR (100 MHz, CDCl_3): δ 212.5, 149.5, 148.6, 147.9, 129.5, 127.5, 123.0, 118.7, 114.2, 111.2, 110.6, 69.9, 56.2, 56.0, 44.4, 39.3, 28.9, 16.9, 13.7; **IR** (NaCl, neat) 2961, 2934, 2835, 1709, 1599, 1515, 1505, 1464, 1384, 1348, 1275, 1252, 1222, 1119 cm^{-1} ; **LRMS** (ESI+) calcd for $\text{C}_{21}\text{H}_{26}\text{NO}_3$, 340.19. Found 340.2.

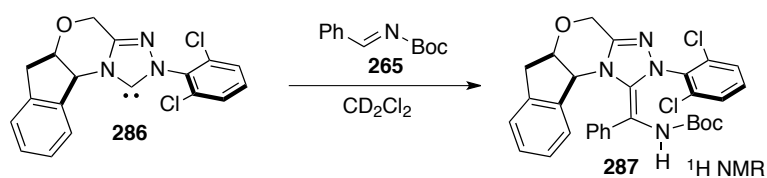
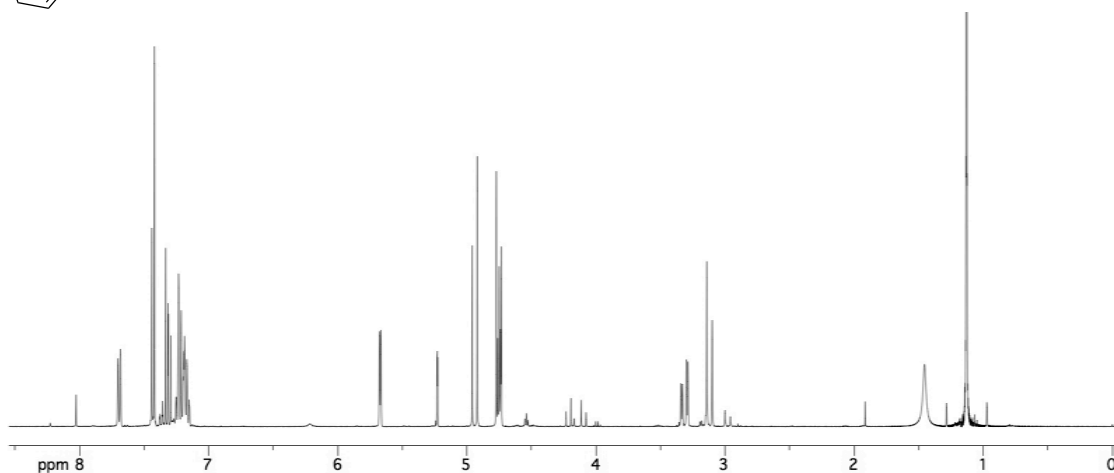
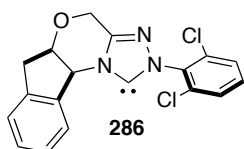


(S)-1-((S)-2-phenyl-1,2,3,4-tetrahydroisoquinolin-1-yl)butan-1-ol (322): To a cooled solution (0 °C) of (S)-1-(2-phenyl-1,2,3,4-tetrahydroisoquinolin-1-yl)butan-1-one (**296**) (0.50 g, 1.79 mmol, 1.0 equiv) in dry MeOH (32 mL) was added NaBH_4 (0.38 g, 8.94 mmol, 5.0 equiv) portionwise. The reaction was stirred at 0 °C until TLC analysis

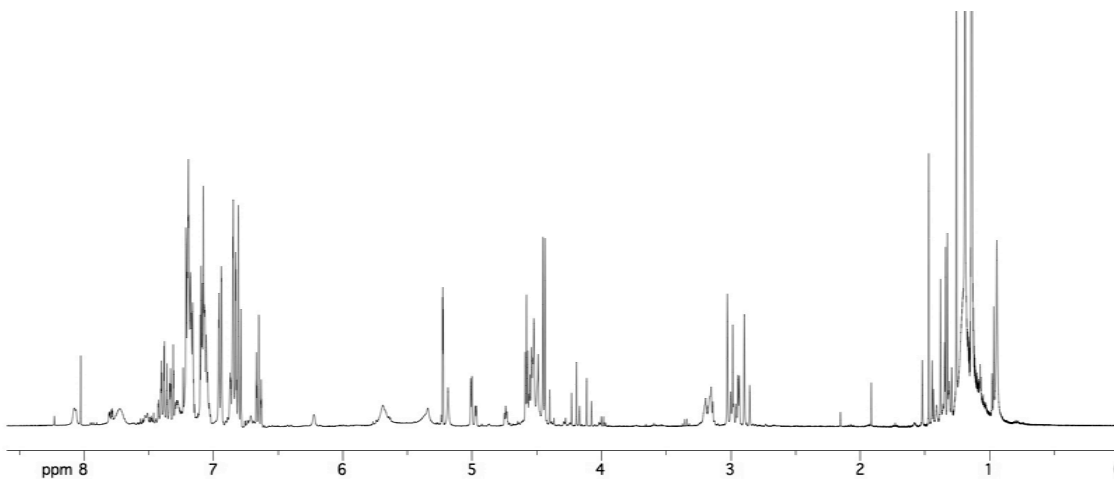
indicated consumption of the starting material. Upon completion, 10% HCl (20 mL) was added and the mixture separated. The aqueous layer was extracted with CH₂Cl₂ (3 x 20 mL), and the combined organic extracts dried, concentrated and purified by chromatography on silica gel (20:1, hex:EtOAc) to yield the alcohol as an off-white amorphous solid (0.38 g, 75%). $R_f = 0.19$ (9:1 hex:EtOAc); $[\alpha]_D^{21} = -28.5$ ($c = 0.009$ g/ml, CHCl₃); **¹H NMR** (400 MHz, CDCl₃): δ 7.24-7.11 (m, 6H), 7.01 (d, $J = 8.2$ Hz, 2H), 6.82 (t, $J = 7.3$ Hz, 1H), 4.41 (d, $J = 8.8$ Hz, 1H), 3.77 (ddd, $J = 12.8, 8.0, 4.9$ Hz, 1H), 3.68 (td, $J = 8.9, 2.2$ Hz, 1H), 3.50 (dt, $J = 12.5, 6.1$ Hz, 1H), 3.40 (bs, 1H), 2.97 (ddd, $J = 16.2, 8.1, 5.4$ Hz, 1H), 2.84 (dt, $J = 16.3, 5.8$ Hz, 1H), 1.71-1.62 (m, 2H), 1.59-1.52 (m, 1H), 1.41-1.34 (m, 1H), 0.91 (t, $J = 7.1$ Hz, 3H); **¹³C NMR** (100 MHz, CDCl₃): δ 150.9, 135.8, 135.1, 129.32, 129.24, 128.7, 127.3, 126.0, 119.5, 116.39, 116.36, 73.91, 73.85, 73.72, 65.9, 44.0, 35.5, 26.7, 19.4, 14.40, 14.35 **IR** (NaCl, neat) 3450, 3060, 3024, 2958, 2870, 1598, 1502, 1390, 1318, 1295, 1217, 1075 cm⁻¹; **LRMS** (ESI+) calcd for C₁₉H₂₄NO, 282.19. Found 282.2.

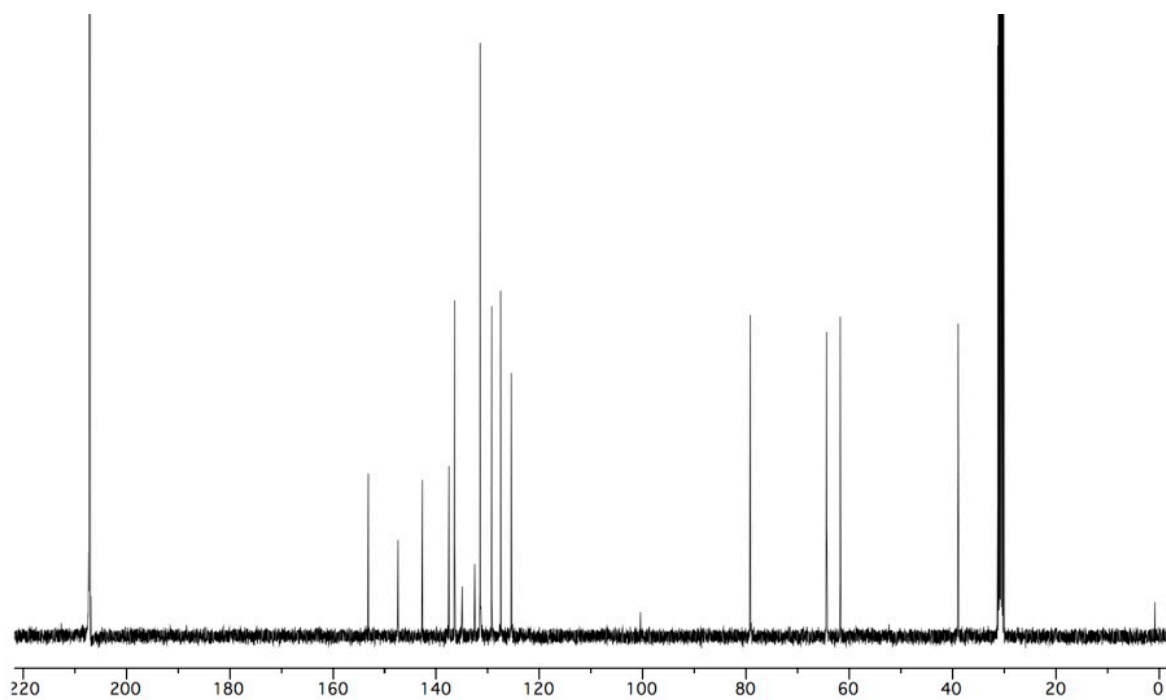
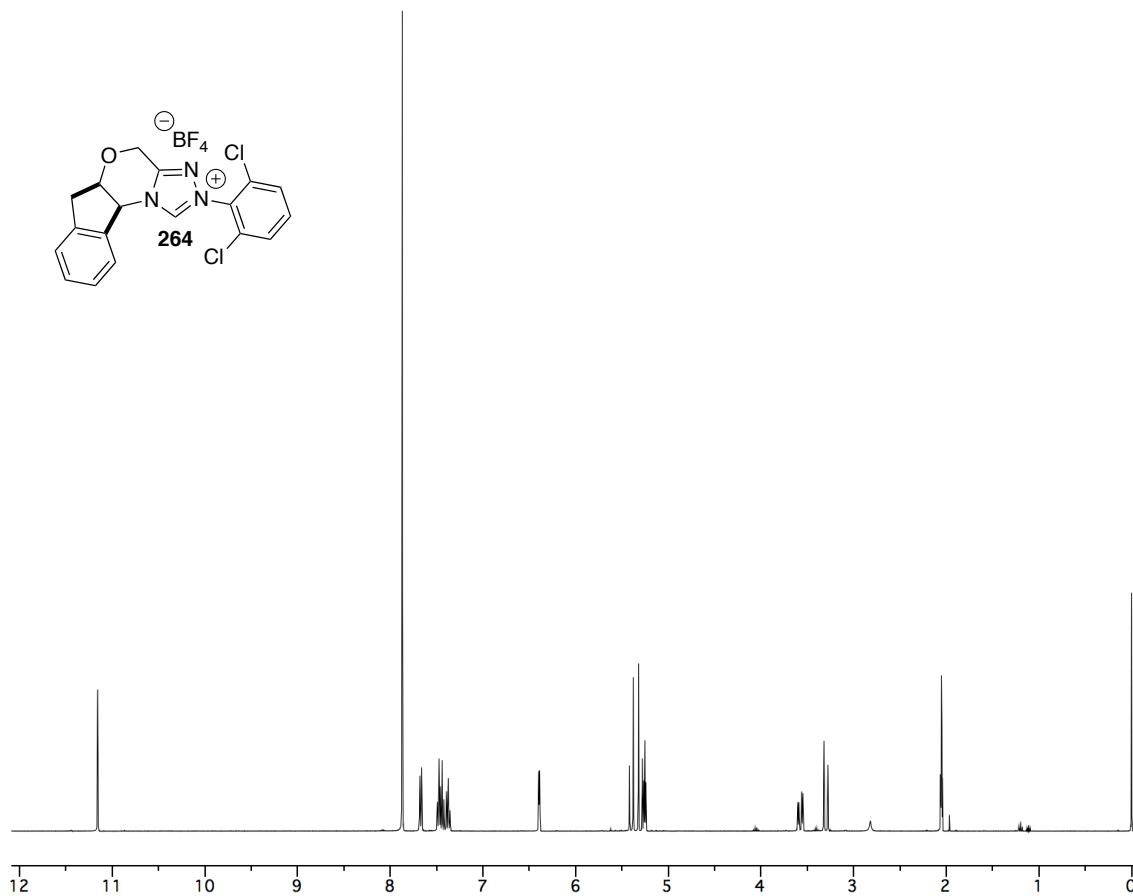
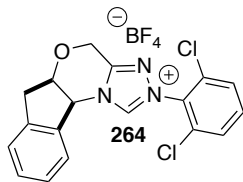
^1H and ^{13}C NMR Spectra

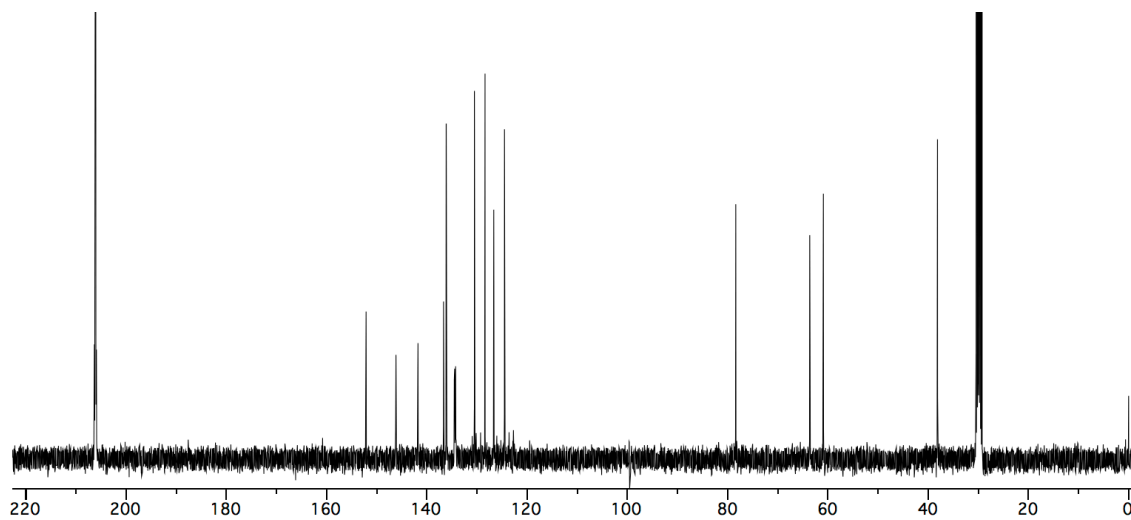
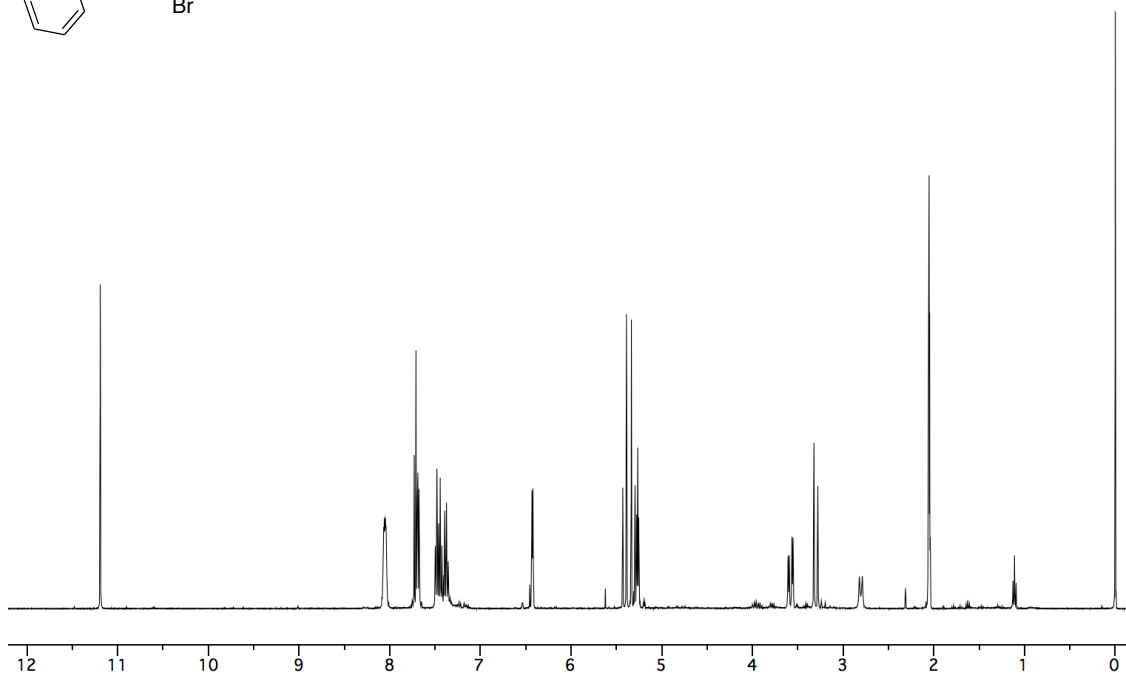
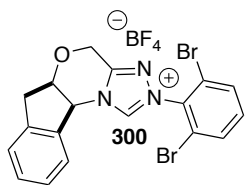
Formation of aza-Breslow Intermediate with *N*-Boc Imines

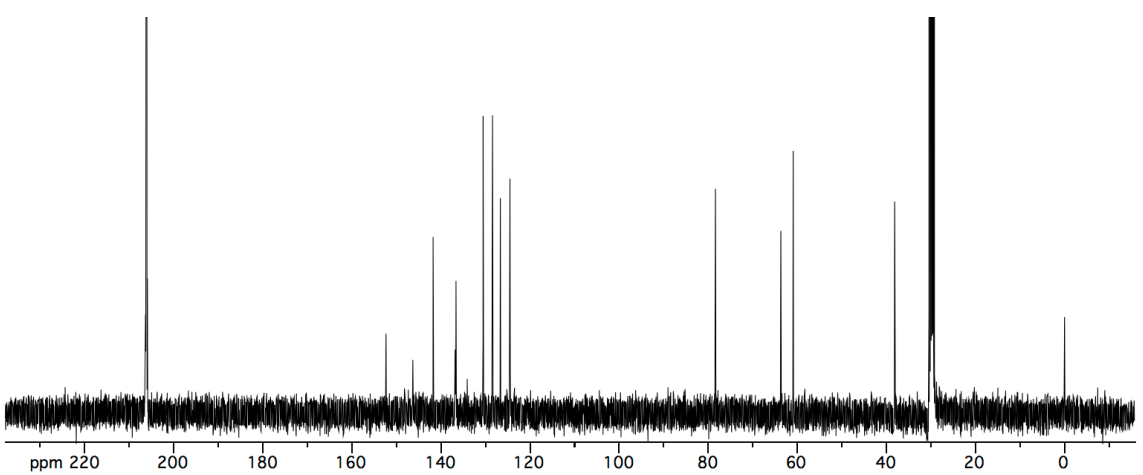
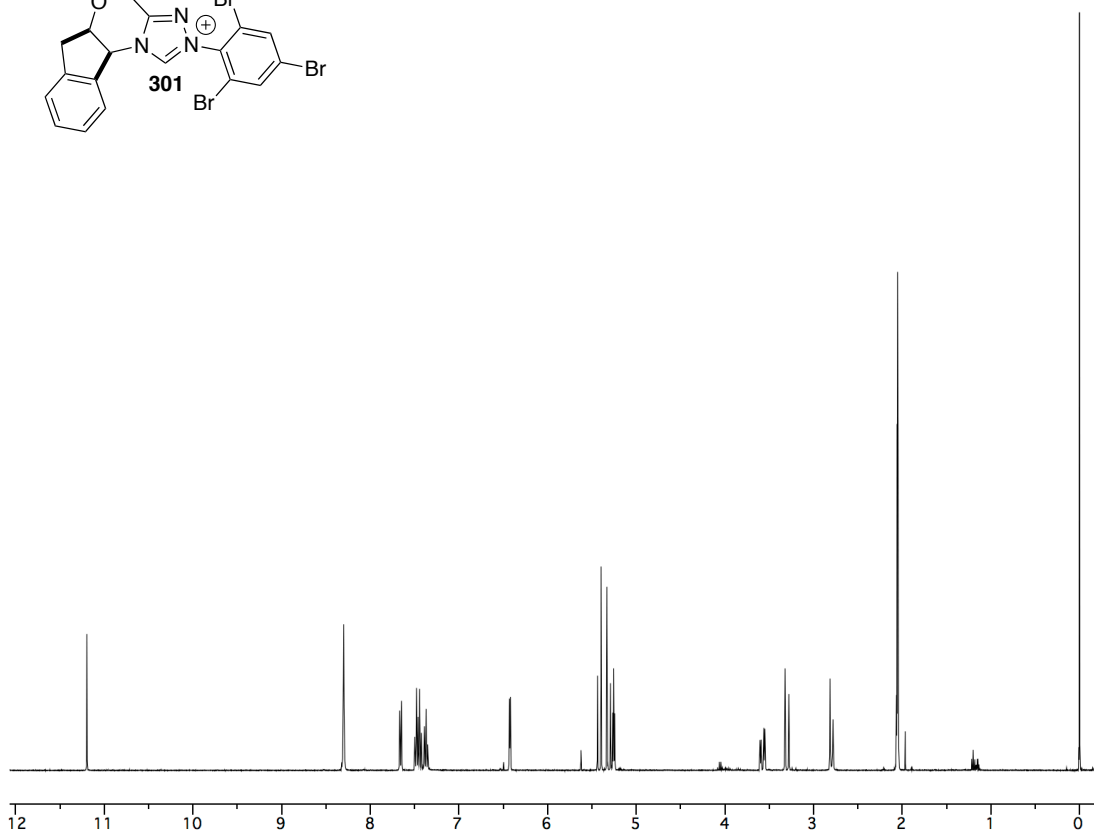
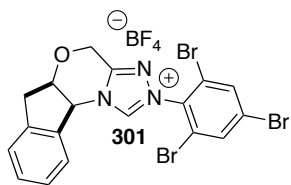


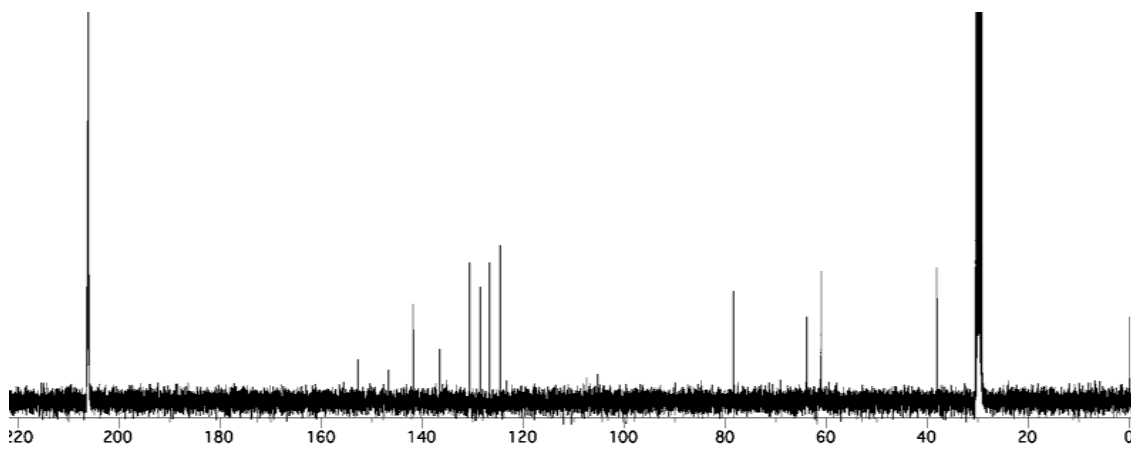
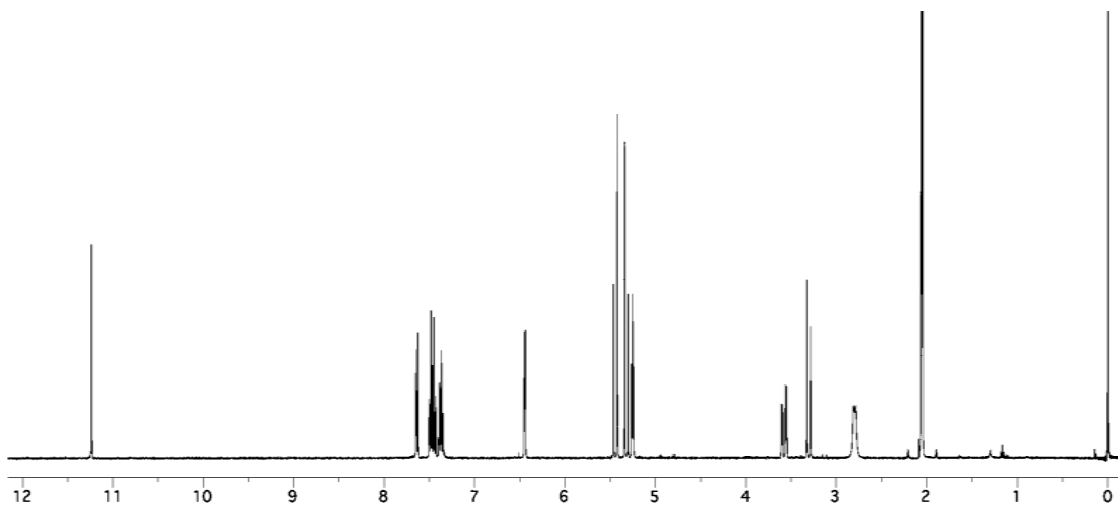
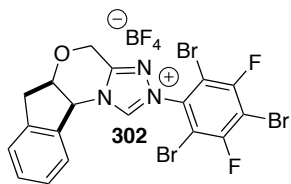
HRMS ESI-APCI
calcd mass = 563.1611 (M+H)
found = 563.1606

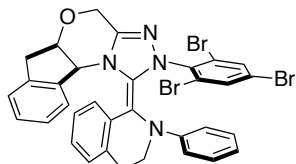




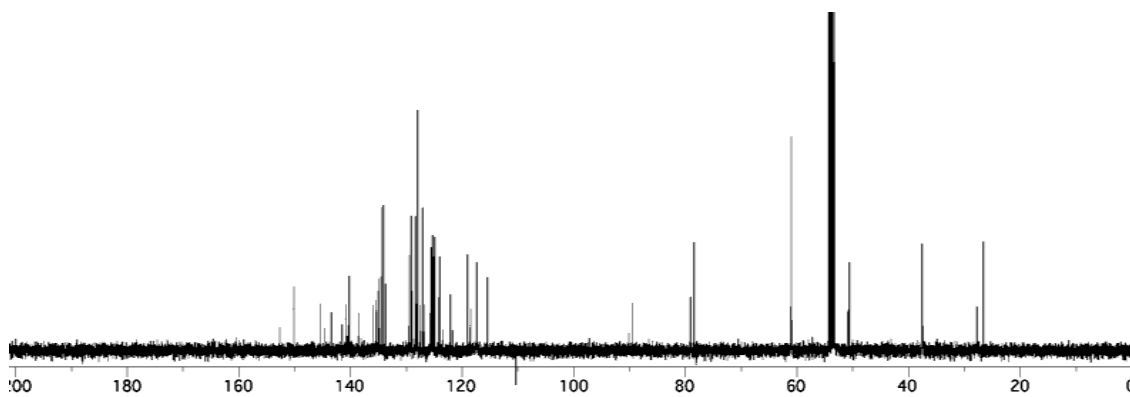
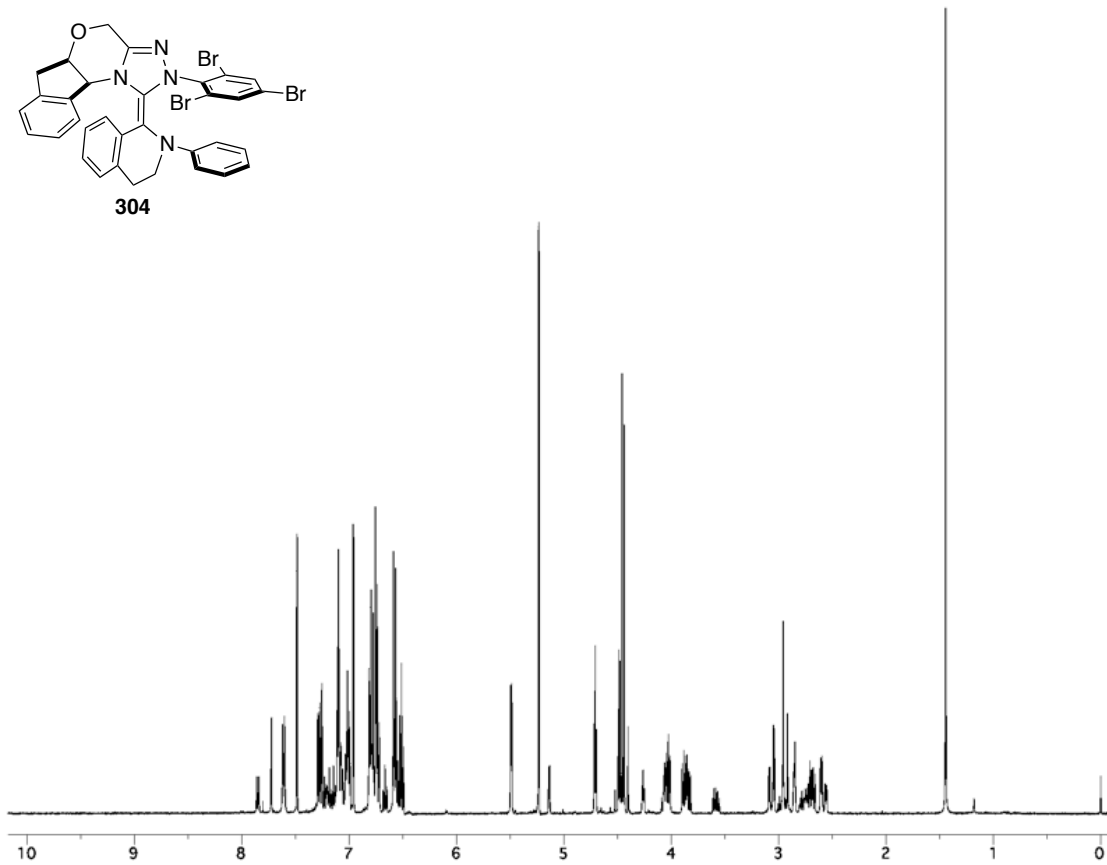


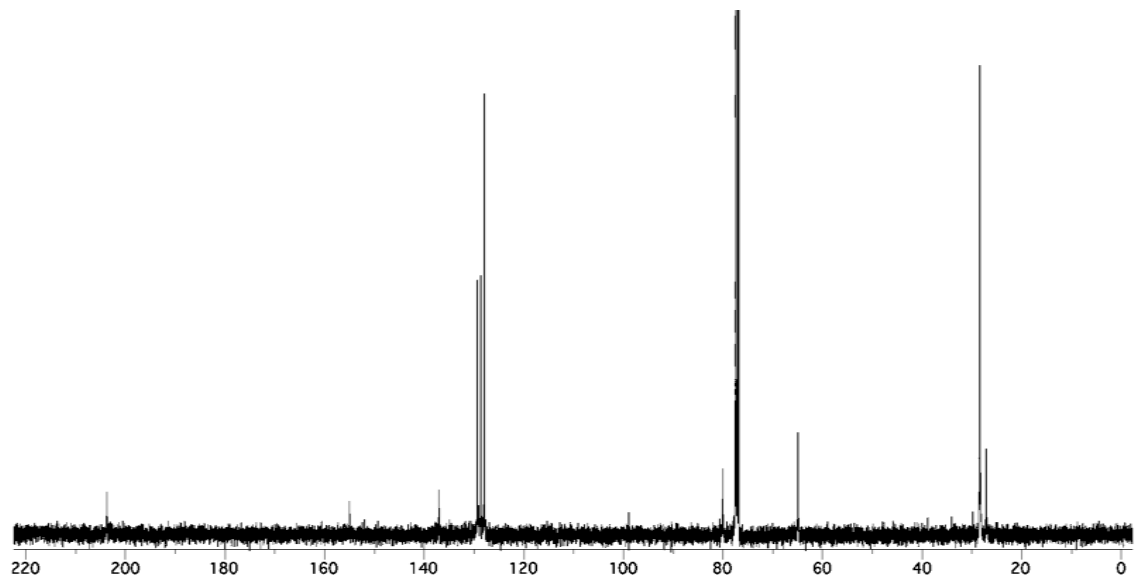
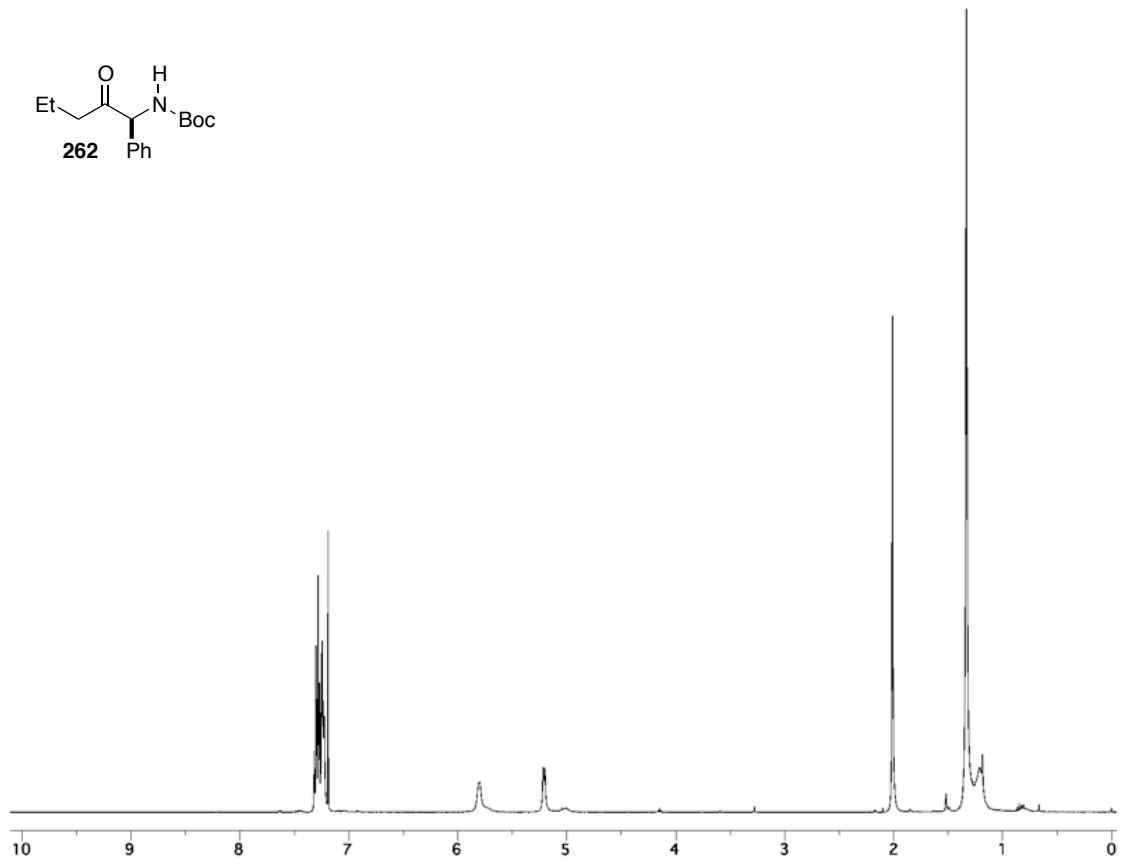
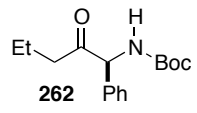


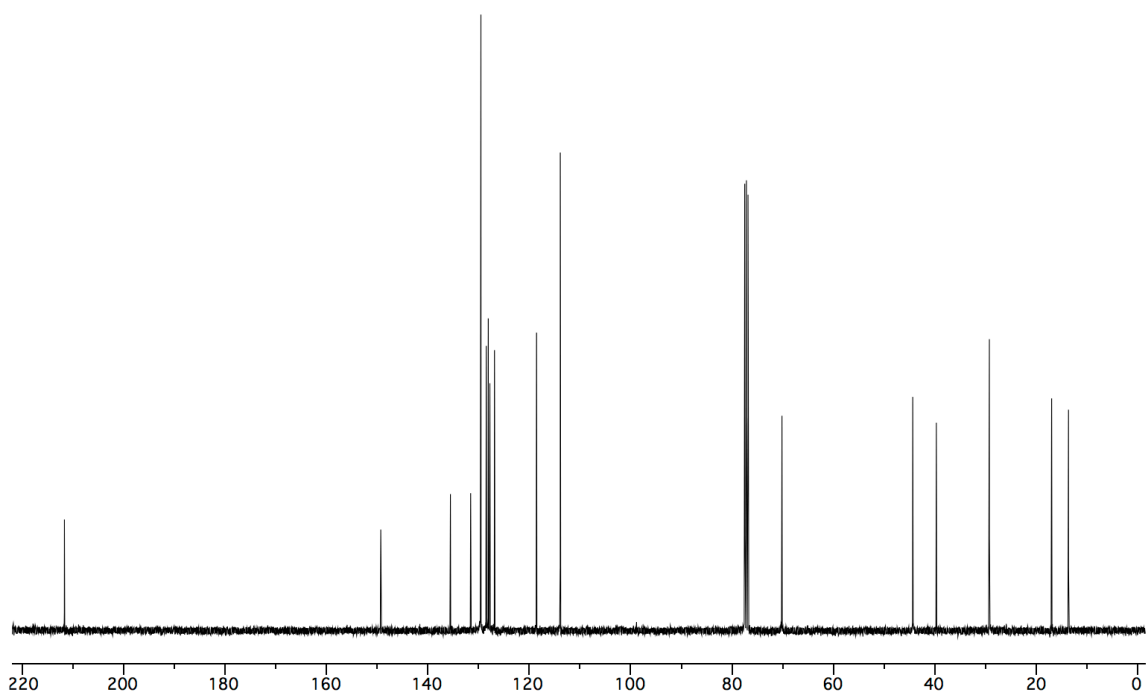
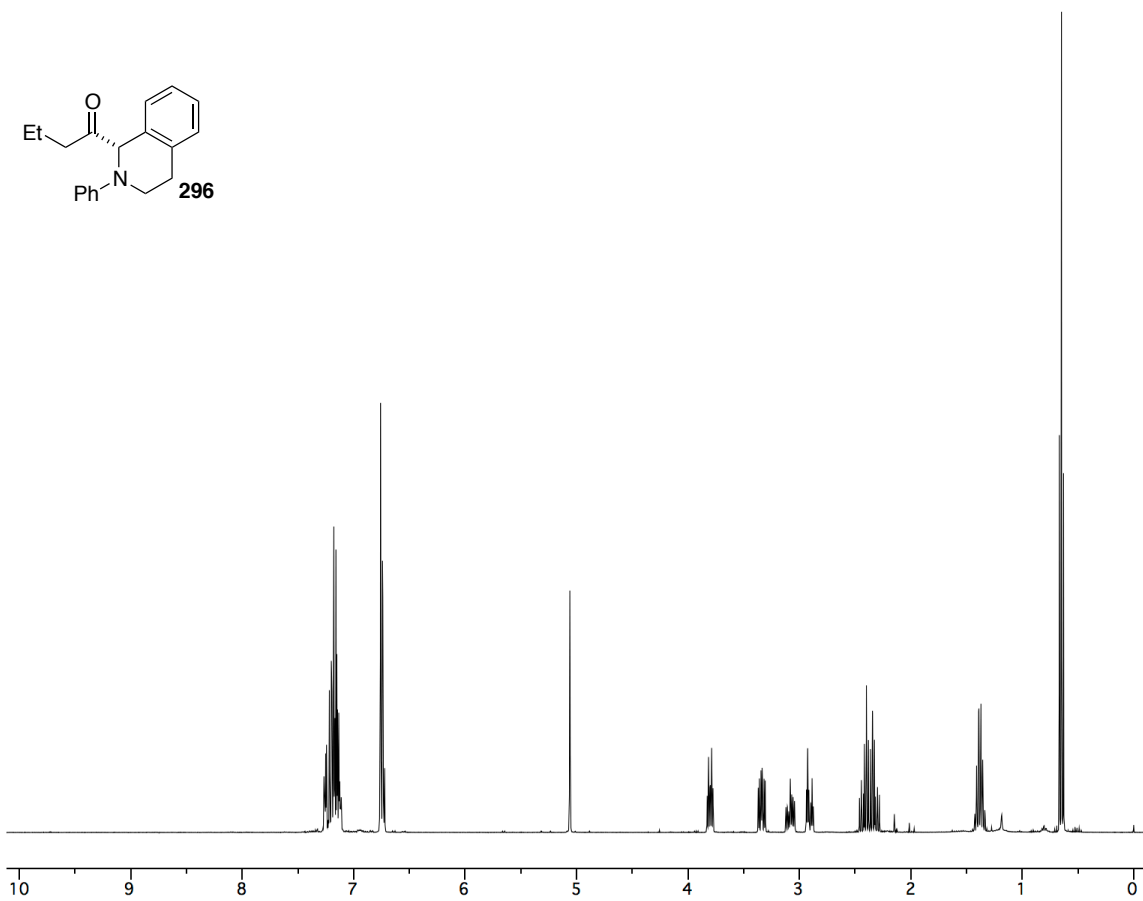
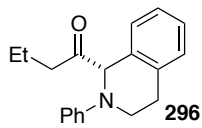




304







Crystallographic Data

Table A3.1 Crystal data and structure refinement for **(304)**.

Identification code	rovis128	
Empirical formula	$C_{33}H_{25}Br_3N_4O$	
Formula weight	733.30	
Temperature	120 K	
Wavelength	0.71073 Å	
Crystal system	Orthorhombic	
Space group	$P2_12_12_1$	
Unit cell dimensions	$a = 9.0959(4)$ Å	$\alpha = 90^\circ$.
	$b = 16.5417(7)$ Å	$\beta = 90^\circ$.
	$c = 18.7217(8)$ Å	$\gamma = 90^\circ$.
Volume	$2816.9(2)$ Å ³	
Z	4	
Density (calculated)	1.729 Mg/m ³	
Absorption coefficient	4.332 mm ⁻¹	
F(000)	1456	
Crystal size	0.26 x 0.12 x 0.09 mm ³	
Theta range for data collection	1.64 to 33.44°.	
Index ranges	$-13 \leq h \leq 14$, $-25 \leq k \leq 25$, $-29 \leq l \leq 28$	
Reflections collected	79444	
Independent reflections	10886 [R(int) = 0.1176]	
Completeness to theta = 33.44°	99.2 %	
Absorption correction	Semi-empirical from equivalents	
Max. and min. transmission	0.6939 and 0.3988	
Refinement method	Full-matrix least-squares on F ²	
Data / restraints / parameters	10886 / 0 / 371	
Goodness-of-fit on F ²	1.017	
Final R indices [I > 2σ(I)]	R1 = 0.0468, wR2 = 0.0912	
R indices (all data)	R1 = 0.1088, wR2 = 0.1277	
Absolute structure parameter	0.006(10)	
Largest diff. peak and hole	0.680 and -0.939 e.Å ⁻³	

Table A3.2 Atomic coordinates ($\times 10^4$) and equivalent isotropic displacement parameters ($\text{\AA}^2 \times 10^3$) for (304). $U(\text{eq})$ is defined as one third of the trace of the orthogonalized U^{ij} tensor.

	x	y	z	$U(\text{eq})$
Br(1)	2038(1)	1405(1)	7495(1)	24(1)
Br(2)	7674(1)	2879(1)	7623(1)	22(1)
Br(3)	4539(1)	2262(1)	10152(1)	31(1)
C(1)	5977(5)	1526(2)	6581(2)	13(1)
C(2)	6528(5)	1524(2)	5240(2)	13(1)
C(3)	5275(5)	1021(2)	4929(2)	14(1)
C(4)	4296(5)	503(2)	5251(2)	17(1)
C(5)	3355(5)	58(3)	4820(3)	22(1)
C(6)	3390(5)	142(3)	4084(3)	21(1)
C(7)	4357(5)	672(3)	3766(2)	20(1)
C(8)	5297(5)	1112(2)	4189(2)	15(1)
C(9)	6465(5)	1710(3)	3967(2)	19(1)
C(10)	6784(5)	2165(2)	4651(2)	15(1)
C(11)	5807(5)	3229(2)	5348(2)	18(1)
C(12)	5588(5)	2660(2)	5961(2)	13(1)
C(13)	4851(4)	2123(2)	7673(2)	14(1)
C(14)	5967(5)	2473(2)	8074(2)	16(1)
C(15)	5879(5)	2535(3)	8814(2)	18(1)
C(16)	4623(5)	2244(3)	9145(2)	18(1)
C(17)	3455(5)	1914(2)	8762(2)	17(1)
C(18)	3586(5)	1859(2)	8025(2)	14(1)
C(19)	6535(5)	820(2)	6844(2)	13(1)
C(20)	6455(5)	481(2)	8122(2)	15(1)
C(21)	7827(5)	836(2)	8228(2)	17(1)
C(22)	8382(6)	928(3)	8920(3)	24(1)
C(23)	7610(6)	662(3)	9505(3)	27(1)
C(24)	6265(6)	277(3)	9401(2)	27(1)
C(25)	5693(6)	177(3)	8719(2)	21(1)
C(26)	5333(5)	-387(2)	7206(2)	20(1)
C(27)	6696(6)	-903(2)	7055(3)	22(1)
C(28)	7958(5)	-440(2)	6719(2)	16(1)

C(29)	9287(6)	-829(3)	6577(2)	22(1)
C(30)	10485(5)	-426(3)	6291(2)	19(1)
C(31)	10371(5)	403(3)	6149(2)	16(1)
C(32)	9070(5)	798(2)	6293(2)	13(1)
C(33)	7845(5)	401(2)	6582(2)	13(1)
N(1)	6269(4)	1913(2)	5934(2)	12(1)
N(2)	4840(4)	2782(2)	6527(2)	15(1)
N(3)	4977(4)	2044(2)	6916(2)	13(1)
N(4)	5772(4)	440(2)	7434(2)	15(1)
O(1)	5692(3)	2795(2)	4695(2)	16(1)

Table A3.3 Bond lengths [\AA] and angles [$^\circ$] for (304).

		C(13)-C(14)	1.389(6)
Br(1)-C(18)	1.880(4)	C(13)-C(18)	1.397(6)
Br(2)-C(14)	1.890(4)	C(13)-N(3)	1.429(5)
Br(3)-C(16)	1.888(4)	C(14)-C(15)	1.391(6)
C(1)-C(19)	1.365(6)	C(15)-C(16)	1.386(7)
C(1)-N(1)	1.397(5)	C(16)-C(17)	1.393(6)
C(1)-N(3)	1.398(5)	C(17)-C(18)	1.387(6)
C(2)-N(1)	1.468(5)	C(19)-N(4)	1.447(5)
C(2)-C(3)	1.526(6)	C(19)-C(33)	1.464(6)
C(2)-C(10)	1.548(5)	C(20)-C(21)	1.394(6)
C(3)-C(4)	1.375(6)	C(20)-C(25)	1.408(6)
C(3)-C(8)	1.395(6)	C(20)-N(4)	1.431(5)
C(4)-C(5)	1.388(6)	C(21)-C(22)	1.399(6)
C(5)-C(6)	1.385(7)	C(22)-C(23)	1.373(7)
C(6)-C(7)	1.378(7)	C(23)-C(24)	1.392(8)
C(7)-C(8)	1.373(6)	C(24)-C(25)	1.389(7)
C(8)-C(9)	1.510(6)	C(26)-N(4)	1.487(5)
C(9)-C(10)	1.513(6)	C(26)-C(27)	1.531(7)
C(10)-O(1)	1.442(5)	C(27)-C(28)	1.517(6)
C(11)-O(1)	1.422(5)	C(28)-C(29)	1.395(6)
C(11)-C(12)	1.496(6)	C(28)-C(33)	1.418(5)
C(12)-N(2)	1.275(5)	C(29)-C(30)	1.386(7)
C(12)-N(1)	1.383(5)	C(30)-C(31)	1.401(6)

C(31)-C(32)	1.379(6)	C(17)-C(16)-Br(3)	119.3(3)
C(32)-C(33)	1.401(6)	C(18)-C(17)-C(16)	118.2(4)
N(2)-N(3)	1.427(4)	C(17)-C(18)-C(13)	121.3(4)
C(19)-C(1)-N(1)	129.4(4)	C(17)-C(18)-Br(1)	119.2(3)
C(19)-C(1)-N(3)	127.2(4)	C(13)-C(18)-Br(1)	119.6(3)
N(1)-C(1)-N(3)	103.3(3)	C(1)-C(19)-N(4)	117.9(4)
N(1)-C(2)-C(3)	117.1(3)	C(1)-C(19)-C(33)	125.9(4)
N(1)-C(2)-C(10)	110.7(3)	N(4)-C(19)-C(33)	116.2(3)
C(3)-C(2)-C(10)	102.3(3)	C(21)-C(20)-C(25)	118.6(4)
C(4)-C(3)-C(8)	120.8(4)	C(21)-C(20)-N(4)	122.5(4)
C(4)-C(3)-C(2)	131.0(4)	C(25)-C(20)-N(4)	118.9(4)
C(8)-C(3)-C(2)	108.0(4)	C(20)-C(21)-C(22)	120.1(4)
C(3)-C(4)-C(5)	118.3(4)	C(23)-C(22)-C(21)	121.3(5)
C(6)-C(5)-C(4)	120.8(4)	C(22)-C(23)-C(24)	119.0(4)
C(7)-C(6)-C(5)	120.5(4)	C(25)-C(24)-C(23)	120.8(5)
C(8)-C(7)-C(6)	119.1(4)	C(24)-C(25)-C(20)	120.2(5)
C(7)-C(8)-C(3)	120.4(4)	N(4)-C(26)-C(27)	110.4(4)
C(7)-C(8)-C(9)	128.8(4)	C(28)-C(27)-C(26)	114.1(3)
C(3)-C(8)-C(9)	110.7(4)	C(29)-C(28)-C(33)	118.7(4)
C(8)-C(9)-C(10)	103.2(3)	C(29)-C(28)-C(27)	120.2(4)
O(1)-C(10)-C(9)	106.0(3)	C(33)-C(28)-C(27)	121.0(4)
O(1)-C(10)-C(2)	110.5(3)	C(30)-C(29)-C(28)	122.2(4)
C(9)-C(10)-C(2)	103.5(3)	C(29)-C(30)-C(31)	119.1(4)
O(1)-C(11)-C(12)	109.4(3)	C(32)-C(31)-C(30)	119.4(4)
N(2)-C(12)-N(1)	114.3(4)	C(31)-C(32)-C(33)	122.4(4)
N(2)-C(12)-C(11)	127.5(4)	C(32)-C(33)-C(28)	118.2(4)
N(1)-C(12)-C(11)	118.3(4)	C(32)-C(33)-C(19)	123.7(3)
C(14)-C(13)-C(18)	118.5(4)	C(28)-C(33)-C(19)	117.5(4)
C(14)-C(13)-N(3)	121.1(4)	C(12)-N(1)-C(1)	107.0(3)
C(18)-C(13)-N(3)	120.4(4)	C(12)-N(1)-C(2)	119.8(3)
C(13)-C(14)-C(15)	121.8(4)	C(1)-N(1)-C(2)	126.6(3)
C(13)-C(14)-Br(2)	120.4(3)	C(12)-N(2)-N(3)	104.0(3)
C(15)-C(14)-Br(2)	117.8(3)	C(1)-N(3)-N(2)	110.7(3)
C(16)-C(15)-C(14)	117.8(4)	C(1)-N(3)-C(13)	123.6(3)
C(15)-C(16)-C(17)	122.4(4)	N(2)-N(3)-C(13)	114.9(3)
C(15)-C(16)-Br(3)	118.3(3)	C(20)-N(4)-C(19)	117.2(3)

C(20)-N(4)-C(26)	114.7(3)	Symmetry transformations used to generate equivalent atoms:
C(19)-N(4)-C(26)	108.0(3)	
C(11)-O(1)-C(10)	111.3(3)	

Table A3.4 Anisotropic displacement parameters ($\text{\AA}^2 \times 10^3$) for (304). The anisotropic displacement factor exponent takes the form: $-2\pi^2 [h^2 a^{*2} U^{11} + \dots + 2 h k a^* b^* U^{12}]$

	U ¹¹	U ²²	U ³³	U ²³	U ¹³	U ¹²
Br(1)	18(1)	32(1)	21(1)	4(1)	-3(1)	-9(1)
Br(2)	15(1)	24(1)	26(1)	-1(1)	1(1)	-5(1)
Br(3)	40(1)	41(1)	12(1)	-4(1)	2(1)	5(1)
C(1)	12(2)	15(2)	12(2)	-5(2)	-1(2)	-1(2)
C(2)	12(2)	17(2)	9(2)	0(2)	2(2)	2(2)
C(3)	15(2)	12(2)	15(2)	0(2)	-2(2)	4(2)
C(4)	18(2)	17(2)	16(2)	-1(2)	4(2)	0(2)
C(5)	21(2)	19(2)	26(2)	-4(2)	2(2)	-1(2)
C(6)	17(2)	20(2)	28(3)	-8(2)	-6(2)	2(2)
C(7)	26(3)	19(2)	16(2)	-2(2)	-3(2)	6(2)
C(8)	15(2)	14(2)	16(2)	-1(2)	0(2)	5(2)
C(9)	23(2)	23(2)	12(2)	3(2)	2(2)	3(2)
C(10)	16(2)	16(2)	14(2)	4(2)	2(2)	1(2)
C(11)	25(2)	15(2)	14(2)	1(2)	-1(2)	-1(2)
C(12)	15(2)	12(2)	13(2)	-1(1)	-2(2)	1(2)
C(13)	14(2)	14(2)	14(2)	0(2)	3(2)	3(2)
C(14)	13(2)	16(2)	20(2)	1(2)	3(2)	1(2)
C(15)	17(2)	20(2)	18(2)	-5(2)	-3(2)	3(2)
C(16)	25(2)	18(2)	11(2)	-2(2)	1(2)	8(2)
C(17)	18(2)	18(2)	16(2)	4(2)	5(2)	3(2)
C(18)	11(2)	13(2)	19(2)	0(2)	-3(2)	2(2)
C(19)	18(2)	8(2)	11(2)	1(1)	0(2)	-2(2)
C(20)	17(2)	11(2)	16(2)	2(2)	2(2)	4(2)
C(21)	20(2)	14(2)	16(2)	-1(2)	3(2)	3(2)
C(22)	26(3)	20(2)	24(3)	-6(2)	-7(2)	9(2)

C(23)	43(3)	22(2)	16(2)	-4(2)	-6(2)	14(2)
C(24)	47(4)	20(2)	15(2)	5(2)	3(2)	8(2)
C(25)	26(3)	16(2)	22(2)	2(2)	8(2)	3(2)
C(26)	25(3)	15(2)	19(2)	1(2)	0(2)	-5(2)
C(27)	31(3)	13(2)	22(2)	-1(2)	3(2)	-6(2)
C(28)	20(2)	15(2)	13(2)	0(2)	-2(2)	1(2)
C(29)	32(3)	17(2)	18(2)	0(2)	0(2)	8(2)
C(30)	18(2)	21(2)	19(2)	-1(2)	3(2)	11(2)
C(31)	12(2)	23(2)	13(2)	0(2)	4(2)	0(2)
C(32)	14(2)	13(2)	11(2)	1(2)	-5(2)	-2(2)
C(33)	18(2)	13(2)	8(2)	-3(1)	-2(2)	4(2)
N(1)	18(2)	11(2)	8(2)	1(1)	0(1)	2(1)
N(2)	18(2)	12(2)	16(2)	1(1)	-5(1)	4(1)
N(3)	15(2)	10(2)	15(2)	4(1)	0(1)	3(1)
N(4)	18(2)	11(1)	16(2)	3(1)	0(2)	-2(1)
O(1)	18(2)	15(1)	13(1)	3(1)	-2(1)	4(1)

Table A3.5 Hydrogen coordinates ($\times 10^4$) and isotropic displacement parameters ($\text{\AA}^2 \times 10^{-3}$) for **(304)**.

	x	y	z	U(eq)
H(2)	7406	1183	5277	15
H(4)	4265	452	5746	20
H(5)	2694	-301	5027	27
H(6)	2756	-163	3802	26
H(7)	4373	732	3272	24
H(9A)	6104	2072	3598	23
H(9B)	7337	1436	3793	23
H(10)	7787	2382	4661	18
H(11A)	5069	3652	5364	21
H(11B)	6768	3480	5382	21
H(15)	6637	2765	9078	22
H(17)	2610	1736	8994	21

H(21)	8375	1012	7838	20
H(22)	9291	1174	8986	28
H(23)	7979	737	9963	33
H(24)	5744	84	9793	33
H(25)	4804	-91	8656	26
H(26A)	4733	-353	6779	23
H(26B)	4752	-638	7579	23
H(27A)	7033	-1138	7501	26
H(27B)	6420	-1342	6740	26
H(29)	9371	-1378	6678	27
H(30)	11353	-702	6194	23
H(31)	11166	685	5960	20
H(32)	9002	1348	6196	15

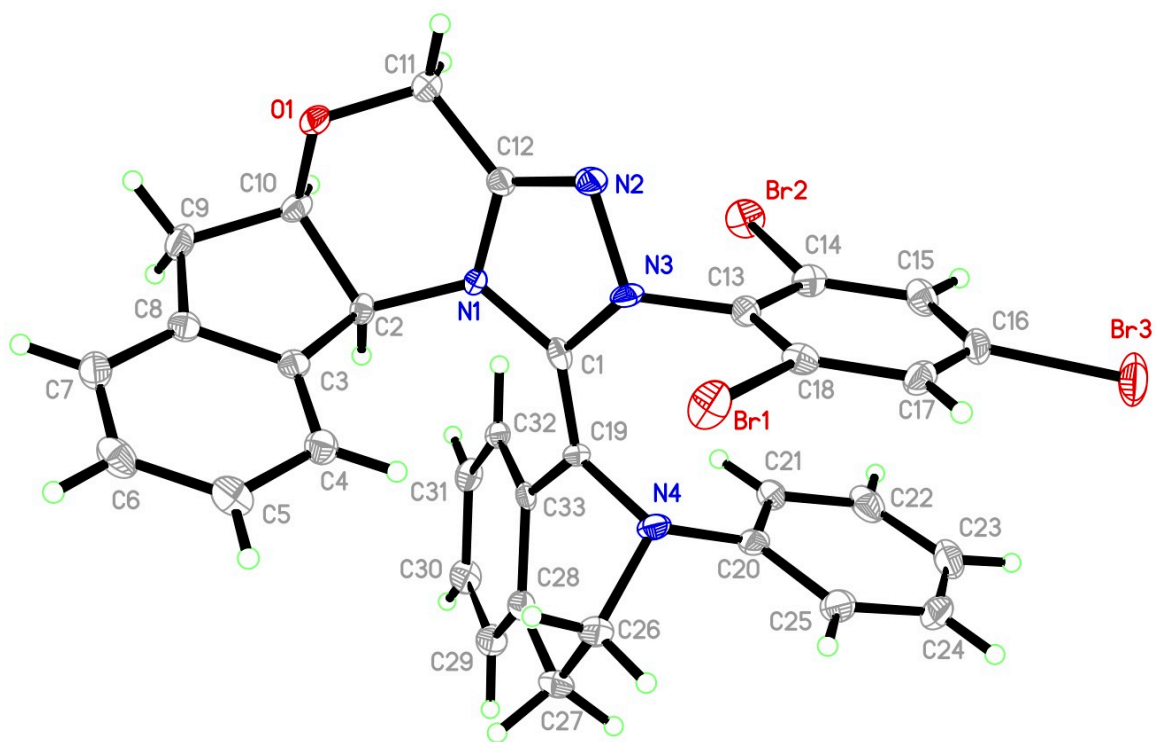


Figure A3.1 Thermal plot of (304). Ellipsoids shown at the 50% probability level.

Table A3.6 Crystal data and structure refinement for (323).

Identification code	rovis147_0m	
Empirical formula	C ₂₆ H ₂₆ BrNO ₂	
Formula weight	464.39	
Temperature	110(2) K	
Wavelength	0.71073 Å	
Crystal system	Orthorhombic	
Space group	<i>P</i> 2 ₁ 2 ₁ 2 ₁	
Unit cell dimensions	<i>a</i> = 6.1152(5) Å	$\alpha = 90^\circ$.
	<i>b</i> = 18.3377(13) Å	$\beta = 90^\circ$.
	<i>c</i> = 20.0164(14) Å	$\gamma = 90^\circ$.
Volume	2244.6(3) Å ³	
Z	4	
Density (calculated)	1.374 Mg/m ³	
Absorption coefficient	1.853 mm ⁻¹	
F(000)	960	
Crystal size	0.20 x 0.16 x 0.14 mm ³	
Theta range for data collection	2.03 to 27.51°.	
Index ranges	-7 ≤ <i>h</i> ≤ 7, -23 ≤ <i>k</i> ≤ 23, -25 ≤ <i>l</i> ≤ 25	
Reflections collected	41125	
Independent reflections	5138 [R(int) = 0.0671]	
Completeness to theta = 27.51°	99.9 %	
Absorption correction	Semi-empirical from equivalents	
Max. and min. transmission	0.7801 and 0.7082	
Refinement method	Full-matrix least-squares on F ²	
Data / restraints / parameters	5138 / 0 / 283	
Goodness-of-fit on F ²	1.037	
Final R indices [I > 2σ(I)]	R1 = 0.0501, wR2 = 0.0995	
R indices (all data)	R1 = 0.0957, wR2 = 0.1143	
Absolute structure parameter	0.024(13)	
Largest diff. peak and hole	0.518 and -0.706 e.Å ⁻³	

Table 7. Atomic coordinates ($\times 10^4$) and equivalent isotropic displacement parameters ($\text{\AA}^2 \times 10^3$) for **(323)**. $U(\text{eq})$ is defined as one third of the trace of the orthogonalized U^{ij} tensor.

	x	y	z	$U(\text{eq})$
Br(1)	12545(1)	6286(1)	9810(1)	60(1)
C(1)	12165(7)	6043(2)	8894(2)	38(1)
C(2)	13807(7)	5680(2)	8565(2)	43(1)
C(3)	13535(7)	5485(3)	7907(2)	42(1)
C(4)	11600(6)	5660(2)	7582(2)	27(1)
C(5)	9951(6)	6027(2)	7918(2)	37(1)
C(6)	10247(6)	6231(3)	8579(2)	39(1)
C(7)	11404(6)	5454(2)	6859(2)	28(1)
C(8)	8974(6)	5322(2)	5929(2)	28(1)
C(9)	7692(8)	4616(2)	5852(2)	34(1)
C(10)	8673(8)	3970(2)	6225(2)	46(1)
C(11)	7654(11)	3244(2)	6019(2)	64(1)
C(12)	7773(7)	6002(2)	5658(2)	24(1)
C(13)	7731(7)	5969(2)	4893(2)	28(1)
C(14)	6006(9)	5637(2)	4566(2)	51(1)
C(15)	5995(11)	5603(3)	3868(2)	65(2)
C(16)	7676(11)	5905(2)	3510(2)	51(1)
C(17)	9339(7)	6248(2)	3830(2)	40(1)
C(18)	9383(6)	6290(3)	4529(2)	38(1)
C(20)	10821(7)	6895(3)	5553(2)	40(1)
C(21)	8111(5)	7027(2)	6464(2)	25(1)
C(22)	9377(8)	7571(3)	6757(2)	59(2)
C(23)	8704(9)	7930(3)	7328(3)	70(2)
C(24)	6753(7)	7775(3)	7627(2)	44(1)
C(25)	5462(7)	7246(2)	7351(2)	32(1)
C(26)	6123(6)	6880(2)	6776(2)	30(1)
N(1)	8787(5)	6688(2)	5877(2)	26(1)
O(1)	9334(4)	5449(2)	6644(1)	31(1)
O(2)	12950(4)	5307(2)	6513(1)	48(1)
C(19A)	10945(16)	6900(9)	4824(5)	28(3)
C(19B)	11267(17)	6474(11)	4939(5)	40(4)

Table A3.8 Bond lengths [\AA] and angles [$^\circ$] for (323).

Br(1)-C(1)	1.901(4)	C(23)-C(24)	1.364(6)
C(1)-C(2)	1.373(6)	C(24)-C(25)	1.368(6)
C(1)-C(6)	1.375(5)	C(25)-C(26)	1.393(5)
C(2)-C(3)	1.376(6)	C(2)-C(1)-C(6)	121.7(4)
C(3)-C(4)	1.389(5)	C(2)-C(1)-Br(1)	119.1(3)
C(4)-C(5)	1.386(5)	C(6)-C(1)-Br(1)	119.2(3)
C(4)-C(7)	1.500(5)	C(1)-C(2)-C(3)	119.8(4)
C(5)-C(6)	1.388(5)	C(2)-C(3)-C(4)	119.4(4)
C(7)-O(2)	1.203(4)	C(5)-C(4)-C(3)	120.3(4)
C(7)-O(1)	1.337(4)	C(5)-C(4)-C(7)	122.2(3)
C(8)-O(1)	1.468(4)	C(3)-C(4)-C(7)	117.5(4)
C(8)-C(9)	1.520(6)	C(4)-C(5)-C(6)	119.9(4)
C(8)-C(12)	1.546(5)	C(1)-C(6)-C(5)	118.7(4)
C(9)-C(10)	1.524(5)	O(2)-C(7)-O(1)	123.9(3)
C(10)-C(11)	1.527(7)	O(2)-C(7)-C(4)	123.3(3)
C(12)-N(1)	1.470(5)	O(1)-C(7)-C(4)	112.8(3)
C(12)-C(13)	1.531(4)	O(1)-C(8)-C(9)	108.1(3)
C(13)-C(18)	1.378(6)	O(1)-C(8)-C(12)	106.6(3)
C(13)-C(14)	1.383(6)	C(9)-C(8)-C(12)	114.0(3)
C(14)-C(15)	1.397(6)	C(8)-C(9)-C(10)	114.2(4)
C(15)-C(16)	1.370(7)	C(9)-C(10)-C(11)	112.7(4)
C(16)-C(17)	1.357(7)	N(1)-C(12)-C(13)	109.8(3)
C(17)-C(18)	1.402(5)	N(1)-C(12)-C(8)	112.6(3)
C(18)-C(19B)	1.453(11)	C(13)-C(12)-C(8)	109.1(3)
C(18)-C(19A)	1.584(11)	C(18)-C(13)-C(14)	119.8(3)
C(20)-N(1)	1.454(5)	C(18)-C(13)-C(12)	119.9(4)
C(20)-C(19A)	1.461(11)	C(14)-C(13)-C(12)	120.3(4)
C(20)-C(19B)	1.477(12)	C(13)-C(14)-C(15)	119.8(5)
C(21)-N(1)	1.392(4)	C(16)-C(15)-C(14)	120.1(5)
C(21)-C(26)	1.393(5)	C(17)-C(16)-C(15)	120.1(4)
C(21)-C(22)	1.393(5)	C(16)-C(17)-C(18)	120.8(4)
C(22)-C(23)	1.381(6)	C(13)-C(18)-C(17)	119.3(4)

C(13)-C(18)-C(19B)	112.5(5)	C(24)-C(23)-C(22)	121.6(5)
C(17)-C(18)-C(19B)	126.2(5)	C(23)-C(24)-C(25)	118.4(4)
C(13)-C(18)-C(19A)	123.2(4)	C(24)-C(25)-C(26)	120.5(4)
C(17)-C(18)-C(19A)	115.0(6)	C(21)-C(26)-C(25)	122.1(4)
C(19B)-C(18)-C(19A)	31.7(4)	C(21)-N(1)-C(20)	121.0(3)
N(1)-C(20)-C(19A)	119.5(5)	C(21)-N(1)-C(12)	120.6(3)
N(1)-C(20)-C(19B)	113.1(6)	C(20)-N(1)-C(12)	116.8(3)
C(19A)-C(20)-C(19B)	33.1(4)	C(7)-O(1)-C(8)	117.2(3)
N(1)-C(21)-C(26)	123.5(3)	C(20)-C(19A)-C(18)	109.6(8)
N(1)-C(21)-C(22)	120.7(3)	C(18)-C(19B)-C(20)	116.3(8)
C(26)-C(21)-C(22)	115.8(3)		
C(23)-C(22)-C(21)	121.6(4)		

Symmetry transformations used to generate equivalent atoms:

Table A3.9 Anisotropic displacement parameters ($\text{\AA}^2 \times 10^3$) for (323). The anisotropic displacement factor exponent takes the form: $-2\pi^2 [h^2 a^{*2} U^{11} + \dots + 2 h k a^* b^* U^{12}]$

	U^{11}	U^{22}	U^{33}	U^{23}	U^{13}	U^{12}
Br(1)	75(1)	67(1)	38(1)	-6(1)	-31(1)	6(1)
C(1)	43(3)	40(2)	32(2)	3(2)	-18(2)	-7(2)
C(2)	28(2)	47(3)	54(3)	-7(2)	-20(2)	10(2)
C(3)	26(2)	51(3)	49(3)	-10(2)	-13(2)	8(2)
C(4)	19(2)	31(2)	31(2)	5(2)	-1(2)	-2(2)
C(5)	25(2)	59(3)	26(2)	7(2)	-6(2)	10(2)
C(6)	34(2)	58(3)	25(2)	3(2)	-4(2)	7(2)
C(7)	18(2)	36(2)	30(2)	5(2)	3(2)	-4(2)
C(8)	23(2)	45(2)	16(2)	4(2)	2(2)	11(2)
C(9)	40(2)	39(2)	24(2)	6(2)	10(2)	10(2)
C(10)	58(3)	55(3)	25(2)	10(2)	11(2)	24(2)
C(11)	77(4)	49(3)	66(3)	30(2)	17(3)	15(4)
C(12)	19(2)	34(2)	20(2)	-4(1)	1(2)	12(2)
C(13)	38(2)	28(2)	18(2)	-1(1)	-2(2)	5(2)
C(14)	76(3)	47(3)	29(2)	7(2)	-15(2)	-24(3)
C(15)	108(5)	57(3)	29(3)	1(2)	-19(3)	-31(3)
C(16)	100(4)	31(2)	21(2)	2(2)	-8(3)	13(3)
C(17)	57(3)	40(2)	24(2)	2(2)	6(2)	15(3)
C(18)	35(2)	54(3)	26(2)	-7(2)	2(2)	14(2)
C(20)	34(2)	51(3)	33(2)	-7(2)	15(2)	-15(2)
C(21)	22(2)	37(2)	16(2)	-5(2)	-4(1)	-2(2)
C(22)	46(3)	85(4)	45(3)	-31(3)	22(2)	-43(3)
C(23)	68(4)	90(4)	53(3)	-47(3)	23(3)	-48(3)
C(24)	46(3)	66(3)	21(2)	-16(2)	4(2)	-9(2)
C(25)	25(2)	44(3)	27(2)	-3(2)	4(2)	3(2)
C(26)	20(2)	40(2)	32(2)	-11(2)	1(2)	-2(2)
N(1)	16(2)	40(2)	21(2)	-6(1)	3(1)	-3(1)
O(1)	16(1)	60(2)	17(1)	4(1)	-1(1)	10(1)
O(2)	17(2)	82(2)	46(2)	-22(2)	5(1)	-1(2)
C(19A)	16(4)	44(8)	25(5)	-1(5)	-3(4)	-1(4)

C(19B) 28(5) 67(10) 26(5) 15(5) 17(4) 9(6)

Table A3.10 Hydrogen coordinates ($\times 10^4$) and isotropic displacement parameters ($\text{\AA}^2 \times 10^{-3}$)
For (323).

	x	y	z	U(eq)
H(2)	15127	5564	8792	51
H(3)	14663	5232	7676	51
H(5)	8620	6139	7695	44
H(6)	9146	6496	8810	47
H(8)	10418	5272	5699	33
H(9A)	7602	4493	5371	41
H(9B)	6183	4697	6016	41
H(10A)	8459	4041	6711	55
H(10B)	10266	3953	6139	55
H(11A)	6070	3262	6091	96
H(11B)	8285	2850	6289	96
H(11C)	7954	3153	5546	96
H(12)	6231	5991	5824	29
H(14)	4832	5433	4814	61
H(15)	4821	5371	3642	78
H(16)	7677	5874	3036	61
H(17)	10488	6461	3578	49
H(20A)	11976	6563	5718	48
H(20B)	11202	7391	5710	48
H(22)	10737	7698	6560	71
H(23)	9622	8293	7517	85
H(24)	6303	8029	8017	53
H(25)	4103	7126	7554	39
H(26)	5188	6520	6590	37
H(19A)	12469	6807	4680	34
H(19B)	10501	7384	4652	34
H(19C)	12305	6756	4661	48

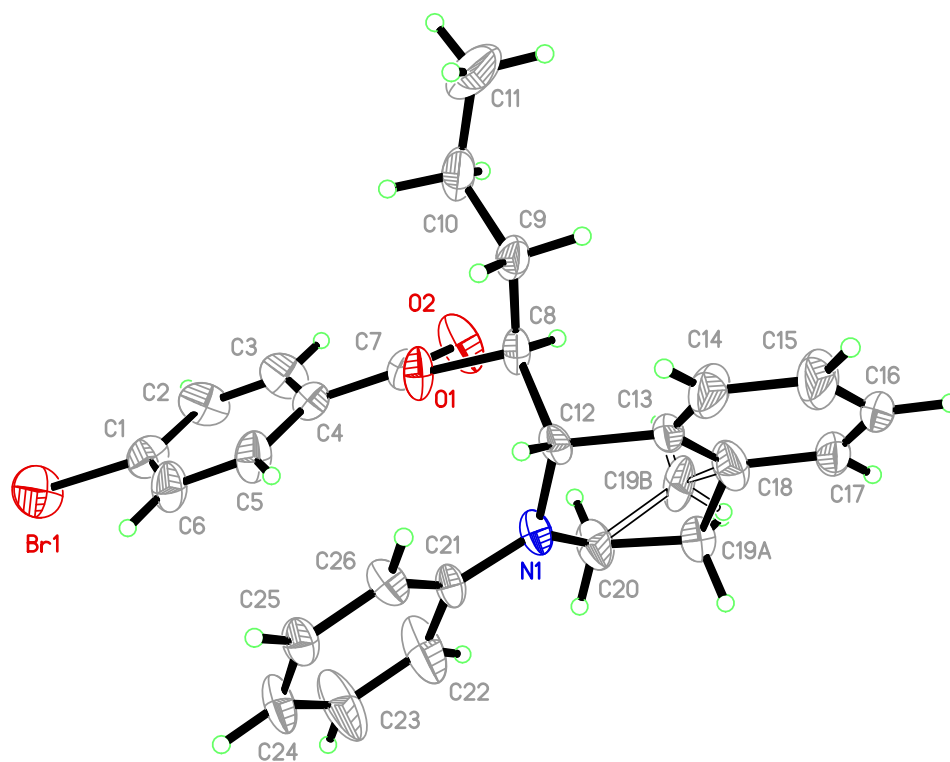


Figure A3.2 Thermal plot of (323). Ellipsoids drawn at the 50% probability level.

REFERENCES

- ¹ Huang, L.; Wulff, W. D. *J. Am. Chem. Soc.* **2011**, *133*, 8892-8895.
- ² Li, Z.; Li, C.-L. *J. Am. Chem. Soc.* **2005**, *127*, 6968-6969.
- ³ M. K. Ghorai, A. Kumar, D. P. Tiwari, *J. Org. Chem.* **2010**, *75*, 137-151.

Appendix 4

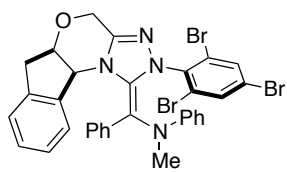
Isolation and Characterization of Aza-Breslow Intermediates

Materials and Methods:

All reactions were carried out under an atmosphere of argon in flame-dried glassware with magnetic stirring. Dichloromethane was degassed with argon and passed through two columns of neutral alumina. Toluene was degassed with argon and passed through one column of neutral alumina and one column of Q5 reactant. Acetonitrile was purchased from Macron Chemicals and used without further purification. N,N-Diisopropylethylamine was purchased from Aldrich and distilled from Calcium hydride prior to use. Column chromatography was performed on SiliCycle®SilicaFlash® P60, 40-63µm 60A. Thin layer chromatography was performed on SiliCycle® 250µm 60A plates. Visualization was accomplished with UV light or KMnO₄ stain followed by heating.

¹H NMR spectra were recorded on Varian 300 or 400 MHz spectrometers at ambient temperature. Data is reported as follows: chemical shift in parts per million (δ , ppm) from toluene-*d*₈ (20.43 ppm) or acetone-*d*₆ (2.03 ppm), multiplicity (s = singlet, bs = broad singlet, d = doublet, t = triplet, q = quartet, and m = multiplet), coupling constants (Hz). ¹³C NMR were recorded Varian 300 or 400 MHz spectrometers (at 75 or 100 MHz) at ambient temperature. Chemical shifts are reported in ppm from CD₂Cl₂ (53.84 ppm) or acetone-*d*₆ (205.87, 30.6 ppm).

Experimental Procedures and Characterization Data

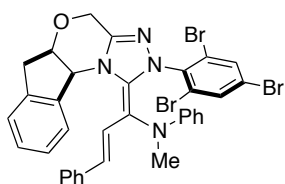


N-methyl-N-((Z)-phenyl((5aR,10bS)-2-(2,4,6-tribromophenyl)-5a,6-dihydroindeno[2,1-b][1,2,4]triazolo[4,3-d][1,4]oxazin-

1(2H,4H,10bH)-ylidene)methyl)aniline (346): To a dry 20 ml

scintillation vial was added trimethyloxonium tetrafluoroborate (48 mg, 0.331 mmol, 1.0 equiv), (E)-N-benzylideneaniline (60 mg, 0.331 mmol, 1.0 equiv) and acetonitrile (4 mL). The reaction was stirred for 18 h at which point triazolium salt (**301**) (200 mg, 0.331 mmol, 1.0 equiv) was added followed by N,N-diisopropylethylamine (0.36 mL, 1.66 mmol, 5.0 equiv). After resting undisturbed for 18 h, a yellow solid crystallized from the reaction mixture which was filtered, washed with acetonitrile followed by diethyl ether and dried to provide **3** as a yellow crystalline solid (162 mg, 68%). $[\alpha]_D^{21} = +242$ ($c = 0.0118$ g/ml, CH_2Cl_2); **m.p.** ($^\circ\text{C}$): 240-242; **$^1\text{H-NMR}$** (400 MHz; toluene- d_8): (mixture of isomers) δ 8.11 (d, $J = 7.5$ Hz, 1H), 7.93 (d, $J = 7.6$ Hz, 0.35H), 7.88 (d, $J = 7.4$ Hz, 0.54H), 7.38-7.24 (m, 4H), 7.22-7.14 (m, 2H), 6.93-6.82 (m, 5H), 6.82-6.76 (m, 1H), 6.74-6.66 (m, 3H), 6.59-6.50 (m, 1H), 6.42-6.38 (m, 0.47H), 6.34-6.32 (m, 0.38H), 5.32-5.29 (m, 0.74H), 5.25-5.24 (m, 0.37H), 5.08 (d, $J = 3.6$ Hz, 1H), 4.28 (s, 0.27H), 4.27-4.23 (m, 0.36H), 4.19 (d, $J = 14.6$ Hz, 1H), 4.13-3.99 (m, 2H), 3.79 (d, $J = 14.7$ Hz, 1H), 3.74-3.73 (m, 1H), 3.41 (s, 1H), 3.37 (s, 0.58H), 2.8 (m, 0.24H), 2.73 (m, 0.15H), 2.68 (m, 0.31H), 2.64 (s, 2H), 2.62 (s, 0.48H), 2.58 (s, 0.76H), 2.47-2.46 (m, 0.65H), 2.44-2.43 (m, 0.56H), 2.39-2.38 (m, 0.39H), 2.35-2.34 (m, 0.33H), 2.33 (s, 0.13H), 2.25 (s, 0.54H); **$^{13}\text{C NMR}$** (100 MHz; CD_2Cl_2): δ 150.6, 150.2, 148.0, 147.8, 146.9, 146.5, 146.23, 146.17, 145.3, 143.4, 141.2, 140.78, 140.75, 140.68, 140.57, 140.40, 140.30, 140.0, 139.58, 139.46, 139.11, 138.97, 138.7, 137.71, 137.59, 137.39, 136.3, 136.0, 135.62, 135.56, 135.52, 135.29, 135.21, 135.16, 134.91, 134.85, 129.6, 129.1, 128.9, 128.63, 128.45, 128.43, 128.34, 128.28, 128.0, 127.7,

127.31, 127.22, 127.18, 127.10, 127.01, 126.94, 126.7, 126.3, 125.96, 125.92, 125.65, 125.57, 125.47, 125.35, 125.30, 125.25, 125.19, 125.10, 125.00, 124.6, 124.26, 124.09, 122.9, 122.5, 122.0, 117.5, 117.2, 116.92, 116.89, 116.78, 114.7, 114.41, 114.38, 113.68, 113.56, 113.2, 96.3, 93.9, 93.3, 92.9, 79.2, 78.8, 78.46, 78.27, 61.27, 61.16, 61.11, 60.95, 60.76, 60.67, 60.53, 60.3, 42.9, 40.4, 38.5, 38.2, 37.9, 37.62, 37.54, 37.36; **IR** (NaCl, neat) 3061, 3023, 2904, 2805, 1633, 1595, 1558, 1537, 1336, 1070 cm^{-1} ; **MS** (ESI+) calcd for $\text{C}_{32}\text{H}_{26}\text{Br}_3\text{N}_4\text{O}$ (M+H), 720.96. Found 721.0.

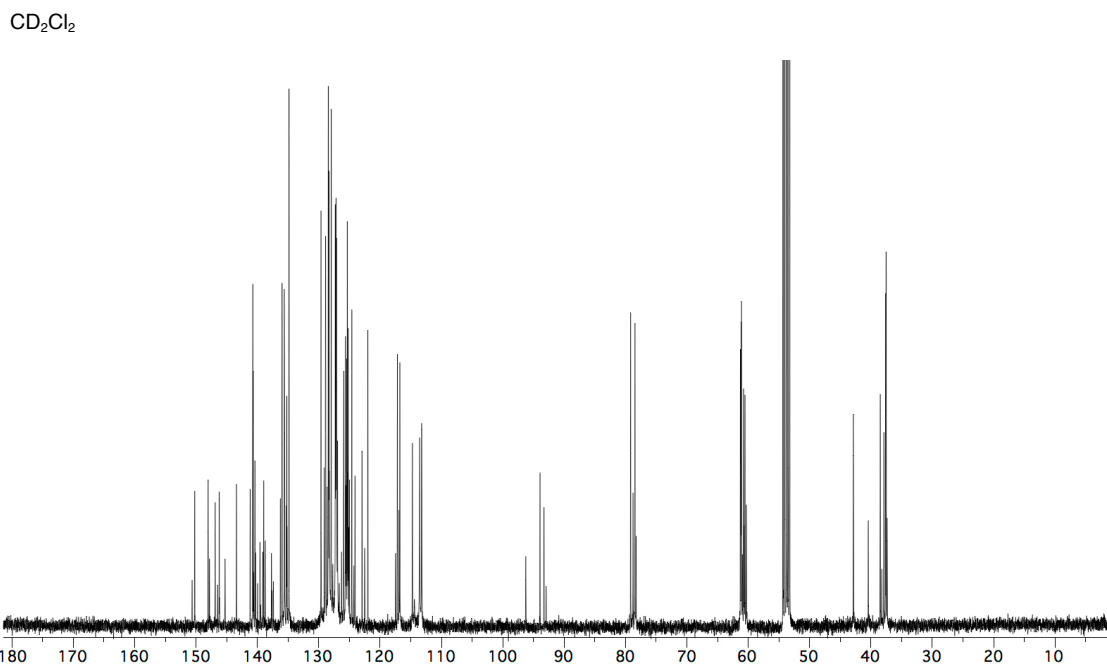
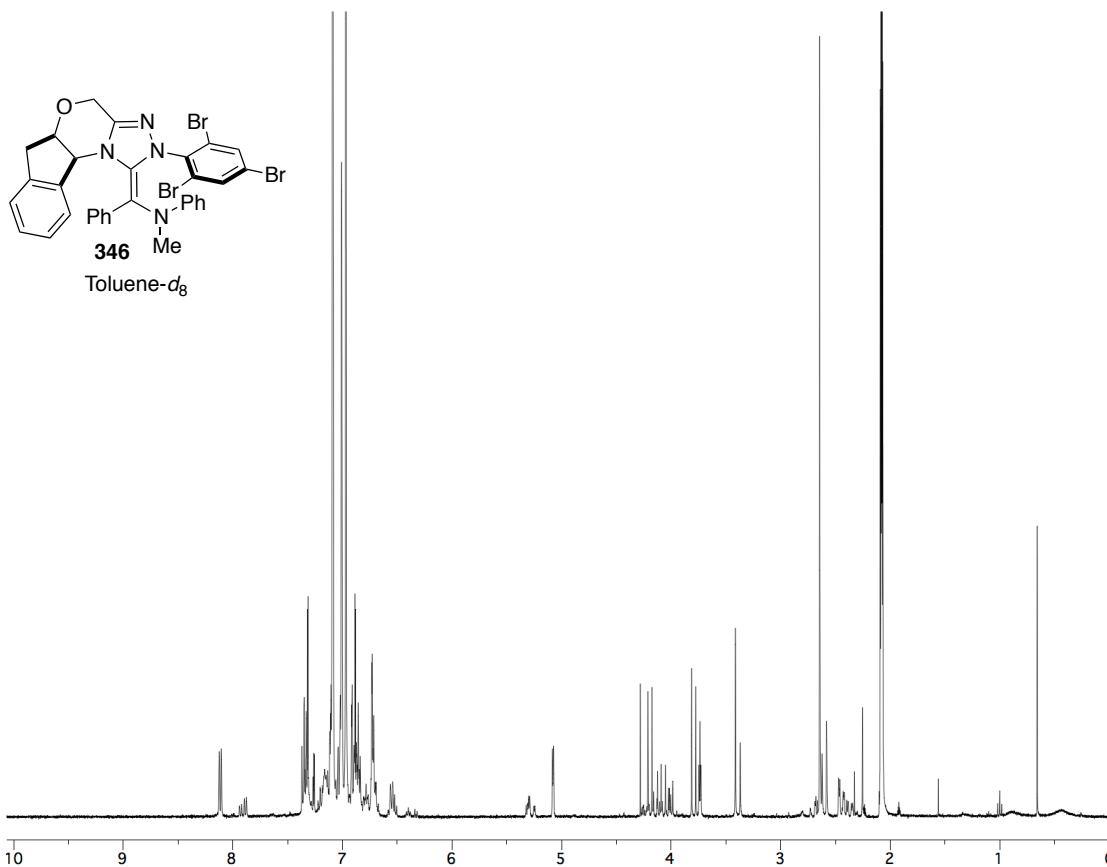


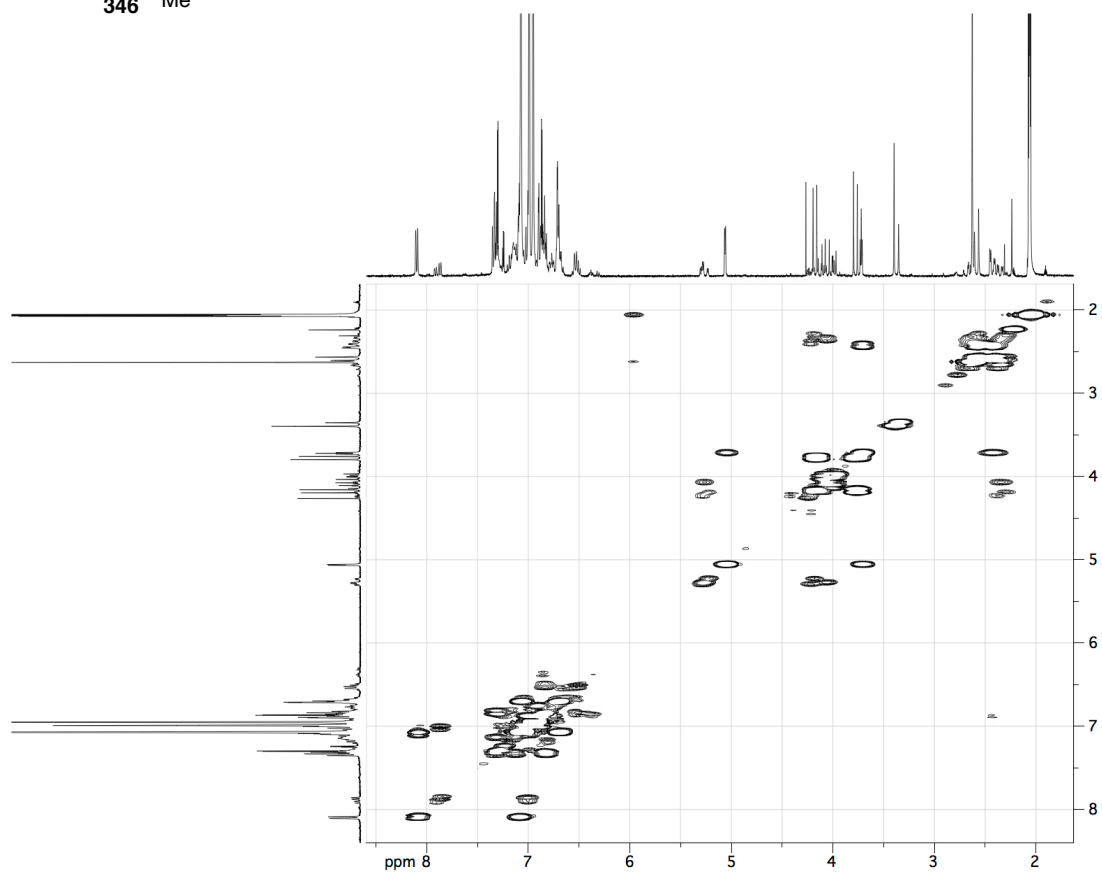
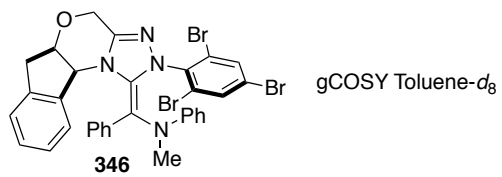
N-methyl-N-((1Z,2E)-3-phenyl-1-((5aR,10bS)-2-(2,4,6-tribromophenyl)-5a,6-dihydroindeno[2,1-b][1,2,4]triazolo[4,3-d][1,4]oxazin-1(2H,4H,10bH)-ylidene)allyl)aniline (348): To a solution

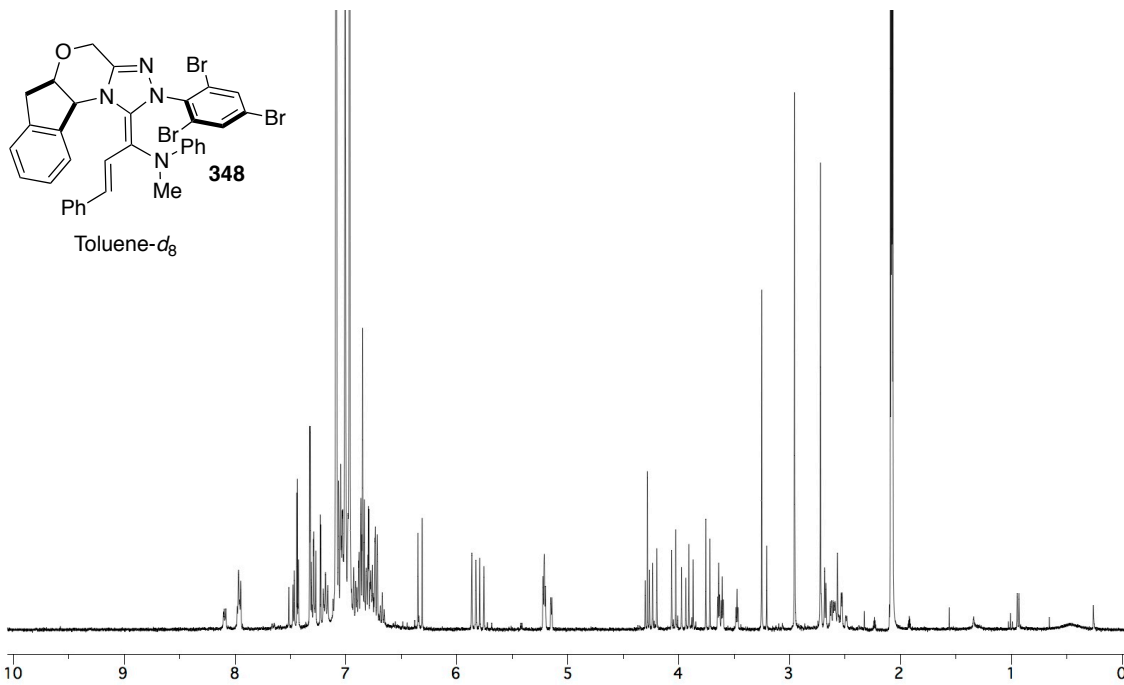
of triazolium salt **1** (0.500 g, 0.815 mmol, 1.0 equiv), and (E)-N-methyl-N-((E)-3-phenylallylidene)benzenaminium perchlorate (0.289g, 0.897 mmol, 1.10 equiv) in acetonitrile (8 mL) was added N,N-diisopropylethylamine (0.71 mL, 4.08 mmol, 5.0 equiv). A yellow precipitate began to form almost instantaneously, which after 2 h was filtered and washed with acetonitrile, followed by ether, and dried to provide **7** as a yellow crystalline solid (468 mg, 77%). $[\alpha]_{\text{D}}^{21} = +754$ ($c = 0.0153$ g/ml, CH_2Cl_2); **m.p.** ($^{\circ}\text{C}$): 212-214; **^1H NMR** (400 MHz, CD_2Cl_2): (mixture of isomers) δ 8.10-8.08 (m, 0.48H), 7.98-7.95 (m, 1H), 7.51-7.43 (m, 1.61H), 7.33-7.27 (m, 2H), 7.23 (d, $J = 2.14$ Hz, 0.55H), 7.21-7.16 (m, 1.16H), 7.06-7.01 (m, 2.7H), 6.93-6.65 (m, 8H), 6.33 (d, $J = 15.1$ Hz, 0.73H), 5.85 (d, $J = 14.9$ Hz, 0.86H), 5.78 (d, $J = 15.1$ Hz, 0.67H), 5.21 (m, 1H), 5.15 (m, 0.44H), 4.30-4.20 (m, 1.4H), 4.06-3.85 (m, 2H), 3.73 (d, $J = 14.9$ Hz, 0.66H), 3.65-3.60 (m, 1H), 3.48-3.46 (m, 0.44H), 3.25 (s, 0.86H), 3.21 (s, 0.31H), 2.96 (s, 1.4H), 2.72 (s, 1.3H), 2.69-2.67 (m, 0.57H), 2.63-2.53 (m, 2H), 2.49-2.48 (m, 0.32H); **^{13}C**

NMR (100 MHz, CD₂Cl₂): δ 149.8, 149.5, 148.5, 148.1, 146.31, 146.25, 145.8, 144.56, 144.44, 144.36, 143.8, 142.8, 141.06, 141.03, 140.55, 140.40, 140.01, 139.99, 139.95, 139.90, 139.78, 139.72, 139.66, 139.1, 138.79, 138.76, 138.2, 136.25, 136.21, 135.9, 135.27, 135.12, 134.8, 134.6, 129.7, 129.24, 129.21, 128.92, 128.77, 128.72, 128.68, 128.61, 128.46, 128.38, 128.1, 127.81, 127.70, 127.04, 126.88, 126.76, 126.67, 125.99, 125.97, 125.87, 125.82, 125.4, 124.93, 124.91, 124.85, 124.76, 124.70, 124.66, 124.61, 124.50, 124.41, 122.28, 122.16, 122.11, 121.6, 121.41, 121.35, 117.25, 117.20, 117.04, 116.6, 116.24, 116.14, 115.2, 112.8, 99.1, 97.5, 97.2, 96.63, 96.49, 79.44, 79.39, 79.0, 78.5, 61.90, 61.85, 61.72, 61.65, 61.3, 60.72, 60.54, 60.1, 41.7, 40.5, 40.2, 39.4, 38.1, 37.80, 37.78, 37.68; **IR** (NaCl, neat) 3061, 3022, 2903, 1623, 1595, 1569, 1552, 1496, 1369, 1287, 1242, 1078 cm⁻¹; **MS** (ESI+) calcd for C₃₄H₂₇Br₃N₄O (M+H), 746.97. Found 747.0.

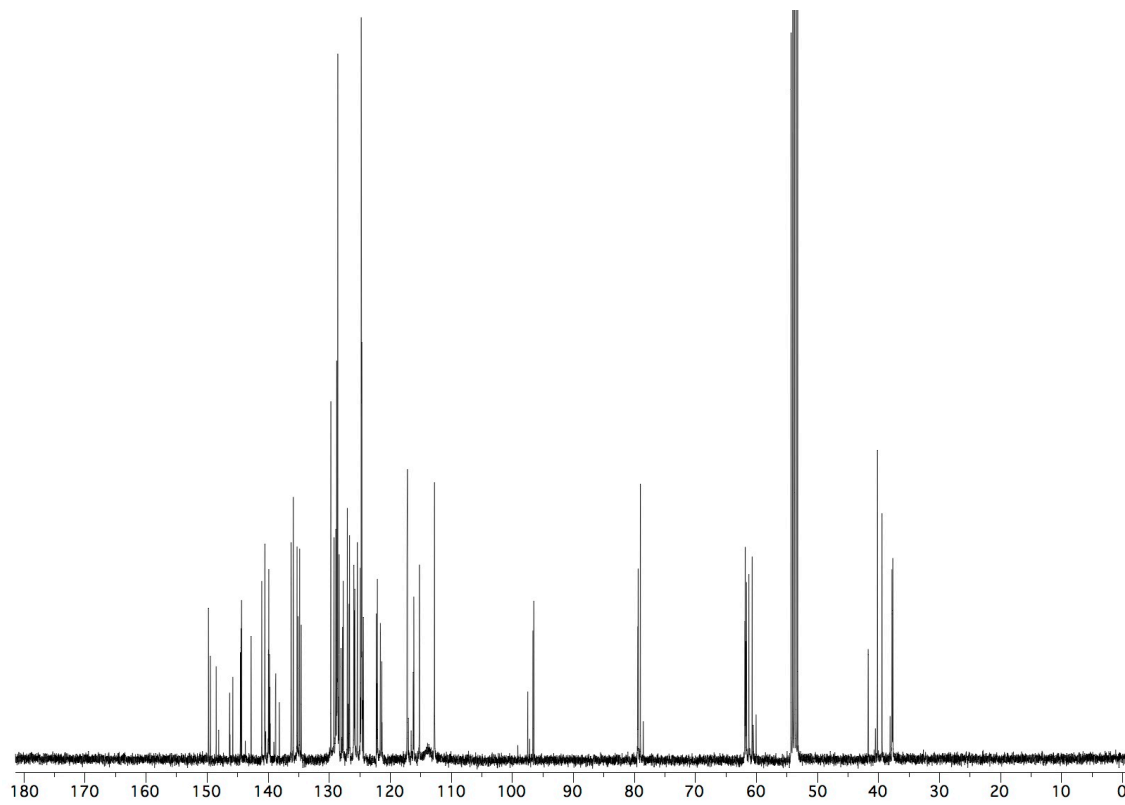
^1H and ^{13}C NMR Spectra



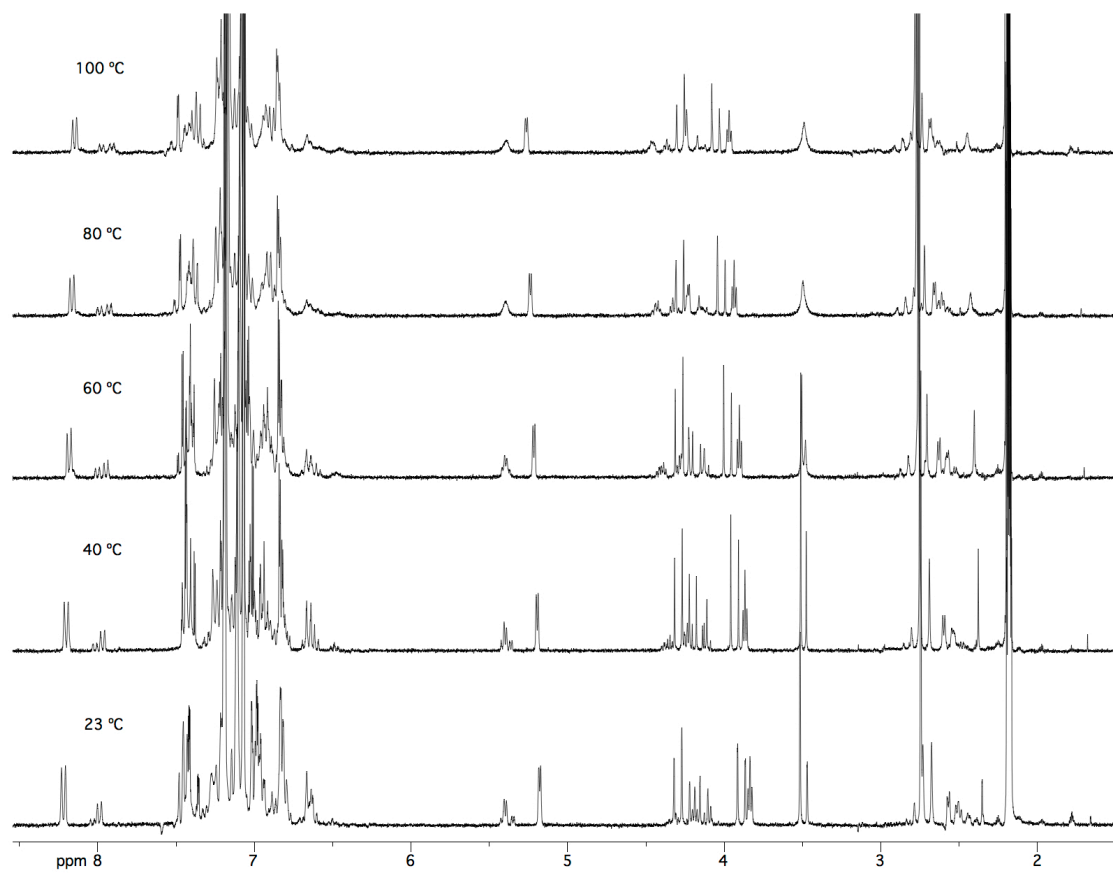
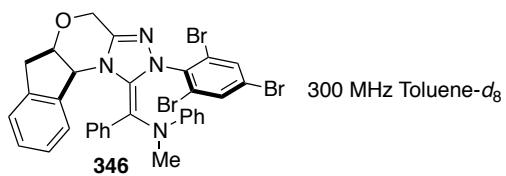


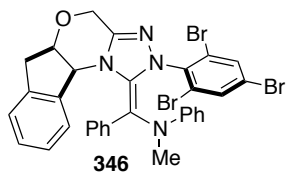


CD_2Cl_2

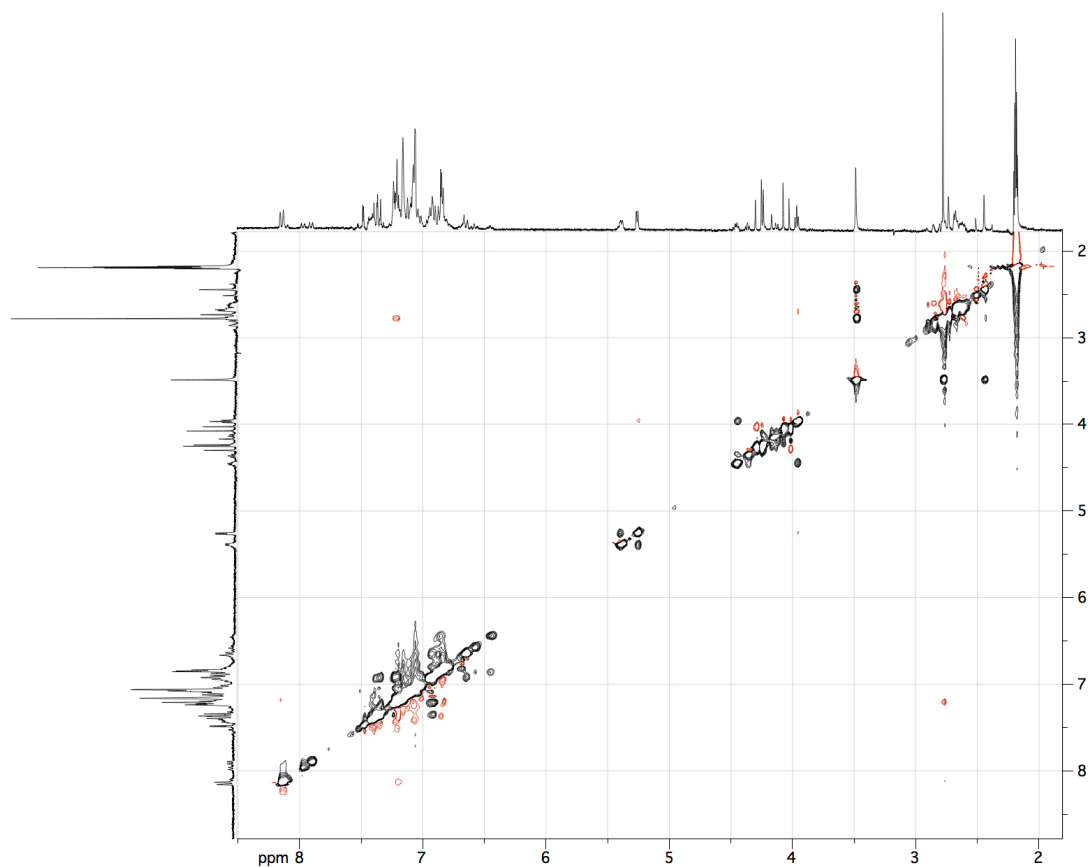


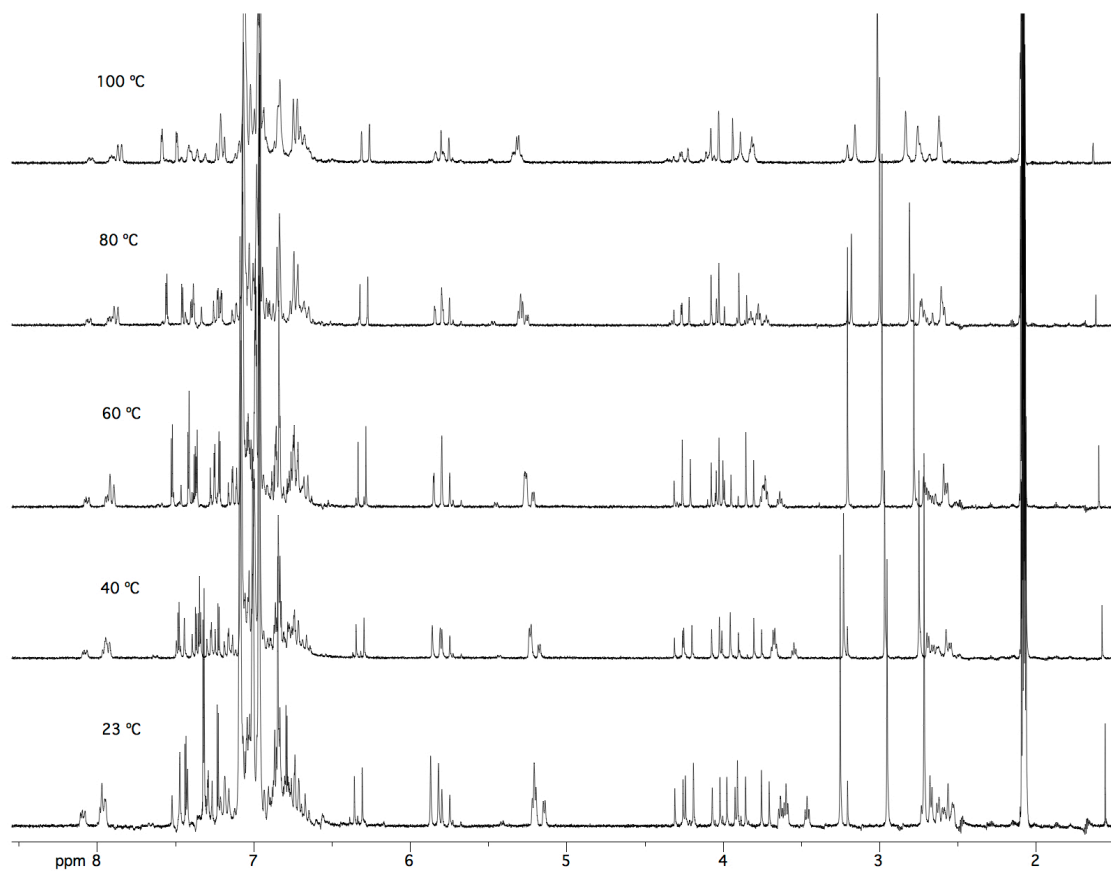
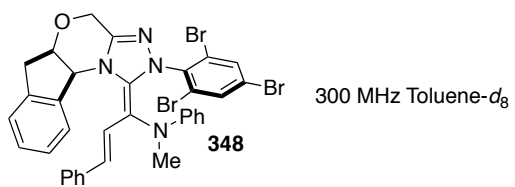
Variable Temperature NMR Studies

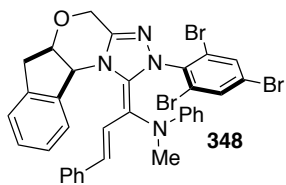




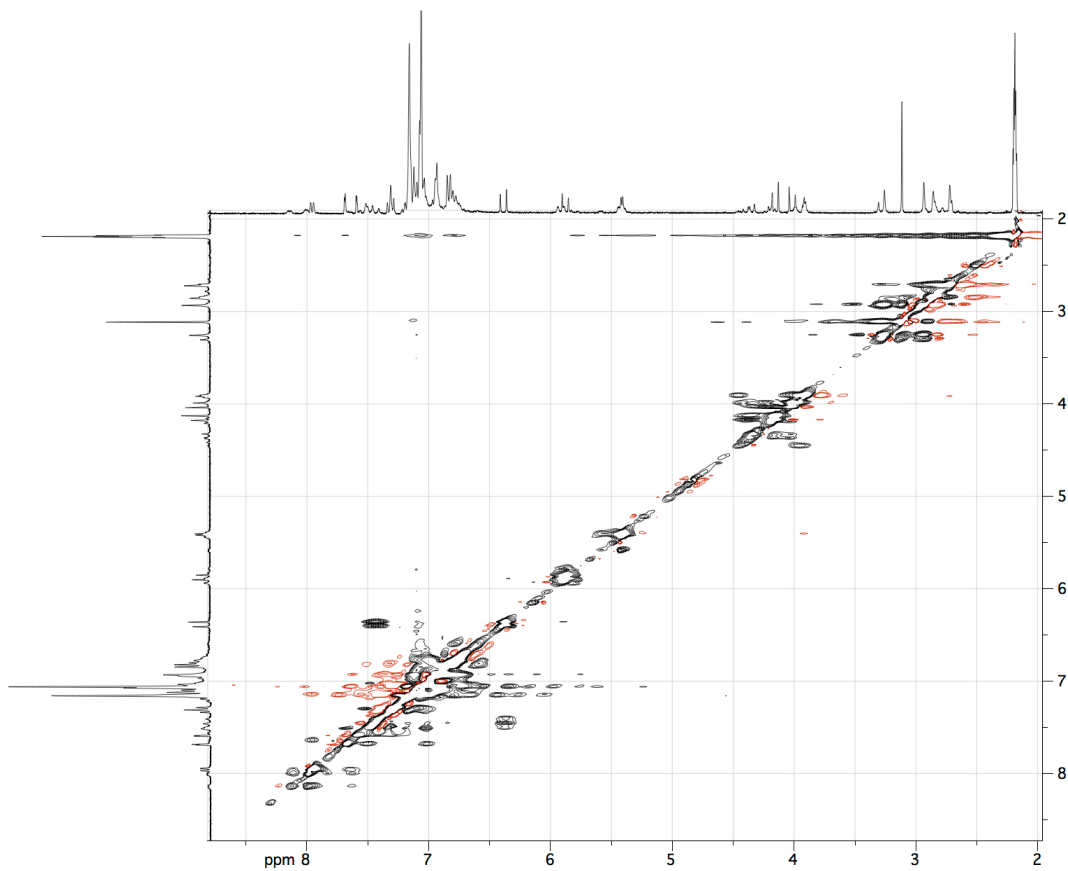
EXSY-NOESY Toluene- d_8 100 °C
Mixing Time = 1000 ms



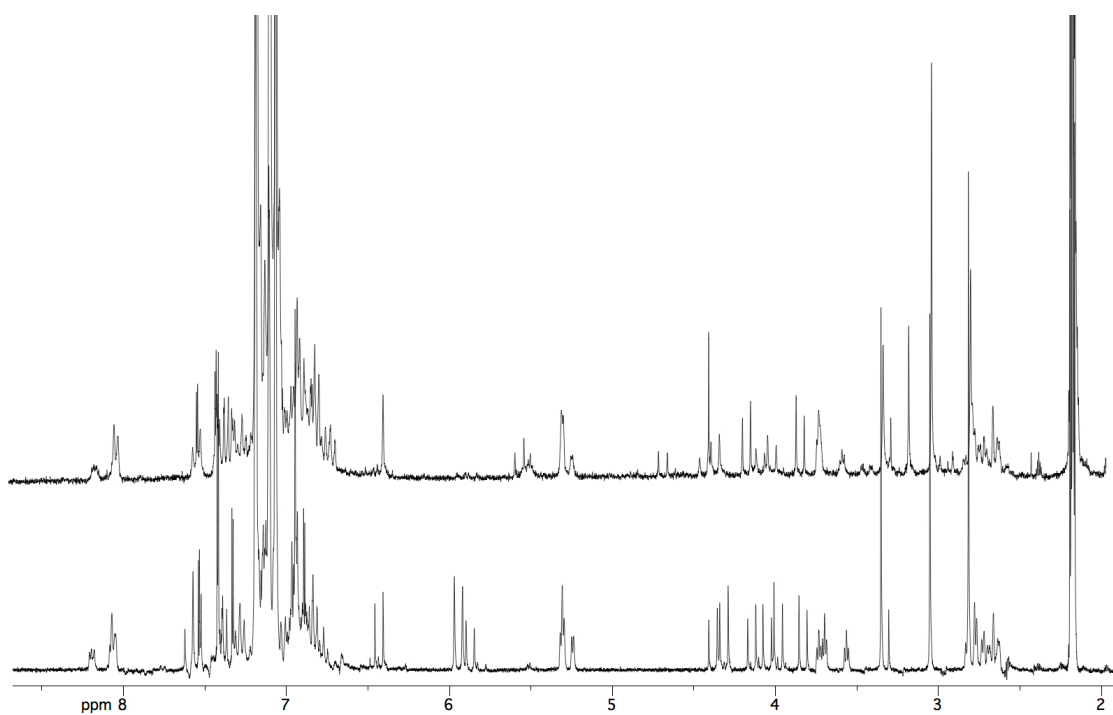
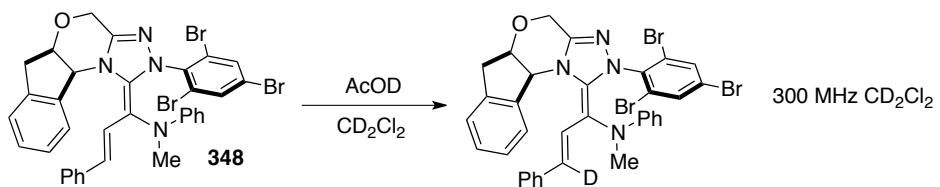




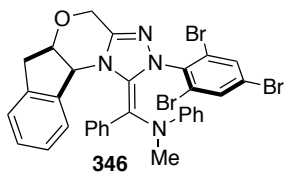
EXSY-NOESY Toluene- d_8 100 °C
Mixing Time = 1000 ms



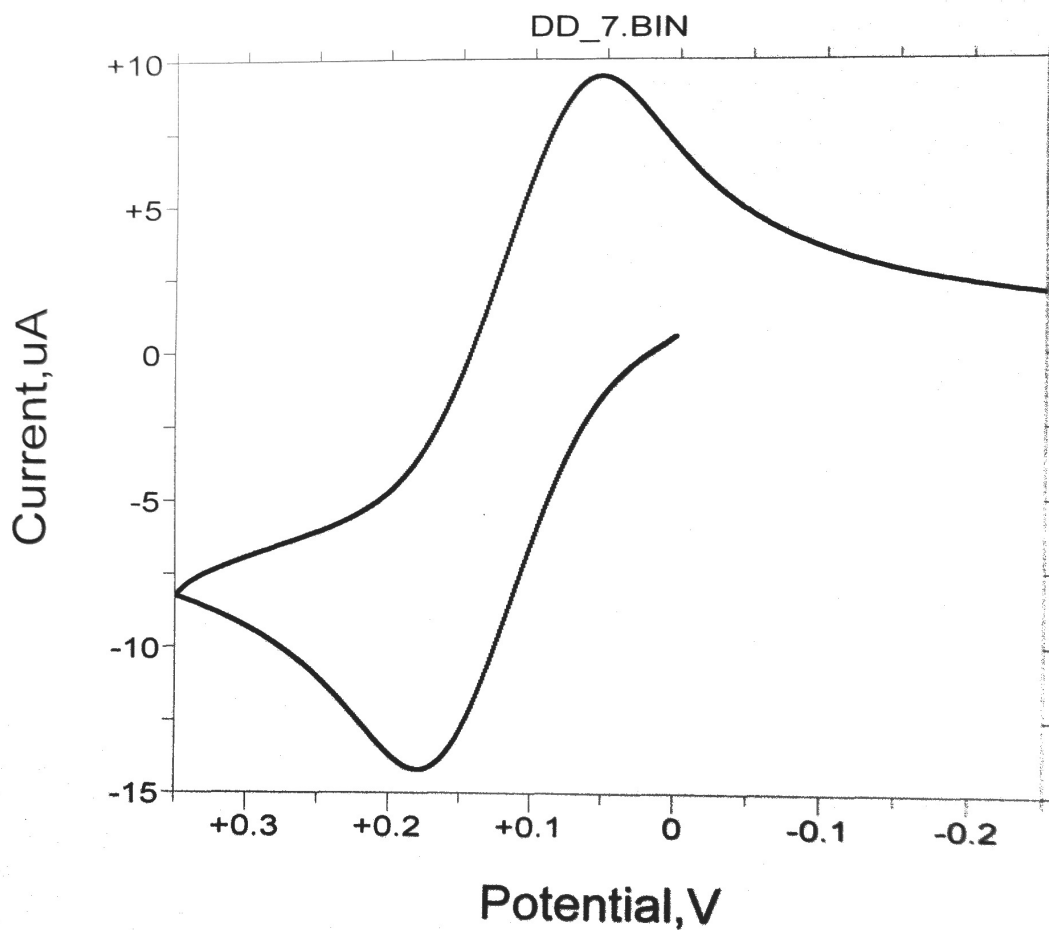
Deuteration Study of (345)



Cyclic Voltammetry Experiments

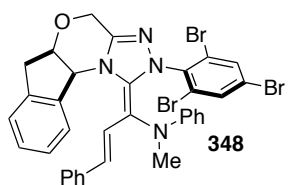


Cyclic Voltammogram in CH₂Cl₂ vs SSCE

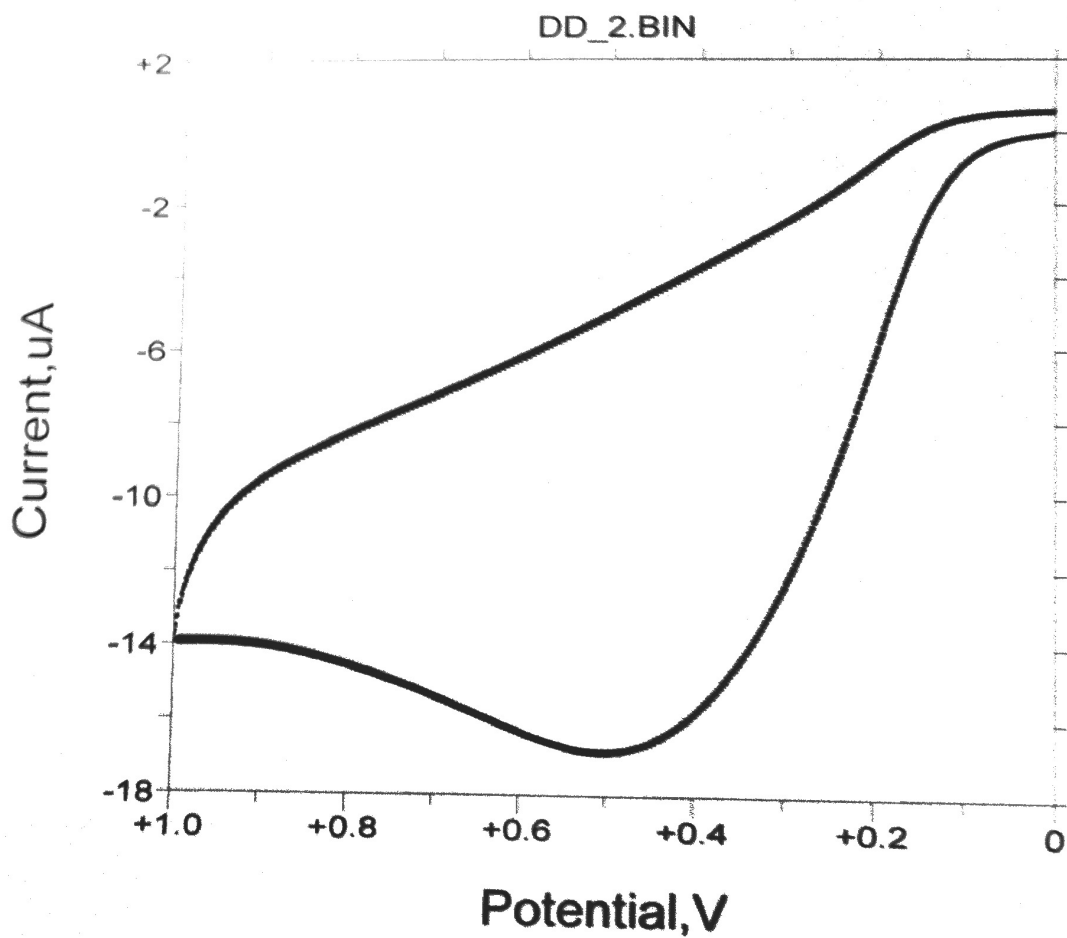


Segment 1:
Ep (mV) = +169
ip (A) = -9.5208E-6

Segment 2:
Ep (mV) = +59
ip (A) = +1.2176E-5



Cyclic Voltammogram in CH₂Cl₂ vs SSCE



Crystallographic Data

Table A4.1 Crystal data and structure refinement for (346).

Identification code	rovis138	
Empirical formula	$C_{32}H_{25}Br_3N_4O$	
Formula weight	721.29	
Temperature	120 K	
Wavelength	0.71073 Å	
Crystal system	Orthorhombic	
Space group	$P2_12_12_1$	
Unit cell dimensions	$a = 9.2723(9)$ Å	$\langle = 90^\circ$.
	$b = 16.0604(16)$ Å	$\oplus = 90^\circ$.
	$c = 18.9428(19)$ Å	$\odot = 90^\circ$.
Volume	2820.9(5) Å ³	
Z	4	
Density (calculated)	1.698 Mg/m ³	
Absorption coefficient	4.324 mm ⁻¹	
F(000)	1432	
Crystal size	0.30 x 0.24 x 0.24 mm ³	
Theta range for data collection	2.15 to 32.04°.	
Index ranges	-13 ≤ h ≤ 13, -23 ≤ k ≤ 23, -28 ≤ l ≤ 28	
Reflections collected	40611	
Independent reflections	9682 [R(int) = 0.0530]	
Completeness to theta = 32.04°	100.0 %	
Absorption correction	Semi-empirical from equivalents	
Max. and min. transmission	0.4272 and 0.3619	
Refinement method	Full-matrix least-squares on F ²	
Data / restraints / parameters	9682 / 0 / 363	
Goodness-of-fit on F ²	0.961	
Final R indices [I > 2σ(I)]	R1 = 0.0371, wR2 = 0.0586	
R indices (all data)	R1 = 0.1035, wR2 = 0.0693	
Absolute structure parameter	-0.004(6)	
Largest diff. peak and hole	0.435 and -0.409 e.Å ⁻³	

Table A4.2 Atomic coordinates ($\times 10^4$) and equivalent isotropic displacement parameters ($\text{\AA}^2 \times 10^3$) for (346). $U(\text{eq})$ is defined as one third of the trace of the orthogonalized U^{ij} tensor.

	x	y	z	$U(\text{eq})$
Br(1)	2695(1)	2845(1)	7541(1)	54(1)
Br(2)	-3094(1)	1678(1)	7528(1)	59(1)
Br(3)	-326(1)	2436(1)	10088(1)	83(1)
C(1)	851(3)	1494(1)	6584(1)	30(1)
C(2)	1391(3)	1441(2)	5247(1)	33(1)
C(3)	182(3)	916(1)	4949(1)	33(1)
C(4)	-769(3)	382(2)	5279(1)	45(1)
C(5)	-1711(3)	-84(2)	4870(2)	58(1)
C(6)	-1694(3)	-18(2)	4146(2)	59(1)
C(7)	-770(4)	526(2)	3814(2)	53(1)
C(8)	183(3)	991(2)	4213(1)	42(1)
C(9)	1321(3)	1593(2)	3984(1)	48(1)
C(10)	1639(3)	2086(2)	4653(1)	42(1)
C(11)	691(3)	3200(2)	5313(1)	46(1)
C(12)	481(3)	2637(1)	5926(1)	34(1)
C(13)	-163(2)	2194(1)	7642(1)	32(1)
C(14)	998(3)	2514(2)	8022(1)	38(1)
C(15)	953(3)	2607(2)	8747(1)	45(1)
C(16)	-283(3)	2390(2)	9091(1)	47(1)
C(17)	-1497(3)	2123(2)	8741(1)	46(1)
C(18)	-1428(3)	2029(2)	8016(1)	37(1)
C(19)	1355(3)	762(2)	6847(1)	31(1)
C(20)	1275(3)	455(2)	8117(1)	35(1)
C(21)	544(4)	172(2)	8717(1)	50(1)
C(22)	1113(4)	289(2)	9384(2)	61(1)
C(23)	2428(4)	658(2)	9480(2)	62(1)
C(24)	3210(4)	895(2)	8892(2)	53(1)
C(25)	2644(3)	796(2)	8218(1)	41(1)
C(26)	-585(3)	-125(2)	7328(1)	60(1)
C(27)	2670(3)	338(2)	6603(1)	31(1)
C(28)	2860(3)	-520(2)	6724(1)	48(1)

C(29)	4139(4)	-908(2)	6594(2)	58(1)
C(30)	5297(4)	-474(2)	6326(1)	54(1)
C(31)	5152(3)	369(2)	6198(1)	43(1)
C(32)	3861(3)	766(2)	6334(1)	35(1)
N(1)	1123(2)	1861(1)	5920(1)	31(1)
N(2)	-215(2)	2802(1)	6495(1)	39(1)
N(3)	-80(2)	2061(1)	6904(1)	34(1)
N(4)	638(2)	431(1)	7452(1)	35(1)
O(1)	588(2)	2742(1)	4678(1)	45(1)

Table A4.3 Bond lengths [\AA] and angles [$^\circ$] for (346).

Br(1)-C(14)	1.895(3)	C(12)-N(1)	1.381(3)
Br(2)-C(18)	1.887(3)	C(13)-C(14)	1.393(3)
Br(3)-C(16)	1.891(2)	C(13)-C(18)	1.395(3)
C(1)-C(19)	1.360(3)	C(13)-N(3)	1.416(3)
C(1)-N(3)	1.394(3)	C(14)-C(15)	1.382(3)
C(1)-N(1)	1.412(3)	C(15)-C(16)	1.363(4)
C(2)-N(1)	1.464(3)	C(16)-C(17)	1.375(4)
C(2)-C(3)	1.512(3)	C(17)-C(18)	1.384(3)
C(2)-C(10)	1.547(3)	C(19)-N(4)	1.427(3)
C(3)-C(4)	1.380(3)	C(19)-C(27)	1.471(4)
C(3)-C(8)	1.400(3)	C(20)-N(4)	1.392(3)
C(4)-C(5)	1.387(4)	C(20)-C(25)	1.397(4)
C(5)-C(6)	1.375(4)	C(20)-C(21)	1.399(4)
C(6)-C(7)	1.376(4)	C(21)-C(22)	1.382(4)
C(7)-C(8)	1.382(4)	C(22)-C(23)	1.368(5)
C(8)-C(9)	1.495(4)	C(23)-C(24)	1.384(4)
C(9)-C(10)	1.522(4)	C(24)-C(25)	1.389(4)
C(10)-O(1)	1.436(3)	C(26)-N(4)	1.462(3)
C(11)-O(1)	1.413(3)	C(27)-C(32)	1.397(3)
C(11)-C(12)	1.484(3)	C(27)-C(28)	1.408(4)
C(12)-N(2)	1.284(3)	C(28)-C(29)	1.363(4)
		C(29)-C(30)	1.378(4)

C(30)-C(31)	1.383(4)	C(17)-C(16)-Br(3)	118.4(2)
C(31)-C(32)	1.379(4)	C(16)-C(17)-C(18)	118.3(2)
N(2)-N(3)	1.426(3)	C(17)-C(18)-C(13)	121.5(2)
C(19)-C(1)-N(3)	128.2(2)	C(17)-C(18)-Br(2)	118.7(2)
C(19)-C(1)-N(1)	128.8(2)	C(13)-C(18)-Br(2)	119.76(18)
N(3)-C(1)-N(1)	102.99(18)	C(1)-C(19)-N(4)	117.1(2)
N(1)-C(2)-C(3)	117.18(19)	C(1)-C(19)-C(27)	124.7(2)
N(1)-C(2)-C(10)	110.53(19)	N(4)-C(19)-C(27)	117.8(2)
C(3)-C(2)-C(10)	102.20(19)	N(4)-C(20)-C(25)	121.3(2)
C(4)-C(3)-C(8)	120.4(2)	N(4)-C(20)-C(21)	121.4(3)
C(4)-C(3)-C(2)	130.6(2)	C(25)-C(20)-C(21)	117.2(3)
C(8)-C(3)-C(2)	108.9(2)	C(22)-C(21)-C(20)	120.9(3)
C(3)-C(4)-C(5)	119.0(2)	C(23)-C(22)-C(21)	121.4(3)
C(6)-C(5)-C(4)	120.6(3)	C(22)-C(23)-C(24)	118.6(3)
C(5)-C(6)-C(7)	120.8(3)	C(23)-C(24)-C(25)	120.8(3)
C(6)-C(7)-C(8)	119.4(3)	C(24)-C(25)-C(20)	120.9(3)
C(7)-C(8)-C(3)	119.9(3)	C(32)-C(27)-C(28)	116.2(2)
C(7)-C(8)-C(9)	130.0(2)	C(32)-C(27)-C(19)	122.9(2)
C(3)-C(8)-C(9)	110.1(2)	C(28)-C(27)-C(19)	120.3(2)
C(8)-C(9)-C(10)	103.4(2)	C(29)-C(28)-C(27)	121.8(3)
O(1)-C(10)-C(9)	106.2(2)	C(28)-C(29)-C(30)	120.9(3)
O(1)-C(10)-C(2)	111.45(19)	C(29)-C(30)-C(31)	118.9(3)
C(9)-C(10)-C(2)	103.2(2)	C(32)-C(31)-C(30)	120.3(3)
O(1)-C(11)-C(12)	109.8(2)	C(31)-C(32)-C(27)	121.7(2)
N(2)-C(12)-N(1)	114.2(2)	C(12)-N(1)-C(1)	107.07(18)
N(2)-C(12)-C(11)	126.6(2)	C(12)-N(1)-C(2)	119.73(18)
N(1)-C(12)-C(11)	119.2(2)	C(1)-N(1)-C(2)	127.83(18)
C(14)-C(13)-C(18)	117.2(2)	C(12)-N(2)-N(3)	103.87(18)
C(14)-C(13)-N(3)	121.6(2)	C(1)-N(3)-C(13)	124.20(19)
C(18)-C(13)-N(3)	121.2(2)	C(1)-N(3)-N(2)	111.33(17)
C(15)-C(14)-C(13)	122.0(2)	C(13)-N(3)-N(2)	113.91(18)
C(15)-C(14)-Br(1)	118.2(2)	C(20)-N(4)-C(19)	121.26(19)
C(13)-C(14)-Br(1)	119.77(18)	C(20)-N(4)-C(26)	119.4(2)
C(16)-C(15)-C(14)	118.2(3)	C(19)-N(4)-C(26)	117.4(2)
C(15)-C(16)-C(17)	122.6(2)	C(11)-O(1)-C(10)	111.4(2)
C(15)-C(16)-Br(3)	119.0(2)		

Symmetry transformations used to generate equivalent atoms:

Table A4.4 Anisotropic displacement parameters ($\text{\AA}^2 \times 10^3$) for **(346)**. The anisotropic displacement factor exponent takes the form: $-2\delta^2[h^2 a^* U^{11} + \dots + 2 h k a^* b^* U^{12}]$

	U ¹¹	U ²²	U ³³	U ²³	U ¹³	U ¹²
Br(1)	40(1)	49(1)	72(1)	-3(1)	4(1)	-10(1)
Br(2)	38(1)	80(1)	60(1)	12(1)	-4(1)	-9(1)
Br(3)	104(1)	106(1)	39(1)	-19(1)	5(1)	15(1)
C(1)	30(1)	30(1)	30(1)	0(1)	-2(1)	-3(1)
C(2)	32(1)	36(1)	31(1)	6(1)	3(1)	5(1)
C(3)	33(1)	30(1)	35(1)	-2(1)	-2(1)	6(1)
C(4)	48(2)	46(2)	40(1)	-5(1)	2(1)	-4(2)
C(5)	50(2)	54(2)	71(2)	-11(2)	4(2)	-12(2)
C(6)	47(2)	57(2)	73(2)	-21(2)	-16(2)	4(2)
C(7)	59(2)	57(2)	42(2)	-8(1)	-19(2)	20(2)
C(8)	42(2)	46(2)	37(1)	1(1)	-2(1)	13(1)
C(9)	60(2)	54(2)	31(1)	5(1)	3(1)	6(2)
C(10)	35(1)	49(2)	44(2)	15(1)	6(1)	4(1)
C(11)	56(2)	34(1)	49(2)	9(1)	-2(1)	1(1)
C(12)	34(1)	32(2)	37(1)	4(1)	-7(1)	0(1)
C(13)	33(1)	27(1)	36(1)	1(1)	1(1)	6(1)
C(14)	36(1)	31(1)	47(1)	0(1)	2(1)	3(1)
C(15)	47(2)	41(2)	46(2)	-11(1)	-7(1)	4(1)
C(16)	63(2)	44(2)	34(1)	-7(1)	3(1)	15(2)
C(17)	46(2)	47(2)	44(2)	4(1)	11(1)	10(1)
C(18)	32(1)	38(2)	41(2)	2(1)	0(1)	5(1)
C(19)	37(2)	26(1)	30(1)	2(1)	-4(1)	-4(1)
C(20)	45(2)	25(1)	34(1)	3(1)	2(1)	8(1)
C(21)	63(2)	41(2)	46(2)	9(1)	10(2)	4(2)
C(22)	100(3)	47(2)	36(2)	10(1)	14(2)	14(2)
C(23)	99(3)	50(2)	38(2)	-1(1)	-12(2)	21(2)
C(24)	59(2)	47(2)	52(2)	-10(1)	-16(2)	15(2)

C(25)	45(2)	39(2)	40(2)	-1(1)	1(1)	3(2)
C(26)	57(2)	60(2)	63(2)	12(2)	-4(2)	-24(2)
C(27)	36(1)	34(1)	24(1)	2(1)	-1(1)	2(1)
C(28)	58(2)	37(2)	49(2)	0(1)	6(2)	3(2)
C(29)	74(2)	37(2)	64(2)	5(1)	13(2)	22(2)
C(30)	52(2)	60(2)	51(2)	2(2)	6(2)	23(2)
C(31)	44(2)	52(2)	33(1)	6(1)	3(1)	6(2)
C(32)	39(2)	38(1)	30(1)	2(1)	-3(1)	4(1)
N(1)	37(1)	28(1)	28(1)	5(1)	0(1)	1(1)
N(2)	43(1)	32(1)	41(1)	5(1)	0(1)	7(1)
N(3)	38(1)	32(1)	31(1)	6(1)	3(1)	4(1)
N(4)	36(1)	33(1)	36(1)	8(1)	2(1)	-6(1)
O(1)	55(1)	40(1)	40(1)	10(1)	-2(1)	4(1)

Table A4.5 Hydrogen coordinates ($\times 10^4$) and isotropic displacement parameters ($\text{\AA}^2 \times 10^{-3}$) for (346).

	x	y	z	U(eq)
H(2)	2256	1094	5293	39
H(4)	-779	336	5768	54
H(5)	-2360	-444	5087	70
H(6)	-2314	-346	3878	71
H(7)	-787	580	3325	63
H(9A)	969	1954	3612	58
H(9B)	2174	1303	3819	58
H(10)	2627	2303	4656	51
H(11A)	-38	3634	5320	55
H(11B)	1630	3463	5343	55
H(15)	1744	2812	8994	54
H(17)	-2343	2007	8986	55
H(21)	-337	-98	8666	60
H(22)	591	113	9776	74
H(23)	2789	748	9932	74

H(24)	4124	1123	8948	63
H(25)	3185	960	7828	49
H(26A)	-1431	101	7548	90
H(26B)	-380	-663	7525	90
H(26C)	-746	-178	6829	90
H(28)	2090	-830	6897	58
H(29)	4232	-1474	6688	70
H(30)	6164	-744	6231	65
H(31)	5927	671	6021	51
H(32)	3782	1333	6243	43

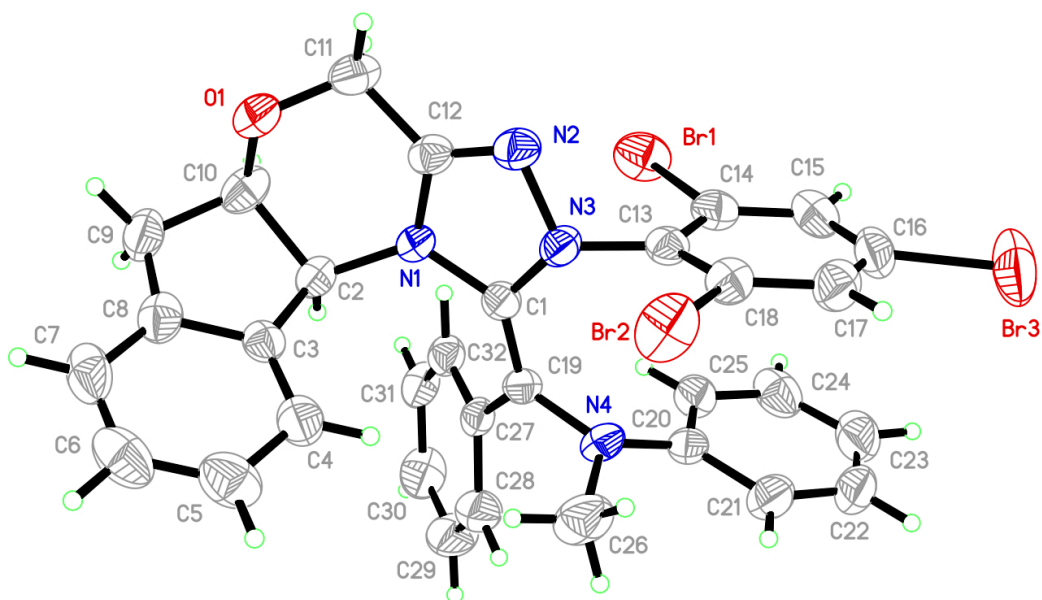


Figure A4.1 Thermal plot of (346). Ellipsoids draw at the 50% probability level.

Table 6. Crystal data and structure refinement for (348).

Identification code	rovis140
Empirical formula	$C_{34}H_{27}Br_3N_4O$
Formula weight	747.33
Temperature	120 K
Wavelength	0.71073 Å
Crystal system	Monoclinic

Space group	$P2_1$	
Unit cell dimensions	$a = 9.8520(4) \text{ \AA}$	$\langle = 90^\circ$.
	$b = 8.8052(4) \text{ \AA}$	$\oplus = 90.677(2)^\circ$.
	$c = 17.8104(7) \text{ \AA}$	$\odot = 90^\circ$.
Volume	$1544.92(11) \text{ \AA}^3$	
Z	2	
Density (calculated)	1.607 Mg/m^3	
Absorption coefficient	3.951 mm^{-1}	
F(000)	744	
Crystal size	$0.30 \times 0.15 \times 0.06 \text{ mm}^3$	
Theta range for data collection	2.07 to 29.58° .	
Index ranges	$-13 \leq h \leq 13$, $-12 \leq k \leq 12$, $-24 \leq l \leq 24$	
Reflections collected	29601	
Independent reflections	8429 [R(int) = 0.0534]	
Completeness to theta = 29.58°	96.8 %	
Absorption correction	Semi-empirical from equivalents	
Max. and min. transmission	0.8091 and 0.3807	
Refinement method	Full-matrix least-squares on F^2	
Data / restraints / parameters	8429 / 1 / 381	
Goodness-of-fit on F^2	1.031	
Final R indices [I > 2sigma(I)]	R1 = 0.0618, wR2 = 0.1507	
R indices (all data)	R1 = 0.1373, wR2 = 0.1760	
Absolute structure parameter	0.015(13)	
Largest diff. peak and hole	1.528 and $-0.620 \text{ e.\AA}^{-3}$	

Table A4.7 Atomic coordinates ($\times 10^4$) and equivalent isotropic displacement parameters ($\text{\AA}^2 \times 10^3$) for (348). $U(\text{eq})$ is defined as one third of the trace of the orthogonalized U^{ij} tensor.

	x	y	z	$U(\text{eq})$
Br(1)	9344(1)	7991(1)	7299(1)	67(1)
Br(2)	4525(1)	4443(1)	7249(1)	69(1)
Br(3)	6120(1)	7615(1)	4670(1)	91(1)
C(1)	8454(6)	4780(6)	8095(3)	36(1)
C(2)	9602(6)	4655(6)	9403(3)	31(1)
C(3)	10997(6)	5424(6)	9409(3)	37(1)

C(4)	11778(6)	5941(7)	8848(4)	44(2)
C(5)	13025(8)	6607(8)	9012(5)	63(2)
C(6)	13480(8)	6742(9)	9747(6)	72(2)
C(7)	12658(7)	6248(9)	10313(5)	65(2)
C(8)	11409(7)	5569(7)	10167(4)	48(2)
C(9)	10366(7)	4953(7)	10682(3)	44(2)
C(10)	9105(6)	4996(6)	10216(3)	39(1)
C(11)	7366(6)	6647(7)	9816(3)	37(1)
C(12)	7569(6)	6189(6)	9023(3)	35(1)
C(13)	6984(7)	6143(7)	7143(3)	41(1)
C(14)	5828(7)	5723(7)	6760(4)	46(2)
C(15)	5531(8)	6179(8)	6041(4)	52(2)
C(16)	6425(9)	7062(7)	5687(4)	54(2)
C(17)	7593(7)	7623(8)	6047(4)	52(2)
C(18)	7831(7)	7177(7)	6784(4)	44(2)
C(19)	9085(7)	3702(7)	7672(3)	39(1)
C(20)	8838(8)	3771(8)	6299(4)	50(2)
C(21)	8087(11)	3446(11)	5632(4)	84(3)
C(22)	8483(17)	3982(16)	4962(5)	113(5)
C(23)	9647(15)	4975(15)	4892(5)	106(4)
C(24)	10371(14)	5208(11)	5540(6)	104(4)
C(25)	10026(9)	4629(9)	6212(4)	70(2)
C(26)	7476(9)	1971(9)	7038(5)	72(2)
C(27)	10357(6)	2982(7)	7861(3)	36(1)
C(28)	10977(7)	1926(7)	7430(3)	41(2)
C(29)	12272(6)	1185(7)	7590(3)	40(1)
C(30)	12785(9)	125(9)	7097(5)	73(3)
C(31)	13974(12)	-613(12)	7203(7)	109(4)
C(32)	14736(8)	-337(11)	7830(6)	80(3)
C(33)	14274(8)	725(14)	8339(5)	90(3)
C(34)	13078(6)	1449(9)	8212(4)	54(2)
N(1)	8638(5)	5172(5)	8853(3)	33(1)
N(2)	6800(5)	6497(5)	8471(3)	38(1)
N(3)	7302(6)	5620(6)	7877(3)	42(1)
N(4)	8401(5)	3277(5)	6978(3)	42(1)
O(1)	8610(4)	6505(4)	10242(2)	37(1)

Table A4.8 Bond lengths [\AA] and angles [$^\circ$] for (348).

Br(1)-C(18)	1.884(6)	C(19)-N(4)	1.449(7)
Br(2)-C(14)	1.924(7)	C(20)-N(4)	1.360(9)
Br(3)-C(16)	1.897(6)	C(20)-C(25)	1.403(12)
C(1)-C(19)	1.367(8)	C(20)-C(21)	1.421(10)
C(1)-N(1)	1.402(7)	C(21)-C(22)	1.345(16)
C(1)-N(3)	1.406(8)	C(22)-C(23)	1.45(2)
C(2)-N(1)	1.431(7)	C(23)-C(24)	1.365(16)
C(2)-C(3)	1.532(8)	C(24)-C(25)	1.348(12)
C(2)-C(10)	1.563(8)	C(26)-N(4)	1.472(10)
C(3)-C(4)	1.348(9)	C(27)-C(28)	1.355(8)
C(3)-C(8)	1.410(9)	C(28)-C(29)	1.458(9)
C(4)-C(5)	1.389(10)	C(29)-C(34)	1.375(9)
C(5)-C(6)	1.384(12)	C(29)-C(30)	1.381(10)
C(6)-C(7)	1.371(13)	C(30)-C(31)	1.351(13)
C(7)-C(8)	1.390(10)	C(31)-C(32)	1.360(14)
C(8)-C(9)	1.489(10)	C(32)-C(33)	1.383(14)
C(9)-C(10)	1.487(9)	C(33)-C(34)	1.357(11)
C(10)-O(1)	1.416(7)	N(2)-N(3)	1.404(7)
C(11)-O(1)	1.440(7)	C(19)-C(1)-N(1)	130.3(5)
C(11)-C(12)	1.485(8)	C(19)-C(1)-N(3)	125.7(5)
C(12)-N(2)	1.263(7)	N(1)-C(1)-N(3)	103.4(4)
C(12)-N(1)	1.418(7)	N(1)-C(2)-C(3)	116.9(4)
C(13)-C(14)	1.371(9)	N(1)-C(2)-C(10)	111.1(5)
C(13)-C(18)	1.395(10)	C(3)-C(2)-C(10)	101.5(4)
C(13)-N(3)	1.418(7)	C(4)-C(3)-C(8)	121.2(6)
C(14)-C(15)	1.371(9)	C(4)-C(3)-C(2)	131.6(5)
C(15)-C(16)	1.337(11)	C(8)-C(3)-C(2)	107.2(5)
C(16)-C(17)	1.400(10)	C(3)-C(4)-C(5)	119.9(7)
C(17)-C(18)	1.388(9)	C(6)-C(5)-C(4)	120.7(8)
C(19)-C(27)	1.441(8)	C(7)-C(6)-C(5)	118.7(8)

C(6)-C(7)-C(8)	121.9(8)	N(4)-C(20)-C(21)	120.8(8)
C(7)-C(8)-C(3)	117.5(7)	C(25)-C(20)-C(21)	116.3(8)
C(7)-C(8)-C(9)	131.1(7)	C(22)-C(21)-C(20)	121.1(12)
C(3)-C(8)-C(9)	111.3(5)	C(21)-C(22)-C(23)	121.8(11)
C(10)-C(9)-C(8)	103.0(5)	C(24)-C(23)-C(22)	115.1(9)
O(1)-C(10)-C(9)	106.9(5)	C(25)-C(24)-C(23)	124.0(12)
O(1)-C(10)-C(2)	108.9(4)	C(24)-C(25)-C(20)	121.4(10)
C(9)-C(10)-C(2)	104.1(5)	C(28)-C(27)-C(19)	124.5(5)
O(1)-C(11)-C(12)	110.7(5)	C(27)-C(28)-C(29)	126.6(5)
N(2)-C(12)-N(1)	114.2(5)	C(34)-C(29)-C(30)	114.5(6)
N(2)-C(12)-C(11)	126.5(5)	C(34)-C(29)-C(28)	125.2(6)
N(1)-C(12)-C(11)	118.9(5)	C(30)-C(29)-C(28)	120.3(6)
C(14)-C(13)-C(18)	116.5(5)	C(31)-C(30)-C(29)	124.0(9)
C(14)-C(13)-N(3)	122.9(6)	C(30)-C(31)-C(32)	119.9(9)
C(18)-C(13)-N(3)	120.5(6)	C(31)-C(32)-C(33)	118.4(8)
C(15)-C(14)-C(13)	123.5(7)	C(34)-C(33)-C(32)	120.1(8)
C(15)-C(14)-Br(2)	117.3(5)	C(33)-C(34)-C(29)	123.1(8)
C(13)-C(14)-Br(2)	119.2(5)	C(1)-N(1)-C(12)	105.8(4)
C(16)-C(15)-C(14)	118.4(7)	C(1)-N(1)-C(2)	131.1(5)
C(15)-C(16)-C(17)	122.1(6)	C(12)-N(1)-C(2)	122.9(4)
C(15)-C(16)-Br(3)	120.0(6)	C(12)-N(2)-N(3)	104.8(4)
C(17)-C(16)-Br(3)	117.8(6)	N(2)-N(3)-C(1)	111.8(4)
C(18)-C(17)-C(16)	117.5(6)	N(2)-N(3)-C(13)	116.1(4)
C(17)-C(18)-C(13)	121.5(6)	C(1)-N(3)-C(13)	126.5(5)
C(17)-C(18)-Br(1)	118.5(5)	C(20)-N(4)-C(19)	121.8(6)
C(13)-C(18)-Br(1)	120.0(4)	C(20)-N(4)-C(26)	121.1(6)
C(1)-C(19)-C(27)	125.2(5)	C(19)-N(4)-C(26)	115.0(5)
C(1)-C(19)-N(4)	116.1(5)	C(10)-O(1)-C(11)	110.8(4)
C(27)-C(19)-N(4)	118.7(5)		
N(4)-C(20)-C(25)	122.9(6)		

Symmetry transformations used to generate equivalent atoms:

Table A4.9 Anisotropic displacement parameters ($\text{\AA}^2 \times 10^3$) for **(348)**. The anisotropic displacement factor exponent takes the form: $-2\delta^2 [h^2 a^{*2} U^{11} + \dots + 2 h k a^* b^* U^{12}]$

	U ¹¹	U ²²	U ³³	U ²³	U ¹³	U ¹²
Br(1)	69(1)	57(1)	76(1)	4(1)	-18(1)	-11(1)
Br(2)	68(1)	75(1)	65(1)	-2(1)	1(1)	-11(1)
Br(3)	132(1)	93(1)	49(1)	20(1)	-24(1)	19(1)
C(1)	45(3)	36(3)	27(3)	1(2)	1(2)	12(3)
C(2)	43(3)	23(2)	28(3)	5(2)	2(2)	4(2)
C(3)	45(4)	29(3)	36(3)	0(2)	-2(3)	7(2)
C(4)	43(4)	45(3)	45(4)	1(3)	13(3)	8(3)
C(5)	44(4)	51(4)	95(6)	3(4)	7(4)	11(3)
C(6)	42(4)	55(5)	120(8)	-3(5)	6(5)	9(3)
C(7)	44(4)	72(5)	77(5)	-15(4)	-24(4)	13(4)
C(8)	41(4)	39(3)	62(4)	-14(3)	-18(3)	12(3)
C(9)	61(4)	40(3)	31(3)	0(3)	-7(3)	11(3)
C(10)	54(4)	28(3)	35(3)	2(2)	12(3)	-5(3)
C(11)	30(3)	43(3)	38(3)	-9(3)	2(2)	4(3)
C(12)	32(3)	26(3)	46(3)	-4(2)	6(3)	9(2)
C(13)	54(4)	34(3)	33(3)	-2(3)	-5(3)	17(3)
C(14)	48(4)	46(3)	45(4)	-6(3)	-5(3)	12(3)
C(15)	68(5)	47(4)	41(4)	-4(3)	-14(3)	22(4)
C(16)	82(5)	39(3)	42(4)	9(3)	-3(4)	28(4)
C(17)	61(4)	43(4)	52(4)	18(3)	-1(3)	-2(3)
C(18)	51(4)	31(3)	50(4)	0(3)	-16(3)	7(3)
C(19)	47(4)	34(3)	35(3)	-2(2)	0(3)	5(3)
C(20)	63(5)	50(4)	38(4)	-9(3)	-9(3)	30(3)
C(21)	121(8)	84(6)	48(5)	-10(4)	-14(5)	49(6)
C(22)	170(13)	134(10)	36(5)	-3(6)	-8(6)	68(9)
C(23)	162(13)	117(9)	40(6)	8(6)	26(7)	35(9)
C(24)	152(11)	67(6)	95(8)	28(6)	66(8)	36(6)
C(25)	90(6)	63(5)	59(5)	27(4)	14(4)	30(5)
C(26)	77(6)	63(5)	76(5)	-18(4)	-25(5)	-6(4)
C(27)	56(4)	29(3)	23(3)	2(2)	-1(2)	10(3)
C(28)	55(4)	38(3)	30(3)	0(2)	-8(3)	9(3)
C(29)	46(3)	35(3)	39(3)	-2(3)	4(3)	8(3)
C(30)	82(6)	52(4)	84(6)	-29(4)	-14(5)	41(4)

C(31)	99(7)	91(8)	138(10)	-44(7)	-8(7)	52(7)
C(32)	39(4)	87(6)	112(7)	25(6)	1(5)	19(4)
C(33)	44(5)	164(11)	60(5)	24(6)	3(4)	17(5)
C(34)	35(4)	82(5)	46(4)	5(4)	6(3)	17(3)
N(1)	38(3)	27(2)	35(3)	-9(2)	0(2)	5(2)
N(2)	47(3)	36(2)	33(3)	-8(2)	-4(2)	22(2)
N(3)	53(3)	40(3)	34(3)	-3(2)	-1(2)	21(2)
N(4)	54(3)	34(3)	37(3)	-3(2)	1(2)	6(2)
O(1)	35(2)	34(2)	41(2)	-10(2)	-1(2)	0(2)

Table A4.10 Hydrogen coordinates ($\times 10^4$) and isotropic displacement parameters ($\text{\AA}^2 \times 10^{-3}$) for (348).

	x	y	z	U(eq)
H(2)	9725	3556	9346	37
H(4)	11483	5853	8352	53
H(5)	13560	6966	8623	76
H(6)	14327	7161	9855	87
H(7)	12945	6371	10809	77
H(9A)	10583	3923	10835	53
H(9B)	10281	5583	11126	53
H(10)	8429	4257	10384	47
H(11A)	7054	7691	9834	44
H(11B)	6673	6011	10038	44
H(15)	4728	5882	5804	63
H(17)	8187	8270	5801	63
H(21)	7308	2852	5660	101
H(22)	7997	3707	4533	136
H(23)	9884	5421	4439	127
H(24)	11150	5802	5516	125
H(25)	10587	4803	6627	85
H(26A)	6619	2219	6807	108
H(26B)	7344	1731	7558	108

H(26C)	7863	1111	6788	108
H(27)	10782	3261	8309	43
H(28)	10531	1646	6988	49
H(30)	12281	-93	6666	87
H(31)	14270	-1309	6848	131
H(32)	15548	-851	7915	95
H(33)	14785	944	8768	107
H(34)	12789	2158	8563	65

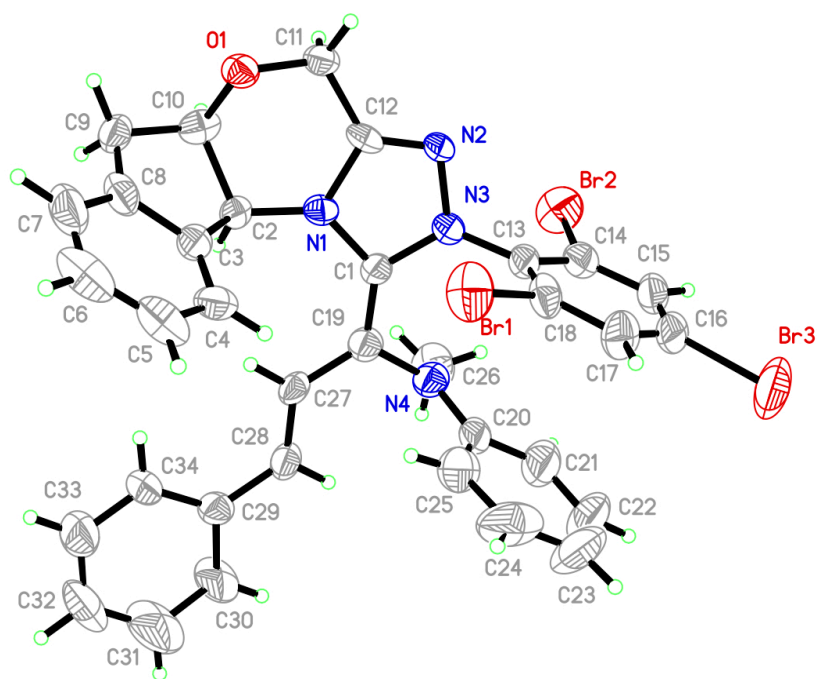


Figure A4.2 Thermal plot of (348). Ellipsoids drawn at the 50% probability level.